HEAVY QUARKS AT FIXED TARGET

FRASCATI PHYSICS SERIES

Series Editor
Vincenzo Valente

Technical Editor
Luigina Invidia

For this Volume:

Editor *B. Cox*
Technical Editor *D. Stokely*

Cover: University of Virginia

Volume III

Istituto Nazionale di Fisica Nucleare – Laboratori Nazionali di Frascati
Divisione Ricerca – SIS – Ufficio Pubblicazioni
P.O. Box 13, I–00044 Frascati (Roma) Italy
email: sispub@vaxlnf.lnf.infn.it

FRASCATI PHYSICS SERIES

HEAVY QUARKS AT FIXED TARGET

ISBN 88–86409–04–4

Printed in Italy

FRASCATI PHYSICS SERIES

Volume III

HEAVY QUARKS AT FIXED TARGET

Editor: B. Cox

Proceedings of the "1994 Workshop on Heavy Quarks Physics at Fixed Target"
University of Virginia, October 7–10, 1994

International Advisory Committee

J. Appel	*Fermilab*
G. Bellini	*University of Milano/INFN*
L. Camilleri	*CERN*
R. Cester	*University of Torino/INFN*
B. Cox	*University of Virginia, Chairman*
F.L. Fabbri	*Laboratori Nazionali di Frascati/INFN*
V. Fitch	*Princeton University*
F. Grancagnolo	*University of Lecce/INFN*
K. Kleinknecht	*Mainz University*
Y. Lemoigne	*Saclay*
V. Luth	*SSC Laboratory*
L. Rossi	*University of Genova/INFN*
D. Websdale	*Imperial College*
J. Wiss	*University of Illinois UC*
S. Bianco	*Laboratori Nazionali di Frascati/INFN, Secretary*

Local Organizing Committee

S. Conetti	*University of Virginia*
P. Fishbane	*University of Virginia*
N. Isgur	*CEBAF*
P. Karchin	*Yale University*
K. Kinoshita	*Virginia Polytechnic Institute*
D. Marlow	*Princeton University*
G. Smith	*Penn State Universtity*
H. Thacker	*University of Virginia*
J. Trischuk	*McGill University*

Graphics
G. Nicoletti
UVa Printing Service

HQ94 Session Convenors

N. Isgur	*CEFAB*
R. Cester	*Torino/INFN*
F. Grancagnolo	*Lecce/INFN*
G. Bellini	*Milano/INFN*
F.L. Fabbri	*Frascati/INFN*
H. Thacker	*University of Virginia*
B. Cox	*University of Virginia*
S. Conetti	*University of Virginia*
K. Kleinknecht	*Mainz*
D. Marlow	*Princeton*
D. Kaplan	*Northern Illinois*
G. Carboni	*Pisa/INFN*

Secretariat
L. Brogiato
D. Stokely

Scientific Secretaries
Z. Cao
K. Hagan–Ingram
P. Hanlet
S. Ledovskoy
V. Pogosyan

INTRODUCTION

Among the most important elementary particle physics topics of the last two decades has been the study of the production and decays of the strange, charm, and beauty quarks, both as they appear in quark-antiquark states in the light meson, charmonium, and bottomonium systems and in their bare quark incarnations in strange, charm, and beauty hadrons. Much of the data on the various quark states has been obtained in fixed target experiments. Accordingly, a series of conferences devoted specifically to discussions of results, ongoing experiments, and future plans for heavy quark fixed target experiments was intitiated in 1993 by the Laboratori Nazionali di Frascati (LNF).

The inaugural conference in this series was held at the Laboratori Nazionali di Frascati from May 31 to June 2, 1993. The second meeting, the subject matter of which is included in this volume, was held at the University of Virginia on October 7-10, 1994.

The richness and breath of the physics addressed by fixed target experiments can be sensed by inspection of the table of contents of this volume. Deep insights into the interactions of quarks and gluons with one another can be obtained by the study of charmonium and bottomonium systems and bare charm and beauty mesons spectroscopy. The experiments in these areas were covered in Sessions I, II, IV and V of the conference. Likewise, the study of the production mechanisms of charm and beauty as discussed by speakers in these sessions and in Session VIII gives insight into the fusion of gluons and quarks to form the meson states. The sensitivity of fixed target experiments to CP violation in electroweak decays of strange, charm, and beauty mesons and hyperons was discussed in Sessions III, VII, IX and X.

Finally, in Sessions XI and XII, two panels discussed the future of fixed target physics in charm and beauty physics as compared to hadron and e^+e^- collider options. The potential for fixed target experiments remains excellent in the area of heavy quark physics with the advent of new fixed charm experiments at Fermilab and the new HERA-B beauty experiment at DESY.

I would like to acknowledge the sponsorship of the University of Virginia, the Istituto Nazionale di Fisica Nucleare of Italy, the U.S. Department of Energy, and the Fermi National Accelerator Laboratory. In particular, I cite the support of the University of Virginia Center for Advanced Studies, the University of Virginia Dean of the Faculty of Arts and Sciences, the University of Virginia Vice-Provost for Research, and the management and staff of the Laboratori Nazionali di Frascati dell' INFN who have made this conference possible. I would like to especially acknowledge the help of Diana Stokely of the University of Virginia HEP group and Stefano Bianco of Frascati in every aspect of the preparations for and the execution of HQ94.

Brad Cox
University of Virginia

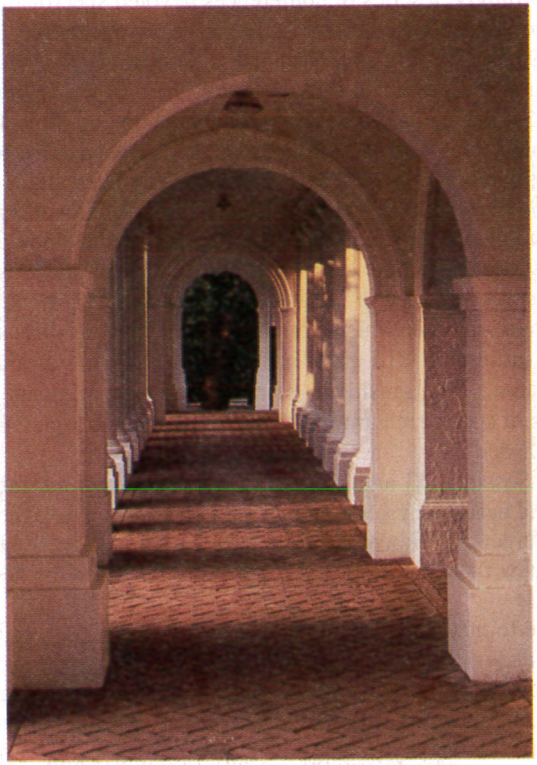

"Rotunda Walkway"

"Mr. Jefferson's Academical Village"

Table of Contents

SESSION I

- M. Wise
  Heavy Quark Theory
- E. Berger
  Heavy Quark Production at Fixed Target Energies
- E. J. Eichten
  Ground State/Excited States of Light-Heavy and Heavy-Heavy Quark Spectroscopy

Frascati Physics Series, Vol. III (1994)
HEAVY QUARKS AT FIXED TARGET
University of Virginia, October 7–10, 1994
(pp. 3–16)

HEAVY QUARK THEORY

Mark B. Wise
California Institute of Technology, Theoretical Physics
Pasadena, California 91125 USA

ABSTRACT

Recent progress in the theory of hadrons containing a single heavy quark is reviewed. Particular attention is paid to those aspects that bear on the determination of the magnitudes of the Cabibbo–Kobayashi–Maskawa matrix elements V_{cb} and V_{ub}.

1 – Introduction

Over the past year there have been several important developments in the theory of hadrons containing a single heavy quark. At the same time there have been significant improvements from experiment in our understanding of the properties of hadrons containing a charm or bottom quark.

The minimal standard model has six quarks that couple to the charged W-bosons through the term

$$\mathcal{L}_{int} = \frac{g_2}{2\sqrt{2}}(\bar{u}, \bar{c}, \bar{t})\gamma_\mu(1-\gamma_5)V \begin{pmatrix} d \\ s \\ b \end{pmatrix} W^\mu + h.c. \qquad (1)$$

in the Lagrange density. Here g_2 is the weak SU(2) coupling, W^μ is the charged W-boson field and V is the Cabibbo–Kobayashi–Maskawa matrix. V arises from the diagonalization of the quark mass matrices. It can be written in terms of three Euler like angles and a complex phase $e^{i\delta}$. In the minimal standard model it is this phase that is responsible for the CP violation observed in kaon decay and CP violation in B decay. Extensions of the standard model with extended Higgs sectors usually have additional sources of CP violation. It is hoped to test the correctness

of the minimal standard model for CP violation in future B decay experiments and elsewhere.

In the minimal standard model the elements of the Cabibbo–Kobayashi–Maskawa matrix are fundamental parameters that must be determined from experiment. In this talk I will concentrate on those issues in heavy quark theory that are related to a determination of $|V_{ub}|$ and $|V_{cb}|$ from B decays. Other interesting areas where progress has occurred will, for the most part, be omitted. Even within the area of those elements of heavy quark physics related to determining the weak mixing angles I will not be able to give a complete review. For example, I will not have time to discuss the implications of sum rules in semileptonic decay and lattice QCD results.

In order to present the new developments in the theory of heavy quarks in their proper context and to fully appreciate their significance I will briefly review some of the key early work on heavy quark theory.

2 – Heavy Quark Effective Theory

The part of the QCD Lagrange density that contains a heavy quark Q is

$$\mathcal{L} = \bar{Q}(i\not{D} - m_Q)Q \ . \tag{2}$$

For situations where the heavy quark Q is interacting with light degrees of freedom (i.e., light quarks and gluons) carrying momentum much less than its mass, m_Q, it is appropriate to take the limit $m_Q \to \infty$ with the heavy quark four-velocity, v^μ, held fixed. [1] In this limit the interactions of the heavy quark become independent of its mass and spin resulting in the approximate heavy quark spin-flavor symmetries of QCD.

To take this limit write

$$Q(x) = e^{-im_Q v\cdot x} h_v^{(Q)}(x) \tag{3}$$

where

$$\not{v} h_v^{(Q)} = h_v^{(Q)} \tag{4}$$

Putting eq. (3) into (2) gives

$$\mathcal{L}_0 = \bar{h}_v^{(Q)}(iD\!\!\!/ + m_Q(\not{v} - 1))h_v^{(Q)} \ . \tag{5}$$

Using the constraint (4) this can be simplified to [2,3]

$$\mathcal{L}_0 = \bar{h}_v^{(Q)} iv\cdot D h_v^{(Q)} \ . \tag{6}$$

Note that the Lagrange density in eq. (6) is independent of the heavy quark's mass and it's spin. Consequently the heavy quark effective theory has a spin flavor symmetry. [1] For charm and bottom quarks moving with the same velocity this is an SU(4) symmetry. Much of the predictive power of the heavy quark effective theory arises because of this symmetry.

The heavy quark field $h_v^{(Q)}$ destroys a quark Q but it does not create the corresponding antiquark. Pair creation does not occur in the heavy quark effective theory.

3 $-1/m_Q$ Corrections

The heavy quark effective theory in (6) represents the $m_Q \to \infty$ limit of QCD. At finite m_Q there are corrections suppressed by powers of $1/m_Q$. These can be included in a systematic fashion. In general

$$Q(x) = e^{-im_Q v\cdot x}[h_v^{(Q)}(x) + \chi_v^{(Q)}(x)] \tag{7}$$

where

$$\not{v} h_v^{(Q)} = h_v^{(Q)} \quad \text{and} \quad \not{v}\chi_v = -\chi_v^{(Q)} \tag{8}$$

The equation of motion for the heavy quark field Q

$$(i\not{D} - m_Q)Q = 0 \tag{9}$$

can be used to express $\chi_v^{(Q)}(x)$ in terms of $h_v^{(Q)}(x)$ order by order in $1/m_Q$. Putting (7) into (9) and using (8) gives

$$\chi_v^{(Q)} = \frac{1}{2m_Q} i\not{D}[h_v^{(Q)} + \chi_v^{(Q)}] \tag{10}$$

which implies that

$$\chi_v^{(Q)} = \frac{1}{2m_Q} i\not{D} h_v^{(Q)} + \mathcal{O}(1/m_Q^2)\,. \tag{11}$$

Using this in eq. (7) and then plugging (7) into the Lagrange density (2) gives the heavy quark effective theory including $1/m_Q$ corrections.

$$\mathcal{L} = \mathcal{L}_0 + \mathcal{L}_1 \tag{12}$$

with $\mathcal{L}_0$ given by eq. (6) and [4,5]

$$\mathcal{L}_1 = \bar{h}_v^{(Q)} \frac{(iD)^2}{2m_Q} h_v^{(Q)} - a_2(\mu)\bar{h}_v^{(Q)} g \frac{G_{\alpha\beta}\sigma^{\alpha\beta}}{4m_Q} h_v^{(Q)} \tag{13}$$

with $a_2(\mu) = 1$. In eq. (13) g is the strong gauge coupling and $G_{\alpha\beta}$ is the gluon field strength tensor. The procedure we have outlined above amounts to matching tree graphs in QCD with those in the heavy quark effective theory. When

loops are included a_2 develops subtraction point dependence because the operator $\bar{h}_v^{(Q)} g G_{\alpha\beta}\sigma^{\alpha\beta} h_v^{(Q)}$ requires renormalization. In the leading logarithmic approximation

$$a_2(\mu) = [\alpha_s(m_Q)/\alpha_s(\mu)]^{9/(33-2n_f)} \tag{14}$$

where n_f is the number of light quark flavors.

The first term in eq. (13) is the heavy quark kinetic energy. It breaks the heavy quark flavor symmetry but not the spin symmetry. The second term in eq. (13) is the energy from the interaction of the heavy quark's color magnetic moment with the chromomagnetic field. It breaks both the spin and flavor symmetries.

4 – Spectroscopy of Heavy Hadrons

In the $m_Q \to \infty$ limit hadrons containing a single heavy quark Q are classified not only by their total spin $\vec{S}$ but also by the spin of their light degrees of freedom [6]

$$\vec{S}_\ell = \vec{S} - \vec{S}_Q \ . \tag{15}$$

Since $s_Q = 1/2$, in this limit hadrons containing a single heavy quark occur in degenerate doublets labelled by the spin of the light degrees of freedom s_ℓ and with total spins

$$s = s_\ell \pm 1/2 \tag{16}$$

An exception occurs for $s_\ell = 0$ where there is only one state with $s = 1/2$. For mesons with $Q\bar{q}$ ($q = u$ *or* d) flavor quantum numbers the ground state doublet has negative parity and $s_\ell = 1/2$ giving a doublet of spin-zero and spin-one mesons. For $Q = c$ they are the D and D^* mesons and for $Q = b$ they are the B and B^* mesons. In the $Q = c$ case an excited doublet of positive parity mesons with $s_\ell = 3/2$ has been observed. The hadrons in this doublet are sometimes called D^{**} mesons and have total spins one and two.

Baryons with Qqq flavor quantum numbers have also been observed. The ground state isospin zero baryons have positive parity and $s_\ell = 0$ and are called Λ_Q baryons. The ground state $I = 1$ baryons have positive parity and $s_\ell = 1$ and come in a doublet with $s = 1/2$ and $3/2$. They are called Σ_Q and Σ_Q^* baryons. For $Q = c$ the Λ_c and Σ_c baryons have been observed and for $Q = b$ the Λ_b baryon has been observed. In the charm case two excited baryons have also been observed. Their properties are consistent with being a negative parity doublet of $I = 0$ baryons with $s_\ell = 1$ giving total spins $1/2$ and $3/2$.

The mass of a hadron H_Q containing a single heavy quark Q can be expanded in powers of $1/m_Q$. Up to order $1/m_Q$ it has the form

$$m_{H_Q} \ = \ m_Q + \bar{\Lambda} - \langle H_Q | \bar{h}_v^{(Q)} \frac{(iD)^2}{2m_Q} h_v^{(Q)} | H_Q \rangle / 2m_H$$

$$+ \quad a_2(\mu)\langle H_Q|\bar{h}_v^{(Q)}\frac{gG_{\alpha\beta}\sigma^{\alpha\beta}}{4m_Q}h_v^{(Q)}|H_Q\rangle/2m_H + \mathcal{O}(1/m_Q^2)\ . \tag{17}$$

The first term on the rhs of equation (17), m_Q, is the heavy quark pole mass. The second $\bar{\Lambda}$ is the mass of the light degrees of freedom in the hadron. It does not depend on the heavy quark mass but does depend on the quantum numbers of the light degrees of freedom. The third term is the heavy quark's kinetic energy and the final term is its chromomagnetic energy. Only the last term depends on the spin of the heavy quark and it causes the splittings in the hadron doublets mentioned earlier. For example

$$m_{B^*} - m_B = -\frac{4}{3}a_2(\mu)\langle B|\bar{h}_v^{(b)}\frac{gG_{\alpha\beta}}{4m_b}\sigma^{\alpha\beta}h_v^{(b)}|B\rangle/2m_B\ . \tag{18}$$

The heavy quark pole mass m_Q is not a physical quantity and its perturbative expansion has an infrared renormalon ambiguity of order Λ_{QCD}. [7,8] Nonetheless, it is very convenient to introduce it. As long as final expressions that are compared with experiment express physical quantities in terms of other physical quantities the fact that the pole mass itself is not really well defined is of no consequence. [9,10]

5 – Exclusive $B \to D^{(*)}e\bar{\nu}_e$ Decay

The rates for $B \to De\bar{\nu}_e$ and $B \to D^*e\bar{\nu}_e$ are determined by the value of $|V_{bc}|$ and the hadronic matrix element of the weak current $\bar{c}\gamma_\mu(1-\gamma_5)b$ between B and $D^{(*)}$ states. The application of heavy quark effective theory involves a two step process. First is matching the current $\bar{c}\gamma_\mu(1-\gamma_5)b$ onto operators in the heavy quark effective theory. In the leading logarithmic approximation this matching takes the simple form [11]

$$\bar{c}\gamma_\mu(1-\gamma_5)b = \left[\frac{\alpha_s(m_b)}{\alpha_s(m_c)}\right]^{-6/25}\left[\frac{\alpha_s(m_c)}{\alpha_s(\mu)}\right]^{a_L}\cdot\bar{h}_{v'}^{(c)}\gamma_\mu(1-\gamma_5)h_v^{(b)} \tag{19}$$

where

$$a_L = \frac{8}{27}[v\cdot v' r(v\cdot v') - 1] \tag{20}$$

and

$$r(v\cdot v') = \frac{1}{\sqrt{(v\cdot v')^2-1}}\ln(v\cdot v' + \sqrt{(v\cdot v')^2-1}). \tag{21}$$

Note that for $v\cdot v' \neq 1$ the coefficient of the current in the effective theory $\bar{h}_{v'}^{(c)}\gamma_\mu(1-\gamma_5)h_v^{(b)}$ depends on the subtraction point μ. In the effective theory where the charm and bottom quarks are both treated as heavy the operator $\bar{h}_{v'}^{(c)}\gamma_\mu(1-\gamma_5)h_v^{(b)}$ requires renormalization. It's matrix elements have a μ dependence that cancels that of its coefficient. However, at zero recoil $v\cdot v' = 1$ the coefficient is independent of μ.

At this kinematic point the operator is the conserved current associated with the spin-flavor symmetries of the heavy quark effective theory and consequently it is not renormalized.

Matrix elements of $\bar{h}^{(c)}_{v'}\Gamma h^{(b)}_v$ in the heavy quark effective theory between B and D^* states are related by heavy quark spin symmetry to a single universal function of $v\cdot v'$,[1]

$$\frac{\langle D(v')|\bar{h}^{(c)}_{v'}\Gamma h^{(b)}_v|B(v)\rangle}{\sqrt{m_B m_D}} = \xi(v\cdot v')Tr\left\{\frac{(\not{v}'+1)}{2}\Gamma\frac{(\not{v}+1)}{2}\right\} \tag{22}$$

$$\frac{\langle D^*(v',\varepsilon)|\bar{h}^{(c)}_{v'}\Gamma h^{(b)}_v|B(v)\rangle}{\sqrt{m_B m_{D^*}}} = \xi(v\cdot v')Tr\left\{\varepsilon^*\frac{(\not{v}'+1)}{2}\Gamma\frac{(\not{v}+1)}{2}\gamma_5\right\}. \tag{23}$$

For $v\cdot v'\neq 1$ the Isgur–Wise function $\xi(v\cdot v')$ depends on the subtraction point μ. However, at zero recoil heavy quark flavor symmetry fixes the normalization [1,12,13] of ξ,

$$\xi(1) = 1. \tag{24}$$

Equations (22) and (23) hold in the $m_{c,b}\to\infty$ limit. In general there are $\Lambda_{QCD}/m_{c,b}$ corrections. However, at zero recoil it has been shown that corrections first arise at order $\Lambda^2_{QCD}/m^2_{c,b}$. [13,14] This important result opens an avenue for the precise determination of $|V_{cb}|$ from exclusive $B\to D^* e\bar{\nu}_e$ decay.

Neglecting nonperturbative corrections, suppressed by powers of $(\Lambda_{QCD}/m_{b,c})$, the zero recoil, the matrix elements of the axial, and vector currents are

$$\frac{\langle D(v)|\bar{c}\gamma_\mu b|B(v)\rangle}{\sqrt{m_B m_D}} = 2\eta_V v_\mu \tag{25}$$

$$\frac{\langle D^*(v,\varepsilon)|\bar{c}\gamma_\mu\gamma_5 b|B(v)\rangle}{\sqrt{m_B m_{D^*}}} = 2\eta_A\varepsilon^*_\mu, \tag{26}$$

where η_V and η_A are QCD correction factors from matching currents in the full theory onto those in the effective theory. In the leading logarithmic approximation where $\ln(m_b/m_c)$ is treated as large and all terms of order $[\alpha_s\ln(m_b/m_c)]^n$ are summed [15,16]

$$\eta_V = \eta_A = \left[\frac{\alpha_s(m_b)}{\alpha_s(m_c)}\right]^{-6/25}. \tag{27}$$

However, since m_b/m_c is not that large a better approximation is to keep the full dependence on m_c/m_b. The coefficients η_V and η_A have been calculated including two loop terms that come from vacuum polarization insertions and are proportional to

$$\beta^{(0)} = 11 - \frac{2}{3}n_f. \tag{28}$$

The result is [13,17,18]

$$\eta_V = 1 + \frac{1}{3}\frac{\bar{\alpha}_s(\sqrt{m_b m_c})}{\pi}\phi(m_c/m_b) + \left(\frac{\bar{\alpha}_s(\sqrt{m_b m_c})}{\pi}\right)^2\left[\frac{1}{72}\phi(m_c/m_b)\beta^{(0)} + ...\right] + ... \ , \tag{29}$$

and

$$\eta_A = 1 + \frac{1}{3}\frac{\bar{\alpha}_s(\sqrt{m_b m_c})}{\pi}[\phi(m_c/m_b) - 2] + \left(\frac{\bar{\alpha}_s(\sqrt{m_b m_c})}{\pi}\right)^2 \cdot \left[\left(\frac{5}{72}\phi(m_c/m_b) - \frac{14}{72}\right)\beta^{(0)} + ...\right] + ... \ , \tag{30}$$

where

$$\phi(z) = -3\left(\frac{1+z}{1-z}\right)\ln z - 6 \ , \tag{31}$$

m_c and m_b are heavy quark pole masses and $\bar{\alpha}_s$ is the $\overline{MS}$ strong coupling. The ellipses in the square brackets are terms independent of n_f. There are reasons to believe that the order $\bar{\alpha}_s^2$ piece proportional to $\beta^{(0)}$ provides a good approximation to the full order $\bar{\alpha}_s^2$ term. That is true for $R(e^+e^- \to \text{hadrons})$, $\Gamma(\tau \to \nu_\tau + \text{hadrons})$ and the relation between the heavy quark pole mass m_Q and the running heavy quark $\overline{MS}$ mass $\bar{m}_Q(m_Q)$:

$$R(e^+e^- \to \text{hadrons}) = 3\left(\sum_i Q_i^2\right)\left[1 + \frac{\bar{\alpha}_s(\sqrt{s})}{\pi} + (0.17\beta^{(0)} + 0.08)\left(\frac{\bar{\alpha}_s(\sqrt{s})}{\pi}\right)^2 + ...\right] \tag{32}$$

$$\frac{\Gamma(\tau \to \nu_\tau + \text{hadrons})}{3\Gamma(\tau \to \nu_\tau \bar{\nu}_e e)} = 1 + \frac{\bar{\alpha}_s(m_\tau)}{\pi} + (0.57\beta^{(0)} + 0.08)\left(\frac{\bar{\alpha}_s(m_\tau)}{\pi}\right)^2 + ... \tag{33}$$

$$m_Q/\bar{m}_Q(m_Q) = 1 + \frac{4}{3}\frac{\bar{\alpha}_s(m_Q)}{\pi} + (1.56\beta^{(0)} - 1.05)\left(\frac{\bar{\alpha}_s(m_Q)}{\pi}\right)^2 + ... \ . \tag{34}$$

Evaluating eqs. (29) and (30) with $m_c/m_b = 0.30$ and $\bar{\alpha}_s(m_b) = 0.20$ gives

$$\begin{aligned} \eta_V &= 1 + 0.02 + 0.004 \\ \eta_A &= 1 - 0.03 - 0.005 \ , \end{aligned} \tag{35}$$

In eqs. (35) the second and third terms are the ones of order $\bar{\alpha}_s$ and $\bar{\alpha}_s^2\beta^{(0)}$ respectively. Also we have taken $n_f = 2$ which gives $\beta^{(0)} = 9$. Note that the two loop term is much smaller than the one loop term indicating that the perturbation series is well behaved.

Nonperturbative corrections to (25) and (26) are of order $(\Lambda_{QCD}/m_{c,b})^{n+2}$, $n = 0, 1, ...$. For $n = 0$ these have been characterized in terms of matrix elements of various operators in the heavy quark effective theory and estimated using

phenomenological models. [19] In addition the corrections to eqs. (25) and (26) that are enhanced by $\ln m_\pi$ or factors of $1/m_\pi$ have been computed using chiral perturbation theory. These have an interesting form. [20] The correction of order $(\Lambda_{QCD}/m_{c,b})^2$ is enhanced by $\ln m_\pi$ but corrections suppressed by higher powers $(\Lambda_{QCD}/m_{c,b})^{n+2}, n = 1, 2, \ldots$ are enhanced by $(\Lambda_{QCD}/m_\pi)^n$. Consequently, power suppressed terms are important for all n. These corrections are calculable in terms of the $D^* D\pi$ coupling. Unfortunately the value of this coupling is not known. This gives one of the major uncertainties in the size of the power correction to eqs. (25) and (26).

6 – Inclusive $B \to X_{c,u} e \bar{\nu}_e$ Decay

Over the past few years there has been great progress in our understanding of inclusive semileptonic B meson decay. [21,22,23,24] The strong interaction physics relevant for this process is parametrized by the hadronic tensor

$$W^{\mu\nu}_{c,u} = (2\pi)^3 \sum_X \delta^4(p_B - q - p_X) \langle B | J^{\mu\dagger}_{c,u} | X \rangle \langle X | J^\nu_{c,u} | B \rangle \tag{36}$$

and

$$J^\mu_c = \bar{c} \gamma^\mu (1 - \gamma_5) b \tag{37}$$

$$J^\mu_u = \bar{u} \gamma^\mu (1 - \gamma_5) b \tag{38}$$

$W^{\mu\nu}$ can be expanded in terms of scalar form factors $W_n, n = 1, 2, \ldots, 5$ that are functions of q^2 and $v \cdot q$.

$$W^{\mu\nu} = -g^{\mu\nu} W_1 + v^\mu v^\nu W_2 - i\varepsilon^{\mu\nu\alpha\beta} v_\alpha q_\beta W_3 + q^\mu q^\nu W_4 + (q^\mu v^\nu + q^\nu v^\mu) W_5 \, . \tag{39}$$

The form factors W_j are the imaginary parts of form factors that occur in the matrix element of the time ordered product of weak currents.

$$T^{\mu\nu}_{c,u} = -i \int d^4x e^{-iq\cdot x} \langle B | T(J^{\mu\dagger}_{c,u}(x) J^\nu_{c,u}(0)) | B \rangle \tag{40}$$

can be expanded in terms of scalar form factors

$$T^{\mu\nu} = -g^{\mu\nu} T_1 + v^\mu v^\nu T_2 - i\varepsilon^{\mu\nu\alpha\beta} v_\alpha q_\beta T_3 + q^\mu q^\nu T_4 + (q^\mu v^\nu + q^\nu v^\mu) T_5 \tag{41}$$

and

$$Im T_{c,u} = -\pi W_{c,u}. \tag{42}$$

Predictions for the form factors T_j can be made by performing an operator product expansion and making a transition to the heavy quark effective theory. The leading operator encountered is $\bar{b}\gamma_\mu b$ and its matrix element is known since it is the conserved b-quark number current. Here there is no need to make the transition to the heavy quark effective theory to understand the m_b dependence. There are no dimension four operators and the dimension 5 operators that occur are the b-quark kinetic energy and the chromomagnetic dipole term that occur in $\mathcal{L}_1$ of eq. (13). Consequently at leading order in $1/m_b$ the differential decay rate $d\Gamma/dq^2dE_e$ for inclusive semileptonic B-decay is given by free b-quark decay. There are no nonperturbative corrections of order (Λ_{QCD}/m_b). Nonperturbative corrections of order $(\Lambda_{QCD}/m_b)^2$ are characterized by the two dimensionless parameters

$$K_b = -\langle B|\bar{h}_v^{(b)}\frac{(iD)^2}{2m_b^2}h_v^{(b)}|B\rangle/2m_B \tag{43}$$

$$G_b = a(\mu)\langle B|\bar{h}_v^{(b)}\frac{gG_{\mu\nu}}{4m_b^2}\sigma^{\mu\nu}h_v^{(b)}|B\rangle/2m_B\ . \tag{44}$$

Including perturbative corrections and nonperturbative corrections suppressed by $(\Lambda_{QCD}/m_b)^2$ the $B \to X_c e\bar{\nu}_e$ semileptonic decay rate is

$$\Gamma(B \to X_c e\bar{\nu}_e) = \Gamma_0[(1 - 8\rho + 8\rho^3 - \rho^4 - 12\rho^2\ln\rho)\eta_{incl}$$
$$+K_b(-1 + 8\rho - 8\rho^3 + \rho^4 + 12\rho^2\ln\rho) + G_b(3 - 8\rho + 24\rho^2 - 24\rho^3$$
$$+ 5\rho^4 + 12\rho^2\ln\rho)] \tag{45}$$

where

$$\rho = m_c^2/m_b^2, \tag{46}$$

and

$$\Gamma_0 = \frac{|V_{cb}|^2 G_F^2 m_b^5}{192\pi^3}\ . \tag{47}$$

In Γ_0 m_b is the b-quark pole mass and η_{incl} gives the effects of perturbative QCD corrections. Results for $B \to X_u e\bar{\nu}_e$ are obtained by taking $\rho = 0$ and $V_{cb} \to V_{ub}$. η_{incl} depends on m_c/m_b so the perturbative QCD corrections are different for $B \to X_c e\bar{\nu}_e$ and $B \to X_u e\bar{\nu}_e$ decay. The nonperturbative corrections are quite small. Furthermore, G_b is known from the $B^* - B$ mass splitting so the only uncertainty in the nonperturbative corrections comes from the size of K_b. In eqs. (45)-(47) m_c and m_b are the charm and bottom quark pole masses. If m_c is eliminated by

$$m_B - m_D = m_b - m_c + m_b K_b - m_c K_c + m_b G_b - m_c G_c, \tag{48}$$

then the decay rate is not too sensitive to the value of m_b. For example, as m_b varies between 5GeV and 4.5GeV the rate $\Gamma(B \to X_c e\bar{\nu}_e)$ changes by only 20%.

Neglecting the nonperturbative corrections the B decay rate equals the b-quark decay rate. The perturbative QCD corrections of order $\bar{\alpha}_s(m_b)$ have been computed and those of order $\bar{\alpha}_s(m_b)^2$ proportional to $\beta^{(0)}$ are also known. We write

$$\eta_{incl} = 1 - \left(\frac{\bar{\alpha}_s(m_b)}{\pi}\right)\frac{2}{3}\left(\pi^2 - \frac{25}{4} + \delta_1(m_c/m_b)\right) - \left(\frac{\bar{\alpha}_s(m_b)}{\pi}\right)^2(\beta^{(0)}\chi_\beta(m_c/m_b) + ...) + ... \quad . \tag{49}$$

The function $\delta_1(x)$ is known analytically. [25] It takes into account the effect of the charm quark mass on the order $\bar{\alpha}_s$ QCD corrections; $\delta_1(0) = 0$. Numerically $\delta_1(0.3) = -1.11$. The function $\chi_\beta(x)$ has been determined numerically yielding $\chi_\beta(0) = 3.2$ and $\chi_\beta(0.3) = 1.7$. Using $\bar{\alpha}_s(m_b) = 0.20$ and $m_c/m_b = 0.30$ gives [26]

$$\eta_{incl} = 1 - 0.11 - 0.06 + ... \tag{50}$$

for $B \to X_c e\bar{\nu}_e$ decay and (using $m_c/m_b = 0$)

$$\eta_{incl} = 1 - 0.15 - 0.11 + ... \ , \tag{51}$$

for $B \to X_u e\bar{\nu}_e$ decay. The second and third terms in eqs. (50) and (51) are the pieces of order $\bar{\alpha}_s(m_b)$ and $\bar{\alpha}_s(m_b)^2\beta^{(0)}$ respectively. In the "two loop" term we have taken $n_f = 2$ which gives $\beta^{(0)} = 9$. For $B \to X_u e\bar{\nu}_e$ the perturbative series is not well behaved and the situation for $B \to X_c e\bar{\nu}_e$ is somewhat marginal. For inclusive semileptonic $D \to X_s\bar{e}\nu_e$ decay similar formulas hold. The perturbative QCD corrections can be deduced from eq. (49) with $\bar{\alpha}_s(m_b) \to \bar{\alpha}_s(m_c)$ and $m_c/m_b \to m_s/m_c \simeq 0$. Here the QCD corrections are also not under control.

The methods outlined above for inclusive semileptonic B decay can also be applied to nonleptonic B-decay. Here one runs into a potential conflict between the measured semileptonic branching ratio and the measured charm multiplicity. [27,28] For the decays that come from $b \to c\bar{c}s$ the charm quark masses take up most of the available energy. Therefore, it is not clear that local duality can be used to relate the quark level decay to the hadron decay. Furthermore, the perturbative QCD corrections in the quark level decay may not be under control. To accommodate the measured semileptonic branching ratio [29] $B_{SL} = (10.4 \pm 0.4)\%$ requires about 40% of the nonleptonic B decays to come from the $b \to c\bar{c}s$ mechanism. This implies a charm multiplicity $\langle n_c \rangle \simeq 1.3$. However, the measured charm multiplicity [30] is only $\langle n_c \rangle_{\rm exp} = 1.04 \pm 0.07$. It will take more data to resolve this issue.

7 – The End Point Region of the Electron Spectrum

The maximum electron energy in the exclusive decay $B \to Xe\bar{\nu}_e$ is

$$E_e^{\max} = \frac{m_B^2 - m_X^2}{2m_B} \,. \tag{52}$$

Therefore, semileptonic B decays with electron energies greater than $(m_B^2 - m_D^2)/2m_B$ must have come from a $b \to u$ transition. This endpoint region of the electron energy spectrum is very important. Understanding it in a model independent way may lead to a precise determination of V_{ub}.

For inclusive $B \to X_u e\bar{\nu}_e$ decay the electron energy spectrum, including nonperturbative effects of order $(\Lambda_{QCD}/m_b)^2$, has been found using the operator product expansion methods outlined in the previous section. Neglecting perturbative QCD corrections [22,23]

$$\begin{aligned} \frac{1}{\Gamma_0}\frac{d\Gamma}{dy} &= \left[2(3-2y)y^2 - \frac{20}{3}y^3 K_b - \left(8 + \frac{20}{3}y\right) y^2 G_b\right]\theta(1-y) \\ &+ \frac{2}{3}[K_b + 11G_b]\delta(1-y) + \frac{2}{3}K_b\delta'(1-y) \,, \end{aligned} \tag{53}$$

where

$$y = (2E_e/m_b) \,, \tag{54}$$

and K_b and G_b are given in eqs. (43) and (44). These matrix elements are of order ε^2 where,

$$\varepsilon = \Lambda_{QCD}/m_b \,. \tag{55}$$

The maximum electron energy for b-quark decay is $y = 1$ (i.e., $E_e = m_b/2$). However, nonperturbative effects (e.g., motion of the b-quark in the B-meson) extend the maximum electron energy for B-meson decay beyond this point. Since we are treating such effects as a power series in ε they are represented by singular terms at $y = 1$. To all orders in ε the decay spectrum obtained from the operator product expansion has the structure [31] (at zero'th order in $\alpha_s(m_b)$)

$$\begin{aligned} \frac{1}{\Gamma_0}\frac{d\Gamma}{dy} &= \theta(1-y)(\varepsilon^0 + 0\varepsilon + \varepsilon^2 + ...) \\ &+ \delta(1-y)(0\varepsilon + \varepsilon^2 + ...) + \delta^{(1)}(1-y)(\varepsilon^2 + \varepsilon^3 + ...) + ... \\ &+ \delta^{(n)}(1-y)(\varepsilon^{n+1} + \varepsilon^{n+2} + ...) + ... \,, \end{aligned} \tag{56}$$

where ε^n denotes a term of that order, which may include a smooth function of y. In eq. (56) $\delta^{(n)}(1-y)$ denotes the n'th derivative of $\delta(1-y)$ with respect to y. The contribution to the total decay rate of a term in $d\Gamma/dy$ of order $\varepsilon^n\delta^{(n)}(1-y)$ is of order ε^n.

The semileptonic decay width for $b \to u$ is difficult to measure because of background contamination from the dominant $b \to c$ semileptonic decays. It is therefore, important to be able to compute the rate in the endpoint region near $y = 1$. One way to calculate the endpoint spectrum is to weight the differential decay distribution $d\Gamma/dy$ in eq. (56) by a normalized function of width σ around $y = 1$. We refer to this process as smearing. Most of the details of the smearing procedure are unimportant; the only quantity of relevance is the width σ of the smearing region.

The singular distribution $\varepsilon^m \delta^{(n)}(1-y)$ (where $m > n$) smeared over a region of width σ gives a contribution of order $\varepsilon^n/\sigma^{n+1}$ to $d\Gamma/dy$. If the width σ of the smearing region is of order ε^p the generic term $\varepsilon^m \delta^{(n)}(1-y)$ yields a contribution of order $\varepsilon^{m-(n+1)p}$. Since $m > n$ this shows that the $1/m_b$ expansion for the spectrum breaks down unless $p \leq 1$, i.e., the smearing region cannot be narrower than ε. The divergence for $p > 1$ is not associated with the failure of the operator product expansion due to resonances with masses of order the QCD scale. The region of the electron energy spectrum for which such resonances dominate the final hadronic states is of width ε^2, while the expansion breaks down upon smearing over any region of size $\varepsilon^{1+\delta}$, where $\delta > 0$.

If the smearing region is chosen of order ε the form of the expansion in eq. (56) shows that the leading terms of the form $\theta(1-y)$ and $\varepsilon^{n+1}\delta^{(n)}(1-y)$ all contribute at order unity to the smeared spectrum. Thus one can obtain the decay spectrum smeared over a width ε if the leading singularities can be summed. The sum of the leading singularities produces a distribution $d\Gamma/dy$ of width ε and height of order unity (i.e., of the same order as the free quark distribution). Neubert and Bigi, et al., have shown how to sum the leading singularities. [32,33] They are characterized by the matrix elements

$$\frac{1}{2m_B}\langle B|\bar{h}_v^{(b)} i D^{\mu_1} \ldots i D^{\mu_n} h_v^{(b)}|B\rangle = A_n v_{\mu_1} \ldots v_{\mu_n} + \ldots \ . \tag{57}$$

The ellipsis on the right side of eq. (57) denote other Lorentz structures. For example, with $n = 2$ the matrix element is,

$$\frac{1}{2m_B}\langle B|\bar{h}_v^{(b)} i D^{\mu_1} i D^{\mu_2} h_v^{(b)}|B\rangle = A_2(v_{\mu_1} v_{\mu_2} - g_{\mu_1\mu_2}) \ , \tag{58}$$

since $v \cdot D h_v^{(b)} = 0$. Contracting on μ_1 and μ_2 gives

$$A_2 = \frac{2}{3} m_b K_b \ . \tag{59}$$

Heavy quark symmetry implies that $A_0 = 1$ and the equation of motion $v \cdot D h_v^{(b)} = 0$ implies that $A_1 = 0$. The quantities A_n have dimensions of mass to the power n.

In terms of them the sum of the leading singularities in the electron spectrum is characterized by a shape function $S(y)$

$$\frac{1}{\Gamma_0}\frac{d\Gamma}{dy} = 2y^2(3-2y)S(y) \tag{60}$$

$$S(y) = \sum_{n=0}^{\infty} \frac{(-1)^n}{n!}\left(\frac{A_n}{m_b^n}\right)\frac{d^n}{dy^n}\theta(1-y) \ . \tag{61}$$

Perturbative QCD corrections are also singular in the endpoint region. Summing the leading perturbative QCD singularities (i.e., the Sudakov double logarithms) changes the shape function to [31]

$$S(y) = \sum_{n=0}^{\infty} \frac{(-1)^n}{n!}\left(\frac{A_n}{m_b^n}\right)\frac{d^n}{dy^n}R(y) \tag{62}$$

where

$$R(y) = \exp\left[-\frac{2}{3\pi}\alpha_s \ln^2(1-y)\right] \ . \tag{63}$$

Recently Korchemsky and Sterman have shown how to sum the next to leading logarithms. [34]

Unfortunately the quantities A_n are not known. However, the same quantities characterize the endpoint photon spectrum in $B \to X_s\gamma$. So there is hope that a detailed study of the photon spectrum in $B \to X_s\gamma$ will determine the endpoint region of the electron spectrum in B decays. [33,34,35]

The methods outlined in this section for describing the endpoint region of the electron spectrum apply when this region is dominated by many states with masses of order $\sqrt{m_b\Lambda_{QCD}}$. In the ISGW [36] model the endpoint region where $b \to c$ transitions are forbidden is dominated by the single decay mode $B \to \rho e\bar{\nu}_e$. If ρ dominance is found to hold experimentally then the sum of the leading singularities is not a valid description of a region of electron energy which is as small as the difference between the $B \to X_u e\bar{\nu}_e$ and $B \to X_c e\bar{\nu}_e$ end points.

If the endpoint region is dominated by the rho meson there are other avenues available to determine V_{ub}. For example, exclusive B and D decays can be used. For $D \to \rho\bar{e}\nu_e$ the weak mixing angles are known and the form factors for this decay mode to determine them for $B \to \rho e\bar{\nu}_e$. Using heavy quark symmetry and isospin symmetry [37]

$$\langle\rho(k)|\bar{u}\gamma_\mu(1-\gamma_5)b|B\rangle/\sqrt{2m_B} = \left(\frac{\alpha_s(m_b)}{\alpha_s(m_c)}\right)^{-6/25} \langle\rho(k)|\bar{d}\gamma_\mu(1-\gamma_5)c|D\rangle/\sqrt{2m_D} \ . \tag{64}$$

In the above perturbative QCD effects have been included in the leading logarithmic approximation. If light quark SU(3) symmetry is applied instead of isospin symmetry then the decay $D \to K^*\bar{e}\nu_e$ can be used (instead of the Cabibbo suppressed

decay $D \to \rho \bar{e} \nu_e$). The form factors for this decay have already been measured. Some problems with this approach are the presence of $1/m_{c,b}$ corrections and possibly large higher order perturbative QCD corrections. [38)]

References

1. N. Isgur and M. Wise, *Phys. Lett.* **B232** (1989) 113; **B237** (1990) 527.
2. E. Eichten and B. Hill, *Phys. Lett.* **B234** (1990) 511.
3. H. Georgi, *Phys. Lett.* **B240** (1990) 447.
4. E. Eichten and B. Hill, *Phys. Lett.* **B243** (1990) 427.
5. A. Falk, et al., *Nucl. Phys.* **B357** (1991) 185.
6. N. Isgur and M. Wise, *Phys. Rev. Lett.* **66** (1991) 1130.
7. I. Bigi, et al., TPI-MINN-94/4-T (1994).
8. M. Beneke, et al., MPI-PhT/94-18 (1994).
9. M. Luke, et al., UTPT-94-21 (1994).
10. M. Neubert and C. Sachrajda, CERN-TH 7312/94 (1994).
11. A. Falk, et al., *Nucl. Phys.* **B343** (1990) 1.
12. S. Nussinov and W. Wetzel, *Phys. Rev.* **D36** (1987) 130.
13. M. Voloshin and M. Shifman, *Sov. J. Nucl. Phys.* **47** (1988) 511.
14. M. Luke, *Phys. Lett.* **B252** (1990) 447.
15. M. Voloshin and M. Shifman, *Sov. J. Nucl. Phys.* **45** (1987) 292.
16. H. Politzer and M. Wise, *Phys. Lett.* **B206** (1988) 681; **B208** (1988) 504.
17. J.E. Paschalis and G. Gounaris, *Nucl. Phys.* **B222** (1983) 473; F. Close, et al., *Phys. Lett.* **B149** (1984) 209.
18. M. Neubert, CERN-TH 7454/94 (1994).
19. For a review of QCD sum rule calculations of $1/m_Q$ corrections see: M. Neubert, *Phys. Rep.* **245** (1994) 261.
20. L. Randall and M. Wise, *Phys. Lett.* **B303** (1993) 135.

HEAVY QUARK PRODUCTION AT FIXED TARGET ENERGIES

E. Berger

Argonne National Laboratory
HEP 362, Argonne, Illinois 60439 (U.S.A.)

No written contribution received

GROUND STATE/EXCITED STATES OF LIGHT-HEAVY AND HEAVY-HEAVY QUARK SPECTROSCOPY

E. Eichten

Fermi National Accelerator Laboratory
MS-106, Theory Group, P.O. Box 500
Batavia, Illinois 60510 (U.S.A.)

No written contribution received

SESSION II

- G. Zioulas
  Onia Experimental Results in E760

- A. McManus
  Results in Charmonium Production at High Energy

- K. Lau
  Rare Charm Decays in E789, E771, and WA92

- M. Sokoloff
  Searching for Flavor-Changing Neutral Currents in Fermilab Experiments E791 and E687

Frascati Physics Series, Vol. III (1994)
HEAVY QUARKS AT FIXED TARGET
University of Virginia, October 7–10, 1994
(pp. 23–38)

ONIA EXPERIMENTAL RESULTS IN E760

George Zioulas
Physics Department, University of California at Irvine
Irvine, California 92717-4575, U.S.A.
(for the E760 Collaboration [1])

ABSTRACT

We present a review of results from E760, a resonant charmonium formation experiment in the Fermilab Antiproton Accumulator. The latest results of the resonance parameters of η_c as measured in the reaction $\bar{p}p \to \eta_c \to \gamma\gamma$, and the results of a search for the η_c' are described. Experiment E835, a continuation of E760, and its physics goals are also presented.

1 – Introduction

Since the discovery of the J/ψ 20 years ago, a large number of experiments have taken data to study the charmonium spectrum. Most of these experiments were done at e^+e^- colliders, where the electron-positron annihilation proceeds through an intermediate virtual photon. This limits the quantum numbers of the final states to be those of the photon ($J^{PC} = 1^{--}$). Thus only $^3S_1$ and $^3D_1$ states, like the J/ψ and ψ', can be produced directly. A major advantage of studying these states in e^+e^- collisions is the high yield relative to the underlying hadronic continuum. Other states, like the $^1S_0$ and the triple P, were observed in e^+e^- collisions through the cascade decays of ψs. In this case, precision measurements of the resonance parameters have been limited by the resolution of the detectors.

A different technique to study charmonium states through proton-antiproton annihilations was first applied by experiment R704 [2] at CERN's ISR and later by experiment E760 [3] at Fermilab. In $\bar{p}p$ annihilations the charmonium states are formed directly through two or three gluon intermediate states and thus, they are not limited to those with quantum numbers of 1^{--}. However, the cross sections

for $\bar{p}p \rightarrow c\bar{c}$ are very small ($\leq 1\ \mu b$) and they have to be extracted from a large non-resonant hadronic background ($\sigma_{\bar{p}p \rightarrow hadrons} \approx 70\ mb$). This background can be reduced significantly if charmonium decays into electromagnetic final states are selected. A large-acceptance electromagnetic calorimeter and a Čerenkov counter are necessary for the rejection of the hadronic background. The success of this technique relies heavily on knowledge of the initial energy. A precise and direct measurement of the mass and width of charmonium resonances is allowed by the precisely defined momentum and the narrow momentum spread of the antiproton beam.

E760 used a beam of antiprotons (typically 3×10^{11}) circulating in the Fermilab Antiproton Accumulator ring and an internal hydrogen gas-jet target of $0.8\ cm$ thickness. The intensity of the jet was adjusted to compensate for the beam loss (beam lifetime $\sim$ 90 *hours*) keeping the instantaneous luminosity to $\sim 7 \times 10^{30}\ cm^{-2} sec^{-1}$. The resonances were scanned by decelerating the $\bar{p}$ beam from the accumulation energy of 8.9 GeV to an energy just above the resonance, and then taking data in steps of 200 to 500 keV (center-of-mass energy) depending on the resonance. The beam was stochastically cooled to $(\Delta p/p)_{rms} \approx 2 \times 10^{-4}$, corresponding to a spread in the center-of-mass energy of 250–350 keV. Data were collected up to an integrated luminosity of $\sim 1.3\ pb^{-1}$ for every beam fill (stack). In the case of a resonance with very small expected cross section (like the $^1P_1$) a whole stack was taken for each energy point.

2 – The E760 detector

The E760 detector [4], shown in fig.1, was a non-magnetic, large acceptance, cylindrical spectrometer, covering the complete azimuth (ϕ) and from 2° to 70° in polar angle (θ). It consisted of a set of proportional and drift chambers, which identified and measured the direction of charged tracks, and two electromagnetic calorimeters, which measured the energies and directions of electrons and photons. It also included, three scintillation-counter hodoscopes for triggering and a multicell threshold Čerenkov counter for electron identification.

The Central CALorimeter (CCAL) consisted of 1280 lead-glass blocks arranged in 64 wedges and 20 rings. Its energy resolution was $\sigma_E/E = 6\%/\sqrt{E(GeV)} + 1\%$ and its position resolution $\sigma_\theta \approx 6\ mrad$ and $\sigma_\phi \approx 12\ mrad$. The position resolution from the tracking was $\sigma_\theta \approx 4\ mrad$ and $\sigma_\phi \approx 7\ mrad$.

Fig.1 also shows the acceptance of the detector for single photons (vertically hatched area), single electrons (horizontally hatched area) and two photons (shaded area) as a function of the production angle and the energy in the center-of-mass. The photon and electron coverage differ due to the aperture of the Čerenkov counter.

In addition to the large acceptance, the detector had a very good separation

of electrons from hadrons. The probability for a hadron to be interpreted as an electron was less than 5×10^{-4}. The CCAL could distinguish between the photons of charmonium decays and those from symmetric as well as highly asymmetric decays of π^0s and ηs due to its granularity and ability to measure photons with energy as low as 20 MeV.

The integrated luminosity for each energy setting was obtained by counting the number of recoil protons from $\bar{p}p$ elastic scattering in a silicon detector located at $\theta = 86.5^o$ from the beam direction. The error in the luminosity measurement was due to the error in the fit to the measured $\bar{p}p$ total cross section and the uncertainty in the detector solid angle. It was estimated to be about $\pm 4\%$.

3 – Event selection

The experimental trigger [5] was designed to select events in which a high mass state decays to an e^+e^- or $\gamma\gamma$ pair. This was implemented by requiring two electron "tracks" as defined by the hodoscopes, the Čerenkov counters and two high-energy clusters in the CCAL for the "charged" trigger, or two high-energy clusters in the CCAL and nothing in the hodoscopes for the "neutral" trigger.

For resonances decaying to $J/\psi + X$, with the J/ψ decaying into e^+e^-, the event selection was based on the discrimination of isolated electron tracks from electron pairs using the pulse height information from the hodoscope and the Čerenkov counter, the dE/dx information from the radial projection chamber, and the transverse shape of the energy deposition in the CCAL. For resonances decaying to $\gamma\gamma$, neutral events with any pair of CCAL clusters having an invariant mass $m_{\gamma\gamma} \geq 2.5\ GeV/c^2$ were selected. Events with more than two clusters were rejected if the invariant mass of any pair of one of the 2 most energetic clusters with any other cluster was in the π^0 (80–200 MeV/c^2) or the η (410–690 MeV/c^2) mass window.

4 – Results

E760 collected data for an integrated luminosity of $\sim 30\ pb^{-1}$ during the 1990-91 Fermilab Fixed Target Run. During this period the experiment took data at the $J/\psi(1^3S_1)$, $\psi'(2^3S_1)$, $\chi_1(^3P_1)$, $\chi_2(^3P_2)$ and $\eta_c(1^1S_0)$ resonances. It also searched for the $h_c(^1P_1)$ and the $\eta_c'(2^1S_0)$ resonances.

4.1 1^3S_1 and 2^3S_1 States

The study of the 1^3S_1 (J/ψ) and 2^3S_1 (ψ') states was done using antiprotons from single stack. The resonance parameters (shown in tab.1) were extracted by fitting the excitation curve to a convolution of the Breit-Wigner cross section, with the energy

Table 1: J/ψ and ψ' resonance masses, widths and branching ratios.

Parameters	J/ψ	ψ'
$M_R\,(MeV/c^2)$	$3096.87 \pm .03 \pm .03$	*input*
$\Gamma_R\,(keV)$	$99 \pm 12 \pm 6$	$306 \pm 36 \pm 16$
$B_{in}B^a_{out}$	$(1.14^{+.16}_{-.12} \pm .10) \times 10^{-4}$	$(1.17^{+.14}_{-.12} \pm .08) \times 10^{-5}$
$B(R \to \bar{p}p)^b$	$(1.82^{+.26}_{-.19} \pm .16) \times 10^{-3}$	$(2.61^{+.31}_{-.27} \pm .17) \times 10^{-4}$

Table 2: χ_1 and χ_2 resonance masses, widths and branching ratios.

Parameters	χ_1	χ_2
$M_R\,(MeV/c^2)$	$3510.53 \pm .04 \pm .12$	$3556.15 \pm .07 \pm .12$
$\Gamma_R\,(MeV)$	$0.88 \pm .11 \pm .08$	$1.98 \pm .17 \pm .07$
$\Gamma_{R\to\bar{p}p}B_{R\to J/\psi\gamma}B_{J/\psi\to e^+e^-}\,(eV)$	$1.29 \pm .09 \pm .13$	$1.67 \pm .09 \pm .12$
$\Gamma(R \to \bar{p}p)^b\,(eV)$	$69 \pm 9 \pm 10$	$180 \pm 16 \pm 26$
$B(R \to \bar{p}p)^b$	$(0.78 \pm .15) \times 10^{-4}$	$(0.91 \pm .15) \times 10^{-4}$

[a] $B(J/\psi \to \bar{p}p)B(J/\psi \to e^+e^-)$ for J/ψ and $B(\psi' \to \bar{p}p)B(\psi' \to e^+e^-)$ for ψ'.
The errors, in the order shown, are statistical and systematic.

[b] Using $B(J/\psi \to e^+e^-)$, $B(\psi' \to e^+e^-)$, $B(\psi' \to J/\psi + X)$ from PDG.

distribution function of the beam. For resonances such as the J/ψ and ψ', whose widths are smaller than the width of the center-of-mass energy distribution, the double scan method [6] was used to determine the beam energy profile. The widths of these resonances were measured, for the first time, directly from an analysis of the line shape. The mass of the ψ' was used as an input in the energy calibration of the Accumulator. Fig.2 shows a comparison of the J/ψ mass and width and the ψ' width as measured by E760 and by other experiments reported in the Review of Particle Properties of the Particle Data Group [7] .

4.2 $^3P_1$ and $^3P_2$ States

E760 studied [4] the χ_1 and χ_2 of the triplet P states in a way similar to the one used in the study of the ψ and ψ' resonances. For each state, a scan across the resonance was performed and the events were selected according to the reaction:

$$\bar{p}p \to \chi_{1,2} \to J/\psi + \gamma \to (e^+e^-)\gamma\,. \qquad (1)$$

A fit to the excitation curves results in the values of the resonance parameters shown in tab.2. A comparison of the E760 results for the mass and width of χ_1 and χ_2 with the results of other experiments is shown in fig.3 and fig.4.

In addition to the mass and total width of the χ_2, the decay rate for $\chi_2 \to \gamma\gamma$ was also measured [8]. The yield of $\bar{p}p \to \gamma\gamma$ events collected in the range

$3520 < E_{cm} < 3690\ MeV$ is shown in fig.5. A 4σ excess over the background is evident at $3556\ MeV$, the energy formation for the χ_2. A fit of these events to a Breit-Wigner with fixed mass and width results in the product of branching ratios $B(\chi_2 \to \bar{p}p) \times B(\chi_2 \to \gamma\gamma) = (1.60 \pm .39 \pm .16) \times 10^{-8}$. Using the values for Γ_{χ_2} and $B(\chi_2 \to \bar{p}p)$ measured by E760, we obtain $B(\chi_2 \to \gamma\gamma) = (1.60 \pm 0.39 \pm 0.23) \times 10^{-4}$ and $\Gamma(\chi_2 \to \gamma\gamma) = 321 \pm 78 \pm 54\ eV$. A comparison of the E760 results with other experiments is shown in fig.6. The dashed [9] and dotted [10] lines are the theoretical predictions of pQCD.

4.3 $^1P_1$ State

One of the primary goals of E760 was to find the missing singlet P state of the charmonium (h_c) and measure its mass and total width. We searched the area around the center-of-gravity mass (m_{cog}) of the three ^3P states by focusing on the decays:

$$\bar{p}p \to h_c \to \eta_c + \gamma \to (\gamma\gamma) + \gamma, \tag{2}$$

$$\bar{p}p \to h_c \to \psi + \pi^0 \to (e^+e^-) + (\gamma\gamma), \tag{3}$$

$$\bar{p}p \to h_c \to \psi + 2\pi \to (e^+e^-) + 2\pi. \tag{4}$$

Fig.7 shows an example of our sensitivity to final states that contain high mass e^+e^- pairs. In fig.7a, the invariant mass m_{ee} is plotted for events at the ψ' formation energy. The large peak at lower masses arises from the decay $\psi' \to \psi + X \to (e^+e^-) + X$, while the small peak is due to the exclusive decay $\psi' \to e^+e^-$. The shaded area represents the residual background estimated by normalizing to equal luminosity events taken outside the ψ' resonance region. In fig.7b, m_{ee} is plotted for events taken during the h_c search. These events were fitted to the reactions $\bar{p}p \to J/\psi + \pi^0$, $\bar{p}p \to J/\psi + 2\pi$, $\bar{p}p \to J/\psi + \gamma$ and $\bar{p}p \to e^+e^-$ whenever the event topology was compatible with the final state hypothesis. Most of the events could be unambiguously defined as either $J/\psi + \gamma$ (cross hatched area) or $J/\psi + \pi^0$ (shaded area). No events were found that could fit the final state $J/\psi + 2\pi$. The $J/\psi + \gamma$ events can be explained as background from the tails of the nearby χ_1 and χ_2 resonances. A few events were identified as $\bar{p}p \to e^+e^-$ (vertically striped area) and can be attributed to the continuum [11]. The cross section as a function of center-of-mass energy for the $J/\psi + \pi^0$ events is shown in fig.8. The data are binned in intervals of $150\ keV$ and clearly show an enhancement around $3526\ MeV$ atop a $\sim 2\ pb$ continuum background. The probability that this structure arose from a statistical fluctuation is less than 1 in 400. This structure has been attributed to the h_c resonance [12] and it was fitted to a mass of $3526.2 \pm 0.15 \pm 0.20\ MeV/c^2$. The upper limit to the width is $\Gamma < 1.1\ MeV$ at the 90% confidence level. The branching

ratio product $B(h_c \to \bar{p}p) \times B(h_c \to J/\psi\pi^0)$ can range from $(1.7 \pm 0.4) \times 10^{-7}$ to $(2.3 \pm 0.6) \times 10^{-7}$. No structure was observed in the reaction (2).

4.4 1^1S_0 State

The 1^1S_0 state (η_c) was observed [13] in the reaction:

$$\bar{p}p \to \eta_c \to \gamma\gamma \tag{5}$$

The cross section for this process is shown in fig.9 as a function of the center-of-mass energy. The events were selected for $|\cos\theta^*_\gamma| \leq 0.25$ to optimize the signal-to-background ratio. The data were fitted with the maximum likelihood method to a Breit-Wigner shape plus a power law background of the form $\sigma_{back} = A \times (2988/E_{cm})^B$. This background is due to misidentified $\pi^0\pi^0$ and $\pi^0\gamma$ events. The values for the resonance parameters that resulted from the fit are $M_{\eta_c} = 2987.5 \pm 2.9\ MeV/c^2$, total width $\Gamma = 23.7^{+11.1}_{-7.0}\ MeV$ and $B(\eta_c \to \gamma\gamma) \times B(\eta_c \to \bar{p}p) = (35.4 \pm 7.6) \times 10^{-8}$. Using the PDG value for $B(\eta_c \to \bar{p}p)$ we obtain $B(\eta_c \to \gamma\gamma) = (3.0 \pm 0.7 \pm 1.0) \times 10^{-4}$ and partial width $\Gamma(\eta_c \to \gamma\gamma) = 7.0^{+2.9}_{-2.0} \pm 2.3\,keV$. The values of the mass, total width and partial width to $\gamma\gamma$ are compared to those measured by other experiments in fig.10. The dotted lines show the theoretical QCD predictions [9] for $\alpha_s = 0.276$.

To understand the background to $\gamma\gamma$, E760 has studied the exclusive $\pi^0\pi^0$ and $\pi^0\gamma$ productions in $\bar{p}p$ annihilations [14]. The feed-down background to $\gamma\gamma$ was calculated by using these cross sections in a Monte Carlo simulation of the detector. The angular distributions for $\gamma\gamma$ are shown in fig.11 for three energies 2.95, 2.99 and 3.1 GeV. The background predictions (dashed lines) are very close to the measured $\gamma\gamma$ distributions. The difference at 2.99 GeV is attributed to the η_c resonance. A comparison between the measured cross sections for $|\cos\theta^*_\gamma| < 0.4$ (filled circles) and the feed-down background (open circles) is shown in fig.12; the data points around the η_c resonance have been suppressed. The dashed line represents a fit of the feed-down cross section to a power law:

$$\sigma_{back} = A \times (\sqrt{s_0}/\sqrt{s})^B. \tag{6}$$

The energy dependence of the non-resonant $\gamma\gamma$ cross section was also parametrized with a power law:

$$\sigma_{\bar{p}p \to \gamma\gamma} = C \times (\sqrt{s_0}/\sqrt{s})^D. \tag{7}$$

A maximum likelihood fit of the data to the superposition of σ_{back} and $\sigma_{\bar{p}p \to \gamma\gamma}$ for $\sqrt{s_0} = 2.988\ GeV$ and various values of exponent D (0 to 10) resulted in an upper limit (90% C.L.) for C ranging from 32 to 43 pb. This is in disagreement with the

result obtained from the CLEO Collaboration [15] for the reaction $\gamma\gamma \to \bar{p}p$. By averaging their data from 2.8 to 3.2 GeV, using their angular distribution to scale down to $|\cos\theta^*| < 0.4$ and applying detailed balance, we estimated the cross section to be about $100pb$, which is 2–3 times our upper limit. Recently, T. Hyer [16] has given an estimate for the ratio $\sigma_{\bar{p}p\to\gamma\gamma}/\sigma_{\bar{p}p\to ee}$, claiming that the prediction for the ratio is less affected by theoretical uncertainties than the predictions for the two separate cross sections. Using the predicted ratio and our measurement [11] for $\sigma_{\bar{p}p\to ee}$, we find $\sigma_{\bar{p}p\to\gamma\gamma}$ to be $5 - 17\ pb$, in very good agreement with our upper limit.

4.5 2^1S_0 State

The 2^1S_0 state (η_c') was observed by the Crystal Ball experiment [17] in 1982. They saw a structure in the inclusive γ spectrum from the ψ' decay which corresponded to a mass of $3594 \pm 5\ MeV/c^2$. Since then, no other experiment has confirmed the η_c'. E760 took data in the energy region where Crystal Ball observed the η_c', but as it is shown in fig.13, no evidence of a signal was seen. The open circles show the Monte Carlo predictions of the feed-down background from $\pi^0\pi^0$ and $\pi^0\gamma$ events; the dotted line is a power law fit of this background.

Since no signal was observed, the data were fitted with a maximum likelihood and upper limits (90% C.L.) for the product of the branching ratios, $B(\eta_c' \to \bar{p}p) \times B(\eta_c' \to \gamma\gamma)$, as a function of the center-of-mass energy and the total width of the resonance. The results are shown in fig.14 for three values of the total width 5, 10 and $15\,MeV$. Assuming that $R_{\eta_c'}/R_{\eta_c} = R_{\psi'}/R_{J/\psi}$, where $R_{\bar{c}c} = \Gamma(\bar{c}c \to \bar{p}p)/\Gamma(\bar{c}c \to gluons)$ and assuming that $B(\eta_c' \to \gamma\gamma) \approx B(\eta_c \to \gamma\gamma)$, then the product of the branching ratios is estimated to be $B(\eta_c' \to \bar{p}p) \times B(\eta_c' \to \gamma\gamma) = (20^{+16}_{-12}) \times 10^{-8}$. This should be compared to our upper limit of 3.4×10^{-8} at $\sqrt{s} = 3594\ MeV$, for $\Gamma = 5\ MeV$. Given the uncertainty of this estimate we cannot claim any compeling evidence against the Crystal Ball measurement.

5 – Experiment E835

Experiment E835 [18] is the approved successor of E760. It was proposed to continue the successful study of the charmonium in the $\bar{p}p$ annihilations that E760 started a few years ago. Its primary goals are to do a precise measurement of the h_c and η_c resonance parameters; to search for the η_c' and measure its mass and width; to precisely measure the mass and total width of the χ_0 and the products of the branching ratios $B(\chi_0 \to \bar{p}p) \times B(\chi_0 \to \gamma\gamma)$ and $B(\chi_0 \to \bar{p}p) \times B(\chi_0 \to J/\psi\gamma)$; and search for the spin 2 charmonium D states.

To perform its ambitious program, E835 will take advantage of the recent

upgrades in the Fermilab Antiproton Accumulator which will triple the $\bar{p}$ beam current. The hydrogen gas jet target has also been upgraded to increase the density by a factor of 3–5. These upgrades will increase the instantaneous luminosity to $\sim 7 \times 10^{31}\ cm^{-2}s^{-1}$ and result in a total integrated luminosity of at least $200\ pb^{-1}$ during the next fixed target period. To handle the higher interaction rate, upgrades in the E760 detector and data acquisition are necessary. The inner tracking will be replaced by 2 double layers of straw tubes, a Silicon barrel detector of high segmentation and a Scintillating Fiber tracker. This upgrade will allow E835 to also study the decay $\eta_c \rightarrow \phi\phi$. The read-out of the central and forward calorimeters will also be upgraded and time information will be recorded for every pulse. The event building, filtering and logging will be Unix based with a sustained throughput rate of about $10\ MB/s$.

Acknowledgements

I wish to thank the U.S. Department of Energy for supporting my participation in the 2nd International Workshop on Heavy Quark Physics. I wish to thank the organizers of the workshop for making this enlightened environment possible. I also wish to thank the other members of the E760 collaboration whose hard work made this presentation possible.

E760's research was supported by the U.S. Department of Energy, the U.S. National Science Foundation, and the Instituto Nazionale di Fisica Nucleare of Italy.

References

1. V. Bharadwaj, M. Church, A. Hahn, S. Hsueh, W. Marsh, J. Peoples Jr., S. Pordes, P.A. Rapidis, R. Ray, S. Werkema (*Fermi National Accelerator Laboratory*), D. Bettoni, G. Borreani, R. Calabrese, P. Dalpiaz, P.F. Dalpiaz, M. Fabbri, A. Gianoli, E. Luppi, M. Martini, F. Petrucci, M. Savrié (*I.N.F.N. and University of Ferrara*), A. Buzzo, M. Macrí, M. Marinelli, M. Pallavicini, C. Patrignani, M.G. Pia, A. Santroni, A. Scalisi (*I.N.F.N. and University of Genoa*), D. Broemmelsiek, J. Fast, K. Gollwitzer, M. Mandelkern, J. Marques, J. Schultz, A. Smith, M.F. Weber, G. Zioulas (*University of California at Irvine*), D. Dimitroyannis, C.M. Ginsburg, M. Masuzawa, J. Rosen, M. Sarmiento, K.K. Seth, S. Trokenheim, J. Zhao (*Northwestern University*), T.A. Armstrong, M.A. Hasan, R. Lewis, A.M. Majewska, J. Reid, G.A. Smith, Y. Zhang (*Pennsylvania State University*), C. Biino, A. Ceccucci, R. Cester, R. Dibenedetto, F. Marchetto, E. Menichetti, A. Migliori, R. Mussa, S. Palestini, N. Pastrone, L. Pesando, G. Rinaudo, B. Roccuzzo, M. Sozzi (*I.N.F.N. and University of*

Turin).

2. C. Baglin et al., CERN Proposal CERN/ISRC/80-14, unpublished (1980).
3. V. Bharadwaj et al., Fermilab Proposal P760, unpublished (1985).
4. T.A. Armstrong et al., Nucl. Phys. **B373**, 35 (1992).
5. R. Ray et al., NIM **A307**, 254 (1991).
6. T.A. Armstrong et al., Phys. Rev. D **47**, 772 (1993).
7. K. Hikasa et al. (Particle Data Group), Phys. Rev. D **45** (1992).
8. T.A. Armstrong et al., Phys. Rev. Lett. **70**, 2988 (1993).
9. W. Kwong et al., Phys. Rev. D **37**, 3210 (1988).
10. T. Barnes, in: Proc. of the IXth International Workshop on Photon-Photon Collisions (eds. D.O Caldwell and H.P. Paar, La-Jolla, 22–26 March 1992), 263 (World Scientific, 1992).
11. T.A. Armstrong et al., Phys. Rev. Lett. **70**, 1212 (1993).
12. T.A. Armstrong et al., Phys. Rev. Lett. **69**, 2337 (1992).
13. T.A. Armstrong et al., Study of the η_c State of Charmonium Formed in $\bar{p}p$ Annihilations and a Search for the η_c', to be submitted to Phys. Rev. D.
14. T.A. Armstrong et al., Meson-Meson and Meson-Photon productions in $\bar{p}p$ Annihilations, to be submitted to Phys. Rev. D.
15. M. Artuso et al., Phys. Rev. D **50**, 5484 (1994).
16. T. Hyer, Phys. Rev. D **47**, 3875 (1993).
17. C. Edwards et al., Phys. Rev. Lett. **48**, 70 (1982).
18. T.A. Armstrong et al., Fermilab Proposal P835(revised), unpublished (1992).

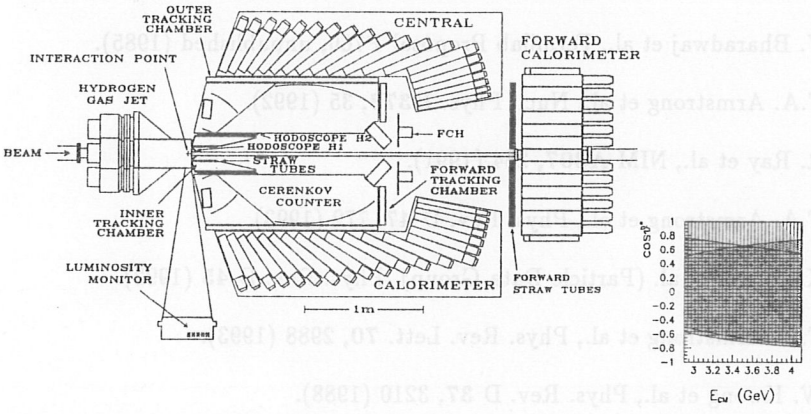

Figure 1: The E760 detector and its acceptance coverage in $\cos\theta^*$ versus the energy in the center-of-mass for single photons (vertically hatched area), single electrons (horizontally hatched area) and two photons (shaded area).

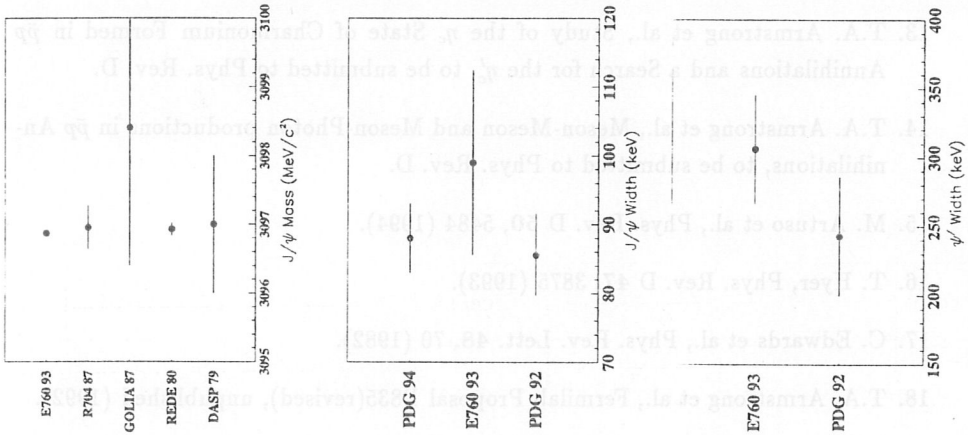

Figure 2: Comparison of the mass and width of J/ψ and the width of ψ' for various experiments and the PDG value.

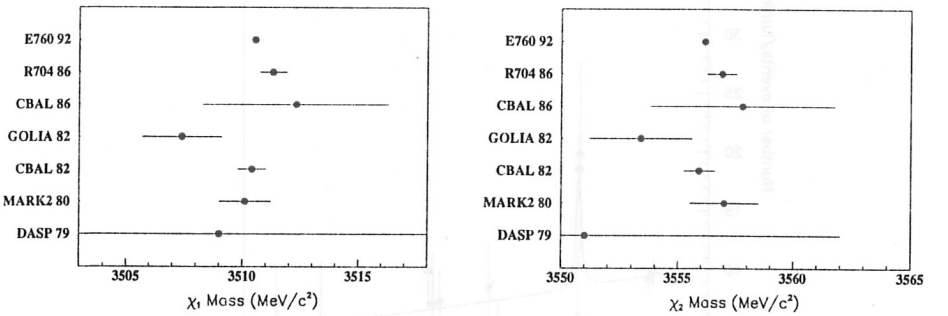

Figure 3: Comparison of the χ_1 and χ_2 masses as measured by E760 and by other experiments.

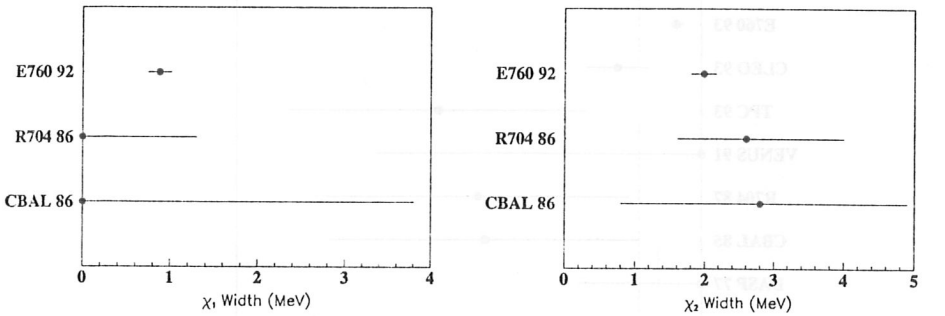

Figure 4: Comparison of the χ_{c1} and χ_{c2} widths as measured by E760 and by other experiments.

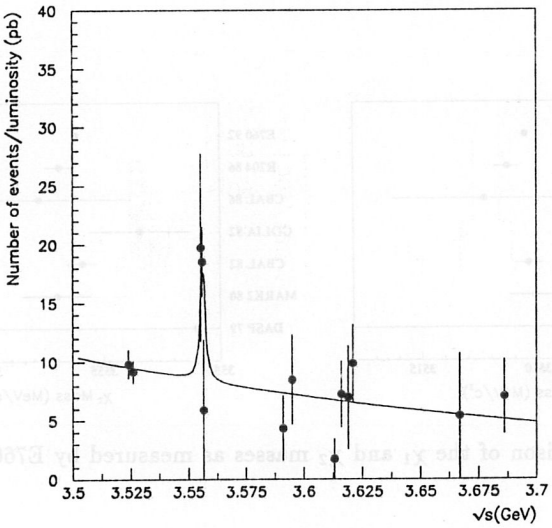

Figure 5: Measured cross section for $\bar{p}p \to \gamma\gamma$ vs center-of-mass energy. The events were selected for $|\cos\theta^*_\gamma| \leq 0.4$.

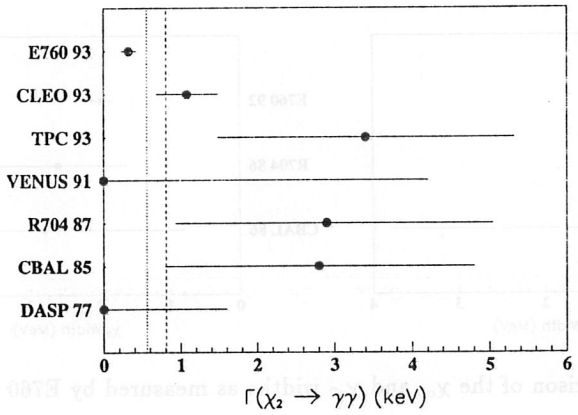

Figure 6: Comparison of the $\chi_2 \to \gamma\gamma$ partial width measured by various experiments. The dashed and dotted lines are the pQCD predictions.

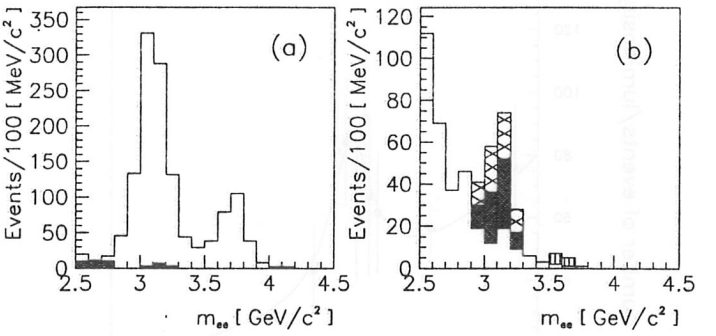

Figure 7: Invariant mass distribution of e^+e^- pairs for events (a) taken at the ψ' ($\int L \approx 1\text{pb}^{-1}$) and (b) taken near the χ_{cog} ($\int L \approx 16\text{pb}^{-1}$).

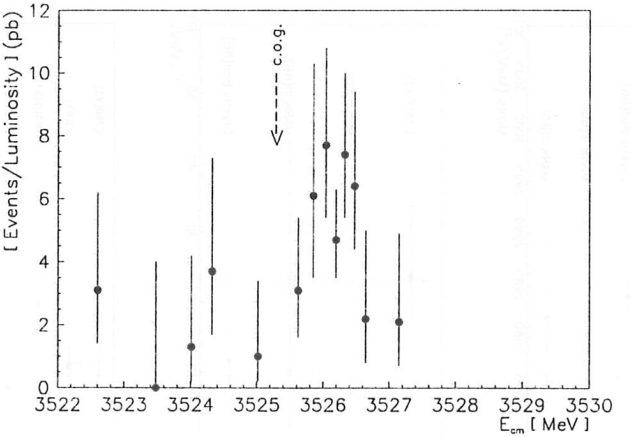

Figure 8: ${}^1P_1$ excitation curve. The number of events per integrated luminosity is plotted in 150 keV bins of the center-of-mass energy.

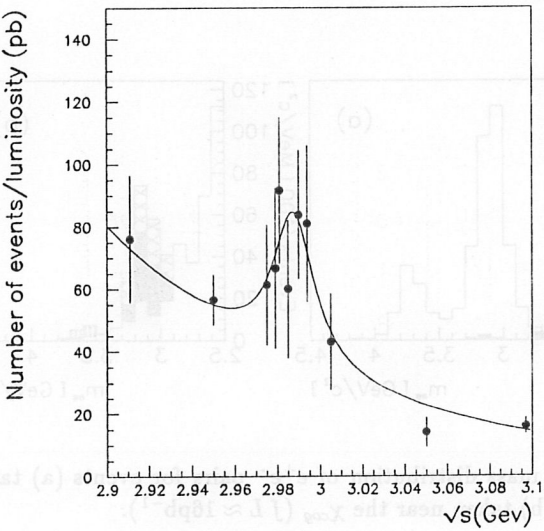

Figure 9: Measured cross section for $\bar{p}p \to \gamma\gamma$ vs center-of-mass energy at η_c. The events were selected for $|\cos\theta^*_\gamma| \leq 0.25$.

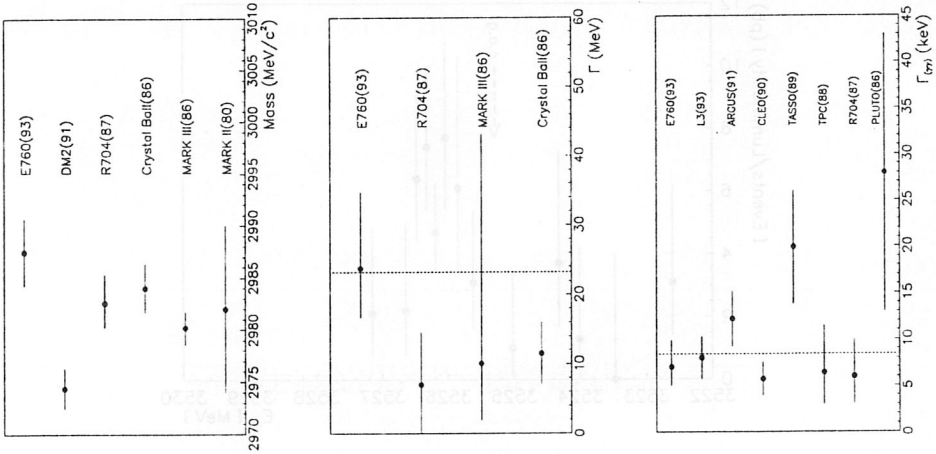

Figure 10: Comparison of the mass, width and partial width to $\gamma\gamma$ of η_c for various experiments. The dotted lines show the theoretical predictions of QCD for $\alpha_s = 0.276$.

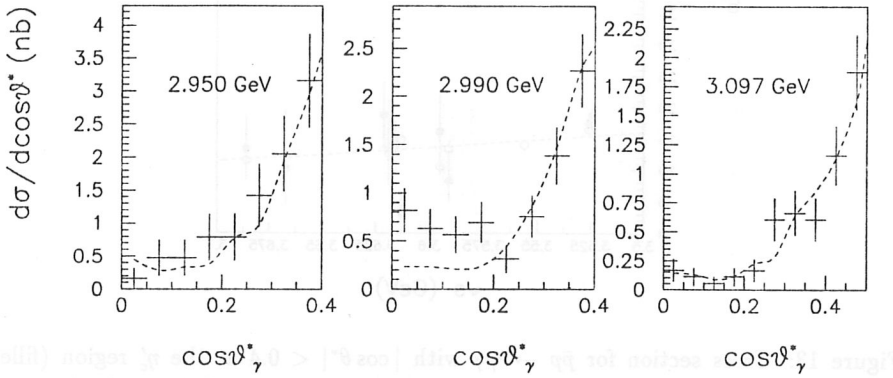

Figure 11: Differential cross section for $\bar{p}p \to \gamma\gamma$. The dashed lines are the Monte Carlo predictions of the $\gamma\gamma$ background from $\pi^0\pi^0$ and $\pi^0\gamma$ events.

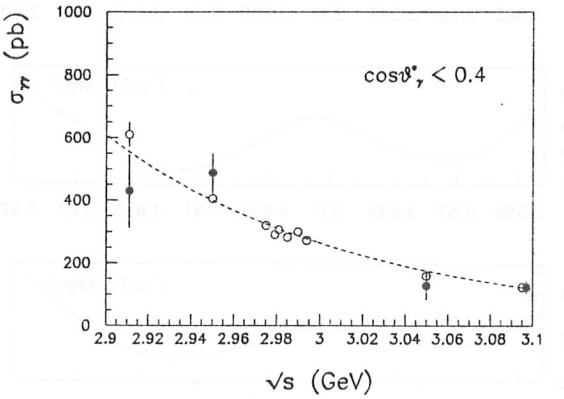

Figure 12: Cross section for $\bar{p}p \to \gamma\gamma$ with $|\cos\theta^*| < 0.4$ at the η_c region (filled circles). The open circles show the Monte Carlo prediction of the $\gamma\gamma$ background from $\pi^0\pi^0$ and $\pi^0\gamma$ events.

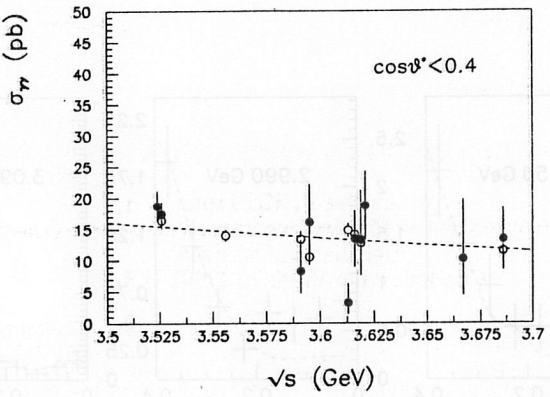

Figure 13: Cross section for $\bar{p}p \to \gamma\gamma$ with $|\cos\theta^*| < 0.4$ at the η_c' region (filled circles). The open circles show the Monte Carlo prediction of the $\gamma\gamma$ background from $\pi^0\pi^0$ and $\pi^0\gamma$ events.

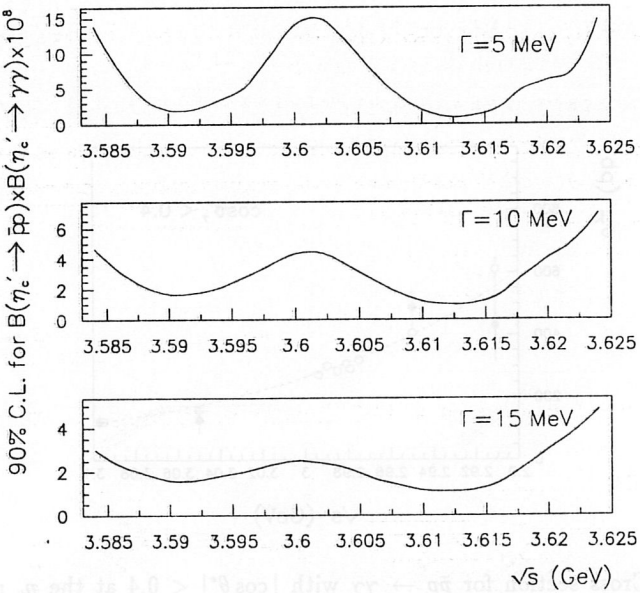

Figure 14: Upper limits on the product $B(\eta_c' \to \bar{p}p) \times B(\eta_c' \to \gamma\gamma) \times 10^8$.

Frascati Physics Series, Vol. III (1994)
HEAVY QUARKS AT FIXED TARGET
University of Virginia, October 7–10, 1994
(pp. 39–52)

RESULTS ON CHARMONIUM PRODUCTION AT HIGH ENERGY

Arthur P. McManus
Physics Department
University of Virginia
Charlottesville Virginia, 22901 U.S.A.

Abstract

A review of Charmonium physics results primarily from fixed target experiments with an emphasis on new results from FNAL experiments E672/E706, E705 and E771 using published papers and other sources. The data is found to be consistent with the latest calculations of the color singlet model

1 Introduction

Since the discovery of charmonium with the J/Ψ resonance at 3.1 GeV/c^2 a number of fixed target experiments have been attempting to fit the experimental data to a model of charmonium production. With the collider experiments using the J/Ψ cross section to calculate the B cross section using J/Ψ and Ψ(2S) decays there has been considerable interest in having a definitive model of charmonium production. It has long been known[1] that J/Ψ production has large contributions from higher charmonium mass states that can decay into J/Ψ but the exact nature of the model is not well understood.

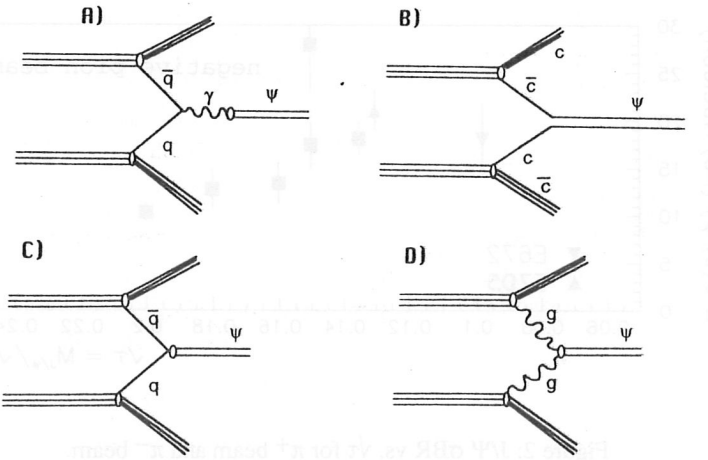

Figure 1: Early models of charmonium production.

In a short review of charmonium models[2,3] several production models can be immediately discarded by experimental evidence or the violation of conservation rules (Figure 1). A Drell Yan process (Figure 1a) can be discounted since the J/Ψ production from a π^- beam would be 4 times the production from a π^+ beam This is not the case as can be seen in Figure 2 where the production from π^- and π^+ beams are nearly identical[4,5,6]. The idea that the J/Ψ is produced via cc quarks from the sea (Figure 1b) is not viable since then charmonium would be produced in conjunction with DD pairs which is also not observed. The interaction of valance quarks and antiquarks (Figure 1c) is a possible process but can not dominate since as can be seen in Figure 3 the production of charmonium from p or p beam is nearly identical after threshold. The direct production of J/Ψ from gluons (Figure 1d) is not allowed because it violates yang's theorem and charge conjugation.

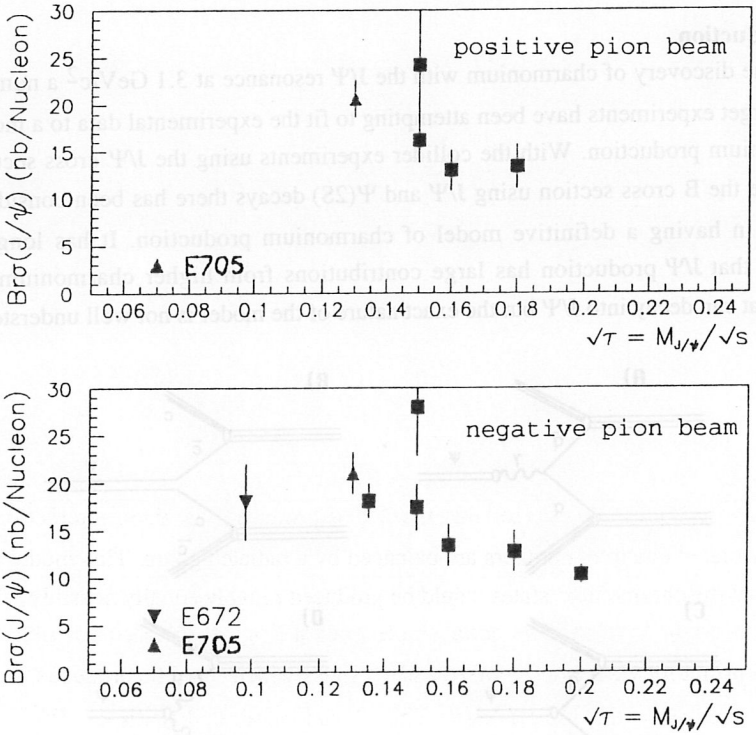

Figure 2: J/Ψ σBR vs. √τ for π^+ beam and π^- beam.

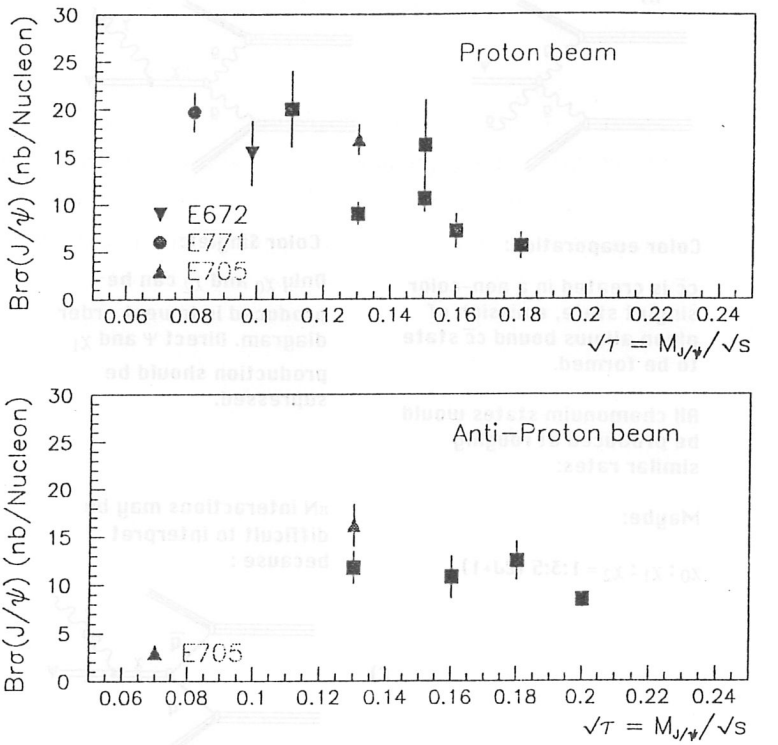

Figure 3: J/Ψ σBR vs. $\sqrt{\tau}$ for proton beam and anti-proton beam.

The production mechanisms shown in Figure 4 represent 2 possible production models with predictions that can be tested. The so-called color evaporation model as represented in Figure 4a assumes that the J/Ψ is produced via gluon interactions and that the violated quantum numbers are balanced by a radiated gluon. This model would predict that the charmonium states would be produced roughly equally possibly with the production going as 2J+1. The color singlet model (Figure 4b) assumes that J/Ψ is produced primarily via the decay of χ_0 and χ_2 states which could be produced via glue-glue interactions at the lowest level. This model predicts that direct J/Ψ and χ_1 production would be suppressed. Unfortunately since valance quark-antiquark (Figure 4c) interactions may make measurements with pion beams difficult to interpret it would be of great interest to use experiments with different beam types to separate the models.

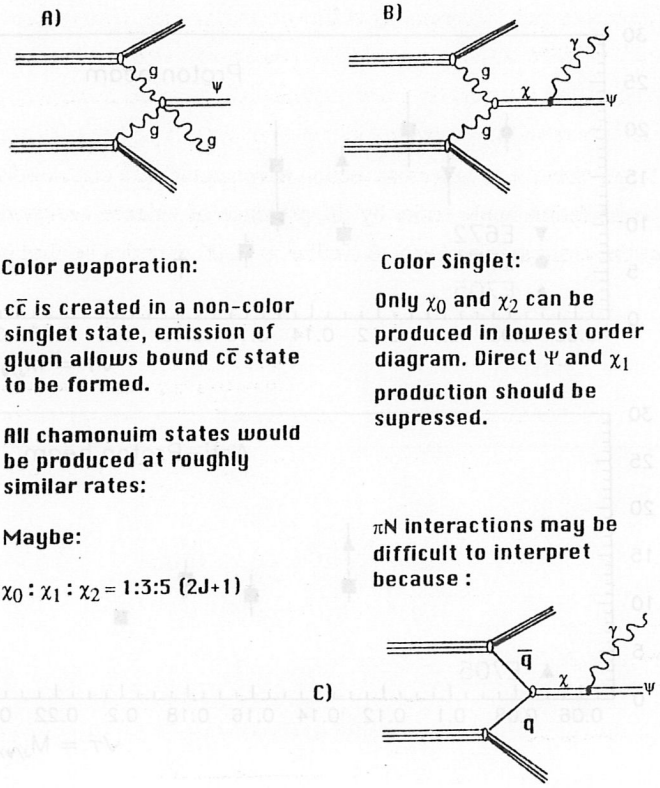

Figure 4: Feynman diagrams for gluon fusion and color singlet models.

2 J/Ψ and Ψ' Production

New preliminary results on various aspects of J/Ψ and Ψ' production have now become available from FNAL experiment E771 in the last year which in conjunction with recent results from E705 will shed some experimental light on production mechanisms. Both E705 and E771 were open geometry experiments with good muon identification performed in the high intensity laboratory at FNAL with various beam types. The E705 experiment accumulated data with proton, antiproton and $\pi^{\pm}$ beams at 300 GeV/c while E771 used a primary 800 GeV proton beam.

The wide range of beam types available to the E705 experiment allows one to look at differences in production for different beam types. Going back to the data in figures 2 and 3, well above threshold the proton and anti-proton cross sections are similar to each other but slightly lower than the $\pi^{\pm}$ cross sections which may imply a harder x_F distribution for the gluons in the pion. Near threshold the anti-proton cross section is larger than the proton cross section which could be a contribution from quark-antiquark annihilation made easier by the presence of valance antiquarks in the anti-protons but the cross section become similar at E705 energies so that is not the main process.

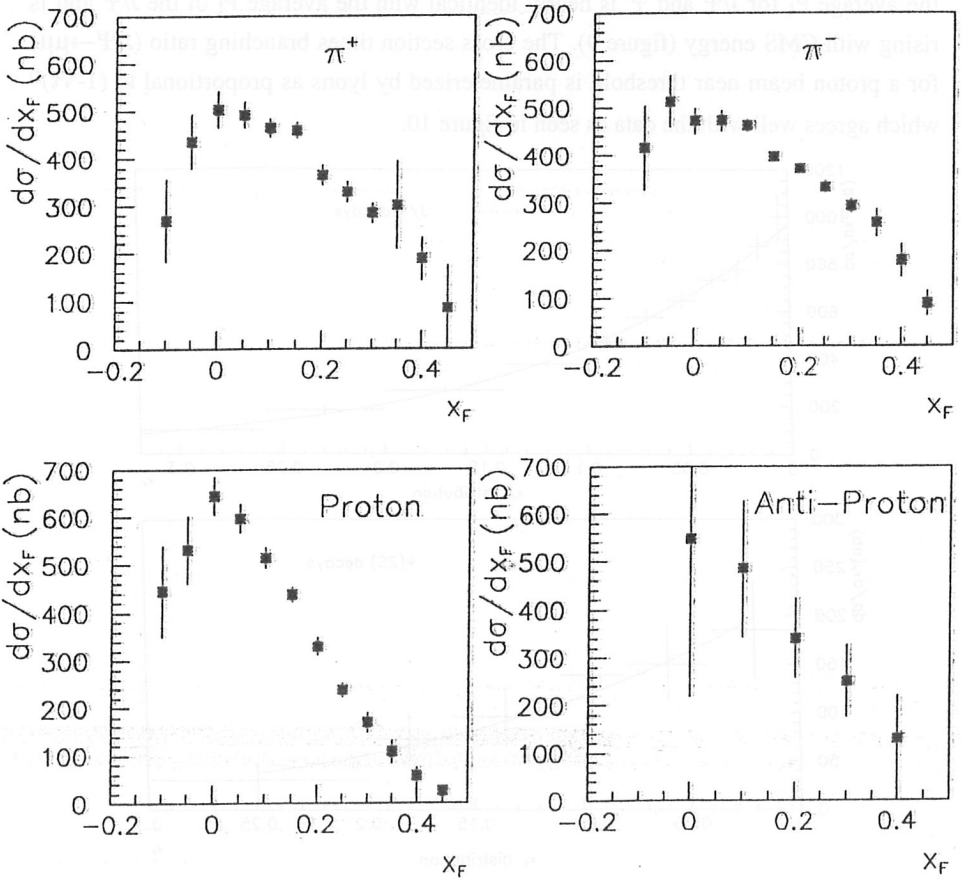

Figure 5: E705 J/Ψ x_F distributions for proton, anti-proton, and pion beams.

Both E771 and E705 reconstructed about 15,000 J/Ψ→μμ events which yields a sample of events sufficient to study the x_F and P_t distributions of the J/Ψ and Ψ' (in the case of E771). The x_F distributions for four beam types from E705 are shown in figure 5. The main difference in beam types from the E705 data is that the slope of the x_F is somewhat larger in protons which may indicate that the patron distribution function in pions are harder. The x_F distributions for J/Ψ and Ψ' from E771 are shown in figure 6 and are fit to a function of the form $(1-x_F)^c$. The distributions are not much different for J/Ψ and Ψ' which could indicate that they are produced in a similar process. The variation of x_F with respect to CMS energy as represented by the exponent c is shown in figure 7. The c exponent is getting larger (x_F getting harder) nearly linearly with increasing energy. The P_t distributions for J/Ψ and Ψ' are shown in figure 8 where again the average P_t for J/Ψ and Ψ' is nearly identical with the average P_t of the J/Ψ and is rising with CMS energy (figure 9). The cross section times branching ratio (J/Ψ→μμ) for a proton beam near threshold is parameterized by lyons as proportional to $(1-\sqrt{\tau})^n$ which agrees well with the data as seen in figure 10.

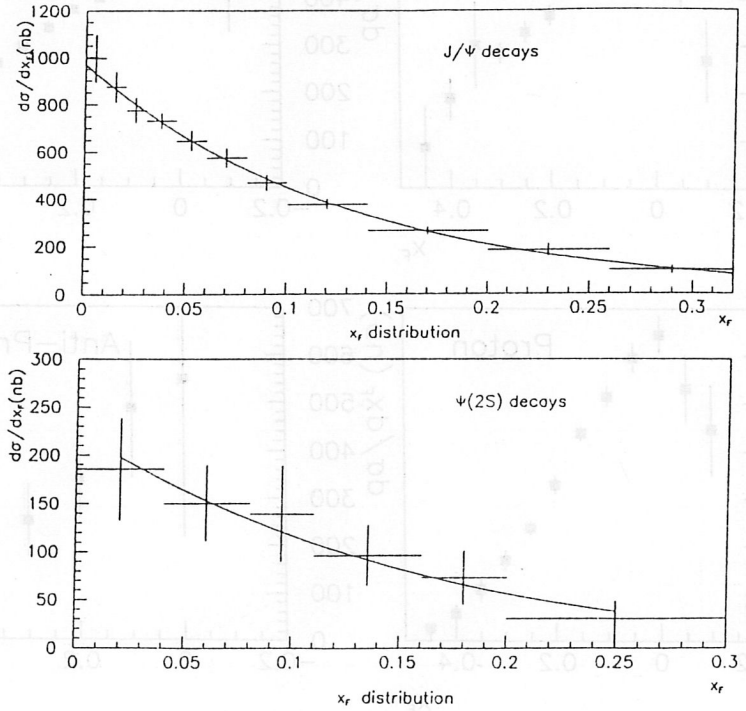

Figure 6: E771 J/Ψ and Ψ(2S) x_F distributions.

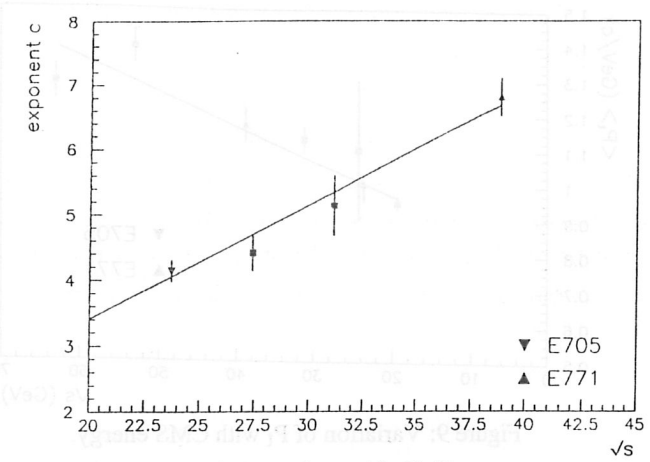

Figure 7: Variation of x_F with CMS energy.

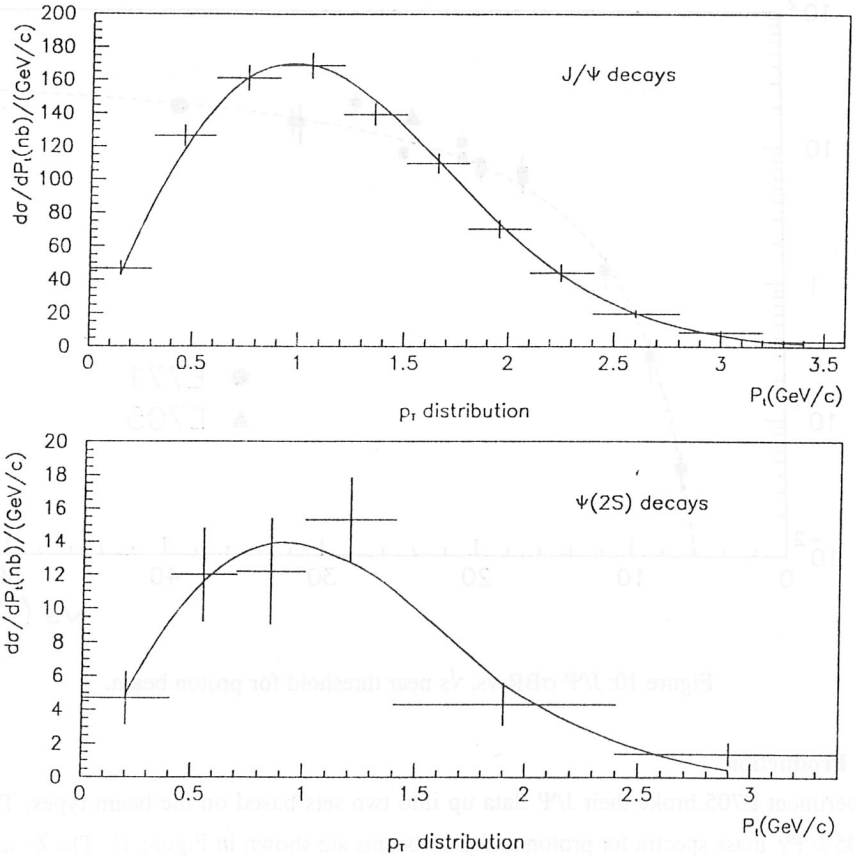

Figure 8: E771 J/Ψ and Ψ(2S) P_t distributions.

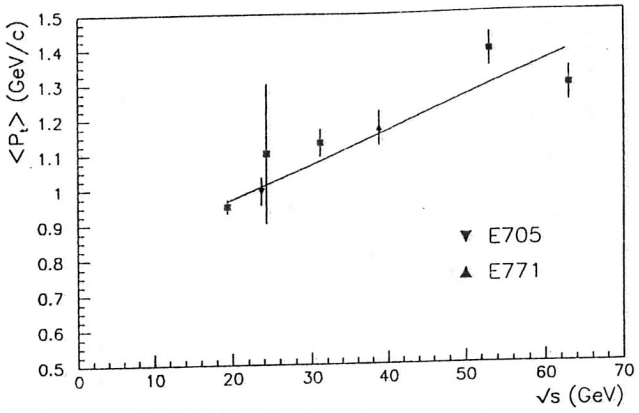

Figure 9: Variation of P_t with CMS energy.

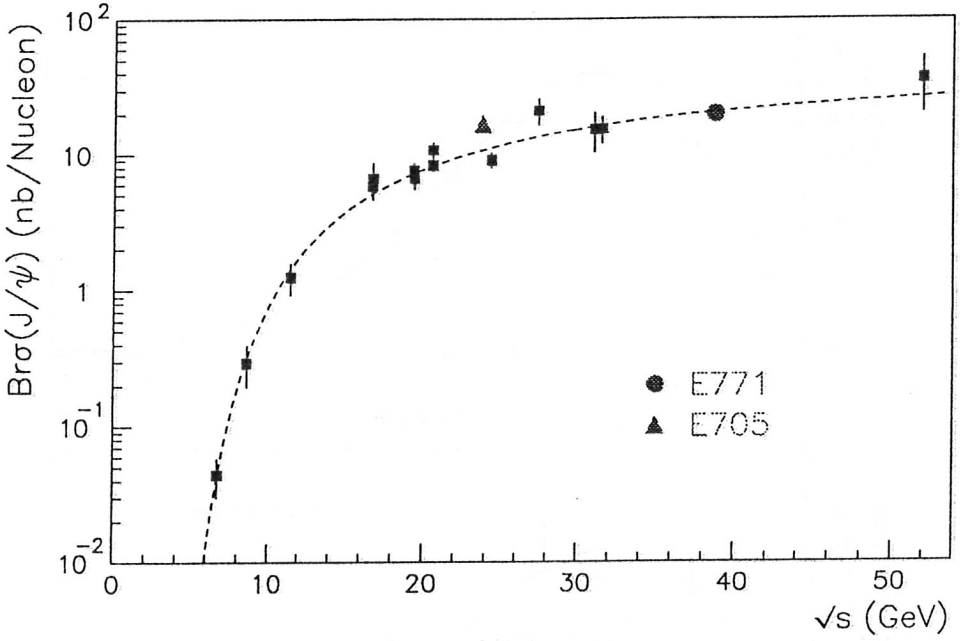

Figure 10: J/Ψ σBR vs. √s near threshold for proton beam.

3 χ Production

Experiment E705 broke their J/Ψ data up into two sets based on the beam types. The E705 J/Ψγ mass spectra for proton and pion beams are shown in Figure 11. The χ_1 and χ_2 peaks are statistically separated for the two beam types. With a pion beam the ratio

of χ_1/χ_2 (figure 12) is near 1/2 but in the proton beam sample the ratio is 0.08 which would imply that the color singlet model would be preferred since the gluon fusion model would predict the ratio to be near one for all beam types. As can be seen in Figure 12 the ratio of χ_1/χ_2 for E705 and E672[7] for pion beams agree very well.

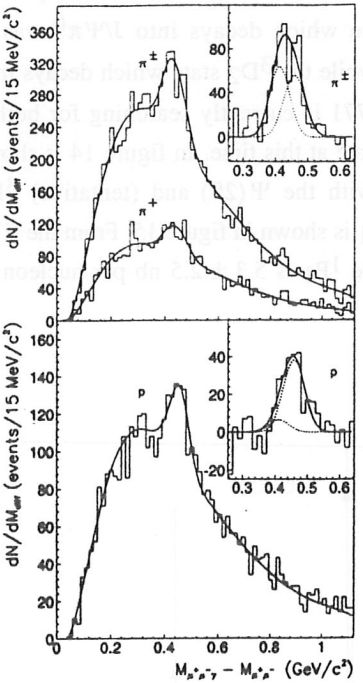

Figure 11: J/Ψγ mass spectra for pion and proton beam.

For a more complete picture using data from E705, E771 and E672 for both pion and proton beams the fraction of J/Ψ from the decays of χ's and Ψ(2S) is shown in figure 13 with some theoretical predictions using one choice of structure functions from a recent paper[8] on the color singlet model (or charmonium model) . In broad details the theory and experiment seem to agree fairly well but further confirmation of the proton beam data would be of great help. One notable disagreement between this theory paper

and experiment is that the production with pion of χ'_2 is predicted to be larger than χ'_1 while experimental evidence indicates that the χ'_1 is larger.

4 New charmonium States

Experiment E705[9] found evidence for two new states of charmonium via their decay into J/Ψ plus pions. These new states were tentatively identified as the $^1P_1$ and the $^3D_2$ states. The $^1P_1$ state which decays into $J/\Psi\pi^0$ was first observed by E760 and confirmed by E705 while the $^3D_2$ state which decays into $J/\Psi\pi^+\pi^-$ was first seen by E705. Experiment E771 is currently searching for both these states but has no firm evidence for either state at this time. In figure 14 is shown the $J/\Psi(\mu^+\mu^-)\ \pi^+\pi^-$ mass spectra for E705 with the Ψ(2S) and (tentative) $^3D_2$ states visible. The E705 observation of the $^1P_1$ is shown in figure 15. From the E705 data the cross section time branching ratio for the $^1P_1$ is 5.3 ± 2.5 nb per nucleon and is 5.3 ± 1.9 ± 1.3 nb per nucleon for the $^3D_2$.

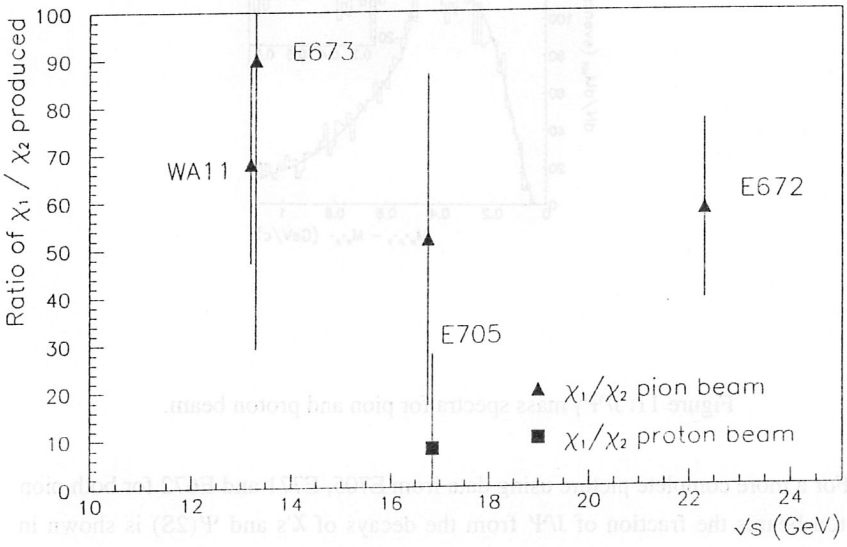

Figure 12:χ_1/χ_2 ratio vs. $\sqrt{s}$ for pion and proton beam.

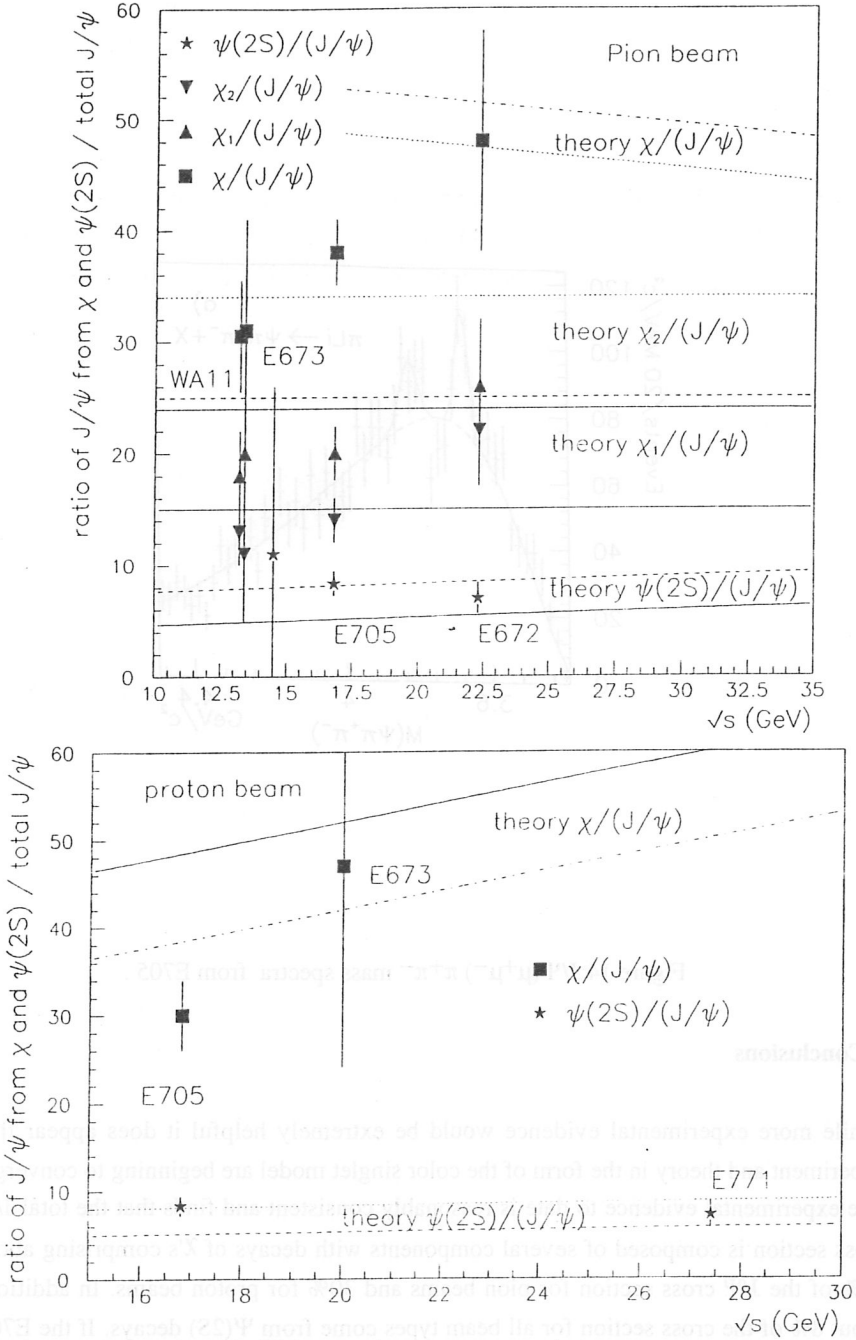

Figure 13: Fraction of J/Ψ from various sources vs. √s for pion and proton beam.

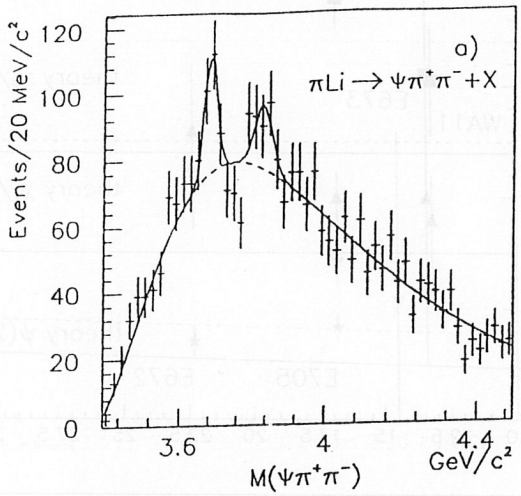

Figure 14:J/Ψ($\mu^+\mu^-$) $\pi^+\pi^-$ mass spectra from E705 .

5 Conclusions

While more experimental evidence would be extremely helpful it does appear that experiment and theory in the form of the color singlet model are beginning to converge. The experimental evidence to date is reasonably consistent and finds that the total J/Ψ cross section is composed of several components with decays of χ's comprising about 40% of the J/Ψ cross section for pion beams and 30% for proton beams. In addition, about 8% of the cross section for all beam types come from Ψ(2S) decays. If the E705 measurements of the $^1P_1$ and $^3D_2$ branching fraction times cross section into J/Ψ is

correct then each would contribute about 5% to the J/Ψ total cross section. All told the direct production of J/Ψ seems to represent only about 40% of the total for pion beams and 50% for proton beams and the story may not be complete.

E771 should is currently analyzing their J/Ψγ, J/Ψπ^0, and J/Ψ$\pi^+\pi^-$ data to measure the $^1P_1$ and $^3D_2$ branching ratio time cross section and the χ fractions for 800 GeV proton beam and may help confirm some of the E705 measurements.

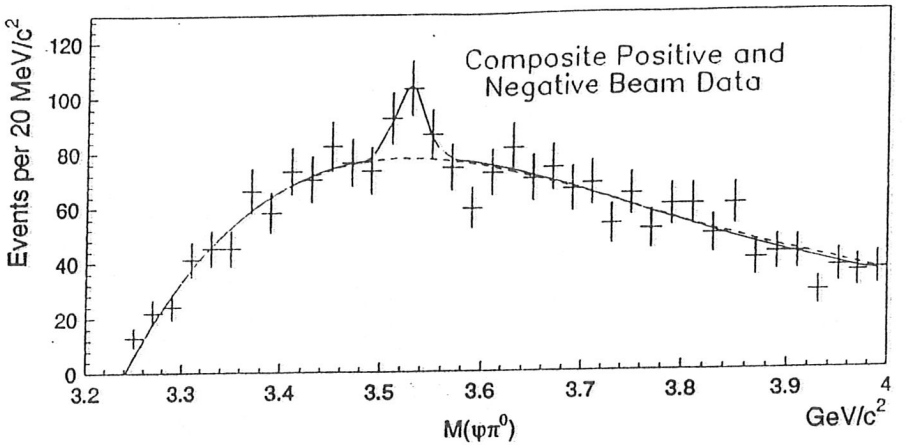

Figure 15:J/Ψπ^0 mass spectra from E705.

6 References

[1] Y. Lemoigne *et. al.* , Phys. Lett. **B113** (1982).

[2] S. Conetti, 'Recent Results on Charmonium Production at High Energy', Frascati Physics Series, Vol. 1, Heavy Quarks at Fixed Target, 19-28 (1993).

[3] S. Conetti, 'Dimuon Experiments at the Fermilab High Intensity Laboratory', Proc. of NATO Advanced Research Workshop on QCD Hard Hadronic Processes (St Croix, USVI Oct 1987), Ed B. Cox 411 (1987).

[4] V. Abramov *et. al.* , 'Properties of J/Ψ Production in π^--Be and p-Be Collisions at 530 GeV', Fermilab Pub 91/62E, March 1991.

[5] L. Antoniazzi *et. al.* , Phys. Rev. **D46**, No 11, 4828 (1992).

[6] L. Antoniazzi *et. al.* , Phys. Rev. Lett. **70**, No 4, 383 (1993) and L. Antoniazzi *et. al.* , Phys. Rev. **D49**, No 1 543 (1994).

[7] R. Jesik *et. al.* ,'Bottom and Charmonium Production in Pion-Nucleon Interactions at 515 GeV/c, 'Proceedings of DPF-94, Abequergue NM (1994).

[8] G. A. Shuler, Quarkonium Production and Decays, CERN-TH.7170/94 (1994).

[9] L. Antoniazzi *et. al.* , 'Search for Hidden Charm Resonance States Decaying into J/Ψ or Ψ' Plus Pions', accepted for publication in Phys. Rev D (1994).

[10] T. Alexopoulus *et. al.* , ' A Search for Charmonium States Decaying into J/Ψ Plus Charged Pions', Proceedings of DPF-94, Abequergue NM (1994).
[11] S.R. Hahn *et. al.* , Phys. Rev. **D30** , 671 (1984).
[12] D. A. Bauer *et. al.* , Phys Rev. Lett. **54**, 753 (1985)

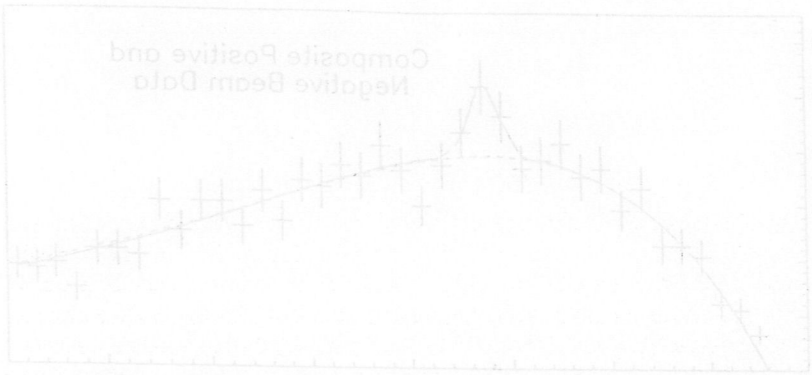

Frascati Physics Series, Vol. III (1994)
HEAVY QUARKS AT FIXED TARGET
University of Virginia, October 7–10, 1994
(pp. 53–62)

RARE CHARM DECAYS IN E789, E771, AND WA92

Kwong Lau
Physics Department, University of Houston, Houston, Texas 77204-5506

ABSTRACT

This talk reviews the current experimental status on searches for the rare charm decays $D^0 \to \mu^+\mu^-$ and $D^\pm \to \mu^+\mu^-\pi^\pm$. Experiment E789 at FNAL has recently published an upper limit of 3.1 x 10^{-5} at 90% confidence level on the branching ratio for $D^0 \to \mu^+\mu^-$ based on its 1990 commissioning run data. This limit is consistent with the Particle Data Group (PDG) limit of 1.1 $\times$ 10^{-5}, obtained by E615 at FNAL. Experiments E771 and WA92, two dedicated heavy quark fixed-target experiments at FNAL and CERN, respectively, have also searched for the decay $D^0 \to \mu^+\mu^-$ in part of their 1991-1992 data, and found no evidence for the decay. Their preliminary upper limits are comparable to the PDG limit. The limits from E771, WA92, and E789 are expected to be improved with the use of the full data and more refined analyses. Based on the same data sample, E771 has also searched and found no evidence for the decay $D^\pm \to \mu^+\mu^-\pi^\pm$, setting a preliminary upper limit of 7.6 $\times$ 10^{-4} on the branching ratio. This limit has surpassed the existing PDG limit of 2.9 $\times$ 10^{-3} by about a factor of four.

1 Introduction

The rare charm decays, $D^0 \to \mu^+\mu^-$ (1) and $D^\pm \to \mu^+\mu^-\pi^\pm$ (2), are sensitive probes to the charm sector of flavor changing neutral currents (FCNCs). Decays (1) and (2) are forbidden at the tree-level by the GIM mechanism [1] in the standard model (SM). Due to the zero spin of the D^0, the decay rate for (1) is further suppressed by angular momentum conservation. At the quark level the decay rate for (1) is given by [2]

$$\Gamma(D^0 \to \mu^+\mu^-) = \frac{G_F^2 m_c^5}{192\pi^3}(\frac{f_D}{m_D})^2(\frac{m_\mu}{m_D})^2|\sum V_{ui}V_{ci}^* C(x_i)|^2, \qquad (3)$$

where G_F is the Fermi coupling constant, f_D is the D^0 decay constant, and V is the CKM matrix. m_D, m_μ, and m_c are the D^0, muon, and charm quark masses, respectively. The function $C(x_i)$ has been evaluated by summing all contributing Feynman diagrams [3], and was found to be proportional to $x_i = (m_i/m_W)^2$; m_i is the quark mass and m_W is the mass of the charged weak boson. Several examples of the contributing Feynman diagrams are shown in Fig. 1. The sum in Eq. (3) is carried over the three down-type quarks ($i = d, s$, and b), and is dominated by contribution from the s quark. Unlike analogous FCNC decays for strange and beauty hadrons, i.e. $K_L \to \mu\mu$ and $B^0 \to \mu\mu$, which have either been observed [4] or are expected to have a branching ratio (BR) of about 10^{-9} [5], the predicted short-distance BR for (1) is extremely small, of the order of 10^{-19} [2]. Even though long-distance effects are expected to enhance the decay rate by several orders of magnitude, decay (1) has no chance of being detected in the near future unless there are other FCNC sources. The best published upper limit for (1) is 1.1 x 10^{-5} [4], obtained almost a decade ago in a fixed-target experiment at FNAL, E615. [6] As a result, there is a huge search window for new physics offered by decay (1). Most extensions of the SM possess FCNC [7]. Even though non-standard strange and beauty changing neutral currents are constrained phenomenologically by $K_L \to \mu\mu$ and the recently observed $B^0 \to \gamma K^*$ decay rates to be insignificant, the charm sector of the FCNC is still wide open.

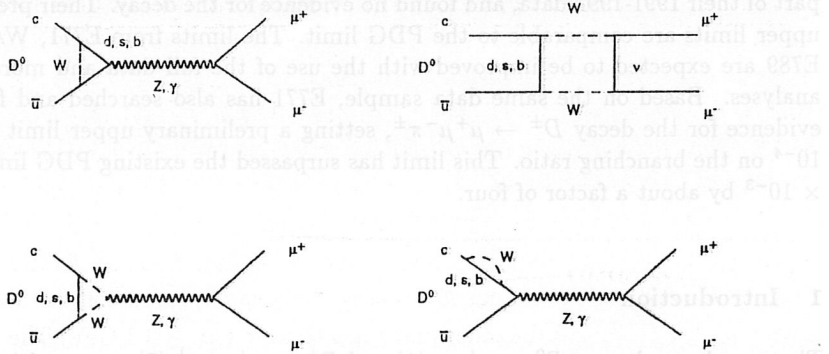

Figure 1: Feynman diagrams contributing to the decay $D^0 \to \mu^+\mu^-$.

Decay (2) is also mediated by charm-changing neutral current (CCNC). The SM prediction of the BR for (2) is considerably larger, of the order of 10^{-10}, as a result of the dominance of the photon propagator in the decay process and the absence of helicity suppression [8]. However, the final state is contaminated by radiative processes and resonance decays. The main long-distance process, $D^\pm \to$

$\phi + \pi^{\pm} \rightarrow \mu\mu\pi$, has a composite BR of 1.7 x 10^{-6}, several orders of magnitude above the non-resonant short-distance rate. A clean search for (2) has to be restricted to kinematic regions with large muon-pair mass which is far away from the ϕ mass. The present upper limit for $D^{\pm} \rightarrow \mu^+\mu^-\pi^{\pm}$ (2.9×10^{-3}) was obtained by the CLEO Collaboration in e^+e^- interactions [9].

This talk reviews the published (E789 and E615) and preliminary results from E771 and WA92 on searches for $D^0 \rightarrow \mu\mu$. Preliminary results from E771 on searches for $D \rightarrow \pi\mu\mu$ and $D \rightarrow K\mu\mu$ are also included. A more sensitive search for $D \rightarrow \pi\mu\mu$ was reported by M. Sokoloff from the FNAL experiment E791 in this workshop [10]. In section 2 the experiments are reviewed. The methods used to arrive at an upper limit for the BR are described in section 3. The results are summarized and briefly compared in section 4.

2 Experiments E771, WA92, and E789

2.1 *E771*

E771 is a fixed-target experiment at FNAL, designed primarily to study beauty hadron production in 800 GeV proton-silicon interactions by detecting J/ψs from decay of beauty hadrons. The detector is a large aperture magnetic spectrometer equipped with a 12-plane precision silicon microstrip vertex detector. The pitch of the silicon strips ranges from 25 to 100 μm, providing impact parameter resolution of about 25 μm. The experiment was conducted with a specialized trigger of requiring either two muons in the final state, or one muon with high transverse momentum, p_t. During the 1992 runs, the experiment recorded about 127 million dimuon triggers and 62 million single muon triggers, corresponding to about 6.6 $\times$ 10^{11} interactions. The results described here are based on about 50% of the dimuon triggers.

The candidates for decay (1) were selected by requiring a fully-reconstructed muon pair in the spectrometer. The information from the silicon detector was not used in this analysis. To reduce K/π decay background, one muon was required to have a $p_t \geq 1$ GeV, and the other muon has to have a $p_t \geq 0.4$ GeV. The invariant mass spectra for opposite-sign (solid histogram) and same-sign (dotted histogram) dimuons are shown in Fig. 2a. The resonances for the well-known vector mesons: J/ψ, ϕ, and ω/ρ are clearly visible in the opposite-sign spectrum.

The mass spectrum in the search region for a D^0 signal is shown in Fig. 2b, where no obvious enhancement is seen at the D^0 mass. The mass spectrum in the search region is well described by a 4th-order polynomial. In order to arrive at an upper limit for the BR, the spectrum is fitted to a Gaussian function at the D^0 mass, superimposed on the 4th-order polynomial. The width of the Gaussian

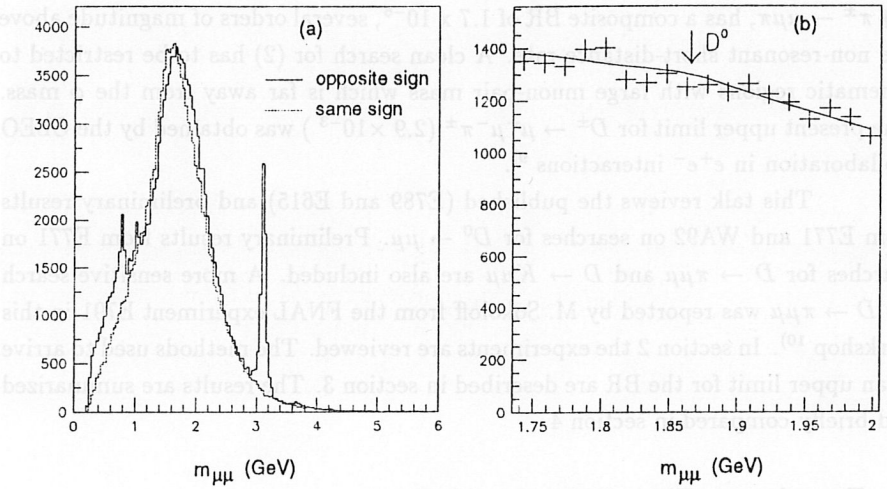

Figure 2: (a) Dimuon mass spectra for opposite (solid) and same (dotted) sign dimuons in E771. (b) The mass spectrum in the search region. The solid line is the 90% confidence level limit for D^0 in the search region as described in the text.

is the mass resolution at D^0, which was determined by interpolating the observed resolutions at ϕ and J/ψ. The fit (soild line) which determines the upper limit on D^0s in the data at 90% confidence level (CL) was obtained by increasing the assumed D^0 signal until the fit reaches a 10% probability. The upper limit on the BR was obtained by normalizing the upper limit on the number of D^0 events (95.4) to the number of J/ψ muon pairs (6258 $\pm$ 91). The J/ψ muon pairs were selected by the same criteria. Based on about 50% of the full data, a preliminary upper limit of 1.7 x 10^{-5} at 90% CL on the BR was obtained [11]. More details of the upper limit calculation are given in Section 3.

The next step in the E771 analysis, which is in progress, is to use the vertex information from the silicon detector. A preliminary study, based on the impact parameter of the muons, revealed that the continuum background is reduced by a factor of about six if a 50 μm cut is applied to the impact parameter of the muon tracks. Since this reduction in background is accompanied by inefficiencies associated with the silicon detector, there is no immediate improvement in the upper limit. The efficiency of the impact parameter cut has been estimated to be about 0.4 which includes silicon tracking inefficiencies and losses due to early decays of the D^0. (The lifetime of $D^0 = 0.42 \times 10^{-12}$ s.) The full exploitation of the vertex information involves reconstructing the vertex of the two muons and requiring a minimum decay distance between the primary interaction point and the muon vertex. This vertex

isolation requirement for the muon pairs should remove most of the prompt muon background. A factor of two to five improvement in the upper limit is expected.

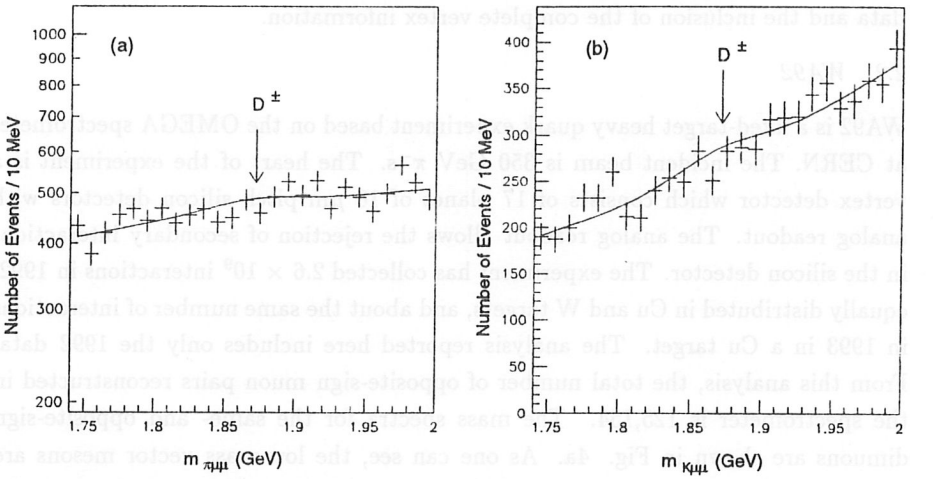

Figure 3: Three-body invariant mass distribution for $\pi\mu\mu$ (a) and $K\mu\mu$ (b) hypotheses for $D^{\pm} \to \mu\mu\pi/K$ search in E771. For both searches, one of the muons was required to have an impact parameter > 50 μm. The solid lines are fits described in the text.

E771 has also used about 40% of the the dimuon sample with large impact parameter to search for (2). Due to the lack of particle identification in E771, each non-muon charged track was tried as a pion or a kaon. The combinatorial background in the search region for the pion (kaon) assumption is shown in Fig. 3a(b). No obvious signal is seen at the $D^{\pm}$ mass in both spectra. The mass spectra were fitted to a polynomial plus a Gaussian function; the polynomial describes the continuum background and the Gaussian function represents the $D^{\pm}$ signal, as in the case of the D^0. The 90% CL upper limit for $D \to \mu\mu\pi$ events is 97.5. The upper limit for the BR was also determined by normalizing to the J/ψ yield. The $D \to \pi\mu\mu$ acceptance times efficiency relative to that of J/ψ muon pairs was determined by a Monte Carlo simulation to be about 0.14. The small acceptance times efficiency for the charged D decays stems from the geometric acceptance for the pion or kaon as well as the effect of the p_t cut on the muons; the p_t of muons from the three-body charged D decay is lower on the average than that of the two-body neutral D decay. Taking these factors into account, the 90% CL upper limit on the BR for $D \to \mu\mu\pi$ was determined to be 7.6×10^{-4}. The corresponding limit for $\mu\mu K$ is 1.0×10^{-3}. These preliminary limits are already three to ten times better than the PDG limit

of 2.9×10^{-3} for $\mu\mu\pi$ and 9.2×10^{-3} for $\mu\mu K$. Again, the vertex constraint on the muons and the companion kaon or pion track has not been fully applied in this analysis. It is expected that this limit will be improved with the use of the entire data and the inclusion of the complete vertex information.

2.2 *WA92*

WA92 is a fixed-target heavy quark experiment based on the OMEGA spectrometer at CERN. The incident beam is 350 GeV π^-s. The heart of the experiment is a vertex detector which consists of 17 planes of 10 μm pitch silicon detectors with analog readout. The analog readout allows the rejection of secondary interactions in the silicon detector. The experiment has collected 2.6×10^9 interactions in 1992, equally distributed in Cu and W targets, and about the same number of interactions in 1993 in a Cu target. The analysis reported here includes only the 1992 data. From this analysis, the total number of opposite-sign muon pairs reconstructed in the spectrometer is 125,154. The mass spectra for the same- and opposite-sign dimuons are shown in Fig. 4a. As one can see, the low-mass vector mesons are clearly visible in the opposite-sign dimuon sample. The number of events in the search region (1.78 to 1.92 GeV) was reduced to 143 by applying additional cuts to the muon vertex kinematics based on information from the silicon detector. The mass spectrum for the 143 events is shown in Fig. 4b, where no enhancement at the D^0 mass is discernible. The 143 events were scanned visually. None of the 143 candidates met the criteria for decay (1). The same scanning criteria, when applied to Monte Carlo events, recovered about 60 % of the decays. Using an upper limit of 2.3 events for zero candidate (at 90% CL) and normalizing to the J/ψ yield, an upper limit of 0.8×10^{-5} was obtained for the BR [12].

2.3 *E789*

A search for the CCNC decay (1) was also performed by E789 [13]. E789 is a special-purpose heavy quark fixed-target experiment at FNAL using 800 GeV protons [14]. The 60 meter long detector is a double-magnet spectrometer equipped with a silicon vertex detector. The spectrometer consists of three tracking stations each with six planes of drift or proportional chambers, followed by a ring-imaging Cherenkov counter, an electromagnetic calorimeter, and a muon identifier. The bending field in the two magnets can be tuned to enhance specific two-body mass in the trigger. The target is a 0.2 mm high $\times$ 1.2 mm long $\times$ 5 cm wide platinum block encapsulated in vacuum. This target geometry provides a precise position for primary interactions along the beam direction and the vertical coordinate. The vertical coordinates of the charged tracks are precisely measured by the silicon microstrip detector which is

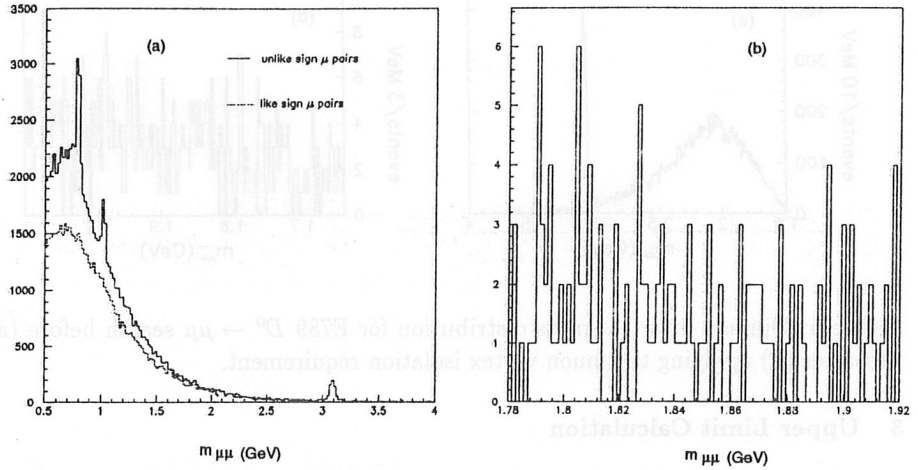

Figure 4: (a) Invariant mass distributions for opposite-sign (solid histogram) and same-sign (dotted histogram) dimuons in WA92. (b) Mass distribution for events after applying the vertex cuts.

composed of eight 5 cm × 5 cm × 300 μm silicon planes with 50 μm pitch, covering the angular regions 20 to 60 and -20 to -60 mrad. There is no silicon tracking in the horizontal direction. The 40 mrad gap along the beamline allows a large number of protons to go through without causing damage to the silicon detector. The data for the search consisted of about 5 x 10^{11} interactions, taken during the commissioning of the experiment in 1990. For the off-line analysis, dimuon events were reconstructed using muon identification and tracking information from the wire chambers and the silicon strip detector. The mass spectrum with loose vertex requirement is shown in Fig. 5a, which contains 1088 ± 36 J/ψ events in the rapidity range $0.1 \leq y \leq 0.4$ where the acceptance is concentrated. To further suppress background, D^0 candidates were required to satisfy additional vertex requirements, consisting of impact parameter cuts and a minimum decay distance (Δz) of 2 mm in the vertex position of the two muons. The mass spectrum for the residual events is shown in Fig. 5b. No signal is seen at the D^0 mass. The number of background-subtracted candidates in the search region (1852-1885 MeV) after applying a tighter vertex isolation cut of $\Delta z \geq 3.25$ mm is -4.1 ± 4.8 events. The resulting upper limit on the branching ratio was calculated to be 3.1 x 10^{-5} at 90% CL [13]. E789 is currently conducting a more thorough search for (1) using the full data.

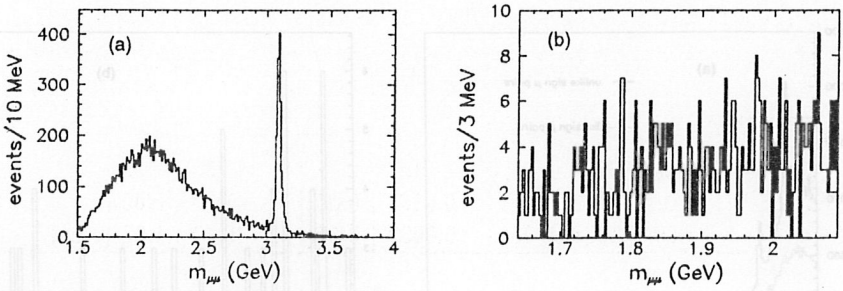

Figure 5: Dimuon invariant mass distribution for E789 $D^0 \to \mu\mu$ search before (a) and after (b) applying the muon vertex isolation requirement.

3 Upper Limit Calculation

Since none of the experiments has found evidence for the decay $D^0 \to \mu\mu$, they all reported an upper limit on the BR. E771 and WA92 have normalized their results to the J/ψ yield according to the following formula.

$$BR(D^0 \to \mu\mu) = BR(J/\psi \to \mu\mu)\frac{\sigma_{J/\psi}}{\sigma_D} A^{-\beta} \frac{A_{J/\psi}}{A_D} \frac{1}{\epsilon} \frac{N_D}{N_{J/\psi}}. \quad (4)$$

The $BR(J/\psi \to \mu\mu) = 0.0597 \pm 0.0025$ [4] is common to all experiments. $\sigma_{J/\psi}$ and σ_D are the production cross sections per nucleon for J/ψ and D^0, respectively. The $A-$dependence of the J/ψ and D^0 cross sections is parametrized as A^α, where A is the atomic weight of the target. The upper limit depends weakly on the target via $A^{-\beta}$, where β is the difference of the αs for J/ψ and D^0 productions. $A_{J/\psi}/A_D$ is the relative acceptance times efficiency of J/ψ to D^0 dimuons. The upper limit on D^0 events is N_D, and the number of reconstructed J/ψs is $N_{J/\psi}$. For WA92 and E789, additional cuts were applied to the D^0 candidates, which were not applied to the J/ψ muons; the efficiency of these cuts is ϵ. E789 has used a different formula to calculate the upper limit, namely by using the differential J/ψ production cross section in pp collisions, $d\sigma/dy$ (y is the rapidity), measured at the ISR [15]. The quoted relative acceptance times efficiency takes into account the losses in the forward region as well as the silicon efficiency ϵ, and is therefore not directly comparable to other experiments. The results for E771, E891, and WA92 are shown in Table 1. The results for E615 are also listed for comparison. Several observations are worth pointing out. The ratio of J/ψ cross section to that of D^0 is fairly constant, in spite of the differences in beam energy and beam particle type. The four experiments have used slightly different values for β, but the target factor varies only from 0.59 to 0.85, under 20% variation from the mean. E615 did not

Table 1: Results from E615, E771, WA92, and E789 on $D^0 \to \mu\mu$ Search

Expt.	N_{int} (10^{11})	$N_{J/\psi}$	$\sigma_{J/\psi}/\sigma_D$	$A^{-\beta}$	$A_{J/\psi}/A_D$	ϵ	N_D	BR (10^{-5})
E615 [6]	0.93	5584 ± 200	0.0177	1.00	1.19	1.00	48.6	<1.1
E771 [11]	3.30	6258 ± 91	0.0150	0.77	1.58	1.00	95.4	<1.7
WA92 [12]	0.01	623 ± 25	0.0167	0.85	1.39	0.60	2.3	<0.8
E789 [13]	5.00	1088 ± 36	0.0030	0.59	48.40	1.00	6.4	<3.1

taken into account the difference in the A-dependence of the J/ψ and D^0 production cross sections, corresponding to $\beta = 0$. The relative J/ψ and D^0 acceptance is also fairly constant, of the order of 1.2 to 1.6, except that of E789 which is not directly comparable. The upper limits on the BR for the four experiments are listed in Table 1. They are all consistent with the PDG limit of 1.1×10^{-5}.

4 Summary and Future Prospects

In summary, most of the current heavy quark fixed-target experiments have the capability to examine decay vertex kinematics of hadrons composed of heavy quarks. This allows them to perform sensitive searches for rare decays of heavy hadrons, in particular FCNC dimuon decays of D^0 and $D^{\pm}$. Experiments E771, E789, and WA92 have searched for such decays in part of their data. No evidence was found. The results are summarized in Table 1 where the PDG limit (E615) is also included for comparision. The preliminary upper limit on the BR is about 1×10^{-5}. By extrapolating the analyses to full data, and speculating on the rejection power of vertex isolation, these limits are expected to be improved, probably by about one order of magnitude in the near future. This, unfortunately, does not provide stringent constraint on the SM, even though some models with FCNC are excluded. On the experimental side, it appears that three-dimensional vertex information is essential in controlling the ultimate background due to double semimuonic decays in these searches. The low level of residual background seen in WA92 and E789 suggests that the limit may be scaled linearly with integrated luminosity by at least another factor of ten. A dedicated fixed-target experiment with a sensitivity of 10^{-7} to 10^{-8} on the BR seems therefore feasible.

5 Acknowledgments

The author thanks his colleagues from E771, especially Guanghui Mo, for discussing the preliminary results. He is also indebted to Dan Kaplan from E789 for discussing

the published results. The result provided by Gianni Penso for WA92 is gratefully acknowleged. The hospitality of the workshop organizers, especially Brad Cox and Diana Stokely, is greatly appreciated. K. L. is supported by a grant from the Texas Advanced Research Program.

References

1. S. L. Glashow, J. Iliopoulos, and L. Maiani, Phys. Rev. D **2,** 1285 (1970).
2. S. Pakvasa, talk presented at Charm 2000, to be published in the proceedings.
3. T. Inami and C. S. Lim, Prog. Theor. Phys. **65** 297 (1981) (E:1772) and references therein.
4. Review of Particle Properties, Particle Data Group, Phys. Rev. D **50,** 1 (1994).
5. See, e.g., M. Savage, Phys. Lett. **B266,** 135 (1991).
6. W. C. Louis *et al.,* Phys. Rev. Lett. **56,** 86 (1027).
7. For a recent review, see J. L. Hewett, talk presented at the *XXI SLAC Summer Institute,* 1993, Stanford, CA.
8. K. S. Babu, X-G. He, Xue-Qian Li, and Sandip Pakavasa, Phys. Lett. **B205,** 540 (1988).
9. P. Haas *et al.,* (CLEO Collaboration), Phys. Rev. Lett. **160,** 88 (1614).
10. M. Sokoloff, this proceedings.
11. G. Mo *et al,* (E771 Collaboration), talk presented at the 1994 DPF meeting; T. Alexopoulos *et al.,* (E771 Collaboration), paper submitted to the 27th Int. Conf. on High Energy Physics, Glasgow, Scotland (GLS0422), FERMILAB-Conf-94/170-E and UHIBPD-HEP-94-003, June 1994.
12. G. Penso, talk presented at the 1994 Italian Physical Society meeting; M. Adamovich *et al.,* (WA92 Collaboration), abstract submitted to the 27th Int. Conf. on High Energy Physics, Glasgow, Scotland (GLS0333), June 1994.
13. C. S. Mishra *et al.,* (E789 Collaboration), Phys. Rev. D **50,** R9 (1994).
14. Y. B. Hsiung *et al.,* Phys. Rev. Lett. **55,** 457 (1985); J. A. Crittenden *et al.,* Phys. Rev. D **34,** 2584 (1986); D.E. Jaffe *et al., ibid* **40,** 2777 (1989).
15. A. G. Clark *et al.,* Nucl. Phys. **B142,** 29 (1978).

Frascati Physics Series, Vol. III (1994)
HEAVY QUARKS AT FIXED TARGET
University of Virginia, October 7–10, 1994
(pp. 63–68)

SEARCHING FOR FLAVOR CHANGING NEUTRAL CURRENTS IN FERMILAB EXPERIMENTS E791 AND E687

Michael D. Sokoloff
Physics Department, University of Cincinnati, Cincinnati, OH 45211–001

Abstract

Fermilab experiments E791 and E687 have been searching for flavor-changing neutral-current charm decays whose observation at the current level of experimental sensitivity would indicate physics beyond the Standard Model. The sensitivity for these new experiments is about an order of magnitude better than previous generations of experiments. Were a signal to be observed in these experiments, it would indicate new physics at the TeV/c^2 mass scale.

1 – Introduction

Flavor-changing neutral-current (FCNC) charm decays are forbidden at the tree level in the Standard Model. Higher-order short-distance amplitudes which mimic FCNC processes give branching ratios between 10^{-11} and 10^{-8} [1]. The sequential decay $D^+ \to \phi\pi^+$; $\phi \to \ell^+\ell^-$ has a branching ratio $\approx 2 \times 10^{-6}$ for either electrons or muons, as was pointed out by one of the participants at this conference. The 1994 Particle Data Group (PDG) compilation of branching ratios [2] reports limits between 1.1×10^{-5} (for $D^0 \to \mu^+\mu^-$) and 9.20×10^{-3} (for $D^+ \to K^+\mu^+\mu^-$) for decay modes being studied by these experiments. This leaves a large window for new physics [3].

E791 and E687 are similar fixed-target experiments which finished taking data at the beginning of 1992. Both use open geometry spectrometers with silicon microstrip detectors, two magnets for momentum analysis, and threshold Cerenkov detectors for particle identification. E687 used a wide-band photon beam incident on an extended beryllium target. E791 used a 500 GeV/c π^- beam incident on five thin foils (one platinum, four diamond) separated by

1.5 cm gaps. Both experiments search for rare decays and normalize branching ratios (or limits) to clean charm signals such as $D^+ \to K^-\pi^+\pi^+$.

2 – Physics Overview

One can argue on dimensional grounds that the matrix element for new physics which leads to FCNC charm decays can be calculated from Feynman diagrams similar to those shown in Figures 1 and 2. The dashed lines represent new heavy exchange bosons with mass m_H. The decay rates for such processes are proportional to the fourth power of m_H. If we assume that the coupling strength of the new interaction is similar to that of the electroweak interaction, then a D^+ branching ratio of 10^{-5} corresponds to an exchange boson mass around 850 GeV/c^2 [1]. If the new interaction is a combination of vector and axial vector currents, then the approximate conservation of helicity will suppress two-body decays such as that shown in Figure 2. Three-body FCNC decays will not suffer from such helicity suppression, so may be more sensitive to new physics.

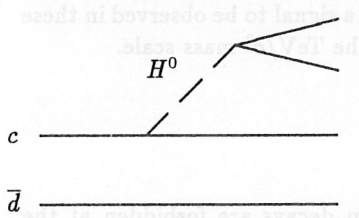

Figure 1: This is the Feynman diagram for a FCNC D^+ decay mediated by a heavy boson H^0.

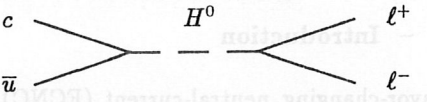

Figure 2: This is the Feynman diagram for a FCNC D^0 decay mediated by a heavy boson H^0.

3 – Results from E791

E791 is searching for the decay $D^+ \to \pi^+\mu^+\mu^-$ using the decay $D^+ \to K^-\pi^+\pi^+$ for normalization. Because the $D^+ \to K^-\pi^+\pi^+$ signal is so large, the experiment has tuned its track and vertex quality cuts on that data. To separate charm candidates from background, the experiment requires that the secondary vertex be well-separated from the primary vertex, that the secondary vertex be located outside the target foils or other solid material, and that the momentum vector of the D candidate point back to the primary vertex. To identify

muons, E791 uses a plane of 16 scintillation counters located behind 15 interaction lengths of shielding. The $\pi^+\mu^+\mu^-$ invariant mass distribution for the first half of the data from E791 is shown in Figure 3.

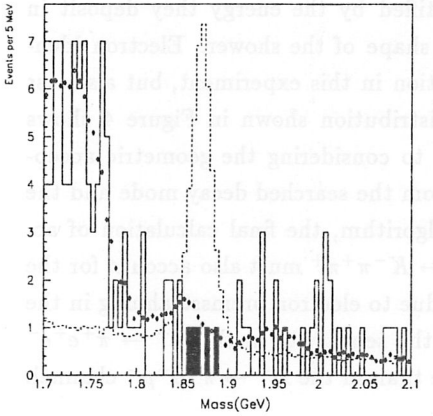

Figure 3: The solid histogram is the $\pi^+\mu^+\mu^-$ invariant mass spectrum after all cuts. The shaded entries are the events in the search window. The dashed histogram is the $K^-\pi^+\pi^+$ normaliztion spectrum scaled by a factor of 600. The small diamonds are the estimated background using the shape of the $\pi^+\mu^+\mu^-$ spectrum before muon identification normalized to the final sample outside the search window.

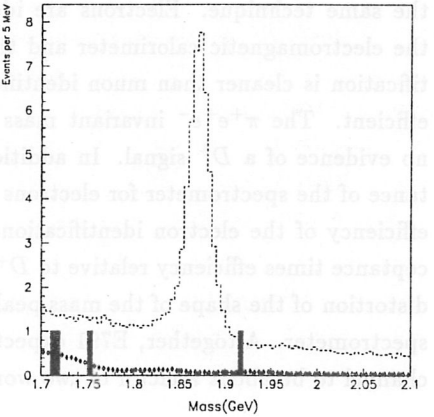

Figure 4: The three shaded entries are the only $\pi^+e^+e^-$ events after vertexing and electron identification cuts. The dashed histogram is the $K^-\pi^+\pi^+$ normaliztion spectrum scaled by a factor of 600. The small diamonds are an estimated background using the shape of the $\pi^+e^+e^-$ spectrum before muon identification normalized to the final sample outside the search window.

The background in the signal region is estimated by assuming the shape of the background is the same as that of the sample passing all cuts except the muon identification cuts and that the normalization is provided by events outside the signal region. This interpolation algorithm predicts 9.5 ± 1.0 events with mass between 1.85 GeV/c^2 and 1.89 GeV/c^2 where five events are observed. The 90% confidence level upper limit is 3.9 signal events. An upper limit on the branching ratio is determined by comparing this number with the 20,000 $D^+ \to K^-\pi^+\pi^+$ events observed in the same data sample. At the time of this conference E791 believed the efficiency for detecting $D^+ \to \pi^+\mu^+\mu^-$ relative to that for detecting $D^+ \to K^-\pi^+\pi^+$ was approximately 85%. The

upper limit for the branching ratio was reported to be 2×10^{-5}. More detailed studies since then indicate that the relative efficiency, given the cuts used at that time, is lower, and the correct upper limit based on the data shown in Figure 3 probably lies between 4.5×10^{-5} and 6.0×10^{-5}.

E791 is also searching for the decay $D^+ \to \pi^+ e^+ e^-$ using essentially the same technique. Electrons are identified by the energy they deposit in the electromagnetic calorimeter and the shape of the shower. Electron identification is cleaner than muon identification in this experiment, but also less efficient. The $\pi^+ e^+ e^-$ invariant mass distribution shown in Figure 4 shows no evidence of a D^+ signal. In addition to considering the geometric acceptance of the spectrometer for electrons from the searched decay mode and the efficiency of the electron identification algorithm, the final calculation of acceptance times efficiency relative to $D^+ \to K^- \pi^+ \pi^+$ must also account for the distortion of the shape of the mass peak due to electron bremsstrahlung in the spectrometer. Altogether, E791 expects the sensitivity in the $D^+ \to \pi^+ e^+ e^-$ channel to be about a factor of two worse than in the $D^+ \to \pi^+ \mu^+ \mu^-$ channel.

4 – Results from E687

E687 searches for FCNC decays and sets upper limits using a relative branching ratios method:

$$\frac{BR(D \to X_{\rm FCNC})}{BR(D \to X_{\rm Norm})} = \frac{N_{\rm obs}(X_{\rm FCNC})}{\epsilon(X_{\rm FCNC})} \frac{\epsilon(X_{\rm Norm})}{N_{\rm obs}(X_{\rm Norm})}$$

similar to that used by E791. The "inner" muon system consists of three planes of scintillator paddles used for triggering and an additional four planes of proportional tubes used for muon identification. The granularity of the proportional tubes was 5 cm, and the hadron misidentification rate was about 1% per track when requiring five of the seven muon system planes to have hits within a 3σ multiple scattering circle. For comparison, the E791 hadron misidentification rate was closer to 5% per track at high momentum.

Upper limit results for several dimuon channels were presented at the CHARM2000 conference in June [4] and are summarized in Table I below. After vertexing and muon identification cuts, E687 has 0 - 3 events in the signal region (1.85 GeV/c^2 - 1.89 GeV/c^2) for each of these decay modes where 1.5 - 2.5 background events are expected. These results should be considered preliminary only – the experimenters hope to optimize cuts and improve sensitivity before publishing a final result.

Mode	E687 Limit	PDG limit
$D^0 \to \mu^+\mu^-$	2.7×10^{-5}	1.1×10^{-5}
$D^+ \to \pi^+\mu^+\mu^-$	9.7×10^{-5}	290×10^{-5}
$D^+ \to K^+\mu^+\mu^-$	8.5×10^{-5}	920×10^{-5}
$D^+ \to \pi^-\mu^+\mu^+$	17×10^{-5}	680×10^{-5}
$D^+ \to K^-\mu^+\mu^+$	20×10^{-5}	430×10^{-5}

Table I: These are the preliminary upper limits on FCNC decays with dimuons in the final state reported by E687 at the CHARM2000 conference [4]. The limits reported by the Particle Data Group in the 1994 compilation [2] are shown for comparison.

5 – Plans for E831

The wide-band photon collaboration plans to run again in 1996 as E831. They expect to increase their luminosity by a factor of ten relative to E687 by improving the beam, by improving the target configuration, and by running longer. Their sensitivity for decays with muons in the final state will be further enhanced by replacing the "outer" muon system which did not work in E687 and by running with an improved "inner" muon system for the full experiment. The inner muon system was not working for the first part of the 1990 run and was operated with a hole in the middle to accomodate another experiment for the whole run. The net result should be a factor of 30 improvement in statistics for decay channels with a single muon and a factor of 50 - 60 improvement for those with two muons. In addition, the experiment will run with more shielding and better tracking which will produce less matching confusion. Altogether, the FCNC sensitivity is expected to improve by a factor of ten.

6 – Summary

E687 and E791 are setting branching ratio limits on FCNC charm decays such as $D^+ \to \pi^+\mu^+\mu^-$ at the $n \times 10^{-5}$ level. These searches are probing physics near the TeV/c^2 mass scale. E831 should be able to push these limits down to the $n \times 10^{-6}$ level, and a fixed target experiment reconstructing 10^8 charm cleanly might push the branching ratio limits to $n \times 10^{-7}$. Such an experiment would be competitive with the LHC, the planned beauty factories, and the proposed τ-charm factories.

7 – Acknowledgements

I would like to thank all my colleagues from E791 for their help in preparing this talk, especially Ai Nguyen and Nick Witchey. I would like to thank Paul Sheldon from E687 who was extremely generous in helping me understand that experiment. This work was supported in part by the U.S National Science Foundation.

References

1. A.J. Schwartz, Mod. Phys. Lett. **A8**, 967 (1993).
2. The Particle Data Group, L. Montanet *et al.*, Phys. Rev. **D50**, Part 1, 1173 (1994).
3. W. Buchmuller and D. Wyler, Phys. Lett. B **177**, 377 (1986);
   A. S. Joshipura, Phys. Rev. D **39**, 878 (1989);
   Miriam Leurer, Phys. Rev. Lett. **71**, 1324 (1993).
4. P.D. Sheldon,"Searching for CP violation, flavor changing neutral currents, and lepton number violation in charm decay," pg. 25 in D.M. Kaplan and S. Kwan, *eds.*, **The Future of High-Sensitivity Charm Experiments: Proceedings of the CHARM2000 Workshop**, Fermilab, June 7–9, 1994, FERMILAB-Conf-94/190.

SESSION III

- G. Valencia
  CP Violation in Hyperon Decays

- K. Luk
  Experimental Prospects for Observing CP Violation in Hyperon Decay

Frascati Physics Series, Vol. III (1994)
HEAVY QUARKS AT FIXED TARGET
University of Virginia, October 7–10, 1994
(pp. 71–80)

$\mathcal{CP}$ VIOLATION IN HYPERON DECAYS

G. Valencia
Department of Physics, Iowa State University, Ames, Iowa 50011

ABSTRACT

In this talk we review the status of the theoretical estimates for $\mathcal{CP}$ violating asymmetries in non-leptonic hyperon decays.

1 – The Decay $\Lambda^0 \to p\pi^-$

The reaction $\Lambda^0 \to p\pi^-$ will be used as an example to set up the model independent formulation of the $\mathcal{CP}$ odd observables in non-leptonic hyperon decays of the form $B_i \to B_f\pi$. In the Λ^0 rest frame, $\vec{\omega}_{i,f}$ will denote unit vectors in the directions of the Λ and p polarizations, and $\vec{q}$ the proton momentum. The isospin of the final state is $I = 1/2$ or $3/2$, and each of these two states can be reached via a $\Delta I = 1/2$ or $3/2$ weak transition respectively. There are also two possibilities for the parity of the final state. They are the s-wave, $l = 0$, parity odd state (thus reached via a parity violating amplitude); and the p-wave, $l = 1$, parity even state reached via a parity conserving amplitude.

We first perform a model independent analysis of the decay by writing the most general matrix element consistent with Lorentz invariance: [1, 2, 3]

$$\mathcal{M} = G_F m_\pi^2 \overline{U}_P (A - B\gamma_5) U_\Lambda. \tag{1}$$

This matrix element reduces to

$$A(B_i \to B_f\pi) = s + p\vec{\sigma}\cdot\vec{q} \tag{2}$$

In terms of these quantities one can compute the decay distribution, and the total decay rate. One finds that the decay is characterized by three independent

observables: the total decay rate and two parameters that determine the angular distribution. The total decay rate is given by:

$$\Gamma = \frac{|\vec{q}|(E_P + M_P)}{4\pi M_\Lambda} G_F^2 m_\pi^4 \left(|s|^2 + |p|^2\right). \tag{3}$$

The angular distribution is proportional to:

$$\frac{d\Gamma}{d\Omega} \sim 1 + \gamma \vec{\omega}_i \cdot \vec{\omega}_f + (1-\gamma)\hat{q}\cdot\vec{\omega}_i \hat{q}\cdot\vec{\omega}_f + \alpha \hat{q}\cdot(\vec{\omega}_i + \vec{\omega}_f) + \beta \hat{q}\cdot(\vec{\omega}_f \times \vec{\omega}_i), \tag{4}$$

where we have introduced the notation:

$$\alpha \equiv \frac{2\mathrm{Re}s^* p}{|s|^2+|p|^2}, \quad \beta \equiv \frac{2\mathrm{Im}s^* p}{|s|^2+|p|^2}, \quad \gamma \equiv \frac{|s|^2-|p|^2}{|s|^2+|p|^2}. \tag{5}$$

However, only two of these parameters are independent, since $\alpha^2+\beta^2+\gamma^2 = 1$. We will treat α and β as the independent ones, although sometimes the parameters α and ϕ, with $\beta = \sqrt{1-\alpha^2}\sin\phi$ and $\gamma = \sqrt{1-\alpha^2}\cos\phi$ are used instead.

The parameter α governs the T-even correlation between the proton momentum and the Λ polarization, whereas β governs the T-odd correlation involving the two polarization vectors and the proton momentum. I use T to indicate the operation that reverses the sign of all momenta and spins in the reaction, and **not** the time reversal operation. The significance of this discrete symmetry is that operators that are even under it can only be used to construct $\mathcal{CP}$ odd observables that require final state interactions, whereas those that are odd can be used to construct $\mathcal{CP}$ odd observables that do not vanish in the absence of final state interactions.

One way to interpret the parameter α follows from considering the angular distribution in the case when the final baryon polarization is not observed:

$$\frac{d\Gamma}{d\Omega} = \frac{1}{16\pi^2}\frac{|\vec{q}|}{M_\Lambda} G_F^2 m_\pi^4 (E_P + M_P)\left(|s|^2+|p|^2\right)(1+\alpha\hat{q}\cdot\vec{\omega}_i). \tag{6}$$

The polarization of the decay proton in the Λ^0 rest frame is given by:

$$\vec{\mathcal{P}}_P = \frac{1}{1+\alpha\vec{\mathcal{P}}_\Lambda\cdot\hat{q}}\left[\left(\alpha + \vec{\mathcal{P}}_\Lambda\cdot\hat{q}\right)\hat{q} + \beta\left(\vec{\mathcal{P}}_\Lambda\times\hat{q}\right) + \gamma\left(\hat{q}\times\left(\vec{\mathcal{P}}_\Lambda\times\hat{q}\right)\right)\right]. \tag{7}$$

From this expression we can relate β to the proton polarization in the direction perpendicular to the plane formed by the Λ polarization and the proton momentum. If the initial hyperon is unpolarized, α gives us the polarization of the proton:

$$\vec{\mathcal{P}}_p = \alpha_\Lambda \hat{q} \tag{8}$$

Since the proton polarization is not measured, the parameter β is not useful for the reaction $\Lambda \to p\pi^-$. It is, however, useful for other hyperon decays, such as the chain:

$$\Xi^- \to \Lambda^0\pi^- \to p\pi^-\pi^- \tag{9}$$

where the second decay analyzes the polarization of the Λ and allows one to observe the parameter β_Ξ.

2 – $\mathcal{CP}$-odd Observables

To construct $\mathcal{CP}$-odd observables we compare the reactions $\Lambda^0 \to p\pi^-$ and $\overline{\Lambda}^0 \to \overline{p}\pi^+$ in terms of the three independent observables. One can show that $\mathcal{CP}$ symmetry predicts that:

$$\begin{aligned} \overline{\Gamma} &= \Gamma \\ \overline{\alpha} &= -\alpha \\ \overline{\beta} &= -\beta \end{aligned} \tag{10}$$

and, therefore, one can construct the following $\mathcal{CP}$-odd observables: [4]

$$\begin{aligned} \Delta &\equiv \frac{\Gamma - \overline{\Gamma}}{\Gamma + \overline{\Gamma}} \\ A &\equiv \frac{\alpha\Gamma + \overline{\alpha}\overline{\Gamma}}{\alpha\Gamma - \overline{\alpha}\overline{\Gamma}} \approx \frac{\alpha + \overline{\alpha}}{\alpha - \overline{\alpha}} + \Delta \\ B &\equiv \frac{\beta\Gamma + \overline{\beta}\overline{\Gamma}}{\beta\Gamma - \overline{\beta}\overline{\Gamma}} \approx \frac{\beta + \overline{\beta}}{\beta - \overline{\beta}} + \Delta \end{aligned} \tag{11}$$

One can show that in the low energy reaction $p\overline{p} \to \Lambda\overline{\Lambda} \to p_f\pi^-\overline{p}_f\pi^+$ it is possible to construct counting asymmetries that measure A and B. [5] If we label each particle's momentum by the particle name, and denote by $N_p^{\pm}$ the number of events with $(\vec{p}_i \times \vec{p}_\Lambda) \cdot \vec{p}_f$ greater or less than zero then: [5]

$$\overline{A} = \frac{N_p^+ - N_{\overline{p}}^- + N_{\overline{p}}^+ - N_p^-}{N_{total}} = \mathcal{P}_\Lambda \alpha_\Lambda A_\Lambda \tag{12}$$

Similarly, in the reaction $p\overline{p} \to \Xi\overline{\Xi} \to \Lambda\pi^-\overline{\Lambda}\pi^+ \to p_f\pi^-\pi^-\overline{p}_f\pi^+\pi^+$, we can define $\overline{N}_p^{\pm}$ to be the number of events with $\mathcal{P}_\Xi \cdot (\vec{p}_f \times \vec{p}_\Lambda)$ greater or less than zero and construct the counting asymmetry: [5]

$$\overline{B} = \frac{\overline{N}_p^+ - \overline{N}_{\overline{p}}^- + \overline{N}_{\overline{p}}^+ - \overline{N}_p^-}{N_{total}} = \frac{\pi}{8}\mathcal{P}_\Xi \alpha_\Lambda \beta_\Xi (A_\Lambda + B_\Xi) \tag{13}$$

3 – Isospin Decomposition

To discuss the final state interaction phases it is convenient to analyze the final pion-nucleon system in terms of isospin and parity eigenstates. In that way we can have in mind the simple picture:

$$\Lambda^0 \underset{H_w}{\overset{t=0}{\longrightarrow}} \left(p\pi\right)_\ell^I \overset{H_s}{\underset{\delta_\ell^I}{\longrightarrow}} \left(p\pi\right)_\ell^I . \tag{14}$$

At $t = 0$ the weak Hamiltonian induces the decay of the Λ^0 into a pion-nucleon system with isospin and parity given by I, ℓ. If there is $\mathcal{CP}$ violation in this decay there will be a $\mathcal{CP}$-odd phase ϕ_ℓ^I. This pion-nucleon system is an eigenstate of the strong interaction. Furthermore, at an energy equal to the Λ mass, it is the only state with these quantum numbers. The pion-nucleon system will then rescatter due to the strong interactions into itself, and in the process pick up a phase δ_ℓ^I. This is an example of what is known as Watson's theorem.

If we parameterize the amplitudes in non-leptonic hyperon decays as:

$$s = \sum_I s_I e^{i(\delta_s^I + \phi_s^I)} \quad p = \sum_I p_I e^{i(\delta_p^I + \phi_p^I)}, \tag{15}$$

then $\mathcal{CPT}$ invariance of the weak Hamiltonian predicts:

$$\overline{s} = \sum_I -s_I e^{i(\delta_s^I - \phi_s^I)} \quad \overline{p} = \sum_I p_I e^{i(\delta_p^I - \phi_p^I)}, \tag{16}$$

whereas $\mathcal{CP}$ invariance of the weak interactions predicts:

$$\overline{s} = \sum_I -s_I e^{i(\delta_s^I + \phi_s^I)} \quad \overline{p} = \sum_I p_I e^{i(\delta_p^I + \phi_p^I)}. \tag{17}$$

From this we see that the ϕ_ℓ^I phases violate $\mathcal{CP}$. We want to extract ϕ_ℓ^I from the $\mathcal{CP}$-odd observables discussed in the previous section.

Introducing the notation used in the literature: [6]

$$\begin{aligned} S(\Lambda_-^0) &= -\sqrt{2/3} S_{11} e^{i(\delta_1 + \phi_1^s)} + \sqrt{1/3} S_{33} e^{i(\delta_3 + \phi_3^s)} \\ P(\Lambda_-^0) &= -\sqrt{2/3} P_{11} e^{i(\delta_{11} + \phi_1^p)} + \sqrt{1/3} P_{33} e^{i(\delta_{33} + \phi_3^p)} \\ S(\Xi_-^-) &= S_{12} e^{i(\delta_2 + \phi_{12}^s)} + \frac{1}{2} S_{32} e^{i(\delta_2 + \phi_{32}^s)} \\ P(\Xi_-^-) &= P_{12} e^{i(\delta_{21} + \phi_{12}^p)} + \frac{1}{2} P_{32} e^{i(\delta_{21} + \phi_{32}^p)} \end{aligned} \tag{18}$$

where Λ_-^0 refers to the reaction $\Lambda^0 \to p\pi^-$ and Ξ_-^- refers to the reaction $\Xi^- \to \Lambda^0 \pi^-$. The notation for the isospin amplitudes is $S_{ij} \equiv S_{2\Delta I, 2I}$, $P_{ij} \equiv P_{2\Delta I, 2I}$, the s-wave phases are denoted by δ_{2I} and the p-wave phases by $\delta_{2I,1}$.

It is useful to construct approximate expressions based on the fact that there are three small parameters in the problem:

- The strong rescattering phases are measured or estimated to be small. Experimentally we know that [7]

$$\delta_1 \approx 6.0^\circ, \quad \delta_3 \approx -3.8^\circ, \quad \delta_{11} \approx -1.1^\circ, \quad \delta_{31} \approx -0.7^\circ \tag{19}$$

with all the errors on the order of 1°. For the Ξ decays there are no experimental results. An early calculation within a model predicted $\delta_{21} = -2.7^\circ$ and

$\delta_2 = -18.7°$. [8] A recent calculation using chiral perturbation theory predicts instead $\delta_{21} = -1.7°$ and $\delta_2 = 0$. [9] Clearly the resulting asymmetries will be completely different depending on which of these results is closer to the true scattering phases.

- The $\Delta I = 3/2$ amplitudes are much smaller than the $\Delta I = 1/2$ amplitudes. Experimentally we know that: [10]

$$S_{33}/S_{11} = 0.027 \pm 0.008, \quad P_{33}/P_{11} = 0.03 \pm 0.037$$
$$S_{32}/S_{12} = -0.046 \pm 0.014, \quad P_{32}/P_{12} = -0.01 \pm 0.04 \tag{20}$$

- The $\mathcal{CP}$ violating phases are presumed to be small.

To leading order in all the small quantities one finds: [4]

$$\begin{aligned} \Delta(\Lambda^0_-) &= \sqrt{2}\frac{S_{33}}{S_{11}} \sin(\delta_3 - \delta_1) \sin(\phi^s_3 - \phi^s_1) \\ A(\Lambda^0_-) &= -\tan(\delta_{11} - \delta_1) \sin(\phi^p_1 - \phi^s_1) \\ B(\Lambda^0_-) &= \cot(\delta_{11} - \delta_1) \sin(\phi^p_1 - \phi^s_1) \end{aligned} \tag{21}$$

and

$$\begin{aligned} \Delta(\Xi^-_-) &= 0 \\ A(\Xi^-_-) &= -\tan(\delta_{21} - \delta_2) \sin(\phi^p_{12} - \phi^s_{12}) \\ B(\Xi^-_-) &= \cot(\delta_{21} - \delta_2) \sin(\phi^p_{12} - \phi^s_{12}) \end{aligned} \tag{22}$$

We can see in these expressions that Δ arises mainly from an interference between a $\Delta I = 1/2$ and a $\Delta I = 3/2$ s-waves, and that it is suppressed by three small quantities. On the other hand, A arises as an interference of s and p-waves of the same isospin and, therefore, it is not suppressed by the $\Delta I = 1/2$ rule. Finally, we can see that B is not suppressed by the small rescattering phases. This is as we expected for a $\mathcal{CP}$ odd observable that is also (naive)-T odd. The hierarchy $B >> A >> \Delta$ emerges. [4] The quantity $\Delta(\Xi^-_-)$ vanishes because there is only one isospin final state in this decay.

This is as far as we can go in a model independent manner. If we want to predict the value of these observables within a model for $\mathcal{CP}$ violation we take the value for the ratio of amplitudes and for the strong rescattering phases from experiment and we try to compute the weak phases from theory.

4 – Standard model calculation

In the case of the minimal standard model, the $\mathcal{CP}$ violating phase resides in the CKM matrix. For low energy transitions, this phase shows up as the imaginary

part of the Wilson coefficients in the effective weak Hamiltonian. In the notation of Buras [11],

$$H_W^{eff} = \frac{G_F}{\sqrt{2}} V_{ud}^* V_{us} \sum_i c_i(\mu) Q_i(\mu) + \text{ hermitian conjugate} \tag{23}$$

$Q_i(\mu)$ are four quark operators, and $c_i(\mu)$ are the Wilson coefficients that are usually written as:

$$\begin{aligned} c_i(\mu) &= z_i(\mu) + \tau y_i(\mu) \\ \tau &= -\frac{V_{td}^* V_{ts}}{V_{ud}^* V_{us}} \end{aligned} \tag{24}$$

with the $\mathcal{CP}$ violating phase being the phase of τ. Numerical values for these coefficients can be found, for example, in Buchalla *et. al.* [12]

The calculation would proceed as usual, by evaluating the hadronic matrix elements of the four-quark operators in Eq. 23 to obtain real and imaginary parts for the amplitudes, schematically:

$$\langle p\pi | \, H_w^{eff} \, | \Lambda^0 \rangle \, |_\ell^I = \mathrm{Re} M_\ell^I + i \mathrm{Im} M_\ell^I, \tag{25}$$

and to the extent that the $\mathcal{CP}$ violating phases are small, they can be approximated by

$$\phi_\ell^I \approx \frac{\mathrm{Im} M_\ell^I}{\mathrm{Re} M_\ell^I}. \tag{26}$$

At present, however, we do not know how to compute the matrix elements so we cannot actually implement this calculation. If we try to follow what is done for kaon decays, we would compute the matrix elements using factorization and vacuum saturation as a reference point, then define some parameters analogous to B_K that would measure the deviation of the matrix elements from their vacuum saturation value. A reliable calculation of the "B" parameters would probably have to come from lattice QCD.

For a simple estimate, we can take the real part of the matrix elements from experiment (assuming that the measured amplitudes are real, that is, that $\mathcal{CP}$ violation is small), and compute the imaginary parts in vacuum saturation. This approach provides a conservative estimate for the weak phases because the model calculation of the real part of the amplitudes is much smaller than the experimental value. Of course, if we cannot predict the real part of the amplitude at all, we might question the reliability of the imaginary part as well.

There are many models in the literature that claim to fit the experimentally measured amplitudes. Without entering into the details of these models, it is obvious that to fit the data, the models must enhance some or all of the matrix elements with

respect to vacuum saturation. Clearly, one would get completely different phases depending on which matrix elements are enhanced. It is not surprising, therefore, that a survey of these models yields weak $\not{CP}$ phases that differ by an order of magnitude [13].

The approximate weak phases estimated in vacuum saturation are: [13]

$$\begin{aligned}
\phi_s^1 &\approx -3y_6 \mathrm{Im}\tau \\
\phi_p^1 &\approx -0.3y_6 \mathrm{Im}\tau \\
\phi_s^3 &\approx \left[3.56(y_1+y_2)+4.1(y_7+2y_8)\frac{m_\pi^2}{m_s(m_u+m_d)}\right]\mathrm{Im}\tau
\end{aligned} \tag{27}$$

To get some numerical estimates we use the values for the Wilson coefficients of Buchalla *et. al.* [12] with $\mu = 1$ GeV, $\Lambda_{QCD} = 200$ MeV. Although quantities such as the quark masses that appear in Eq. 27 are not physical [14], we will use for an estimate the value $m_\pi^2/(m_s(m_u+m_d)) \sim 10$. For the quantity $\mathrm{Im}\tau$ we use the current upper bound $\mathrm{Im}\tau \leq 0.0014$. Putting all the numbers together yields:

$$\begin{aligned}
\Delta(\Lambda_-^0) &= \begin{cases} -1.4\times 10^{-6} & \text{for } m_t = 150 \text{ GeV} \\ -9.1\times 10^{-7} & \text{for } m_t = 200 \text{ GeV} \end{cases} \\
A(\Lambda_-^0) &= 3.7\times 10^{-5} \\
B(\Lambda_-^0) &= 2.4\times 10^{-3}
\end{aligned} \tag{28}$$

A poor man approach to the problem of the hadronic matrix elements consists of surveying several models. Combining this with a careful analysis of the allowed range for the short distance parameters that enter the calculation yields results similar to that of Eq. 28: that A is in the range of "a few" $\times 10^{-5}$ and that Δ is almost two orders of magnitude smaller. The rate asymmetry exhibits a strong dependence on the top-quark mass: for a certain value of m_t, the two terms in Eq. 27 cancel against each other. The angular correlation asymmetries, on the other hand, depend mildly on the top-quark mass. This is understood from the point of view that the most important effect of a large top-quark mass is to enhance electroweak corrections to the effective weak Hamiltonian. This is important for the $\Delta I = 3/2$ amplitudes but not for the $\Delta I = 1/2$ amplitudes.

5 – Other Models of $\not{CP}$ Violation

Other models of $\not{CP}$ violation contain additional short distance operators with $\not{CP}$ violating phases. [15, 16] Some of these have been analyzed in the literature fixing the strength of the $\not{CP}$ violating couplings from the parameter ϵ in kaon decays. [4] A summary of those results is shown in Table 1, taken from a recent talk by He. [17]

Table 1. Sample of models of CP violation in hyperon decays.

Λ decay	KM model	Weinberg Model	Left-Right Model
$\Delta(\Lambda^0_-)$	$< 10^{-6}$	-0.8×10^{-5}	0
$A(\Lambda^0_-)$	$-(1 \sim 5) \times 10^{-5}$	-2.5×10^{-5}	-1.1×10^{-5}
$B(\Lambda^0_-)$	$(0.6 \sim 3) \times 10^{-4}$	1.6×10^{-3}	7.0×10^{-4}
Ξ decay			
$\Delta(\Xi^-_-)$	0	0	0
$A(\Xi^-_-)$	$-(1 \sim 10) \times 10^{-5}$	-3.2×10^{-4}	2.5×10^{-5}
$B(\Xi^-_-)$	$(1 \sim 10) \times 10^{-3}$	3.8×10^{-3}	-3.1×10^{-4}

An important point is that the numbers for the $\Xi^- \to \Lambda\pi^-$ decay were obtained using the early model calculation. [8] With the chiral perturbation theory numbers [9] $A(\Xi^-_-)$ would be smaller by a factor of 10.

Acknowledgements

I would like to thank J. F. Donoghue, X. G. He, B. R. Holstein and H. Steger for pleasant collaborations on the subject of this talk.

References

1. T. D. Lee, *Particle Physics and Introduction to Field Theory*(Harwood, New York, 1982).
2. R. E. Marshak, Riazuddin and C. P. Ryan, *Theory of Weak Interactions in Particle Physics* (Wiley, New York, 1969).
3. E. Commins and P. Bucksbaum, *Weak Interactions of Leptons and Quarks* (Cambridge, New York, 1983).
4. J. F. Donoghue and S. Pakvasa, *Phys. Rev. Lett.* **55**, 162 (1985); J. F. Donoghue, X. G. He and S. Pakvasa, *Phys. Rev.* **D34**, 833 (1986).
5. J. F. Donoghue, B. R. Holstein and G. Valencia, *Phys. Lett.* **178B**,319 (1986).
6. O. E. Overseth and S. Pakvasa, *Phys. Rev.* **184**, 1663 (1969).
7. L. Roper, *et. al.*, *Phys. Rev.***138**, 190 (1965)
8. R. Nath and B. Kumar, *Nuov. Cim.* **36**, 669 (1965).
9. M. Lu, M. Savage and M. Wise, *Phys. Lett.* **337B**,133 (1994).
10. O. E. Overseth, *Phys. Lett.* **111B**,286 (1982).

11. A recent review with a complete list of references is A. Buras and M. Harlander in *Heavy Flavors*, ed. A. Buras and M. Lindner (WS, Singapore, 1992).

12. G. Buchalla, A. Buras and M. Harlander, *Nucl. Phys.* **B337**,313 (1990).

13. X G. He, H. Steger and G. Valencia, *Phys. Lett.* **272B**,411 (1991).

14. J. F. Donoghue, E. Golowich and B. R. Holstein, *Dynamics of the Standard Model* (Cambridge, Cambridge, 1992).

15. S. Weinberg, *Phys. Rev. Lett.* **37**, 657 (1976).

16. R. N. Mohapatra and J. C. Pati, *Phys. Rev.* **D11**, 566 (1975).

17. X. G. He and S. Pakvasa, UH-511-802-94, OITS-550.

Frascati Physics Series, Vol. III (1994)
HEAVY QUARKS AT FIXED TARGET
University of Virginia, October 7–10, 1994
(pp. 81–93)

Experimental Prospects for Observing CP Violation in Hyperon Decay*

Kam-Biu Luk
University of California and Lawrence Berkeley Laboratory, Berkeley, CA 94720

Abstract

The status and prospect of studying CP invariance by determining the difference in the decay angular distributions between the hyperon and the antihyperon are presented. Current experimental limits are at least two orders of magnitude away from theoretical predictions that range from 10^{-3} to 10^{-5}. There is no dedicated experiment except one recently approved fixed target experiment at Fermilab, E871, that will search for CP violation in charged-Ξ and Λ hyperon decays down to the 10^{-4} level.

1. Introduction

Shortly after parity nonconservation in weak interactions was questioned, possible violation of time reversal T -- or CP symmetry assuming CPT invariance holds -- as well as charge conjugation C was also suggested.[1] Okubo pointed out that CP violation would lead to a difference in the branching ratio of a given decay mode for the Σ^+ and $\overline{\Sigma}^-$ hyperons.[2] In 1959, Pais noted that when the decay angular distributions of the Λ^0 and $\overline{\Lambda}^0$ are compared, any inequality would signal breaking of CP invariance.[3] These conjectures triggered experimental searches for discrete symmetry breaking which is still actively pursued today. The early tests of CP conservation in hyperon decay were performed by determining the time reversal parameter, β, in the decay of polarized Λ^0 which were produced in exclusive reactions.[4] These experiments suffered from limited statistics and could only reach a level of the order of a few percents.

*Invited talk presented at The Second International Workshop on Heavy Quark Physics in Fixed Target Experiments, Charlottesville, Virginia, October 7, 1994.

Recently there is renewal of interest in testing CP invariance in hyperon decay. This is motivated by the fact that with new accelerator facilities and better instrumentation, it is experimentally feasible to check the validity of some theoretical estimations of the CP-odd effect with good sensitivity. In this talk, the experimental status of such tests is briefly reviewed and the prospect of performing dedicated experiments is presented.

2. Theoretical Motivation

For the parity violating nonleptonic decay of a $J^P = \frac{1}{2}^+$ hyperon into a $J^P = \frac{1}{2}^+$ baryon and a $J^P = 0^-$ meson, the final state can be in orbital angular momentum states of 0 and 1 with the corresponding S- and P-waves. It can be shown that the decay rate is given by:[5]

$$\Gamma = G_F^2 m_\pi^4 \frac{p_d (E_d + m_d)}{4\pi m_p} \left(|S|^2 + |P|^2 \right) \tag{1}$$

where G_F is the Fermi constant, m_π is the mass of the charged pion, m_p is the mass of the hyperon, m_d is the mass of the baryon, p_d and E_d are the magnitude of the momentum and energy of the baryon in the rest frame of the hyperon respectively. In the hyperon rest frame, the angular distribution the daughter baryon is:

$$\frac{dN_d}{d\cos\theta_d} = \frac{1}{2}\left(1 + \alpha_p \vec{P}_p \cdot \vec{p}_d\right) \tag{2}$$

where θ_d is the angle between the polarization of the hyperon, $\vec{P}_p$, and the momentum unit vector of the decay baryon, $\vec{p}_d$. Furthermore, the polarization of the baryon, $\vec{P}_d$, is related to the polarization of the hyperon by:

$$\vec{P}_d = \frac{1}{\left(1 + \alpha_p \vec{P}_p \cdot \vec{p}_d\right)} \left[\left(\alpha_p + \vec{P}_p \cdot \vec{p}_d \right) \vec{p}_d + \beta_p \vec{P}_p \times \vec{p}_d + \gamma_p \vec{p}_d \times \left(\vec{P}_p \times \vec{p}_d \right) \right] \tag{3}$$

where the decay asymmetry parameters α_p, β_p, and γ_p are defined in terms of the parity-violating S-wave and the parity-conserving P-wave:

$$\alpha_p = \frac{2\,\mathrm{Re}(S^* P)}{|S|^2 + |P|^2}, \quad \beta_p = \frac{2\mathrm{Im}(S^* P)}{|S|^2 + |P|^2}, \quad \gamma_p = \frac{|S|^2 - |P|^2}{|S|^2 + |P|^2} \tag{4}$$

with $\alpha_p^2 + \beta_p^2 + \gamma_p^2 = 1$.

For a given two-body nonleptonic hyperon decay and that of its antiparticle, in terms of Γ, α and β, some observables that are sensitive to CP violation in the decay can be defined as:

$$\Delta = \frac{\Gamma - \overline{\Gamma}}{\Gamma + \overline{\Gamma}}, \quad A = \frac{\alpha + \overline{\alpha}}{\alpha - \overline{\alpha}}, \quad B' = \frac{\beta + \overline{\beta}}{\alpha - \overline{\alpha}}, \quad B = \frac{\beta + \overline{\beta}}{\beta - \overline{\beta}}, \tag{5}$$

where the overlined quantities refer to the antihyperon. If CP is conserved in the decay, $\Gamma = \overline{\Gamma}$, $\alpha = -\overline{\alpha}$, and $\beta = -\overline{\beta}$.

To date, reliable calculations of CP violation in hyperon decays are not available. This is because exact evaluation of the hadronic matrix elements cannot be implemented. Estimations of Δ, A, B and B' have been obtained by using different models to calculate the hadronic matrix elements.[6] Some predictions of the CP violation in the $\Lambda^0 \to p\pi^-$ and $\Xi^- \to \Lambda^0\pi^-$ decays in the standard model, the multi-Higgs model and the isoconjugate Left-Right symmetric model are shown in Table 1.[7] It should note that superweak models[8] do not have $\Delta S = 1$ CP-odd effects (direct CP violation) and thus all observables in equation (5) are expected to be very small or zero.

Table 1. Some estimations of CP violation in $\Lambda^0 \to p\pi^-$ and $\Xi^- \to \Lambda^0\pi^-$ decays[7]

	Δ_Λ	A_Λ	B_Λ
Standard Model	$< 10^{-6}$	$-(5\sim1) \times 10^{-5}$	$(3\sim0.6) \times 10^{-4}$
Multi-Higgs	-0.8×10^{-5}	-2.5×10^{-5}	1.6×10^{-3}
Left-Right	0	-1.1×10^{-5}	7.0×10^{-4}

	Δ_Ξ	A_Ξ	B_Ξ
Standard Model	0	$-(10\sim1) \times 10^{-5}$	$(10\sim1) \times 10^{-3}$
Multi-Higgs	0	-3.2×10^{-4}	3.8×10^{-3}
Left-Right	0	-2.5×10^{-5}	-3.1×10^{-4}

3. Experimental activities

From Table 1, it is obvious that in general Δ is too small to measure. Determination of the other observables requires hyperon samples with precisely known polarization. Although it is the most sensitive to CP violation, the polarization of the daughter baryons must also be measured in order to determine B. In addition, to reach a sensitivity of 10^{-4} in B, at least 10^8 to 10^9 polarized hyperon and antihyperon decays are needed because the statistical error in B is inversely proportional to β which is usually a small number. Therefore, A is the most promising observable for searching for CP violation in hyperon decays.

3.1 Past searches

There were three tests of CP conservation in the hyperon sector from experiments R608 at ISR, DM2 at Orsey, and PS185 at LEAR. These studies focussed on the determination of A_Λ by detecting $\Lambda^0 \to p\pi^-$ and $\bar{\Lambda}^0 \to \bar{p}\pi^+$ decays. Limited by statistics, the average of their results compiled by the Particle Data Group is $A_\Lambda = -0.03 \pm 0.06$.[9] We are going to briefly describe the technique of these three experiments.

3.1.1 R608 at ISR[10]

Polarized Λ^0 and $\bar{\Lambda}^0$ were produced in the forward beam fragmentation region in the following inclusive reactions:

$$pp \to \Lambda^0 + X \quad (6)$$
$$\bar{p}p \to \bar{\Lambda}^0 + X. \quad (7)$$

Assuming charged-conjugation conservation in strong interactions, polarization of Λ^0 in $p \to \Lambda^0$ is identical to that of $\bar{\Lambda}^0$ in $\bar{p} \to \bar{\Lambda}^0$. This assumption was checked by comparing the momentum distributions of the charged particles, and of the Λ^0 and $\bar{\Lambda}^0$ between these reactions. Excellent agreement was observed from the central region to x_F of 0.8. Based on 17,028 $\Lambda^0 \to p\pi^-$ and 9,553 $\bar{\Lambda}^0 \to \bar{p}\pi^+$ events, the ratio $\alpha_\Lambda/\bar{\alpha}_\Lambda$ was found to be -1.04 ± 0.29 which is equivalent to $A_\Lambda = -0.02 \pm 0.14$.

3.1.2 DM2 at Orsey[11]

A total of 1,847 $\Lambda^0\bar{\Lambda}^0$ pairs coming from the decays of J/ψ's produced in unpolarized e^+e^- collisions was used to study the differential cross section:

$$\frac{d\sigma}{d\cos\theta_\Lambda\, d\Omega_p d\Omega_{\bar{p}}} \propto 2\left(1-\frac{p_\Lambda^2}{E_\Lambda^2}\sin^2\theta_\Lambda\right)\left[1-\alpha_\Lambda\bar{\alpha}_\Lambda(\boldsymbol{p}\cdot\boldsymbol{n})(\bar{\boldsymbol{p}}\cdot\boldsymbol{n})\right] + \frac{p_\Lambda^2}{E_\Lambda^2}\sin^2\theta_\Lambda\left\{1-\alpha_\Lambda\bar{\alpha}_\Lambda\left[\boldsymbol{p}\cdot\bar{\boldsymbol{p}}-2(\boldsymbol{p}\cdot\boldsymbol{x})(\bar{\boldsymbol{p}}\cdot\boldsymbol{x})\right]\right\} \quad (8)$$

where θ_Λ is the emission angle of the Λ^0 with respect to the e^+ beam direction, p_Λ and E_Λ are the momentum and energy of the Λ^0 in the J/ψ decay, $\boldsymbol{p}$ and $\bar{\boldsymbol{p}}$ are the p and $\bar{p}$ momentum in the Λ^0 and $\bar{\Lambda}^0$ rest frame respectively, $\boldsymbol{x}$ is normal to the $\Lambda^0\bar{\Lambda}^0$ direction and to the beam axis, and $\boldsymbol{n}$ is defined as unit vector that suppresses the 0 spin projection in the J/ψ decay and is degenerated with the beam axis at $\theta_\Lambda = 0°$ and 90°. By fixing the parity asymmetry parameter α_Λ at the canonical value of 0.642,[9] the observed distribution for $\boldsymbol{p}\cdot\bar{\boldsymbol{p}}$ was fitted to the theoretical expectation by varing $\bar{\alpha}_\Lambda$. The least squares minimization yielded $\bar{\alpha}_\Lambda = -0.63\pm0.13$. This determination gives $A_\Lambda = 0.01\pm0.10$.

3.1.3 PS185 at LEAR

In this experiment, polarized $\Lambda^0\bar{\Lambda}^0$ pairs were produced in low energy $\bar{p}p$ exclusive reactions at threshold. Again, conservation of charge-conjugation in the production process guarantees that the polarizations of Λ^0 and $\bar{\Lambda}^0$ be the same. From the products $\alpha_\Lambda P_\Lambda$ for $\Lambda^0 \to p\pi^-$ and $\bar{\alpha}_\Lambda \bar{P}_\Lambda$ for $\bar{\Lambda}^0 \to \bar{p}\pi^+$ decays, the observable A_Λ can be determined. By combining 4,063 events taken at 1.546 GeV/c incident $\bar{p}$ momentum[12] and 11,362 events at 1.695 GeV/c, a result of -0.024 ± 0.057 for A_Λ was obtained.[13]

3.2 Prospects

There has been considerable interest at CERN, at Fermilab, and at a future tau-charm factory in pursuing searches for CP violation in non-leptonic hyperon decay to better precision, on the order of 10^{-4} in A and 10^{-3} in B. Most of these proposed experiments require either upgrade of the existing facilities or construction of new storage rings in order to accumulate enough events in a finite amount of time to reach the goal. Presently, none of these new programs is approved.

An alternative approach is to exploit hyperon beams. Strange baryons are known to be copiously produced in high energy fixed target experiments. It is relatively easy to obtain large samples of longitudinal polarized Λ^0 and $\bar{\Lambda}^0$ from unpolarized Ξ^- and $\bar{\Xi}^+$ decays. Since $\bar{P}_\Lambda = \alpha_\Xi \hat{\Lambda}$ in this case, the polarizations of Λ^0 and $\bar{\Lambda}^0$ are identical up to the level of CP symmetry breaking in the charged Ξ decay. This is the technique used by the recently approved experiment, E871, at Fermilab. We now turn to the details of these new initiatives.

3.2.1 Low energy $\bar{p}p$ experiments

The promising results of PS185 at LEAR have prompted an investigation of the feasibility of measuring A_Λ with better precision.[14] The new experiment requires an upgrade of LEAR to LEAR-2 so that the number of $\bar{p}$'s in a stack will be increased by ten fold to more than 2×10^{11}. A hydrogen jet target with a surface density of 10^{14} atoms/cm^2 is used to intercept the 1.642 GeV/c $\bar{p}$ beam. This energy is chosen to suppressed the production of $\bar{\Lambda}^0\Sigma^0+\Lambda^0\bar{\Sigma}^0$ which is an important background to the measurement. At this beam energy, a peak luminosity of greater than 6.6×10^8 cm^{2}s^{-1} can be achieved. With a production cross section for the reaction $\bar{p}p \rightarrow \Lambda^0\bar{\Lambda}^0$ of 65 μb, the maximum production rate of $\Lambda^0\bar{\Lambda}^0$ pairs is ≈ 4,250 s^{-1}. But only events with the $\bar{\Lambda}^0$ in the range of $-0.75 < \cos\theta_{cm} < 0.3$ will be accepted because, in this kinematic region, the average polarization of the Λ is the highest, about 46%. Furthermore, in the region of interest, the momentum distributions in the laboratory frame of the decay protons and antiprotons are quite similar. Assuming an overall efficiency of 35%, similar to what has been achieved in PS185, the production rate of $\bar{p}p \rightarrow \Lambda^0\bar{\Lambda}^0 \rightarrow \bar{p}\pi^+p\pi^-$ events is dropped to 154 s^{-1}. In order to obtain an error of 10^{-4} in A_Λ, 1.2×10^7 s of running time at the peak luminosity is needed.

In principle, the cleanest signal of CP violation in hyperon decays is given by the observables B and B', which are independent of the poorly known final state phase shift difference. The most accessible process to do this is the charged Ξ decay which can be considered as a double self analyzer (Λ^0 decay is a single self analyzer). Due to the required beam momentum is about 3.5 GeV/c, the $\bar{p}p \rightarrow \Xi^-\bar{\Xi}^+$ process is beyond the capability of LEAR. Thus, determination of B_Ξ and B'_Ξ can only be done at SuperLEAR.

It is important to realize that in the exclusive production of hyperon-antihyperon pairs, all the decay particles are unambiguously identified. The key of the measurement is counting the number of decay protons and antiprotons above and below the production plane which is defined by the vertices of the hyperon decays and the interaction point. Any asymmetry or inefficiency in the apparatus could then lead to (1) moving protons and antiprotons to the wrong side of the production plane, (2) misconstructing the production plane. Some examples of the systematic problems are residual magnetic field near the production point, different chamber inefficiency in different part of the spectrometer, interactions with matter in the apparatus. Worst of all, due to the nature of the process, for instance $\bar{p}p \rightarrow \bar{\Lambda}^0\Lambda^0$ in fixed target mode, the leading particle effect will give rise to asymmetric momentum distributions between particles and antiparticles that tend to probe different part of the apparatus. This is one of the reasons why the region of interest is chosen in such a way to reduce this bias.

A similar low energy $\bar{p}p$ experiment to measure A_Λ has also been considered at Fermilab.[15] With the commission of the Main Injector, a total of about 4.7×10^8 $\bar{p}$'s/sec will be available. By colliding the stored $\bar{p}$ beam at 1.641 GeV/c with an internal hydrogen gas jet target of 10^{14} atoms/cm^2, about 7,500 $\Lambda^0\bar{\Lambda}^0$ pairs/sec can be produced. Only the charged decay mode of both Λ^0 and $\bar{\Lambda}^0$ is detected. By choosing the same kinematic region of interest as the

LEAR-2 experiment and with some assumptions about the overall efficiency, it is claimed that in sixteen days of data taking, observable A_Λ can be measured to a precision of 10^{-4}. To reach the 10^{-5} level, a dedicated $\bar{p}$ storage ring will be needed.

3.2.2 J/ψ decays at tau-charm factory[16]

It has been argued that the tau-charm factory can provide very clean and systematic free conditions for investigating CP violation in Λ^0 and Ξ^- decays. When a tau-charm factory is operated at the J/ψ peak, the production cross section of J/ψ strongly depends on the beam energy spread. By using monochromators the beam energy spread can be reduced from 1.3 MeV to 0.1 MeV and the expected luminosity is about 4×10^{32} $cm^{-2}s^{-1}$. In a year of running (1 year ≡ 10^7s), as shown in Table 2, the number of $\Lambda^0\bar{\Lambda}^0$ and $\Xi^-\,\bar{\Xi}^+$ pairs coming from J/ψ decays is estimated to be 1.1×10^8 and 1.4×10^8 respectively.

Since the rate of good J/ψ decays is about 500 times higher than that for CP violation studies, an efficent trigger scheme must be employed. It has be proposed that the proton and antiproton from the decays will be identified by TOF in the first level trigger. Then the decay of the hyperons will be selected in the second level by searching for multiplicity jump in the number of tracks in the drift chamber which has very low mass. The trigger rate should be decreased to about 100 Hz. Online reconstruction will then be used as a third level trigger to identify the presence of hyperon pairs. The spectrometer will have excellent momentum resolution which is crucial in determining angles and planes used in the measurements of the decay parameters.

What CP observables that the tau-charm factory can measure depends on the polarization of the beam which is defined by:

$$P_{beam} = \frac{P_+^L + P_-^L}{1 + P_+^L P_-^L} \,. \tag{9}$$

where P_+^L and P_-^L are the longitudinal polarization of the e^+ and e^- respectively. The hyperon polarization is related to the beam polarization by

$$\bar{P}_Y = \frac{\left(P_{beam}\hat{e}^+ \cdot \hat{Y}\right)\hat{Y} - \beta_\psi\left(\hat{e}^+ \cdot \hat{Y}\right)\left(\hat{e}^+ \times \hat{Y}\right) - \alpha_\psi P_{beam}\left(\hat{e}^+ \times \hat{Y}\right)\times \hat{Y}}{\frac{1}{2}\left(1+\cos^2\theta_Y\right) + \left|\frac{A_{++}}{A_{+-}}\right|^2 \sin^2\theta_Y} \tag{10}$$

where $\hat{Y}$ is the momentum unit vector of the hyperon in the laboratory frame, θ_Y is the emission angle of the hyperon with respect to the e^+ beam direction, A_{++} and A_{+-} are the helicity decay amplitudes of the J/ψ. The parameters, α_ψ and β_ψ, are defined as:

$$\alpha_\psi = \frac{\sqrt{2}\,\mathrm{Re}\left(A_{++}^{*}A_{+-}\right)}{|A_{+-}|^2}\,, \qquad \beta_\psi = \frac{\sqrt{2}\,\mathrm{Im}\left(A_{++}^{*}A_{+-}\right)}{|A_{+-}|^2} \tag{11}$$

If the beams are not polarized and β_ψ is zero, only the product $\alpha_\Lambda \bar{\alpha}_\Lambda$ can be measured in the Λ decay. This will require input of α_Λ from other experiments. This drawback does not exist when the beams are polarized. In the case of Ξ decay, independent of the beam polarization, the angular distributions and correlations of the daughter baryons, Λ and p, in the decay sequence are sufficient for extracting values for the decay asymmetry parameters without replying on another experiments.

However, as shown in Table 2, the precision in determining the CP observables at the tau-charm factory is poorer than those at low energy $\bar{p}p$ experiments.

Table 2. Sensitivities of CP observables in 1 year of running with monochromators at tau-charm factory. Beam polarization is assumed to be 40%.

J/ψ decay mode	Beam polarization	Measured parameters	CP observables	Sensitivity at τ-charm fac.
$\Lambda^0\bar{\Lambda}^0$	No	$\alpha_\Lambda\bar{\alpha}_\Lambda$ †	A_Λ	5×10^{-3} *
$\Lambda^0\bar{\Lambda}^0$	Yes	α_Λ, $\bar{\alpha}_\Lambda$	A_Λ	$\leq 10^{-3}$
$\Xi^-\bar{\Xi}^+$	No	α_Λ, $\bar{\alpha}_\Lambda$ α_Ξ, $\bar{\alpha}_\Xi$ β_Ξ, $\bar{\beta}_\Xi$	A_Λ A_Ξ B'_Ξ	$\approx 10^{-3}$ $\approx 10^{-3}$ $\approx 5 \times 10^{-3}$
$\Xi^-\bar{\Xi}^+$	Yes	α_Λ, $\bar{\alpha}_\Lambda$ α_Ξ, $\bar{\alpha}_\Xi$ β_Ξ, $\bar{\beta}_\Xi$	A_Λ A_Ξ B'_Ξ	$\leq 10^{-3}$ $\leq 10^{-3}$ $\approx 5 \times 10^{-3}$

† requires input value of α_Λ from other experiments

* sensitivity is limited by the precision of the input α_Λ

3.2.3 Experiment 871 at Fermilab[17]

The goal of E871 is to search for CP violation in charged Ξ and Λ hyperon decays by measuring A_Λ and A_Ξ to better than 10^{-4}. In this experiment, both Ξ^- and $\bar{\Xi}^+$ hyperons will be produced with no polarization by 800 GeV protons hitting the target at zero degree (parity

conservation in strong interactions demands the polarization be zero). The Λ from the weak decay of an unpolarized Ξ is in a pure helicity state which is related to the decay parameter of the parent Ξ: $\bar{P}_\Lambda = \alpha_\Xi \hat{\Lambda}$. The angular distributions of the proton and antiproton in the Λ^0 and $\overline{\Lambda}^0$ helicity frames are thus given by:

$$\frac{dN}{d(\cos\theta)} = \frac{N_0}{2}(1+\alpha_\Lambda P_\Lambda \cos\theta) = \frac{N_0}{2}(1+\alpha_\Lambda \alpha_\Xi \cos\theta) = \frac{N_0}{2}(1+\overline{\alpha}_\Lambda \overline{\alpha}_\Xi \cos\theta). \qquad (12)$$

If CP invariance is good in both Λ and Ξ decays, then $\overline{\alpha}_\Lambda = -\alpha_\Lambda$ and $\overline{\alpha}_\Xi = -\alpha_\Xi$, and the proton and antiproton distributions are identical, as is every other kinematic parameters in the decay process. It is evident from Equation (12) that differences between the slopes of the two $cos\theta$ distributions can be due to CP violation in either the Ξ or Λ decay:

$$A' = \frac{\alpha_\Lambda \alpha_\Xi - \overline{\alpha}_\Lambda \overline{\alpha}_\Xi}{\alpha_\Lambda \alpha_\Xi + \overline{\alpha}_\Lambda \overline{\alpha}_\Xi} = A_\Lambda + A_\Xi. \qquad (13)$$

that is, the experiment is sensitive to CP violation in both hyperon decays.

This experiment is scheduled to run in the 1996 fixed target period. The plan and elevation views of the E871 apparatus are shown in Figure 1. The apparatus has been kept simple in order to facilitate its understanding at the level of the expected asymmetry. The apparatus consists of two targets of different interaction lengths,* followed by a curved collimator embedded in a 6 m long dipole magnet. Behind a vacuum decay region is a conventional magnetic spectrometer employing high-rate, narrow pitch multiwire proportional chambers. The spectrometer momentum analyzing magnets have sufficient strength to ensure that the proton from the Λ^0 decay is always bent to one side of the spectrometer and that the two pions from the Ξ^- and Λ^0 decays are always bent to the opposite side, and both are well separated from the charged beam exiting the collimator. A simple, yet selective trigger for collecting Ξ^- decays is formed by requiring the coincidence of signals from a scintillator hodoscope on the pion side, from the hodoscope on the proton side and from the hadronic calorimeter. The calorimeter is used to make the trigger "blind" to muons which are one of the dominant background. The requirement of certain amount of energy deposited in the calorimeter also reduces the trigger rate due to secondary interactions of the charged beam with material in the spectrometer. When the polarities of the magnets in the apparatus are reversed and the target is switched, identical trigger, thus a CP invariant trigger, can be used to collect $\overline{\Xi}^+$ decays. In addition, p and $\bar{p}$ (π^- and π^+) always sample the same region of the spectrometer, thus minimizing systematic bias. With 10^{10} protons/sec on target, the trigger rates for both the negative and positive running, tabulated in Table 3, have been estimated

* These targets are chosen in such a way that the spectrometer will always see similar singles rate between Ξ^- and $\overline{\Xi}^+$ runs without changing the incident proton intensity.

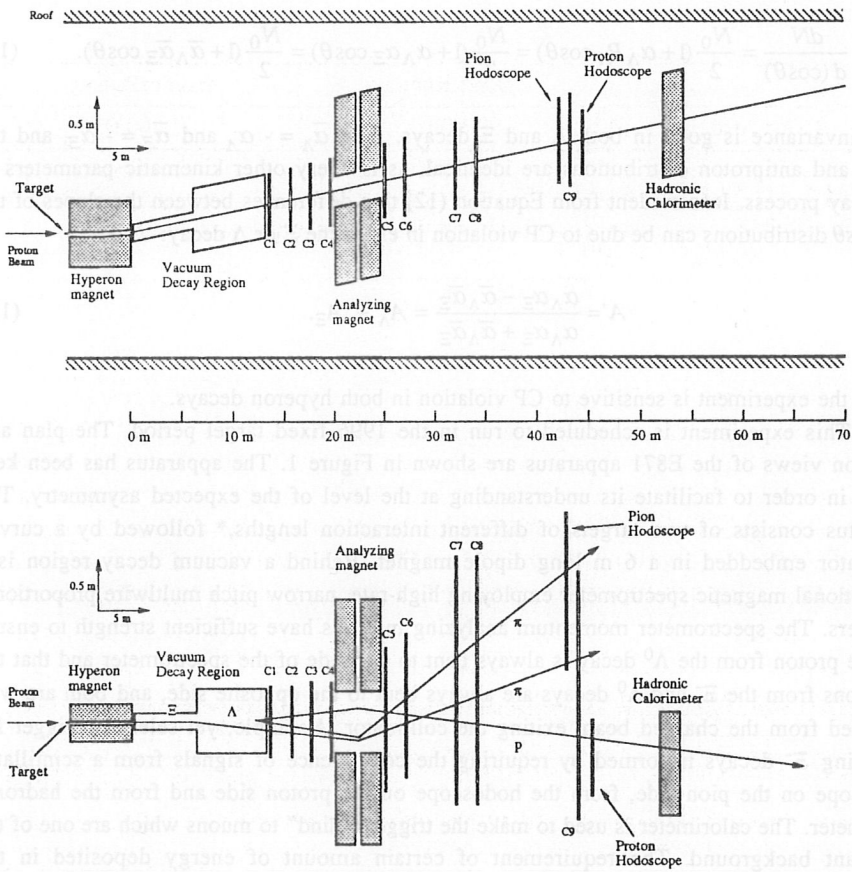

Figure 1. Plan and elevation views of E871 spectrometer

with Monte Carlo simulations. In 200 days of running, with a duty factor of 50%, a total of 2.9 x 10^9 each of the $\Xi^- \rightarrow \Lambda^0\pi^- \rightarrow p\pi^-\pi^-$ and $\bar{\Xi}^+ \rightarrow \bar{\Lambda}^0\pi^+ \rightarrow \bar{p}\pi^+\pi^+$ events, after reconstruction and event selection requirements, will be obtained.

Table 3. Trigger rate per 10^{10} protons/sec on target

	Negative Running	PositiveRunnig
Background	22,000 Hz	22,200 Hz
$\Xi \rightarrow \Lambda\pi \rightarrow p\pi\pi$	11,000 Hz	2,300 Hz
$K \rightarrow 3\,\pi$	2,400 Hz	2,000 Hz
Total	35,400 Hz	26,500 Hz

The data acquisition system, based on multiple VME crates, is designed to handle a maximum trigger rate of 100,000 Hz. The event size is expected to be about 600 bytes, resulting in a sustained data logging rate of about 20 Mbyte/sec. This is high rate, but is only a factor of two larger than has been previously logged at Fermilab fixed target experiments.

Systematic effects which have the potential to cause false asymmetries are of great concern. Sources of biases fall into three classes: (1) differences in acceptance between the Ξ^- and $\bar{\Xi}^+$ decays, (2) nonzero polarization of the Ξ^- and $\bar{\Xi}^+$, and (3) differential differences between the p and $\bar{p}$, π^+ and π^-, cross sections. While every effort will be made to minimize the former two classes of biases, class (3) is intrinic and the only way to reduce its effect is to minimize the mount of material in the spectrometer. In the momentum range accepted by the experiment, the differential change in the particle and antiparticle cross section is less than 5%. Because the experiment will have approximately 1.5% of an interaction length of material, this bias will give a false asymmetry A' of about 7 x 10^{-5}.

In order to get a quantitative estimate of the effects of the first two classes of biases on the CP asymmetry measurement, pairs of Ξ^- data sets from a previous experiment, E756, with large acceptance differences in the laboratory and polarization differences are used to compare their proton distributions in the Λ^0 rest frame. Since all of the events are Ξ^-'s, any difference between the proton distributions is solely due to acceptance differences between the two samples and not due to CP violation. No attempt was made to correct for acceptance before the comparison of the data sets. Approximately 14 millions of $\Xi^- \rightarrow \Lambda^0\pi^- \rightarrow p\pi^-\pi^-$ events were analyzed. Down to the 10^{-3} level, none of the biases due to acceptance differences in the laboratory or polarization differences caused any difference in the proton distributions. The biases have such a small impact on the CP observable measurement is due to the fact that the proton and antiproton angular distributions are in the parent helicity frames which are changing from event to event. Any fixed asymmetry in the apparatus does

not uniquely map into a particular region of the $cos\theta$ distributions of interest. By extrapolation from the studies of the E756 data, these two kinds of biases will contribute less than 10^{-4} to the measurement of A' in E871.

4. Conclusion

Searching for CP violation outside K_L^0 decays is a very important and challenging issue in particle physics. Nonleptonic decays of hyperons and their antiparticles provide us an opportunity to address this outstanding problem. Current limits in testing CP invariance in hyperon decay are poor, only at the 10^{-2} level. There is no dedicated experiment with better precision in the near future except experiment E871 at Fermilab. The results from E871 will certainly play an important role in defining the future program in the study of CP non-conservation in hyperon decay.

5. Acknowledgements

I would like to thank the organizer, Brad Cox, for inviting me to participate in this interesting workshop. I also would like to express my gratitude to Craig Dukes, David Hertzog, Sandip Pakvasa, and Mahiko Suzuki for many fruitful discussions. This work was supported by the Department of Energy.

6. References

1. T. D. Lee, R. Oehme, and C. N. Yang, Phys. Rev. **106**, 340 (1957).
2. S. Okubo, Phys. Rev. **109**, 984 (1958).
3. A. Pais, Phys. Rev. Lett. **3**, 242 (1959).
4. J. W. Cronin and O. E. Overseth, Phys. Rev. **129**, 1795 (1963); O. E. Overseth and R. F. Roth, Phys. Rev. Lett. **19**, 391 (1967); W. E. Cleland et al., Phys. Lett. **B26**, 45 (1967).
5. E. Commins and P. Bucksbaum, *Weak Interactions of Leptons and Quarks* (Cambridge, New York, 1983).
6. T. Brown, S. F. Tuan, and S. Pakvasa, Phys. Rev. Lett. **51**, 1823 (1983); L. L. Chau and H. Y. Cheng, Phys. Lett. **B131**, 202 (1983); J. F. Donoghue and S. Pakvasa, Phys. Rev. Lett. **55**, 162 (1985); J. F. Donoghue, X. G. He, and S. Pakvasa, Phys. Rev. **D34**, 833 (1986); J. F. Donoghue, B. R. Holstein, and G. Valencia, Phys. Lett. **B178**, 319 (1986); M. J. Iqbal and G. A. Miller, Phys. Rev. **D41**, 2817 (1990); X. G. He, H.

Steger, and G. Valencia, Phys. Lett. B272, 411 (1991).
7. X. G. He and S. Pakvasa, 1994 preprint, UH-511-802-94, OITS-550; and references therein.
8. L. Wolfenstein, Phys. Rev. Lett. **13**, 562 (1964); T. Brown, N. Desphande, S. Pakvasa, and H. Sugawara, Phys. Lett. **B141**, 95 (1984); R. N. Mohapatra, J. C. Pati, and L. Wolfenstein, Phys. Rev. **D11**, 3319 (1975).
9. Particle Data Group, Phys. Rev. **D50**, 1173 (1994).
10. P. Chauvat et al., Phys. Lett. **B163**, 273 (1985).
11. M. H. Tixier et al., Phys. Lett. **B212**, 523 (1988).
12. P. D. Barnes et al., Phys. Lett. **B199**, 147 (1987).
13. P. D. Barnes et al., Nucl. Phys. **A526**, 575 (1991).
14. N. Hamann et al., 1992 CERN preprint, CERN/SPSLC 92-19.
15. S.Y. Hsueh, Nucl. Phys., A558, 561c (1993).
16. E. M. Gonzalez-Romero, **A558**, 579c (1993); E. Gonzalez and J. I. Illana, 1994 CERN preprint, CERN-PPE/94-33.
17. J. Antos et al., Fermilab E871 proposal, March 26, 1994.

SESSION IV

- M. Purohit
  Charm Results from E791
- T. Handler
  Hadronic Decay of Charm Mesons: Results from E687
- C. Lazzeroni
  Study of Charm Correlations in π^- - N Interactions at $\sqrt{s} \approx 26$ GeV
- V. Kekelidze
  Observation of Charmed Baryon Λ^+_c and Ξ^+_c Decays

Frascati Physics Series, Vol. III (1994)
HEAVY QUARKS AT FIXED TARGET
University of Virginia, October 7–10, 1994
(pp. 97–105)

Charm Results from E791

Milind Purohit*
Department of Physics & Astronomy, University of South Carolina

ABSTRACT

Preliminary results from Fermilab experiment E791 are presented. Results are available on $D^0 - \overline{D}^0$ mixing, on the Doubly Cabibbo Suppressed Decays (DCSD) $D^+ \to K^+\pi^+\pi^-$ and $D^+ \to K^+K^+K^-$, on a search for the Flavor Changing Neutral Current (FCNC) decay $D^+ \to \pi^+\mu^+\mu^-$, and on asymmetries in charm production. We comment on upcoming results.

1. Introduction

E791, a fixed-target pion-production charm experiment used a 10.5 Mbytes/s data acquisition system[1] and logged over 20,000,000,000 events to tape in our 1991-92 run. The experiment used a segmented target with five thin foils (each about 1.2 mm thick) with about 1.5 cm center-to-center separation. This target configuration allowed us to select charm decays outside the target with high efficiency thereby suppressing the large background due to secondary interactions. Six 25-μm pitch silicon micro-strip planes in the beam and 17 silicon micro-strip planes downstream of the target comprised our vertex detector.

Reconstruction of the large data sample collected is now complete and stripping of the reconstructed data into smaller subsets suitable for data analysis will be complete by Dec. 1994. Most analyses available at the present time use between 1/3 to 2/3 of the data set.

The high statistics of our sample allow us to study new branching modes and determine branching ratios. However, present interest focuses on searches for rare decays which have eluded us in the past. In this context our most interesting results are the searches for FCNC in the $D^+ \to \pi^+\mu^+\mu^-$ channel, for $D^0 - \overline{D}^0$ mixing and for DCSD in the $D^+ \to K^+\pi^+\pi^-$ and $D^+ \to K^+K^+K^-$ modes. We have also used our high statistics to examine antiparticle / particle asymmetries in charm production. These results are summarized below.

*Representing the E791 Collaboration: Centro Brasileiro de Pesquisas Fisicas, Brazil, University of California, Santa Cruz, University of Cincinnati, CINVESTAV, Mexico, Fermilab, Illinois Institute of Technology, Kansas State University, University of Mississippi, Princeton University, Universidad Autonoma de Puebla, Mexico, Tel Aviv University, Israel, University of South Carolina, Tufts University, University of Wisconsin, Yale University.

2. Search for FCNC in the $D^+ \to \pi^+\mu^+\mu^-$ mode

Evidence for flavor changing neutral currents would, of course, present an exciting window into physics beyond the standard model. Such decays have been extensively searched for in rare kaon decays where experiments have continually improved the limits thereby ruling out exchange bosons up to masses of around 100 TeV/c^2. However, it is possible that different bosons mediate the exchange in charm FCNC decays. The present PDG limit[2] for the $D^+ \to \pi^+\mu^+\mu^-$, for instance, is 2.9×10^{-3}.

In searching for this decay we used the Cabibbo-favored decay $D^+ \to K^-\pi^+\pi^+$ for normalization. All cuts are identical on the search sample as well as this normalization sample except for muon identification cuts. We require the secondary vertex to be well separated from the primary vertex and from target foils. Decay tracks must have a significant impact parameter to the primary and the momentum transverse to the D^+ line of flight must be less than 250 MeV/c.

Muons are identified by a set of scintillation hodoscopes downstream of shielding equivalent to 2.5 metres of steel. Muon candidates are required to have a minimum momentum of 7 GeV/c and are tagged by a scintillation counter hit. The hit counter must have an edge within 1.64 multiple-scattering σ of the predicted position. The two oppositely charged muon candidates are not allowed to be tagged by the same counter.

The mass-dependence of the background is assumed to be the same as the normalizing signal prior to muon identification cuts and the background rate is estimated by the effect of the muon requirements on the wings of the $D^+ \to K^-\pi^+\pi^+$ signal. By this procedure we determine the upper limit on B($D^+ \to \pi^+\mu^+\mu^-$) to be 2×10^{-5}. Since this conference however, we have revised this estimate upwards by a factor of about 2 - 3. For figures and other details the reader is referred to a talk on this topic by M. Sokoloff[3] in these proceedings.

3. $D^0 - \overline{D}^0$ mixing

$D^0 - \overline{D}^0$ mixing is expected to be very small in the standard model which predicts mixing rates in the range 10^{-10} to 10^{-7}. This provides us with a large window to study effects beyond the standard model. For instance, recently Lawrence Hall and Steven Weinberg[4] have explored the consequences of an extension of the standard model involving charged Higgs bosons. They predict an extremely small amount of direct CP violation in neutral kaon decays and also very small CP violating effects in decays of B mesons. Interestingly however, they predict a large amount ($\sim$ 0.2%) of $D^0 - \overline{D}^0$ mixing. Other models also predict large $D^0 - \overline{D}^0$ mixing relative to the standard model. These include supersymmetric models, models involving a fourth generation and models with left-right symmetry,[5,6]

Recently CLEO II[7] published evidence for a wrong-sign signal in the decays of a D^0 to a charged Kaon and a charged pion. The expected sign ("right-sign") is tagged by choosing decays of the D^0 from $D^{*\pm}$ mesons and using the charge of the D^* as a tag. These wrong sign decays could be due to the Doubly Cabibbo Suppressed decays $D^0 \to K^+\pi^-$ or due to mixing in which the D^0 mixes to a $\overline{D}^0$ before decay. CLEO II

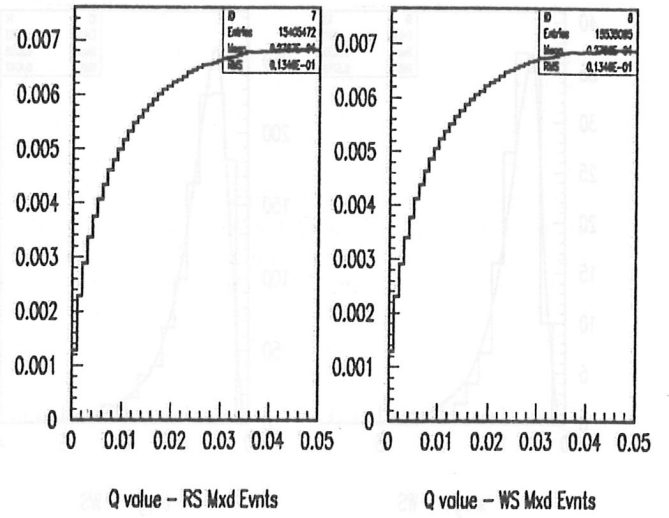

Fig. 1. The q-value distribution for D^0's combined with random pions from other events, for both right and wrong signs.

cannot distinguish between these possibilities but find that

$$\frac{\Gamma(D^0 \to K^+\pi^-)}{\Gamma(D^0 \to K^-\pi^+)} = (0.77 \pm 0.25 \pm 0.25)\%$$

E791, like the other fixed-target experiments E687, E691 etc. can distinguish between DCSD and mixed decays by using the different time-dependence of the two decays. DCSD decays should have the usual exponential time decay while mixed decays, in a simple approximation, should behave like $t^2 \exp(-t/\tau)$ which peaks at $2\tau = 0.83$ps. For comparison, our resolution in lifetime is around 0.04 ps.

We examine our D^0 decays to $K\pi$ in both the right- and wrong-sign by using the D^* (or, equivalently, the pion from the D^*) as a tag as described above. We fit simultaneously to the D^0 mass, the q-value in the D^* decay and the proper time of the D^0 decay. The fit includes various terms. For instance, there is a term which describes the Cabibbo-favored right sign decays. This term has the exponential decay time distribution and Gaussians which describe the D^0 mass and D^* q-value. The main background in wrong-sign decays comes from combining D^0's with wrong-sign pions. This background can be studied using D^0's from one event and pions from other events using our data. The resultant shape is shown in figure 1 and provides a good fit to our actual background. We do a 3-dimensional maximum likelihood fit and the resultant fit quality can be judged by the plots in figure 2 which show the fit overlayed on time distributions of the wrong-sign data.

Very preliminary results of this fit using 1/3 of our data in the $K\pi$ mode and

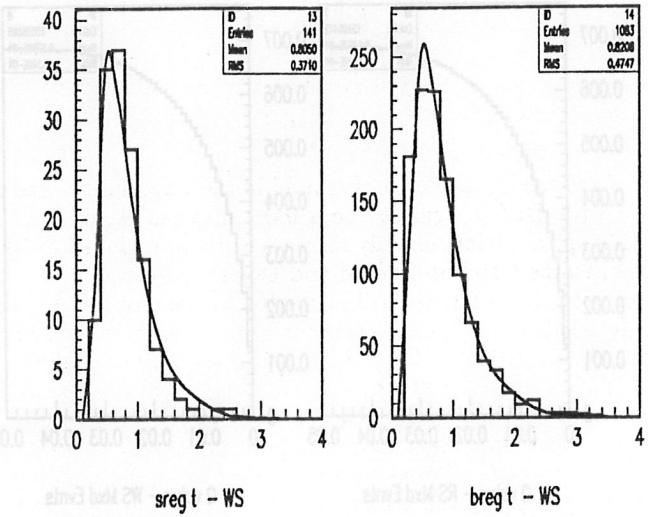

Fig. 2. Projections of the fit to the wrong sign time distributions in the signal and background regions. Both histograms show the proper time in units of picoseconds.

1/4 of our data in the $K\pi\pi\pi$ mode (being carried out by Guy Blaylock at UC, Santa Cruz) are listed below.

In the $K\pi$ mode when we do not allow interference between DCSD decays and mixing, we get a limit of 0.5% for $r_{\rm mix}$ which is defined as the ratio

$$r_{\rm mix} \equiv \frac{\Gamma(D^0 \to \overline{D}^0 \to \overline{f})}{\Gamma(D^0 \to f)}$$

When we allow DCSD and mixing terms to interfere, we get a limit of 1.0%. Similarly, in the $K\pi\pi\pi$ mode, we get limits of 0.3% and 3.0% with and without interference allowed. In the $K\pi$ mode, the limit on DCSD decays is $r_{\rm DCSD} < 2.7\%$ at the 90% CL. (The fit gives $r_{\rm DCSD} = (1.9^{+0.6}_{-0.8})\%$ which is consistent with the CLEO result $r_{\rm DCSD\ /\ mix} = (0.77 \pm 0.25 \pm 0.25)\%$.

4. DCSD decays

DCSD decays of D mesons are naively expected to occur at a rate of $\tan^4\theta_c$ relative to the Cabibbo-favored decays, but can be enhanced in the decays of the D^+. This is because the usual hadronic decays of the D^+ are suppressed due to interference of the color-allowed and color-suppressed spectator diagrams. This interference does not occur for DCSD decays.

We can now report on a preliminary analysis of ~40% of E791's data set which has now been completed.[8] Since the DCSD signal is expected (and known) to be small

compared to the Cabibbo-favored signal, the analysis requires much tighter cuts than those used for the Cabibbo-favored decay $D^+ \to K^-\pi^+\pi^+$. The tighter cuts ensure lower backgrounds. The analysis is further complicated by reflections due to particle misidentification from decays such as $D^+ \to K^-\pi^+\pi^+$ and $D_s^+, D^+ \to K^-K^+\pi^+$.

In searching for the DCSD signal, we tuned our analysis cuts using the Cabibbo-favored signal by maximizing the quantity $5 \times \tan^4\theta_C \times S/\sqrt{5 \times \tan^4\theta_C \times S + B}$, (where S and B are the signal and background in the Cabibbo-favored mode) since we naively expected the DCSD signal to be a few times $\tan^4\theta_C$ of the Cabibbo-favored signal. After this optimization, exactly the same cuts are applied (with one exception discussed below) to the Cabibbo-favored and DCSD samples.

The main cuts are as follows. All decay tracks are required to travel through at least one magnet, to have a χ^2/DOF less than 5 and a contribution of greater than 25 to the χ^2 if they are forcibly included in the primary vertex fit. The decay vertex is required to be at least 20σ downstream of the production vertex, the p_T-balance around the D flight direction is required to be less than 250 MeV/c, the impact parameter of the D-meson is required to be less than 30 microns at the production vertex, no more than one additional track is allowed within 50 microns of the D decay vertex and the decay vertex is required to be at least 2σ outside any target. Further, the product of the ratios of each decay track's impact parameter to the secondary and primary vertices is required to be less than 0.001.

In the Cabibbo-favored decays, the kaon was identified by charge alone as the particle with charge opposite to that of the D-meson. In the DCSD decays, of the two particles with the same charge as the D-meson the kaon was taken to be the one with larger Čerenkov probability to be a kaon. In both cases however, tracks considered pions are required to have a pion Čerenkov probability greater than 0.55 and similarly the kaon is required to have a kaon probability greater than 0.30. In Figure 3 we show the invariant mass distribution for the Cabibbo-favored decays $D^+ \to K^-\pi^+\pi^+$.

Using Monte Carlo we showed that the background contributions from the decays $\overline{D}^0 \to K^+\pi^+\pi^-\pi^-$, $\overline{D}^0 \to K^+\pi^-$, $\overline{D}^0 \to K^+\pi^-\pi^0$, $D^+ \to \pi^+\pi^-\pi^+$, $D^+ \to K^-\pi^+\pi^+\pi^0$, $D_s^+ \to \phi e^+\nu_e$ and $\Lambda_c^+ \to pK^-\pi^+$ were all negligible. However, the 3-body decays $D^+ \to K^-\pi^+\pi^+$ and $D_s^+, D^+ \to K^-K^+\pi^+$ contribute significantly to the background. Therefore, we *explicitly cut out* such decays by discarding events which have a candidate $KK\pi$ or Cabibbo-favored $K\pi\pi$ mass in the signal region. Figures 4a and 4b show the candidate DCSD events with the alternate 3-body mass hypotheses just described. It is clear that there is significant contamination. Events that fall in the shaded regions are removed. However, these cuts remove not only the true $K^+\pi^+\pi^-$ and $K^+K^-\pi^+$ decays from D-mesons but also background under those peaks. Hence parts of the "true" (or combinatoric) background under the candidate DCSD signal are also removed.

We have simulated the resulting background shape in three different ways: (1) by mixing D decay tracks from different data events, (2) from Monte Carlo and (3) by fitting the background away from peaks in two-dimensional plots with the DCSD mass on one axis and the reflected mass on the other. All three methods give identical results within errors and we choose the fitting technique to obtain our central values. Figure 5a shows the DCSD invariant mass with the shaded region showing the expected background shape. It is clear that there is a 4σ signal.

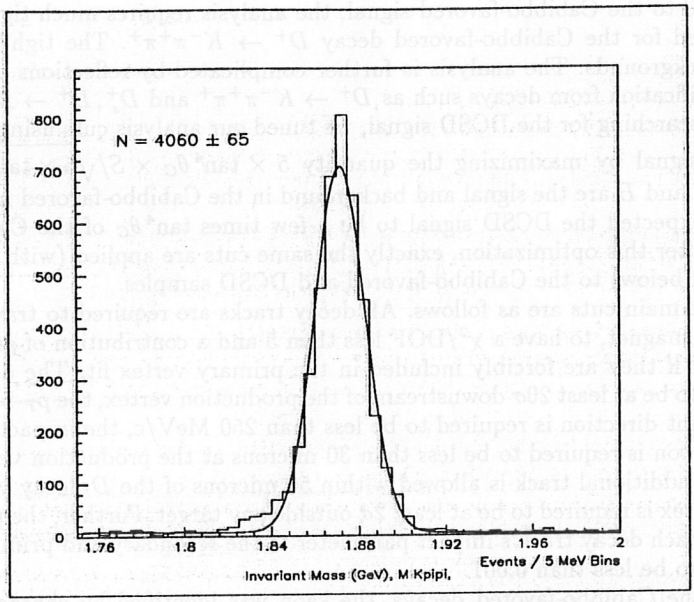

Fig. 3. Invariant mass distribution for the Cabibbo-favored decay $D^+ \to K^-\pi^+\pi^+$ from ~40% of the E791 data sample. This is used as normalization for the doubly Cabibbo-suppressed signal.

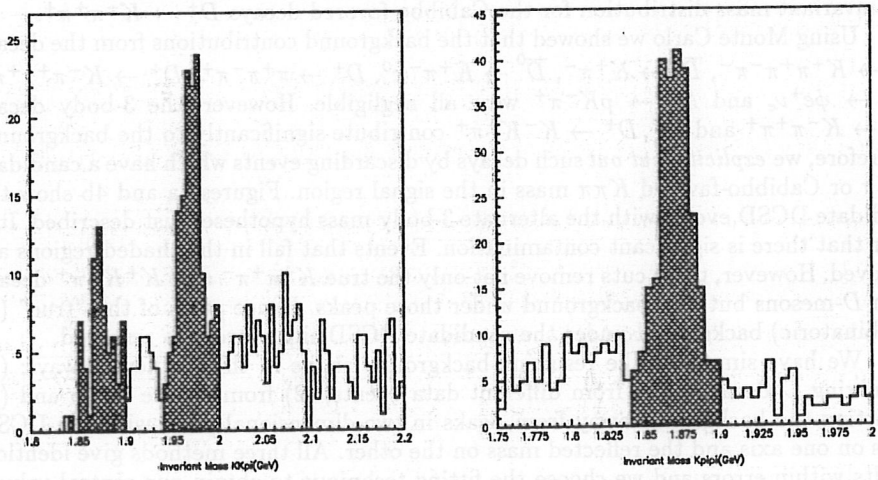

Fig. 4. The DCSD candidate events with a) a $K^-K^+\pi^+$ mass hypothesis and b) a $K^-\pi^+\pi^+$ mass hypothesis. Clear reflected signals can be seen in both cases. Events in the shaded regions are explicitly removed from the DCSD sample.

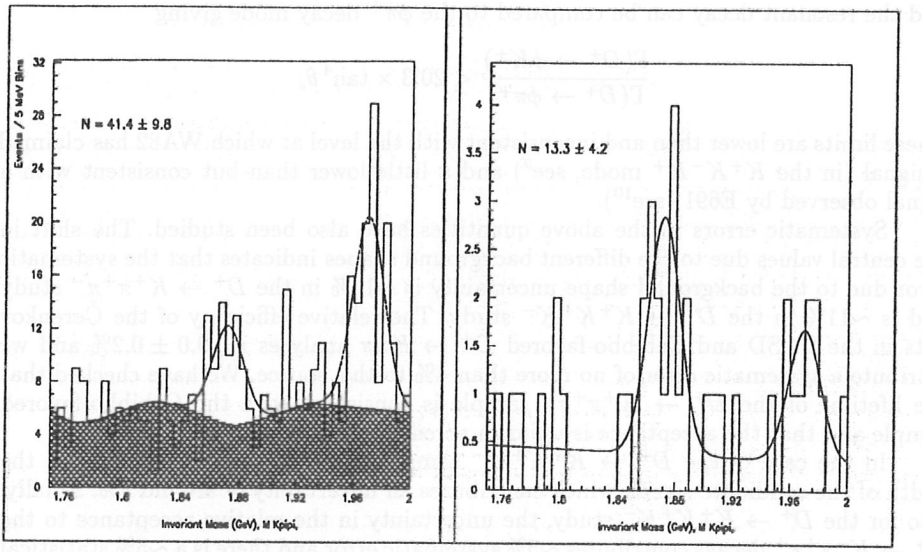

Fig. 5. Invariant mass distributions for a) the doubly Cabibbo-suppressed decay $D^+ \to K^+\pi^+\pi^-$ and b) for the doubly Cabibbo-suppressed decay $D^+ \to K^+\pi^+\pi^-$ with the $K\pi$ mass required to lie in the interval 840 - 945 MeV/c^2 and the cosine of the angle the Kaon makes with the D-direction in the K^* rest frame required to be greater than 0.5. Both figures are for data from ~40% of the E791 sample.

From fits to data displayed in the figures above, we obtain the ratio[8]

$$\frac{\Gamma(D^+ \to K^+\pi^-\pi^+)}{\Gamma(D^+ \to K^-\pi^+\pi^+)} = (3.9 \pm 0.9 \pm 0.5) \times \tan^4\theta_c$$

This is already a much better limit/signal than the Particle Data booklet[2] limit of $20 \times \tan^4\theta_c$.

A preliminary examination of the resonant subcomponents has been done and we find that

$$\frac{\Gamma(D^+ \to K^{*0}\pi^+)}{\Gamma(D^+ \to K^-\pi^+\pi^+)} < 2.9 \times \tan^4\theta_c$$

If this is considered to be a signal, we obtain

$$\frac{\Gamma(D^+ \to K^{*0}\pi^+)}{\Gamma(D^+ \to K^-\pi^+\pi^+)} = (1.9 \pm 0.6) \times \tan^4\theta_c$$

(statistical error only). Figure 5b shows the DCSD signal after the K^* selection.

Similarly, an examination of decays to three charged kaons has revealed that

$$\frac{\Gamma(D^+ \to K^+K^-K^+)}{\Gamma(D^+ \to K^-\pi^+\pi^+)} < 1.7 \times \tan^4\theta_c$$

and the resonant decay can be compared to the $\phi\pi^+$ decay mode giving

$$\frac{\Gamma(D^+ \to \phi K^+)}{\Gamma(D^+ \to \phi\pi^+)} < 20.3 \times \tan^4\theta_c$$

These limits are lower than and inconsistent with the level at which WA82 has claimed a signal (in the $K^+K^-K^+$ mode, see[9]) and a little lower than but consistent with a signal observed by E691 (see[10]).

Systematic errors in the above quantities have also been studied. The shift in the central values due to the different background shapes indicates that the systematic error due to the background shape uncertainty is ~10% in the $D^+ \to K^+\pi^+\pi^-$ study and is ~11% in the $D^+ \to K^+K^+K^-$ study. The relative efficiency of the Čerenkov cuts in the DCSD and Cabibbo-favored $D^+ \to K\pi\pi$ analyses is $99.0 \pm 0.2\%$ and we attribute a systematic error of no more than 4% to this source. We have checked that the lifetime of the $D^+ \to K^+\pi^+\pi^-$ sample is consistent with the Cabibbo-favored sample and that the acceptance is uniform across the Dalitz plot.

In the case of the $D^+ \to K^+K^+K^-$ sample, there is some uncertainty in the width of the candidate signal, which contributes an uncertainty of around 3%. Finally, also for the $D^+ \to K^+K^+K^-$ study, the uncertainty in the relative acceptance to the $D^+ \to K^-\pi^+\pi^+$ decays contributes ~5% systematic error and there is a ~5% statistical error due to Monte Carlo statistics.

5. Other analyses and future results

Using about 1/2 of our data set, we have examined the D^+ production asymmetry, i.e., the ratio

$$A \equiv \frac{N_{D^-} - N_{D^+}}{N_{D^-} + N_{D^+}}$$

With our incoming π^- ($\bar{u}$ d) beam, we expect an excess of D^- ($\bar{c}$ d) which shares a quark with the incoming particle over D^+ ($c\bar{d}$), at least in the forward direction. This effect can also be explained by next-to-leading order calculations and by the presence of intrinsic $c\bar{c}$ pairs in the target nucleon. Using over 20,000 $D^\pm$ decays, we see a definite indication of a rise of A with incresing x_F, but do not obtain good agreement with either PYTHIA[11] (string fragmentation explanation) or with the intrinsic charm model of Vogt and Brodsky.[12] Figure 6 below shows the D^+ mass plot and the A measurement compared to predictions by PYTHIA and by Vogt and Brodsky.

We continue our studies of charm production, charm semileptonic decays, rare decays, charm baryon decays etc. We are interested in measuring charm baryon lifetimes, particularly those of the Ξ_c^0, the Ξ_c^+ and the Ω_c^0. We are encouraged by the observation of over a million Ξ^- and about 16,000 Ω^- in our full data sample.

6. Acknowledgements

I would like to thank the entire E791 collaboration for their efforts in collecting and analysing these data. Special thanks to Ai Nguyen and Nick Witchey for the $\pi\mu\mu$ results, to Jim Wiener for his DCSD results, to Tom Carter for his D^+ production asymmetry results and to Guy Blaylock for his $D^0 \to K\pi\pi\pi$ mixing results. This work was supported by the U.S. Department of Energy.

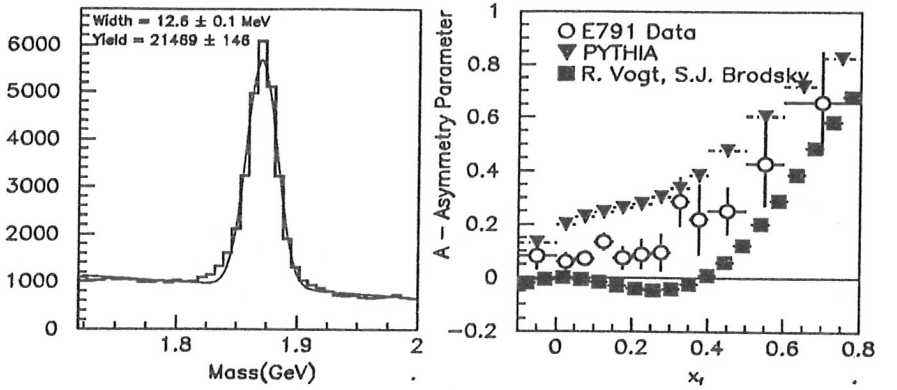

Fig. 6. a) The invariant mass distribution for all $D^+ \to K^-\pi^+\pi^+$ decays. b) The asymmetry parameter A (defined in the text) as a function of x_F and compared to model predictions.

References

1. S. Amato et al., "The E791 parallel architecture data acquisition system", NIM **A324** (1993) 535.
2. The Particle Data Group in the "Review of Particle Properties", Phys. Rev. **D50**, (1994) 1177.
3. M. D. Sokoloff "Searching for Flavor-changing Neutral Currents in Fermilab Experiments E791 and E687" in these proceedings.
4. L. Hall and S. Weinberg, Phys. Rev. **D48**, 979 (1993).
5. K. S. Babu et al., Phys. Lett. **B205**, 540 (1988).
6. E. Ma, Mod. Phys. Lett. **A3**, 319 (1988).
7. D. Cinabro et al., Phys. Rev. Lett. **72**, (1994) 1406.
8. J. S. Wiener "Doubly Cabibbo Suppressed Decays of the Charged D Meson", Princeton University Ph. D. thesis, unpublished (1994).
9. M. Adamovich et al., Phys. Lett. **B305** (1993) 177.
10. J. C. Anjos et al., Phys. Rev. Lett. **69** (1992) 2892.
11. T. Sjostrand CERN-TH.6488/92 (PYTHIA 5.6 Manual).
12. R. Vogt and S. J. Brodsky "QCD and Intrinsic Heavy Quark Predictions for Leading Charm and Beauty Hadroproduction", SLAC-PUB-6468, Apr. 1994.

Frascati Physics Series, Vol. III (1994)
HEAVY QUARKS AT FIXED TARGET
University of Virginia, October 7–10, 1994
(pp. 107–116)

Hadronic Decay of Charm Mesons: Results from E687

Thomas Handler
for the E687 Collaboration*
Physics Dept., University of Tennessee
Knoxville, TN 37996-1200

Abstract

Recent experimental results on several hadronic decay modes of D and D_s from the E687 collaboration at Fermilab are presented and compared with data from other experiments. In addition to the decay modes, branching ratios and resonance substructure analyses will be presented.

1 - Introduction

The E687 collaboration has collected approximately 10^5 charmed particles in the wide band photon beam at Fermilab. The mean photon beam energy was ~220 GeV. The E687 detector[1] is a large aperture spectrometer, having excellent charged particle identification and vertexing capabilities. The vertexing is done using a high resolution silicon microstrip detector. Further details concerning the E687 spectrometer can be found in Reference [1]. The E687 experiment is characterized by its good statistics and a good understanding of the systematics of its detector. In addition to the topics presented in this talk, other results on semi-leptonic decays. lifetimes, baryonic states and photoproduction dynamics from E687 are available.

2 - Hadronic Decays of D and D_s

The importance of final state interactions and non-spectator contributions to the decay of D mesons can be addressed through the hadronic decays of the D mesons.

---

* Co-authors are: P. L. Frabetti, **Bologna**; H. W. K.Cheung, J. P. Cumalat, C. Dallapiccola, J. F. Ginkel, S. V. Greene, W. E. Johns, M. S. Nehring, **Colorado**; J. N. Butler, S. Cihangir, I. Gaines, P. H. Garbincius, L. Garren, S. A. Gourlay, D. J. Harding, P. Kasper, A. Kreymer, P. Lebrun, S. Shukla, M.Vittone, **Fermilab**; S. Bianco, F. L. Fabbri, S. Sarwar, A. Zallo, **Frascati**; R. Culbertson, R. W. Gardner, R. Greene, J. Wiss, **Illinois**; G. Alimonti, G. Bellini, B. Caccianiga, L. Cinquini, M. Di Corato, M.Giammarchi, P. Inzani, F. Leveraro, D. Menasce, E. Meroni, L. Moroni, D. Pedrini, L. Perasso, A. Sala, S. Sala, D. Torretta, **Milano**; D. Buchholz, D. Claes, B. Gobbi, B. O'Reilly, **Northwestern**; J. M. Bishop, N. M. Cason, C. J. Kennedy, G. N. Kim, T. F. Lin, D. L. Puseljic, R. C. Ruchti, W. D. Shephard, J. A. Swiatek, Z. Y. Wu, **Notre Dame**; V. Arena, G. Boca, C. Castoldi, G. Gianini, S. Malvezzi, S. P. Ratti, C. Riccardi, P. Vitulo, **Pavia**; A. Lopez, **Puerto Rico**; G. P. Grim, V. S. Paolone, P. M. Yager, **U. C. Davis**; J. R. Wilson, **South Carolina**; P. D. Sheldon, **Vanderbilt**; F. Davenport, **North Carolina**; G. R. Blackett, K. A. Danyo, M. Pisharody, **Tennessee**; B. G. Cheon, J. S. Kang, K. Y. Kim, **Korea**

2.1 - $D^0 \rightarrow K^+K^-$ and $\pi^+\pi^-$

The data sample[2] for these two decays consists of 580 ± 39 events for the decay $D^0 \rightarrow K^+K^-$ and 179 ± 31 events for the decay $D^0 \rightarrow \pi^+\pi^-$ yielding a ratio of

$$\frac{\Gamma(D^0 \rightarrow K^+K^-)}{\Gamma(D^0 \rightarrow \pi^+\pi^-)} = 2.53 \pm 0.46 \pm 0.19.$$

This result is consistent with other experimental results which are presented in Table I.

Table I

Mark II[3]	3.4 ± 1.8
Mark III[4]	3.7 ± 1.4
ARGUS[5]	2.5 ± 0.7
CLEO[6]	2.35 ± 0.37 ± 0.28
E691[7]	1.95 ± 0.34 ± 0.22
WA82[8]	2.23 ± 0.81 ± 0.46

What is expected for this decay ratio? Theoretical models[9] with SU(3) breaking predict a value of approximately 1.4. This is clearly in disagreement with the measured results. Several theoretical approaches have been tried to more closely approximate the measured value for this relative branching ratio. Theoretical calculations[10] using final state interactions which shift the relative rates into the various two body channels differently for $\pi\pi$ and KK final states have been tried. Other theoretical calculations[11] use penguin diagrams which interfere destructively for $\pi\pi$ but constructively for KK

2.2 - $D^0 \rightarrow \overline{K}^0K^0$ and $K_s^0K_s^0K_s^0$

Simple spectator diagrams do not contribute to these two decay modes and therefore provide information about the importance of other decay processes[12]. The decay $D^0 \rightarrow K_s^0K_s^0K_s^0$ is Cabibbo allowed and could possibly be due to W exchange. The decay $D^0 \rightarrow \overline{K}^0K^0$ probably occurs through final state interactions as the two possible W exchange diagrams for this decay almost cancel due to the Glashow-Iliopoulos-Maiani mechanism.

E687 has measured the rates for the these two decay processes relative to $D^0 \rightarrow \overline{K}^0\pi^+\pi^-$. The results are presented in Table II along with the results from other experiments. As can be seen they are all in relative agreement.

Table II

	$\frac{\Gamma(D^0 \to \overline{K}^0 K^0)}{\Gamma(D^0 \to \overline{K}^0 \pi^+ \pi^-)}$	$\frac{\Gamma(D^0 \to K_s^0 K_s^0 K_s^0)}{\Gamma(D^0 \to \overline{K}^0 \pi^+ \pi^-)}$
ARGUS[5]	< 0.16	$0.017 \pm 0.007 \pm 0.005$
CLEO[6,13]	$0.021^{+0.011+0.002}_{-0.008-0.002}$	0.016 ± 0.005
E687[14]	$0.039 \pm 0.013 \pm 0.013$	$0.035 \pm 0.012 \pm 0.006$

2.3 - $D^{\pm}, D_s^{\pm} \to K_s^0 K^{\pm}$, $K_s^0 K^{*\pm}$, and $K_s^0 \pi^{\pm}$

The decay $D^{\pm} \to \overline{K}^0 K^{\pm}$ has a Cabibbo suppressed diagram while the decay $D^{\pm} \to \overline{K}_s^0 \pi^{\pm}$ has two Cabibbo allowed diagrams which can interfere destructively with each other. As a result of this destructive interference, final state interactions and differences in phase space, the branching ratio of the Cabibbo suppressed to Cabibbo allowed can be larger than naively expected. For the decay $D^{\pm} \to K_s^0 K^{*\pm}$, the $K^{*\pm}$ decays into $K_s^0 \pi^{\pm}$. The branching ratios relative to the decay mode $K_s^0 \pi^{\pm}$ are given in Table III.

Table III

	$D^{\pm}$	$D_s^{\pm}$
$\frac{K_s^0 K^{\pm}}{K_s^0 \pi^{\pm}}$	$0.25 \pm 0.04 \pm 0.02$ world averge[15]: 0.28 ± 0.06	
$\frac{K_s^0 \pi^{\pm}}{K_s^0 K^{\pm}}$		0.18 ± 0.21 < 0.53 (90% C.L.) existing limit[15]: < 0.21 (90% C.L.)
$\frac{\overline{K}_s^0 K^{*\pm}}{\overline{K}^0 \pi^{\pm}}$	$1.1 \pm 0.3 \pm 0.4$	< 0.9 (90% C.L.)

How do these results compare with theoretical predictions? The quark factorization model of BSW[16] predicts a value of 0.33 for the ratio of $D^+ \to \overline{K}^0 K^+$ to $D^+ \to \overline{K}^0 \pi^+$, while Kamal and Verma[17] (KV), in the frame of SU(3), taking into account final state interactions plus SU(3) breaking in the final state interactions obtain a value of 0.26. As for the D_s ratio, these two theoretical methods yield values of 0.19 and 0.068, respectively. The experimental results from E687 agree

favorably with these theoretical calculations for the $D^{\pm}$. However there seems to be some disagreement with regards to the value for the $D_S^{\pm}$ These comparisons are summarized in Table IV.

Table IV

	BSW	KV	E687
$\frac{D^{\pm} \to \overline{K}^0 K^{\pm}}{D^{\pm} \to K^0 \pi^{\pm}}$	0.33	0.26	0.25 ± 0.04
$\frac{D_s^{\pm} \to \overline{K}^0 \pi^{\pm}}{D_s^{\pm} \to \overline{K}^0 K^{\pm}}$	0.19	0.068	0.33 ± 0.14

2.4 - $D^0 \to 4\pi, K^+K^-\pi^+\pi^-, K^-K^+K^-\pi^+$

The 4π and $K^+K^-\pi^+\pi^-$ decay modes of the D^0 are both Cabibbo suppressed, while the $K^-K^+K^-\pi^+$ decay mode is Cabibbo allowed but phase space suppressed. This is the first observation of $K^-K^+K^-\pi^+$ decay mode for the D^0. The various mass spectra are presented in Figure 1. We find for the relative width for the $3K\pi$ to $K3\pi$ to be

$$\frac{\Gamma(D^0 \to K^-K^+K^-\pi^+)}{\Gamma(D^0 \to K^-\pi^+\pi^-\pi^+)} = 0.0028 \pm 0.0007 \pm 0.002.$$

For our measured relative width of the 4π to $K3\pi$ and its comparison to other experimental values, see Table V. For the measured relative width of $2K2\pi$ to $K3\pi$ and its comparison to other measured values see Table VI.

Previously we showed a comparison of the experimental data for the relative rate of $D^0 \to K^+K^-$ to $D^0 \to \pi^+\pi^-$ which was found to be $2.53 \pm 0.46 \pm 0.19$. This was above the theoretical predictions which were in the range 1.4 - 2.0. To this we can add a comparison of the rate of $D^0 \to K^+K^-\pi^+\pi^-$ to $D^0 \to \pi^+\pi^-\pi^+\pi^-$. The value that we obtain is $0.35 \pm 0.05 \pm 0.02$. Whereas the first one, with only two particles in the decay mode, was higher, the addition of a pion pair to the initial particles brings the ratio lower than the prediction. The implication of the fact that the two relative rates are not the same is that simple spectator diagrams do not dominate the decay process.

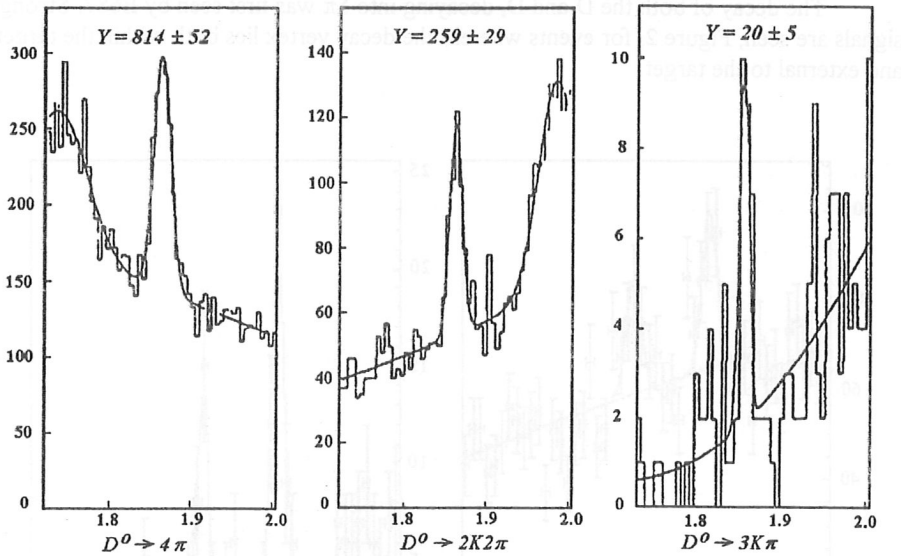

Figure 1: Four body invariant mass distributions for the D^0.

Table V

	$\frac{\Gamma(D^0 \to \pi^-\pi^+\pi^-\pi^+)}{\Gamma(D^0 \to K^-\pi^+\pi^-\pi^+)}$
E687	$0.097 \pm 0.006 \pm 0.002$
E691[18]	$0.096 \pm 0.018 \pm 0.007$
CLEO[13]	0.102 ± 0.013

Table VI

	$\frac{\Gamma(D^0 \to K^+K^-\pi^+\pi^-)}{\Gamma(D^0 \to K^-\pi^+\pi^-\pi^+)}$
E687	$0.034 \pm 0.004 \pm 0.002$
E691[18]	$0.028\ ^{+0.008}_{-0.007}$
CLEO[13]	0.0314 ± 0.010
ARGUS[19]	$0.041 \pm 0.007 \pm 0.005$

2.5 $D^{\pm}, D_s^{\pm} \rightarrow 5\pi$

The decay of both the D and D_s decaying into 5π was first seen by E687. Strong signals are seen, Figure 2, for events wherein the decay vertex lies both within the target and external to the target.

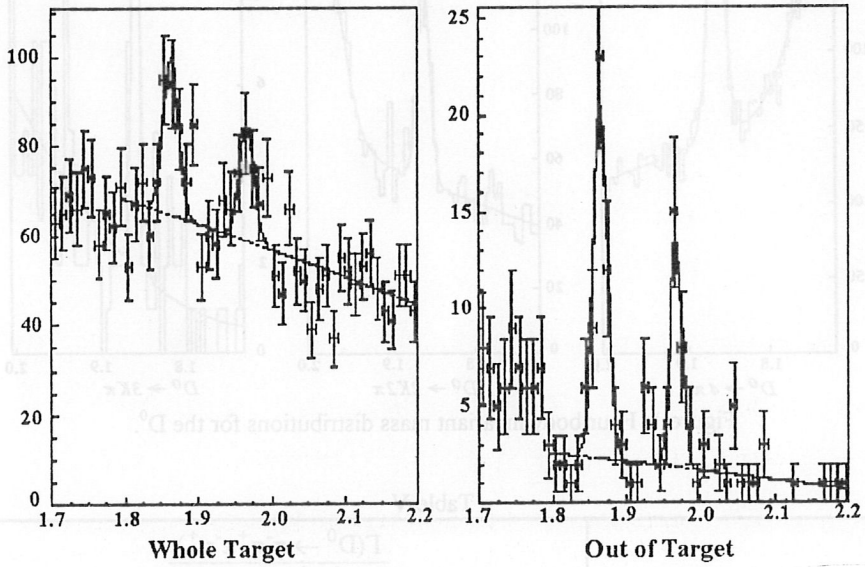

Figure 2: 5π Mass plot.

3 - Dalitz Plot Analyses

We have carried out Dalitz plot analyses on several three body decay modes of the D and D_s charmed mesons. The decay modes for which the analysis has been completed are: $D^0 \rightarrow K_s^0\pi^+\pi^-$, $D^0 \rightarrow K^-\pi^+\pi^0$, and $D^+ \rightarrow K^-\pi^+\pi^+$. Analysis is still in progress on the decays $D^{\pm}, D_s^{\pm} \rightarrow K^{\mp}K^{\pm}\pi^{\pm}$. The decay amplitude function used was of the form

$$A(D) = a_0 \exp(i\delta_0) + \sum_i a_i \exp(i\delta_i) B(abc|r)$$

with

$$B(abc|r) = BW(ab|r)L(a,c)$$

and

$$BW(ab|r) = \frac{F_D F_r}{M_r^2 - M_{ab}^2 - i\Gamma M_r}$$

and L(a,c) a spin dependent function

3.1 - General Observations on D to $K\pi\pi$

$D^0 \rightarrow K_s^0\pi^+\pi^-$

This decay mode is dominated by intermediate two-body resonances of which the $K^*(890)$ is the most prominent.

$D^0 \rightarrow K^-\pi^+\pi^0$

This decay mode is also dominated by intermediate two-body resonances with the ρ being predominate. This decay mode has consdierable non-resonant behavior.

$D^+ \rightarrow K^-\pi^+\pi^+$

This decay mode for the D^+ is dominated by the non-resonant behavior.

The E687 results[20] agree with E691 as far as the branching ratios are concerned but not with the phases. For a complete list of the fitted decay fractions, the relative phases and the branching ratios please see Reference [20].

3.2 - $D^\pm, D_s^\pm \rightarrow K^\mp K^\pm \pi^\pm$

Strong signals are seen for both the $D^\pm$ and $D_s^\pm$ in the $KK\pi$ invariant mass plots, Figure 3. Preliminary Dalitz plot fits indicate that the presence of ϕ, K^{*0} and non-resonant behavior. To get a satisfactory fit to the Dalitz plot it is necessary to include the $f_0(975)$. The non-resonant contribution is small for the $D_s^\pm$ while for the $D^\pm$ it is comparable to the ϕ, K^{*0}.

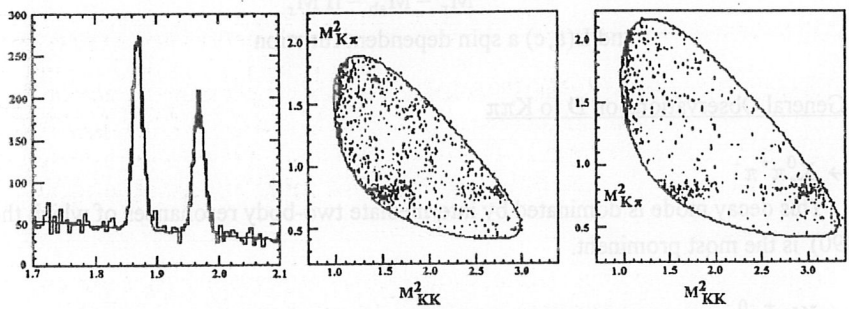

Figure 3: Invariant Mass plot for KKπ and Dalitz plots for D and D_s.

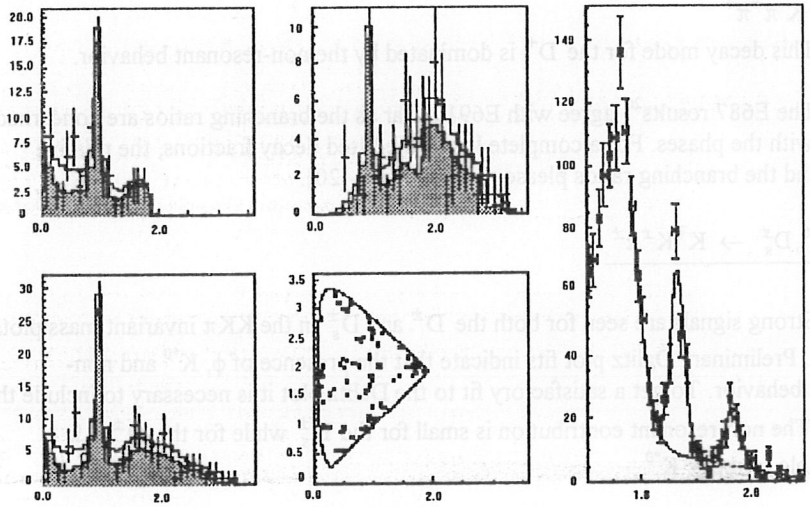

Figure 4: Invariant mass plot for 3π and Dalitz plot for D_s.

3.3 - $D^{\pm}, D_s^{\pm} \rightarrow 3\pi^{\pm}$

Clean $D^{\pm}$ and $D_s^{\pm}$ signals can be observed in the 3π invariant mass plot, Figure 4. A Dalitz plot analysis is under way with preliminary results indicating that $f_0(975)$ dominates as can be seen in the D_s Dalitz plot.

4 - CP Violation

It has been suggested[21] that CP violation would be significantly enhanced in the decays of charmed particles. This violation would show itself as an asymmetry in the decay rates of CP conjugate states. It is also required that two independent weak decay amplitudes contribute to same final state and that final state interactions should induce a strong phase shift between the two weak amplitudes.

It is necessary to account for the differing D and $\overline{D}$ production rates in this experiment. To do this, the decay rate asymmetry can be written as

$$A_{cp} = \frac{\eta(D) - \eta(\overline{D})}{\eta(D) + \eta(\overline{D})},$$

with η being the decay channel yield normalized to a Cabibbo allowed channel.

The E687[22] measured limits are given in Table VII

Table VII

Decay	Limit at 90% C.L.
$D^0 \rightarrow K^-K^+$	$-11\% < A_{cp} < 16\%$
$D^+ \rightarrow K^-K^+\pi^+$	$-14\% < A_{cp} < 8.1\%$
$D^+ \rightarrow \overline{K}^{*0}K^+$	$-33\% < A_{cp} < 9.4\%$
$D^+ \rightarrow \phi\pi^+$	$-7.5\% < A_{cp} < 21\%$

References

1 . P. L. Frabetti et al., Nucl. Instrum. Methods **A320**, 519 (1992).
2 . P. L. Frabetti et al., Phys. Lett. **B321**, 295 (1994).
3 . G. S. Abrams et al., Phys. Rev. Lett. **43**, 481 (1979).
4 . R. M. Baltrusaitis et al., Phys. Rev. Lett. **55**, 150 (1985).

5 . H. Albrecht et al., Z. Phys. **C46**, 9 (1990).
6 . J. Alexander et al., Phys. Rev. Lett. **65**, 1184 (1990).
7 . J. C. Anjos et al., Phys. Rev. **D44**, R3371 (1991).
8 . M. Adamovich et al., Phys. Lett. **B280**, 163 (1992).
9 . A. Buras et al., Nucl. Phys. **B268**, 16 (1986);
M. Bauer et al., Z. Phys. **C34**, 103 (1987).
10 . A. N. Kamal et al., Phys. Rev. **D35**, 3515 (1987);
Phys. Rev. **D36**, 3510 (1987);
A. Czarnecki et al., Z. Phys. **C54**, 411 (1992);
L. L. chau et al., Phys. Lett. **B280**, 281 (1992).
11 . M. Gluck, Phys. Lett. **B88**, 145 (1979);
J. Finjord, Nucl. Phys. **B181**, 74. (1981)
12 . X. Y. Pham, Phys.Lett. **B193**, 331 (1987);
H. J. Lipkin, Phys. Rev. Lett. **44**, 710 (1980).
13 . H. Ammar et al., Phys. Rev. **D44**, 3383 (1991).
14 . P. L. Frabetti et al., Submitted to Physics Letters.
15 . Particle Data Group, K. Hikasa et al., Phys. Rev. **D45**, 1 (1992).
16 . M. Bauer et al., Z. Phys. **C34**, 103 (1987).
17 . A. Kamal and R. Verma, Phys. Rev. **D35**, 3515 (1987).
18 . J. C. Anjos et al., Phys. Rev. **D43**, R635 (1991).
19 . ARGUS Coll. preprint DESY 94-052.
20 . P. L. Frabetti et al., Phys. Lett. **B331**, 217 (1994).
21 . M. Golden and B. Grinstein, Phys. Lett. **B222**, 501 (1989).
F. Buccella et al., Phys. Lett. **B302**, 319 (1993).
22 . P. L. Frabetti et al., Phys. Rev. **D50**, R2953 (1994).

Frascati Physics Series, Vol. III (1994)
HEAVY QUARKS AT FIXED TARGET
University of Virginia, October 7–10, 1994
(pp. 117–126)

STUDY OF CHARM CORRELATIONS IN $\pi^- - N$ INTERACTIONS AT $\sqrt{s} \approx 26$ GeV

Cristina Lazzeroni
Università degli Studi di Pisa and INFN-Pisa
for BEATRICE Collaboration*

ABSTRACT

We report on the associated production of charmed hadrons in π^- nucleon interactions at $\sqrt{s} \approx 26$ GeV at the CERN Ω' spectrometer. Results are presented on the azimuthal correlation of charm particle pairs and are compared to Next-to-Leading-Order QCD calculations.

1 – Introduction

Hadronic interactions at high energy are commonly described by the so called "QCD improved parton model" [1]. In this model the scattering process is the result of elementary interactions between quarks and gluons in the hadrons. At Leading Order (LO) the processes contributing to the production of heavy quark pairs are quark-antiquark annihilation and gluon-gluon fusion, the latter being dominant at $\sqrt{s} \approx 26$ GeV.

*M.Adamovich, M.Adinolfi, Y.Alexandrov, C.Angelini, C.Bacci, D.Barberis, D.Barney, J.Batten, W.Beusch, C.Bruschini, R.Cardarelli, A.Cardini, V.Casanova, F.Ceradini, G.Ciapetti, M.Dameri, G.Darbo, A.Di Ciaccio, A.Duane, J.P.Dufey, Ph.Farthouat, V.Flaminio, A.Forino, B.R.French, A.Frenkel, C.Gemme, R.Gessaroli, K.Harrison, R.Hurst, A.Kirk, F.Lacava, C.Lazzeroni, L.Malferrari, S.Maljukov, G.Martellotti, P.Martinengo, P.Mazzanti, J.G.McEwen, I.Minashvili, P.Nechaeva, A.Nisati, D.Orestano, B.Osculati, M.Passaseo, G.Penso, E.Petrolo, L.Pontecorvo, A.Quareni, P.Ragni, H.Rotscheidt, V.Ryzhov, C.Roda, L.Rossi, N.Russakovich, C.Salvo, R.Santonico, G.Schuler, A.Semenov, A.Solovjev, M.Torelli, S.Veneziano, M.Verzocchi, D.Websdale, M.Weymann, L.Zanello, M.Zavertyaev

Such LO processes produce $c\bar{c}$ pairs where the c and the $\bar{c}$ quarks are emitted back-to-back in the parton-parton centre-of-mass system. As a result the D and $\bar{D}$ particles tend to be emitted in opposite directions in the plane perpendicular to the beam. The distribution of their opening angle $\Delta\phi$ in this plane should then be sharply peaked at 180°. However, because of the relatively small mass of the charmed quark, the LO approximation may not describe adequately the production process. It may, in particular, happen that effects normally suppressed by powers of the heavy quark mass contribute in a significant way in the case of charm. Thus large contributions from Next-to-Leading-Order (NLO) corrections are likely.

Recently, detailed calculations at order $O(\alpha_S{}^3)$ of charm production in hadronic interactions have been carried out [2, 3, 4, 5]. These calculations have compared the predictions at the LO and at the NLO varying the renormalisation scale μ_R, the charm mass m_c , the parton distribution functions and Λ_{QCD}. The results show that relatively large uncertainties remain in the predictions of the charm production cross-section, when going from LO to NLO approximation. Smaller uncertainties affect the $\Delta\phi$ distribution, which should be widened by higher than NLO processes. However, other effects such as the parton transverse momentum, the radiation of soft gluons and the parton fragmentation may lead to similar broadening.

We report in this letter on a measurement of the azimuthal angle correlation of charm particle pairs produced in the reaction :

$$\pi^- + N \rightarrow \mathrm{D} + \bar{\mathrm{D}} + anything$$

at an incident momentum of 350 GeV/c.
The results are discussed in the framework of perturbative QCD and compared with other measurements done in hadroproduction and photoproduction experiments.

2 – The experimental setup

The WA92 experiment was performed at the Ω' magnetic spectrometer at CERN. The main motivation of the experiment was the study of hadroproduction of beauty particles. For this purpose the experiment was equipped with a high resolution imaging detector and a selective trigger to detect secondary vertices, charged particles emitted at large transverse momentum and leptons. The acceptance of the trigger and the capability of the detector to reconstruct decay vertices allow the selection of a large sample of fully reconstructed charmed particles.

Beam tracks were measured by 10 planes of 20 μm pitch silicon microstrip detectors (SMDs) before hitting a 2 mm thick copper target. Tracks emerging from the interaction were measured using a vertex detector, which consisted of 12 planes of 25 μm pitch and 5 planes of 50 μm pitch SMDs. The region between the target and the vertex detector, where most of the beauty and charm decays occur, was equipped with 17 10 μm pitch analogue readout SMDs closely packed so as to give a high resolution picture of the event. This device, named decay detector (DkD) [6], allows the detailed reconstruction of beauty and charm decays. The target and the SMDs were located upstream of the Ω' spectrometer in a region of very low magnetic field.

The Ω' spectrometer consists of several drift and multiwire proportional chambers placed in a 1.8 T dipolar magnetic field giving a $\Delta p/p^2$ resolution of 1.6 10^{-4} $(\mathrm{GeV}/c)^{-1}$. A lead-glass electromagnetic calorimeter and a muon filter [7] follow the magnetic spectrometer, as shown schematically in figure 1. Between the spectrometer and the calorimeter a finely segmented butterfly-shaped scintillator hodoscope [8] is used to select charged particles emitted at large transverse momentum.

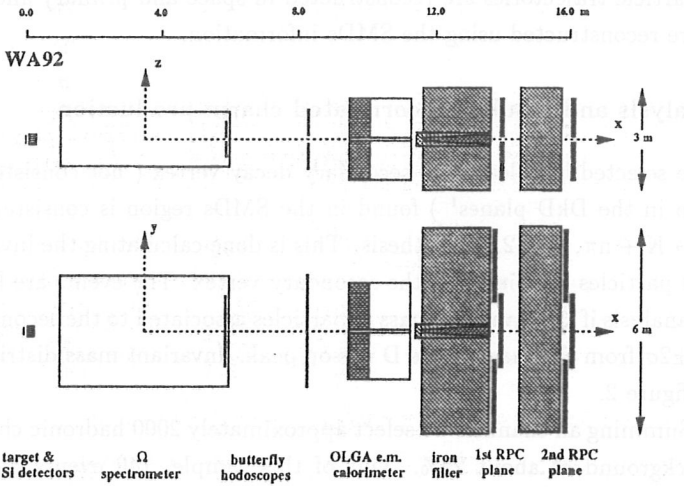

Figure 1: Schematic view of the WA92 setup.

We used a multilevel trigger; events are recorded if at least two of the following conditions are verified simultaneously:

- At least one secondary vertex is present in the DkD region. The search for secondary vertices is done by a fast processor that selects tracks with large impact parameter with respect to the interaction vertex [9, 10].
- There is at least one charged particle with a $p_T > 0.6$ GeV/c with respect to the beam direction.
- There is at least one muon pointing to the interaction region.

The rejection factor of the trigger for minimum bias event is about 30, the acceptance for charm events is about 10%.

The experiment has collected data during two periods, in 1992 and in 1993, when 90 million and 60 million triggers where recorded on tape respectively. Results presented here refer only to half of the 1992 data sample.

The data were processed in two steps. In the first step events are passed through a filter, which verifies the trigger conditions by means of a fast reconstruction program which is able to reject some trivial background that escaped the online processors. This step reduces the data sample by a factor of three. In the second step charged particle trajectories are reconstructed in space and primary and secondary vertices are reconstructed using the SMDs information.

3 – Analysis and results on correlated charm production

Events are selected if at least one secondary decay vertex (not consistent with an interaction in the DkD planes[1]) found in the SMDs region is consistent with the decay $D \to K + n\pi$, n=1,2,3 hypothesis. This is done calculating the invariant mass of charged particles associated to the secondary vertex. The events are kept for the following analysis if the invariant mass of particles associated to the secondary vertex is within $\pm 2\sigma$ from the mass of the D meson peak. Invariant mass distributions are shown in figure 2.

Summing all channels we select approximately 2000 hadronic charm decays over a background of about 25%. Out of this sample, 140 events have another secondary vertex reconstructed in the SMDs region. It is first checked that these secondary vertices identified only topologically are not due to an interaction in the DkD planes or to a decay of a strange hadron. In addition a cut has been applied

[1] An interaction is recognized because of the high energy release in the silicon detector due to a nuclear break-up.

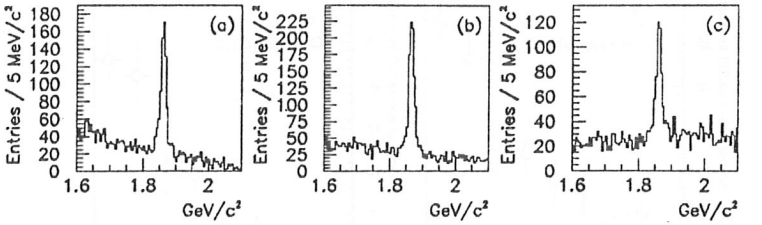

Figure 2: Invariant mass distributions: $D^o \to K^-\pi^+$ (a), $D^+ \to K^-\pi^+\pi^+$ (b), $D^o \to K^-\pi^-\pi^+\pi^+$ (c) and charge conjugate hypothesis: a clean peak corresponding to D mesons is visible over a combinatorial background.

on the distance R between the two secondary vertices in the plane perpendicular to the beam direction. The rejection of events with R < 100 μm has been chosen on the basis of the distribution of errors on vertex coordinates in this plane. As a result of this cut the error on the azimuthal angle difference has a mean value of 1 degree and is always much smaller than 10 degrees.

These cuts reduce the sample to 113 events. A further reduction has been performed through a visual scanning of the events in the SMDs, looking for possible tracking or vertex finding errors. After this step the sample reduces to 102 events compatible with the $D\bar{D}$ hypothesis. This will be referred to in the following as the signal sample.

The background left after these selections has been evaluated as follows. Two-secondary-vertex events have been selected requiring one of the two vertices to have 2, 3 or 4 prongs and a K nπ (n=1,2,3 as appropriate) effective mass in the D side band (1.75 < M < 1.80 GeV/c^2 or 1.94 < M < 2.1 GeV/c^2) and subsequently applying the same cuts used for the signal sample. All distributions relative to the control sample have been normalised to 25% of the signal sample.

The azimuthal angle difference $\Delta\phi$ between the two charm hadrons is evaluated using the position of the two secondary decay vertices with respect to the primary interaction vertex, in the plane transverse to the beam direction.

The raw data distribution for the azimuthal angle between charmed pairs is shown in figure 3(a). Figure 3(b) shows the same distributions after subtraction of background computed as explained above.

We have performed a detailed simulation to evaluate the acceptances for charm events. We have generated $c\bar{c}$ events using a combination of Pythia 5.4 [11]

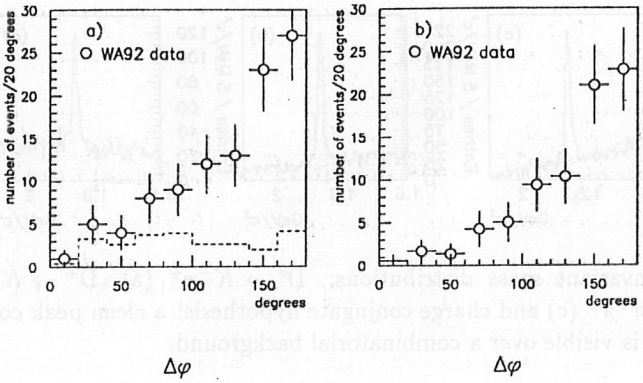

Figure 3: Charm pair azimuthal correlation : WA92 data before background subtraction and background distribution (a), data after background subtraction (b)

and Fluka [12]. The simulation predicts a constant acceptance of associated charm particle production as a function of the azimuthal angle difference. It can be noticed that NLO calculations predict c and $\bar{c}$ quarks to be produced more back-to-back than what is observed in the experimental data for charmed hadrons, as shown in figure 4(a).

Higher order corrections, as well as nonperturbative effects, such as the transverse momenta of the incoming partons or the fragmentation, can cause a broadening of the $\Delta\phi$ distribution. The effect of fragmentation of charm quarks has been evaluated with the simulation chain described above. The comparison of the $\Delta\phi$ distributions of $c\bar{c}$ generated pairs and of hadron pairs that result from the hadronization of the quarks (fig 5) shows that this effect cannot account for the difference between the data and the NLO calculation.

To quantify the size of the effects which widened the azimuthal angle distribution the experimental data are compared with a model [5] where a transverse component p_T, distributed as $dN/dp_T^2 \propto e^{-p_T^2/<p_T^2>}$, is added to the incoming parton momentum and then the NLO perturbative QCD calculations are performed. This comparison is shown in figure 4(b) for two different values of $< p_T^2 >$. A value $< p_T^2 >$ of 0.3 $(\mathrm{GeV}/c)^2$ can account for non perturbative and perturbative (beyond

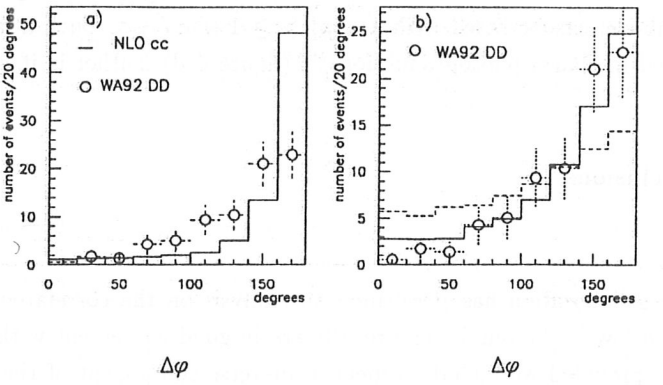

Figure 4: Charm pair azimuthal correlation: WA92 data are compared to NLO perturbative QCD calculation (a), and to a simple model where a transverse momentum component of the parton is added to the NLO perturbative QCD quark predictions (b) (dotted line : $< p_T{}^2 > = 1.0$ (GeV/c)^2, solid line : $< p_T{}^2 > = 0.3$ (GeV/c)^2).

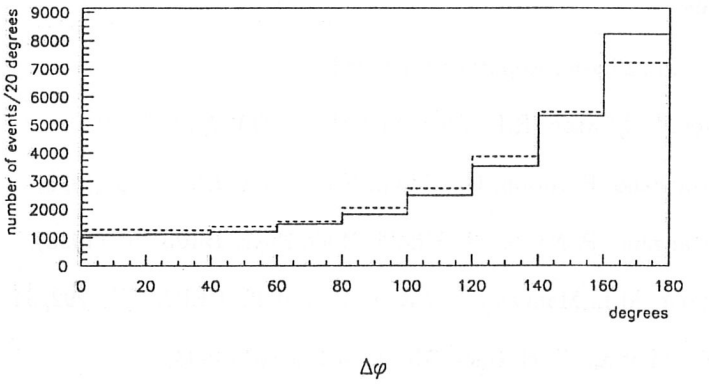

Figure 5: Charm pair azimuthal correlation of simulated $c\bar{c}$ (solid line) and $D\bar{D}$ (dotted line) pairs.

NLO) effects which boost the $c\bar{c}$ system in the transverse plane[2].

Data from other charm hadroproduction experiments [13, 14, 15] (figure 6 a-c) seem to favour rather broad correlations, which, assuming the validity of the model described above, can be fitted with a $< p_T^2 > \geq 1$ (GeV/c)^2. Such a large effect is not observed in charm photoproduction [16] (figure 6 d) neither is it confirmed by our result.

4 – Conclusions

The WA92 collaboration has performed an analysis on the correlated charm production on a low background. The results are in good agreement with NLO QCD calculations provided we include a mean transverse component of the parton momentum of about 0.5 GeV/c.

Acknowledgements

We thank S. Frixione, M. Mangano, P. Nason and G. Ridolfi for useful discussions and for providing us with unpublished results of their calculations.

References

1. G.Altarelli , Physics Reports **81** 1 (1982).
2. P. Nason, S. Dawson, R.K. Ellis, Nucl. Phys. **B327** 49 (1989).
3. M.L. Mangano, P. Nason, G. Ridolfi, Nucl. Phys. **B373** 295 (1992).
4. M.L. Mangano, P. Nason, G. Ridolfi, Nucl. Phys. **B405** 507 (1993).
5. S. Frixione, M.L. Mangano, P. Nason, G. Ridolfi, CERN-TH.7292/94 (1994).
6. M. Adinolfi et al., Nucl. Instr. Meth. **A329** 117 (1993).
7. C. Bacci et al., Nucl. Instr. Meth. **A324** 83 (1993).
8. W. Beusch et al., Nucl. Instr. Meth. **A249** 391 (1986).

[2] Former results [17, 5] had been obtained without background subtraction

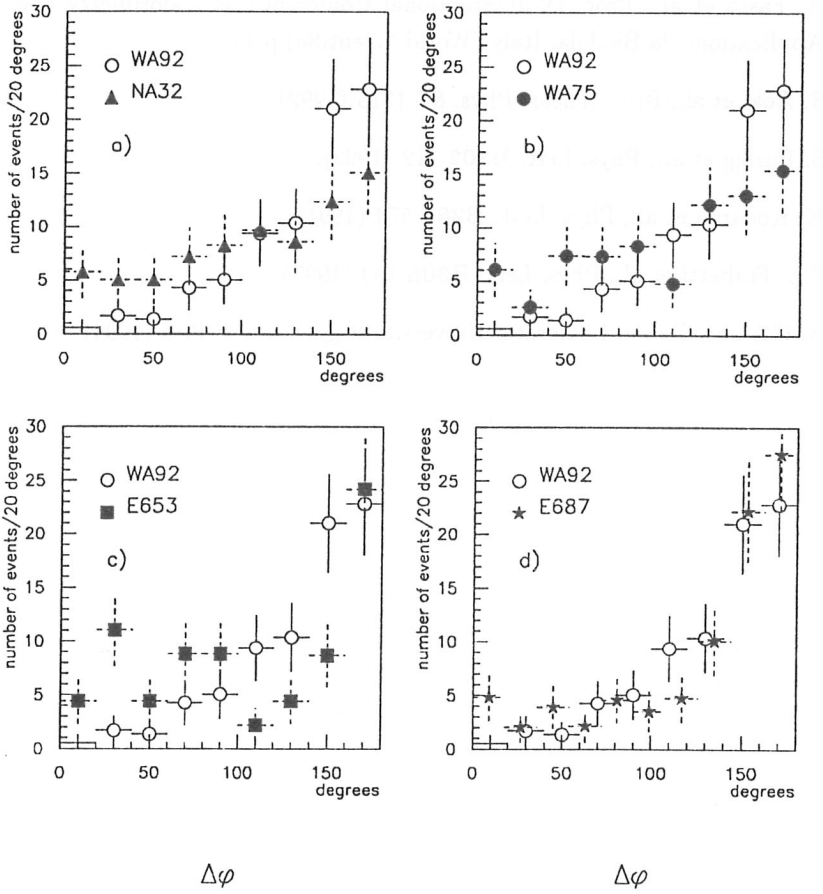

Figure 6: WA92 data are compared to NA32 (a), WA75 (b), E653 (c) and E687 (d) data. All distributions are normalized to the WA92 data sample.

9. G. Darbo et al., Nucl. Instr. Meth. **A351** 225 (1994).

10. G. Darbo, L. Rossi, Nucl. Instr. Meth. **A289** 584 (1990).

11. H.-U. Bengtsson and T.Sjöstrand, Comput. Phys. Commun. **46** 43 (1987).

12. A. Fassò et al., Proc. IV International Conference on Calorimetry and their Applications, la Biodola, Italy (World Scientific) p.493.

13. S. Aoki et al., Prog. Theor. Phys. **87** 1315 (1992).

14. S. Barlag et al., Phys. Lett. **B302** 112 (1993).

15. K. Kodama et al., Phys. Lett. **B263** 579 (1991).

16. P.L. Frabetti et al., Phys. Lett. **B308** 193 (1993).

17. A. Cardini, Tesi di Dottorato, Università degli Studi di Pisa (1994).

Frascati Physics Series, Vol. III (1994)
HEAVY QUARKS AT FIXED TARGET
University of Virginia, October 7–10, 1994
(pp. 127–139)

OBSERVATION OF CHARMED BARYON Λ_C^+ AND Ξ_C^+ DECAYS

EXCHARM Collaboration *†‡§

Presented by V. Kekelidze

ABSTRACT

Preliminary results on the decays of charmed baryons Λ_C^+ and Ξ_C^+ observed in two different runs of the EXCHARM experiment at the Serpukhov accelerator are reported. These baryons were produced by neutrons with mean momenta of 37 GeV/c and 45 GeV/c on a carbon target. The decay mode $\Xi_C^+ \to \bar{K}^0 p K^- \pi^+$ was observed for the first time. The ratios of branching ratios were estimated for several observed decay modes.

Although two decades have passed since the discovery of particles with charmed quarks, charmed baryon decays have been observed only via some modes which are rather far from the completeness. New experimental data in this study are necessary to test and develop models of heavy quark physics.

Some of the charmed baryon decays have been observed in [1)–12)] and indications for these decays have been presented in [13), 14)].

Preliminary results on the decays of Λ_C^+ and Ξ_C^+, inclusively produced by neutrons on carbon, are presented in this paper.

The experiment is performed in the neutral beam 5N of the Serpukhov accelerator using the magnetic spectrometer EXCHARM. The beam particles, mainly neutrons, are produced by protons on the internal beryllium target at 0°. The mean values of the neutron momenta are respectively $\approx$ 37 GeV/c and $\approx$ 45 GeV/c for

[1]A.N.Aleev, V.P.Balandin, A.Bragadireanu, I.I.Evsikov, P.Z.Hristov, I.M.Ivanchenko, A.M.Kalinin, A.F.Kamburyan, M.N.Kapishin, N.N.Karpenko, V.D.Kekelidze, I.G.Kosarev, Yu.A.Koshevnikov, Yu.A.Kretov, N.A.Kuz'min, G.A.Kvirikashvili, A.L.Lyubimov, A.S.Mestvirishvili, P.V.Moisenz, A.N.Morozov, A.K.Odishvili, V.V.Pal'chik, Yu.K.Potrebenikov, T.B.Progulova, V.A.Sashin, V.E.Simonov, L.A.Slepets, V.N.Spaskov, G.T.Tatishvili, A.I.Zinchenko
Joint Institute for Nuclear Research, Joliot Curie 6, 141980 Dubna, Russia
A.A.Loktionov
Institute of High Energy Physics of the Rep.Kaz.Academy of Sciences, 480082 Alma-Ata, Kazakhstan
T.Ponta
Institute of Nuclear Physics, P.O.Box MG-6, Magurele, Bucharest, Rumania
A.S.Kurilin
Institute of Nuclear Problems, Byelorussian State University, Leninsky pr. 4, 220080 Minsk, Byelorussia
M.V.Belov, E.G.Devitsin, V.A.Kozlov, S.Yu.Potashov, M.V.Zavertyaev
Lebedev Physical Institute of the Russian Academy of Sciences, Leninsky pr. 53, 117924 Moscow, Russia
J.Hladky, A.Prokes
Institute of Physics of the Czech Academy of Sciences, Na Slovance 2, 180 40 Prague, Czech Republic
A.P.Bugorsky
High Energy Physics Institute, 142284 Protvino, Russia
V.I.Zayachky
Higher Chemical-Technological Institute, Blvd. Kl.Ohridsky 8, Sofia, Bulgaria
I.M.Geshkov, A.C.Vylov
Institute for Nuclear Research and Nuclear Energetics of the Bulgarian Academy of Sciences, Tsarigradsko chaussee 72, 1784 Sofia, Bulgaria
L.N.Abesalashvili, N.S.Amaglobeli, B.G.Chiladze, R.A.Kvatadze, M.V.Kopadze, N.L.Lomidze, M.D.Mosidze, T.G.Pitskhelauri, R.G.Shanidze
Institute of High Energy Physics, Tbilisi State University, Universitetskaia 6, 380086 Tbilisi, Georgia

[2]Supported by Russian Fund of Fundamental Research (grants 93-02-03987 and 93-02-03989) and International Science Foundation (grant RFP000)
[3]Supported by Bulgarian National Fund "Scientific Investigations"
[4]Supported by International Science Foundation (grant RVN000)

50 GeV/c and 70 GeV/c incident protons [15]. The corresponding energy spectra of the beam are presented in fig.1.

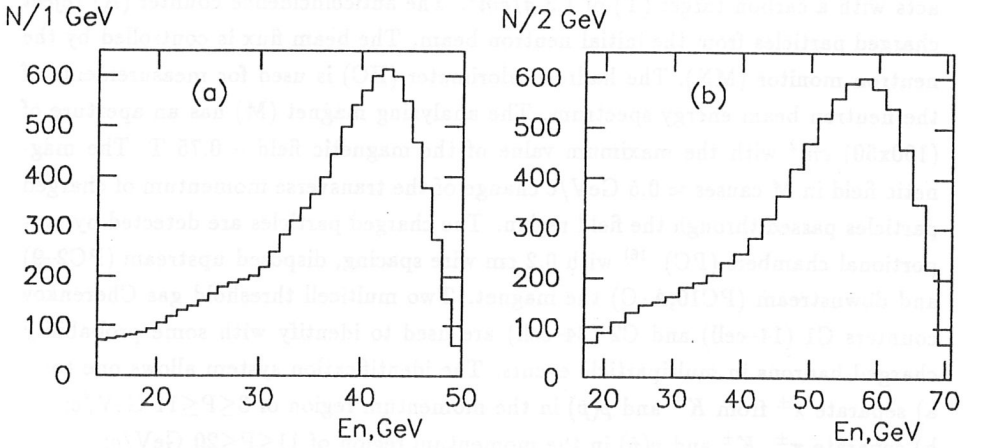

Figure 1: The energy spectra of neutrons produced by protons of: (a) $P_p = 50$ Gev/c and (b) $P_p = 70$ Gev/c.

A layout of the main elements of the EXCHARM spectrometer is presented in fig.2.

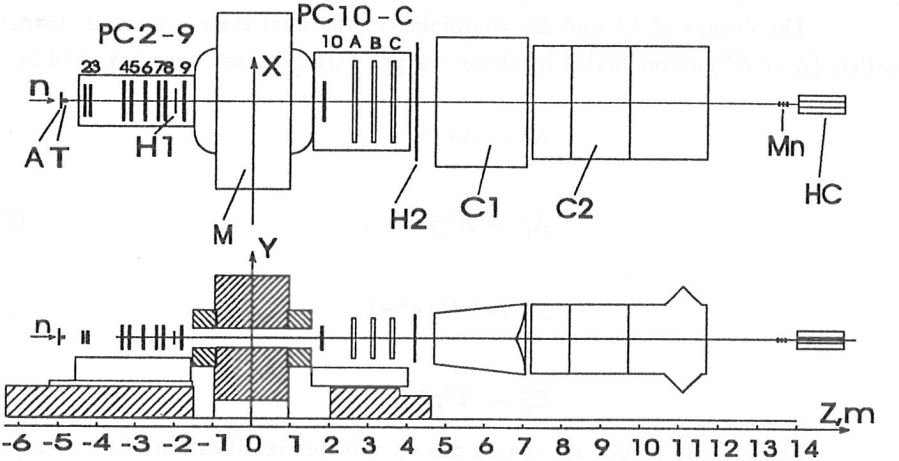

Figure 2: Arrangement of the EXCHARM spectrometer elements at the 5N channel of the Serpukhov accelerator: n – neutron beam; A – anticoincidence counter; T – target; M – magnet; PC – multiwire proportional chambers; H1,H2 – scintillation hodoscopes; C1,C2 – Cherenkov threshold counters; Mn – neutron monitor; HC - hadron calorimeter

The neutron beam (n) with an intensity of about 10^7 neutrons/burst interacts with a carbon target (T) of 1.3 g/cm^2. The anticoincidence counter (A) reject charged particles from the initial neutron beam. The beam flux is controlled by the neutron monitor (MN). The hadron calorimeter (HC) is used for measurements of the neutron beam energy spectrum. The analyzing magnet (M) has an aperture of (100x50) cm^2 with the maximum value of the magnetic field – 0.75 T. The magnetic field in M causes $\approx$ 0.5 GeV/c change of the transverse momentum of charged particles passed through the field region. The charged particles are detected by proportional chambers (PC) [16] with 0.2 cm wire spacing, disposed upstream (PC2–9) and downstream (PC10,A–C) the magnet. Two multicell threshold gas Cherenkov counters C1 (14–cell) and C2 (34–cell) are used to identify with some probability charged hadrons in multiparticle events. The identification system allows one to:
a) separate $\pi^{\pm}$ from $K^{\pm}$ and $p(\bar{p})$ in the momentum region of $3 \leq P \leq 11$ GeV/c;
b) separate $\pi^{\pm}$, $K^{\pm}$ and $p(\bar{p})$ in the momentum region of $11 \leq P \leq 20$ GeV/c;
c) separate $p(\bar{p})$ from $\pi^{\pm}$ and $K^{\pm}$ in the momentum region of $20 \leq P \leq 40$ GeV/c.

Two hodoscope planes of scintillation counters (H1 and H2) with dimensions (600x320x10) mm^3 and (3000x1200x10) mm^3, consisting of 15 and 60 counters, respectively, are used in the trigger system. The trigger condition requires at least four charged particles passed through the spectrometer. The trigger signal is formed by the hodoscopes of PCś and the planes of scintillation counters H1 and H2.

The decays of Λ_C^+ and Ξ_C^+ containing in the final state a neutral strange particle (Λ or $\bar{K}^0$) accompanied by three charged particles have been searched for:

$$\Lambda_C^+ \to \Lambda\pi^+\pi^+\pi^-, \tag{1}$$

$$\Lambda_C^+ \to \bar{K}^0 p\pi^+\pi^-, \tag{2}$$

$$\Xi_C^+ \to \Lambda K^-\pi^+\pi^+, \tag{3}$$

$$\Xi_C^+ \to \bar{K}^0 pK^-\pi^+. \tag{4}$$

These decay modes are chosen due to reliable identification of the decays

$$K_S^0 \to \pi^+\pi^- \tag{5}$$

and

$$\Lambda \to p\pi^- \tag{6}$$

using only geometric and effective mass criteria, and to the appropriate multiplicity of charged particles in the final states.

The effective mass resolution for the states (1)–(4), estimated by Monte–Carlo simulation is around 12 MeV/c^2. Such a resolution and the relatively low mean multiplicity of the charged particles produced at the Serpukhov energies, make the combinatorial background in the studied spectra of the final states (1)–(4) insignificant. Therefore, it is possible to search for charmed particles without usage of a vertex detector, i.e. not distinguishing their production and decay vertices.

The presented results are based on $\approx 4 \cdot 10^7$ nC interactions recorded during two runs of the experiment. $\approx 10^7$ recorded events are produced by neutrons from 50 GeV/c protons (run#1) and $3 \cdot 10^7$ events – by neutrons from 70 Gev/c protons (run#2)[1]. The other experimental conditions such as magnetic field, Cherenkov counter ussage, etc., for run#1 and run#2 were slightly different.

To identify Λ and K^0_S decays, (5) and (6), neutral Vee's (V^0) have been selected with the effective mass of $(p\pi^-)/(\pi^+\pi^-)$ system differed from the Λ/K^0 mass less than 7/10 MeV/c^2 respectively. The experimental resolutions for these masses are: $\approx$ 1.6 MeV/c^2 for Λ and $\approx$ 4.0 MeV/c^2 for K^0_S.

In total, $4.6 \cdot 10^5/7.7 \cdot 10^5$ events with Λ/K^0_S candidates have been selected respectively.

To select the final states (1)–(4), Λ / K^0_S and charged hadrons $h^\pm$ are required to have a common interaction vertex in the target region. The mean quadratic distance between the reconstructed particle trajectories in this vertex must not exceed the fourfold space resolution which is about 0.1 cm. After these conditions $1.8 \cdot 10^5/3.1 \cdot 10^5$ events containing, respectively, Λ/K^0_S and three or more charged particles have been chosen.

It was also required that the reconstructed vertices of Vee's were placed not less than 5cm downstream the target.

To distinguish the π^+ and p in (2), identify p in (4), and reject π^- among K^- candidates in (3) and (4), the information from Cherenkov counter have been analyzed.

Combinations where either the negative particles – candidates to K^-, could be identified with π^-, or π^-, K^- and $\bar{p}$ are not distinguished, were excluded. Almost 85% of π^-'s among K^- candidates have been excluded from the final states (3) and about 40% from (4). The efficiency of K^- identification in the final states (3) and (4) was 0.70, and 0.80, respectively [17]. The π^+'s were identified only in the state (2). This allowed to exclude about 25% of K^+ and p and select real π^+ with an efficiency of about 0.85. The p's were identified in (2) and (4) and as a result about

[1]The results, obtained for the final state (1) in run #2, are based only on $\approx 10^7$ nC interactions

50% of π^+'s and K^+'s were rejected. Real p's have been selected with an efficiency of about 0.70.

The obtained invariant mass spectra of the final states (1) and (2) are presented in fig.3, (a) and (b), and in fig.4, (a) and (b), for run#1 and run#2, respectively. Peaks at the Λ_C^+ mass region are observed. These peaks have been identified with the Cabibbo favored Λ_C^+ decays (1) and (2). The spectra have been approximated by Gauss distribution for the signals and smooth function for the background representation.

The invariant mass spectra of the final states (3) and (4) are presented in fig.5, (a) and (b), and in fig.6, (a) and (b), for run#1 and run#2 respectively. These spectra were approximated like ones described above. Significant peaks are seen at the Ξ_C^+ mass in all spectra. These peaks indicate the Cabibbo favored decays (3) and (4) of Ξ_C^+. The Ξ_C^+ decay mode into $\bar{K}^0 p K^- \pi^+$ has been observed for the first time.

The characteristics of these signals, obtained in run#1 and run#2, are shown in table 1 and 2 respectively. The systematic error of invariant mass is estimated to be around 15 MeV/c^2. This error is caused mainly by both: uniform approximation of the magnetic field and the limited accuracy of detector alignments.

The combinatorial background in all the presented spectra is insignificant and does not exceed 1.01 in the mass region of the signals.

The observation of different decay channels allows to evaluate some ratios of branching ratios (Br). The ratio of branching ratios of the decays (2) to (1) has been calculated according to the expression

$$R_{21} = \frac{N_2}{N_1} \cdot \frac{Br_1(V^0)}{Br_2(V^0)} \cdot r_{12}, \tag{7}$$

where N_1 and N_2 are the numbers of observed decays of (1) and (2) modes respectively; $Br_1(V^0)$ and $Br_2(V^0)$ – the branching ratios of V^0's decays ($Br(\Lambda \to p\pi) = 0.641$ and ($Br(\bar{K}^0 \to \pi^+\pi^-) = 0.343$); r_{12} – ratio of the acceptances (1) to (2).

It has been obtained that:

$$R_{\Lambda_c^+} = \frac{Br(\Lambda_c^+ \to \bar{K}^0 p\pi^+\pi^-)}{Br(\Lambda_c^+ \to \Lambda\pi^+\pi^+\pi^-)} = \begin{cases} 2.4 \pm 1.0, & \text{for run\#1,} \\ 2.0 \pm 0.9, & \text{for run\#2.} \end{cases} \tag{8}$$

The combined value of $R_{\Lambda_c^+}$ is equal to 2.2±0.7.

The same expression (7) has been used to calculate the ratio of branching ratios of the decays (4) to (3):

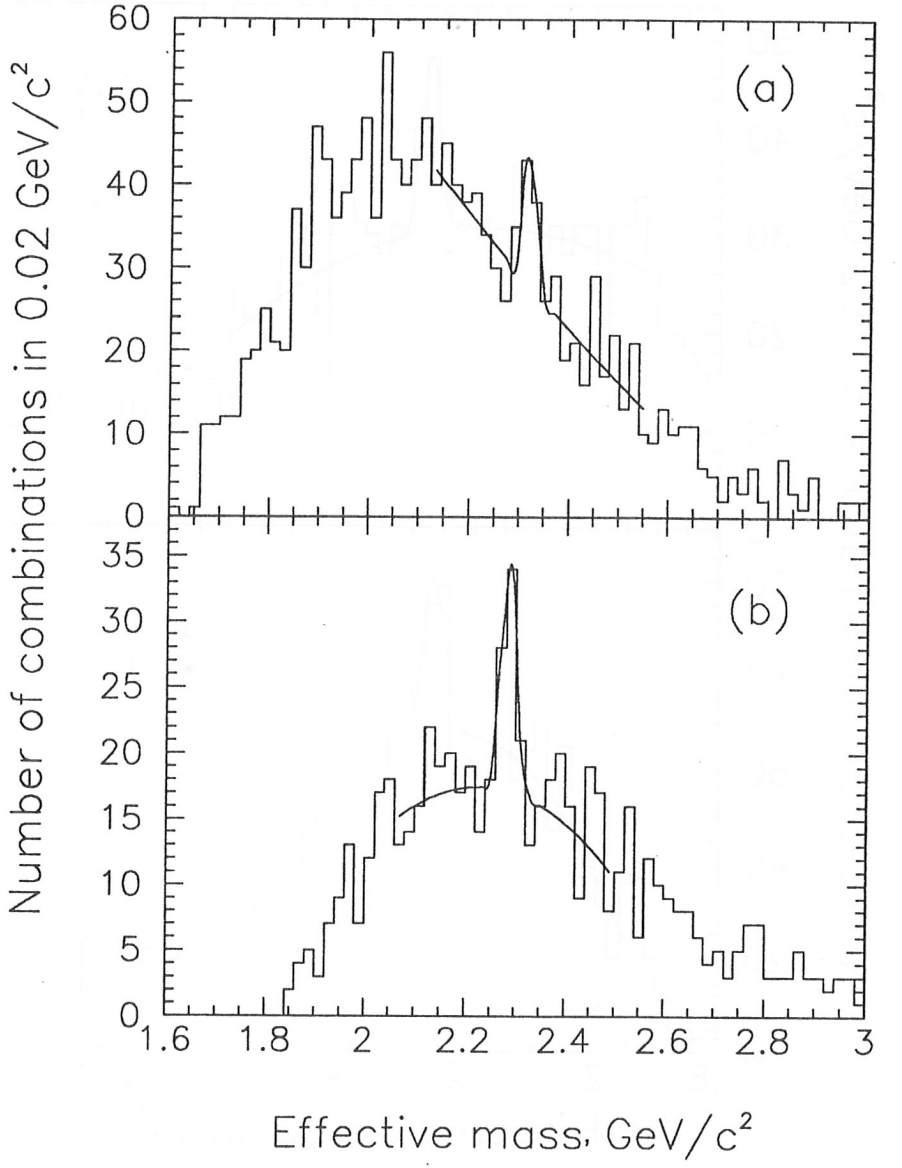

Figure 3: Effective mass spectra of $\Lambda\pi^+\pi^+\pi^-$ (a) and $K^0_S p\pi^+\pi^-$ (b), run#1.

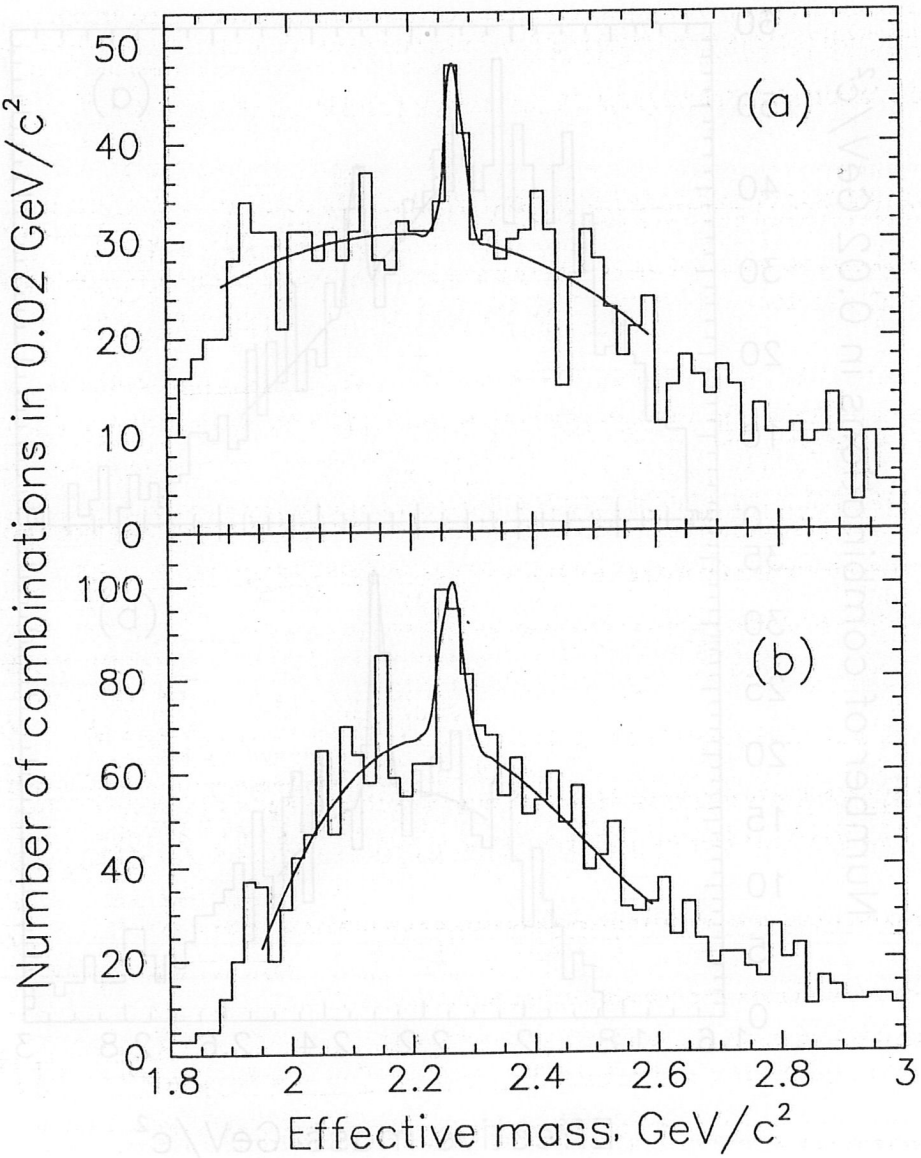

Figure 4: Effective mass spectra of $\Lambda\pi^+\pi^+\pi^-$ (a) and $K^0_S p\pi^+\pi^-$ (b), run#2.

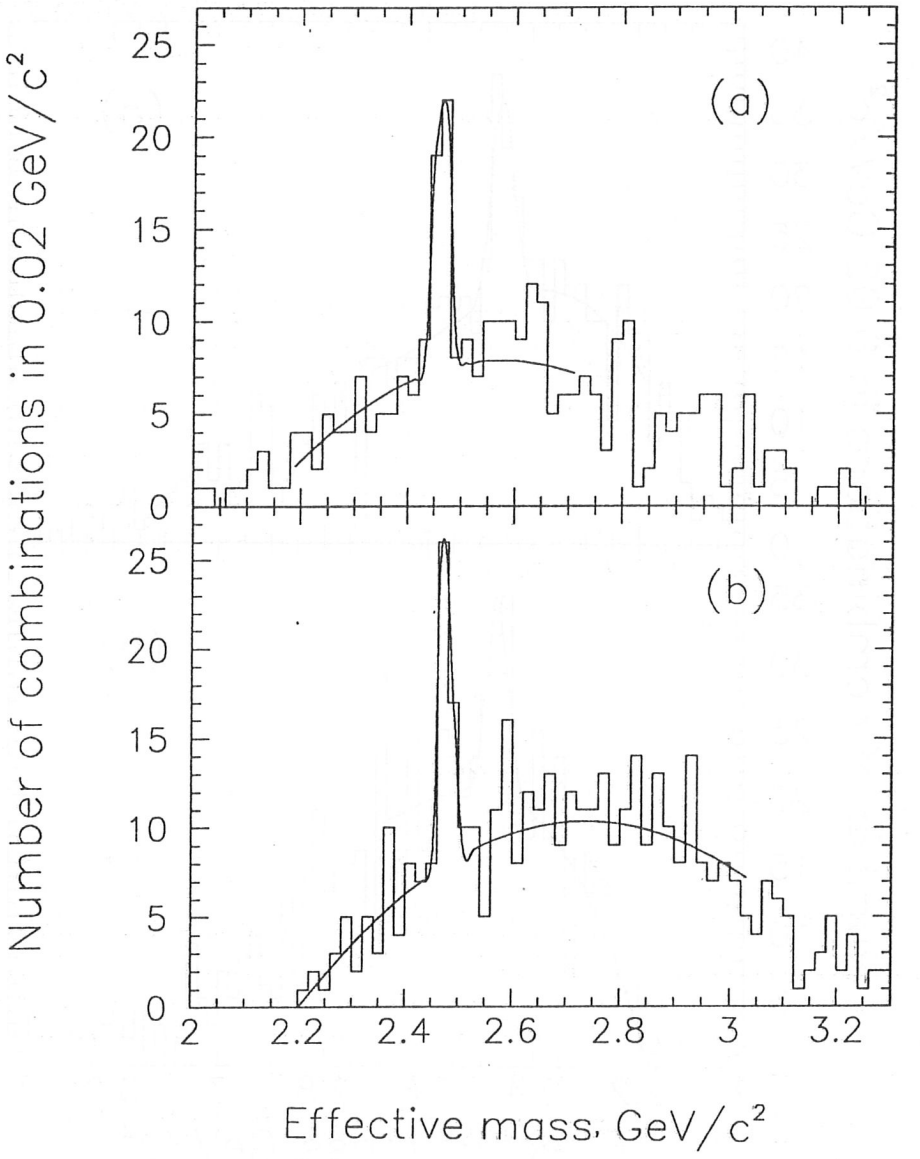

Figure 5: Effective mass spectra of $\Lambda K^- \pi^+ \pi^+$ (a) and $K^0_S p K^- \pi^+$ (b), run#1.

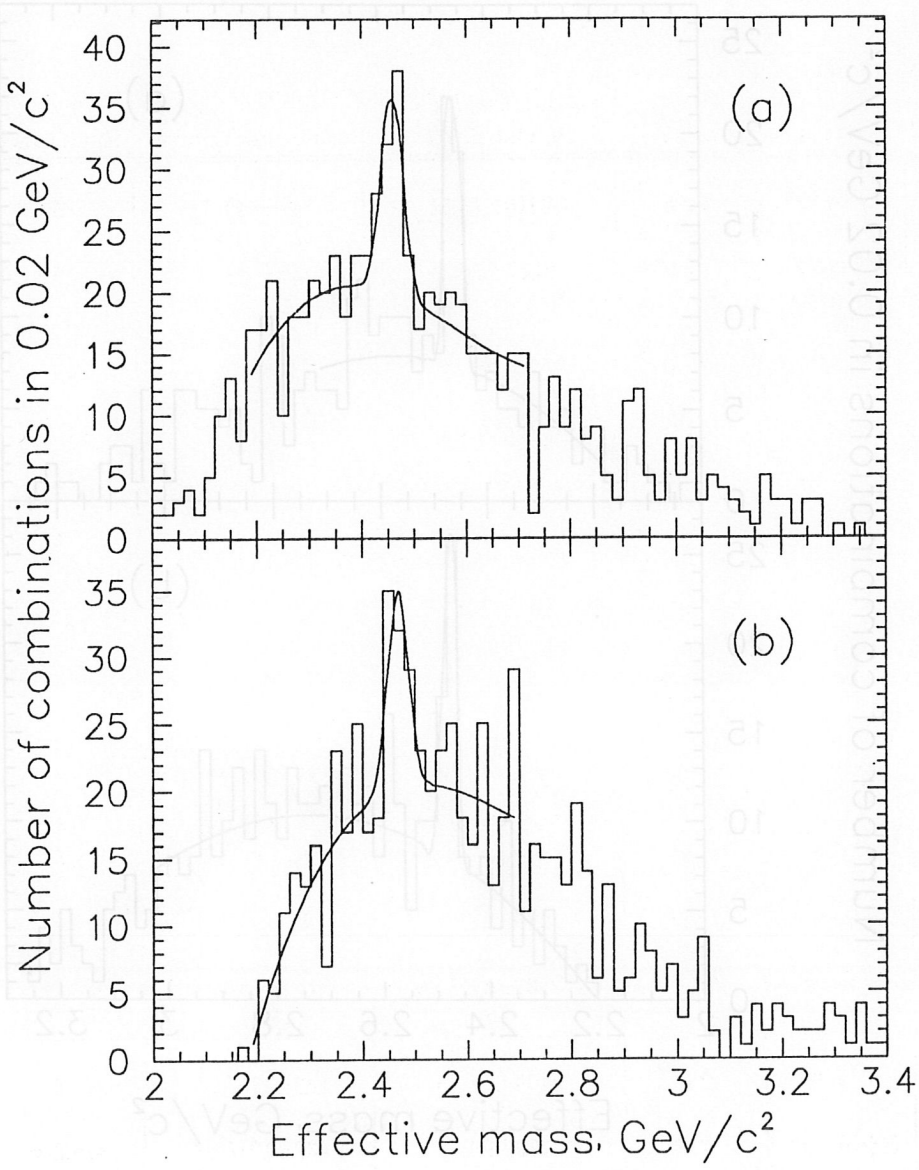

Figure 6: Effective mass spectra of $\Lambda K^-\pi^+\pi^+$ (a) and $K^0_S p K^-\pi^+$ (b), run#2.

Table 1:

Final states	Number of comb.	Signals		
		Mean mass, MeV/c^2 ± stat ± syst	Number of comb./background	Stat. significance
$\Lambda\pi^+\pi^+\pi^-$	1485	2310±7±15	(41±11)/75	$\approx 5\cdot\sigma$
$K^0_S p\pi^+\pi^-$	656	2287±7±15	(35± 9)/48	$\approx 5\cdot\sigma$
$\Lambda K^-\pi^+\pi^+$	317	2465±4±15	(27± 6)/14	$\approx 7\cdot\sigma$
$K^0_S pK^-\pi^+$	436	2472±7±15	(27± 7)/16	$\approx 7\cdot\sigma$

Table 2:

Final states	Number of comb.	Signals		
		Mean mass, MeV/c^2 ± stat ± syst	Number of comb./background	Stat. significance
$\Lambda\pi^+\pi^+\pi^-$	1449	2275±6±15	(30±13)/92	$\approx 3.1\cdot\sigma$
$K^0_S p\pi^+\pi^-$	2413	2265±6±15	(75±17)/186	$\approx 5.5\cdot\sigma$
$\Lambda K^-\pi^+\pi^+$	747	2460±8±15	(43±11)/ 60	$\approx 5.6\cdot\sigma$
$K^0_S pK^-\pi^+$	713	2470±9±15	(39±10)/ 63	$\approx 5.0\cdot\sigma$

$$R_{\Xi_c^+} = \frac{Br(\Xi_c^+ \to \bar{K}^0 p K^- \pi^+)}{Br(\Xi_c^+ \to \Lambda K^- \pi^+ \pi^+)} = \begin{cases} 2.3 \pm 1.1, & \text{for run\#1,} \\ 2.6 \pm 1.0, & \text{for run\#2.} \end{cases} \quad (9)$$

The combined value of $R_{\Xi_c^+}$ is equal to 2.4±0.7.

Possible cascade decay of Ξ_C^+ via $\bar{K}^*(892)^0$ has been searched for among the final states (3).

The fractions of the cascade decays:

$$R_{\Xi_c^+}(\bar{K}^{*0}) = \frac{Br(\Xi_c^+ \to \Lambda \bar{K}^{*0} \pi^+ \to \Lambda K^- \pi^+ \pi^+)}{Br(\Xi_c^+ \to \Lambda K^- \pi^+ \pi^+)} \quad (10)$$

has been evaluated in accordance with (7).

The obtained value $R_{\Xi_c^+}(\bar{K}^{*0})$ for run#1, run#2 and the combined results is presented in table 3.

Table 3:

	Run#1	Run#2	Combined
$R_{\Xi_c^+}(\bar{K}^{*0})$	0.4±0.2	0.4±0.2	0.40±0.14

Conclusion

The charmed baryon Λ_C^+ and Ξ_C^+ decays (1–4) have been observed. Among those the decay mode $\Xi_C^+ \to \bar{K}^0 p K^- \pi^+$ is a new one. The decays of both Λ_C^+ and Ξ_C^+ via p are more favorable then the ones via Λ. An appreciable fraction of Λ_C^+ and Ξ_C^+ decays via intermediate resonant states have been observed.

The authors are greatly indebted to A.A.Logunov, Yu.D.Prokoshkin, I.A.Savin, A.N.Sissakyan and N.E.Tyurin for their support and permanent interest in the study.

References

1 . S. Barlag et al., Phys.Lett. **B218** 374 (1989).

2 . S. Barlag et al., Phys.Lett. **B233** 522 (1989).

3 . P.L. Frabetti et al., Phys.Lett. **B251** 639 (1990).

4 . P. Avery et al., Phys.Rev.Lett. **65** 2842 (1990).

5 . Alvarez et al., Z.Phys. **C47** 539 (1990).

6 . H. Albrecht et al., Phys.Rev. **B274** 239 (1992).

7 . H. Albrecht et al., Phys.Lett. **B247** 121 (1990).

8 . S.R. Klein, Int.J.Mod.Phys. **A8** 1457 (1990).

9 . S.F. Biagi et al., Z.Phys. **C28** 175 (1985).

10 . P. Coteus et al., Phys.Rev.Lett. **59** 1530 (1987).

11 . M.S. Alam et al., Phys.Lett. **B226** 401 (1989).

12 . A.N. Aleev et al., Z.Phys. **C23** 333 (1984).

13 . G.T. Tatishvili, in: Proc. of the XI International Seminar on High Energy Physics Problems (ed. A.M.Baldin and V.V.Burov, Dubna, 1993), 152 (JINR, Dubna, 1994).

14 . V.D. Kekelidze, in: Proc. of the XXVI International Conference on High Energy Physics (ed.J.R. Sanford, Dallas, August 1992), **1**, 1066 (North-Holland, Amsterdam, 1993).

15 . A.N. Aleev et al., JINR preprint **P13–94–312** (1994).

16 . A.N. Aleev et al., JINR preprint **P13–94–124** (1994).

17 . A.F. Kamburyan et al., JINR preprint **P13–93–362** (1993).

SESSION V

- E. Chudakov
  Charmed Baryon Production in the CERN Hyperon Beam
- M. Procario
  Charmed from Hyperons in the Future: Fermilab Experiment 781
- J. Wiss
  Charm Semi-Leptonic Physics
- S. Shukla
  Excited Charm States
- G. Bellini
  Charm Spectroscopy and Lifetime

Frascati Physics Series, Vol. III (1994)
HEAVY QUARKS AT FIXED TARGET
University of Virginia, October 7–10, 1994
(pp. 143–156)

CHARMED BARYON PRODUCTION IN THE CERN HYPERON BEAM

WA89 collaboration
Presented by E.Chudakov,
Institut für Kernphysik, University of Mainz, D-55099, Mainz, Germany

ABSTRACT

The WA89 experiment studies charmed particles produced in the forward direction by a 330GeV/c hyperon beam. Various decays of charmed-strange baryons Ξ_c and Ω_c^0 have been observed. The lifetime of Ξ_c^+ baryons has been measured. Measurements of the Λ_c^+ Σ_c and Ξ_c inclusive x_F and p_T distributions indicate a leading particle effect.

1 – Introduction

The experiment WA89 uses a Σ^- beam with an energy of 330GeV and the upgraded Ω facility at CERN. The goal of the experiment in the charm sector is to study the hadroproduction mechanisms of charmed particles with and without strangeness at x_F>0.2, where the charmed particle may share a spectator quark with the beam particle. If such a leading effect is strong the hyperon beam may provide an advantage for the study of the charmed-strange particles, especially the charmed-strange baryons.

2 – Experiment WA89

Hyperons were produced by 450 GeV/c protons impinging on a 40 cm long beryllium target with a diameter of 0.2 cm. A magnetic channel consisting of 3 magnets with an integrated field of 8.4 Tm selected negative particles with a momentum of 330 GeV/c and a momentum spread of $\sigma(p)/p = 7\%$ which hit the experimental target about 16 m downstream. The size of the beam at the target was 3.6 cm horizontally

and 1.5 cm vertically, and its dispersion was 0.6 mrad in the horizontal plane and 1.0 mrad in the vertical plane. An average beam spill of 2.1 s contained about $1.8 \cdot 10^5$ Σ^- hyperons and about $4.5 \cdot 10^5$ π^- at the experimental target for an incoming intensity of $3.0 \cdot 10^{10}$ protons per spill. A transition radiation detector was used to discriminate online between π^- and hyperons. The remaining high-momentum pion contamination was less than 10% of the hyperon sample, which contained mainly Σ^- and about 2% of Ξ^- hyperons. The experimental target consisted of copper and carbon plates and had a thickness of about 4% of an interaction length.

The experiment had three major runs of data taking. In 1991, about 120 million events were recorded. In 1993, about 180 million events were recorded with a considerably upgraded setup, and about 320 million events were recorded in 1994. The results presented are based on the full 1991 data sample and on a part of the 1993 data sample.

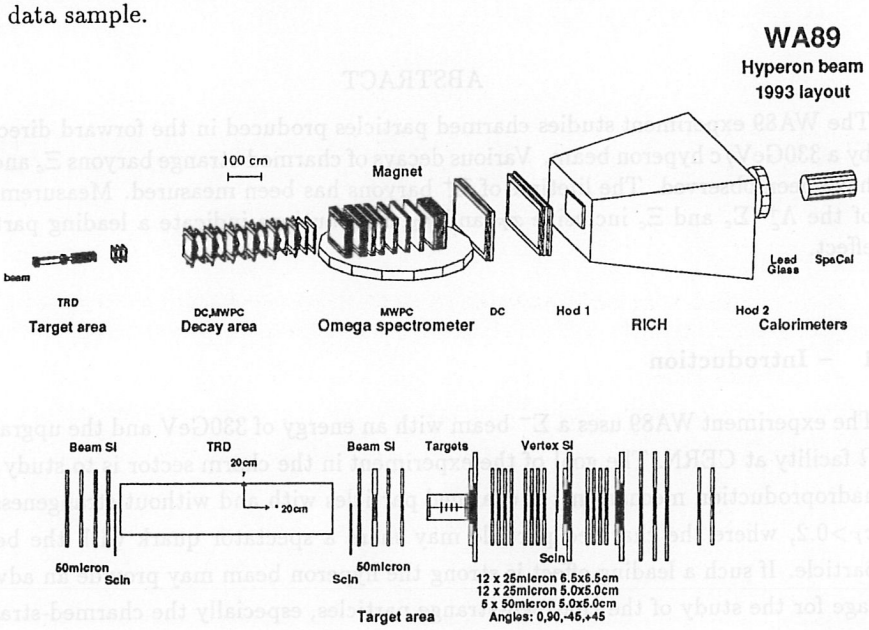

Figure 1: WA89 experimental set-up in 1993

Fig. 1 shows a sketch of the experimental setup used in the 1993 run. The secondary particles were detected by 24 silicon micro-strip planes with 25μm and 5 planes with 50μm pitch. Positioning the target about 14 m upstream of the center of the Ω-spectrometer provided a 10 m long decay area for short living strange particles. The products of these decays along with the particles coming directly from the target were detected by 36 planes of drift chambers with a spatial resolution of about 300 μm and 20 planes of MWPC with a pitch of 1 mm. The particle momenta

were measured by the Ω-spectrometer [1] consisting of a super-conducting magnet with a field integral of 7.5 Tm and a tracking detector consisting of 45 MWPC planes inside the field area and 8 drift chamber planes at the exit of the magnet. The momentum resolution was $\sigma(p)/p^2 \approx 10^{-4}$ (GeV/c)$^{-1}$. Charged particles were identified using a ring imaging Cherenkov (RICH) detector [2]. It had a threshold of $\gamma = 42$ and provided K/π separation up to about 100 GeV/c. Downstream of the RICH a lead glass electromagnetic calorimeter was positioned for photon and electron measurement [3]. The electromagnetic calorimeter was followed by a hadron calorimeter.

The trigger was relatively open. It selected about 20% of all Σ^- induced interactions using multiplicities measured in scintillator hodoscopes and proportional chambers downstream of the magnet and correlations of hits in these detectors to select particles with high momenta. More than 2 particles at the exit of the magnet were required.

In the 1991 run the microvertex detector consisted of 4 silicon micro-strip planes with 25μm and 8 planes with 50μm pitch. The decay area contained only the drift chambers.

3 – Event reconstruction

The charged tracks were reconstructed in the Ω-spectrometer and matched to the tracks reconstructed in the decay region and in the vertex detector. For the charm search a candidate-driven approach was applied. Charm decays were selected using cuts on the separation of the charm vertex from the primary vertex (typically 6σ, $\sigma \approx 550\mu m$) and on the impact parameter of the charm particle relative to the primary vertex (< 60μm), also the unambiguous association of tracks to the vertices was required. For charged kaons and protons the RICH identification was used.

4 – Charmed baryon spectroscopy

All $1/2^+$ ground state charmed baryons (Fig. 2) but for the two states Ξ_c' have been discovered. Our goal is to observe all established ground states and to search for still undiscovered states.

4.1 Non–strange charmed baryons

Using the 1991 data we have observed signals of D-mesons, Λ_c^+ and Σ_c^0 baryons [14]. Using about 25% of the 1993 data we also observe signals of Σ_c^{++} and

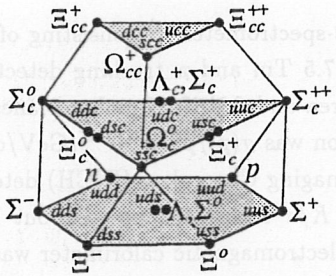

Figure 2: SU(4) baryon multiplet

Σ_c^+ (fig.3). The mass difference of Σ_c^{++} and Σ_c^+ to Λ_c^+ is measured to be 168.1± 2.0 and 166.8± 3.0 Mev/c^2.

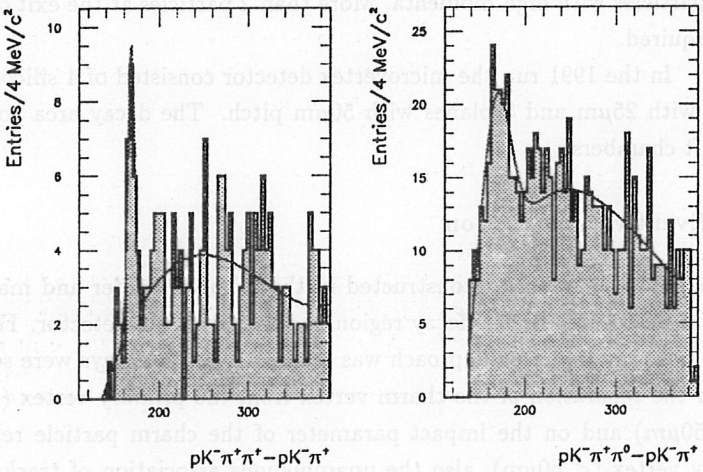

Figure 3: Mass differences (in MeV/c^2) for a) M($K^-p\pi^+$ π^+) - M($K^-p\pi^+$) and b) M($K^-p\pi^+$ π^0) - M($K^-p\pi^+$), for $K^-p\pi^+$combinations taken from the Λ_c^+ mass peak. About 25% of the 1993 data were used.

4.2 Single-strange charmed baryons

Figure 4 (upper row) depicts signals for the Ξ_c^+ decaying into $\Lambda K^-\pi^+\pi^+$ and $\Xi^-\pi^+\pi^+$ from the 1991 data set. The lower row of the same figure presents signals for Ξ_c^0 decaying into $\Lambda K^-\pi^+$ and $\Xi^-\pi^+$. The masses measured are 2454± 3.0± 7.0 and 2451± 4.0± 7.0 MeV/c^2 for Ξ_c^+ and 2465± 3.0± 7.0 and 2455± 4.0± 7.0 MeV/c^2 for Ξ_c^0 , which is about 2σ lower than the PDG masses [4]. These mass shifts are

not in the 1993 data which is illustrated by the Ξ_c^+ signals (Fig.5). The measured masses are 2462± 3.0 and 2465± 3.0 MeV/c^2. The systematic error has not yet been evaluated.

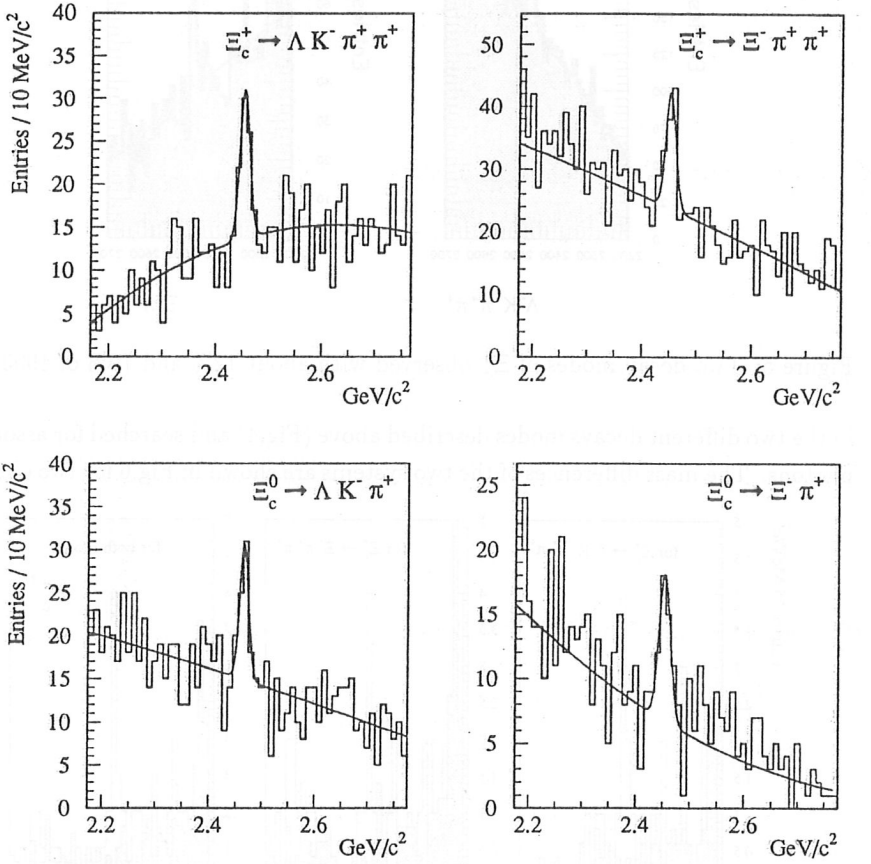

Figure 4: Decay modes of Ξ_c^+ and Ξ_c^0 observed in 1991.

4.3 Search for Ξ_c'

Single-strange charmed baryons have so far only been observed as members of a SU(3) triplet with antisymmetric spin and flavor wavefunctions in the two lighter quarks. The flavor sextet states Ξ_c' with symmetric wavefunction are expected to have a mass larger by about the size of the Λ^0 -Σ^0 mass splitting. Most calculations predict a mass difference only allowing radiative decay into the antisymmetric triplet state [5, 6, 7, 8, 9, 10]. In order to search for those states we have selected Ξ_c^+ candidates

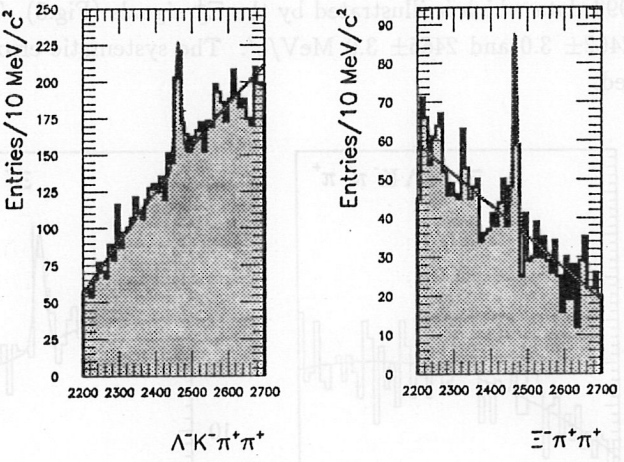

Figure 5: Two decay modes of Ξ_c^+ observed with about 12% and 70% of 1993 data.

in the two different decays modes described above (Fig.4) and searched for associated photons. The mass differences of the two systems are shown in Fig.6 for two observed

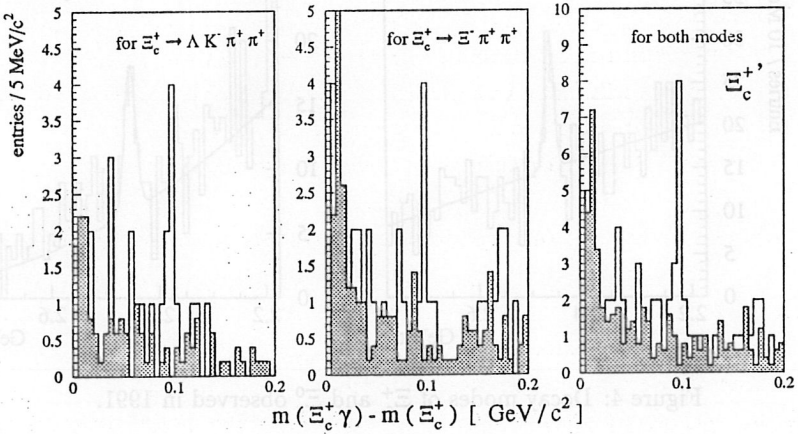

Figure 6: Mass difference $\Xi_c^+\gamma$-Ξ_c^+ in two decay modes for Ξ_c^+ and summed signal

decays of Ξ_c^+ . A small signal can be observed in both spectra at the same energy difference. The summed spectrum is also shown in Fig.6. Although statistically still weak we interpret this signal as first evidence for the observation of a $\Xi_c^{+\prime}$ state. It should be noticed, however, that no evidence could yet be observed for the neutral charge state.

Table 1: Parameters of the Ω_c^0 peaks observed. The errors are statistical only

decay mode	part of used statistics	signal/background	mass MeV/c^2
$\Omega^-\pi^+$	40%	10/3	2723±4
$\Omega^-\pi^-\pi^+\pi^+$	40%	16/8	2714±3
$\Xi^- K_s^0\pi^+$	60%	14/7	2701±3
$\Xi^- K_s^0\pi^+\pi^+\pi^-$	60%	18/8	2706±3
$\Xi^- K^-\pi^+\pi^+$	80%	60/60	2703±3
$\Lambda^0 K_s^0 K^-\pi^+$	40%	22/34	2705±4
$\Lambda^0 K^- K^-\pi^+\pi^+\pi^-$	40%	22/17	2704±3

4.4 Observation of Ω_c^0

Almost ten years after its first evidence from the WA62 hyperon beam experiment [15], which observed a cluster of 3 events at 2740±20 MeV/c^2, the Ω_c^0 remains a poorly known object of which only several dozen decays have been observed in 4 different decay modes by three different experiments. The observation was later confirmed by the ARGUS collaboration which observed 12.2±4.5 events in the channel $\Xi^- K^-\pi^+\pi^+$ [16] and presented evidence for 6.5±3.2 events in the $\Omega^-\pi^-\pi^+\pi^+$ final state [17]. More recently, the tagged photon beam experiment E687 has published evidence for the decay Ω_c^0 to $\Omega^-\pi^+$ (10.3± 3.9 events) [18]. The best mass measurement so far has been performed by the E687 using about 40 decays Ω_c^0 to $\Sigma^+ K^- K^-\pi^+$ [19] obtaining a mass of 2700±1.5±2.5 MeV/c^2. No relative branching ratios for the different decay modes observed have so far been determined, neither has the lifetime been measured. No particular decay mode has yet been seen by at least two experiments.

The preliminary WA89 results on the Ω_c^0 search are presented in the Fig.7. We observe mass peaks of different statistical significance for various decay modes containing Ω^- , Ξ^- and Λ^0 , obtained using from 40% to 80% of the 1993 data for different modes. The results are summarized in Tab.1. Systematic errors of the mass measurement have not been evaluated yet.

In summary, we have observed Ω_c^0 signals in 7 different decay modes. Three of them ($\Omega^-\pi^+$,$\Omega^-\pi^-\pi^+\pi^+$ and $\Xi^- K^-\pi^+\pi^+$) had been observed by other experiments.

5 – Decays of charmed baryons

We have measured the lifetime of Ξ_c^+ , estimated the ratio of two observed branching ratios and searched for possible resonance components of the observed decays.

obtained a preliminary value of $\tau_{\Xi_c^+} = 0.32^{+0.08}_{-0.06} \pm 0.05$ ps in good agreement with existing measurements (Fig.8) [15, 11, 12, 13].

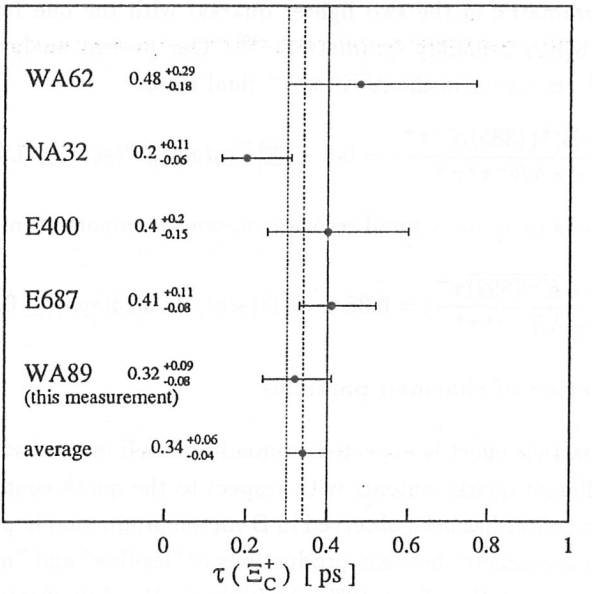

Figure 8: Comparison of all existing life time measurements for Ξ_c^+

The present status of the analysis has not yet allowed a similar study for the neutral Ξ_c^0 partner.

5.2 Decays of Ξ_c^+

Using the Ξ_c^+ lifetime measured we have estimated the relative branching ratios of two decay modes observed in the data from 1993. From this still preliminary analysis we infer that

$$BR(\frac{\Xi_c^+ \to \Lambda K^- \pi^+ \pi^+}{\Xi_c^+ \to \Xi^- \pi^+ \pi^+}) \approx 4 \qquad (1)$$

with large systematic uncertainties. This value could be interpreted such that the association of the resulting two strange quarks to different hadrons is preferred and could be understood from a large recoil transferred to the strange quark in the c-quark decay process.

In D-meson decays two body final states are largely enhanced over many-body decays. Observed multihadronic final states very often stem from the decay of intermediate resonances. Simple considerations predict that in the case of the

Ξ_c^+ baryon resonances should largely be suppressed and can only come from short range spin-spin interactions or from a mixing of the Ξ_c^+ wavefunction (which is mainly antisymmetric in the two lighter quarks) with the one from its multiplet partner $\Xi_c^{+\prime}$ (which is mainly symmetric) [20]. Our present analysis has shown no sign for a Σ^{*+} resonance in the $\Lambda^0 K^- \pi^+ \pi^+$ final state:

$$BR(\frac{\Xi_c^+ \to \Sigma^{*+}(1385) K^- \pi^+}{\Xi_c^+ \to \Lambda K^- \pi^+ \pi^+}) = 0.0 \pm .^{+0.17}_{-0}(stat)^{+0.06}_{-0}(sys), \leq 0.33(90\% c.l.) \quad (2)$$

However there is room for a small resonant mesonic component in

$$BR(\frac{\Xi_c^+ \to \Lambda \overline{K^{*0}(892)} \pi^+}{\Xi_c^+ \to \Lambda K^- \pi^+ \pi^+}) = 0.38 \pm 0.38(stat) \pm 0.15(sys), \leq 0.9(90\% c.l.) \quad (3)$$

6 – Production of charmed particles

The leading particle effect is expected to manifest itself in x_F distributions of particles with different quark contents with respect to the quark content of the beam. Indeed, such an effect has been observed in D-meson production in pion beams [21, 22]. At $x_F \approx 0.5$ the asymmetry between productions of "leading" and "non-leading" particles was measured to be about 10%. At lower x_F the asymmetry is considerably lower.

In order to look for the leading particle effect we have studied x_F distributions for D-mesons, Λ_c^+ and Σ_c using the 1991 data set, and also made a comparison with preliminary results for for Ξ_c^+ obtained with the 1993 data set. The corresponding mass distributions and acceptance corrected x_F distributions are presented in the Fig.9. The usual parametrization of the differential cross-section was used:

$$\frac{d\sigma}{dx_f dp_t^2} = A \cdot (1 - x_f)^n \cdot e^{-bp_t^2} \quad (4)$$

The measured values of the parameters are presented in Tab.2. Within the still

Table 2: Fitted values for the slope parameters n and b. Quark contents of particles may be compared with the quark content of the beam - sdd

particle	quarks	n	b
D^-	$\bar{c}d$	$5.1 \pm 1.9 \pm 0.4$	$1.1 \pm 0.3 \pm 0.2$
Λ_c^+	cud	$4.9 \pm 1.2 \pm 0.4$	$1.1 \pm 0.3 \pm 0.1$
Σ_c^0	cdd	$4.6 \pm 2.3 \pm 0.6$	$1.8 \pm 0.3 \pm 0.2$
Ξ_c^+	csu	$4.7 \pm 1.6 \pm 0.6$	

large errors for the slope n no influence of the quark content seems visible. However

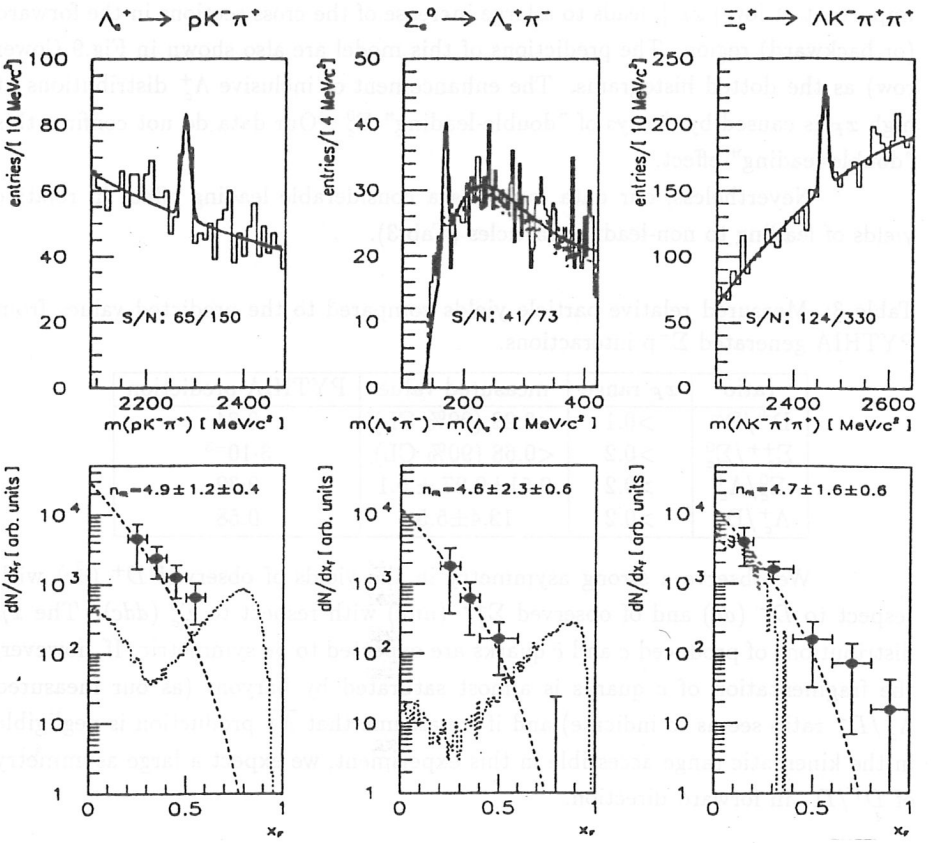

Figure 9: Mass distributions and x_F spectra for Λ_c^+, Σ_c^+ and Ξ_c^+. The solid lines represent the results of a fit, the dotted histograms are the predictions of the PYTHIA–LUND model with arbitrary normalization.

the simple parametrization used might be not sensitive to possible differences of x_F distributions in the high x_F range. The low statistics available does not allow us to make an asymmetry measurement as it has been done elsewhere [21, 22].

In NLO-QCD calculations charm quark production is described via the 'dominant' QCD processes $q\bar{q}$ annihilation and gg-fusion which lead to a general value for n=6.9 [23]. The PYTHIA-Lund model describing the hadronization of charm quarks predicts a very strong "double-leading" effect via a color flow mechanism if the charmed particle may share two quarks with the beam particle. Assuming a "hard" interaction of 2 partons only, the spectator quarks (diquarks) remain undisturbed keeping their initial colour. This way a colour correlation between the produced c-quarks and the spectator quarks can be kept which leads to an efficient recombination of the c-quark with the beam remnant. This process, although not

important at low $|x_F|$, leads to a large increase of the cross sections in the forward (or backward) region. The predictions of this model are also shown in Fig.9 (lower row) as the dotted histograms. The enhancement of inclusive Λ_c^+ distributions at high x_F is caused by decays of "double-leading" Σ_c^0 . Our data do not confirm this "double-leading" effect.

Nevertheless, our data indicates a considerable leading effect in relative yields of leading to non-leading particles (Tab.3).

Table 3: Measured relative particle yields compared to the predicted values from PYTHIA generated Σ^-p interactions.

ratio	x_F range	measured value	PYTHIA prediction
D^+/D^-	>0.1	<0.28 (90% CL)	0.84
Σ_c^{++}/Σ_c^0	>0.2	<0.68 (90% CL)	$3{\cdot}10^{-3}$
Σ_c^0/Λ_c^+	>0.2	$0.51\pm0.27\pm0.1$	0.32
Λ_c^+/D^-	>0.2	12.4 ± 5.5	0.58

We observe a strong asymmetry in the yields of observed D^+ $(\bar{d}c)$ with respect to D^- $(d\bar{c})$ and of observed Σ_c^{++} (uuc) with respect to Σ_c^0 (ddc). The x_F distributions of produced c and $\bar{c}$ quarks are expected to be symmetric. If, however, the fragmentation of c quarks is almost saturated by baryons (as our measured Λ_c^+/D^- ratio seems to indicate) and if we assume that $\overline{\Lambda_c^+}$ production is negligible in the kinematic range accessible in this experiment, we expect a large asymmetry of D^+/D^- in forward direction.

7 – Conclusion

We have measured relative particle rates and relative inclusive differential cross sections in x_F and $p_\perp^2$ for $\Sigma^- N$ interactions at 330 GeV/c. Our results indicate a leading particle effect in hadroproduction, which is a pronounced influence of the quark structure of the beam particle on the yield of charm final states. We observe a significant enhancement of D^- mesons relative to D^+ in the range $x_F > 0.1$, and an enhancement of Σ_c^0 relative to Σ_c^{++} in the range $x_F > 0.2$. The data indicate that in our acceptance ($x_F \geq 0.2$) most of the charm quarks are bound in charm baryons with the $\bar{c}$ quarks hadronizing to a charm meson. Such an effect may be expected for a baryon beam in forward direction.

A big sample of charmed–strange baryons has been detected. Five new decay channels of Ω_c^0 have been observed.

The lifetime of Ξ_c^+ has been measured which is in good agreement with other measurements.

References

1. W.Beusch, CERN-SPSC/77-70, CERN, Geneva, Switzerland (1977)
2. W. Beusch et al., Nucl. Instrum. Methods **A323** (1992) 373.
3. W.Brückner et al., Nucl. Instrum. Methods **A313** (1992) 345.
4. Particle Data Group; L. Montanet et al., Phys. Rev. **D50** (1994) n.3, part I.
5. A. De Rujula, H. Georgi and S. L. Glashow, Phys. Rev. **D12** (1975) 147
6. K. Maltman and N. Isgur, Phys. Rev. **D22** (1980) 1701
   S. Capstick and N. Isgur, Phys. Rev. **D34** (1986) 2809
7. W-Y. P. Hwang and D. P. Lichtenberg, Phys. Rev. **D35** (1987) 3526
8. C. Itoh et al., Phys. Rev. **D40** (1989) 3660
9. S. Fleck and J. M. .Richard, Particle World vol. 1, no. 3 (1990) 67
   J. M. Richard and P. Taxil, Phys. Lett. **B128** (1983) 453
10. J. G..Körner, M. Krämer and D. Pirjol, DESY-94-095, MZ-THEP-94-08
11. P. Coteus et al., Phys. Rev. Lett. **59** (1987) 1530.
12. S. Barlag et al., Phys. Lett. **B233** (1989) 522
13. P.L. Frabetti et al., Phys. Rev. Lett. **70** (1993) 1381.
14. WA89 collaboration (S. Brons et al.), in: Proc. Heavy Quarks at Fixed Target (ed. S. Bianco and F.L. Fabbri, Frascati 1993), **1**, 181 (SIS Ufficio Pubblicazioni, Frascati (Roma), 1993)
15. S. Biagi et al., Zeitschr. f. Phys. **C28** (1985) 175.
16. H. Albrecht et al., Phys. Lett. **B288** (1992) 367.
17. J. Stiewe, Proc. 26th int. Conf on High Energy Physics, AIP Conf. Proc., New York (1993) 1076.
18. P.L. Frabetti et al., Phys. Lett. **B300** (1993) 190.
19. P.L. Frabetti et al., Phys. Lett. **B338** (1994) 106.
20. J.G. Körner et al., Zeitschr. f. Phys. **C55** (1992) 659.
21. M. Adamovich et al., Phys. Lett. **B305** (1993) 402.

22. G.A. Alves et al., Phys. Rev. Lett. **72** (1994) 812.

23. P. Nason et al., CERN-TH/94-7134.

Frascati Physics Series, Vol. III (1994)
HEAVY QUARKS AT FIXED TARGET
University of Virginia, October 7–10, 1994
(pp. 157–165)

Charm From Hyperons in the Future: Fermilab Experiment 781

Michael Procario
Carnegie Mellon University

ABSTRACT

Recent results from CERN experiment WA89 have shown that charmed baryons and particularly charmed-strange baryons have a significant cross section in Σ^- beams. Fermilab experiment 781, which is currently under construction, will utilize this fact to pursue a broad program of high statistics studies of charmed baryons in the next Fermilab fixed target run.

1 – Introduction

As the previous speaker has clearly shown, charmed baryons and particularly charmed-strange baryons are copiously produced in Σ^- beams at $x_F > 0.2$. CERN experiment WA89 already has a sample of reconstructed charmed-strange baryons that is is as good as any in the world, despite having a relatively small sample of charmed mesons. Fermilab experiment 781 [1] will pursue this technique for studying charmed baryons with higher beam fluxes, larger acceptance, and a better vertex detector. This will make E781 a second generation charmed baryon experiment, and allow the systematic, in-depth study of charmed baryon production and decay physics.

The are a variety of physics goals in charmed baryon studies. The first is a complete understanding of the weak decays. Charmed baryons like charmed mesons have large QCD effects in their weak decays, and to understand these effects will require a broad program of measurements. The first measurements should be precision lifetimes of all weakly decaying charmed baryons. Today, only the Λ_c^+

is measured to better than 10%. Bigi has called for all weakly decaying charmed baryon lifetimes to be measured to better than 10%. [2]

A very important complement to lifetimes are the semileptonic decays. Currently, CLEO and ARGUS have evidence for $\Lambda_c^+ \to X\Lambda\ell\nu$ and $\Xi_c^0 \to X\Xi^-\ell\nu$ decays and CLEO also has observed $\Xi_c^+ \to X\Xi^0\ell\nu$ decays. [3] There is currently no evidence of a semileptonic decay where the final state baryon is not a ground state hyperon.

Non-leptonic decays will be needed to sort out all of the nonfactorizing effects that are expected in charmed baryons. Only in the case of the Λ_c^+ have significant non-leptonic decays been observed. Many of these are multibody decays which may have resonance structure, but very little is known about that now.

The second major area of physics that can be addressed with charmed baryons is spectroscopy. Heavy Quark Effective Theory (HQET) has made a variety of predictions about the spectrum of charmed mesons, and similar predictions about baryons should be possible. There are extra degrees of freedom in the baryon sector which can be used to more stringently test the potential models, lattice calculations, and HQET predictions. Experimentally, most of the spectrum is unknown. Three of the four the ground state baryons are firmly established, as are the isospin 1 triplet of Σ_c's. New results on the Ω_c [4], excited Λ_c's [5], and the Ξ_c' are statistically limited and will need to followed up. The rest of the spectrum is unknown.

The simple predictions of charm production from perturbative QCD do not agree with the data, although these predictions have been successfully corrected by modeling the non-perturbative effects. Most of this work has been done for mesons where the hadronization of the quark into the meson has been accounted for with fragmentation models. Currently, the production of charmed baryons seems to pose many more puzzles than have been seen in the mesons. NA32 has reported observing equal rates of Λ_c and $\bar{\Lambda}_c$ at large x_F from a π^- beam, which is hard to understand in terms of perturbative QCD. WA89 has seen strong leading particle effects in a Σ^- beam. They observe a much larger $\Sigma_c^0(cdd)$ signal than $\Sigma^+ +_c (cuu)$. [6] Both particles decay to Λ_c^+ and a charged π so their acceptances are similar. One thing that is different is that $\Sigma_c^0(cdd)$ has the same light diquark (dd) as the Σ^-.

2 – The Detector

E781 is a three-stage forward charge-particle spectrometer with particle identification and electromagnetic calorimetry. The detector has acceptance of $0.1 < x_F < 1.0$. The overall layout of the detector is shown in figure 1. The are a variety of reasons for choosing this geometry.

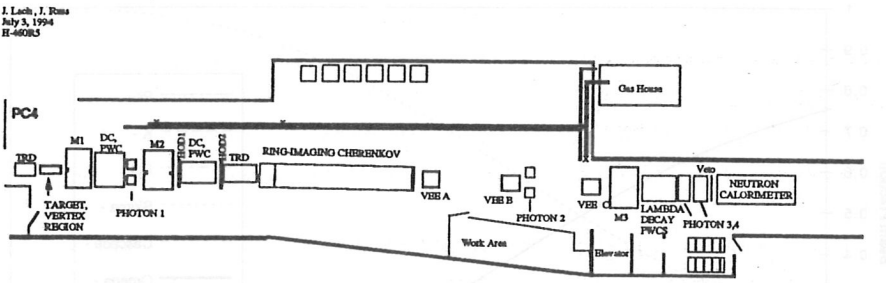

Figure 1: The layout of E781

- At high x_F the tracks have higher momentum and lower multiple scattering. This improves the vertex resolution, and allows us to trigger on large miss distance tracks.

- For the high momentum tracks we have a small solid angle to cover. This allows the use of a RICH with phototubes as the photon detector. Phototubes are easier to use and build than to TAMI or CsI photocathodes.

- It has been previously measured that the ratio of baryons to mesons increases with x for strange particles, and the recent WA89 results have shown the same effect for charmed particles.

The philosophy of the detector's design could be stated as: We know that there is charm there and we should optimize on signal/background not signal.

The beam is predominantly mixture of π^- and Σ^- with a small admixture of Ξ^- and Ω^-. The ratio, $n(\Sigma^-)/n(\pi^-)$ can be adjusted by varying the momentum that is accepted as shown in figure 2. We plan to run with a ratio $n(\Sigma^-)/n(\pi^-) \geq 1$. The Σ flux will be 10^6 MHz.

The first stage of the spectrometer has large acceptance with a 2.5 GeV/c momentum cutoff. This stage measures soft pions from D^*'s, Σ_c's and other decays of excited charm states. It also can measure the tracks from the other charm particle which is produced at lower x_F than the trigger charm particle, so that we can study charm pairs.

The second stage of the spectrometer has a 15 GeV/c momentum cutoff. This stage is used for the trigger, which will be fully discussed in the next section. There is a RICH detector with useful p/K separation from 20 GeV/c to 225 GeV/c and K/p separation from 40 GeV/c to 480 GeV/c. There is a transition radiation detector for electron identification.

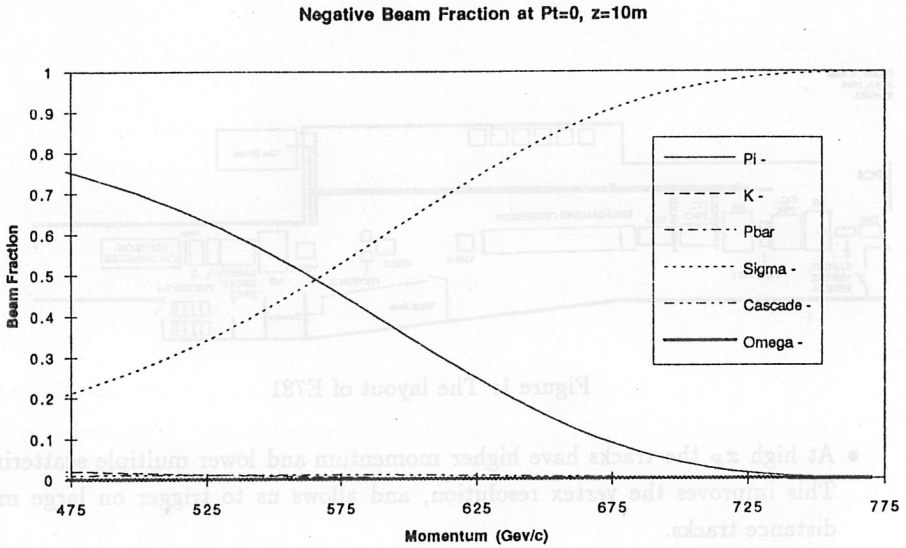

Figure 2: Particle fractions in Fermilab proton center hyperon beam

The last stage measures the decay products of Λ's that decay very far downstream. Charmed strange baryon decays can decay Ξ^- and Ω^- which produce Λ's very far downstream. This last stage is needed to achieve high efficiency for these decays.

The beam is measured with a silicon strip system to provide high accuracy predictions of $x-y$ position the primary vertex. The vertex region also has a silicon strip detector. This detector has 20 planes in 4 views to provide highly redundant tracking information to simplify track-finding and track-matching both in the online software filter and offline reconstruction. The performance of an eight plane system using an earlier generation of VLSI readout was run in a test beam. It achieved excellent hit resolution of 4μm for planes with 20μm pitch by interpolating the charge deposited in adjacent strips.

There are three lead glass photon detectors for the reconstruction of π^0s and photons. One array of lead glass is associated with each stage of the spectrometer. The most downstream array will detect the radiative decay photons like $\Sigma^0 \to \Lambda\gamma$ or the not yet confirmed $\Xi_c' \to \Xi_c\gamma$.

3 – Charm Trigger

The heart of E781 is the hardware trigger and online software filter. Both of these processes rely on the fact that the multiplicity is low in the second stage spectrometer and that these tracks are high enough momentum that they are well measured. The

typical multiplicity of non-charm events is 15 at the primary vertex but only 5 in our second stage spectrometer.

Two scintillator hodoscopes combined with matrix logic can count the number, measure the charge, and roughly estimate the momentum of tracks in the second spectrometer. By requiring 3 positive tracks in the second spectrometer, the hardware trigger rejects non-charm by a factor of 8-10. Typically the charmed baryon will contribute 2 of these positive tracks and the underlying event will contribute the other. Events passing this trigger are fully read out and passed on the online software filter.

The software filter runs in real time and only those event passing the filter are written to tape. This greatly reduces the offline analysis load after the experiment finishes its run, but it is critical that the quality of data is closely monitored to insure that data is not lost.

The software filter is topological looking for evidence of a secondary vertex. The filter searches for tracks after the second magnet. Those that are found are projected back into the vertex detector. Since the multiplicity is low after the second magnet the track finding is simplified there, and by looking only along the projected tracks in the vertex detector the track finding is also simplified in the vertex detector. These tracks are compared with the intersection of the beam track and the target foils. If any of the tracks miss this intersection by a significant amount then there is evidence of a secondary vertex.

The angular acceptance of the second stage of the spectrometer is 30 mrad and the targets are at most 1.5 mm thick, so the worst case geometric effect is 22μm. Multiple scattering errors are minimized by using only high momentum tracks. Simulations studies have shown that a 30μm cut on the miss distance keeps the non-charm background trigger rate below 1%, if there are no tracking error. The fake trigger rate will be dominated by tracking errors not measurement errors.

A test was performed with an eight plane silicon vertex detector and single magnet spectrometer of similar angular acceptance as the full experiment. Data was taken with a 400 GeV pion beam striking a thick target (6% λ_{int} of Al). Figure 3 shows the maximum miss distance per event from the test run. The measured rejection was good, and the E781 trigger should do better. A number of the events in the tail of the distribution had hit confusion that will be helped by the stereo planes and the extra planes in the full vertex detector.

The miss distance filter is fully efficient for charmed baryon decays with lifetimes than 100 fs. It will also be very efficient for charmed meson decays, since the filter requirement is just a secondary vertex. The sample of charmed mesons should be comparable to the sample of charmed baryons. It should be very good for

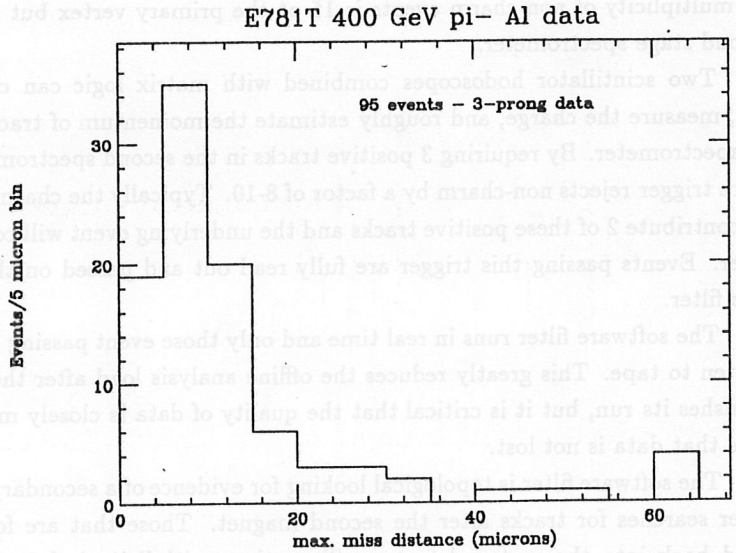

Figure 3: Test run results for maximum miss distance from primary of high momentum tracks using an 8 plane silicon strip detector

calibrating our detector, and we may be able to some small amount of physics with it.

Events which pass the miss distance filter are very useful for physics analysis. The filter indirectly requires requires a secondary vertex. In most analyses of charmed produced in fixed target experiments, the most powerful rejection of background is achieved by requiring that the secondary vertex be separated from primary vertex. This is usually expressed as the distance from the primary vertex to the secondary divided by the resolution on the vertices (L/σ). A simulation of $\Lambda_c^+ \to pK^-\pi^+$ with $x_F = 0.3$ shows the effect of the miss distance trigger. Figure 4 shows that events with low L/σ have been removed, so they events that pass our trigger are easier to analyze.

Some charmed baryons such as the Ω_c may have shorter lifetimes. We can also use other software filters designed around different event characteristics. In Ω_c and Ξ_c decays there is multiple strangeness. Using the RICH to identify protons and kaons and select events having both, and have sufficient rejection of background to not need the miss distance requirement.

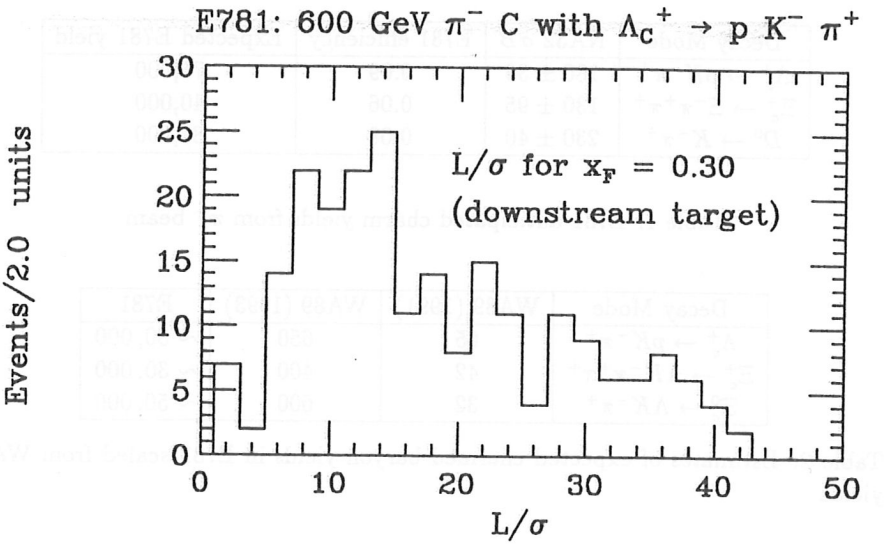

Figure 4: Monte Carlo results for the significance of Λ_c^+ vertices that pass the trigger

4 – Yields

E781 plans to accumulate more than 10^6 reconstructed charmed hadrons, with over 100,000 in the large charmed baryon decay modes. Using NA32 π^- production cross sections [7] we can predict what E781 can expect from running with a π^- beam. We scale up the cross section by 2 to account for our higher energy beam. The x_F distribution is different. The power is 4.2 instead of 3.5. We use the same p_t spectrum.

The assumptions about the run are 1000 hours of data with 1000 seconds of livetime per hour; 4% interaction probability; and that charmed production scales like $A^{1/3}$. The average A of the E781 target is 32.8. The trigger and reconstruction efficiencies have been calculated. The trigger efficiency weighted by the cross section

$$\frac{d\sigma}{dx_F} = (1 - x_F)^{4.2}.$$

The reconstruction efficiencies were calculated using all necessary effects, such as detector resolution, multiple Coulomb scattering, primary and secondary vertex assignment, but not pattern recognition mistakes. The results for π^- data are shown in table 1.

The calculation of expected yields from the Σ^- beam is more difficult than for the π^- beam because the WA89 cross section analysis is not complete. We

Decay Mode	NA32 σB	E781 efficiency	Expected E781 yield
$\Lambda_c^+ \to pK^-\pi^+$	180 ± 36	0.09	75,000
$\Xi_c^+ \to \Xi^-\pi^+\pi^+$	130 ± 95	0.06	40,000
$D^0 \to K^-\pi^+$	230 ± 40	0.08	86,000

Table 1: E781 anticipated charm yields from π^- beam

Decay Mode	WA89 (1991)	WA89 (1993)	E781
$\Lambda_c^+ \to pK^-\pi^+$	65	650	$\sim 50,000$
$\Xi_c^+ \to \Lambda K^-\pi^+\pi^+$	42	400	$\sim 30,000$
$\Xi_c^0 \to \Lambda K^-\pi^+$	32	600	$\sim 50,000$

Table 2: Estimates of expected charmed baryon yields in E781 scaled from WA89 yields

attempt to scale their yields by taking into account the relative acceptances, rejection factors and number of triggered events. The assumptions used are itemized below.

- The WA89 efficiency for $\Lambda_c \to pK^-\pi^+$ is 1% in 1991, 2.5% in 1993 and 1994 for $x_F > 0.2$.
- WA89 trigger rejected inelastic events five times the rate it rejected charm events.
- WA89 uses a L/σ cut of 5, which is similar to the E781 online filter.
- E781 will have 15 times more interactions.
- E781 average efficiency per mode is 8%.
- The cross section at 600 GeV is 1.5 times greater than at 330 GeV.

Using these assumptions we arrive at the estimates in table 4. These estimates are only good to a factor of 2-3.

E781 will be able to take data with both beams simultaneously. This will allow for systematic comparisons of the production from both beams. Since the software filter gives us the ability to find charm while still running, we will able to choose the beam that best optimizes our charmed baryon yields.

5 – Conclusions

Charmed baryon physics is maturing. Results are now coming in from a variety of experiments on weak decays, spectroscopy and production mechanisms, which is stimulating theoretical work in the is area. However, most of the current results still have poor statistics compared to charmed mesons. The interesting questions like the differences in charmed baryon lifetimes, the possible leading particle effects, and many others will need higher statistics to be answered.

An experiment optimized for the study of charmed baryons can significantly improve this situation. E781 has set out to optimize the observation of charmed baryons through the use of a Σ^- beam, a very forward geometery, excellent particle identification, and a topological trigger. The yields expected in E781 will by on the order of 100,000 reconstructed charmed hadrons in the large decay modes. This sample will have similar numbers of charmed mesons and baryons and the charmed-strange baryons will be similar in number as the charmed baryons.

References

1. E781 Collaboration: Carnegie Mellon University, Fermilab, University of Iowa, University of Rochester, University of Washington, Petersburg Nuclear Physics Institute, ITEP(Moscow), IHEP(Protvino), Moscow State University, University of São Paulo, Centro Brasileiro de Psequisas Fisicas, Univeridade Federale de Paraiba, IHEP(Beijing), University of Bristol, Tel Aviv University, Max-Plank-Institut für Kernphysik-Heidelberg, Universidad Autonoma de San Luis Potosi.

2. I.I. Bigi, CERN-Th.7370/94 .

3. H. Albrecht *et. al.* (ARGUS Collaboration), Phys. Lett. **B269** p. 234 (1991).
   H. Albrecht *et. al.* (ARGUS Collaboration) Phys. Lett. **B303** p. 368 (1993)
   T. Bergfeld *et. al.* (CLEO Collaboration) Phys. Lett. **B303** p. 368 (1993)
   J. Alexander *et. al.* (CLEO Collaboration) CLNS 94-1288.

4. P. Frabetti *et. al.* (E687 Collaboration), Phys. Lett. **B300** p. 190 (1993).

5. H. Albrecht *et. al.* (ARGUS Collaboration), Phys. Lett. **B317** p. 277 (1993).
   P. Frabetti *et. al.* (E687 Collaboration), Phys. Rev. Lett. **72** p. 961 (1994).
   K. Edwards *et. al.* (CLEO Collaboration), CLNS 94-1304.

6. R. Werding (WA89 Collaboration), talk given at the International Conference on High Energy Physics, Glasgow, Scotland, 1994.

7. S. Barlag *et. al.* (NA32 Collaboration), Phys. Lett. **B247** 113 (1990)

Frascati Physics Series, Vol. III (1994)
HEAVY QUARKS AT FIXED TARGET
University of Virginia, October 7–10, 1994
(pp. 167–182)

CHARM SEMILEPTONIC PHYSICS

Jim Wiss
Department of Physics
University of Illinois at Urbana-Champaign
1110 W. Green St.
Urbana IL. 61801-3080

ABSTRACT

We review recent data on semileptonic decays of charmed mesons and baryons. These data provide tests of lattice guage theories, HQET and unique estimates of absolute branching fractions for several baryon and meson states.

1 – Introduction

There have been a huge number of new and interesting results on charm semileptonic physics even since the CHARM2000 conference earlier this summer.

$e^{\pm}$, ft	$D^o \to K^- \ell\nu$	$f_+(q^2)$	$\surd$
ft	$D^+ \to K^* \ell\nu$	$A_1(0), V_1(0), V_2(0)$	$\surd$
$e^{\pm}$, ft	$D_s^+ \to \phi\ell\nu$	$\mathcal{B}$, $A_1(0), V_1(0), V_2(0)$	$\surd$
$e^{\pm}$	$D^+ \to \pi\ell\nu$	V_{cd}/V_{cs} $(f_+(q^2))$	X
$e^{\pm}$, ft	$D_s^+ \to \eta$ & η' $\ell\nu$	Vec/PS	$\surd$
$e^{\pm}$	$\Lambda_c^+ \to \Lambda\ell\nu$	$\mathcal{B}$, HQET	$\surd$
$e^{\pm}$	$\Xi_c \to \Xi\ell\nu$	$\mathcal{B}$	$\surd$

Above is a highly schematic table which summarizes the states which have been studied, how they have been studied, and either the realized or future () physics potential of such measurements. Results from fixed target experiments (ft) continue to complement those from e^+e^- annihilation ($e^{\pm}$). Charm semileptonic studies provide a wealth of information including: important probes of quark dynamics through

measurements of form factors ($f_+(q^2)$) and ($A_1(0), V_1(0), V_2(0)$), model dependent information on the absolute branching ratios ($\mathcal{B}$) for the D_s^+, Λ_c^+ and Ξ_c, information on CKM matrix elements (V_{cd}/V_{cs}), and tests of HQET. Determination of CKM matrix elements (V_{bu}) and more stringent tests of HQET will be possible through the interplay of studies of both charm and beauty semileptonic decay results.

At present there is a long standing theoretical problem with the observed ratio of vector to pseudoscalar decay widths for $D^+ \to K^*\ell\nu$ relative to $D^+ \to K\ell\nu$ [1] which has recently been confirmed through comparisons of the width for $D_s^+ \to \phi\mu\nu$ to $D_s^+ \to (\eta + \eta')\mu\nu$ (Vec/PS). Because of the undetected ν, one only partially reconstructs the final state leaving the important experimental challenge of proving exclusivity of the final state; *ie* one must establish that one is observing the claimed final state without additional, undetected neutrals. A variety of experimental techniques can be brought to bear on the problem of isolating semileptonic decays from both non-charm and charm backgrounds. Frequent use is made of D^* tagging. One often has the ability to exploit the charge correlations between leptons and kaons or D^* decay pions and thus eliminate backgrounds through a wrong sign subtraction. Often, in fixed target experiments, Cabibbo forbidden decays (X) are subject to particle mis-identification backgrounds from the much more copious Cabbibo allowed decays ($\surd$).

2 $D \to$ pseudoscalar $\ell^+\nu$

These decays are particularly interesting to study since they can provide detailed information on the q^2 dependence of the charm semileptonic form factors, $f_+(q^2)$. The decay rate expression for PS $\ell\nu$ is:

$$\frac{d\Gamma}{dq^2} = \frac{G_F^2 |V_{cq}|^2 P^3}{24\pi^3} \{|f_+(q^2)|^2 + m_\ell^2 \, |f_-(q^2)|^2 ...\} \qquad (1)$$

where P is the D frame momentum of the pseudoscalar particle and one of the two possible form factors $f_-(q^2)$ becomes unimportant in the limit of zero lepton mass. Two parameterizations are used for $f_+(q^2)$:

$$f_+(q^2) = \frac{f_+(0)}{(1 - q^2/m_{pole}^2)} \quad \text{or} \quad f_+(q^2) = f_+(0)e^{\alpha q^2} \qquad (2)$$

The first form is motivated by the belief that the coupling of the $c\bar{q}$ quarks to the virtual $W^\pm$ should be dominated by bound states [1] of the $c\bar{q}$ system; the second form is motivated [2] by the ISGW model. Figure 1(a) illustrates the difference

[1] Hence for the case of $D \to K\ell\nu$ decay, one expects that m_{pole} should be set to the mass of the vector $D_s^*(2110)$ since it has the same spin-parity as the $c\bar{s}$ current of the form factor.

between $f_+^2(q^2)$ for a pole form, an exponential form, and a linear form. Over the restricted q^2 range available for the presently studied $D^o \to K^-\ell^+\nu$ decay, one is primarily measuring just the slope ratio, $(df_+/dq^2(0))/f_+(0)$. To go futher, we will probably have to wait for the future for measurements of $D \to \pi e^+\nu$ so that the q^2 domain can extend much closer to the location of the anticipated D^{+*} (rather than D_s^{+*}) pole. Figure 1(b) illustrates that $f_+^2(q^2)$ has a rather subtle, asymmetric, and

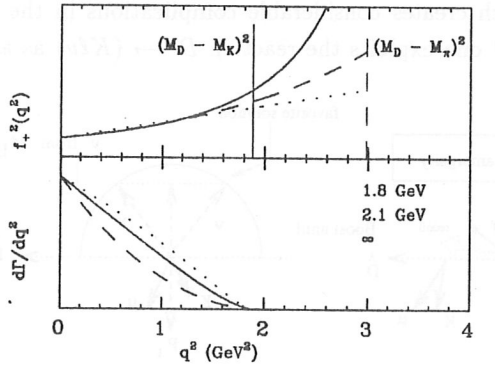

Figure 1: (a) Various parameterizations of $f_+^2(q^2)$ over the kinematic range for $D^o \to Ke^+\nu$ (vertical solid) and $D \to \pi e^+\nu$ (vertical dashed). The pole form (solid), exponential form (dashed) and a linear form (dotted) are displayed. (b) $d\Gamma/dq^2$ for $m_{pole} = 2.1\ GeV$ (solid), $m_{pole} = \infty$ (dashed) , $m_{pole} = 1.8\ GeV$ (dotted)

difficult to measure influence on $d\Gamma/dq^2$. Most of one's ability to measure beyond $f_+(0)$ and $df_+/dq^2(0)$ occurs at large q^2 where the rate is low.

One can measure the product of $f_+^2(0)$ and the appropriate CKM matrix element by integrating the $d\Gamma/dq^2$ expression given by Eqn. (1) using the measured $f_+(q^2)/f_+(0)$ shape and setting the integrated width to the measured total width for $\Gamma(\text{PS}\ \ell\nu)$. Experiments generally measure a given final state semileptonic width $\Gamma(f\ \ell\nu)$ by first determining the absolute branching fraction of the decay $\mathcal{B}(f\ \ell\nu)$ from the yield of the $X\ell\nu$ state relative to the yield of a decay with a known absolute branching ratio. Γ then follows from $\mathcal{B}$ and the lifetime of the particular charm species (C):

$$\Gamma(C \to f\ell\nu) = \hbar\mathcal{B}(f\ \ell\nu)\ /\ \tau_C \qquad (3)$$

2.1 $D \to K\ell^+\nu$

Much of the information on the detailed decay shapes originally came from fixed target experiments which exploit their generally excellent vertexing capability in order to "close" the decay kinematics and measure q^2. The momentum of the unobserved neutrino can be measured to within a two fold ambiquity by balancing p_t

about the line between the primary and secondary vertex. The kinematics is most easily done by boosting along the D direction until the sum of the longitudinal kaon and lepton momentum vanishes. The CLEO Collaboration [2] devised a way of obtaining q^2 information without relying on knowlege of the D momentum direction for events from $D^{*+} \to \tilde{\pi}^+(K^-\ell^+\nu)$ decay. Figure 2 contrasts these two methods for obtaining information about the missing neutrino. In both cases q^2 smearing is considerable which creates considerable complications in the fitting procedure. Traditionally [3] [4] [2] one exploits the reaction $D^* \to (K\ell\nu)$ as a method to elimi-

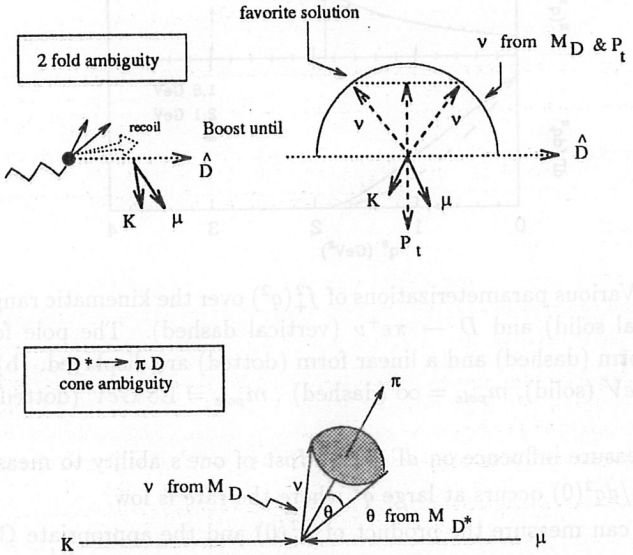

Figure 2: In the upper figure, the kaon and lepton are boosted along the $\hat{D}$ direction into a frame where their momentum sum lies transverse to the $\hat{D}$ direction. The neutrino P_t balances the P_t of the kaon + lepton and its energy can be computed from the P_t and mass of the D. The neutrino momentum is then known to a 2-fold ambiguity corresponding to the intersection of the P_t line and the energy circle. The favorite solutions used by most groups is marked. For the case of *eg* $D^{*+} \to \tilde{\pi}^+(K^-\ell^+\nu)$ decay (lower figure) boosts the $\tilde{\pi}$ to the $K^-\mu^+$ rest frame. The ν momentum can be computed from the D^o mass; and the angle θ between the $\tilde{\pi}$ and the ν can then be computed from the D^{*o} mass. q^2 is bounded by minimum q^2 on the neutrino cone closest to μ and a maximum q^2 furthest from μ.

nate backgrounds from other charm semileptonic sources. The most recent results employing a D^* tag come from CLEO [2] (Fig. 3) and E687 [5] (Fig. 4).

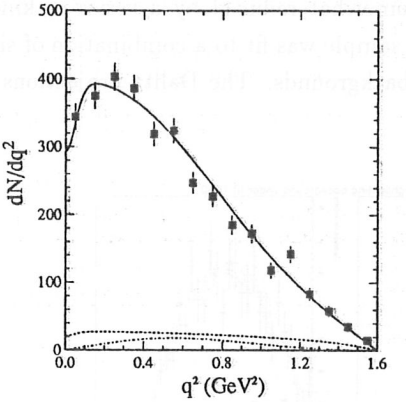

Figure 3: The uncorrected q^2 dependence from CLEO's 2700 event sample D^* tagged sample where the modes $D^o \to K^-\ell^+\nu$ and $D^+ \to K_s\ell^+\mu$ are combined.

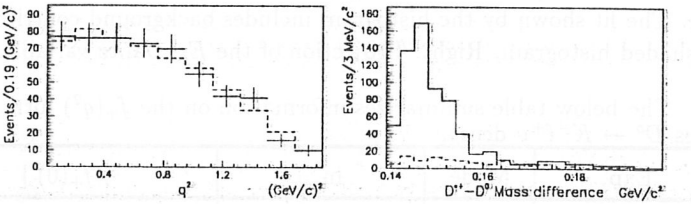

Figure 4: Left: The uncorrected q^2 distribution for $K^-\mu^+\nu$ events from the E687, $\approx$ 500 event, D^* tagged sample. Right: The $D^{*+} - D^o$ mass difference for right sign (solid) and wrong sign (dashed) events.

Recently E687 [5] greatly increased their statistics for this mode by including a sample of $\approx$ 1850 inclusive $D^o \to K^-\mu^+\nu$ events where a D^* tag was not required. Of course without the cleansing power of a D^* tag there will be an inevitable increase in backgrounds from both misidentified muons and other semileptonic decay processes such as $D^+ \to (K^-\pi^+)\mu^+\nu$, $D^0 \to (K^-\pi^o)\mu^+\nu$,and $D_s^+ \to \phi\mu^+\nu$.

Background was somewhat reduced by a series of kinematic cuts. The Dalitz plot for the surviving sample was fit to a combination of signal, and semileptonic and misidentification backgrounds. The Dalitz projections are shown in Fig. 5.

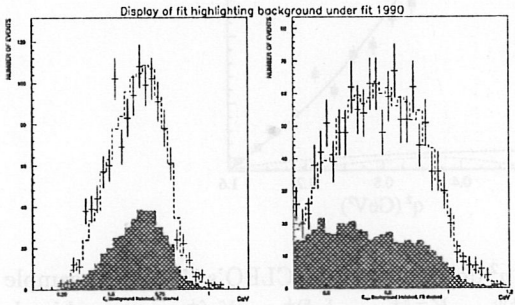

Figure 5: Left: Projection of the E_μ (muon energy in the D rest frame) Dalitz variable. The fit shown by the histogram includes background contributions shown by the shaded histogram. Right: Projection of the E_K Dalitz variable.

The below table summarizes information on the $f_+(q^2)$ form factor which describes $D^o \to K^-\ell^+\nu$ decay.

Exp.	Mode	m_{pole}	$\mid f_+(0) \mid$
E691 [3]	$K^-e^+\nu_e$	$2.1^{+0.4}_{-0.2} \pm 0.2$	$0.79 \pm 0.05 \pm 0.06$
CLEO(91) [4]	$K^-e^+\nu_e$	$2.1^{+0.4+0.3}_{-0.2-0.2}$	$0.81 \pm 0.03 \pm 0.06$
CLEO(93) [2]	$K^-\ell^+\nu_l$	$2.00 \pm 0.12 \pm 0.18$	$0.77 \pm 0.01 \pm 0.04$
MKIII [6]	$K^-e^+\nu_e$	$1.8^{+0.5+0.3}_{-0.2-0.2}$	$\mid V_{cs} \mid (0.72 \pm 0.05 \pm 0.04)$
E687 (prelim)†	$K^-\mu^+\nu_\mu$	$2.01^{+0.35+?}_{-0.19-?}$	$0.73 \pm 0.04 \pm ?$
E687 (prelim)‡	$K^-\mu^+\nu_\mu$	$1.91^{+0.13+?}_{-0.10-?}$	$0.75 \pm 0.02 \pm ?$

† D^{*+} tagged sample (450 events) ‡ Inclusive sample (1850 events)

All results appear consistent with the expected D_s^{*+} pole mass of 2.1 GeV, however this is little more than a measurement of the slope of $f_+(q^2)$ near $q^2 = 0$. CLEO obtains an exponential fit to the alternative form: $f_+(q^2) \propto \exp(0.29 \pm 0.04 \pm 0.06)\, q^2$, which, as illustrated in Figure 1 (a) , is nearly indistinquishable from the pole form but has more symmetrical error bars. The $f_+(0)$ values are also consistent with theoretical estimates: $f_+(0) \approx 0.7 - 0.9$.

2.2 $\underline{D \to \pi \ell^+ \nu}$

CLEO [7] has recently made a measurement of $D^+ \to \pi^\circ \ell \nu / K^\circ \ell \nu$ which is substantially free of the usual misidentification background expected for a $\pi^\pm$. Their signal (Fig. 6) is brought out through tagging via $D^{*+} \to \pi^\circ D^+$ decay. They summarize

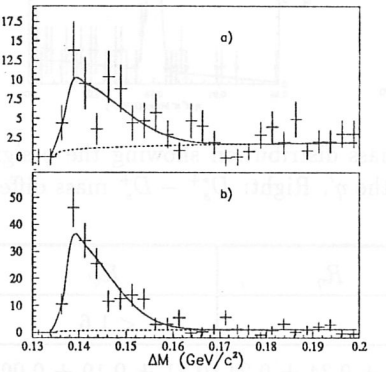

Figure 6: Upper: $D^{*+} - D^+$ mass difference for CLEO tagged $\pi \ell \nu$ candidates. Lower: $D^{*+} - D^+$ mass difference for the normalizing mode $K_s \ell \nu$

their measurement as: $|f_\pi / f_K|^2 \ |V_{cd}/V_{cs}|^2 = .085 \pm .027 \pm 0.014$ since present theoretical uncertainties in the form factors exceed uncertainties in the CKM matrix ratio. Using $|V_{cd}/V_{cs}|^2 = 0.051 \pm .002$ obtained from neutrino produced charm data [8] , CLEO obtains a form factor ratio consistent with unity as expected theoretically. A big increase in statistics for a $\pi \ell \nu$ mode could potentially settle the issue of the q^2 dependence of semileptonic form factors.

2.3 $\underline{D_s^+ \to \eta \mu \nu \ , \ \eta' \mu \nu}$

This work by the CLEO II Collaboration [9] represents a real tour de force for their electromagnetic calorimeter. The D_s^+ signal (Fig. 7) is tagged through $D_s^{*+} \to \gamma D_s^*$ and both the η and η' are reconstructed through decays involving final state photons. The width for the η and η' semileptonic decays is reported relative to the width for $D_s^+ \to \phi \mu^+ \nu$ in terms of the variables R_η and $R_{\eta'}$:

$$R_\eta = \frac{\Gamma(D_s^+ \to \eta \mu \nu)}{\Gamma(D_s^+ \to \phi \mu \nu)} \quad , \quad R_{\eta'} = \frac{\Gamma(D_s^+ \to \eta' \mu \nu)}{\Gamma(D_s^+ \to \phi \mu \nu)} \tag{4}$$

The values of R_η and R'_η are compared to previous values obtained by E653 and two theoretical estimates in the below table:

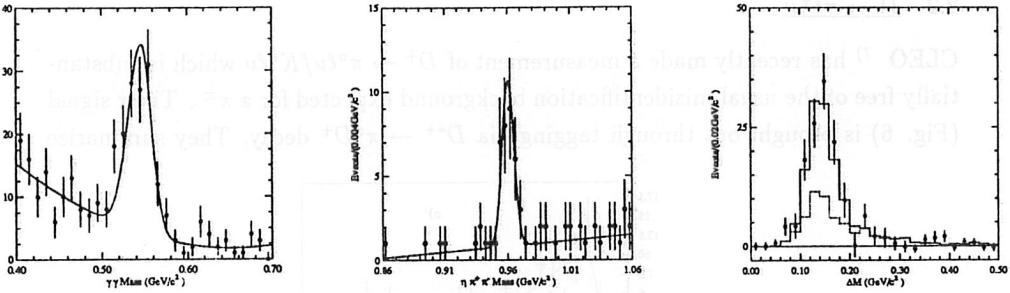

Figure 7: Left: $\gamma\gamma$ mass distribution showing the η signal. Center: $\eta\pi^+\pi^-$ mass distribution showing the η'. Right: $D_s^{*+} - D_s^+$ mass difference.

	R_η ,	$R_{\eta'}$	$R_\eta + R_{\eta'}$
E653		< 1.6	3.9 ± 1.6
CLEO [9]	$1.74 \pm 0.34 \pm 0.24$	$0.71 \pm 0.19 \pm 0.09$	$2.46 \pm 0.39 \pm 0.26$
ISWG [10]	0.39	0.34	0.73
Kamal [11]	$1.85 \pm 0.41 \pm 0.37$	$2.22 \pm 0.57 \pm 0.44$	$4.07 \pm 0.70 \pm 0.57$

Both R_η , R'_η and their sum are substantially lower than the predictions of the modified ISWG model as calculated by D. Scorna. We note that this discrepancy is in the same direction as the well known [1] problem that the width ratio for $D \to \overline{K}\mu\nu$ compared $\overline{K}^*\ell\nu$ is larger than expected theoretically.

3 $D \to$ Vector $\ell\nu$ Decays

The vector $\ell\nu$ decay process involves a hadronic current describing the overlap of the D and vector meson wave functions which (in the limit of zero lepton mass) can be described by two axial and one vector form factor.

A variety of theoretical methods including QCD sum rules [12] , quark models [13] [14] [15], and lattice gauge theory [16] [17] have been brought to bear on the prediction of these three form factors. Although the full expression for the decay width is rather lengthy, a clear exposition can be found in the seminal reference [18]. It has become customary to assume that q^2 dependence of the form factors is dominated by the poles of the cq system with the same spin-parity as the form factor. Hence for $D \to K^*\ell\nu$ decays one expects the $D_s^{*(*)}$ spectrum of poles (2.1 GeV for the vector and 2.5 GeV for the axial). Given the narrow q^2 domain, this is tantamount to assuming values for the form factor q^2 slope near 0. This leaves

one with three measurements $A_1(0)$, $A_2(0)$, and $V(0)$. It has become traditional to factor out $A_1^2(0)$ from the decay width, leaving two ratios: $R_V = V(0)/A_1(0)$ and $R_2 = A_2(0)/A_1(0)$ which serve to describe the *shape* of the decay distribution. The R_v and R_2 values can be used to obtain Γ_ℓ/Γ_t which is the ratio of the q^2

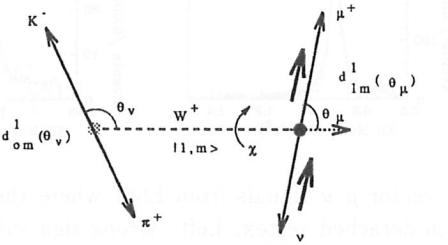

Figure 8: Illustration of the three decay angles used in describing the decay of *eg* $D \to K\ell\nu$. The form factors determine a q^2 dependent spin of the virtual W^+ which then dictates the decay distribution in terms of θ_v – the polar angle describing the vector $\to$ two pseudo-scalar decay, θ_μ – the polar angle describing the decay of the virtual $W \to \ell\nu$, and χ – the azimuthal acoplanarity angle between the vector meson and virtual W decay planes.

integrated widths for the W^+ to be longitudinally polarized ($|1,0>$) as opposed to transversely polarized ($|1,\pm 1>$) with respect to its D frame momentum axis.

The value of $A_1(0)$ then follows from the decay width which can be estimated by measuring the branching ratio of the semileptonic decay with respect to a reference state and then using the absolute branching fraction of the reference state and D lifetime to compute a total decay width (eq. 3).

Form factor measurements have been made for both $D^+ \to K^{*+}\ell\nu$ decay [18) 19) 20)] as well as for the $D_s^+ \to \phi\ell^+\nu$ decay [21) 22) 25)]. Figure 9 shows two representative vector $\mu^+\nu$ signals from E687.

3.1 $D^+ \to \overline{K}^{*o}\ell^+\nu$

At present, information on the form factors comes primarily from: E691 [18)] , E653 [19)], and E687 [20)]. These fixed target experiments use vertexing methods to estimate the ν momentum and thus measure considerably smeared values of q^2 and the three decay angles. All three published measurements are consistent. The below table compares the average [8)] along with a recent, representative Lattice Gauge Theory calculation [16)].

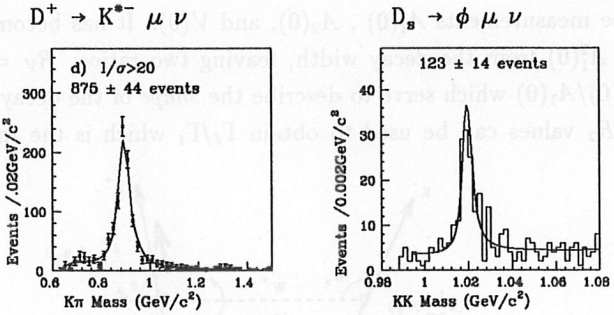

Figure 9: Two vector μ ν signals from E687 where the vector daughters and a μ are in a common detached vertex. Left: Wrong sign subtracted $K^-\pi^+$ mass distribution showing a prominent $\overline{K}^{*o}$ (896). Right: K^+K^- mass distribution showing a prominent ϕ (1020).

	R_2	R_v	Γ_l/Γ_t
< E687/E691/E653 >	$0.74 \pm .14$	1.86 ± 0.20	1.21 ± 0.10
BES [16]	$0.70 \pm .16\ ^{+0.20}_{-0.15}$	$1.99 \pm .22\ ^{+0.31}_{-0.35}$	$1.21 \pm .12\ ^{+0.15}_{-0.13}$

When these shape parameters are fed back into the decay rate expression to obtain values for $A_1(0)$, the agreement with theory is not good.

Exp	$A_1(0)$	$A_2(0)$	$V(0)$
E691	$0.49 \pm .07$	0.0 ± 0.2	1.2 ± 0.3
E653	0.57 ± 0.08	0.47 ± 0.16	1.2 ± 0.3
E687	0.59 ± 0.05	0.46 ± 0.11	1.0 ± 0.30
Average	0.56 ± 0.04	0.40 ± 0.08	1.1 ± 0.2
LGT (BES)	$0.83 \pm .14 \pm 0.28$	$0.59 \pm 0.14\ ^{+0.24}_{-0.23}$	$1.43 \pm 0.45\ ^{+0.48}_{-0.49}$

Other theoretical estimates for $A_1(0)$ tend to cluster around 0.8. This indication of a $K^*\ell\nu$ shortfall is borne out by directly comparing the ratio of $K^*\ell\nu/K\ell\nu$ which experimentally ranges from 0.4 - 0.6 where it is expected to be much closer to ≈ 1. Recall that there is fair agreement between theory and experiment for the value of the $f_+(0)$ form factor which controls the rate for $D \to K\ell\nu$ decay.

3.2 $D_s^+ \to \phi\ell^+\nu$

The rate for decay $D_s^+ \to \phi\ell^+\nu$ decay is frequently used to obtain estimates of $\mathcal{B}(D_s^+)$. A model is used to relate $\Gamma(D_s^+ \to \phi\ell^+\nu)$ to the width of a reference state with a well measured absolute branching fraction and eq. 3 is used to compute the unknown branching ratio.

Experiment	$B(D_s \to \phi\pi)$ (%)
CLEO	$5.1 \pm 0.4 \pm 0.4 \pm 0.7$
E687†	$2.90 \pm .5 \pm 0.45 \pm 0.39$
E687	$3.1 \pm 0.9 \pm 0.5 \pm 0.4$
ARGUS	2.4 ± 1.0
E691	> 3.4 at 90% CL
World average [8]	3.5 ± 0.4

† Neglecting possible OZI suppressed backgrounds

E687 [24] assumes that $\Gamma(\phi\ell\nu) = (0.9 \pm 0.12) \times \Gamma(\overline{K^{*o}}\mu^+\nu)$ based on a composite [8] of theoretical estimates.

The difference between the recent E687 and CLEO values partially reflect differences in their assumptions and normalization. CLEO [25] references their $\phi\mu\nu$ width to $\Gamma(D^o \to K^{*-}\ell^+\nu)$ and uses a $\phi\mu^+\nu/K^{*-}\mu^+\nu$ ratio of 1.0 which is the prediction of the modified ISGW model. They obtain $B(D_s^+ \to \phi\pi^+) = (5.1 \pm 0.4 \pm 0.4 \pm 0.7)\%$ assuming a negligible level for OZI suppressed backgrounds.

A recent, unresolved experimental controversy has arisen concerning the relationship between the form factors for $D_s^+ \to \phi\mu^+\nu$ and $D^+ \to \overline{K^{*o}}\mu^+\nu$ decay which are expected [16] [26] to be very close.

Below are three recent measurements:

	R_v	R_2	Γ_ℓ/Γ_t
E653 [21]	$2.3\ ^{+1.1}_{-0.9} \pm 0.4$	$2.1\ ^{+0.6}_{-0.5} \pm 0.2$	$.54 \pm .21 \pm .10$
E687 [22]	$1.8 \pm 0.9 \pm 0.2$	$1.1 \pm 0.8 \pm 0.1$	$1.0 \pm .5 \pm .1$
CLEO [25]	$0.9 \pm 0.6 \pm 0.3$	$1.4 \pm 0.5 \pm 0.3$	$1.1 \pm 0.3 \pm 0.2$
<informal >	1.43 ± 0.5	1.63 ± 0.37	0.74 ± 0.18
PDG D^+ [8]	1.89 ± 0.25	0.73 ± 0.15	$1.23 \pm .13$

To my mind the situation remains rather murky. Given the large size of the errors, the measurements from all three experiments are consistent but the

form factors measured for $D_s^+ \to \phi\mu^+\nu$ are inconsistent with those measured for $D^+ \to \overline{K}^{*o}\mu^+\nu$ at about the 2σ level. The new CLEO numbers have brought the R_v average for $\phi\ell\nu$ below the value for $\overline{K}^{*o}\ell\nu$; while E653 has brought the R_2 average for $\phi\ell\nu$ above the value for $\overline{K}^{*o}\ell\nu$.

4 $\Lambda_c^+ \to \Lambda\ell^+\nu$ and $\Xi_c \to \Xi\ell^+\nu$

The data on Λ_c^+ comes from both CLEO [27] and ARGUS [28] while the data on Ξ_c comes exclusively from CLEO [29]. Evidence for these baryonic semileptonic decays is an observed excess shown in Fig. 10 of the right sign compared to wrong sign baryon-lepton correlations after the imposition of kinematic cuts designed to eliminate possible charmed backgrounds with additional neutrals. As is the case

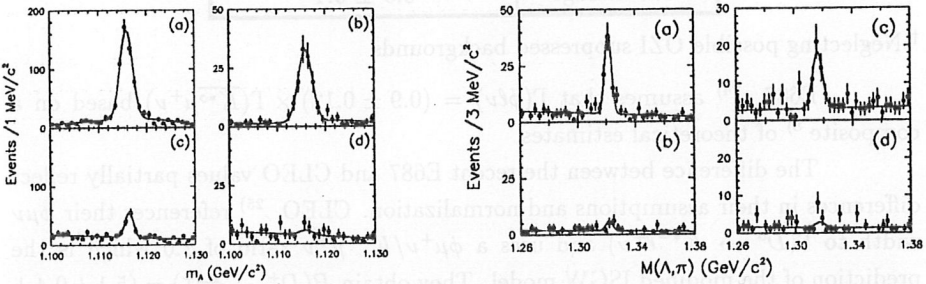

Figure 10: The illustrated data is from CLEO. Left: Excess Λ signal for right sign $\Lambda\ell\nu$ candidates (a) + (b) compared to wrong sign (c) + (d). Plots (a) and (c) show signals for Λ 's produced with electrons; Plots (b) and (d) show signals for Λ's produced with muons. Right: Excess Ξ signal for right sign $\Xi e^+\nu$ candidates (a) + (c) compared to wrong sign (b) + (d). Plots (a) and (b) show signals for $\Xi_c^- \to \Lambda\pi^-$. Plots (c) and (d) show signals for $\Xi_c^o \to \Lambda\pi^o$.

with the D_s^+, the rate for baryonic semileptonic decay provides information on the baryon absolute branching fractions using an assumption of a universal charm semileptonic width , $\Gamma(C \to X\ell\nu)$. This width can be estimated as the average of the (consistent) inclusive widths for the D^+ and D^o. Eq. 3 allows one to measure the inclusive semileptonic $\mathcal{B}(X\ell\nu)$ in terms of the the universal $\Gamma(C \to X\ell\nu)$ and baryon lifetime. The $\mathcal{B}$ for a given hadronic decay can be estimated from measured yield of these decays relative to an observed semileptonic mode if one knows the fraction of total inclusive $X\ell\nu$ decays which decay via the observed semileptonic mode. Using this technique CLEO [27] measures $B(\Lambda_c \to \Lambda\ell^+\nu) = (6.67 \pm .35 \pm 1.35)\% \times \Gamma(\Lambda\ell\nu)/\Gamma(X\ell\nu)$ where the last width ratio is the unknown fraction of inclusive $X\ell\nu$ which are exclusively $\Lambda\ell^+\nu$. Similarly they [29] measure

$B(\Xi_c^o \to \Xi^-\pi^+) = (0.52 \pm 0.16 \pm 0.13)\%\ \Gamma(\Xi\ell\nu)/\Gamma(X\ell\nu)$. The ratio of exclusive over inclusive semileptonic decay widths for these modes might be near unity in light of the analogous ratio for D decay: $\Gamma(D \to (K + K^*)\ell\nu)/D \to X\ell\nu) = 0.89 \pm 0.12$.

4.1 Λ polarization in $\Lambda\ell\nu$ decays

An even more interesting result concerns the polarization of the final state Λ which is predicted [30] to be large in HQET. Use of HQET for the heavy charmed quark reduces the four possible helicity form factors to just two, and allows one to predict the polarization as a function of q^2 in terms of the unknown ratio of the remaining form factors $R = f_2/f_1$. As $q^2 \to 0$ the longitudinal helicity dominates and $\alpha \to -1$ irrespective of the value of R as shown in Figure 11. In the limit of infinite product baryon mass $f_2(q^2) \to 0$, while $f_1(q^2)$ remains finite and thus one expects $|R| < 1$. At the average probed q^2 range of $\approx .7$ GeV^2 , one would expect $\alpha \approx -0.9$ in agreement with the measurements.

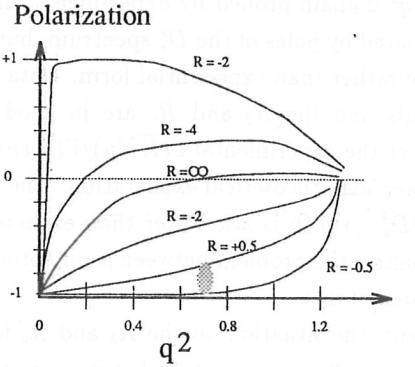

Figure 11: A sketch of the expected q^2 dependence of the Λ polarization for various possible ratios of $R = f_2(0)/f_1(0)$. The shaded region shows the typical q^2 domain probed by the experiments.

Both CLEO and ARGUS measure the decay asymmetry for $\Lambda\ell\nu$ by fitting their data to the the form: $d\Gamma/d\cos\theta \propto 1 + \alpha\ \alpha_\Lambda\ \cos\theta$ where θ is the angle between $\vec{p}$ (the Λ decay proton) and $-(\vec{\ell} + \vec{\nu})$ evaluated in the Λ rest frame; and $\alpha_\Lambda = .64$ is the well known self-analyzing asymmetry of the Λ . The Λ_c momentum can be estimated both from the thrust axis and visible decay products. CLEO (Fig. 12)obtains $\alpha = -0.89^{+0.17+0.09}_{-0.11-0.05}$; while ARGUS obtains -0.91 ± 0.49.

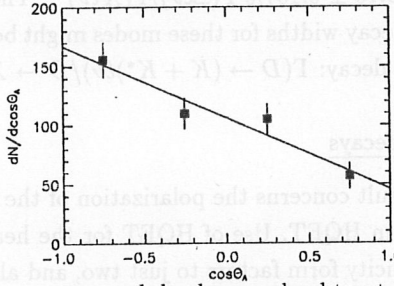

Figure 12: Acceptance corrected, background subtracted $dN/d\cos\theta$ distribution for CLEO $\Lambda\ell\nu$ candidates indicating a large (-89 %) longitudinal polarization for the Λ.

5 Summary

The recent data on $D \to K\ell\nu$ agrees reasonably well among experiments and with theory. Over the q^2 domain probed by experiments, the data are consistent with a form factor dominated by poles of the D_s^* spectrum, but the q^2 domain is insufficient to establish a pole rather than exponential form. Data on $D \to \overline{K}^*\ell\nu$ are consistent among experiments and the R_2 and R_v are in good agreement with theoretical expection. However the experimental $\Gamma(\overline{K}^*\ell\nu)/\Gamma(\overline{K}\ell\nu)$ ratio continues to be nearly a factor of two lower than theoretical expectation. The ratio of $D_s^+ \to \phi\ell\nu$ compared to $D_s^+ \to \eta\ell\nu$ or $D_s^+ \to \eta'\ell\nu$ is also lower than expected in theories such as ISWG which tends to confirm the problem between semileptonic decays into vector relative to pseudoscalar final states.

At present, the situation on the R_2 and R_v form factors for $D_s^+ \to \phi\ell\nu$ is rather murky. The results are consistent between experiments, but are inconsistent by about 2σ with the form factor ratios measured for $D^+ \to \overline{K^*}\ell\nu$ which runs counter to theoretical expectations. There is interesting new data on Λ_c and Ξ_c which provides new information on charmed baryon absolute branching fractions. The Λ from $\Lambda_c \to \Lambda\ell\nu$ decay is very highly polarized against its helicity axis which confirms the expectations of HQET.

Acknowledgements

I would like to acknowledge the efforts of my many E687 colleagues including Ray Culbertson, Rob Gardner, John Cumalat, and Will Johns.

References

1. J.P. Cumalat , in **The Fermilab Meeting DPF92**, 10-14 November 1992, published by World Scientific Publishing Co, edited by Carl H. Albright, Peter H. Kasper , Rajendran Raja, John Yoh.

2. CLEO Collab., Phys. Lett. B317 (1993) 647.

3. E691 Collab., J.C. Anjos *et al.*, Phys. Rev. Lett. 62 (1989) 1587.

4. CLEO Collab.,Phys. Rev. D44 (1991) 3394.

5. E687 Collab., W. Johns *et al.*, submitted to *The Albuquerque Meeting - Particles and Fields '94*

6. Mark III Collab., Phys. Rev. Lett. 66 (1991) 1011.

7. CLEO Collab., Phys. Rev. Lett. 71 (1993) 1311.

8. Particle Data Group, M. Aguilar-Benitez *et al.*,Review of Particle Properties, Phys. Rev. D 50 (1994) 1173

9. CLEO Collab., (M. Battle, et al.), CLEO-CONF-94-18, Jul 1994. 17pp. Submitted to Int. Conf. on High Energy Physics, Glasgow, Scotland, Jul 20-27, 1994.

10. D. Scora, Ph.D. thesis, University of Toronto, 1993

11. A. N. Kamal *et al.*, Phys. Rev. D 49 (1994)1330

12. P. Ball, V.M. Braun, H.G. Dosch, M. Neubert, Phys. Lett. B 259 (1991) 481; P. Ball, V.M. Braun, H.G. Dosch, Phys. Rev. **D** 44 (1991) 3567.

13. J.G. Korner and G.A. Schuler, Z. Phys. **C46** (1990) 93.

14. M. Bauer, B. Stech, M. Wirbel, Z. Phys. **C29** (1985) 637; M. Bauer and M. Wirbel, Z. Phys. **C42** (1989) 671.

15. F.J. Gilman and R.L. Singleton, Phys. Rev. **D41** (1990) 142.

16. C.W. Bernard, A.X. El-Khadra, and A. Soni, Phys. Rev. D 45 (1992) 869.

17. V. Lubicz, G. Martinelli, M.S. McCarthy, C.T. Sachrajda, Nucl. Phys. **B356** (1991) 301.

18. E691 Collab., J.C. Anjos *et al.*, Phys. Rev. Lett. 65 (1990) 2630.

19. E653 Collab., K. Kodama *et al.*, Phys. Lett. B 274 (1992) 246.

20. E687 Collab., P.L. Frabetti *et al.*, Phys. Lett. B 307 (1993) 262.

21. E653 Collab., K. Kodama *et al.*, Phys. Lett. B 309 (1993) 483.

22. E687 Collab., P.L. Frabetti, *et al.*, Physics Letters B 328 (1994) 187

23. CLEO Collab., J. Alexander, *et al.*, Phys. Lett. B337:(1994) 405

24. E687 Collab., P.L. Frabetti *et al.*, Phys. Lett. B 313 (1993) 253.

25. CLEO Collab., F. Butler *et al.*, Phys. Lett. B 324 (1994) 255

26. V. Lubicz, G. Martinelli, M.S. McCarthy, and C.T. Sachrajda, Phys. Lett. B 274 (1992) 415

27. CLEO Collab.,T. Bergfeld, *et al.* , Phys. Lett. B323 (1994) 219.

28. ARGUS Collab., H. Albrecht *et al.*, Phys. Lett. B326 (1994) 320

29. CLEO Collab., J. Alexander *et al.*, CLNS-94-1288, Jul 1994. 10pp.

30. W. Roberts, Phys. Lett. B282 (1992) 593
T. Mannel, W. Roberts and Z. Ryzak, Nucl. Phys. B335 (1992)38
J.C. Korner and M. Kramer, Phys. Lett. B275 (1992)495.

Frascati Physics Series, Vol. III (1994)
HEAVY QUARKS AT FIXED TARGET
University of Virginia, October 7–10, 1994
(pp. 183–194)

EXCITED CHARM STATES

Shekhar Shukla
Fermi National Accelerator Laboratory
Batavia, IL 60510, U.S.A.

ABSTRACT

Characteristics of mass spectra and decays of orbitally excited charm mesons and baryons, expected on the basis of quark models and Heavy Quark Symmetry, are briefly described. The difficulties associated with measurements on these excited states are discussed. The accuracy and reliability of currently available experimental information is examined. The reasons, for the widely accepted spin-parity assignments to the observed excited mesons and baryons, are stated. Finally, the experimental data, with the accepted spin-parity assignments, is compared with expectations based on quark models and Heavy Quark Symmetry.

1 - Introduction

The first orbitally excited charm meson was observed by ARGUS[1] in 1986. Since then, five more excited charmed mesons have been observed. We are beginning to see excited charm baryons. Two excited baryon states have been observed so far.

1.1 Motivation

The motivation for studying excited charm states is two-fold. A study of these states helps the understanding of strong interactions via quark models or via more model independent calculations using Heavy Quark Symmetry. Recent examples of the former are calculations of Godfrey and Kokoski[2], and, Capstick and Isgur[3]. Some recent examples using Heavy Quark Symmetry are the work by Eichten, Hill and Quigg[4], and Isgur and Wise[5]. The other reason for studying charm hadrons is that they help the study of beauty hadrons. The charm and beauty quarks are both considerably heavier than the u,d and s quarks and are also heavy on the QCD scale, which is determined by Λ_{QCD}. As a result, the charm system, with much more experimental data available, turns out to be especially useful in getting a reasonably good idea of the properties of beauty hadrons. An understanding of the charm hadrons is also needed because the beauty hadrons decay to charm hadrons and, for making measurements on beauty hadrons, a good knowledge of the decay products is essential.

1.2 Lowest Excitations of Mesons and Baryons

Excited charm mesons have a charm quark and a lighter quark (u, d or s) in a bound state with relative orbital angular momentum, L>0. For a given quark pair with a radial excitation number, n, and an orbital angular momentum, L, there are four possible total angular momentum states. There is one state corresponding to the case when the sum of quark spins, $\vec{S} = \vec{S_c}+\vec{S_q}$, $\vec{S_c}$ and $\vec{S_q}$ being the spin of the charm quark and the lighter quark respectively, has the value S=0. The total angular momentum $\vec{J}=\vec{L}+\vec{S}$ has the value J=L in this case. There are three states, with J=L-1, L, and L+1, corresponding to S=1.

There are experimental measurements on six of the twelve excited charm mesons with L=1. None of the higher excited charm mesons have been observed as yet. The excited charm baryons discussed here have three quarks with flavors c, u and d. The light-quark pair has an orbital angular momentum L>0, relative to the charm quark. For the lowest orbital excitation, L=1, the three quark spins and the orbital angular momentum combine to give seven states with isospin, I=0 (excited states of Λ_c^+) and seven states with isospin, I=1 (excited states of Σ_c^+). The two new baryon states observed recently are identified as the L=1 excitations[6] above the Λ_c^+.

1.3 Heavy Quark Approximation

The system containing one heavy quark and one or more lighter quarks simplifies considerably[5] if the mass, m_Q, of the heavy quark is large on the QCD mass scale, which is determined by Λ_{QCD}. In this case, which we will henceforth refer to as the *heavy quark approximation*, the motion of the heavy quark can be ignored. The spin of the heavy quark, $\vec{S_Q}$, and the total angular momentum of the light quarks, $\vec{j}$, are separately conserved. The energy spectrum is determined by j. There are two degenerate states for each value of j, corresponding to the two values, $J=j\pm\frac{1}{2}$ of the total angular momentum, $\vec{J} = \vec{j}+\vec{S_Q}$. Since the energy spectrum is determined by the dynamics of the light quark, the spectra of systems, where the heavy-quark approximation is valid, are expected to be identical except for a constant mass shift due to the difference in the mass of the heavy quark. For a finite mass of the heavy quark, corrections of order $O(\Lambda_{QCD}/m_Q)$ result in a mass-splitting between the two states. Again the splitting in systems with different varieties of the heavy quark is related. It is inversely proportional to the mass of the heavy quark. The existing experimental data suggests that the heavy-quark approximation is valid for calculations involving B and D mesons and perhaps for the K mesons.

2 - Challenges faced in Observation

The lowest excited charm hadrons decay strongly to a ground state charmed hadron and lighter mesons. The factors that make excited states more difficult to observe than the weakly decaying ground state are, 1) Larger Combinatoric background, 2) peaks due to other excited states overlapping with, or being in the vicinity of, the peak of interest, and 3) lower reconstruction efficiency. We dwell on these three factors in the remainder of this section.

2.1 Combinatoric Background

The higher combinatoric background results from more numerous decay products and larger intrinsic widths of the states. In fixed target experiments, there is an additional source contributing to the combinatoric background - one that perhaps dominates the other two sources in some cases. The additional background arises from the fact that there is no observable separation between the locations of production and decay of the state being studied. In case of a weakly decaying hadron, the production and decay vertices are visibly separated. Only tracks from the decay are used to construct candidates for the charm state. In case of the decay of an excited state, tracks from the decay of the excited state as well as those from fragmentation following charm production, can be used to construct candidates for the state. The background increases with primary vertex multiplicity. Consequently, it is expected to be worse in charm from hadroproduction than that from photoproduction.

2.2 Other Structures

When observing a peak due to an excited state in a mass distribution, structures in the vicinity due to other excited states, partially or fully reconstructed, can make it difficult to estimate the background shape under the peak. At times they can actually overlap with the state under study. An example is the two peaks in the $D^{*+}\pi^-$ mass distribution arising from the decay of the members of the $j^P=\frac{3}{2}^+$ doublet (see section 3.3.2). When ARGUS[1] observed the first signal due to an excited charm state, it was interpreted as being due to the decay of a broad state of width ~40 MeV. As we know now, the broad peak is due to the two overlapping $j^P=\frac{3}{2}^+$ states.

Determination of the background under the peak requires a region of smoothly varying background around the peak. If there are structures in the vicinity of the peak of interest, they can hamper this determination. An example is the bumps close to the D_2^{*+} peak in the $D^0\pi^+$ mass plot (see section 3.2.1).

2.3 Reconstruction Efficiency

The excited states, in general, have a lower reconstruction efficiency. It is partly due to the larger number of decay products and partly, in case of current experiments, because the apparatus was probably not designed with much attention to the acceptance for these states.

3 - The Lowest Excited (L=1) Mesons

Popularly known as $D^{**}(c\bar{u}$ and $c\bar{d})$ or $D_s^{**}(c\bar{s})$, these mesons consist of a charm quark and a lighter quark with relative orbital angular momentum, L=1. Phenomenological models usually parameterize the spin-independent part of the inter-quark interaction with a Coulomb-type potential due to a single-gluon vector exchange and a linear confining potential arising from a multi-gluon scaler exchange. One of the quarks being light, the two quarks venture farther from each other than those in a similar charmonium. Consequently, the L=1 charmed mesons probe the inter-quark potential at larger distances than charmonium.

In the heavy-quark approximation, the energy levels are characterized by the two values, $\frac{1}{2}$ and $\frac{3}{2}$, of the total angular momentum of the light quark, $\vec{j} = \vec{L}+\vec{S_q}$, where $\vec{S_q}$ is the spin of the light quark. For each value of j, there are two degenerate states corresponding to the two values, $J=j\pm\frac{1}{2}$, of the total angular momentum, $\vec{J} = \vec{j}+\vec{S_c}$, $\vec{S_c}$ being the spin of the charm quark. The finite mass of the charm quark leads to a splitting, of order $O(\Lambda_{QCD}/m_Q)$, between the the two levels. The two members of the $j^P=\frac{3}{2}^+$ doublet have been observed for all three flavors of the light meson. The J=2 members are referred to as D_2^{*o}, D_2^{*+}, and D_{s2}^{*+} for the light quark flavors u, d and s respectively. The corresponding J=1 members are named D_1^o, D_1^+, and D_{s1}^+. The measured masses and widths are listed in Tables II and III. Members of the $j^P=\frac{1}{2}^+$ doublet, being wide, are difficult to observe and none has been observed so far.

3.1 Decays

The L=1 charmed mesons decay strongly, mostly through 2-body decays. The allowed 2-body decays are listed in Table I. Strong decays of D_s^{**+} to $D_s^+\pi$ or $D_s^{*+}\pi$ are prohibited by conservation of isospin in strong interactions. Other 2-body decays are prohibited due to conservation of parity in strong interactions and conservation of angular momentum. It should be noted that the D^{**} is only ~450 MeV more massive than the D^*. So the decays to $D\rho$ and $D^*\rho$ are possible only due to the large width of the ρ.

The J=2 state decays to $D\pi$ or $D^*\pi$ through a D-wave and is fairly narrow. The J=0 state decays to $D\pi$ through an S-wave and is expected to be wide (several hundreds of MeV according to Godfrey and Koksoki[2]). The J=1 states can decay to $D^*\pi$ through an S-wave or a D-wave. However, the J=1 state belonging to the $j^P=\frac{3^+}{2}$ doublet decays predominantly through a D-wave (only through a D-wave in the heavy-quark approximation) and is narrow, while that belonging to the $j^P=\frac{1^+}{2}$ doublet decays predominantly through an S-wave (only through an S-wave in the heavy-quark approximation) and its width is expected to be large (several hundreds of MeV according to Godfrey and Koksoki[2]).

Table I. Allowed 2-body strong decays of L=1 charmed mesons

j^P	J^P	D^{**}	D_S^{**}
$\frac{3^+}{2}$	2^+	$D\pi$, $D^*\pi$, $D\rho$, $D^*\rho$	D^*K, DK
$\frac{3^+}{2}$	1^+	$D^*\pi$, $D\rho$, $D^*\rho$	D^*K
$\frac{1^+}{2}$	1^+	$D^*\pi$, $D\rho$, $D^*\rho$	D^*K
$\frac{1^+}{2}$	0^+	$D\pi$, $D^*\rho$	DK

3.2 Spin-parity Assignment

3.2.1 *The $J^P=2^+$ States (D_2^{*o}, D_2^{*+} and D_{s2}^{*+})*

The state D_2^{*o} was observed in the $D^+\pi^-$ mass spectrum[7–11], while its isospin partner, D_2^{*+}, was observed in the $D^o\pi^+$ spectrum[10,12,13]. The following is a statement of the reasons for the assignment L=1, J=2 to the observed state, D_2^{*o}. The lowest excited states that can decay to $D^+\pi^-$ are the two L=1 states with J=0 and J=2. These states are expected to be separated by ~100 MeV. The J=0 states are expected to be several hundreds of MeV wide, while the J=2 state is expected to be narrow (a few tens of MeV). The mass and width of the observed state are consistent with the expected values for the J=2 state and inconsistent with those for the J=0 state. The higher excited states are expected to be ~300 MeV heavier than the observed state[4].

Now, if the observed state is indeed an L=1, J=2 state, it should also decay to $D^{*+}\pi^-$. A shoulder observed in the $D^{*+}\pi^-$ mass spectrum next to the peak due to another state (D_1^o), is consistent with arising from the decay of the D_2^{*o} to $D^{*+}\pi^-$. There is additional information available from an angular distribution of events in the shoulder (see section 3.3.2). The information is consistent with the decay of an L=1, J=2 state. However, its quality is not good enough to help significantly in the identification of the

state. Considering all the available evidence, the state D_2^{*0} is accepted as the lowest L=1, J=2 state. Similar arguments lead to the assignment L=1, J=2 to the D_2^{*+}.

The state D_{s2}^{*+} was observed recently[14] in a decay to D^0K^+. The possible spin assignments for the D_{s2}^{*+} corresponding to the lowest orbital excitation are J=0 and J=2, since it is observed to decay to DK. The narrow width supports a J=2 assignment. The decay of the state to D*K has not been observed. This, however, does not conflict with the J=2 assignment, since the decay to D*K is expected to be highly supressed due to a limited available phase space.

3.2.2 The $J^P=1^+$ States (D_1^0, D_1^+ and D_{s1}^+)

The state D_1^0 was observed[9–11,15] in the decay to $D^{*+}\pi^-$. Apart from the D_2^{*0}, the lowest excited states that can decay to $D^{*+}\pi^-$ are the two L=1 states with J=1. Owing to its narrow observed width and some decay angular distributions (see section 3.3.2), the observed state is identified as the J=1 member of the $j^P=\frac{3}{2}^+$ doublet. The state is not observed in the $D^+\pi^-$ mass spectrum. This agrees with the expectation for a J=1 state. The state D_1^+ observed recently[13] in the decay to $D^{*0}\pi^+$ is, based on similar considerations, identified as the charged isospin partner of the D_1^0.

The D_{s1}^+ has been observed[9,10,16] in the decay to D*K but not to DK. Since it is observed to decay to D*K, its possible spin assignments corresponding to the lowest orbital excitation are J=1 and J=2. The fact that it has not been observed to decay to DK, indicates that it has J=1. The narrow measured width indcates that it is a member of the $j^P=\frac{3}{2}^+$ doublet decaying through a D-wave. Thus the state is identified as the J=1 member of the $j^P=\frac{3}{2}^+$ doublet.

3.3 Measurement of Masses and Widths

3.3.1 D_2^{*0} and D_2^{*+}

Fig. 1 shows distributions, from CLEO and E687, in the difference, $\Delta M=M(D^0\pi^+)-M(D^0)$, between the measured masses, $M(D^0\pi^+)$ and $M(D^0)$, of the D_2^{*+} candidate and the D^0 from its decay. The peak due to the D_2^{*+} is seen at $\Delta M=600$ MeV. There is no known state with a mass very close to that of the D_2^{*+} mass that can decay to $D^0\pi^+$. The J=0 state, which has not been observed as yet, is expected to be only ~100 MeV lighter. But it is expected to be very broad (several 100 MeV) and should not interfere with the observation of D_2^{*+}.

Unfortunately, the mass spectrum is marred by structures due to partially reconstructed states on the low-mass side of the peak of interest. These structures

hamper accurate background determination. The enhancement at ΔM~450 MeV is due to the decay of the state being investigated, D_2^{*+}, and the other member of the $j^P=\frac{3}{2}^+$ doublet, the D_1^+, to $D^{*0}\pi^+$. The D^{*0} decays to $D^0\pi^0$, the π^0 escaping detection in the apparatus. Owing to the small q-value of the π^0 from the D^{*0} decay, the enhancement in the $D^0\pi^+$ mass spectrum has the same shape as it would have had, were the decay to $D^{*0}\pi^+$ fully reconstructed, but is shifted down in mass by approximately one pion mass. The gap, between the structure at ~450 MeV and the D_2^{*+}, is not large enough to allow a reliable background determination. It is necessary to use the mass range beyond this structure.

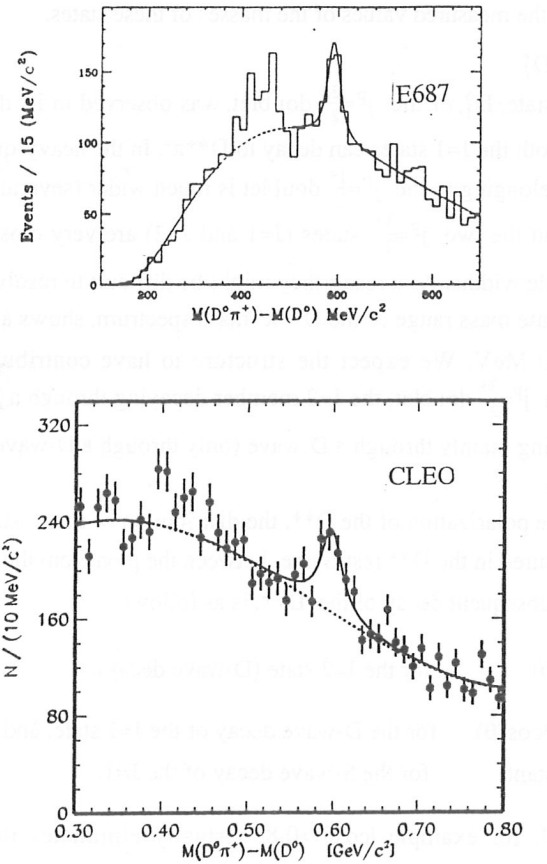

Fig.1 Distributions in the mass difference $\Delta M=M(D^0\pi^+)-M(D^0)$, from E687 and CLEO, showing the peak due to D_2^{*+} along with another structure due to partially reconstructed states.

However, there might be other structures that prevent extension of the mass range on the low mass side. One source that may lead to such a structure, is the decay of the D_1^+ to $D^o\rho^+$, or, of the D_1^o to $D^o\rho^o$. Partial reconstruction of the state, using the D^o and one of the pions from the ρ-decay, causes a broad enhancement at lower masses. The significance of the enhancement in the observed mass distribution depends on the fashion in which the charm is produced, and the acceptance of the apparatus. The study of the D_2^{*o} using the $D^+\pi^-$ mass spectrum entails tackling problems similar to those faced in the study of D_2^{*+}. Table II shows the experimental results on the masses and widths of the J=2 states. The problems in background determination are probably responsible for the large spread in the measured values of the masses of these states.

3.3.2 D_1^o and D_1^+

The J=1 state, D_1^o, of the $j^P=\frac{3^+}{2}$ doublet, was observed in its decay to $D^{*+}\pi^-$. The J=2 state and both the J=1 states can decay to $D^{*+}\pi^-$. In the heavy-quark approximation, the J=1 state belonging to the $j^P=\frac{1^+}{2}$ doublet is much wider (several 100 MeV) than the $j^P=\frac{3^+}{2}$ states. But the two $j^P=\frac{3^+}{2}$ states (J=1 and J=2) are very close to each other and have comparable widths. As a result they might be difficult to resolve. Indeed, a display of the appropriate mass range of the $D^{*+}\pi^-$ mass spectrum, shows a broad structure at a mass of ~2420 MeV. We expect the structure to have contributions from the two members of the $j^P=\frac{3^+}{2}$ doublet, the J=2 member decaying through a D-wave and the J=1 member decaying mainly through a D-wave (only through a D-wave in the heavy-quark approximation).

Due to the polarization of the D^{*+}, the distribution of these states in $\cos\theta$, θ being the angle, measured in the D^{*+} rest frame, between the pion from the decay of the D_1^o and that from the subsequent decay of the D^{*+}, is as follows.

$$\frac{dN}{d\cos\theta} \propto \begin{cases} \sin^2\theta & \text{for the J=2 state (D-wave decay),} \\ (1+3\cos^2\theta) & \text{for the D-wave decay of the J=1 state, and,} \\ \text{constant} & \text{for the S-wave decay of the J=1.} \end{cases} \quad (1)$$

A cut on $\cos\theta$, for example $|\cos\theta|>0.8$, virtually eliminates the J=2 state, while preserving a large part of the contribution from the J=1 state, thus enabling the measurement of the mass and width of the latter. Measurement on the isospin partner,

D_1^+, of the D_1^0 is made in a similar fashion. Results of measurement of the masses and widths of these states by ARGUS, CLEO and E687 are listed in Table III. The recent measurements by CLEO and E687 are in fairly good agreemment.

3.3.3 The Strange States

There is no perceivable problem due to partially reconstructed states in the observation of the D_s^{**+}. The fundamental reason is that the states are very close to the edge of phase space, causing the J=1 state to be very narrow and the decay of the J=2 state to D*K to be highly supressed relative to that to DK. There is no reflection in the DK spectrum due to a partially reconstructed J=2 state. The reflection due to a partially reconstructed J=1 state is extremely narrow and easily identified. The results of measurements on the J=2 and J=1 states are listed in Tables II and III respectively. There is excellent agreement among the measurements on the J=1 state. The J=2 state has been observed only by CLEO[14] so far.

Table II. Masses and widths in (MeV/c^2) of the $J^P = 2^+$ mesons, along with the decay modes used for measurement.

	D_2^{*0}		D_2^{*+}		D_{s2}^{*+}	
	$(D_2^{*0} \to D^+\pi^-)$		$(D_2^{*+} \to D^0\pi^+)$		$(D_{s2}^{*+} \to D^0K^+)$	
Experiment	Mass	Width	Mass	Width	Mass	Width
ARGUS	2455±3±5	15^{+13+5}_{-10-10}	2469±4±6	27±12		
CLEO I.5	2461±3±1	20^{+9+9}_{-12-10}				
CLEO II	2465±3±3	28^{+8+6}_{-7-6}	2463±3±3	27^{+11+5}_{-8-5}	$2573.2^{+1.7+0}_{-1.6-0.9}$	16^{+5+3}_{-4-3}
E687	2453±3±2	25±10±5	2453±3±2	23±9±5		
E691	2459±3±2	20±10±5				

Table III. Masses and widths in (MeV/c^2) of the $J^P=1^+$ states, along with the decay modes used for measurement.

	D_1^0		D_1^+		D_{s1}^+	
	$(D_1^0 \to D^{*+}\pi^-)$		$(D_1^+ \to D^{*0}\pi^+)$		$(D_{s1}^+ \to D^{*0}K^+, D^{*+}K^-)$	
Experiment	Mass	Width	Mass	Width	Mass	Width(90%CL)
ARGUS	2414±2±5	13^{+6+10}_{-6-5}			2535.5±0.4±1.3	<3.9
CLEO I.5	2428±3±2	23^{+8+10}_{-6-4}			2536.6±0.7±0.4	<5.4
CLEO II	2421^{+1+2}_{-2-2}	20^{+6+3}_{-5-3}	2425±2±2	26^{+8+4}_{-7-4}	2535.1±0.2±0.5	<2.3
E687	2422±2±2	15±8±4			2535.0±0.6±1.0	<3.2

3.4 Branching Ratios

The statistical uncertainties in the number of events for the observed states in any decay mode are of the order of 25%. In addition, there are comparable systematic uncertainties. Consequently, with the currently available statistics, the ratio of rates for any two decays is not known to better than ~50%. The statistics and the understanding of the background will have to improve considerably before the data on ratios of decay rates can be used effectvely for developing theoretical models or making theoretical predictions.

4 - Charmed Baryons

A narrow (width<3.2 MeV at 90% CL) excited charmed baryon of mass ~2626 MeV was observed by ARGUS[17] in a decay to $\Lambda_c^+\pi^+\pi^-$. The state has since been confirmed by CLEO[18] and E687[19]. The decay allows its identification as one of the excited states of Λ_c^+ or Σ_c^+, or the ground state, $J^P=\frac{3^+}{2}$, of Σ_c^+. Were it Σ_c^+ or one of its excited states, it would have favored the decay through $\Lambda_c^+\pi^o$, rather than $\Lambda_c^+\pi^+\pi^-$, since its mass is only slightly above the $\Lambda_c^+\pi\pi$ threshold. On the other hand, if it is an L=1 excitation of the Λ_c^+, it is prohibited from decaying to $\Lambda_c^+\pi^o$ due to conservation of isospin. Then it should decay to $\Lambda_c^+\pi\pi$ ($\Lambda_c^+\pi^+\pi^-$ or $\Lambda_c^+\pi^o\pi^o$). Thus the observed state is likely to be an excited Λ_c^+. The observed mass is close to the value expected for the lighter L=1 excited states of Λ_c^+.

Recently, another state was observed by CLEO[20] and then by E687[21], in the $\Lambda_c^+\pi^+\pi^-$ mass distribution at a mass of ~2593 MeV. This state, like the one at 2626 MeV, has not been observed to decay to $\Lambda_c^+\pi^o$. It is found to decay preferentially to $\Sigma_c\pi$, with the Σ_c subsequently decaying to $\Lambda_c^+\pi$. The two states, $\Lambda_c^{*+}(2593)$ and $\Lambda_c^{*+}(2626)$, have been interpreted as the two members with, $J^P=\frac{1^-}{2}$ and $J^P=\frac{3^-}{2}$, of the doublet with L=1, j=1. The state with $J^P=\frac{1^-}{2}$ decays preferentially to $\Sigma_c\pi$. Were Σ_c^* light enough, the state with $J^P=\frac{3^-}{2}$ would have favored the decay to $\Sigma_c^*\pi$. However, Σ_c^* is too heavy[22] for the decay to be possible. Consequently the state is expected to decay to $\Lambda_c^+\pi\pi$. Table IV summarizes the results of measurements on the two states.

Table IV. Measured Mass in (MeV/c^2) for $\Lambda_c^{*+}(2626)$ and $\Lambda_c^{*+}(2593)$

	$\Lambda_c^{*+}(2626)$		$\Lambda_c^{*+}(2593)$	
Experiment	Decay Mode	Mass	Decay Mode	Mass
ARGUS	$\Lambda_c^+\pi^+\pi^-$	2626.6±0.5±1.5		
CLEO II	$\Lambda_c^+\pi^+\pi^-$	2627.2±0.4±1.1	$\Sigma_c^{++}\pi^-$, $\Sigma_c^{0}\pi^+$	2593.1±0.4±2.6
CLEO II	$\Lambda_c^+\pi^0\pi^0$	2625.8±0.9±2.0		
E687	$\Lambda_c^+\pi^+\pi^-$	2625.5±0.6±0.9	$\Lambda_c^+\pi^+\pi^-$	2593.2±0.8±0.9

5 -Conclusions

5.1 Comparison of Experimental Measurements with Theoretical Predictions

The isospin splitting between the charged and neutral states is consistent with zero as expected. Table V shows the measured masses and widths averaged over the various experiments, compared with the predictions from Godfrey and Kokoski[2] and Eichten, Hill and Quigg[4]. Godfrey and Kokoski use a QCD-inspired model. Their two predicted values in the table for the width of each state correspond to two different models used for the decay - the pseudo-scaler emission model and the flux tube breaking model. Eichten, Hill and Quigg use Heavy Quark Symmetry and the experimental data on the excited K and D mesons to predict the properties of the excited D_s, B and B_s mesons.

Table V. Comparison of the measured masses and widths (MeV/c^2) with Recent Theoretical Predictions

	$D_2^*(2^+)$		$D_1(1^+)$		$D_{s2}^{*+}(2^+)$		$D_{s1}^+(1^+)$	
	Mass	Width	Mass	Width	Mass	Width	Mass	Width
Experiment	2460±5	24±5	2423±3	18±6	2473±3	16±6	2435.3±.4	<2.3
Godfrey&Kokoski[3]	2500	63, 37	2460	26,38	2590	21,16	2555	0.4,1.9
Eichten,Hill&Quigg[4]					2561	11	2526	<1

5.2 Measurements desirable and probably feasible in the near future

None of the higher excited mesons (2S, 3D e.t.c.) has been observed as yet. They are expected to be wider than the L=1 states observed so far[4]. Some of them might be observable in the near future.

It is important to have better measurements of branching ratios for several of the observed decays, and some decays like $D^{**}\rightarrow D\rho$, that have not been observed as yet. A large part of the background in the mass distributions used to study the L=1 mesons arises from decays of other excited charmed mesons. As new excited states are observed

and their decays understood, the background in these distributions will be known better, making more accurate measurements on the L=1 states possible.

The dominant problem with measurements on excited charm baryons so far, is low statistics. As we accumulate higher statistics in charm experiments we will observe more excited baryon states.

References

1 ARGUS Collab., H. Albrecht et al, Phys. Rev. Lett. **56**, 549 (1986).
2. S. Godfrey and R. Kokoski, Phys. Rev. D **43**, 1679 (1991).
3. S. Capstick and N. Isgur Phys. Rev. D **34**, 2809 (1986).
4 E. J. Eichten, T. Hill and C. Quigg, Phys. Rev. Lett. **71** (1994) 4116.
E. J. Eichten, T. Hill and C. Quigg, FERMILAB-CONF-94/118-T.
5. N. Isgur and M. B. Wise, Phys. Rev. Lett. **66**, 1130 (1991) .
6. P. Chao, Phys. Rev. D **50**, 3295 (1994).
7 E691 Collab., J.C. Anjos et al, Phys. Rev. Lett. **62**, 1717 (1989)
8 ARGUS Collab., H. Albrecht et al Phys. Lett. B **221** (1989) 422
9 CLEO Collab, P. Avery et al, Phys. Rev. D **41** 774 (1990)
10 E687 Collab., P. L. Frabetti et al, Phys. Rev. Lett. **72** (1994) 324.
11 CLEO Collab, P. Avery et al, Phys. Lett. B **331**(1994) 236
12 ARGUS Collab., H. Albrecht et al, Phys. Lett. B **231** (1989) 208
13 CLEO Collab, T. Bergfeld et al, Cornell Report CLNS 94 / 1298
14 CLEO Collab, Y. Kubota et al, Phys. Rev. Lett. **72** (1994) 1972
15 ARGUS Collab., H. Albrecht et al Phys. Lett. B **232** (1989) 398
16 ARGUS Collab., H. Albrecht et al Phys. Lett. B **230** (1989) 162
ARGUS Collab., H. Albrecht et al, Phys. Lett. B **297**, 425 (1993).
CLEO Collab, J. P. Alexander et al, Phys. Lett. B **303** (1993) 377
BEBC. A.E. Asratyan, et al, Z. Phys. C 61, **563** (1994).
17 ARGUS Collab., H. Albrecht et al, Phys. Lett. B **317**, 227 (1993).
18 CLEO Collab., D. Acosta et al, Proc. of the 16th International Symposium on Lepton and Photon Interactions, Ithaca, New York, 1993.
19 E687 Collab., P. L. Frabetti et al, Phys. Rev. Lett. **72** (1994) 961.
20 CLEO Collab., M. Battle et al, Proc. of the 16th International Symposium on Lepton and Photon Interactions, Ithaca, New York, 1993.
21 Private Communication.
22 V.V Ammosov. et al. JETP Lett. **58**, 249 (1993).

Frascati Physics Series, Vol. III (1994)
HEAVY QUARKS AT FIXED TARGET
University of Virginia, October 7–10, 1994
(pp. 195–210)

CHARM SPECTROSCOPY AND LIFETIME

G. Bellini
Dipartimento di Fisica dell'Universitá e
Istituto Nazionale di Fisica Nucleare

ABSTRACT

A review of the charm state lifetimes and of the charm baryon masses is presented. The $\frac{\tau(D^{\pm})}{\tau(D^0)}$ and $\frac{\tau(D_s^{\pm})}{\tau(D^0)}$ are now known with an accuracy of 1.7% and 3.6%, respectively, and the baryon lifetime hierarchy seems well established. The measurements of the Ω_c^0 mass converge to a value in the range $2700 - 2710\ MeV/c^2$.

1 Introduction

In the last two years a large improvement has been achieved in the charm particle lifetime. The E687 data gave a very important contribution.
In this paper I am trying to give an up to date picture of the status of the art in this field.
The paper consists of four sections. In the first I discuss the methods adopted to measure the times of life and to fit the mean lifetime value of the charm states. In the sections 2. and 3. I discuss the lifetime measurements of the charmed mesons and baryons and the mass values of the charged and neutral cascades and Ω_c^0. Finally in the fourth section I will present some conclusions.

2 Lifetime measurement

The distance $\ell = \beta\gamma ct = \frac{P}{M}ct$ has to be measured for each charm state. Due to the short τ_c $[10^{-12} - 10^{-13}s]$, the measurements depend crucially upon the spatial resolution. Then a high precision vertex detector is needed. Just as an example the resolution of the E687 microvertex detector is $\sigma_l \simeq$ few hundreds of microns and $\sigma_t \simeq$ few tens of microns.

2.1 Vertexing

As it is well known two different approaches can be used to reconstruct the vertices: the "stand alone" and the "candidate driven" approach.
The "stand alone" method starts with an hypothesis for the primary vertex, then removes worst tracks and looks for a secondary vertex with the rejected tracks.
In the "candidate-driven" method, first the charm candidate forms a "seed" track, then tracks around the "seed" are nucleated to find the primary vertex.
A comparison between the two methods shows that the "stand alone" vertexing is inefficient for short lifetimes, but allows the reconstruction of decays with missing neutrals (ν, π^0, etc..) and does not require specific decay modes for the skims. On the other hand the candidate driven method has the advantage to allow the identification of primary vertices with even only one track belonging to them. In addition its efficiency at short lifetime is definitively better.

2.2 Vertex cutting tools

Various cuts are used to reconstruct and select the primary and secondary vertices. I will discuss them here briefly:

- *a. The detachment cut* $\ell/\sigma_\ell > N$. ℓ is the distance in the space between the primary and the secondary vertex. This cut is very usefull in enhancing the signal with respect to the background. Its effectiveness is weakened of course if the lifetime is very short.

- *b. Pointing back to primary.* We impose a cut on d/σ_d, where d is the distance in the space between the primary vertex and the direction of the momentum vector of the reconstructed charmed state.

- *c,d. Secondary vertex confidence level* and *primary vertex confidence level.* They concern cuts on the confidence level of the vertex fits.

- *e. No charm daugther in primary vertex.* We require a very low probability that tracks, produced in the charm decay, belong to the primary vertex.

- *f. No extra tracks near the secondary vertex.* In this case we impose a lower cut on the distance between the secondary vertex and extra tracks.

These last two requirements, which are usually called "isolation cuts", are particularly important to select charmed particles with short lifetime.

2.3 The reduced proper time

The detachment cut distorts heavily the proper time $t = \ell/\beta\gamma c$. Then to extract the lifetime a strong correction function f(t) is needed. f(t) is evaluated by means of MC simulations, which in any case involve some uncertainties on the assumed parameters and corrections, and produces systematic biases. As a consequence it is suitable to reduce as much as possible the weight of the corrections.
An important improvement can be achieved by replacing the proper time with the reduced proper time

$$t' = t - t_{min} = \frac{\ell - N\sigma_\ell}{\beta\gamma c} \tag{1}$$

where N is the significance of the detachment cut, which has been adopted. If σ_ℓ is independent of ℓ [as it can be assumed in a restricted range, at least] we succeed, to restore the exponential dependence $e^{-t'/\tau}$, using t'.
f(t') is very weakly dependent on t'. Then the systematic errors connected to it are drastically reduced.
Two t' distributions are used to measure the lifetime; they concern the signal region and the background events, respectively. The signal region is typically chosen as a region $\pm 2\sigma_m$ wide around the mass mean value M of the charm signal.
The t' distribution from the background is obtained from the sidebands, chosen not too far away from the signal region, because the background time evolution can depend on the invariant mass. Typical sidebands are two regions, $2\sigma_m$ wide, $4\sigma_m$ far from the signal peak.

2.4 The Maximum Likelihood Functions

The Maximum Likelihood Functions usually used to fit the lifetime are: the binned M.L.F. and the continuous M.L.F.

2.4.1 Binned Maximum Likelihood

The Binned M.L.F. is based upon the Poisson probability of observing s_i signal events in a bin i centered around t_i', when n_i events are predicted, in presence of B_i background events.
The number of events in the bin i of the t_i' signal distribution can be written in the following way:

$$n_i = S \times P^s(t_i') + B \times P^{bg}(t_i') \tag{2}$$

S= total signal events in the signal region; B= total background events in the signal region; P^s, P^{bg}= probabilities for an event, of signal and background, respectively, to have a decay time between t_i and $t_i + \Delta t_i$.

$P^s(t_i')$ can be parametrized as $e^{-t_i'/\tau}$; $P^{bg}(t_i')$ is obtained by the sidebands.
Then:

$$n_i = S\frac{f(t_i')\cdot e^{-t_i'/\tau}}{\Sigma f(t_i')\cdot e^{-t_i'/\tau}} + B\frac{b_i}{\Sigma b_i} \tag{3}$$

b_i=number of events in the bin i of the sideband hystogram; τ and B are the fit parameters; S is constrained to be $S = N_{tot}^{obs} - B$, where N_{tot}^{obs} is the total number of events in the signal region.
Assuming a Poisson distribution of the entries in the signal distribution:

$$L_{signal} = \prod_{i=1}^{\sharp bins} \frac{n_i^{s_i}}{s_i!}e^{-n_i} \tag{4}$$

s_i= number of events in the bin i of the signal hystogram.
For the background:

$$L_{bg} = \frac{(\mu_{bg})^{\Sigma bi}}{(\Sigma bi)!}e^{-\mu_{bg}} \tag{5}$$

where

$$\mu_{bg} = B/R \tag{6}$$

and

$$R = \frac{\text{signal width}}{\text{sideband width}} \tag{7}$$

Finally the total M.L.F. is:

$$L = L_{signal} \times L_{bg} \tag{8}$$

The advantage of the Binned M.L. is that it does not need a parametrization for the background.

2.4.2 *Continuous Maximum Likelihood*

In this case the contribution to the likelihood is calculated for each event in the signal region.
The probability for the event i is:

$$P(m_i, t_i') = \frac{Aexp[-(m_i - M)^2/2\sigma_m]}{\sqrt{2\pi}\ \sigma_m} f(t')e^{-t_i'/\tau} + C(m_i)T_b(t_i') \tag{9}$$

- m_i, t_i' are referred to the event i;
- M is the mean value of the invariant mass;
- $T_b(t_i')$ is the t' distribution for the background events as obtained from a fit to the sidebands.

The values of A, M, σ_m, $C(m_i)$ are fixed from a fit to the invariant mass plot and the probability $P(m_i, t_i')$ is normalized to that:

$$\int_{M-2\sigma_m}^{M+2\sigma_m} P(m_i, t_i') dm_i dt_i' = 1 \tag{10}$$

Finally the M.L.F. is:

$$L = \prod_i P(m_i, t_i) \tag{11}$$

3 Measurement of the lifetime of $D_0^{\pm}, D_s, \Lambda_c$

A big improvement in the precision of the lifetime measurements has been achieved with the E687 data. In Figs. 1,2,3,4 the lifetime measurements are presented with the statistical errors and, when available, the systematic errors. The decay channels and the number of events in the yields for the more accurate measurements are also mentioned. The world mean values of the Particle Data Group '92 and Particle Data Group '94 are quoted; the difference between these two quotations is due only to the E687 ('94) results with full statistics. The accuracy of our present experimental knowledge of the lifetimes is: $\sim$ 1.4% for $D^{\pm}$,$\sim$ 1% for D^0, $\sim$ 3.6% for D_s, $\sim$5% for Λ_c.

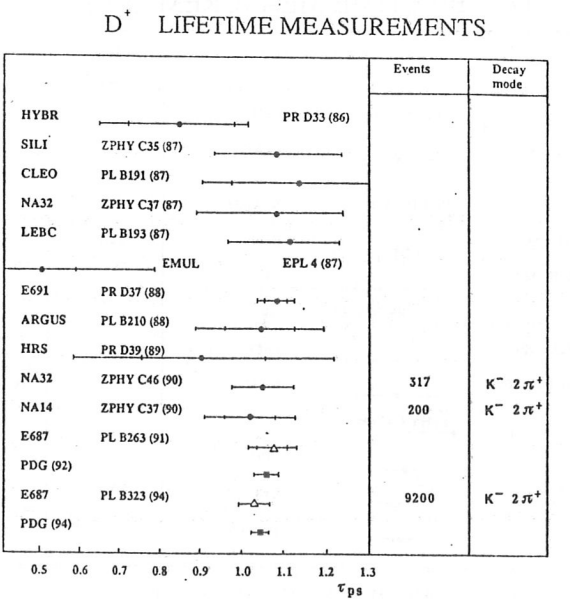

Fig. 1

D^0 LIFETIME MEASUREMENTS

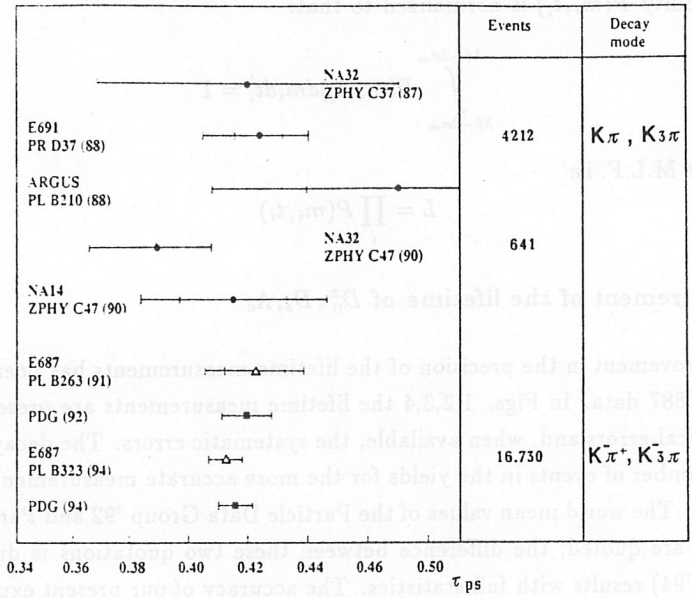

Fig. 2

D_S LIFETIME MEASUREMENTS

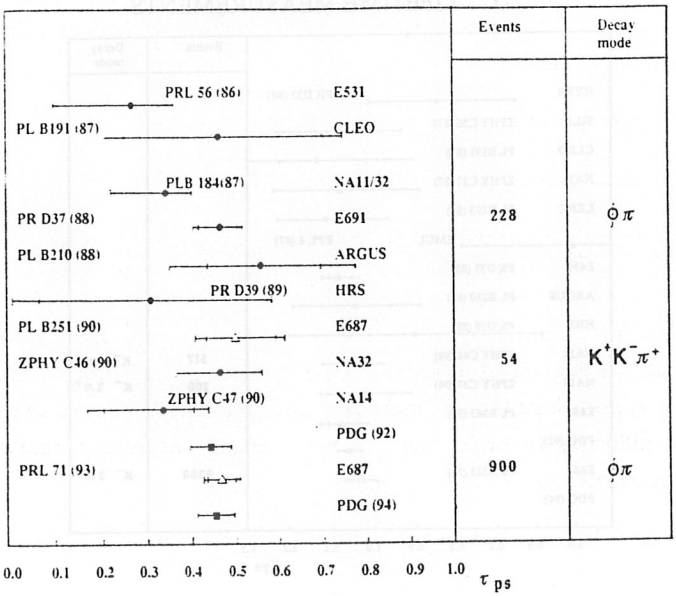

Fig. 3

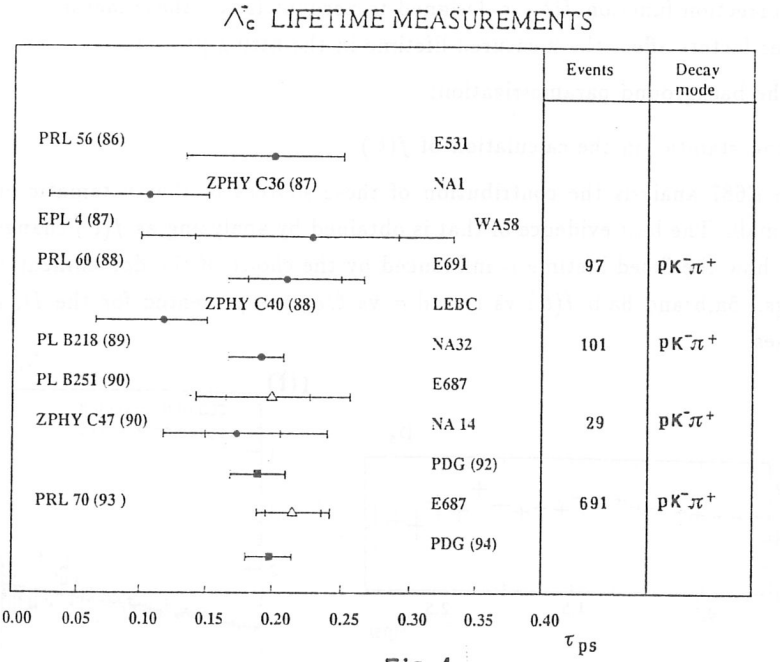

Fig. 4

In the E687 analysis a special accuracy has been devoted to the study of the systematic uncertainty. Possible contributions to the systematic errors concern the proper time distribution and the fitting procedure. The factors, which can affect the proper time distributions, are:

- the transverse profile of the photon beam;
- the momentum spectrum of the charmed states;

(both these sources are connected to possible inaccuracies of the acceptance calculations);

- the hadronic absorption of the charmed particles and their secondaries. In this case the uncertainties are due to the fact that the absorption cross section for the charmed states are unknown and, for what concern the secondaries, to the difficulty to understand to what extent the elastic scattering causes mismeasurements;
- acceptance of the detector;
- analysis cuts.

The correction function $f(t')$ is designed to account for all these factors.
Further factors affect the measured lifetime in the fitting procedure:

- the background parametrization;
- uncertainties in the calculation of $f(t')$.

In the E687 analysis the contribution of these sources to the systematic errors is very small. The best evidence of that is obtained by analyzing as $f(t')$ changes with t' and how the fitted lifetime is influenced by the choice of the detachment cut.
In Figs. 5a,b and 6a,b $f(t')$ vs t' and τ vs ℓ/σ_ℓ are presented for the D_s and Λ_c analyses.

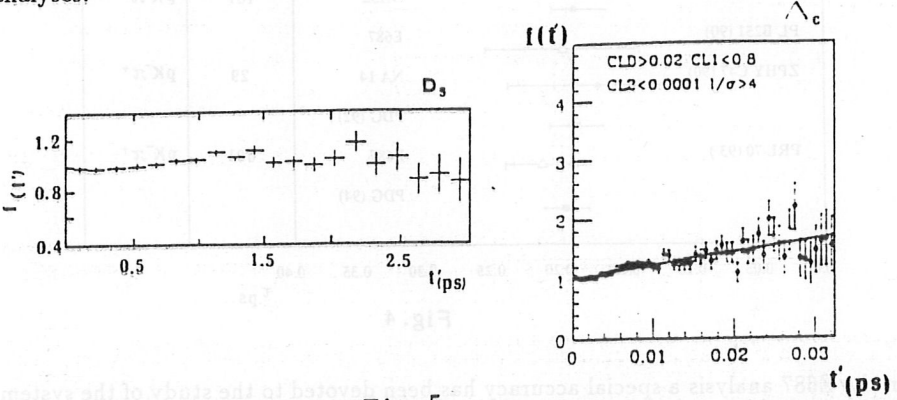

Fig. 5

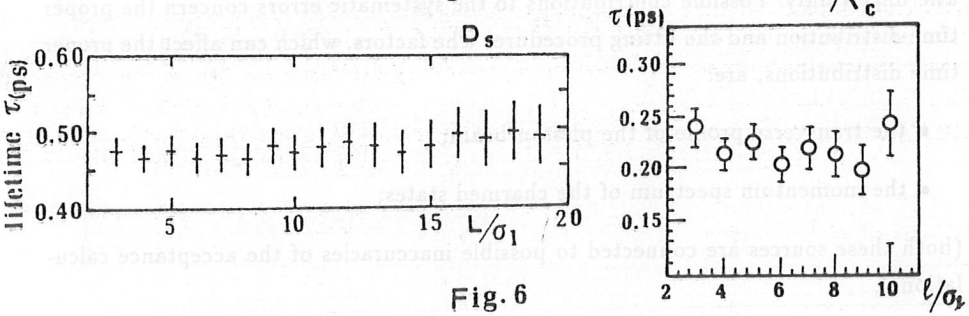

Fig. 6

We can observe that f(t') is always a very smooth function of t' and that the fitted values of the lifetime are not influenced by the detachment cut.
The systematic effects have been studied by the E687 collaboration also doing the same lifetime analyses for subsamples, defined in various ways. In Figs. 7a and 7b the results of these systematic studies are shown, as an example, for D_s and Λ_c: the lifetimes obtained by the subsamples are fully compatible with the values quoted for the full samples.

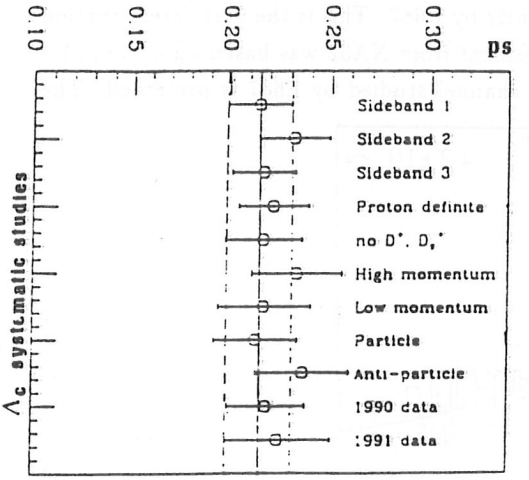

Fig. 7a

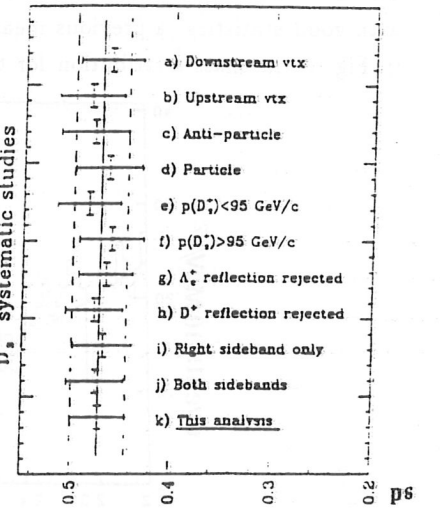

Fig. 7b

4 Study of the cascades and Ω_c^0

4.1 Ξ_c^0

In Table I a compilation of the Ξ_c^0 mass values measured up to now, are presented. The mass quoted by PDG'94 is also shown; it does not take into account the recent WA89 data.

Table I

EXPERIMENT	MODE	YIELD (events)	MASS (MeV/c^2)
CLEO	$\Xi^-\pi^+$	14	$2471 \pm 3 \pm 4$
CLEO	$\Xi^-\pi^+$	19	$2472 \pm 3 \pm 4$
NA32	$pK^-\bar{K}^{*0}$	4	$2473.3 \pm 1.9 \pm 1.2$
ARGUS	$\Xi^-\pi^+$ $\Xi^-\pi^+\pi^+\pi^-$	54	$2472.1 \pm 2.7 \pm 1.6$
E687	$\Xi^-\pi^+$	42 ± 10	$2462.1 \pm 3.1 \pm 1.4$
PDG'94			2470 ± 1.8
WA89	$\Xi^-\pi^+$	22/25	$2455 \pm 4 \pm 7$
WA89	$\Lambda K^-\pi^+$	32/37	$2465 \pm 3 \pm 7$

The Ξ_c^0 lifetime has been measured recently by E687. This is the first determination with good statistics (a previous measurement from NA32 was based on 4 events). In Fig. 8 the mass distribution for the channel studied by E687 is presented. The

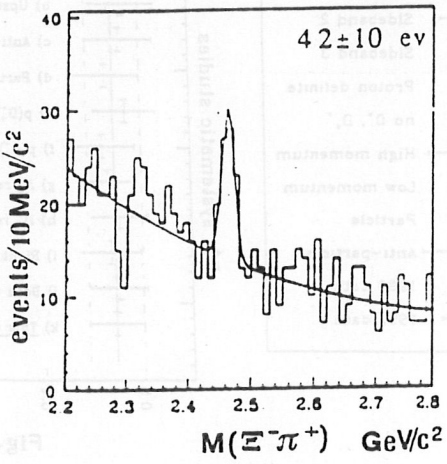

Fig. 8

decay is $\Xi_c^0 \to \Xi^-\pi^+$, where $\Xi^- \to \Lambda_0\pi^-$ and $\Lambda_0 \to p\pi^-$. In this analysis only Ξ^- decays downstream of the vertex detector are taken into account to have a high resolution track for the charmed state[1]. The yield consists of 42±10 events.
The distribution of the times of life, the correction function f(t') and τ vs ℓ/σ_ℓ are shown in Fig. 9. The correction function is very smooth and the fitted lifetime value is very stable as ℓ/σ_ℓ cut changes. This is a good demonstration that the systematic effects are small.
The Ξ_c^0 lifetime quoted by E687 is: $1.01^{+0.025}_{-0.017} \pm 0.05 ps$.

5 $\Xi_c^\pm$

The charged cascade has been measured more extensively than the neutral cascade, due to its longer lifetime.
In Table II the mass measurements are presented. The PDG'94 quotation does not take into account yet the Excharm and the WA89 data. In Table III the lifetime measurements are summarized, together with the decay channel, which has been analyzed, and the statistics of signal events used to measure the lifetime.

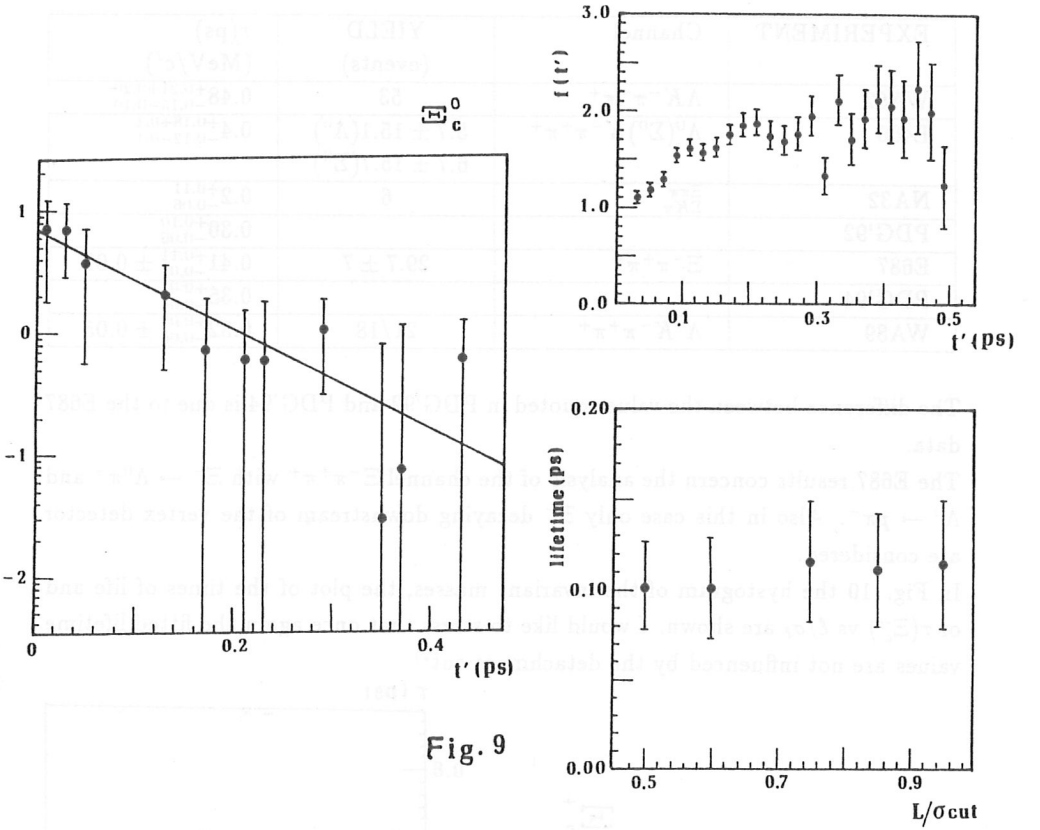

Fig. 9

Table II

EXPERIMENT	MASS (MeV/c^2)
CLEO	$2467 \pm 3 \pm 4$
ARGUS	$2465.1 \pm 3.6 \pm 1.9$
WA62	2460 ± 25
E400	$2459 \pm 5 \pm 30$
NA32	$2466.5 \pm 2.7 \pm 1.2$
E687	$2464.4 \pm 2.0 \pm 1.4$
PDG'94	2465.1 ± 1.6
Excharm	2465 ± 4
Excharm	2472 ± 4
WA89	2462 ± 3
WA89	2465 ± 3

Table III

EXPERIMENT	Channel	YIELD (events)	τ(ps) (MeV/c^2)
WA62	$\Lambda K^-\pi^+\pi^+$	53	$0.48^{+0.21+0.20}_{-0.15-0.10}$
E400	$\Lambda^0(\Sigma^0)K^-\pi^+\pi^+$	$5.7 \pm 15.1(\Lambda^0)$ $6.7 \pm 15.7(\Sigma^0)$	$0.4^{+0.18+0.1}_{-0.12-0.1}$
NA32	$\frac{\Xi\pi\pi}{\Sigma K\pi}$	6	$0.2^{+0.11}_{-0.06}$
PDG'92			$0.30^{+0.10}_{-0.06}$
E687	$\Xi^-\pi^+\pi^+$	29.7 ± 7	$0.41^{+0.11}_{-0.08} \pm 0.02$
PDG'94			$0.35^{+0.07}_{-0.04}$
WA89	$\Lambda^0 K^-\pi^+\pi^+$	21/18	$0.32^{+0.08}_{-0.06} \pm 0.05$

The difference between the values quoted in PDG'92 and PDG'94 is due to the E687 data.

The E687 results concern the analysis of the channel $\Xi^-\pi^+\pi^+$ with $\Xi^- \to \Lambda^0\pi^-$ and $\Lambda^0 \to p\pi^-$. Also in this case only Ξ^- decaying downstream of the vertex detector are considered.

In Fig. 10 the hystogram of the invariant masses, the plot of the times of life and of $\tau(\Xi_c^-)$ vs ℓ/σ_ℓ are shown. I would like to stress that once again the fitted lifetime values are not influenced by the detachment cut[2].

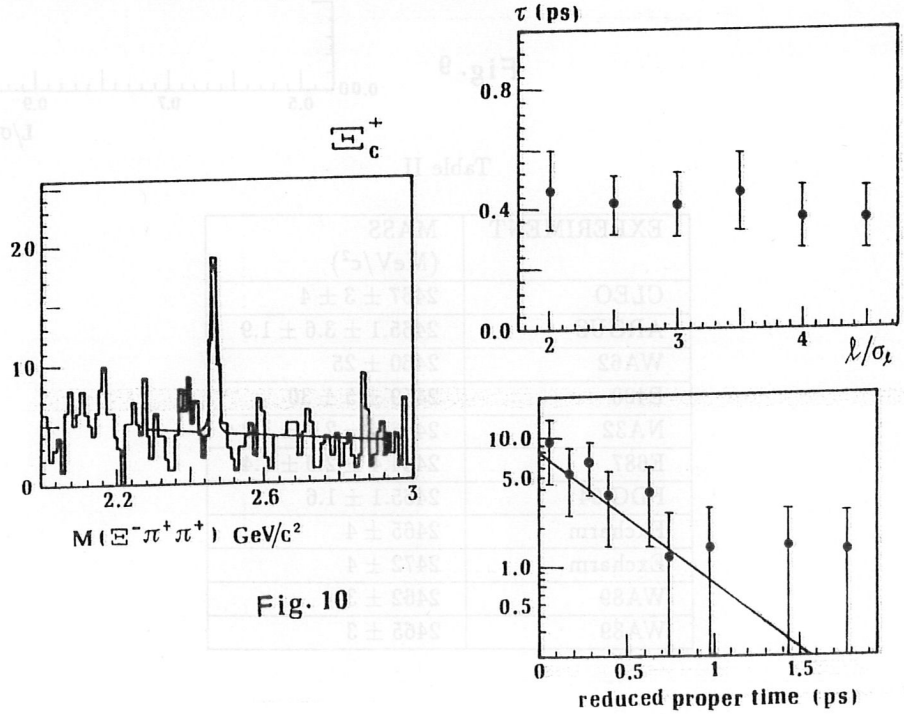

Fig. 10

6 Ω_c^0

After the first evidence provided by WA62 (with only 3 events), in 1992 ARGUS and E687 obtained a peak having ~2.7 s.d. of statistical significance in the channels $\Xi^- K^- \pi^+ \pi^+$ (12±7 events) and $\Omega^- \pi$ with $\Omega^- \to \Lambda^0 K^-$ (10±4 events), respectively. But later the decay channel $\Xi^- K^- \pi^+ \pi^+$ was studied by CLEO and E687, and the channel $\Omega^- \pi^- \pi^+ \pi^+$ by E687; in all three cases no evidence has been found.

More recently E687 reached a good statistical significance for the presence of Ω_c^0 in the channel $\Sigma^+ K^- K^- \pi^+$ with Σ^+ decaying both to $p\pi^+$ and $n\pi^+$. The total yield consists of ~ 42.5±8.8 events.

A further preliminary evidence has been obtained by E687 in the channel $\Sigma^+ K^- K_s^0$, with 21.34±8.3 events in the yield.

Up to this moment 4 independent evidences of Ω_c^0 were obtained, but no one channel was observed by two different experiments.

Very recently WA89[3] found good evidence for Ω_c^0 in the following channels: $\Omega^- \pi^+$, $\Omega^- \pi^- \pi^+ \pi^+$, $\Xi^- K^- \pi^+ \pi^+$, $\Xi^- K^0 \pi^+$, $\Xi^- K^0 \pi^- \pi^+ \pi^+$, $\Lambda K^- K^- \pi^+ \pi^+$, $\Lambda K^0 K^- \pi^+$.

Then now we have two channels showing an Ω_c^0 peak from the analysis of two different experiments: $\Omega^- \pi^+$ by E687 and WA89; $\Xi^- K^- \pi^+ \pi^+$ by ARGUS and WA89.

In Fig. 11 the Ω_c^0 invariant mass, as reconstructed in the various channels, are shown.

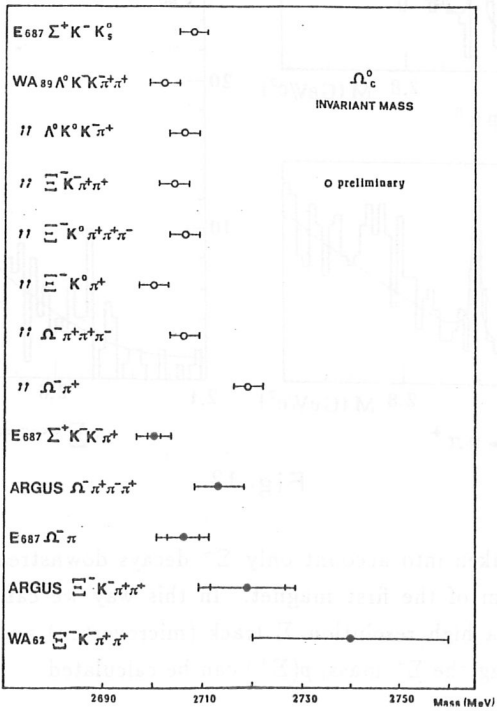

Fig. 11

The values quoted fluctuate in a large range, but if we take into account only the more recent values, included the preliminary ones, we can observe that the mass values range within the interval 2700-2710 MeV/c^2.

6.0.1 Ω_c^0 lifetime

The E687 collaboration studied the Ω_c^0 lifetime analyzing the channel: $\Omega_c^0 \rightarrow \Sigma^+ K^- K^- \pi^+$ in both the Σ^+ decay modes: $\Sigma \rightarrow p\pi^0$ and $\Sigma \rightarrow n\pi^+$. In Fig. 12 the two subsamples, obtained selecting the $\Sigma \rightarrow p\pi^0$ and the $\Sigma \rightarrow n\pi^+$ decay modes, are shown together with the full sample. The Ω_c^0 mass is: $M(\Omega_c^0) = 2698.8 \pm 2.5 MeV/c^2$ (width=6.4±1.9 MeV/c^2) for the sample with $\Sigma \rightarrow p\pi^0$, and $M(\Omega_c^0) = 2700.0 \pm 2.0$ (width=5.6±1.3 MeV/c^2) for the sample considering the $n\pi^+$ decay mode. Finally the full sample gives: $M(\Omega_c^0) = 2699 \pm 1.5 \pm 2.5 MeV/c^2$. The consistency is very good. The mass widths have to be compared with the resolution alone, which is 8.0±2. MeV/c^2.

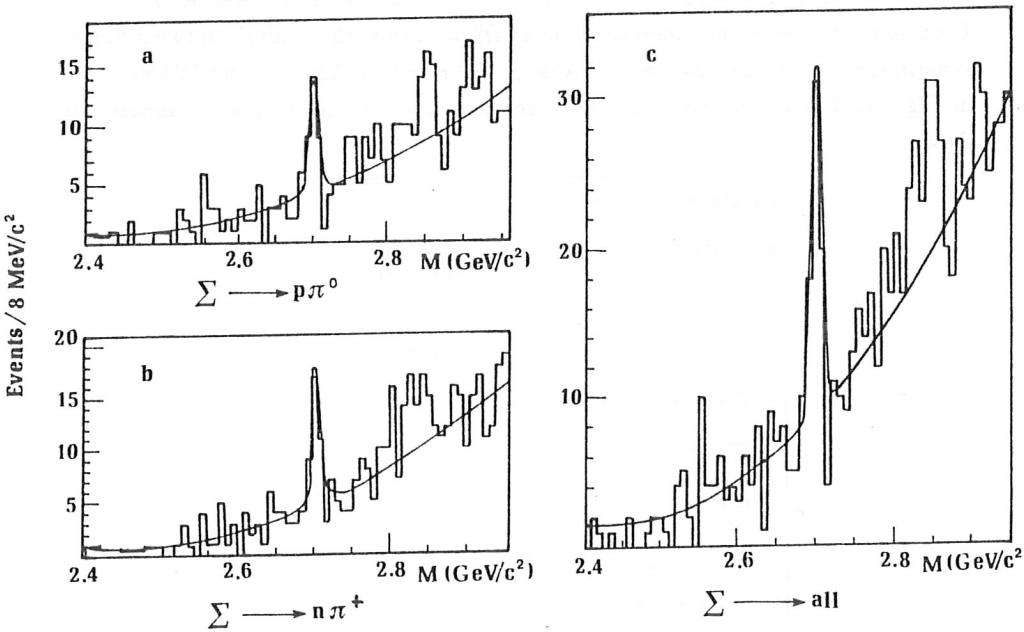

Fig. 12

In this analysis we taken into account only Σ^+ decays downstream of the vertex detector and upstream of the first magnet. In this way we can reconstruct the intersection between a high resolution Σ track (microvertex) and a p or π track (MWPC). Constraining the Σ^+ mass, $p(\Sigma^+)$ can be calculated.

The confidence level helps in solving the two-fold ambiguity, which remains at 35% for the $(p\pi^0)$ sample and at 10% for the $(n\pi^+)$ one. This difference between the two subsamples is due to the larger π^+ decay angle, if compared to the p one, and to the use of the calorimeters in checking the n direction.

Various methods are used to account for possible double candidates; the results are quite equivalent and introduce a systematic uncertainty of $\sim 0.1 MeV/c^2$. Possible contamination from other channels, as $\Xi_c^0 \rightarrow \Sigma^+ K\pi^-\pi^+$, has been studied and it has been found to be negligible.

The measurement of the Ω_c^0 lifetime presents many difficulties because, from the preliminary results, it appears to be very close to the resolution of the E687 experimental set up, which is $\sim$ 0.05 ps for the lifetime reconstruction.

As a consequence the cut on ℓ/σ_ℓ cannot be used or can be used very weakly $(\ell/\sigma_\ell > 0)$ and the simple correction function f(t') is not valid anymore. In fact the corrections obtained via MC simulations are heavily influenced by the lifetime and the resolution in t' (or t;t'$\equiv$t without detachment cuts), which have been assumed for the generation.

Various approaches are used to solve these problems. An iterative method makes use of several f(t'), calculated with different τ_{gen}. An other approach adopts a two-dimension simultaneous parametrization of $f(t', \tau_{gen})$. In addition both the Binned and the Continuous Maximum Likelihood methods are used.

The E687 collaboration has not yet given a final quotation. But what is possible to adfirm already is that the Ω_c^0 lifetime ranges between 0.05 and 0.1 ps, with a statistical error of $\sim$0.02 ps. The systematic error is still under study.

7 Conclusion

In Table IV I summarize the lifetime results obtained by E687, which up to now are the most accurate and in Table V their accuracy.

Table IV

	E687 λ(psec)	PDG94 λ(psec)
$D^\pm$	$1.048 \pm .015 \pm .011$	$1.057 \pm .015$
D^0	$.413 \pm .004 \pm .003$	$.415 \pm .004$
$D_S^\pm$	$.475 \pm .020 \pm .007$	$.467 \pm .017$
Λ_C^+	$.215 \pm .016 \pm .008$	$.200^{+.011}_{-.010}$
Ξ_C^+	$.410^{+.11}_{-.08} \pm .02$	$.35^{+.07}_{-.04}$
Ξ_C^0	$.101^{+.025}_{-.017} \pm .005$	$.098^{+.023}_{-.015}$
Ω_C^0	$.05 - .1$	

Table V

	Accuracy (E687)	Accuracy (PDG94)
$D^{\pm}$	1.8%	1.4%
D^0	1.2%	1.0%
$D_S^{\pm}$	4.5%	3.6%
Λ_C^+	8.3%	5.2%
Ξ_C^+	27.2%	15.7%
Ξ_C^0	25.2%	19.4%

The quotations of PDG'94, which include the E687 measurements, are also shown. From these results we can extract the best quotations of the ratios between D^+ and D^0, D_s and D^0 lifetimes:

$$\frac{\tau(D^{\pm})}{\tau(D^0)} = 2.547 \pm 0.043 \tag{12}$$

and

$$\frac{\tau(D_s^{\pm})}{\tau(D^0)} = 1.12 \pm 0.04 \tag{13}$$

Taking into account that the semileptonic widths, still from PDG' 94, give:

$$\frac{\Gamma(D^0 \to eX)}{\Gamma(D^+ \to eX)} = \frac{\Gamma(D^0 \to eX)/\Gamma_{tot}(D^0)}{\Gamma(D^+ \to eX)/\Gamma_{tot}(D^+)} \times \frac{\Gamma_{tot}(D^0)}{\Gamma_{tot}(D^+)} = \tag{14}$$

$$= \frac{BR(D^0 \to eX)}{BR(D^+ \to eX)} \times \frac{\tau(D^+)}{\tau(D^0)} = 1.14 \pm 0.22$$

it is clear that the extra rate of the charged D's with respect to the neutral ones is not due to the semileptonic process.

In addition the baryon lifetime hierarchy can be considered settled enough in the following way: $\tau(\Omega_c^0) \leq \tau(\Xi_c^0) < \tau(\Lambda_c^+) < \tau(\Xi_c^+)$

References

1. P.L. Frabetti et al., Phys. Rev. Lett. **70**, 2058 (1993).
2. P.L. Frabetti et al., Phys. Rev. Lett. 1381 (1993).
3. E. Chudakov - this Conference.

SESSION VI

- J. Simone
  Progress in Lattice Gauge Calculations of Heavy Quark Properties

- M. Greco
  Large p_T Hadroproduction of Heavy Quarks and Quarkonia

PROGRESS IN LATTICE GAUGE CALCULATIONS OF HEAVY QUARK PROPERTIES

J. Simone

MS-106, P.O. Box 500, Batavia, Illinois 60510 (U.S.A.)

No written contribution received

Frascati Physics Series, Vol. III (1994)
HEAVY QUARKS AT FIXED TARGET
University of Virginia, October 7–10, 1994
(pp. 215–232)

LARGE p_T HADROPRODUCTION OF HEAVY QUARKS AND QUARKONIA

Mario Greco
Dipartimento di Fisica, Università di Roma III
and
INFN, Laboratori Nazionali di Frascati, Italy

ABSTRACT

The production of heavy quarks at large p_T ($p_T \gg m$) in hadronic collisions is considered in the framework of perturbative fragmentation functions, allowing a resummation at the NLO level of final state large mass logarithms of the kind $\log(p_T/m)$. The resulting theoretical uncertainty from factorization/renormalization scales at large p_T is shown to be much smaller than that shown by the full $O(\alpha_s^3)$ perturbative calculation. Then the production of heavy quarkonia at large tranverse momenta is discussed by including the mechanism of fragmentation, in particular the direct fragmentation to J/ψ and the fragmentation to χ states followed by radiative decay to J/ψ. The overall theoretical estimate is shown to be nearly consistent with the experimental observation for J/ψ. On the contrary the situation is quite unsatisfactory for the ψ', demanding for a new mechanism dominating the production process.

The hadroproduction of heavy quarks has recently been a subject of intense studies both experimentally and theoretically, in particular as an important testing ground for QCD. Also the study of the production properties of bound states of heavy quarks plays a central role in our understanding of the theory on the very border between the perturbative and non perturbative domains. A large amount of experimental data on the hadroproduction of b and c quarks and their bound states has been accumulated so far, to be compared with next-to-leading order (NLO) calculations recently available on the market. In this talk I will not attempt to review the full range of theoretical predictions on the production processes, the

general properties having been already discussed nicely by Berger [1]. Rather I will concentrate on some new results on the production of heavy quarks and quarkonia at collider energies and large transverse momenta, which go beyond the strict realm of fixed order perturbation theory, giving more precise predictions and also some new ideas for the production mechanisms.

We consider first the production of heavy quarks in hadronic collisions. On the theoretical side the calculation in perturbative QCD of the differential and total cross sections to order α_s^3 has been performed [2-6], providing a firm basis for a detailed study of the properties of the bottom and charm quarks, and leading to reliable predictions for the production rate of the top quark [8-10].

These results do however present a non-negligible residual factorization/renormalization (f/r) scale dependence, particularly at large p_T. Furthermore, the validity of this NLO $O(\alpha_s^3)$ calculation is limited when $p_T \gg m$, m being the large quark mass, by the appearance of potentially large logarithms of the type $\log(p_T/m)$, which have to be resummed to all orders. The physical reason for that is quite clear. For example, terms of order $(\alpha_s^3)\log(p_T/m)$ or $(\alpha_s^4)\log(p_T/m)^2$ are simply related to the mass singularities originating from collinear configurations when $m \to 0$ for fixed p_T. The theoretical uncertainty associated to those corrections has been roughly estimated in [3]. Whereas for top quark production this uncertainty is irrelevant, this is not the case for the production of bottom and charm quarks at large p_T, leading to relevant phenomenological consequences.

A solution to this problem has recently been considered [7], following an approach based on the properties of fragmentation of a generic parton p ($p = q, g, Q$) in the heavy quark Q, after the parton has been produced inclusively in the hard collision of the two initial hadrons. The basic formula is represented by eq. (1), where the partonic cross sections $\hat{\sigma}_{ij\to kX}$ at $O(\alpha_s^3)$ have been given in ref. [11] in the massless quark limit. $\hat{\sigma}_{ij\to kX}$ introduces an explicit dependence on p_T and on factorization/renormalization mass scales. The dependence on the heavy quark mass is then obtained through the fragmentation function of the parton $p \to Q + X$, evolved at NLO accuracy from an initial scale $\mu_0 \sim m$ (see below) to $\mu \sim p_T$. This approach explicitly resums potentially large terms ot the kind $[\alpha_s \log(p_T/m)]^n$, giving a better description of the theoretical predictions at large p_T. Indeed the corresponding uncertainty is quite reduced in this region with respect to the fixed order result, due to a significantly smaller sensitivity to the relevant scales. On the other hand, because of the massless limit used for the $O(\alpha_s^3)$ kernel cross sections

$\hat{\sigma}_{ij\to kX}$, this approach does not allow to recover in a simple way the limit $p_T \lesssim m$ of the perturbative calculation.

I will briefly review the main ideas of this analysis. According to factorization theorems [12] the cross section for the inclusive hadroproduction of a hadron at high transverse momentum, i.e. for the process

$$H_1 + H_2 \to H_3 + X$$

can be written as

$$\mathrm{d}\sigma = \sum_{i,j,k} \int \mathrm{d}x_1\, \mathrm{d}x_2\, \mathrm{d}x_3\, F^i_{H_1}(x_1,\mu_F) F^j_{H_2}(x_2,\mu_F) \mathrm{d}\hat{\sigma}_{ij\to kX}(x_1,x_2,x_3,\mu_R,\mu_F) D^{H_3}_k(x_3,\mu_F) \tag{1}$$

As usual, the F's are the distribution functions of the partons in the colliding hadrons, $\hat{\sigma}$ is the kernel cross section and D is the fragmentation function of the observed hadron. The factorization mass scales μ_F of the structure and fragmentation functions are assumed to be equal for the sake of simplicity. μ_R is the renormalization scale.

Due to the presence of collinear singularities both in the initial and final state this process is not fully predictable by QCD itself. We can actually calculate the kernel cross section and the evolution of the structure and fragmentation functions, but we have to rely on some phenomenological input to obtain the latter at some given initial scale.

This situation changes drastically when we come to consider the inclusive production of a heavy quark. In this case its mass, being finite and considerably greater than Λ, makes the perturbative expansion feasible and prevents collinear singularities from appearing in the splitting vertices which involve the heavy quark. Having this in mind two approaches can be pursued in the calculation of heavy quark production.

The first one is to directly calculate in perturbation theory the process $\mathrm{d}\hat{\sigma}_{ij\to QX}$, Q being the heavy quark and i,j the initial state *light* partons (i.e. light quarks and gluons). This kernel cross section will then be convoluted with initial state structure functions only, the final state showing no singularities of any kind. This approach has been followed in the past [2-5], providing a full perturbative $O(\alpha_s^3)$ calculation. In the following we shall use for comparisons the results of Nason, Dawson and Ellis, and refer to them as NDE. In this fixed order approach, as stated earlier, terms of the kind $\alpha_s \log(p_T/m)$ will appear. They are remnant of the collinear

singularity screened by the finite quark mass. As noted in ref. [3] they can grow quite large at high tranverse momenta, thereby spoiling the validity of the expansion in α_s. Therefore they have to be summed to all orders.

The alternative way is to consider that when a quark, of whichever flavour, is produced at very high transverse momentum $p_T \gg m$ its mass plays almost no role at all in the scattering process. This is to say that mass effects in the kernel cross section are suppressed as power ratios of mass over the scale of the process. We can therefore devise a picture in which all quarks are produced in a massless fashion at the high scale $\mu_F \sim p_T \gg m$ and only successively, as their virtuality decreases, they can *fragment* into a massive heavy quark. The cross section can therefore be described by a formula analogous to eq. (1), with $H_3 = Q$. The key difference to the hadron production case considered in eq. (1) is that initial state conditions for the heavy quark fragmentation functions are now calculable from first principles in QCD (hence the definition of "perturbative" fragmentation functions, PFF) and do not have to be taken from experiment.

Actually, the following set of next-to-leading initial state conditions can be obtained [13] in the $\overline{MS}$ scheme for the fragmentation function of a heavy quark, gluon and light quark respectively, in the heavy quark Q

$$D_Q^Q(x,\mu_0) = \delta(1-x) + \frac{\alpha_s(\mu_0)C_F}{2\pi}\left[\frac{1+x^2}{1-x}\left(\log\frac{\mu_0^2}{m^2} - 2\log(1-x) - 1\right)\right]_+ \quad (2)$$

$$D_g^Q(x,\mu_0) = \frac{\alpha_s(\mu_0)T_f}{2\pi}(x^2+(1-x)^2)\log\frac{\mu_0^2}{m^2} \quad (3)$$

$$D_{q,\bar{q},\bar{Q}}^Q(x,\mu_0) = 0 \quad (4)$$

where μ_0 must be taken of the order of the heavy quark mass.

Then using the usual Altarelli-Parisi evolution equations at NLO accuracy one finds the fragmentation functions set at any desired factorization scale μ_F. An important feature of this approach can now be appreciated. The "almost-singular" logarithmic term $\log(p_T/m)$ splits into two, as follows. A $\log(p_T/\mu_F)$ will be found in the kernel cross section $\hat{\sigma}$ which has no dependence on the heavy quark mass, according to the assumption that it is produced in a *massless* way). Moreover, by choosing $\mu_F \sim p_T$ it will not contain large logarithms and its perturbative expansion will behave correctly. The remaining part of the log will instead be lurked into the fragmentation function $D(x_3,\mu_F)$. The large $\log(\mu_F/\mu_0)$ is resummed to all orders by the evolution equations, and only the small $\log(\mu_0/m)$ provided by the initial state condition is treated at fixed order in perturbation theory. Therefore one expects

a better control of the theoretical uncertainty at large p_T. On the other hand, for $p_T \lesssim m$ the fragmentation approach does not allow to recover easily the $O(\alpha_s^3)$ result, which, of course, holds exactly.

In order to implement the "perturbative fragmentation function (PFF) approach" at a numerical level we need three ingredients, which are all available at the next-to-leading level:

i) the distribution functions of any parton (including the heavy flavour in question) in the hadrons (proton or antiproton), evolved at NLO accuracy. All modern sets satisfy this requirement. An important point must however be made clear. A heavy quark present in the initial state can be directly brought to the final state where it is fragmented to the detected heavy flavour through the D_Q^Q, and therefore with high probability. This means that the resulting cross section is particularly sensitive to the overall heavy flavour content of the colliding hadrons. In the Parton Distribution Functions (PDF) sets available this content is generated through perturbative gluon splitting above a given threshold. The total yield will therefore depend on the choice made. For instance, the HMRS-B set [14] ($\Lambda_5^{\overline{MS}} = 123$) takes $F_b(x, 2m_b) = 0$ as initial condition, whereas the MT-B2 [15] ($\Lambda_5^{\overline{MS}} = 124$) and the CTEQ1M [16] ($\Lambda_5^{\overline{MS}} = 152$) ones choose, according to ref. [17], $F_b(x, m_b) = 0$.

ii) the kernel cross section for the scattering of any two massless partons into another massless parton. This calculation is provided at the NLO in various renormalization/factorization schemes in ref. [11].

iii) the fragmentation functions of any parton into the heavy flavour. They are obtained by evolving the initial conditions given above (eqs. 2,3,4) with NLO accuracy [18]. This is done through numerical inversion of the Mellin moments of the evolved distributions.

With these ingredients at our disposal we can now evaluate the cross section for the high p_T inclusive hadroproduction of a bottom quark. Figure 1 shows, from ref. [7] and for the b-quark production, the comparison of the result of ref. [3] with our calculations for two different PDF sets, for $p\bar{p}$ collisions at the Cern and Fermilab colliders energies of 630 Gev and 1800 GeV respectively, for $\mu = \sqrt{m_b^2 + p_T^2}$. We can see that in the high p_T region the fixed order cross section is quite sensitive to the structure function set choice, the MT one giving a markedly lower result. The

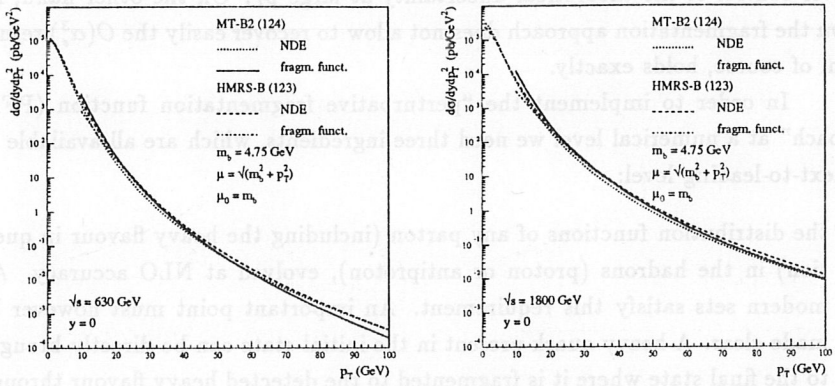

Figure 1: Results from the PFF approach compared to the fixed order prediction of NDE, with the MT-B2 and the HMRS-B sets, at 1800 and 630 GeV for $p\bar{p}$ collisions.

opposite happens in the PFF approach, which becomes very sensitive in the low p_T region to the neglect of the heavy quark mass terms in the partonic cross sections and to the threashold behaviour of the PDF sets in the heavy quark content. Our calculation, on the other hand, leads to substantially identical predictions obtained in the high p_T region with the two PDF sets.

Next we consider the dependence on the choice of the f/r mass scale μ. Figure 2 shows, for $p\bar{p}$ collisions at 1800 GeV and with the MT-B2 and HMRS-B sets, the theoretical uncertainty resulting from the variation of the factorization and renormalization mass scales between $\mu_{ref}/2$ and $2\mu_{ref}$, where μ_{ref} is defined as $\sqrt{m_b^2 + p_T^2}$ and we have taken $\mu = \mu_F = \mu_R$. As expected the band of the NDE calculation is sensibly larger than ours, showing the improvement brought by the resummation of the large logarithms of p_T/m_b. These features can be better appreciated in figure 3, where the cross section at 1800 GeV with the MT-B2 set is plotted, at fixed y and p_T, as a function of $\mu = \xi\mu_{ref}$, for ξ varying between 0.25 and 4. This figure also shows a comparison with the factorized calculation with a Born (i.e. LO) cross section kernel (but with two-loop α_s and NLO structure and fragmentation functions). As expected, the lack of the next-to-leading terms strongly enhances the scale dependence. The similarity between the NDE result and the fragmentation

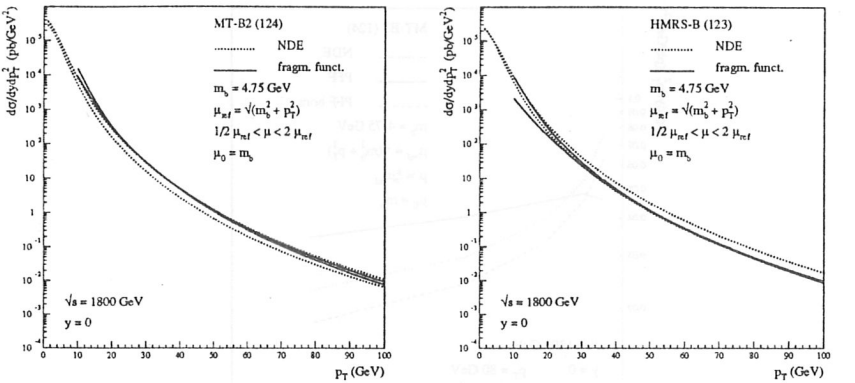

Figure 2: Scale dependence at 1800 GeV, with MT-B2 and HMRS-B structure functions sets.

function approach with Born kernel cross section is striking. The small scale sensitivity of our full NLO calculation shows that the factorization/renormalization scale dependence is a real $O(\alpha_s^4)$ effect, whereas in the fixed order approach (e.g. NDE) the presence of large $\log(p_T/m)$ results in an effective $O(\alpha_s^3)$ dependence.

We can now turn to quantities of more direct experimental interest and see how the advantages of our approach are reflected onto them. Namely, we will consider the total cross section for one particle inclusive heavy quark production, integrated above a given p_T^{min} and within a rapidity region $|y| < y_{max}$. Only the variation of the theoretical prediction due to changes in the factorization/renormalization scale and in the PDF set used will be studied. Other possible sources of uncertainties, aside the change of μ_0 which has been shown to be almost neglibible, are the value of the QCD scale Λ and of the bottom mass m_b. They should however be common to both the fixed order and the fragmentation function approach, and have been studied in detail in ref. [3].

The overall smaller theoretical uncertainty of the PFF result can be appreciated in fig. 4, where the highest and lowest predictions of the two approaches, out of the six curves previously considered, have been plotted. Note that we have not considered in detail the uncertainties for $p_T \lesssim 10$ GeV. The CDF experimental data [19] are also shown. Similarly in fig. 5 the comparison is shown with UA1 data

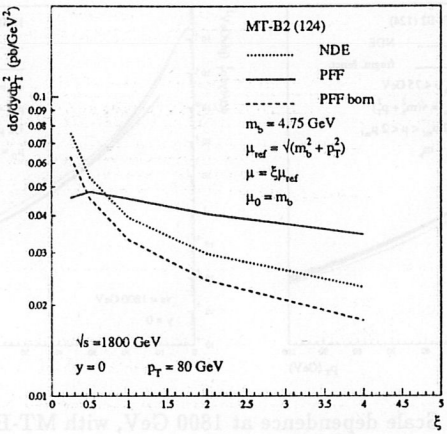

Figure 3: Scale dependence of the cross section as a function of $\mu = \xi\mu_{ref}$, at $y = 0$ and $p_T = 80$ GeV. "NDE" and "PFF" refer to the full NLO calculations, whereas "PFF born" is the result of the fragmentation function approach with LO kernel cross section.

[20] at 630 GeV.

The same kind of result is obtained for charm production. Figure 6 compares compares our predictions to NDE and also in this case we find a sizeable reduction in the uncertainty of the theoretical prediction. An independent analysis has been carried out [21] for the hadronic production of the charmed mesons D and D^*, using phenomenological inputs for the fragmentation functions in e^+e^- annihilation and NLO evolution equations. The predicted tranverse momentum distributions behave similarly to the open charm results.

We consider now the production of the bound states of heavy quarks which plays a central role in our understanding of QCD on the very border between the perturbative and non-perturbative domain. In particular it is of key importance to have accurate estimates of the production cross sections at large tranverse momenta for precision tests of the theory and possible evidence of new phenomena.

So far there has been an intensive experimental study of the $c\bar{c}$ $1S$ vector bound state, namely J/ψ and ψ', both at UA1 [22] and CDF [23]. The results have

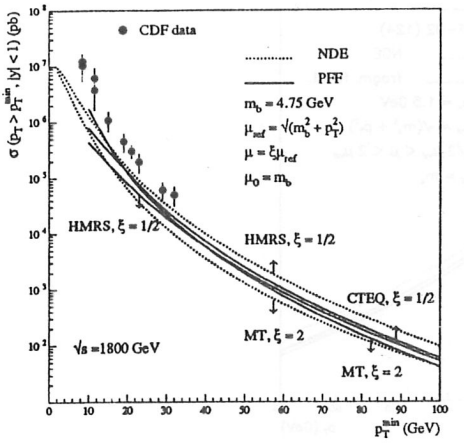

Figure 4: Comparison of the overall theoretical uncertainty of inclusive high p_T heavy quark production at 1800 GeV in the PFF and fixed order approaches. CDF experimental data are also shown.

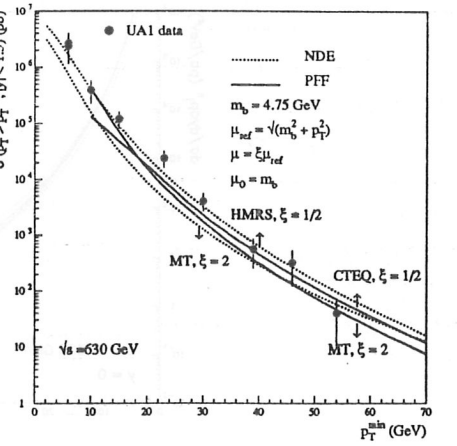

Figure 5: Comparison of the overall theoretical uncertainty of inclusive high p_T heavy quark production at 630 GeV in the PFF and fixed order approaches. UA1 experimental data are also shown.

been compared with theoretical calculations [24,2,25] which take into account two different mechanisms for J/ψ production: direct charmonium production, including the contribution from the χ states, i.e.

$$gg \to J/\psi\, g \qquad gg, q\bar{q} \to \chi g \hookrightarrow J/\psi\,\gamma \qquad qg \to \chi q \hookrightarrow J/\psi\,\gamma \tag{5}$$

and the production resulting from B mesons decay

$$p\bar{p} \to bX \hookrightarrow B \to J/\psi\, X \tag{6}$$

These calculations are in disagreement with the results from CDF, the J/ψ rate observed being actually higher, by a factor of two or more, than the predicted one [23,25,26].

It has however recently been pointed out by E. Braaten and T.C. Yuan [27] that at large p_T an additional production mechanism comes into play, namely the fragmentation of a gluon or a charm quark into a charmonium state. While being of higher order with respect to direct production by a power of the running coupling constant α_s, this mechanism becomes dominant at large p_T because of a factor

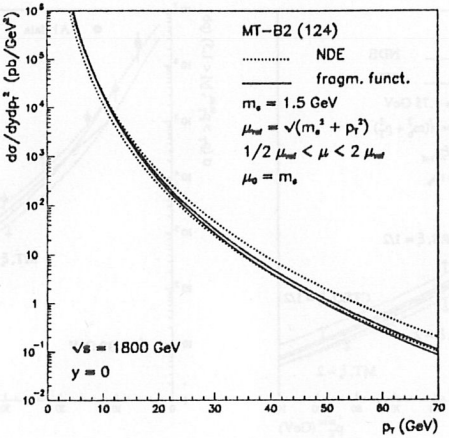

Figure 6: Results from the PFF approach to c quark production compared to the fixed order prediction of NDE, with the MT-B2 set, at 1800 GeV for $p\bar{p}$ collisions.

$O(p_T^2/m_c^2)$ which overcomes the extra power of α_s. The fragmentation functions describing these processes can be calculated perturbatively. Indeed it has been argued in [27] and subsequently shown at LO in [28] that J/ψ production via fragmentation will overcome the direct one (i.e. $gg \to J/\psi g$) at $p_T \sim$ 6-8 GeV. A similar exercise for the χ production, when the total fragmentation probability $\int D_g^\chi$ (see below) times the $gg \to gg$ cross sections is compared to the direct production $gg \to \chi g$, reveals that fragmentation should dominate for p_T already at $\sim$ 2 GeV. Since this result is at the limit of validity of the fragmentation function approach, we can however still expect that the fragmentation mechanism will dominate over the direct one at p_T values as low as 5-6 GeV.

These ideas have been recently applied [36,37,39] to a more quantitative determination of the J/ψ production rate in hadron collisions, taking also into account the production via fragmentation processes of the χ states and subsequent radiative decays to J/ψ.

To this aim the following fragmentation functions play a major role: the gluon fragmentation to J/ψ [27], $D_g^{J/\psi}$ (see fig. 7); the charm (or anticharm) fragmentation to J/ψ [29], $D_c^{J/\psi}$ (see fig. 8); the charm fragmentation to χ states [30,31], D_c^χ;

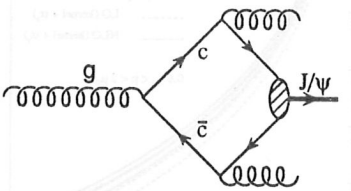

Figure 7: One of the diagrams for the gluon fragmentation function at the scale $\mu = 2m_c$.

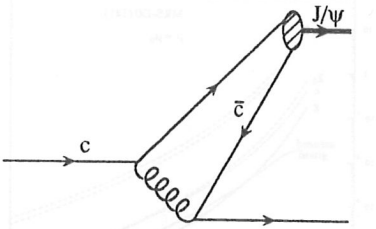

Figure 8: One of the diagrams for the charm fragmentation function, at the scale $\mu = 3m_c$.

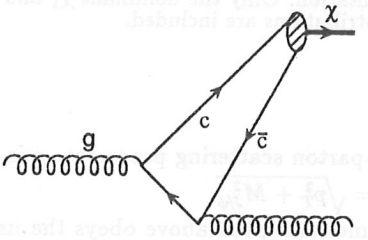

Figure 9: One of the diagrams for the gluon fragmentation function to the χ states, at the scale $\mu = 2m_c$.

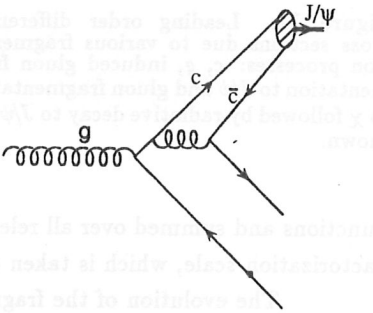

Figure 10: One of the "perturbative" contributions to the induced gluon fragmentation function, at the scale $\mu = 4m_c$.

and finally the gluon fragmentation to χ states [32], D_g^χ (see fig. 9).

They have been all calculated by perturbative techniques at an initial scale of the order of the mass of the J/ψ. Of course in the evaluation of the actual cross sections they must be evolved to the appropriate scale, and one gets to the usual expression

$$d\sigma(p\bar{p} \to J/\psi(p_T) + X) = \sum_i \int_{z_{min}}^1 dz\, d\sigma(p\bar{p} \to i(p_T/z) + X, \mu) D_i^{J/\psi}(z, \mu) \qquad (7)$$

for the J/ψ production, the sum running over g, c and $\bar{c}$. A similar formula does hold for χ production. The cross section on the right hand side corresponds to the inclusive production of the parton i, convoluted with the appropriate structure

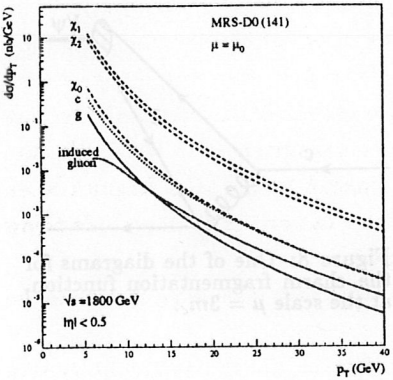

Figure 11: Leading order differential cross sections due to various fragmentation processes: c, g, induced gluon fragmentation to J/ψ and gluon fragmentation to χ followed by radiative decay to J/ψ are shown.

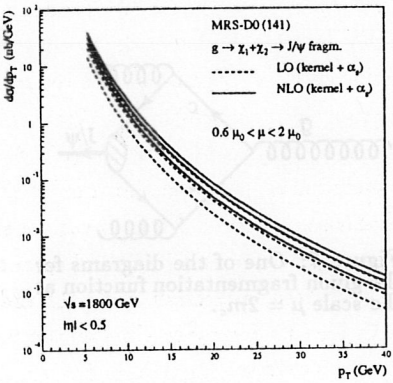

Figure 12: Leading vs. next-to-leading cross section for producing a J/ψ via fragmentation. Only the dominant χ_1 and χ_2 contributions are included.

functions and summed over all relevant parton-parton scattering processes. μ is the factorization scale, which is taken of order $\mu_0 = \sqrt{p_T^2 + M_{J/\psi}^2}$.

The evolution of the fragmentation functions given above obeys the usual Altarelli-Parisi (AP) equations

$$\mu \frac{\partial}{\partial \mu} D_i^{J/\psi}(z,\mu) = \sum_j \int_z^1 \frac{dy}{y}\, P_{i\to j}(z/y,\mu)\, D_j^{J/\psi}(y,\mu) \qquad (8)$$

Furthermore it has been pointed out in ref. [33] that when one considers the whole set of the AP equations, with the appropriate mixings taken into account, the evolution of the $D_c^{J/\psi}$ will induce a gluon fragmentation function through the splitting $g \to c\bar{c}$ and subsequent fragmentation of one of the quarks into a J/ψ (see fig. 10). This process is of order α_s^3 but, being enhanced by a factor $\log(\mu/M_{J/\psi})$, will dominate over the the contribution from $D_g^{J/\psi}$ at large p_T.

We present first the leading order (LO) results using the Born partonic cross sections and then, to reduce the theoretical uncertainty, by taking into account the full NLO [11] information on the partonic scattering processes.

From ref. [36] we plot in fig. 11 the LO cross sections, differential in p_T and

integrated over the $\eta < |0.5|$ range, for producing a J/ψ via fragmentation, either directly or after radiative decay of a χ state. The values of the various parameters entering into the calculation are reported in ref. [36], and we are using $\mu = \mu_0$ for the factorization/renormalization (f/r) scales. We also use the MRS-D0 set of structure functions. The curves labeled by χ are due to gluon fragmentation only. We have not included $c \to \chi$ fragmentation contributions since, from the total fragmentation probabilities listed in [30], they can be predicted to lie two orders of magnitude below the $c \to J/\psi$ curve and be therefore surely negligible.

From inspection of fig. 11 the contributions from χ_1 and χ_2 states can be clearly seen to dominate all over the p_T range considered.

Next we compare, in fig. 12, the results obtained for the dominant $\chi_1 + \chi_2$ contribution in the LO approach with those obtained by inserting also the next-to-leading (NLO) partonic cross sections, to order α_s^3, with α_s evaluated to two loop accuracy. Figure 12 clearly shows that the higher order terms enhance the cross section by a factor about 1.5. This is consistent with previous studies of higher order corrections in heavy quark [2-5] and inclusive jets [11,34] production in hadron collisions. The effect of variations of the f/r scales μ between $0.6\,\mu_0$ and $2\mu_0$ is also shown. As expected, the inclusion of the NLO terms reduces the sensitivity to scale variations.

Finally we show, in fig. 13 and from ref. [36] prediction for J/ψ production by adding the mechanism of fragmentation to the direct one [35] and to the production from B decays as taken from ref. [25], together with the reported theoretical uncertainty. The bands are made by choosing the highest and lowest curve which could be obtained by varying some of the parameters. The total result is obtained by adding togheter the two highest and the two lowest curves respectively. The size of the the fragmentation contribution is seen to be comparable with the previous estimate for the sum of the two mechanisms considered up to now, leading therefore to a sizeable enhancement of the predicted overall production rate, which we also show in the figure. Similar results have been obtained in ref. [37].

When we compare with CDF data points [23] we see that they are now more compatible with the theoretical band. This improves sensitivly the previous situation, where only by making very extreme choices of the parameters one could get close to the experimental findings. In addition the new set of CDF data [38], which selects out via a microvertex detector the fraction of J/ψ coming from B decays, also agrees better with the theoretical predictions after fragmentation has

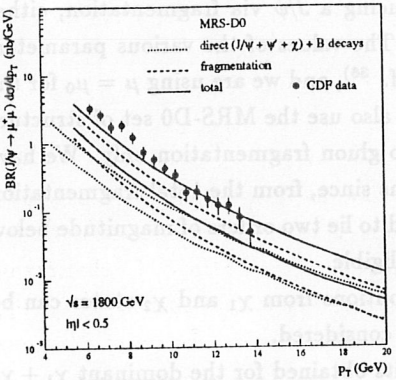

Figure 13: Theoretical prediction for J/ψ production at Tevatron, compared to experimental data from CDF [23]. Both the old result (dotted line) from ref. [25,35] (upper curve: $\mu = m_T/4$, $\Lambda = 275$ MeV; lower curve $\mu = m_T$, $\Lambda = 215$ MeV) and the new fragmentation (dashed line) contribution (upper curve: $\mu = 0.6\mu_0$, $\mu^g_{ini} = 4$ GeV; lower curve: $\mu = 2\mu_0$, $\mu^g_{ini} = 2$ GeV) are included.

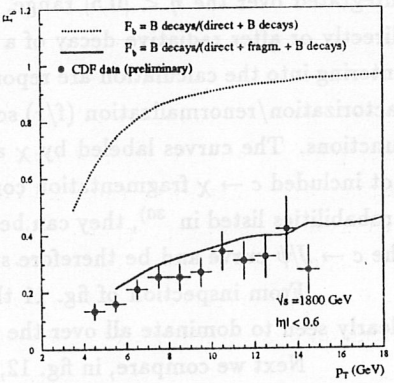

Figure 14: Fractional contribution to the J/ψ production cross section from B decays and prompt sources.

been taken into account, as shown in fig. 14.

Whereas the fragmentation mechanism discussed above seems to give a better description of the J/ψ production, the situation concerning the ψ' on the contrary is still far from our present understanding. Indeed the the production rate of prompt ψ' at the Tevatron is larger than the theoretical prediction at large p_T by about a factor of thirty. This large discrepancy clearly demands for a new mechanism dominating the production process. Indeed very recently new proposals have been put forward as, for example, the existence of higher P-wave or D-wave states which decay into the ψ', similarly to the χ states decaying into the J/ψ [39,40]. Also the existence of new metastable charmonium states or hybrid charmonium states [41], and, more recently, the contribution of colour octet states [42] which subsequently evolve non perturbatevely into a ψ' or J/ψ plus light hadrons, have been advocated as possible candidates for solving this ψ' anomaly. A more accurate analysis of ψ'

production data could certainly shade some light on the relative importance ot the above mentioned mechanisms in the production of S-wave states of heavy quarkonia.

To conclude, we have discussed the production of heavy quarks at large p_T ($p_T \gg m$) in hadronic collisions. In order to make the theoretical predictions more reliable, we have studied this problem in the framework of the perturbative fragmentation functions, which allow a NLO evaluation of the potentially large logarithms of the kind $\log(p_T/m)$, which are resummed to all orders. Our analysis for the b and c quarks leads to much more stable results with respect to changes of the factorization/renormalization scales compared to what is obtained in the $O(\alpha_s^3)$ calculation. Also the theoretical uncertainty related to different choices of PDF sets is reduced. Other possible sources of uncertainties, like the scale μ_0 of the initial state condition in the fragmentation functions evolutions, are negligible.

We have also considered the inclusive production of J/ψ in hadron collisions in the framework of fragmentation functions. We have shown explicitly that the production and successive radiative decays of the χ states plays a dominant role. The overall theoretical estimate, including the contribution from B decays, is nearly consistent with the experimental observations. The situation for ψ', on the contrary, clearly demands for new mechanisms of production which might explain the large discrepancy with the experimental observation.

I'm grateful to Matteo Cacciari for comments and his valuable help in preparing the written version of this talk.

References

1. E. L. Berger, these Proceedings.
2. P. Nason, S. Dawson and R.K. Ellis, Nucl. Phys. **B303** (1988) 607.
3. P. Nason, S. Dawson and R.K. Ellis, Nucl. Phys. **B327** (1989) 49.
4. W. Beenakker, H. Kuijf, W.L. van Neerven and J. Smith, Phys. Rev. **D40** (1989) 54.
5. W. Beenakker, W.L. van Neerven, R. Meng, G.A. Schuler and J. Smith, Nucl. Phys. **B351** (1991) 507.
6. M.L. Mangano, P. Nason and G. Ridolfi, Nucl. Phys. **B373** (1992) 295.
7. M Cacciari and M. Greco, Nucl. Phys. **B421** (1994) 530.
8. G. Altarelli, M. Diemoz, G. Martinelli and P. Nason, Nucl. Phys. **B308** (1988) 724.
9. E. Laenen, J. Smith and W.L. van Neerven, Phys. Lett. **B321** (1994) 254.
10. R.K. Ellis, Phys. Lett. **B259** (1991) 492.
11. F. Aversa, P. Chiappetta, M. Greco and J.Ph. Guillet, Nucl. Phys. **B327** (1989) 105.
12. See, e.g., J.C. Collins, D.E. Soper and G. Sterman, in *Perturbative QCD* (Singapore, World Scientific, 1989), p. 1.
13. B. Mele and P. Nason, Nucl. Phys. **B361** (1991) 626.
14. P.N. Harriman, A.D. Martin, W.J. Stirling and R.G. Roberts, Phys. Rev. **D42** (1990) 798.
15. J.G. Morfin and W.K. Tung, Zeit. Phys. **C52** (1991) 13.
16. J. Botts, J.G. Morfin, J.F. Owens, J. Qiu, W.K. Tung and H. Weerts, Phys. Lett. **B304** (1993) 159
17. J.C. Collins and W.K. Tung, Nucl. Phys. **B278** (1986) 934.

18. G. Curci, W. Furmanski and R. Petronzio, Nucl. Phys. **B175** (1980) 27
W. Furmanski and R. Petronzio, Phys. Lett. **B97** (1980) 437.

19. F. Abe *et al.* (CDF coll.), Phys. Rev. Lett. **68** (1992) 3403
S. Vejcik (CDF), presented at DPF Meet. Am. Phys. Soc., Batavia (1992), to appear in the Proceedings
B.T. Huffman (CDF), presented at DPF Meet. Am. Phys. Soc., Batavia (1992), FNAL-CONF-92/337-E (1992), to appear in the Proceedings
See also F. Abe *et al.* (CDF coll.), Phys. Rev. Lett. **71** (1993) 2396 and references therein.

20. C. Albajar *et al.* (UA1 coll.), Phys. Lett. **B213** (1988) 405; Phys. Lett. **B256** (1991) 121.

21. M. Cacciari, M. Greco and A. Tanzini, in preparation.

22. C. Albajar *et al.*, UA1 Coll., Phys. Lett. **B256** (1991) 112.

23. F. Abe *et al.*, CDF Coll., Phys. Rev. Lett. **69** (1992) 3704.

24. E.L. Berger and D. Jones, Phys. Rev. **D23** (1981) 1521, Phys. Lett. **B121** (1983) 61
R. Baier and R. Rückl, Z. Phys. **C19** (1983) 251
F. Halzen, F. Herzog, E.W.N. Glover and A.D. Martin, Phys. Rev. **D30** (1984) 700
E.W.N. Glover, A.D. Martin and W.J. Stirling, Z. Phys. **C38** (1988) 473
B. van Eijk and R. Kinnunen, Z. Phys. **C41** (1988) 489.

25. M.L. Mangano, Z. Phys. **C58** (1993) 651.

26. J.E. Huth and M.L. Mangano, Annu. Rev. Nucl. Part. Sci. **43** (1993) (585).

27. E. Braaten and T.C. Yuan, Phys. Rev. Lett. **71** (1993) 1673.

28. M.A. Doncheski, S. Fleming and M.L. Mangano, FERMILAB-CONF-93/348-T

29. E. Braaten, K. Cheung and T.C. Yuan, Phys. Rev. **D48** (1993) 4230.

30. Yu-Qi Chen, Phys. Rev. **D48** (1993) 5181, erratum Phys. Rev. **D50** (1994) 6013

31. T.C. Yuan, Phys. Rev. **D50** (1994) 3176

32. E. Braaten and T.C. Yuan, Phys. Rev. **D50** (1994) 3176

33. A.F. Falk *et al.*, Phys. Lett. **B312** (1993) 486.

34. S.D. Ellis, Z. Kunszt and D.E. Soper, Phys. Rev. Lett. **64** (1990) 2121.

35. M.L. Mangano, private communication.

36. M. Cacciari and M. Greco, Phys. Rev. Lett. **73** (1994) 1586.

37. E. Braaten, M.A. Doncheski, S. Fleming and M. Mangano, Phys. Lett. **B333** (1994) 548.

38. A. Zieminski, Proceedings of "Les Rencontres de Physique de la Vallée d'Aoste", La Thuile (1994), M. Greco ed., Editions Frontieres, 1994.

39. D.P. Roy and K. Sridhar, Phys. Lett. **B339** (1994) 141.

40. P. Cho, M.B. Wise and S. Trivedi, FERMILAB-PUB-94/256-T (hep-ph 9408352).

41. F.E. Close, Phys. Lett. **B342** (1995) 369.

42. E. Braaten and S. Fleming, NUHEP-TH-94-26.

SESSION VII

- I.I. Bigi
  The Expected, the Promised and the Conceivable - On CP Violation in Beauty and Charm Decays

- H. Albrecht
  Prospects for CP Measurements in HERA-B

Frascati Physics Series, Vol. III (1994)
HEAVY QUARKS AT FIXED TARGET
University of Virginia, October 7–10, 1994
(pp. 235–248)

THE EXPECTED, THE PROMISED AND THE CONCEIVABLE – ON CP VIOLATION IN BEAUTY AND CHARM DECAYS

I.I. Bigi
Dept. of Physics, Univ. of Notre Dame du Lac, Notre Dame, IN 46556, U.S.A.
e-mail address: BIGI@UNDHEP.HEP.ND.EDU

Abstract

The general CP phenomenology for beauty and charm decays is sketched and the KM expectations of large CP asymmetries in B decays are reviewed. I describe some observable signatures for the intervention of New Physics and list benchmarks defining the 'ultimate' measurements in beauty physics. I also stress the need for dedicated searches for CP asymmetries in D decays; attaining a sensitivity level of 10^{-3} could well reveal New Physics and thus lead to a new paradigm.

1 – Introduction

The three basic messages I want to convey in this talk are contained in the title:
• We can confidently *expect* large CP asymmetries to occur in B decays.
• I feel almost justified to *promise* that New Physics (NP) will reveal itself there.
• It is quite *conceivable* that CP asymmetries will become observable in charm decays – in particular if an intervention of NP will enhance their size above the levels expected within the KM ansatz.

The talk will be organized as follows: the general phenomenology is sketched in Sect. 2 and the KM expectations for B decays are stated in Sect. 3; signatures for NP are listed in Sect. 4; Sect. 5 contains the 'HERA-B menu' while the 'ultimate' measurements are defined in Sect. 6; after describing the most promising ways to search for CP violation in charm decays in Sect. 7, I give an outlook in Sect. 8.

2 – General Phenomenology of CP Violation

There are five different classes of CP asymmetries that can emerge in meson decays, and they fall into two groups.

The first group involves comparing partial rates. The decay rate for two CP conjugate channels as a function of proper time t can be written as

$$\Gamma(B[D] \to f;t) = e^{-\Gamma_{B[D]}t} G_f(t)\,, \quad \Gamma(\bar{B}[\bar{D}] \to \bar{f};t) = e^{-\Gamma_{B[D]}t} \bar{G}_{\bar{f}}(t) \tag{2.1}$$

If $\bar{G}_{\bar{f}}(t)/G_f \neq 1$ is observed, CP violation has been discovered. Three classes can be distinguished:

(a):

$$\frac{\bar{G}_{\bar{f}}(t)}{G_f(t)} \neq 1\,, \quad \frac{d}{dt}\left(\frac{\bar{G}_{\bar{f}}(t)}{G_f(t)}\right) \neq 0 \tag{2.2}$$

This represents 'CP violation involving $B^0 - \bar{B}^0[D^0 - \bar{D}^0]$ oscillations and it can manifest itself in non-leptonic decays: e.g., $B_d \to \psi K_S$ or $D^0 \to K^+K^-, \pi^+\pi^-$ [1].

(b):

$$\frac{\bar{G}_{\bar{f}}(t)}{G_f(t)} \neq 1\,, \quad \frac{d}{dt}\left(\frac{\bar{G}_{\bar{f}}(t)}{G_f(t)}\right) \equiv 0\,, \quad \frac{d}{dt}G_f(t) \neq 0 \tag{2.3}$$

It constitutes 'CP violation in $B^0 - \bar{B}^0[D^0 - \bar{D}^0]$ oscillations' which can most clearly be studied in semileptonic decays, in particular to 'wrong-sign' leptons: $B^0 = (b\bar{q}) \to l^+X$ or $D^0 \to l^-X$.

(c):

$$\frac{\bar{G}_{\bar{f}}(t)}{G_f(t)} \neq 1\,, \quad \frac{d}{dt}\left(\frac{\bar{G}_{\bar{f}}(t)}{G_f(t)}\right) \equiv 0\,, \quad \frac{d}{dt}G_f(t) \equiv 0 \tag{2.4}$$

This case is called 'direct' CP violation and it can also arise in charged meson and baryon decays: e.g., $B \to K\pi$, $D^{neut}K$ or $D \to K_S\pi$.

The second group involves observables other than a ratio of partial widths.

(d): CP violation can reveal itself in final-state distributions: there can be telling asymmetries in the Dalitz plot, or T odd correlations can arise.

(e): CP violation can be established also through the observation of a special transition rather than an asymmetry. Consider

$$e^+e^- \to B^0\bar{B}^0[D^0\bar{D}^0]|_{J^{CP}=1^{--}} \to f_1 f_2 \tag{2.5}$$

with f_1 and f_2 being CP eigenstates of the *same* CP parity. Reaction (2.5) can proceed only through CP violation since the initial and final state CP parities differ.

The prospects for observing such phenomena vary considerably from case to case: class (e) will presumably remain academic since its rate depends on the product of two small branching ratios like for $f_{1,2} = \psi K_S \to (l^+l^-)K_S$ or $D^+D^- \to (K^-\pi^+\pi^+)(K^+\pi^-\pi^-)$. Class (d) represents a very wide and promising field; some interesting theoretical studies have been made [2], but it is still too early to draw

Table 1:

Class	Advantages	Drawbacks
CP violation involving oscillations	• reliable theoretical predictions • large effects • striking experimental signature • access to all three angles of the KM triangle	• flavour tagging required • asymmetric B factory needed
direct CP violation	• self-tagging • can be done at a symmetric B factory	• less clean theoretical interpretation • smaller effects • less striking experimental signature • access to only one angle in the KM triangle

firm conclusions, and I will not pursue it any further here. As far as class (b) is concerned, existing predictions are not very precise, but it is very hard to see how CP asymmetries in semileptonic B^0 decays could exceed 0.1 %.

In the following I will focus on classes (a) and (c), which have complementary advantages and drawbacks, as sketched in Table 1.

3 – KM Expectations in B Decays

3.1 Generalities

Within the KM ansatz the CP asymmetries are described in terms of relative phases of various KM parameters. Weak universality imposes unitarity constraints on them that are expressed by triangle relations[3]:

$$0 = V^*(ud)V(ub)+V^*(cd)V(cb)+V^*(td)V(tb) \simeq V(ub)-\lambda V(cb)+V^*(td),\ \lambda \simeq \sin\theta_C \tag{3.1}$$

Since the three sides of this triangle are all $\sim \mathcal{O}(\lambda^3)$, its angles are naturally large, see Fig. 1.

This is in marked contrast to the situation in charm decays where the relevant triangle is given by

$$0 = V^*(ud)V(cd) + V^*(us)V(cs) + V^*(ub)V(cb) \simeq \mathcal{O}(\lambda) + \mathcal{O}(\lambda) + \mathcal{O}(\lambda^5) \tag{3.2}$$

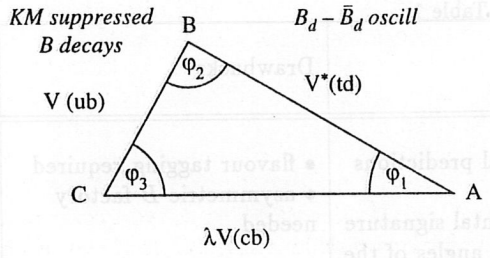

Figure 1: The KM triangle relevant for B transitions

which represents a very 'squashed' triangle with one angle necessarily tiny and the other two accessible only through highly suppressed transitions with an amplitude of relative strength $\mathcal{O}(\lambda^4) \sim 3 \cdot 10^{-3}$.

The foremost goal is of course to find CP violation. Yet one can define a more specific and detailed program of inquiry, namely to first determine and then probe the KM triangle with utmost sensitivity. For that purpose one aims at extracting the values of the KM parameters $|V(cb)|$, $|V(ub)|$ and $|V(td)|$ from various sets of data[4]. For these quantities determine the lengths of the three sides of the relevant KM triangle and thus allow to infer the values of the angles. Next one undertakes to measure the angles ϕ_1 and ϕ_2 (also known as β and α). If their measured values differed significantly from their infered values, one would have established the intervention of New Physics (NP). There is a clear prescription of how to measure these angles through CP asymmetries. Consider for simplicity only final states f that are CP self-conjugate; one then obtains

$$\Gamma(B^0[\bar{B}^0] \to f;t) = K_f[\bar{K}_f]e^{-\Gamma_B t}\left(1 - [+]Im\frac{q}{p}\bar{\rho}_f \cdot \sin\Delta m_B t\right), \; \bar{\rho}_f = \frac{T(\bar{B}^0 \to f)}{T(B^0 \to f)} \tag{3.3}$$

For $f = \psi K_S$ one finds that the asymmetry parameter can be expressed – to a high degree of accuracy – as a combination of KM parameters only: $(q/p) \cdot (T(\bar{B}^0 \to \psi K_S)/T(B^0 \to \psi K_S)) = (V^*(td)/V(td)) \cdot (V^*(cb)V(cs)/V(cb)V^*(cs))$; therefore

$$\Gamma(B_d[\bar{B}_d] \to \psi K_S;t) = K_1 e^{-\Gamma_B t}(1 - [+]\sin 2\phi_1 \sin\Delta m_B t) \tag{3.5}$$

Similarly

$$\Gamma(B_d[\bar{B}_d] \to \pi^+\pi^-;t) = K_2[\bar{K}_2]e^{-\Gamma_B t}(1 - [+]"\sin 2\phi_2" \sin\Delta m_B t) \tag{3.6}$$

As far as $B_d \to \pi^+\pi^-$ is concerned there arise two complications. On the one hand the quantity "$\sin 2\phi_2$" measured in $B_d \to \pi^+\pi^-$ is not identical to the genuine

KM parameter $\sin 2\phi_2$. The difference between the two can be ascribed to Cabibbo suppressed Penguin transitions $b \to d$ or to rescattering $B_d \to "D\bar{D}" \to \pi^+\pi^-$. While I do not expect this difference to be big, it exists and provides a limiting factor in the theoretical interpretation. This added complexity will typically (though not necessarily) also lead to direct CP violation in $B_d \to \pi^+\pi^-$ decays as allowed in eq. (3.6) through $K_2 \neq \bar{K}_2$. Measuring $BR(B_d \to \pi^0\pi^0)$ and $BR(B^- \to \pi^-\pi^0)$ will however enable us to extract $\sin 2\phi_2$ reliably from the CP asymmetry in $B_d \to \pi^+\pi^-$[5]. In addition to this theoretical complication there exists an experimental one as well: it is obviously important to have particle identification that can reliably distinguish $B \to K\pi$ and $B \to \pi\pi$ modes.

There is also some good news which I will only state: there exists a host of additional exclusive channels that can be employed here: $B_d \to \psi K_L$, $\psi' K_S$, $\psi' K_L$, $\psi(K_S\pi^0)_{K^*}$, $D^{(*)}\bar{D}^{(*)}$ etc. for $\sin 2\phi_1$ and $B_d \to \pi\rho$, $\pi\omega$, πa_1 etc. for $\sin 2\phi_2$.

3.2 – Determining the KM Triangle

The baseline of the triangle can conveniently be normalized to unity without affecting the angles. The other two sides are then given by $V(ub)/V(cb)$ and $V^*(td)/\lambda V(cb)$; those ratios are more directly observable than $V(ub)$ and $V(td)$ themselves.

Our present information on the normalized KM triangle is as follows:

- Present data on charmless semileptonic B decays *suggest* $|V(ub)/V(cb)| \simeq 0.08 \pm 0.03$. I am somewhat skeptical that the stated error properly reflects the present experimental and theoretical uncertainties; yet I am confident that the situation will be clarified in the next few years due to considerably more sensitive data and a judicious application of heavy quark expansions[4].
- The quantity $\sin 2\phi_1$ controling the CP asymmetry in $B_d \to \psi K_S$ can in principle be extracted from the observed value of $\epsilon_K/\Delta m(B_d)$ with little sensitivity to the (heavy) top quark mass. Yet this procedure at present suffers from grave theoretical uncertainties in the size of the hadronic matrix element:

$$\frac{\epsilon_K}{\Delta m(B_d)} \propto \sin 2\phi_1 \simeq 0.42 \cdot UNC \qquad (3.7a)$$

$$UNC \simeq \left(\frac{0.04}{|V(cb)|}\right)^2 \left(\frac{0.72}{x_d}\right) \left(\frac{\eta_{QCD}^{(B)}}{0.55}\right) \left(\frac{0.62}{\eta_{QCD}^{(K)}}\right) \left(\frac{2B_B}{3B_K}\right) \left(\frac{f_B}{160\ \text{MeV}}\right)^2 \qquad (3.7b)$$

Nevertheless two things should be noted here:

– $\sin 2\phi_1$ is *large* for reasonable values of f_B; for $f_B = 220$ MeV one actually obtains $\sin 2\phi_1 \simeq 0.8$!

– Once $\sin 2\phi_1$ has been measured, one can infer the value required for f_B from eqs.(3.7) with good accuracy.

The present information on the KM triangle is summarized in Fig. 2: the top of the triangle has to lie in the shaded area.

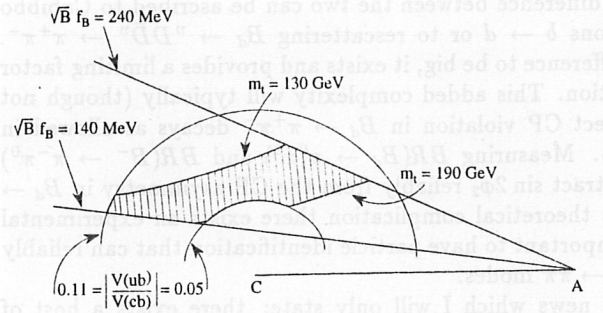

Figure 2: Shape of the KM triangle inferred from present phenomenology

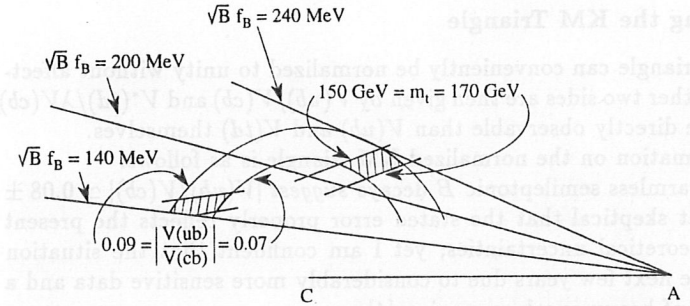

Figure 3: Shape of the KM triangle after future measurements of $V(ub)/V(cb)$ and m_t

I anticipate that over the next few years $|V(ub)/V(cb)|$ will be extracted with a realistic error of 10% or less. It is hoped that the top quark mass will be known to within ± 10 GeV. The resulting KM landscape is illustrated in Fig. 3. The allowed area for the top of the triangle is now greatly reduced, and consists of two disjoint subdomains; one requires $f_B \simeq 210 \div 240$ MeV and the other $f_B \simeq 140 \div 170$ MeV.

Knowing $|V(td)/V(cb)|$ and thus the third side would provide another powerful constraint; yet that information will not come easily. There are three avenues towards this goal: (i) It has been suggested [6] to extract it from the observed ratio $R_\gamma \equiv BR(B \to \gamma\rho/\omega)/BR(B \to \gamma K^*)$. This is based on the assumption that both radiative transitions are driven mainly by a Penguin operator reflecting short distance dynamics; in that case one would have $R_\gamma = |V(td)/V(ts)|^2 \times SU(3)$ breaking. Unfortunately it has not been established that in particular the mode $B \to \gamma\rho/\omega$ is Penguin dominated. One can actually advance various arguments why long distance dynamics make quite significant contributions that do not depend on $V(td)$. I am skeptical that such contributions can reliably be computed from first

principles in the near future; on the other hand one can gauge their weight once $BR(D \to \gamma K^*, \gamma\rho/\omega)$ and $BR(B \to \gamma D^*)$ have been measured since these modes cannot be driven by Penguin operators[7]. (ii) Determining the $B_s - \bar{B}_s$ oscillation rate would allow a fairly reliable extraction:

$$\frac{\Delta m(B_d)}{\Delta m(B_s)} \simeq \frac{Bf_B^2|_{B_d}}{Bf_B^2|_{B_s}} \cdot \frac{|V(td)|^2}{|V(ts)|^2} \tag{3.8}$$

where it is understood that the *ratio* of the B_d and B_s matrix elements can be calculated more reliably than the matrix elements themselves. (iii) My own favourite is to employ a measurement of $BR(K^+ \to \pi^+\nu\bar{\nu})$ once that becomes available. For the width of that rare transition can reliably be expressed as a function of m_{top} and $|V(td)|$ with the remaining uncertainty mainly due to the size of m_{charm} [8, 9].

4 – Signatures for New Physics

The best way in which searches for NP are to be conducted will depend on how much is known at the time about which KM parameter. I will describe here two typical scenarios to illustrate the basic features on which any search would be based.

4.1 Typical Search Scenarios

(1) With $|V(ub)/V(cb)|$ and $|V(td)/V(cb)|$ known the KM triangle has been determined. Actually it would already have been overconstrained without data on CP violation in B decays: for with eqs.(3.7) one can infer the necessary size of f_B from the resulting angle ϕ_1. With it and the measured top mass one computes $\Delta m(B_d)$ and confronts it with the experimental value. Measuring the CP asymmetry in $B_d \to \psi K_S$ then yields a second sensitive constraint: if it is found to differ from $\sin 2\phi_1$ as infered from the triangle, one has established the intervention of NP.

(2) If $V(td)/V(cb)$ were remain to be largely undetermined, one had to use the measured CP asymmetry in $B_d \to \psi K_S$ to fix $\sin 2\phi_1$ and thus the triangle. As before it would then actually have been overdetermined: inferring the size of f_B from $\sin 2\phi_1$ one can compute $\Delta m(B_d)$ and compare it with the data. Measuring $\sin 2\phi_2$ to obtain a second constraint would then become even more mandatory.

4.2 The ϕ_3 (or γ) Saga

The third angle ϕ_3 can be measured via CP violation involving $B^0 - \bar{B}^0$ oscillations or via direct CP violation. The first method searches for a CP asymmetry in, e.g., $B_s \to K_S\rho^0$ decays. However it does not strike me as particularly promising. For by then the other two angles ϕ_1 and ϕ_2 will have been determined with a higher accuracy than can realistically be expected for ϕ_3 measured in this way; ϕ_3 will then be known as $\pi - \phi_1 - \phi_2$ – unless there is NP lurking below the surface! Yet then

it makes more sense to analyze a channel with (a) a higher branching ratio, (b) a more striking experimental signature and (c) a cleaner theoretical interpretation. The mode $B_s \to \psi\phi$ (or $B_s \to \psi\eta$) fits this bill[10]. For the KM ansatz predicts a small asymmetry here

$$Im\frac{q}{p}\bar{\rho}(B_s \to \psi\phi)|_{KM} \sim 2\% \tag{4.1}$$

as is easily understood: for on the leading KM level only quarks of the second and third family contribute in the transitions $B_s \to \psi\phi$ and $B_s \to \bar{B}_s \to \psi\phi$; a CP asymmetry then has to be Cabibbo suppressed. New Physics on the other hand could quite naturally produce an asymmetry well in excess of 10%! A note of caution: if B_s mesons oscillated too rapidly, the asymmetry in $B_s \to \psi\phi$ would get washed out – yet this would also happen in $B_s \to K_S\rho^0$.

The angle ϕ_3 can be measured also via a direct CP asymmetry in $B^\pm \to D_{neut}K^\pm$ modes[11]. This represents a sounder approach, in particular since it can be undertaken already at a *symmetric* B factory. Furthermore it is at least intellectually 'cute'. For it makes use of the fact that for neutral mesons flavour eigenstates and mass eigenstates are in general distinct (although they can be expressed as linear combinations of each other) with the former defined by the flavour-specific decays $D^0 \to K^-\pi^+$ and $\bar{D}^0 \to K^+\pi^-$ [1] and the latter by decays into CP eigenstates: $D_1 \to K_S\pi^0$, $D_2 \to K_L\pi^0$, K^+K^-. A comparison of $B^- \to D_1K^-[D_2K^-]$ with $B^+ \to D_1K^+[D_2K^+]$ can then reveal a CP asymmetry for these channels reflecting the coherent interplay of $B^\pm \to D^0K^\pm$ and $B^\pm \to \bar{D}^0K^\pm$ transitions. It should be noted as a point of general interest that the quantum mechanical realization of particle-antiparticle identity for B^0, D^0 and K^0 mesons plays an essential role in CP asymmetries of B decays: (i) Applied to B^0 states it constitutes a pre-requisite for $B^0 - \bar{B}^0$ oscillations. (ii) It leads to distinct states K_S and K_L to provide the second pre-requisite for the observability of a CP asymmetry in $B_d \to \psi K_S$. (iii) Applied to D^0 mesons it is essential for the emergence of direct CP violation in $B_d \to DK$ decays, as dicussed above.

The latter is proportional to $\sin\phi_3$ [2]; it also depends on the phaseshift $\Delta\phi_{str}$. Yet it is a gratifying feature [12] of these reactions that they allow the experimental isolation of $\sin\phi_3$ from the hadronic matrix elements. Due to CPT invariance one has four independant amplitudes, namely for $B^- \to D^0K^-$, $B^- \to \bar{D}^0K^-$, $B^- \to D_{1,2}K^-$ and $B^+ \to D_{1,2}K^+$. Measuring them allows one to extract $\sin\phi_3$, $\Delta\phi_{str}$, $|T(B^- \to D^0K^-)|$ and $|T(B^- \to \bar{D}^0K^-)|$ (up to a discrete ambiguity)!

4.3 New Physics Scenarios

One can easily give explicit dynamical scenarios of NP that would have an observable impact on the CP phenomenology in B decays.

[1] Due to doubly Cabibbo suppressed decays these channels do not provide a perfect filter, yet one of sufficient quality.

[2] It is also amusing to note that $\sin\phi_3 = 1$, $\sin 2\phi_3 = 0$ for $\phi_3 = 90^\circ$ as implied by the 'Stech' matrix.

As usual, the Minimal Supersymmetric Standard Model (MSSM) plays the role of the standard extension of the Standard Model. Since it does not introduce any appreciable new phase, there is still *no* sizeable CP asymmetry in $B_s \to \psi\phi$. Yet MSSM can have an indirect impact [13]. For it can provide a significant contribution to $\Delta m(B_d)$ and $\Delta m(B_s)$, though not to their ratio. With $\Delta m(B_d)/\Delta m(B_s)$ and thus $|V(td)/V(ts)|$ measured in addition to $|V(ub)/V(cb)|$ one would observe the following in the MSSM scenario: the angles ϕ_1 and ϕ_2 as infered from the KM trigonometry would agree with the observed CP asymmetries in $B_d \to \psi K_S$ and $B_d \to \pi^+\pi^-$; yet with the value infered for f_B from $\sin 2\phi_1$ one would fail to reproduce $\Delta m(B_d)$! The discrepancy would be due to SUSY contributions.

A *non-minimal* implementation of SUSY on the other hand would open the floodgates for additional CP phases[13] – as would horizontal interactions etc. etc. In general NP is most likely to make its presence felt first in the highly forbidden $\Delta B = 2$ transitions driving $B^0 - \bar{B}^0$ oscillations. In that case it would affect all B_d decays in a uniform manner; likewise for B_s decays. It would thus represent a dynamical realization of the 'Superweak Scenario'.

5 – The HERA-B Menu

Contrary to widely held beliefs good food can be found at DESY. I am actually referring to food for the mind that is being offered on the HERA-B menu. It consists of three main courses:
(i) $B_s - \bar{B}_s$ oscillations,
(ii) $B_d \to \psi K_S$ vs. $\bar{B}_d \to \psi K_S$,
(iii) $B_s \to \psi\phi$ vs. $\bar{B}_s \to \psi\phi$,
and one side dish:
(iv) $\tau(B_s \to l\nu D_s^{(*)})$ vs. $\tau(B_s \to \psi\phi)$.

Observing a positive signal in all three cases (i) - (iii) would represent a 'Beyond your wildest dreams' scenario: as discussed before, the results from (i) would yield the final element for the KM triangle together with one constraint from $\Delta m(B_d)$; course (ii) would provide a second constraint. Taken together (i) and (ii) represent probes for NP in $\Delta m(B^0)$ and $\mathrm{Im}\Delta m(B_d)$. Course (iii) constitutes a clean and direct probe for NP in $\mathrm{Im}\Delta m(B_s)$. Concerning the side dish (iv): $B_s - \bar{B}_s$ oscillations generate two states differing also in their lifetimes: $B_s^{(short)}$ and $B_s^{(long)}$. The $B_s^{(short)}$ lifetime reveals itself, to a good approximation, in $B_s \to \psi\phi$, whereas the semileptonic channels $B_s \to l\nu D_s^{(*)}$ reflect the lifetime averaged over $B_s^{(short)}$ and $B_s^{(long)}$. A state of the art calculation yields [14]

$$\frac{\tau(B_s \to l\nu D_s^{(*)}) - \tau(B_s \to \psi\phi)}{\tau(B_s \to l\nu D_s^{(*)})} \simeq 0.1 \cdot \left(\frac{f_{B_s}}{200\ \mathrm{MeV}}\right)^2 \qquad (5.1)$$

Such a small difference in lifetimes would escape detection. Yet it is conceivable that the real difference is considerably larger since the computation yielding eq.(5.1) is

Table 2: Possible scenarios for the KM matrix for $m_{top} = 180$ GeV.

	A	B	C	D	E	I	II	III
$\|V(ub)/V(cb)\|$	0.06	0.062	0.068	0.059	0.089	0.046	0.059	0.071
x_s/x_d	25	25	22	26	35			
$\sin 2\phi_1$	0.52	0.54	0.58	0.51	0.71	0.39	0.49	0.59
$\sin 2\phi_2$	-0.15	-0.11	0.30	-0.40	-0.62	-0.32	-0.46	-0.14
$\sin 2\phi_3$	0.65	0.71	0.30	0.81	0.99	0.66	0.84	0.70
$\sin \phi_3$	0.94	0.94	0.99	0.89	0.75	0.93	0.88	0.93

not gold-plated. Searching for the lifetime difference in $B_s^{(short)}$ vs. $B_s^{(long)}$ thus represents a probe not for NP, but of our computational control over hadronization effects.

6 – The Ultimate Challenge in B Physics

There is good reason for the hope that the asymmetric B factories at KEK and SLAC will establish CP violation in B decays. Nevertheless it is unlikely that they will provide also the ultimate measurements. Those are defined by the following considerations:

(i) Some of the theoretical predictions – like the asymmetry parameter in $B_d \to \psi K_S$ being $\sin 2\phi_1$ – enjoy a high parametric accuracy. Furthermore there exists the expectation that an increasingly detailed database coupled with refined theoretical tools will allow us to translate this parametric accuracy into a numerical one of a few per cent[4]. This opens up the possibility to search for NP contributing as little as 10% in amplitude.

(ii) It is quite possible that no CP violation were found in B decays, with an upper bound of, say, a very few per cent. In that case we would have established that $K_L \to \pi\pi$ transitions are predominantly driven by a source (or sources) other than the KM mechanism, i.e NP!

(iii) Even finding the CP phenomenology in B decays to be fully consistent with the KM framework could provide us with seeds of more profound knowledge: analyses of SUSY GUT scenarios lead to an apparently rather limited set of allowed KM matrices. Prominent examples [15, 16] are listed in Table 2 for $m_{top} = 180$ GeV in a way that is convenient for my discussion, where I have assumed $[B_s f^2(B_s)]/[B_d f^2(B_d)] = 1.1$ to translate $|V(ts)/V(td)|^2$ into x_s/x_d. The symbols $A-E$ and $I-III$ refer to different classes of mass matrices analysed in ref. [15] and [16]. The details are not important here [3], and I anticipate considerable theoretical evolution to take place over the next few years; but I want to use these numbers to illustrate important benchmarks for the ultimate measurements:

[3] It takes, of course, the trained eye of a theorist to discern the simple pattern underlying these values for the KM parameters.

- $B_s - \bar{B}_s$ oscillations might be extremely rapid!
- The business at hand remains unfinished in an essential way until also $\sin 2\phi_2$ has been measured with good accuracy.
- To differentiate completely among these scenarios requires the experimental uncertainties to lie below a few per cent.

Obviously only dedicated experiments performed at the LHC have the statistical muscle to achieve such goals. The question is: can they develop the systematic brain that is up to this task?

7 – CP Violation in Charm Decays

It has been stated quite often that without NP $D^0 - \bar{D}^0$ oscillations proceed very slowly and CP asymmetries in D decays are small. Yet: How small is small? This has to be addressed on a case-by-case basis.

7.1 CP Violation Involving $D^0 - \bar{D}^0$ Oscillations

The rate for D^0 decays into CP eigenstates like K^+K^- or $\pi^+\pi^-$ as a function of proper time t is given by

$$\Gamma(D^0 \to f;t) \propto e^{-\Gamma_D t}\left(1 + \sin\Delta m_D t\, Im\frac{q}{p}\bar{\rho}(D \to f)\right) \simeq$$

$$\simeq e^{-\Gamma_D t}\left(1 + \frac{\Delta m_D}{\Gamma_D}\frac{t}{\tau_D} Im\frac{q}{p}\bar{\rho}(D \to f)\right) \qquad (7.1)$$

In the Standard Model one expects $\Delta m_D/\Gamma_D \sim 0.01$ and $Im\bar{\rho}(D \to f) \sim \mathcal{O}(\lambda^4) \leq 0.01$; i.e. such a CP asymmetry will not exceed the 10^{-4} level, and it is so tiny since it represents the product of two small effects, namely $D^0 - \bar{D}^0$ oscillations and CP violation.

7.2 Direct CP Violation

Direct CP violation can become observable only if two different amplitudes contribute coherently to a certain decay. This can happen for once Cabibbo suppressed modes, but neither for Cabibbo allowed nor twice forbidden channels. Rough estimates tell us that direct CP asymmetries can be as 'large' as $\mathcal{O}(\lambda^4) \sim \mathcal{O}(10^{-3})$ in $D \to [S = 0]$ and $D_s \to [S = +1]$ channels. It will be possible to refine these predictions in the future through 'theoretical engineering' [17], i.e. one matches theoretical predictions for two-body modes against a host of well-measured branching ratios to extract the size of transition amplitudes (including absorption) and strong phase shifts. Present data limit direct CP asymmetries to roughly the 10% level, as shown in Table 3.

Table 3: Present bounds on CP asymmetries in D decays

Decay mode	Measured asymmetry	90% C.L. limit
$D^0 \to K^+K^-$	0.024 ± 0.084 [18]	$-11\% < A_{CP} < 16\%$
	0.071 ± 0.065 [19]	$-3.6\% < A_{CP} < 17.8\%$
$D^+ \to K^-K^+\pi^+$	-0.031 ± 0.068 [18]	$-14\% < A_{CP} < 8.1\%$
$D^+ \to K^{*0}K^+$	-0.12 ± 0.13 [18]	$-33\% < A_{CP} < 9.4\%$
$D^+ \to \phi\pi^+$	0.066 ± 0.086 [18]	$-7.5\% < A_{CP} < 21\%$
$D^0 \to K_S\phi$	-0.005 ± 0.067 [19]	$-11.5\% < A_{CP} < 10.5\%$
$D^0 \to K_S\pi^0$	-0.011 ± 0.030 [19]	$-6\% < A_{CP} < 3.8\%$

7.3 Possible Impact of NP

The intervention of NP could have a two-fold impact on CP violation involving $D^0 - \bar{D}^0$ oscillations: it could quite conceivably increase $\Delta m_D/\Gamma_D$ to around 0.1, its present upper bound; secondly, it could generate $Im(D^0 \to K^+K^-, \pi^+\pi^-) \sim 0.1$. Taken together, it would produce a CP asymmetry $\sim \mathcal{O}(1\%)$ in reaction (7.1).

A new element overlooked so far emerges for direct CP asymmetries in $D \to K_S + \pi's$ transitions[20]. I will describe it here specifically for $D^\pm \to K_S\pi^\pm$ decays. There are two different amplitudes contributing to this mode, namely the Cabibbo allowed channel $D^+ \to \bar{K}^0\pi^+$ and the doubly Cabibbo suppressed one (DCSD) $D^+ \to K^0\pi^+$:

$$\Gamma(D^+ \to K_S\pi^+) \simeq \frac{1}{2}\Gamma(D^+ \to \bar{K}^0\pi^+)\left(1 - 2Re\frac{T(D^+ \to K^0\pi^+)}{T(D^+ \to \bar{K}^0\pi^+)}\right) \tag{7.2}$$

Four consequences arise from the coherent contribution of the DCSD amplitude:
- $\Gamma(D^+ \to K_S\pi^+) \neq \Gamma(D^+ \to K_L\pi^+)$ even ignoring CP violation in the $K^0 - \bar{K}^0$ system.
- The difference is linear in the DCSD amplitude and thus of order $2\tan^2\theta_C = 0.1$.
- With the isospin structure differing for $D^+ \to \bar{K}^0\pi^+$ and $D^+ \to K^0\pi^+$ one can expect different strong phase shifts to occur in the two amplitudes. Those can actually be determined experimentally. Thus a CP asymmetry can emerge:

$$\Gamma(D^+ \to K_S\pi^+) \neq \Gamma(D^- \to K_S\pi^-) \tag{7.3}$$

- An asymmetry of equal size, but opposite sign occurs for the final state where K_L replaces K_S:

$$\Gamma(D^+ \to K_L\pi^+) - \Gamma(D^- \to K_L\pi^-) = -[\Gamma(D^+ \to K_S\pi^+) - \Gamma(D^- \to K_S\pi^-)] \tag{7.4}$$

Such an asymmetry arises already within the KM ansatz. Yet it is tiny, namely $\leq 10^{-4}$, again reflecting the product of two small quantities $\sim \lambda^2 \cdot \lambda^4$. Yet if NP contributes a mere 10% to the DCSD amplitude, one would have an asymmetry of around 1%!

8 – Outlook

It is quite evident that the insights to be gained from a comprehensive and dedicated study of CP violation

- are of fundamental importance;
- cannot be obtained any other way, and
- cannot become obsolete.

The phenomenon of CP violation can be put also into a wider context. There are two central mysteries in the Standard model. One concerns the origin of masses: while the generation of mass can be implemented by the Higgs mechanism in a gauge invariant way, there is no direct experimental evidence for it; furthermore it is also quite unsatisfactory from a theoretical point of view. The second central mystery – not unrelated to the first one – concerns the family replication, the pattern of the fermion masses and the origin of CP non-invariance. There we are even more at a loss for a real understanding; we can only state that since there are three families, CP violation can be implemented via the KM mechanism. In short our answer to the question of why there are families and why there is CP violation is – 'why not?'

There are certainly enough mysteries to ponder. It would be wonderful if they could be solved by pure thinking – and preferably all of them in one fell swoop! Indeed, it would be miraculous. For the history of our discipline teaches us that progress occurs through a succession of paradigms with each new one encompassing the previous one and the shifts most of the time being caused by unexpected empirical input.

It is actually the motivation for the LHC to gain new insights into the problem of mass generation by directly probing physics at the 1 TeV scale. Likewise a thorough analysis of CP violation in heavy flavour decays will provide new perspectives onto the family problem in general and CP violation in particular. I for myself have little doubt that these studies will lead to a new paradigm – in particular if we commit ourselves to a truly comprehensive analysis, i.e. one that includes detailed studies of the charm system (and the τ lepton and top quark for that matter).

Acknowledgements This work was supported by the National Science Foundation under grant number PHY 92-13313. I enjoyed the format and the efficient running of the meeting created by the organizers. It is also always a pleasure to visit the house that 'Old Tom' built!

References

[1] A. Carter, A. Sanda, Phys. Rev. **D23** (1981) 1567; I.I. Bigi, A. Sanda, Nucl. Phys. **B193** (1981) 85; I.I. Bigi, V. Khoze, N.G. Uraltsev, A. Sanda, in: "CP Violation", C. Jarlskog (ed.), World Scientific, Singapore, 1989, p.175.

[2] see, e.g.: G. Kramer, W. Palmer, H. Simma, Nucl. Phys. **B428** (1994) 77.

[3] For a general introduction, see the article by C. Jarlskog, in: "CP Violation", C. Jarlskog (ed.), World Scientific, Singapore, 1989.

[4] I.I. Bigi, Invited Talk given at the International Workshop on B Physics, Nagoya, Japan, Oct. 26-28, 1994, preprint UND-HEP-94BIG12.

[5] M. Gronau, Phys. Lett. **B265** (1991) 389.

[6] A. Ali et al., preprint CERN-TH.7118/93, to appear in Z. Phys. C.

[7] I.I. Bigi, T. Mannel, in preparation.

[8] A. Buras et al., Phys. Rev. **D50** (1994) 3433.

[9] I.I. Bigi, F. Gabbiani, Nucl.Phys. **B367** (1991) 3.

[10] I. I. Bigi, A. I. Sanda, Nucl. Phys. **B193** (1981) 85; Phys. Rev. **D29** (1984) 1393; Nucl. Phys. **B281** (1987) 41.

[11] I. I. Bigi, A. I. Sanda, Phys. Lett. **B211** (1988) 213; Nucl. Phys.**B281** (1987)41.

[12] M. Gronau, D. Wyler, Phys. Lett. **B265** (1991) 172.

[13] I.I.Bigi, F. Gabbiani, Nucl.Phys. **B352** (1991) 309.

[14] M. Voloshin, M. Shifman, N. Uraltsev, V. Khoze, Sov. J. Nucl. Phys. **46** (1987) 112; I. Bigi, B. Blok, M. Shifman, N. Uraltsev, A. Vainshtein, in: 'B Decays', 2nd edition, S. Stone (ed.), World Scientific, pg. 132.

[15] P. Ramond, R. G. Roberts, G. G. Ross, Nucl. Phys. **B406** (1993) 19.

[16] G. Anderson et al., Phys. Rev. **D49** (1994) 3660.

[17] For a first attempt see: F. Buccella et al., Phys. Lett. **B302** (1993) 319.

[18] P.L. Frabetti et al., preprint Fermilab-Pub-071-E (1994)

[19] M.S. Alam et al., preprint CLEO CONF 94-14 (1994)

[20] I.I. Bigi, H. Yamamoto, preprint UND-HEP-94-BIG09.

PROSPECTS FOR CP MEASUREMENTS IN HERA-B

H. Albrecht

DESY, F-15, 22603, Hamburg, Germany

No written contribution received

SESSION VIII

- R. Jesik
  B Cross Section Results from E672/E706

- M. Dameri
  A Measurement of the Total Beauty Cross Section in 350 GeV/c π^- Cu Interactions

- D. Kaplan
  B Cross Section from E789

Frascati Physics Series, Vol. III (1994)
HEAVY QUARKS AT FIXED TARGET
University of Virginia, October 7–10, 1994
(pp. 253–262)

B CROSS SECTION RESULTS FROM FERMILAB E672/E706.

RICHARD JESIK*
University of Illinois at Chicago, Chicago, IL 60607

ABSTRACT

We report on a sample of twelve thousand reconstructed $J/\psi \to \mu^+\mu^-$ events produced in π^--nucleon collisions at 515 GeV/c. Bottom-quark states are identified by J/ψs originating from secondary vertices. Based upon 8 signal events in which the J/ψ vertex occurs in an air-gap region, we obtain an inclusive bottom cross section of $(75 \pm 31 \pm 26)$ nb/nucleon. This result is compared to recent QCD predictions. We have also observed several events in the exclusive decay modes $B^\pm \to J/\psi + K^\pm$ and $B^0 \to J/\psi + K^{0*}$

1 – Introduction

Next-to-leading-order calculations for the production of heavy quarks have become available during the past few years [1]. Recent collider data have shown that these predictions underestimate bottom production [2]. The calculations require the convolution of hard-scattering cross sections with parton distribution functions, and uncertainties result from the choice of gluon distribution functions, scale factors, and b-quark mass. Calculations by Berger [3] and by Mangano, Nason, and Ridolfi (MNR) [4] also provide predictions at fixed-target energies. Consequently, our measurement of the bottom cross section for 515 GeV/c incident pions provides another opportunity to test these calculations.

In this paper, we report on a measurement of the cross section for $\pi^- + \mathrm{Be} \to b + X$, with $b \to J/\psi + X$ and $J/\psi \to \mu^+\mu^-$. These events are uniquely tagged by a J/ψ emerging from a secondary vertex. Although the branching ratio into J/ψ

*Representing the E672 and E706 collaborations. Work supported by the NSF and DOE.

is small (1.3%) [5], this decay is advantageous since the resulting dimuons provide a clean trigger and signal. A significant background to secondary-vertex J/ψs from b-decays is, however, produced by events in which a high-momentum particle from the primary collision interacts further downstream in the target and produces a J/ψ (secondary interactions).

2 – Experiment E672/E706

The experiment was carried out in the Fermilab Meson West beamline using a large-aperture, open-geometry spectrometer with the capability of studying high-mass muon pairs. The muon detector, located 20 m downstream of the target, consisted of two muon PWC stations, a beam dump, a toroid magnet with an average p_T impulse of 1.3 GeV/c, four more muon PWC stations separated by iron and concrete shielding, and two muon hodoscopes [6]. The upstream part of the spectrometer consisted of 16-planes of silicon-strip detectors (SSDs), a dipole magnet with a p_T impulse of 0.45 GeV/c, 16 planes of PWCs and 16 planes of straw drift tubes, a liquid-argon calorimeter with electromagnetic and hadronic sections, and a forward calorimeter [7]. Dimuon pretriggers required coincidences between interaction counter and muon hodoscope signals. A fast (10 μs) processor was used to trigger on the effective mass of track combinations in the muon PWCs. Data were collected during the 1990 Fermilab fixed-target run with a 515 GeV/c π^- beam incident on beryllium and copper targets. Approximately 10^7 dimuon triggers were recorded (corresponding to a luminosity of 8 pb^{-1} per nucleon), yielding 10^6 events with a reconstructed dimuon combination originating from the target region.

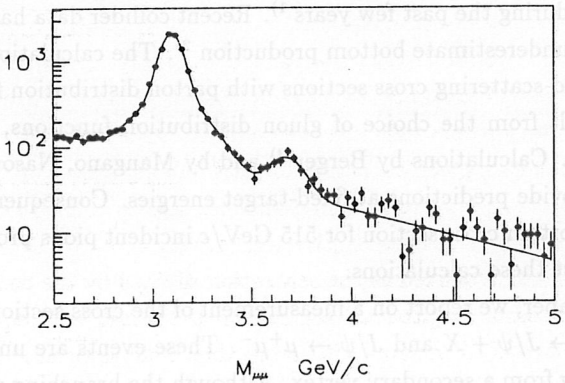

Figure 1: Opposite-sign dimuon invariant mass.

A fit was performed to link muon tracks through the entire detector. This fit included multiple-scattering considerations and a consistency requirement for the track momentum as measured via the dipole magnet and by the toroid. Only events with at least two fully-linked muons were kept. The remaining segments in the SSDs and upstream PWCs were used to find the hadronic tracks and event vertices. Figure 1 shows the reconstructed opposite-sign dimuon invariant-mass distribution in the J/ψ region. A fit to this data yields $12,640 \pm 50$ J/ψs with a mass resolution of 68 MeV/c^2, and 387 ± 79 $\psi(2S)$s. The measured J/ψ mass is (3.097 ± 0.001) GeV/c^2, and that of the $\psi(2S)$ is (3.67 ± 0.01) GeV/c^2.

3 – J/ψs from secondary vertices

To increase the efficiency and precision for finding a secondary vertex, the origin of the J/ψ was found by a muon-oriented vertex refitting procedure. Opposite-sign muon pairs in the reconstructed mass range 2.85 GeV/c^2 $< M_{\mu\mu} <$ 3.35 GeV/c^2 with consistent intersections in the x-z and y-z planes were fit with simultaneous vertex and J/ψ mass constraints. The resulting vertex served as a seed for an iterative vertex-fitting procedure which associated other tracks to this vertex. Only SSD-PWC linked tracks with transverse impact parameter within 1.5 standard deviations of the J/ψ vertex seed position were used in the fit. This procedure increased the secondary J/ψ vertex finding efficiency by 26% over the initial vertex finding. The average vertex resolution was 14 μm and 350 μm in the transverse and longitudinal directions, respectively. Figure 2 shows the difference, in the longitudinal direction, between the reconstructed primary and J/ψ vertices. The shaded area represents the expected vertex resolution for direct J/ψ production. As is shown, most of our J/ψs are produced in the primary interaction, there is, however, a clear excess of events in which the J/ψ vertex is well downstream of the primary. This signal is not, unfortunately, all due to b-decays; secondary interactions are responsible for a significant number of these events. Several cuts were applied to clean this sample. Only events with at least three fully reconstructed tracks from the primary were kept, yielding 631 events. Fiducial volume cuts for both primary and secondary vertices passed 577 events. A significance greater than 3 was required for both the longitudinal and transverse separation between the primary and secondary vertices, with significance defined as the separation divided by the combined vertex uncertainty. An absolute longitudinal separation of 2.5 mm was required, leaving 121 events. Secondary J/ψ vertices with more than four associated hadrons were discarded to reduce the background from secondary interactions; 73 events passed this cut. The primary- and secondary-vertex z-position distributions for these events are shown in Figs. 3b and 3c, respectively.

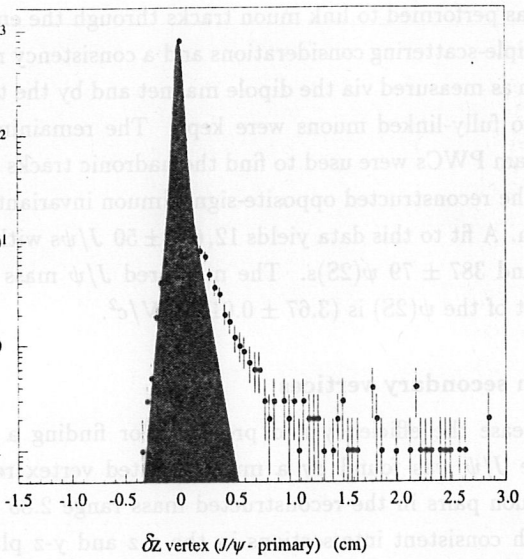

Figure 2: Differences between reconstructed primary and J/ψ vertices in the longitudinal (z) direction.

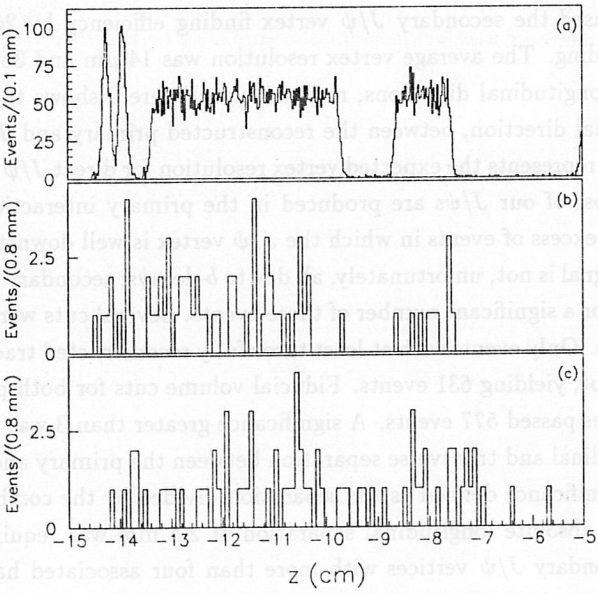

Figure 3: Vertex z coordinate distributions: (a) all refit J/ψs; (b) primary vertex for the 73 events passing the cuts; (c) secondary J/ψ vertex for these events.

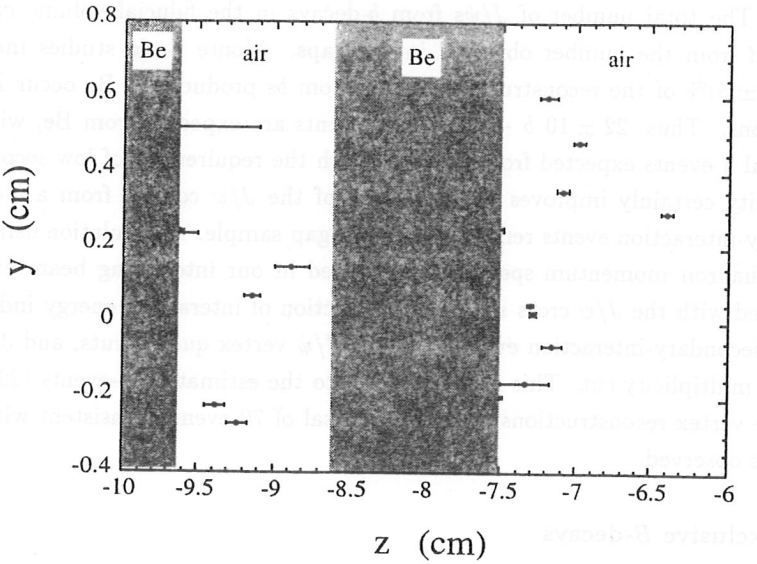

Figure 4: J/ψ secondary vertex positions in the y-z plane showing events in the air-gap regions

In several events, the secondary J/ψ vertex occurs in an air gap region; the background from secondary interactions is negligible for such events. The positions in the y-z plane of the J/ψ vertices in these gaps are shown in Fig. 4 (with z error bars). In ten of these events, the J/ψ vertex is at least three standard deviations away from the Be target elements. The background to this signal from false vertex reconstruction was estimated using GEANT-based, full-detector, Monte Carlos that included detector noise as observed in the data. The Monte Carlo events agree with our direct J/ψ events in terms of hit and track multiplicities, as well as position and momentum resolutions. The resulting background to the secondary-vertex J/ψ sample was found to be 11 ± 2 events, with 2 ± 1 events occurring in the gap regions. Additional background contributions were checked for by searching the data, itself, for dimuons with invariant mass in the J/ψ side bands from secondary vertices in the air-gap region (no events were found), and for reconstructed J/ψ vertices upstream of the primary vertex (one event was found, consistent with Monte Carlo expectations). From these considerations, we obtain a background subtracted signal (attributed to b-decays) of 8 ± 3.3 events in which the J/ψ vertex occurs in a region where only air is present.

The total number of J/ψs from b-decays in the fiducial volume can be estimated from the number observed in the gaps. Monte Carlo studies indicate that $(37 \pm 5)\%$ of the reconstructed vertices from bs produced in Be occur in the gap regions. Thus, 22 ± 10 $b \to J/\psi + X$ events are expected from Be, with an additional 4 events expected from Cu. Although the requirement of low secondary multiplicity certainly improves the likelihood of the J/ψ coming from a b-decay, secondary-interaction events remain in the non-gap sample. A simulation using the forward hadron momentum spectrum (measured in our interacting beam events) convoluted with the J/ψ cross section as a function of interaction energy indicates that 80 secondary-interaction events pass the J/ψ vertex quality cuts, and 33 also pass the multiplicity cut. This number added to the estimate of b-events $(22 + 4)$ and false vertex reconstructions (11) gives a total of 70 events, consistent with the 73 events observed.

4 – Exclusive B-decays

We searched this sample of secondary J/ψs for the exclusive channels $B^{\pm} \to J/\psi + K^{\pm}$ and $B^0 \to J/\psi + K^{0*}$. Events with three-prong secondaries (2 muons plus another track) were selected as candidate $B^{\pm} \to J/\psi + K^{\pm}$ decays. To reduce background, only combinations with a secondary hadron having $p_T > 0.5$ GeV/c were considered. This track was assumed to be a kaon, and its momentum was added to that of the J/ψ to form a candidate B momentum vector. The vector was projected back from the secondary to the primary vertex, and a transverse impact parameter, δ_v, was calculated; only events with $\delta_v < 80$ μm were kept. Since tracks from the underlying event can be coincidentally associated with a secondary vertex, 4-prong secondary vertices were also included in the selection. None of the 4-prong vertex events in the sample had both secondary hadron tracks pass the $p_T > 0.5$ GeV/c cut. The secondary vertices for these events were refit omitting the low p_T track, and the events were analyzed under the hypothesis of 3-prong B decays. Four events survived the above cuts (three having 3-prong secondary vertices, and one with a 4-prong secondary). Two events fell in the B-mass region, one in each charged K mode.

In the search for neutral B-decays, K^{0*}s were observed by their decays into $K^{\pm}\pi^{\mp}$ pairs. Kaon mass was assigned only to tracks with momentum greater than half that of the other track, and pairs having mass consistent with the K^{0*} were combined with the J/ψ in the same manner as in the $B^{\pm}$ analysis. Momentum vectors of B^0 candidates were required to satisfy $\delta_v < 100$ μm. Five events passed these cuts (none had double $K\pi$ combinations), and three have reconstructed masses in the B-mass region. One of these 3 events occurred in an air gap region.

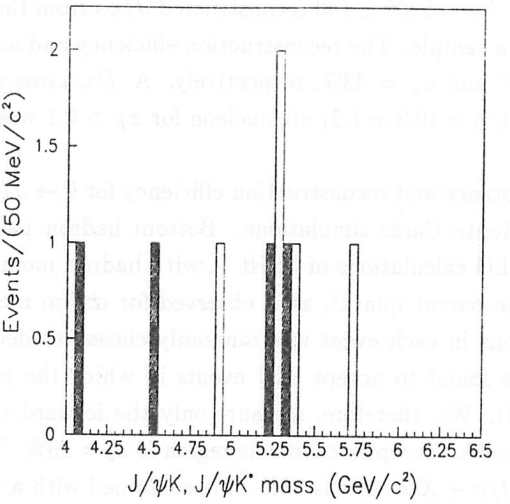

Figure 5: Combined $J/\psi + K^{\pm}$ and $J/\psi + K^{0*}$ invariant mass; the shaded entries are $J/\psi K^{\pm}$ combinations.

The combined $J/\psi + K^{\pm}$ and $J/\psi + K^{0*}$ invariant-mass distribution is shown in Fig. 5. The expected B mass resolution is 35 MeV/c^2. There are 5 events near the nominal B-meson mass. A background analysis using primary-vertex events subject to the same cuts as the B-candidate sample shows no evidence for arbitrary enhancement in the B-mass region due to the imposed cuts. Because of the small number of events in each decay mode, the exclusive decays are not used to determine the cross section. This measurement was done, instead, using the air-gap signal.

5 – Bottom cross section

Based upon the background subtracted signal of 8 $b \to J/\psi + X$ air gap events (and using J/ψ production as normalization), the bottom cross section is given by

$$\sigma_{b\bar{b}} = \frac{N_{b\to\psi}}{\epsilon_{b\to\psi} a_{b\to\psi} 2Br(b \to \psi \to \mu\mu)} \frac{\sigma_\psi Br(\psi \to \mu\mu)}{A} \frac{\epsilon_\psi a_\psi}{N_\psi}, \qquad (1)$$

where ϵ_b and ϵ_ψ are reconstruction efficiencies, a_b and a_ψ are detector acceptances, and A is the target atomic mass. The factor of 2 arises since either the b or the $\bar{b}$ in an event can result in a J/ψ. The branching ratios $Br(b \to J/\psi + X) = 1.3\%$ [5], and $Br(J/\psi \to \mu\mu) = 5.9\%$ [8] give a combined branching ratio of $Br(b \to J/\psi \to \mu\mu) = 7.7 \times 10^4$, averaged over all b-hadron species, including baryons.

There are $N_\psi = 9800 \pm 130$ reconstructed J/ψs from the Be target having $x_F > 0.1$ in the data sample. The reconstruction efficiency and acceptance for these J/ψs are $\epsilon_\psi = 64\%$ and $a_\psi = 43\%$, respectively. A J/ψ cross section (on Be) of $\sigma_\psi \cdot Br(J/\psi \to \mu\mu)/A = (9.2 \pm 1.2)$ nb/nucleon for $x_F > 0.1$ was measured by this experiment.

The acceptance and reconstruction efficiency for $b \to J/\psi + X$ events were calculated using Monte Carlo simulations. Bottom hadron pairs were generated according to the NLO calculations of MNR [4], with hadron momentum taken to be equal to that of the parent quark[1], as is observed for charm meson production [9]. One of the b-hadrons in each event was randomly chosen to decay into $J/\psi + X$. Our apparatus was found to accept only events in which the parent b-quark had $x_F > 0$ (see Fig. 6). We, therefore, measure only the forward part of the bottom cross section; the overall acceptance in this region is $a_b = 19\%$. The reconstruction efficiency for $b \to J/\psi + X$ events is 39%, this combined with a 27% probability of a decay occurring in an air gap region, yields an effective efficiency $\epsilon_b = 15\%$.

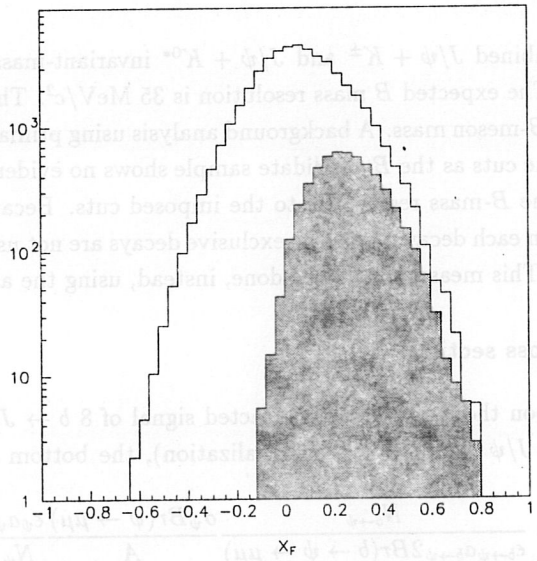

Figure 6: Monte Carlo generated b-quark x_F distribution, shaded histogram is for events accepted by our apparatus.

[1]Inclusion of a Peterson type fragmentation to the quarks momentum reduces the detection acceptance by 9%, this variation is included in the reported cross section's systematic uncertainty.

Using these values, and $N_{b\to\psi} = 8 \pm 3.3$, we obtain a bottom cross section in the forward direction ($x_F > 0$) of $\sigma_{b\bar{b}} = (47 \pm 19 \pm 14)$ nb/nucleon (assuming A^1-dependence) for π^--N collisions at 515 GeV/c, where the first uncertainty is statistical and the second is systematic. The main sources of systematic uncertainty are in the normalization (13%), branching ratios (13%), b production, hadronization, decay properties (16%), and reconstruction efficiencies (18%). For comparison with theory and other experiments, this measurement is extrapolated from $x_F > 0$ to all values. Based on x_F distribution predictions by MNR [4], a multiplicative factor of 1.58 is required. Thus, we obtain a total cross section of $\sigma_{b\bar{b}} = (75 \pm 31 \pm 26)$ nb/nucleon. Extrapolations based on Berger's predictions [3], and a measurement by Fermilab experiment E653 [10] are reflected in the quoted systematic uncertainty. With this cross section, we expect a total of 3 or 4 events in the exclusive decay modes, which is consistent with the observed excess in Fig. 5.

A comparison of our measurement to predictions for bottom cross sections in π-N collisions made by MNR [4] and Berger [3], and to those of previous experiments [10, 11], is shown in Fig. 7. Our measurement is on the high side of the theoretical predictions, favoring predictions with smaller b-quark mass values, and renormalization scales that are a smaller fraction of the mass scale. This is consistent with recent analysis of collider bottom-quark data [12].

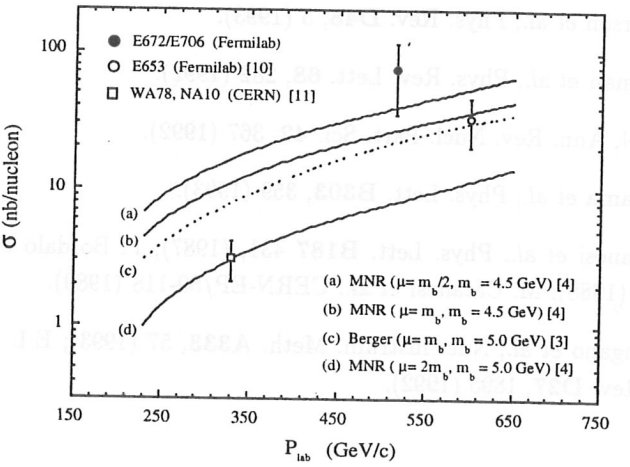

Figure 7: Total bottom cross sections in πN collisions, compared with several theoretical predictions.

Acknowledgements

We gratefully acknowledge the efforts of Fermilab's staff. We also thank MNR for their assistance and the use of their programs.

References

1. P. Nason, S. Dawson, and R.K. Ellis, Nucl. Phys. **B303**, 607 (1988); **B327**, 49 (1989); **B335**, 260 (1990).
2. F. Abe *et al.*, Phys. Rev. Lett. **71**, 50 (1993).
3. E.L. Berger, Phys. Rev. **D37**, 1810 (1988); ANL-HEP-CP-88-26, (1988).
4. M. Mangano, P. Nason, G. Ridolfi, Nucl. Phys. **B405**, 507 (1993); **B373**, 295 (1992).
5. O. Adriani, *et al.*, Phys. Lett. **B288**, 412 (1992).
6. V. Abramov *et al.*, FERMILAB-Pub-91/62-E, (1991); S. Kartik *et al.*, Phys. Rev. **D41**, 1 (1990).
7. G. Alverson *et al.*, Phys. Rev. **D48**, 5 (1993).
8. D. Coffman *et al.*, Phys. Rev. Lett. **68**, 282 (1992).
9. J. Appel, Ann. Rev. Nucl. Part. Sci. **42**, 367 (1992).
10. K. Kodama *et al.*, Phys. Lett. **B303**, 359 (1993).
11. M. Catanesi *et al.*, Phys. Lett. **B187** 431, (1987); P. Bordalo *et al.*, Z. Phys. **C39**, 7 (1988); M. Catanesi *et al.*, CERN-EP/89-118 (1989).
12. M. Mangano *et al.*, Nuc. Instrum. Meth. **A333**, 57 (1993); E.L. Berger, *et al.*, Phys. Rev. **D27**, 1895 (1992).

Frascati Physics Series, Vol. III (1994)
HEAVY QUARKS AT FIXED TARGET
University of Virginia, October 7–10, 1994
(pp. 263–274)

A MEASUREMENT OF THE TOTAL BEAUTY CROSS SECTION IN 350 GeV/c π^- Cu INTERACTIONS

Mauro Dameri
INFN, Sezione di Genova
via Dodecaneso 33, I-16132 Genova, (ITALIA)
on behalf of the Beatrice Collaboration*

ABSTRACT

Beauty production in π^--copper interactions has been observed at 350 GeV beam energy looking at multivertex events with and without high transverse momentum muon. The measured cross section for all x_F, assuming linear A-dependence, is $\sigma_{b\bar{b}} = 6.6 \pm 1.8 \pm 2.0$ nb per nucleon.

1 Introduction

Since the discovery of the Υ resonance [1], several experiments have studied open beauty production in hadronic interactions. After the first controversial observations at the CERN Intersecting Storage Rings (ISR) [2], a few positive results have been reported [3, 4, 5]. In fixed target experiments at the CERN Super Proton Syncrotron (SPS) and at the FNAL Tevatron, hadroproduction of BB pairs has been observed

*M.Adamovich, M.Adinolfi, Y.Alexandrov, C.Angelini, F.Antinori, C.Bacci, D.Barberis, D.Barney, J.Batten, W.Beusch, C.Bruschini, R.Cardarelli, A.Cardini, V.Casanova, F.Ceradini, G.Ciapetti, M.Dameri, G.Darbo, A.Di Ciaccio, A.Duane, J.P.Dufey, Ph.Farthouat, V.Flaminio, A.Forino, B.R.French, A.Frenkel, C.Gemme, R.Gessaroli, K.Harrison, R.Hurst, A.Kirk, F.Lacava, J.C.Lassalle, C.Lazzeroni, L.Malferrari, S.Maljukov, G.Martellotti, P.Martinengo, P.Mazzanti, J.G.McEwen, I.Minashvili, P.Nechaeva, A.Nisati, D.Orestano, B.Osculati, M.Passaseo, G.Penso, E.Petrolo, L.Pontecorvo, A.Quareni, P.Ragni, H.Rotscheidt, V.Ryzhov, C.Roda, L.Rossi, N.Russakovich, C.Salvo, R.Santonico, G.Schuler, A.Semenov, A.Solovjev, M.Torelli, S.Veneziano, M.Verzocchi, D.Websdale, M.Weymann, L.Zanello, M.Zavertyaev

in nuclear emulsions targets [6] and indirect measurements of the beauty production cross section at beam momenta in the range 140-800 GeV/c the current fixed target energies, have been published. At these energies measurements of the B production are made difficult by the tiny cross section which entails a very small signal-to-noise ratio ($\sigma_{b\bar{b}}/\sigma_{tot} \simeq 10^{-6}$ at $\sqrt{s} = 26$ GeV) and by the restrained acceptance that ranges from some 10^{-3} to 10^{-6} for exclusive decay channels. Two factors are important for finding a beauty signal in a fixed-target environment: the selectivity of the trigger and the reconstruction efficiency for decay vertices. The experiment WA92 has been designed to have a large acceptance for beauty particles and a high background rejection : the acceptance of the trigger for beauty events was of the order of 33% and the capability of the detector to reconstruct decay vertices allowed the selection of a large fraction of the beauty signal and an important and clean sample of fully reconstructed charmed particles.

2 The experimental setup

Experiment WA92, designed to study the hadroproduction and the decay of particles containing b quarks, took data at the Ω' magnetic spectrometer facility in the CERN West Area. The measuring apparatus, described in detail elsewhere [7], was characterized by two peculiar devices: a high resolution imaging detector to study secondary vertices and a selective trigger to collect events with a secondary activity downstream of the primary interaction and with leptons and charged particles emitted at large transverse momentum. In this paper we simply recall the description of these two devices and of the detectors relevant for this analysis based on events produced by a 350 GeV/c π^- beam in a 2 mm thick copper target. Beam tracks were measured by 10 planes of 20 μm pitch silicon microstrip detectors (SMDs). The energy released by interactions in the target and escaping it was detected by a silicon 300 μm thick detector (IT) glued to the downstream face of the target. Tracks emerging from the interaction were measured using a vertex detector, which consisted of 12 planes of 25 μm pitch and 5 planes of 50 μm pitch SMDs. The region between the target and the vertex detector, where most of the beauty and charm decays occur, was equipped with the Decay Detector (DD) [8], which is a sort of *electronic bubble chamber* able to visualize the complex topologies (i.e. chained decays, kinks) typical of beauty decays, otherwise difficult to be detected. DD allows therefore the observation of decay channels other than B $\Rightarrow J/\Psi$. The DD is

made of 17 10 μm pitch detectors covering an area of $5 \times 5\,\mathrm{mm}^2$. The spacing along the beam direction is 1.2 mm for the first 14 planes and 5 mm for the following ones; the first 6 detectors are 150 μm thick and the others 300 μm thick. Thirteen planes measure the Z (vertical) coordinate, two the Y (horizontal) coordinate and two are inclined for projection matching. All strips are individually read out into 8-bit ADC's; with thresholds set for each strip at 4 times the pedestal RMS we obtain efficiencies of 93% and 97% for the thin and the thick planes respectively with a noise level of 10^{-3} per strip. The measured single-point resolution is between 2 and 3 μm and the two-track resolution is of the order of 30 μm .

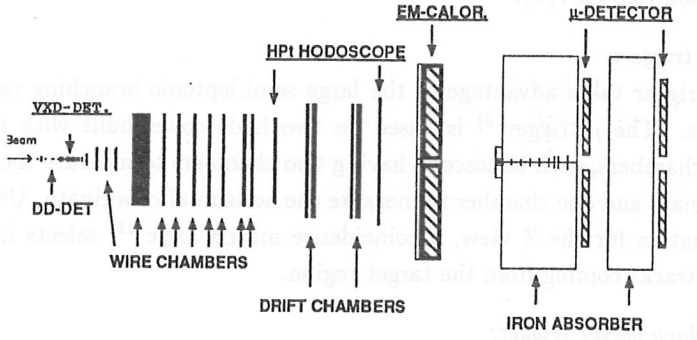

Figure 1: *Schematic view of the WA92 setup.*

The target and the SMDs were located upstream of the Ω' spectrometer in a region of very low magnetic field. The Ω' spectrometer consisted of 8 drift and 44 multiwire proportional chambers placed in a 1.8 T dipolar magnetic field (directed along the Z coordinate) giving a $\Delta p/p^2$ resolution of 1.6 10^{-4} $(\mathrm{GeV}/c)^{-1}$. A lead-glass electromagnetic calorimeter and a muon filter [9] followed the magnetic spectrometer, as shown schematically in figure 1. Between the spectrometer and the calorimeter a finely segmented butterfly-shaped scintillator hodoscope [10] was used to select charged particles emitted at large transverse momentum.

3 The trigger

To counter the unfavorable signal-to-noise ratio we used of a combination of several independent trigger components:

- *High transverse momentum Trigger:*
  This trigger selects, in less than 250 ns, events having particles with $p_T \geq 0.6$ GeV/c with respect to the beam direction, which can be produced in decays of high-mass particles. The trigger uses two so-called butterfly hodoscopes [10]; as a result of the deflection in the magnetic field of the Ω spectrometer, a charged particle that originates in or close to the target can cross the butterfly hodoscopes, and thus give a trigger, only if it has p_T larger than the set threshold (0.6 GeV/c).

- *Muon trigger:*
  This trigger takes advantage of the large semi-leptonic branching ratio of B mesons. The μ-trigger [9] is based on two hodoscopes built with resistive-plate chambers, each hodoscope having two chambers to measure the vertical coordinate and one chamber to measure the horizontal coordinate. Using only information for the Z view, a coincidence matrix logic [11] selects in 250 ns muon tracks coming from the target region.

- *Secondary-vertex trigger:*
  The secondary-vertex trigger or beauty contiguity trigger (BCT) exploits the long B lifetime ($c\tau \simeq 450\,\mu$m) which allows decay vertices to be well separated from the primary interaction point. The BCT hardware and the implemented algorithm have been extensively described elsewhere [12, 13, 14, 15] and only their performance will be discussed here.

A multilevel trigger selected events only if at least two of the above conditions were verified simultaneously. The rejection factor of the trigger for minimum bias event was about 30 and the acceptance for charm events about 10%.

The experiment has collected data during two periods, in 1992 and in 1993, when 90 million and 60 million triggers where recorded on tape respectively. Results presented here refer only to half of the 1992 data sample.

Trigger Type	*Data*	*Min.Bias*	$c\bar{c}$	$b\bar{b}$
INT/σ_{tot}	65 %	67 %	75 %	75 %
$1\mu/INT$	2.7 %	2.5 %	8.0 %	18.3 %
$2\mu/INT$	0.08 %	0.06 %	0.1 %	1.6 %
$1HP_T/INT$	41.0 %	41.0 %	45.0 %	62.7 %
$2HP_T/INT$	12 %	11.2 %	10.4 %	28.1 %
BCT/INT	5.4 %	5.4 %	13.5 %	49.3 %
1992 Tri/σ_{tot}	2.5 %	2.2 %	8.2 %	31.6 %

Table 1: *Trigger rates for 1992. The first column is for real data, the others are from simulation. For the definition of the trigger components see the text.*

3.1 Trigger Performance

In triggering on secondary vertices there is a trade-off between beauty acceptance and background reduction, and some attention is needed to avoid (or at least reduce) possible trigger biases. The BCT track reconstruction algorithm is carefully designed to minimize the effects of detector inefficiencies and noise and to correctly count and classify tracks according to their impact parameter(IP). The BCT trigger provided an IP selection that is uniformly efficient between 100 μm and 1 mm.

To understand the trigger behaviour we have fully simulated minimum-bias, $c\bar{c}$ and $b\bar{b}$ events. Minimum-bias events were generated using Fluka [16] as interfaced with Geant 3.21 [17]. This reproduced well the experimentally measured charged particle multiplicities and kinematics, and also the production of heavily ionizing particles. We generated $c\bar{c}$ and $b\bar{b}$ events using a combination of Pythia 5.4 [18] and Fluka. In the generation process up to 98.5% of the centre-of-mass energy was available for the simulation of hard processes by Pythia; the remaining energy was used to simulate soft processes with Fluka. The passage of generated particles through the experimental apparatus was simulated in detail using Geant 3.21. Non-interacting beam particles, detector inefficiencies and random noise were added in accordance with experimental measurements.

In Table 1 we present the trigger rates obtained for background and signal with the different triggers and in Fig. 2 we represent the beauty acceptance of the trigger. The interaction pretrigger (INT) required the presence of an incoming beam particle, incident on the target, and outgoing interaction products, together with a

signal of more than 5 m.i.p. in the IT; the 1μ (2μ) trigger required the presence of at least one (two) muon(s); the $1HP_T$ ($2HP_T$) trigger required that there should be at least one (two) particle(s) having a transverse momentum with respect to the beam ≥ 0.6 GeV/c; the BCT required at least three primary and two secondary tracks. The trigger was the logical 'OR' of the 'AND' of any two of the 1μ, $1HP_T$, BCT triggers; all events satisfying the 2μ trigger were accepted. As the acceptance of INT is 75% the global acceptance corresponds to about 1/3 of $\sigma(B)$.

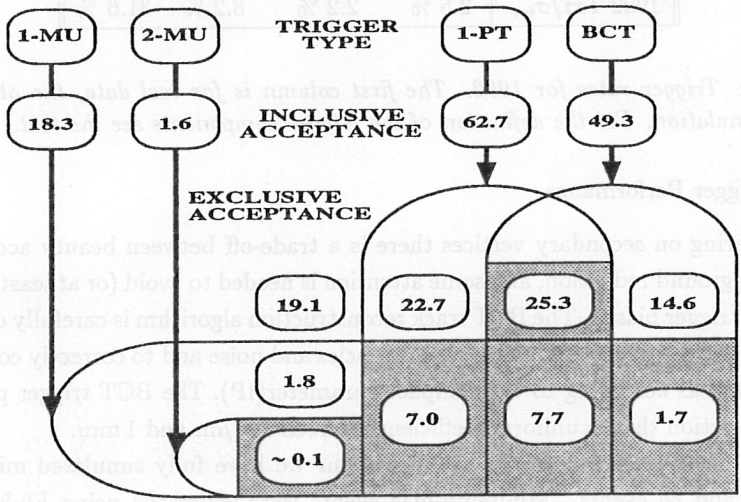

Figure 2: *The grey regions represent the trigger acceptances for beauty events with respect to the INT trigger, which had an efficiency of* 75% *for events occurring in the target.*

4 Rejection of secondary interactions

As shown in Fig. 3.a, most secondary vertices reconstructed in the decay detector region are hadronic interactions in the silicon planes. The DD represents 0.6% of a π interaction length and 4.5% of a radiation length. Given the small beauty production cross section, the ratio between the number of secondary vertices due to beauty cascade decays and those due to secondary interactions in minimum bias events is of the order of 10^{-5}. A simple cut on the vertex position cannot be used because of the small spacing between the DD planes. Thanks to the DD

analogue read-out we could develop a method based on the large energy release due to nuclear fragments and slow tracks which accompany most of the interactions in the Si planes. Cuts based on the distance between the reconstructed vertex position and the centroid of the large energy deposits reject 91% of the vertices due to secondary interactions while loosing only 3% of K_s^0 and Λ^0 and 8% of $D^{0,\pm}$ decays (Fig. 3.b). Some secondary vertices are due to coherent or low-multiplicity hadronic interactions surviving the pulse height cuts and others are fake vertices due to high hit densities (mostly interactions).

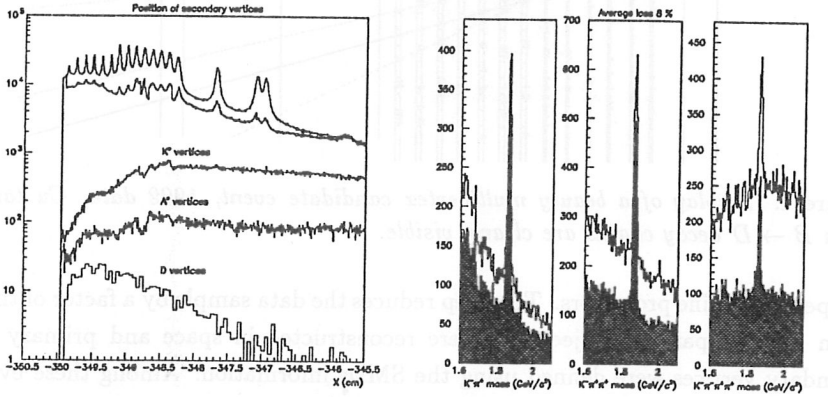

Figure 3: *a) Position of reconstructed secondary vertices in the DD region. The vertices between the two upper curves are rejected as due to secondary interactions in the Si planes. b) D^0 and $D^{\pm}$ invariant mass distributions showing the effect of the algorithm rejecting secondary interactions.*

5 Search for beauty decays

This analysis is based on 40×10^6 events corresponding to about 1.6×10^9 inelastic interactions and equivalent to about 20% of the global statistic on tape. Assuming a cross section of 5 nb/nucleon and a linear dependence on the atomic number, 1200 B events were produced in the target: the estimated sensitivity is 80 ev/nb after the trigger. The data were filtered by a fast reconstruction program which verified the trigger conditions in order to reject some trivial background that

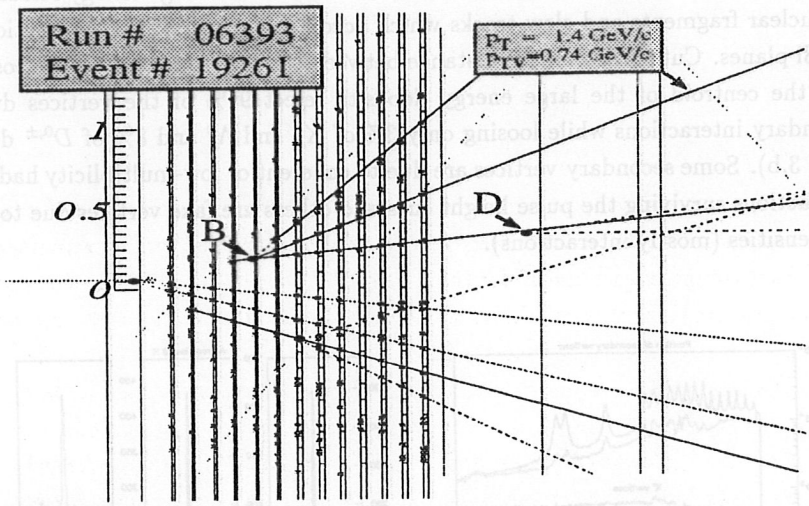

Figure 4: *Display of a beauty multivertex candidate event, 1992 data, Cu target. Both $B \rightarrow D$ decay chains are clearly visible.*

escaped the online processors. This step reduces the data sample by a factor of three. Then charged particle trajectories were reconstructed in space and primary and secondary vertices were defined using the SMDs information. Among these events the Trident reconstruction program [19] found 6×10^6 events with a well reconstructed secondary vertex, containing an estimated sample of 350 beauty events . The cut on hadronic interactions reduced the data sample to 1×10^6 events. The events were then separated into 2 streams to be analyzed with a graphical display program, in order to exploit the visualizing capabilities of the DD:

- events with at least 3 secondary vertices in the DD region (*multivertex* events);
- events with at least 2 secondary vertices and a high transverse momentum muon associated to one of them($\mu - events$).

These strict selection criteria gave about 2000 events amongst which we were expecting to observe 10 beauty decays. Then the graphical analysis allowed us to search for additional secondary activity and kinks and to check the reconstruction of the tracks and vertices in the DD region, and thus to achieve a larger background reduction. We were eventually left with 25 *multivertex* events and 31 $\mu - events$.

As above-mentioned, one of the major sources of background were produced by the secondary interactions which have a probability of be reconstructed $P_{rt} \simeq 10^{-3}$ and a probability to survive the cut on the pulse height $P_{ph} \simeq 9 \cdot 10^{-2}$. In the selected samples the number of background events produced by secondary interactions is:

$$N_{bsec} = N_{tot} \times (P_{rt} \times P_{ph})^{N_{sv}}$$

where N_{tot} is the total number of interactions and N_{sv} is the number of requested secondary vertices per event. Thus for the *multivertex* selection we remained with 10^{-3} background events and 13 for the $\mu-events$. Moreover for this last category we should also consider the probability to have a *collinear* μ identified and reconstructed back to the DD. They come mostly from the π(K)$\Rightarrow \mu$ decays whose probability is estimated to be of the order of 10^{-2} and thus the in the μ selection the background events are less than 1. We could conclude that secondary interactions are not an important background source. As a confirmation we observed in the selected samples the same number of charged and neutral secondary vertices whereas for secondary interactions the population of charged vertices is 10 times that of the neutral ones. The second and, as indicated by the simulation, the main background source are the charm decays. Using a sample of 1.5×10^5 simulated charm events we got a value of $4 \cdot 10^{-3}$ for the probability $P(p_{tv})$ that at least one secondary track satisfies the requirement $p_{tv} > 1.0$ GeV/c, where p_{tv} is the transverse momentum of a secondary particle relative to the line of flight of the secondary vertex to which it is associated. Taking into account that the data correspond to 3×10^6 charm events, this background entails a 90% CL limit of 0.5 background events in the *multivertex* sample and 0.4 in the μ one.

The cut $p_{tv} > 1.0$ GeV/c reduced our samples to 5 *multivertex* and 9 $\mu-events$. Once correcting for the acceptances which are $0.28 \pm 0.02\%$ for *multivertex* and $0.62 \pm 0.02\%$ for $\mu - events$, we obtained:

$$\sigma(B_{mvtx}) = 7.6 \pm 3.4 nb \qquad (multivertex \text{ sample})$$

$$\sigma(B_{\mu}) = 6.3 \pm 2.1 nb \qquad (\mu \text{ sample})$$

and, combining the results which are compatible with each other, we finally obtain:

$$\sigma(B) = 6.6 \pm 1.8(stat) \pm 2.0(syst) nb$$

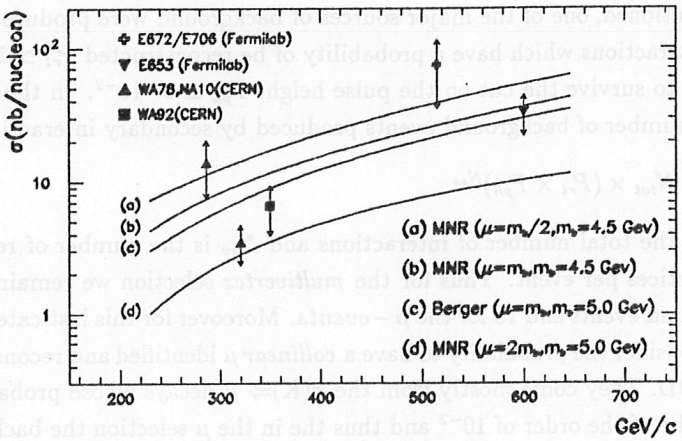

Figure 5: *Experimental results versus NLO QCD theoretical predictions for the B production in πN collisions as a function of the beam momentum.*

which is in good agreement with the next-to-leading order perturbative QCD calculations [20] as shown in Fig. 5. As a check we have also measured the production cross section for D^0, $D^{\pm}$ and J/ψ. From a estimated population of 3×10^6 D events and $7.4 \times 10^4 J/\Psi$ produced in target we obtained : $\sigma(D^0) = 9.6 \pm 2.4 \mu b$ and $\sigma(D^{\pm}) = 4.8 \pm 1.3 \mu b$ both for $x_F > 0$; while $\sigma(J/\psi)$ =300 $\pm$ 20 nb for all x_F. The above results are all in good agreement with other experiments.

6 Conclusions

A trigger looking for secondary vertices has been used for the first time in an experiment to search for beauty particles. The trigger was able to reject 94.2% of the background keeping $\sim$ 30% of the beauty signal. A high precision (10 μm pitch) Si telescope has been operated and used to observe directly the cascade decays of beauty particles. Secondary hadronic interactions have been rejected efficiently with cuts correlating the vertex position to the large energy deposits.

The topological trigger, together with the high resolution of the decay

detector, enabled us to see beauty events with the help of interactive graphics. More sophisticated code is being developed to improve the event selection and allow us to relax some cuts, thus gaining in acceptance and efficiency. The measurement of the beauty cross section based on two independent samples of events yielded values compatible with each other and in good agreement with other experiments and with QCD calculations. The result presented, which is still preliminary, has been extracted using 20% of the WA92 statistics. The full analysis of WA92 data should give an error on $\sigma(B) < 10\%$.

References

1. S.W.Herb et al., *Phys.Rev.Lett.* **39** (1977) 252;
   W.R.Innes et al., *Phys.Rev.Lett.* **39** (1977) 1240.

2. M.Basile etal., *Lett.Nuovo Cimento* **31** (1981) 97; *Nuovo Cimento* **68A** (1982) 289:
   D.Drijard et al., *Phys.Lett.* **B108** (1982) 361.

3. A. Diamant-Berger et al., *Phys.Rev.Lett.* **44** (1980) 507;
   A.Bodek et al., *Phys.Lett.* **B113**(1982) 82;
   R.Barate et al., *Phys.Lett.* **B121**(1983) 449;
   J.Badier et al., *Phys.Lett.* **B124**(1983) 535; Phys.Lett. **B158** (1985) 85.

4. A.Ereditato et al., *Phys.Lett.* **B157** (1985) 463.

5. M.G.Catanesi et al., *Phys.Lett.* **B187** (1987) 431.

6. J.P.Albanese et al., *Phys.Lett.* **B158** (1985) 186.
   K.Kodama et al., *Phys.Lett.* **B303** (1993) 359.

7. D.Barberis et al., Proc. CHARM2000 Workshop, Fermilab,USA, June 7-9,1994,213.

8. M. Adinolfi et al., *Nucl. Instr. Meth.* **A329** (1993) 117.

9. C. Bacci et al., *Nucl. Instr. Meth.* **A324** (1993) 83.

10. W. Beusch et al., *Nucl. Instr. Meth.* **A249** (1986) 391.

11. E. Petrolo and S. Veneziano, *Nucl. Instr. and Meth. Phy. Res.* **A315** (1992) 95.
E. Gennari, E. Petrolo and S. Veneziano, *IEEE Trans. Nucl. Sci.* **NS-39** (1992).

12. G. Darbo and L. Rossi, *Nucl. Instr. and Meth. Phys. Res.* **A289** (1990) 584.

13. A. Beer, et al., The beauty contiguity trigger of the BEATRICE experiment: detector, readout and processor overview, *Nucl. Instr. and Meth. Phys. Res.* **A337** (1994) 280.

14. C. Bruschini, "Studio di un Trigger rapido su vertici secondari per la ricerca di particelle dotate di Beauty", *Thesis, University of Genova.*

15. G. Darbo et al., *Nucl. Instr. Meth.* **A351** (1994) 225.

16. A. Fassò et al., "FLUKA: present status and future developments", proceedings of the IV International Conference on Calorimetry High Energy Physics, la Biodola, Italy, 21-26 September 1993.(World Scientific) p.493.

17. GEANT Detector Description and Simulation Tool, CERN Program Library Long Writeup W5013 (1994).

18. H.-U. Bengtsson and T. Sjöstrand, *Comput. Phys. Commun.* **46** (1987) 43.

19. J.-C. Lassalle et al., *Nucl. Instr. and Meth. Phy. Res.* **A176** (1980) 371.
D. Barberis, M. Dameri and B. Osculati, *private communication.*

20. P. Nason, S. Dawson, R.K. Ellis, *Nucl. Phys.* **B327** (1989) 49;
M.L. Mangano, P. Nason, G. Ridolfi, *Nucl. Phys.* **B373** (1992) 295;
M.L. Mangano, P. Nason, G. Ridolfi, *Nucl. Phys.* **B405** 507 (1993);
S. Frixione, M.L. Mangano, P. Nason, G. Ridolfi, CERN-TH.7292/94 (1994);
M.L. Mangano,P. Nason,G. Ridolfi, *IFUP-TH-37/92 GEF-TH-15/1992* (1992).

Frascati Physics Series, Vol. III (1994)
HEAVY QUARKS AT FIXED TARGET
University of Virginia, October 7–10, 1994
(pp. 275–281)

B CROSS SECTION FROM E789

Daniel M. Kaplan
Illinois Institute of Technology

for the Fermilab E789 Collaboration*

ABSTRACT

Using an 800 GeV proton beam, Fermilab E789 has observed a signal of $J/\psi \to \mu^+\mu^-$ decays occurring in vacuum downstream of a gold-wire target. We obtain a doubly-differential cross section for J/ψ's originating from B decays $d^2\sigma/dx_F\,dp_t^2 = 94 \pm 25 \pm 19\,\mathrm{pb/GeV^2/nucleon}$ at $x_F = 0.05$ and $p_t = 1$ GeV. This is compared with QCD predictions and the results of other experiments. Extrapolating over all x_F and p_t, our result implies $\sigma(pN \to b\bar{b} + X) = 5.0 \pm 1.3 \pm 1.2\,\mathrm{nb/nucleon}$.

1 – Introduction

Using the upgraded E605 spectrometer [1] (Fig. 1), Fermilab E789 has made the first measurement of the B cross section in proton interactions at fixed-target energies. We observe B production via the process $p + \mathrm{Au} \to B + X$, $B \to J/\psi + X$, $J/\psi \to \mu^+\mu^-$. (B here denotes any hadron containing a beauty quark or antiquark.) The B cross section is of interest both as a test of QCD and as an "engineering" number for use e.g. in planning the HERA-B experiment [2]. A more detailed discussion of the data analysis than presented here may be found in Ref. [3].

*C. N. Brown, T. A. Carey, Y. C. Chen, R. Childers, W. E. Cooper, C. W. Darden, G. Gidal, K. N. Gounder, P. M. Ho, L. D. Isenhower, D. M. Jansen, R. G. Jeppesen, D. M. Kaplan, J. S. Kapustinsky, G. C. Kiang, M. S. Kowitt, D. W. Lane, L. M. Lederman, M. J. Leitch, J. W. Lillberg, W. R. Luebke, K. B. Luk, P. L. McGaughey, C. S. Mishra, J. M. Moss, J. C. Peng, R. S. Preston, D. Pripstein, J. Sa, M. E. Sadler, R. Schnathorst, M. H. Schub, V. Tanikella, P. K. Teng, J. R. Wilson; Abilene Christian University, Academia Sinica (Taiwan), University of California at Berkeley, University of Chicago, Fermi National Accelerator Laboratory, Lawrence Berkeley Laboratory, National Cheng Kung University, Northern Illinois University, University of South Carolina.

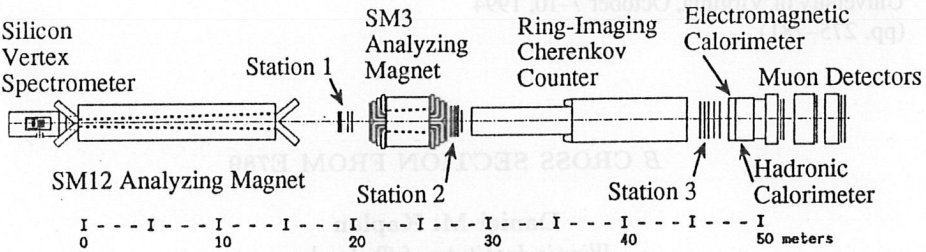

Figure 1: E789 apparatus (plan view).

2 – Apparatus

The spectrometer upgrade included installation of an array of sixteen silicon-microstrip detectors (SMDs) downstream of the target, replacement of the multiwire proportional chambers with small-cell drift chambers, and an order-of-magnitude increase in the data-acquisition capacity. The SMDs were arrayed from 37 – 94 cm downstream of the target in two arms covering the angular ranges $\pm(20 - 60)$ mr above and below the beam axis; they thus instrumented the clear apertures above and below the beam dump suspended within the SM12 analyzing magnet. The detectors, type "B" from Micron Semiconductor, were of $5 \times 5\,\mathrm{cm}^2$ area, $300\,\mu$m thickness, and $50\,\mu$m pitch. To minimize multiple-scattering and radiation-damage effects, they were immersed in helium gas cooled to 10° C. In each arm, planes measuring the bend (y-z) view alternated with planes at $\pm 5°$ stereo angles. Signals from 8,544 strips were individually read out via Fermilab 128-channel amplifier cards [4] and LBL discriminators [5] synchronized to the accelerator RF. The discriminated signals were transmitted through $\approx$ 400 ns of multiconductor cable to coincidence registers. The system provided decay-distance resolution of $\approx$ 0.7 mm rms, compared to the typical 1.3 cm B decay distance.

3 – Data sample

Data were taken separately in charm and beauty spectrometer settings. Results from the charm running have already been published [6, 7]. In the beauty running, 800 GeV primary proton beam of intensity $\approx 6 \times 10^{10}$ protons per 20 s spill was incident on a gold-wire target 0.2 mm high and 3 mm thick. Since $\approx$ 60% of the beam was focussed onto the target, the typical interaction rate was $\approx$ 50 MHz. The SM12 current was set to 1500 amperes, optimizing acceptance for J/ψ decays. Some 9×10^8 events were recorded on 770 8 mm tapes.

4 – Results

Fig. 2 shows the dimuon invariant-mass spectrum before decay-vertex cuts. To enhance the $B \rightarrow J/\psi$ signal/background we cut on the reconstructed-vertex z coordinate (z_v) of the muon pair and on the vertical impact parameters (δ_i) of the two muon tracks. The impact-parameter requirements ensure that neither the μ^+ nor the μ^- track points to the target. Fig. 3 shows the dimuon mass spectra for successively tighter z_v and impact parameter cuts. We attribute the net excess of J/ψ events with downstream vertices to the $B \rightarrow J/\psi$ process[1]. In addition, a significant downstream excess is evident in the continuum, presumably due to double-semileptonic $B\overline{B}$ decays.

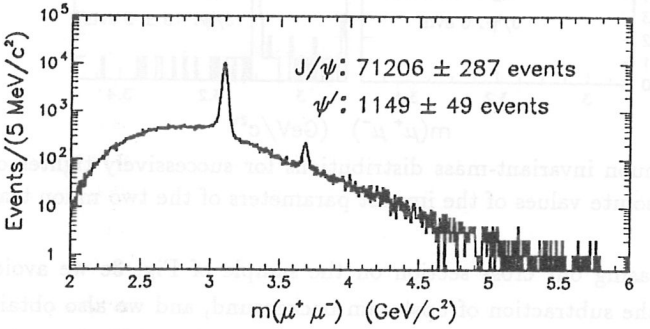

Figure 2: Dimuon invariant-mass distribution.

To convert these event yields to cross sections, we simulate geometrical acceptance using the following model of b-quark production, hadronization, and decay to $J/\psi + X$: 1) we generate b-quark x_F and p_t distributions according to the next-to-leading-order calculation by Mangano, Nason, and Ridolfi [8]; 2) the b-quark momentum vector is smeared[2] with Gaussian parton intrinsic-transverse-momentum distributions of $< k_T^2 >= 0.5$ GeV^2; 3) b-quark fragmentation is modeled using the Peterson function [9], with $\epsilon = 0.006 \pm 0.002$ as determined from e^+e^- annihilation [10]; 4) we use 1.537 ± 0.021 ps [11] as the average B lifetime; 5) since a b quark fragments dominantly into a B_d or a B_u, we use a distribution from the CLEO collaboration [12] to simulate the momentum of J/ψ's originating from B decays; 6) a decay-angle distribution $1 - \lambda \cos^2\theta$, with $\lambda = 0.436 \pm 0.115$ [12], is used to simulate the J/ψ polarization.[3]

[1] Monte Carlo studies show that the relative lack of upstream events is not due to analysis bias [3].

[2] As suggested to us by E. Berger. This increases our cross section by only a few percent, given the substantial smearing due to fragmentation and decay.

[3] We have also checked that b-quark production and fragmentation according to the PYTHIA

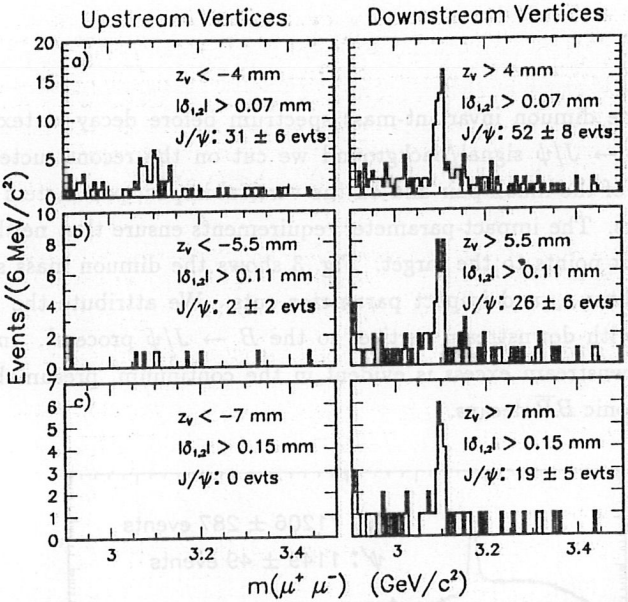

Figure 3: Dimuon invariant-mass distributions for successively tighter cuts on z_v and on the absolute values of the impact parameters of the two muon tracks $|\delta_{1,2}|$.

By basing our cross section on the sample of Fig. 3c we avoid any uncertainties in the subtraction of upstream background, and we also obtain optimal statistical significance. We assume linear target-atomic-weight dependence for B production since recent experiments have shown no nuclear suppression of D production [6]. We obtain $< d^2\sigma|_{J/\psi \text{ from } B}/dx_F\, dp_t^2 >= 71 \pm 19 \pm 14\,\text{pb/GeV}^2\text{/nucleon}$ averaged over the J/ψ-x_F and p_t bin $0 < x_F < 0.1$, $p_t < 2\,\text{GeV}$. The cross section is stable as we vary our vertex cuts. A separate analysis using a different SMD track reconstruction program also yields a consistent result.

5 – Discussion and Conclusions

To compare with theory it is convenient to interpolate the cross section to the point $x_F = 0.05$ and $p_t = 1\,\text{GeV}$. Using our model we find that the interpolated cross section is 1.32 times the average cross section, i.e. $94 \pm 25 \pm 19\,\text{pb/GeV}^2\text{/nucleon}$, and that the interpolation has negligible systematic uncertainty. Fig. 4 compares the interpolated cross section with representative predictions of the model. The predictions contain substantial uncertainties due to choices for the b mass (37% decrease at our x_F and p_t as m_b varies from 4.75 to 5.00 GeV), the QCD scale (45% decrease as μ varies from $\sqrt{m_b^2 + p_t^2}$ to $2\sqrt{m_b^2 + p_t^2}$), and the parton distribution functions (±30%

Monte Carlo gives results consistent with our model.

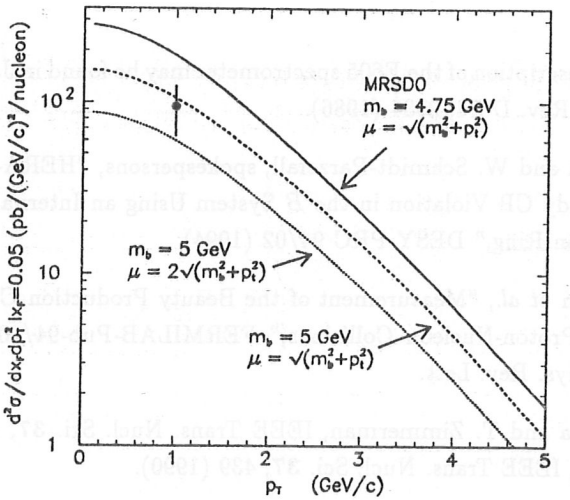

Figure 4: $d^2\sigma/dx_F\,dp_t^2$ for J/ψ's originating from B decays compared to predictions of the model described in the text for various values of the b mass and QCD scale.

variation with respect to the MRSD0 [13] set). The solid curve in Fig. 4 is based on the same assumptions as used recently by the CDF collaboration [14]. Compared to this prediction, our measurement is a factor of two low, while theirs is high by a similar factor. While the sensitivities of the predictions to the model assumptions differ between $\sqrt{s} = 1.8$ TeV and fixed-target energies, within the model no set of assumptions appears to be consistent with both our measurement and CDF's.

Despite the wide range of predictions for the *size* of the differential cross section at our x_F and p_t, the *shapes* vs. these variables are relatively insensitive to the input assumptions. We can thus use the model to extrapolate over all x_F and p_t with only a slight increase in systematic uncertainty. Using $B(b\bar{b} \to J/\psi + X) = (2.60 \pm 0.34)\%$ (twice the inclusive branching ratio for $B \to J/\psi + X$ [11]), we thus obtain $\sigma(pN \to b\bar{b} + X) = 5.0 \pm 1.3 \pm 1.2$ nb/nucleon.

The B cross sections measured by various groups (using a variety of techniques, beams, and energies) suggest a developing puzzle: while many groups observe a cross section higher than predicted (NA10 [15], CDF [14, 16], E653 [17], E672 [18]), others find values at (WA75 [19], WA78 [20], UA1 [21], WA92 [22]) or below (E789) QCD expectations. The large uncertainties of many of the results may mean that there is no substantial discrepancy among comparable measurements. However, there is some indication of a need for modification of the gluon structure function in the proton, as suggested by Berger and Meng [23], to steepen the energy dependence of the proton-induced cross section.

References

1. A detailed description of the E605 spectrometer may be found in J. A. Crittenden *et al.*, Phys. Rev. D **34**, 2584 (1986).

2. W. Hofmann and W. Schmidt-Parzefall, spokespersons, "HERA-B: An Experiment to Study CP Violation in the B System Using an Internal Target at the HERA Proton Ring," DESY-PRC 94/02 (1994).

3. D. M. Jansen *et al.*, "Measurement of the Beauty Production Cross Section in 800 GeV/c Proton-Nucleon Collisions," FERMILAB-Pub-94/403 (1994), submitted to Phys. Rev. Lett.

4. R. J. Yarema and T. Zimmerman, IEEE Trans. Nucl. Sci. **37**, 430 (1990); T. Zimmerman, IEEE Trans. Nucl. Sci. **37**, 439 (1990).

5. B. T. Turko *et al.*, IEEE Trans. Nucl. Sci. **39**, 758 (1992).

6. M. J. Leitch *et al.*, Phys. Rev. Lett. **72**, 2542 (1994).

7. C. S. Mishra *et al.*, Phys. Rev. D **50**, 9 (1994).

8. P. Nason, S. Dawson, and R. K. Ellis, Nucl. Phys. **B303**, 607 (1988); M. Mangano, P. Nason, and G. Ridolfi, Nucl. Phys. **B405**, 507 (1993).

9. C. Peterson *et al.*, Phys. Rev. D **27**, 105 (1983).

10. J. Chrin, Z. Phys. C **36**, 165 (1987); D. Decamp *et al.*, Phys. Lett. B **244**, 551 (1990). This is also the value of ϵ used in Reference [14].

11. Particle Data Group, L. Montanet *et al.*, Phys. Rev. D **50**, Part 1 (1994).

12. D. Besson, CLEO collaboration, private communication.

13. A. D. Martin, W. J. Stirling, and R. G. Roberts, Phys. Lett. B **306**, 145 (1993).

14. F. Abe *et al.*, FERMILAB-Conf-94/136-E (1994).

15. P. Bordalo *et al.*, Z. Phys. C **39**, 7 (1988).

16. F. Abe *et al.*, Phys. Rev. Lett. **69**, 3704 (1992); M. Mangano *et al.*, Nucl. Instr. Meth. **331**, 57 (1993).

17. K. Kodama *et al.*, Phys. Lett. B **303**, 359 (1993).

18. R. Jesik *et al.*, this Conference and FERMILAB-Pub-94/095-E (1994).
19. J. P. Albanese *et al.*, Phys. Lett. **158B**, 186 (1985).
20. M. G. Catanesi *et al.*, Phys. Lett. B **231**, 328 (1989).
21. C. Albajar *et al.*, Phys. Lett. B **256**, 121 (1991).
22. M. Dameri, this Conference.
23. E. L. Berger and R. Meng, "The Gluon Density," in **The Fermilab Meeting: DPF '92**, C. H. Albright *et al.*, *eds.*, World Scientific, Singapore (1992), p. 954; Phys. Lett. B **304**, 318 (1993).

RESULTS FROM E-731 / PROSPECTS FOR CP MEASUREMENTS IN KTEV

D. Jensen

Fermilab National Accelerator Laboratory
MS-231, P.O. Box 500, Batavia, Illinois 60510 (U.S.A.)

No written contribution received

Frascati Physics Series, Vol. III (1994)
HEAVY QUARKS AT FIXED TARGET
University of Virginia, October 7–10, 1994
(pp. 287–300)

CP VIOLATION IN K DECAYS : RESULTS FROM NA31, PROSPECTS IN NA48.

P.Buchholz
CERN, CH 1211 Geneva 23, Switzerland

ABSTRACT

The origin of direct CP violation and its precise magnitude are still open questions in the standard model. At the CERN Super Proton Synchroton (SPS), the NA31 collaboration[1] has performed a first measurement of direct CP violation. Another collaboration, NA48[2], is preparing a future experiment to measure direct CP violation in the kaon system with a precision of $\mathrm{Re}(\epsilon'/\epsilon)$ of about 2×10^{-4}. The results obtained by NA31 and the status of NA48 are presented here.

1 – CP violation in the neutral K system

CP violation was discovered by J.H.Christenson, V.Fitch, J.Cronin and R.Turlay in 1964 [1]. Since then, both experimental and theoretical aspects of CP violation have been studied continously. The mass and lifetime eigenstates K_S and K_L are mixtures of the CP eigenstates K_1 and K_2 which are themselves mixtures of the strong interaction eigenstates K^0 and $\overline{K^0}$.

$$K_S \propto K_1 + \epsilon K_2 \propto 1/\sqrt{2}\,[K^0 + \overline{K^0} + \epsilon(K^0 - \overline{K^0})] \quad (1)$$

$$K_L \propto K_2 + \epsilon K_1 \propto 1/\sqrt{2}\,[K^0 - \overline{K^0} + \epsilon(K^0 + \overline{K^0})] \quad (2)$$

CP violation can occur in two ways, indirect (via the decay of the admixture of the opposite CP eigenstate (ϵ)) and direct (via the direct decay of a CP eigenstate into a final state of opposite CP (ϵ')). Unfortunately, the study of direct

[1]CERN, Edinburgh, Mainz, Orsay, Pisa, Siegen

[2]Cagliari, Cambridge, CERN, Dubna, Edinburgh, Ferrara, Mainz, Orsay, Perugia, Pisa, Saclay, Siegen, Torino and Vienna

CP violation has turned out to be difficult (both experimentally and theoretically), and the understanding of its magnitude and origin still is far from satisfactory. Experimentally the double ratio :

$$R = \frac{N_{(K_L \to \pi^0\pi^0)}}{N_{(K_S \to \pi^0\pi^0)}} \Big/ \frac{N_{(K_L \to \pi^+\pi^-)}}{N_{(K_S \to \pi^+\pi^-)}} \approx 1 - 6\mathrm{Re}(\epsilon'/\epsilon) \qquad (3)$$

is measured.

Different experiments determine the double ratio R (3) in different ways. The NA31 collaboration at CERN chose to use separate K_L and K_S beams and to measure the charged and neutral decays concurrently. The E731 collaboration at FNAL measured charged and neutral decays separately but in concurrent beams. The last twenty percent of the data was taken measuring all four decay modes concurrently. Both next generation experiments, NA48 at CERN and KTEV at FNAL, will also use this approach.

Due to the different approaches, the systematic error sources are very different. The method adopted by the NA31 collaboration keeps Monte Carlo corrections to a minimum and there are no tagging ambiguities, but it puts severe requirements on detector stability and the understanding of accidental events. In contrast to NA31, the E731 approach keeps the sensitivity to detector and beam variations to a minimum but involves a-priori large Monte Carlo corrections and requires an excellent understanding of the regenerator background and tagging ambiguities. For the new generation of experiments (NA48 and KTEV) the largest single difference is the way in which the K_S beam is produced. The NA48 collaboration uses a bent crystal and a separate target, whereas KTEV will use a regenerator.

2 – The NA31 experiment

The NA31 proposal dates from the end of 1981. After a first run in 1985 data for the double ratio measurement was taken in 1986 and data for the measurement of the phases Φ_{+-} and Φ_{00} [2] was taken in 1987. The detector was upgraded in 1988 and the "first evidence for direct CP violation" [3] was published. A new round of data taking for the double ratio measurement with the improved detector followed in 1989 and 1990. In addition to the ϵ'/ϵ and phase measurements, the collaboration published many results concerning rare K decays [4] including the first observations of $K_S \to \gamma\gamma$ [5], $K_L \to \pi^0\gamma\gamma$ [6] and $K_L \to eeee$ [7]. There are more results to be published in the near future [8].

2.1 The NA31 detector

The main features of the NA31 apparatus [9] are :

- the concurrent detection of charged $K \to \pi^+\pi^-$ and neutral $K \to \pi^0\pi^0$ decay modes running alternately in K_L and K_S beams,
- a long fiducial region of 50 m to maximize the $K_L \to \pi^+\pi^-, \pi^0\pi^0$ statistics,
- no regenerator to keep the background low,
- a movable K_S target to cover the K_L decay region to keep acceptance corrections minimal,
- a highly efficient and stable detector,
- no magnet, two wire chambers with a position resolution of about 0.5 mm per projection,
- a good electromagnetic liquid argon/lead calorimeter with an energy resolution of $\sigma(E)/E = 7.5\ \%/\sqrt{E\ [\mathrm{GeV}]} \oplus 140\ \mathrm{MeV}/E\ [\mathrm{GeV}] \oplus 0.5\ \%$,
- a scintillator/iron hadron calorimeter with an energy resolution for pions of $\sigma(E)/E = 65\ \%/\sqrt{E\ [\mathrm{GeV}]}$,
- a transition radiation detector [10] to obtain additional e π separation (added in 1988).

Figure 1 shows the NA31 detector arrangement.

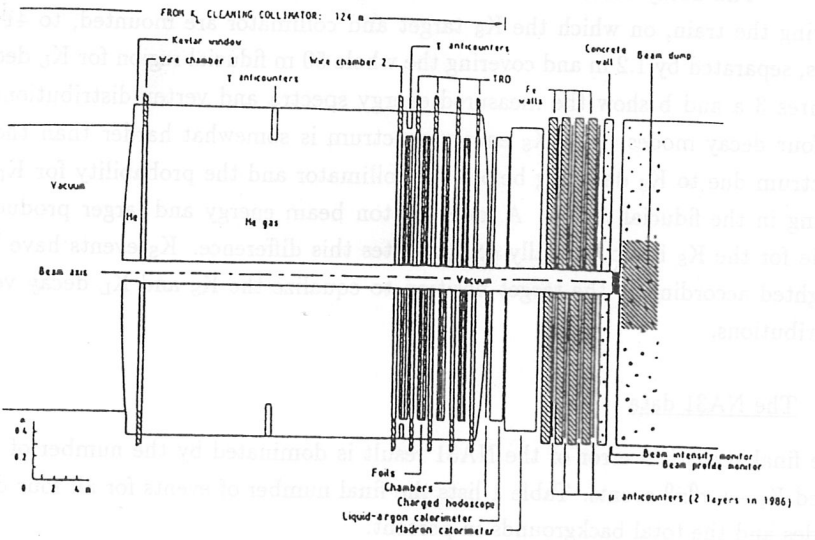

Figure 1: NA31 detector arrangement.

Figure 2 shows a schematic overview of the NA31 experiment with the movable K_S target.

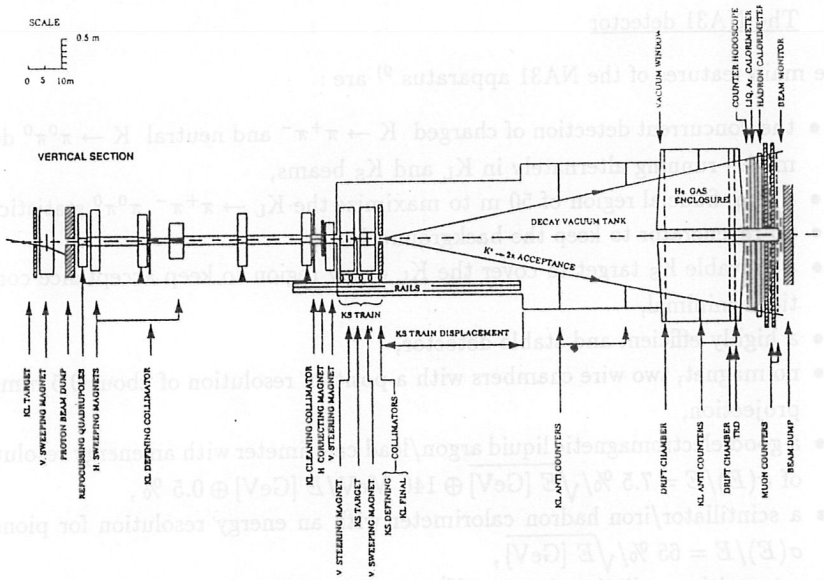

Figure 2: Schematic overview of experiment NA31.

The decay vertex distributions of K_L and K_S decays are made similar by moving the train, on which the K_S target and collimator are mounted, to 41 stations, separated by 1.2 m and covering the whole 50 m fiducial region for K_L decays. Figures 3 a and b show the measured energy spectra and vertex distributions for all four decay modes. The K_S energy spectrum is somewhat harder than the K_L spectrum due to K_S decaying before the collimator and the probability for K_L decaying in the fiducial region. A lower proton beam energy and larger production angle for the K_S beam partially compensates this difference. K_S events have been weighted according to the target position to equalize the K_S and K_L decay vertex distributions.

2.2 The NA31 data

The final statistical error of the NA31 result is dominated by the number of measured $K_L \to \pi^0\pi^0$ events. Table 1 lists the final number of events for all four decay modes and the total backgrounds in percent.

The largest background originates from $K_L \to \pi^0\pi^0\pi^0$ events in the $K_L \to \pi^0\pi^0$ sample. Figures 4 a and b show the distributions of (a) $K_S \to \pi^0\pi^0$ events and (b) $K_L \to \pi^0\pi^0$ events as a function of the χ^2 of the two π^0 masses.

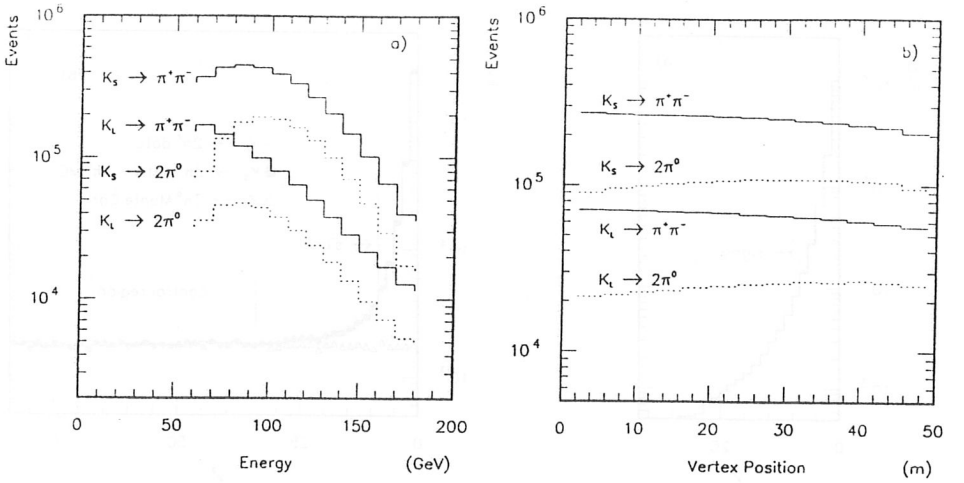

Figure 3: Measured energy spectra (a) and vertex distributions (b).

Table 1: Final NA31 event statistics.

decay mode	number of events	total background (%)
$K_L \to \pi^0\pi^0$	319 000	2.67
$K_L \to \pi^+\pi^-$	847 000	0.63
$K_S \to \pi^0\pi^0$	1 322 000	0.07
$K_S \to \pi^+\pi^-$	3 241 000	0.03

Table 2 lists the different backgrounds for the $K_L \to \pi^+\pi^-$ sample. It is dominated by the K_{e3} background. All systematic uncertainties and magnitudes of corrections are given in table 3.

Table 2: $K_L \to \pi^+\pi^-$ background.

source	contribution (%)
$\pi^+\pi^-\pi^0$	0.04
$\pi e \nu$	0.40
$\pi \mu \nu$	0.10
neutron interactions	0.09

A crucial point of the experiment is a good understanding of the correction for changes in the measured double ratio R introduced by accidental activity in the detector. Figures 5 a and b show the amount of accidental losses and the corrected

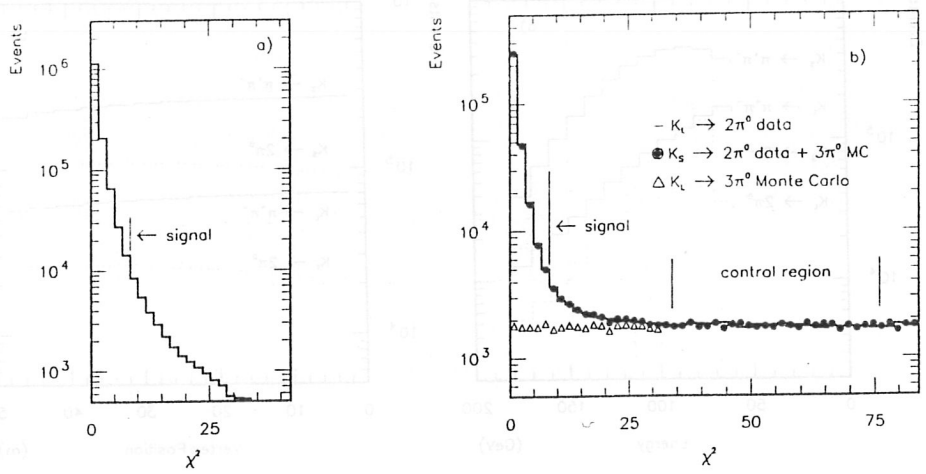

Figure 4: Distributions of (a) $K_S \rightarrow \pi^0\pi^0$ and (b) $K_L \rightarrow \pi^0\pi^0$ events as a function of the χ^2 of the two π^0 masses.

double ratio R as a function of the beam intensity. The losses increase with the beam intensity as expected and are nearly identical for charged and neutral decays. No intensity dependence of the double ratio R remains after correction for accidental losses.

2.3 The final NA31 results

The final result obtained from the 1988 and 1989 data samples [11] is :

$$R = 0.9878 \pm 0.0026 \pm 0.0030, \tag{4}$$

$$\mathrm{Re}(\epsilon'/\epsilon) = (2.0 \pm 0.7) \times 10^{-3}. \tag{5}$$

Table 3: Summary of sources and magnitudes of corrections and systematic uncertainties in the double ratio R.

source	correction (%)	systematic uncertainty (%)
background to $K_L \rightarrow \pi^0\pi^0$	2.67	0.13
background to $K_L \rightarrow \pi^+\pi^-$	0.63	0.10
accidental activity	0.16	0.14
energy scale calibration and stability		0.13
trigger and K_S anticounter inefficiencies	0.51	0.09
Monte Carlo acceptance	0.14	0.10
wire chamber inefficiency		0.10
total systematic uncertainty on R		0.30

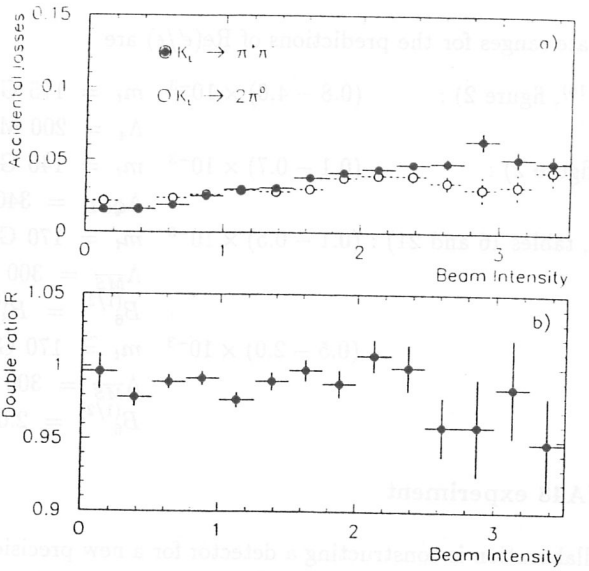

Figure 5: Accidental losses (a) and the double ratio R (b) as a function of the beam intensity.

Combining this result with the previous result from the 1986 data [3] leads to :

$$R = 0.9862 \pm 0.0039, \tag{6}$$

$$\mathrm{Re}(\epsilon'/\epsilon) = (2.3 \pm 0.65) \times 10^{-3}. \tag{7}$$

A common systematic uncertainty of 0.0028 in R has been taken into account.

2.4 Summary of experimental and theoretical results

The latest and most precise measurements are :

$$\mathrm{Re}(\epsilon'/\epsilon) = (2.30 \pm 0.65) \times 10^{-3} \quad \text{CERN NA31 [11]},$$
$$\mathrm{Re}(\epsilon'/\epsilon) = (0.74 \pm 0.59) \times 10^{-3} \quad \text{FNAL E731 [12]}.$$

Theoretical predictions [13, 14, 15, 16] involve the calculation of penguin diagrams (electroweak and QCD) and of hadronic matrix elements. The accuracy of the result depends mainly on the uncertainties of m_t, $\Lambda_{\overline{MS}}$, m_s, $B_6^{(1/2)}$, $B_8^{(3/2)}$, B_K, $|V_{cb}|$ and $|V_{ub}/V_{cb}|$ [15]. Two groups, Rome [14] and Munich [15], have done next to leading order (NLO) calculations, whereas the Dortmund group [16] argues that the uncertainties of the hadronic matrix elements are too large to go to NLO calculations.

The approximate ranges for the predictions of $\mathrm{Re}(\epsilon'/\epsilon)$ are :

Dortmund ([16], figure 2) :	$(0.8 - 4.6) \times 10^{-3}$	$m_t = 175$ GeV, $\Lambda_4 = 200$ MeV,
Rome ([14], figure 2) :	$(0.1 - 0.7) \times 10^{-3}$	$m_t = 140$ GeV, $\Lambda_{QCD} = 340$ MeV,
Munich ([15], tables 16 and 21) :	$(0.1 - 0.5) \times 10^{-3}$	$m_t = 170$ GeV, $\Lambda_{\overline{MS}} = 300$ MeV, $B_6^{(1/2)} = B_8^{(3/2)} = 1.0$,
	$(0.5 - 2.0) \times 10^{-3}$	$m_t = 170$ GeV, $\Lambda_{\overline{MS}} = 300$ MeV, $B_6^{(1/2)} = 2.0$, $B_8^{(3/2)} = 1.0$.

3 – The NA48 experiment

The NA48 collaboration is constructing a detector for a new precision measurement of direct CP violation at the CERN SPS [17]. The main aim of the experiment is to measure $\mathrm{Re}(\epsilon'/\epsilon)$ to better than 2×10^{-4}. This precision requires more than 2×10^6 $\mathrm{K_L} \to \pi^0\pi^0$ decays which will be obtained by running the experiment with ten times the intensity and event rates as compared to NA31 [9]. Therefore, again compared to NA31, all systematic uncertainties will be decreased by a factor of three. The NA48 collaboration intends to achieve these improvements by :

- the concurrent detection of all four decay modes ($\mathrm{K_{L,S}} \to \pi^0\pi^0, \pi^+\pi^-$) in the same detector,
- using nearly collinear $\mathrm{K_L}$ and $\mathrm{K_S}$ beams,
- tagging the proton which produces the $\mathrm{K_S}$,
- using a magnet spectrometer to reduce the background for the charged decays ($\mathrm{K_{L,S}} \to \pi^+\pi^-$) to the per mille level,
- using a fast liquid krypton calorimeter to detect the gammas from the π^0 decays with an excellent energy and space resolution,
- using a fully pipelined 40 MHz FADC readout and trigger,
- weighting the $\mathrm{K_L}$ decays to obtain a similar vertex distribution in z as for the $\mathrm{K_S}$.

Figure 6 shows a schematic overview of the NA48 experiment.

3.1 The NA48 proton tagging counter

The proton tagging counter [17, 18] upstream of the $\mathrm{K_S}$ target will measure the time of passage of the proton producing the $\mathrm{K_S}$. The corresponding event seen in the

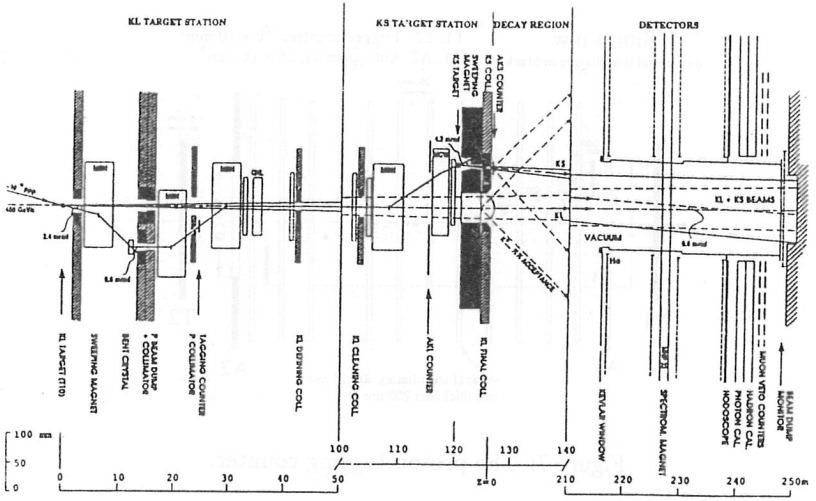

Figure 6: Schematic overview of experiment NA48.

detector will be identified by requiring the difference of the proton's time of passage and the event time in the detector to be equal to the time of flight between the tagging counter and the detector (about 250 m). The performance requirements are :

- a high rate capability (3×10^7 protons per 2.5 s pulse) with deadtime-less readout,
- a time resolution of better than 500 ps,
- resolving overlapping pulses down to 5 ns,
- using light material to preserve the proton beam quality,
- radiation hardness (1 SPS burst corresponds to 1 Gy),
- high efficiency.

In order to fulfill these requirements a design was chosen which consists of two sets of twelve staggered scintillation counters arranged alternately in horizontal and vertical orientation. Figure 7 shows the arrangement of the scintillation counters in the tagging counter.

A prototype of the tagging counter system was tested successfully [18]. A geometrical alignment of better than 0.5 mrad, a light yield of more than 300 photoelectrons and a time resolution of better than 100 ps were achieved. In addition a 6 bit 450 MHz FADC system was tested. It showed an intrinsic time resolution of 50 ps and overlapping pulses could be separated down to 7 ns. This figure will be improved by using 8 bit 1 GHz FADC's of which a prototype was tested successfully.

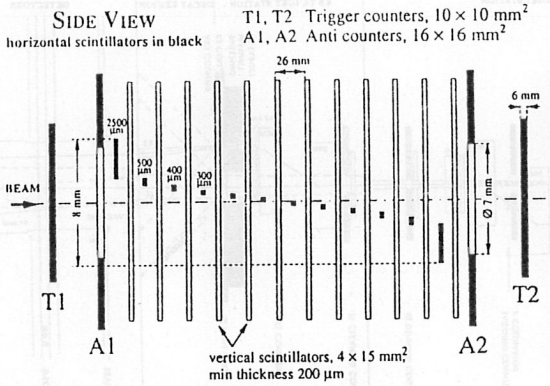

Figure 7: The proton tagging counter.

3.2 The NA48 magnetic spectrometer

The magnetic spectrometer [17] consists of a large aperture (2.4 m) dipole magnet and four high precision, high rate drift chambers. The magnetic field (corresponding to about 250 MeV transverse momentum) was measured. The field map agrees with the TOSCA simulation everywhere in the fiducial area to within 3 parts per thousand. All four drift chambers consist of four double planes. The orientations of the planes are : xx (0°), yy (90°), uu (-45°) and vv (45°). Each plane has a central hole for the neutral-beam pipe. A small prototype of the chamber gave a resolution of better than 100 μm and a full scale mechanical model of the central ring showed that the wires can be positioned on the ring with the same precision as in the small prototype. The production of the large chambers has started and the spectrometer should be completed during 1995.

3.3 The NA48 electromagnetic liquid krypton calorimeter

The proposed electromagnetic calorimeter [17, 19, 20] has an active volume of liquid krypton with an octagonal fiducial area 2.4 m across (diameter of an inscribed circle). The depth is 27 radiation lengths corresponding to 1.25 m of liquid krypton. The singles rate is expected to be about 1 MHz. The photon energy range is 2 to 100 GeV with an average of about 25 GeV. The energy resolution is required to be significantly better than $7.5\ \%/\sqrt{E[\mathrm{GeV}]}$ as achieved in NA31 [9]. The pulse height response must be calibrated and stable to better than one per mille. The space resolution should be better than 1 mm and it should be possible to resolve two photons separated by more than about 4 cm. The time resolution should be

better than 1 ns for photon energies above 10 GeV.

To achieve these design goals, a liquid krypton calorimeter of high granularity with a 2 cm × 2 cm readout tower structure is being built. Altogether there will be about 13500 towers. This segmentation ensures the high rate capability, good space resolution and photon separation. The use of liquid krypton in a quasi-homogeneous structure (the only other materials are thin readout electrodes) minimizes sampling fluctuations as needed to achieve the excellent energy resolution required. The total volume of liquid krypton will be about 10 m^3 (24 tons). Low detector capacitance of about 80 pF per cell and the use of cold preamplifiers with short connections result in a high speed readout. The initial current readout technique [21, 22] is used with a pulse shaping of 40 ns peaking time and total width of about 160 ns (the total drift time across the gap has been measured to be 3.0 μs at 3000 V [20]).

The design adopted for the full-size calorimeter consists of tower cells formed by single full-metal strips tensioned in beam direction with a slight zigzag of 50 mrad. Figure 8 shows the prototype which was tested in an electron beam.

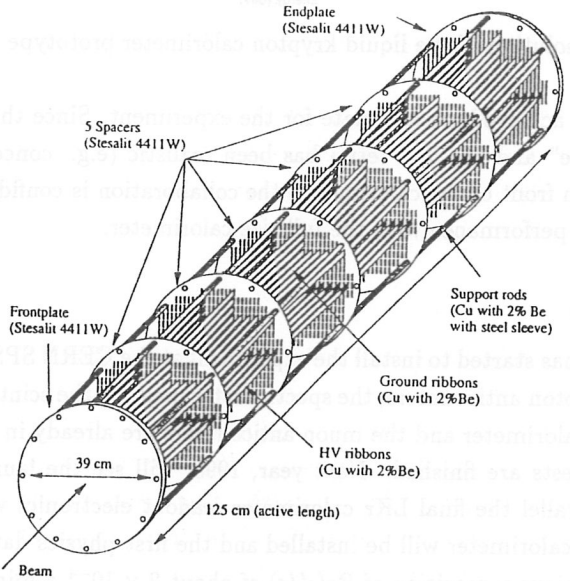

Figure 8: Liquid krypton calorimeter prototype.

The main results obtained with the prototype calorimeter are :

energy resolution : $\sigma(E)/E = 3.5\ \%/\sqrt{E\ [\mathrm{GeV}]} \oplus 40\ \mathrm{MeV}/E\ [\mathrm{GeV}] \oplus 0.4\ \%$,

space resolution : $\sigma_x(E) = 4.1\ \mathrm{mm}/\sqrt{E\ [\mathrm{GeV}]} \oplus 0.5\ \mathrm{mm}$,

$\sigma_y(E) = 4.5\ \mathrm{mm}/\sqrt{E\ [\mathrm{GeV}]} \oplus 0.5\ \mathrm{mm}$,

time resolution : $\sigma(E) < 300$ ps for $E > 10\mathrm{GeV}$.

The energy resolution achieved with a prototype is shown in figure 9 as a function of energy. It is in good agreement with the results of a detailed Monte Carlo simulation.

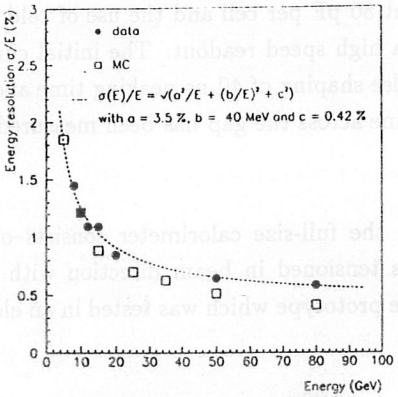

Figure 9: Energy resolution of the liquid krypton calorimeter prototype.

The resolutions achieved are adequate for the experiment. Since the prototype design is "scalable" and the test setup has been realistic (e.g. concerning the amount of material in front of the calorimeter) the collaboration is confident of achieving the same good performance with the full-size calorimeter.

3.4 The NA48 schedule

The NA48 collaboration has started to install the experiment at the CERN SPS. The beam line, part of the photon anticounters, the spectrometer magnet, the scintillator hodoscope, the hadron calorimeter and the muon anticounters are already in place. All detector prototype tests are finished. Next year, 1995, will see the launch of the spectrometer. In parallel the final LKr calorimeter readout electronics will be tested. In 1996 the LKr calorimeter will be installed and the first physics data will be taken. In order to achieve a precision of $\mathrm{Re}(\epsilon'/\epsilon)$ of about 2×10^{-4} a minimum of three years of data taking is required.

3.5 Prospects for rare K decay physics in NA48

Table 4 lists the main properties of the K_L and K_S beams. The beams are not optimised for rare K decay physics. The strength of the experiment will be the background rejection due to the excellent photon energy and position resolutions and the good two photon separation.

Table 4: Characteristics of the NA48 K_L and K_S beams.

	K_L	K_S
protons per pulse	1.5×10^{12}	3×10^7
spill length	≈ 2.5s	
cycle time	14.4s	
accepted K^0 momentum range	70 - 170 GeV/c	
fiducial region	$2\tau_s \approx 12$m	
number of K^0 per pulse	$\approx 2 \times 10^7$	≈ 300
number of K^0 in accepted momentum range per pulse	$\approx 6.4 \times 10^6$	≈ 220
number of K^0 decaying in fiducial region per pulse	$\approx 2.2 \times 10^4$	≈ 190
number of $K^0 \to \pi^0\pi^0$ per pulse	≈ 20	≈ 60
detector acceptance for $K^0 \to \pi^0\pi^0$ decays	20%	
number of accepted $K^0 \to \pi^0\pi^0$ per pulse	≈ 4	≈ 12
number of accepted $K^0 \to \pi^0\pi^0$ per hour	≈ 1000	≈ 3000
number of accepted $K^0 \to \pi^0\pi^0$ per year	$\approx 1.5 \times 10^6$	$\approx 4.5 \times 10^6$
(assuming 120 days with 50 % efficiency)		

The detector acceptances and trigger efficiencies for different rare decay modes are being studied. The main goals are :

- a precise measurement of $\Gamma_{(K_S \to \gamma\gamma)}/\Gamma_{(K_L \to \gamma\gamma)}$,
- a limit on the branching ratio for $K_L \to \gamma\gamma\gamma$ in the order of 10^{-9},
- about 1000 $K_L \to \pi^0\gamma\gamma$ events,
- the observation of $K_L \to \pi^0\pi^0\gamma$,
- a large sample of $K_L \to ee\gamma$ and $K_L \to \mu\mu\gamma$ events,
- a limit on the branching ratio for $K_L \to \pi^0 ee$ in the order of 10^{-10},
- limits on or measurements of $K_L \to \pi^0\mu\mu$, $K_L \to \pi^0\nu\bar{\nu}$, $K_L \to eeee$, $K_L \to ee\mu\mu$, $K_L \to \pi\pi ee$, $K_L \to \pi\pi\mu\mu$, $K_L \to \pi e\nu\gamma$ and $K_L \to \pi\mu\nu\gamma$ decays,
- limits on K_S decays.

Acknowlegdements

The help of G.Barr is gratefully acknowlegded. I would like to thank B.Cox for the invitation and him and all organizers for making the meeting such a successful and enjoyable event.

References

1. J.H.Christenson et al., PRL **13**, 138 (1964).
2. R.Carosi et al., PL B **237**, 303 (1988).
3. H.Burkhardt et al., PL B **206**, 169 (1988).
4. G.D.Barr et al., PL B **214**, 303 (1988).
   G.D.Barr et al., PL B **240**, 283 (1990).
   G.D.Barr et al., PL B **284**, 440 (1992).
   G.D.Barr et al., PL B **304**, 381 (1993).
   G.D.Barr et al., PL B **328**, 528 (1994).
5. H.Burkhardt et al., PL B **199**, 139 (1987).
6. G.D.Barr et al., PL B **242**, 523 (1990).
7. G.D.Barr et al., PL B **259**, 389 (1991).
8. K.Kleinknecht, these proceedings.
9. H.Burkhardt et al., NIM A **268**, 116 (1988).
10. G.D.Barr et al., NIM A **294**, 465 (1990).
11. G.D.Barr et al., PL B **317**, 233 (1993).
12. L.K.Gibbons et al., PRL **70**, 1203 (1993).
13. T.Inami and C.S.Lim, Prog.Theor.Phys. **65**, 297, 1772(E) (1981).
    J.M.Flynn and L.Randall, PL B **224**, 221 (1989), B **235**, 412(E) (1990).
14. M.Ciuchini et al., PL B **301**, 263 (1993).
15. A.J.Buras et al., MPI-Ph/93-11.
16. J.Heinrich et al., PL B **279**, 140 (1992).
17. G.D.Barr et al., CERN/SPSC/90-22/P253.
18. P.Grafström et al., NIM A **344**, 487 (1994).
19. P.Buchholz, NIM A **316**, 1 (1992).
    G.D.Barr et al., NIM A **323**, 393 (1992).
    A.Ceccucci, Proceedings of the 6th Pisa Meeting on Advanced Detectors, La Biodola, Isola d'Elba, May 1994.
    M.Martini, Proceedings of the 4th International Conference on Advanced Technology and Particle Physics, Como, October 1994.
20. V.Fanti et al., NIM A **344**, 507 (1994).
21. C.Cerri et al., NIM **227**, 227 (1984).
22. V.Radeka et al., NIM A **265**, 228 (1988).

SESSION X

- L. Littenberg
  Overview of Rare K Decays
- D. Lazarus
  Results/Prospects in E777/851/865
- W. Molzon
  Leptonic Decays of Neutral Kaons - Recent Results and Expected Experimental Progress
- M. Ito
  Results from BNL E787, a Search for $K^+ \rightarrow \pi^+ \nu \bar{\nu}$
- R. Tschirhart
  The Fermilab Rare Kaon Decay Program
- K. Kleinknecht
  Results on Rare Decays of Neutral Kaons from the NA31 Experiment at CERN

Frascati Physics Series, Vol. III (1994)
HEAVY QUARKS AT FIXED TARGET
University of Virginia, October 7–10, 1994
(pp. 303–326)

OVERVIEW OF RARE K DECAYS

Laurence Littenberg
Physics Department, Brookhaven National Laboratory
Upton, NY 11973

ABSTRACT

The status and future prospects of searches for and studies of forbidden and highly suppressed K decays are reviewed.

1 – Introduction

In this review I discuss three areas of recent activity in rare K decay. These are lepton-flavor violating decays, which are entirely forbidden in the Standard Model, $K_S \to \pi^+\pi^-\pi^0$, which is of interest from the point of view of CP-violation, and "one loop" decays of the form $K^{0,\pm} \to (\pi^{0,\pm})\ell\bar{\ell}$, that can throw light on Standard Model CP-violation and determine parameters such as V_{td}.

2 – Lepton flavor violation

Although the violation of separate lepton flavor (LFV) is not allowed in the Standard Model, we know of no fundamental reason why such processes should not exist [1] and most proposed extensions [2] of the Standard Model predict LFV at some level. The search for LFV in the decays of muons and kaons has a long history and has been pursued to remarkable sensitivities. Fig. 1 depicts $K_L \to \mu e$ via the exchange of a hypothetical horizontal gauge boson, X, compared to $K^+ \to \mu\nu$ via W exchange.

Assuming a V-A interaction:

$$\begin{aligned} B(K_L \to \mu e) &= \left(\frac{g^X_{sd} g^X_{\mu e}}{g^2 sin\theta_C}\right)^2 \left(\frac{M_W}{M_X}\right)^4 \frac{\tau_{K_L}}{\tau_{K^+}} B(K^+ \to \mu^+\nu) \\ &= 3.3 \times 10^{-11} \left(\frac{91\ TeV}{M_X}\right)^4 \left(\frac{g^X_{sd} g^X_{\mu e}}{g^2}\right)^2 \end{aligned} \quad (1)$$

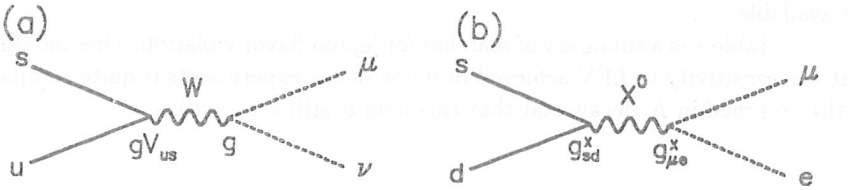

Figure 1: (a) $K^+ \to \mu^+\nu$ decay, (b) $K_L \to \mu e$ via the exchange of a boson, X.

Since the latest limit [3] on $B(K_L \to \mu e)$ is 3.3×10^{-11}, assuming that $g^X_{sd} \approx g^X_{\mu e} \approx g$, one is already probing scales of order 100 TeV for a LFV interaction. Sensitivity to $B(K_L \to \mu e)$ is expected to reach $\sim 10^{-12}$/event in the next couple of years. The corresponding exercise on $B^0 \to \mu e$ yields:

$$B(B^0 \to \mu e) = 10^{-14}\left(\frac{91\ TeV}{M_X}\right)^4 \left(\frac{g^X_{bd} g^X_{\mu e}}{g^2}\right)^2 \tag{2}$$

This comparison can also be expressed as [4]:

$$\frac{B(B^0 \to \mu e)}{B(K_L \to \mu e)} \approx \frac{\tau_B}{\tau_{K_L}} \frac{m_B}{m_K} \left(\frac{g^X_{bd}}{g^X_{sd}}\right)^2 \tag{3}$$

$$\approx 3 \times 10^{-4} \left(\frac{g^X_{bd}}{g^X_{sd}}\right)^2 \tag{4}$$

Therefore one would need $B(B^0 \to \mu e) < 10^{-14}$ to compete with $B(K_L \to \mu e) < 3.3 \times 10^{-11}$, unless g^X_{bd} is significantly larger than g^X_{sd},

In three-body decays, where the helicity suppression that penalizes heavy parent mass is absent, a similar comparison yields a result more favorable to B's [4]:

$$\frac{B(B \to K\mu e)}{B(K \to \pi\mu e)} \approx \frac{1}{10} \frac{\tau_B}{\tau_{K_L}} \left(\frac{m_B}{m_K}\right)^5 \left(\frac{g^X_{bd}}{g^X_{sd}}\right)^2 \tag{5}$$

$$\approx \left(\frac{g^X_{bd}}{g^X_{sd}}\right)^2 \tag{6}$$

The factor $\frac{1}{10}$ reflects the B's preference for decaying to heavy hadronic systems. Thus for the three-body decays, equal branching ratios have about equal reach for LFV. The comparative experimental situation is illustrated by Fig. 2 which shows the most recent data on $B^- \to K^- e\mu$ from CLEO [5] and on $K^+ \to \pi^+ e\mu$ from AGS-777 [6]. Each plot is a distribution of the final state effective mass versus a second variable that also distinguishes signal from background. In each case background events approach or even enter the signal region. The difference is that the K sensitivity is roughly five orders of magnitude better than that of the B result (it will soon almost seven orders of magnitude, if AGS-865 meets its goal). This is primarily due to the current relative abundance of Ks and Bs. However, even if one had the requisite 50,000-fold increase in B-statistics, the signal box would contain 10^5 background events. This illustrates the advantages of a dedicated detector, where particle identification factors of $\geq 10^7$ are available.

Table 1 is a summary of searches for lepton flavor violation. One should note that the sensitivity to LFV achieved in muon decay experiments is quite comparable to that reached in K decay, and that this field is still very active.

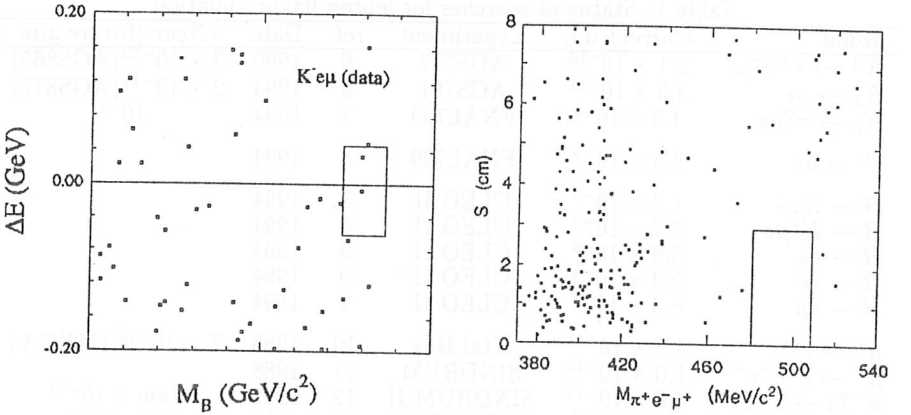

Figure 2: Search for lepton flavor violation in Bs and Ks. The left hand plot shows the result of the CLEO search for $B^- \to K^- e\mu$. The ordinate is the difference between the energy of the beam and that of the final state particles and the abscissa is the $Ke\mu$ effective mass. The right hand plot shows the result of the AGS-777 search for $K^+ \to \pi^+ e\mu$. The ordinate is the rms distance of closest approach of the three tracks to a common vertex and the abscissa is the three body effective mass.

3 $K_S \to 3\pi$

One should keep in mind how little we actually know about CP-violation if we don't beg the question by assuming that the Standard Model is right. All confirmed observations are consistent with the superweak model [17], *i.e.* they can be explained by state-mixing alone. A number of modern theoretical approaches [18] have consequences very similar to superweak, at least for the K and B systems. Moreover, even if the superweak model is disproved and the KM mechanism [19] turns out to successfully describe the CP-violation we observe, it probably can't account for the baryon asymmetry of the universe [20]. This motivates the search for CP violation in areas where the KM mechanism predicts undetectably small effects.

Two experiments, CPLEAR and FNAL-621 have recently reported results on $K_S \to \pi^+\pi^-\pi^0$. The 3π state is to K_S more or less what the 2π state is to K_L, but there has been far less work on on the former relative to the latter. The reasons are not hard to find. For K_S one must work close to the production target, usually a poor environment. In the case of $K_L \to 2\pi$, one can easily remove K_S "background" by moving a few τ_S downstream, whereas even in the first τ_S, $K_S \to 3\pi$ is overwhelmed

Table 1: Status of searches for lepton flavor violation

Mode	Current u.l.	Experiment	ref.	Date	(Near-)future aim
$K^+ \to \pi^+ e^- \mu^+$	2.1×10^{-10}	AGS777	6	1990	3×10^{-12}(AGS865)
$K_L \to \mu e$	3.3×10^{-11}	AGS791	3	1993	2×10^{-12}(AGS871)
$K_L \to \pi^0 \mu e$	3.5×10^{-9}	FNAL799	7	1994	10^{-11}
$\pi^0 \to \mu e$	8.6×10^{-9}	FNAL799	8	1994	
$B \to K \mu e$	1.2×10^{-5}	CLEO II	5	1994	
$B \to K^* \mu e$	2.7×10^{-5}	CLEO II	5	1994	
$B \to \mu e$	5.9×10^{-6}	CLEO II	9	1994	
$B \to \tau e$	5.3×10^{-4}	CLEO II	9	1994	
$B \to \tau \mu$	8.3×10^{-4}	CLEO II	9	1994	
$\mu^+ \to e^+ \gamma$	4.9×10^{-11}	Xtal Box	10	1988	7×10^{-13} (MEGA)
$\mu^+ \to e^+ e^- e^+$	1.0×10^{-12}	SINDRUM	11	1988	
$\mu^- Ti \to e^- Ti$	4.3×10^{-12}	SINDRUM II	12	1993	$few \times 10^{-14}$
$\mu^+ e^- \to \mu^- e^+$	3.3×10^{-7}	PSI R-89-06	13	1994	3×10^{-9}
$Z^0 \to \mu e$	3.9×10^{-6}	L3	14	1994	
$Z^0 \to e \tau$	8.6×10^{-6}	L3	14	1994	
$Z^0 \to \mu \tau$	1.1×10^{-5}	L3	14	1994	
$\tau \to \mu \gamma$	4.2×10^{-6}	CLEO II	15	1993	
$\tau \to \mu \mu \mu$	4.3×10^{-6}	CLEO II	16	1994	
$\tau \to \mu \mu e$	3.5×10^{-6}	CLEO II	16	1994	
$\tau \to \mu e e$	3.4×10^{-6}	CLEO II	16	1994	
$\tau \to e e e$	3.3×10^{-6}	CLEO II	16	1994	

by $K_L \to 3\pi$. Moreover, only the $3\pi^0$ state is pure CP $-$. The $J = 0$ $\pi^+\pi^-\pi^0$ system is quite complicated. There is a CP+ component which, although suppressed by angular momentum (since $\ell_{\pi^+\pi^-} = 1, 3, ..$) and the $\Delta I = \frac{1}{2}$ rule (since $I = 2$), still dominates the CP-violating ($\ell = 0$, $I = 1$) component. From state-mixing alone, one predicts a CP-violating branching ratio, $B(K_S \to \pi^+\pi^-\pi^0)_\epsilon = |\epsilon|^2 \frac{\Gamma_L}{\Gamma_S} B(K_L \to \pi^+\pi^-\pi^0) \approx 10^{-9}$, while theoretical estimates [21] of the CP-conserving branching ratio are in the $few \times 10^{-7}$ range. In practice, one measures the interference between the K_S and K_L, so that the CP-conserving component can be removed by integrating over the Dalitz Plot (assuming that the acceptance is well enough understood). Then, by analyzing separately the proper time distribution of the halves of the Dalitz Plot with $E_{\pi^+} - E_{\pi^-} > 0$ and < 0, the CP-conserving branching ratio can be extracted. Figs. 3 and 4 show the results of this procedure for the two experiments. In each case evidence for a signal can be seen at early proper time. The branching ratios calculated from the observed interference amplitudes are: $B(K_S \to \pi^+\pi^-\pi^0)_{CPcons.} = (3.9^{+5.4\,+0.9}_{-1.8\,-0.7}) \times 10^{-7}$ (FNAL 621 [22]) and $B(K_S \to \pi^+\pi^-\pi^0)_{CPcons.} = (8.2^{+6.0\,+7.3}_{-4.4\,-4.9}) \times 10^{-7}$ (CPLEAR [23]) where in each case the first error is statistical and the second systematic. Thus, $K_S \to \pi^+\pi^-\pi^0$ has been seen for the first time.

However, the primary objective of these experiments is to search for the

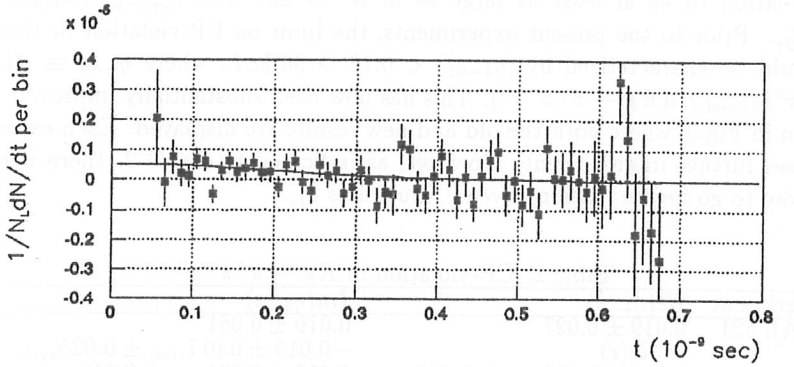

Figure 3: FNAL-621: difference of time distributions of $K \to \pi^+\pi^-\pi^0$ with $E^{cm}_{\pi^+} > E^{cm}_{\pi^-}$ and those with $E^{cm}_{\pi^-} > E^{cm}_{\pi^+}$

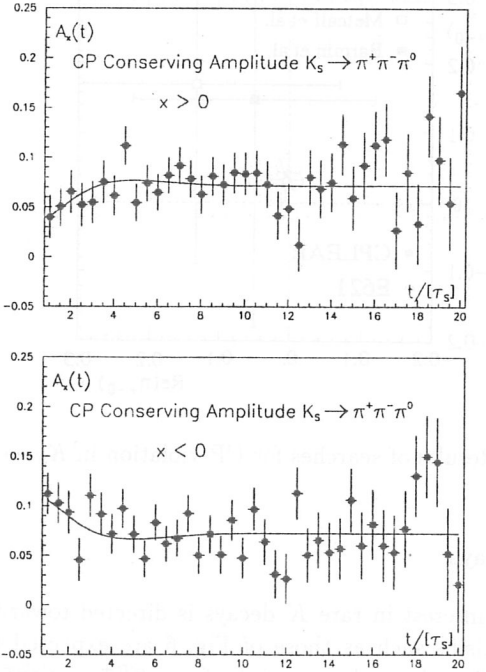

Figure 4: CPLEAR: Decay rate asymmetry for $K \to \pi^+\pi^-\pi^0$ with $E^{cm}_{\pi^+} > E^{cm}_{\pi^-}$ and for $E^{cm}_{\pi^-} > E^{cm}_{\pi^+}$

CP-violating component of this decay. The Standard Model predicts [24] the direct CP-violation to be at least as large as in $K \to 2\pi$, with $\epsilon'_{\pi^+\pi^-\pi^0}$ ranging up to $\geq 10\epsilon'_{2\pi}$. Prior to the present experiments, the limit on CP-violation in this channel could be characterized by $|\eta_{+-0}|^2 < 0.12$ @ 90%c.l., where $\eta_{+-0} \equiv A(K_S \to \pi^+\pi^-\pi^0)_{CPviol.}/A(K_L \to \pi^+\pi^-\pi^0)$. This has now been substantially improved, as can be seen in Fig.5, where both the old and new results are displayed. Each experiment promises further improvement. However, as indicated by Table 2, there is quite a long way to go before reaching even ϵ, much less $\epsilon'_{2\pi}$.

Table 2: CP-violation in $K_S \to \pi^+\pi^-\pi^0$

Experiment	$Re(\eta_{+-0})$	$Im(\eta_{+-0})$	ref.
FNAL 621	0.019 ± 0.027	0.019 ± 0.061	25
"	$\equiv Re(\epsilon)$	$-0.015 \pm 0.017_{stat.} \pm 0.025_{syst.}$	25
CPLEAR	$0.005 \pm 0.022_{stat.} \pm 0.007_{syst.}$	$0.016 \pm 0.024_{stat.} \pm 0.018_{syst.}$	23
ϵ	0.0016	0.0017	26

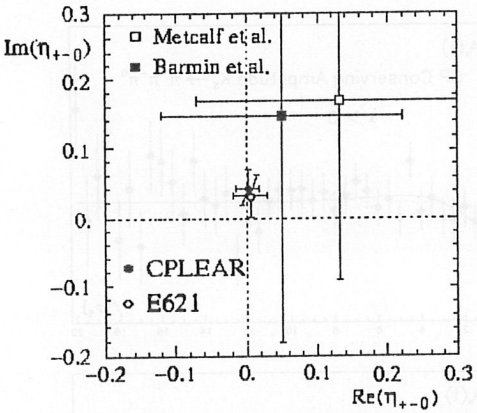

Figure 5: Results of searches for CP-violation in $K_S \to \pi^+\pi^-\pi^0$

4 – One-loop decays

Much of the current interest in rare K decays is directed toward the study of one-loop effects. Mechanisms such as those of Fig. 6 are expected to dominate, or at least contribute significantly to decays of the form $K^{0,\pm} \to (\pi^{0,\pm})\ell\bar{\ell}$. In the SM the calculation of these diagrams is very clean; QCD corrections are small or moderate, and hadronic matrix elements can be reliably obtained from the rates of common K decay modes. The t-quarks in the loops make the processes sensitive to parameters

like m_t and V_{td}. $K_L \to \pi^0 \ell\bar{\ell}$ is CP-violating to first order, and provides potentially very useful probes of this phenomenon. In addition, numerous non-SM contributions to $K^{0,\pm} \to (\pi^{0,\pm})\ell\bar{\ell}$ have been predicted over the years. Since experiments have not yet reached the Standard Model level for most of these modes, the potential for the discovery of new physics remains.

The exploration of these modes motivates the study of a number of other decays. In some cases these constitute experimental backgrounds to the one-loop processes (e.g. $K_L \to \ell^+\ell^-\gamma\gamma$ as background to $K_L \to \pi^0\ell^+\ell^-$ or $K^+ \to \pi^+\gamma\gamma$ as background to $K^+ \to \pi^+\nu\bar{\nu}$). Others can be used to establish the size of possible long-distance competition to the one-loop effects (e.g. $K_L \to \pi^0\gamma\gamma$, which scales the CP-conserving contribution to $K_L \to \pi^0\ell^+\ell^-$).

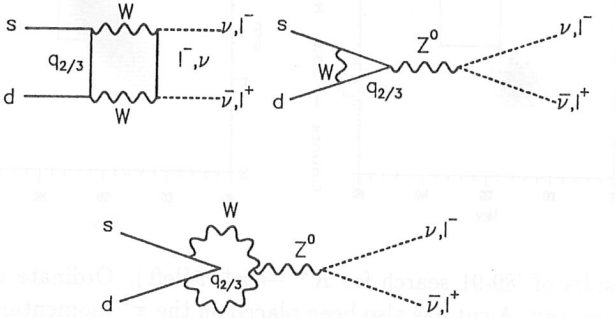

Figure 6: One-loop contributions to $K^{0,\pm} \to (\pi^{0,\pm})\ell\bar{\ell}$

4.1 $K^+ \to \pi^+\nu\bar{\nu}$

In $K^+ \to \pi^+\nu\bar{\nu}$, long-distance 'background' is negligible [27] so that the short-distance contributions (SM or non-SM) are completely unobscured. The QCD corrections are relatively small and well determined. Recent calculations by Buchalla and Buras [28] beyond leading logarithms indicate theoretical uncertainties $\leq 7\%$ for typical SM parameters. The branching ratio is particularly sensitive to the value of $|V_{td}|$, and offers perhaps the cleanest way of determining this parameter.

The branching ratio is given by:

$$B(K^+ \to \pi^+\nu\bar{\nu}) = \frac{\alpha^2 B(K^+ \to \pi^0 e^+\nu)}{V_{us}^2 2\pi^2 sin^4\theta_W} \sum_\ell |V_{cs}^* V_{cd} X_{NL}^\ell + V_{ts}^* V_{td} X(x_t)|^2 \quad (7)$$

where $x_t \equiv (m_t/m_W)^2$. For $m_t \sim 174$GeV, $X(x_t) \approx 1.6$. Note that V_{td} occurs in the product $V_{ts}^* V_{td}$. If one assumes a unitary CKM matrix, Eq. 7 can be rewritten:

$$B(K^+ \to \pi^+\nu\bar{\nu}) = 1.2 \times 10^{-10} A^4 [\eta^2 + \frac{2}{3}(\rho_o^e - \rho)^2 + \frac{1}{3}(\rho_o^\tau - \rho)^2] \quad (8)$$

where $\rho_o^\ell \equiv 1 + \frac{X_{NL}^\ell}{A^2\lambda^4 X(x_t)}$ and $X_{NL}^\ell \approx 10^{-3}$.

In leading order in Wolfenstein parameters, $B(K^+ \to \pi^+\nu\bar{\nu})$ determines a circle in the ρ, η plane with center $(\rho_o, 0)$; $\rho_o \equiv \frac{2}{3}\rho_o^e + \frac{1}{3}\rho_o^\tau \approx 1.4$ and radius $= \frac{1}{A^2}\sqrt{\frac{B(K^+\to\pi^+\nu\bar{\nu})}{1.2\times10^{-10}}}$

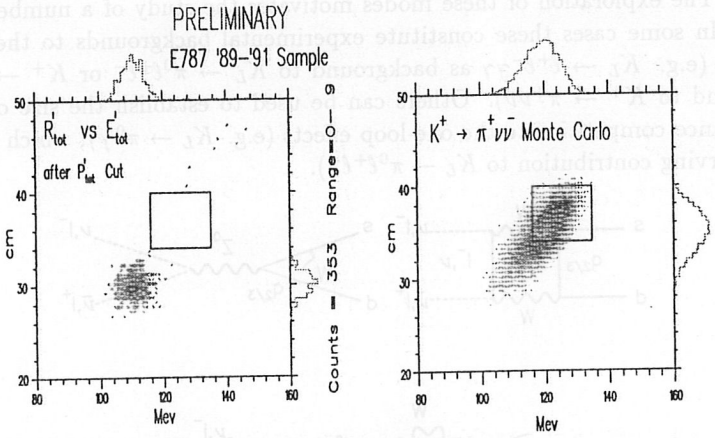

Figure 7: Results of '89-91 search for $K^+ \to \pi^+\nu\bar{\nu}$(left). Ordinate is π^+ range and abscissa is π^+ energy. A cut has also been placed on the π^+ momentum. Signal region is outlined. Peak at lower left is $K^+ \to \pi^+\pi^0$. Events at upper right are from tail of $K^+ \to \mu^+\nu$ and $K^+ \to \mu^+\nu\gamma$. The right hand plot shows a Monte Carlo simulation of the signal. The falloff of events with range < 30cm is due to the trigger.

Detecting this decay at the 10^{-10} level is rather challenging. The only detectable particle, the π^+, is a very common decay product of the K^+. The other two final state particles are undetectable, so there is no kinematic constraint (other than $p^*_{\pi^+} \leq 227\ MeV/c$). The major backgrounds are the common two-body decay modes $K^+ \to \pi^+\pi^0$ (21.2%) and $K^+ \to \mu^+\nu$ (63.5%). To eliminate the former one needs a γ veto capable of suppressing π^0s by a factor of $\sim 10^6$. To eliminate the latter one needs particle identification capability to reject μ^+ by $> 10^8$. AGS-787 has been pursuing this decay mode for several years now. This experiment, currently a collaboration of BNL, INS/Tokyo, KEK, Osaka, Princeton, and TRIUMF, searches for $K^+ \to \pi^+\nu\bar{\nu}$ and related decays with a solenoidal spectrometer [29] in a stopping K^+ beam. Preliminary results from three years' running are now available. Fig. 7 shows a plot of π^+ kinetic energy versus range for $K^+ \to \pi^+\nu\bar{\nu}$ candidates passing particle ID, photon veto and event quality cuts. No candidates survive, resulting in a 90% c.l. upper limit of 3.6×10^{-9}. Combining this with the limit [30] 1.8×10^{-8} previously obtained by E787 for a different kinematic region ($p_{\pi^+} < p_{K\pi 2}$), yields $B(K^+ \to \pi^+\nu\bar{\nu}) < 3.0 \times 10^{-9}$ (@ 90% c.l.). A limit on the process $K^+ \to \pi^+ + X^0$,

where X^0 is a single massless unseen neutral, can also be extracted. The new limit on this SM-violating process is $B(K^+ \to \pi^+ X^0) < 6.1 \times 10^{-10}$ (@ 90% c.l.). These limits represent 50-fold improvements in the sensitivity to $K^+ \to \pi^+ +$ 'nothing' with respect to previous experiments. However, an additional factor 10 in sensitivity will be required to reach the prediction of the Standard Model for $K^+ \to \pi^+ \nu\bar{\nu}$. Therefore an upgraded beam and detector were built to continue this search. The aim is to reach a sensitivity of at least 4×10^{-11}/event. The first run in the new configuration was completed in July 1994.

4.2 $K_L \to \pi^0 \nu\bar{\nu}$

In the Standard Model $K_L \to \pi^0 \nu\bar{\nu}$ is virtually 100% direct CP-violating [31]. There are no significant long distance contributions or indirect CP-violating "background", and only tiny QCD corrections. The branching ratio is given by:

$$B(K_L \to \pi^0 \nu\bar{\nu}) = \frac{\tau_{K_L}}{\tau_{K^+}} \frac{\alpha^2 B(K^+ \to \pi^0 e^+ \nu)}{V_{us}^2 2\pi^2 sin^4\theta_W} \sum_\ell |Im V_{ts}^* V_{td} X(x_t)|^2 \quad (9)$$

$$= 5 \times 10^{-10} A^4 \eta^2 \quad (10)$$

where Eq. 10 assumes CKM unitarity and the CDF value for m_t. Thus a measurement of this branching ratio directly determines η (*modulo* A^2). However, the experimental difficulty of this extremely desirable measurement is even greater than in the charged analog. The initial state energy is difficult or impossible to measure, there is no visible vertex, two of the final state particles cannot be detected so that there are no kinematic constraints, and many backgrounds produce apparently unaccompanied π^0's. Yet one needs to get to the 10^{-12} level. The latest limit is from FNAL 799, in which a search was made for the Dalitz converted version, $K_L \to \pi^0 \nu\bar{\nu} \to e^+ e^- \gamma \nu\bar{\nu}$. This allows a vertex to be obtained at the cost of a factor 80 in statistics. Fig. 8 shows a plot of $ee\gamma$ p_T *vs* mass for candidates from this experiment. The signal box is centered on the π^0 mass and on a p_T beyond that possible for π^0's from most potential backgrounds. The events just below the signal box come from $\Lambda \to n\pi^0$. $Ke3$ events populate the region above and to the right of the signal region. It's clear that future progress will depend on detector improvements as well as on increased K flux. With no events in the signal box, a 90% c.l. limit of $B(K_L \to \pi^0 \nu\bar{\nu}) < 5.8 \times 10^{-5}$ was obtained [32]. Thus there are still 7 orders of magnitude needed to reach the SM level. Many clever schemes for measuring this process have been discussed, but thus far the only proposal for a dedicated experiment has been one at KEK [33]. I believe that this process presents a great opportunity for a relatively small group to do a very important experiment.

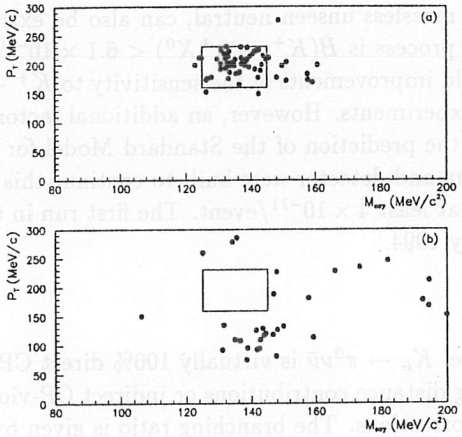

Figure 8: Results of $K_L \to \pi^0\nu\bar{\nu}$ search (from FNAL-799). (a) Monte Carlo, (b) candidates

4.3 $K_L \to \pi^0\ell^+\ell^-$

Since $K_L \to \pi^0\nu\bar{\nu}$ is so hard to detect, how about replacing the elusive neutrinos with charged leptons? Unfortunately, the same interaction that renders the charged leptons detectable complicates the theory considerably. This is not so serious in the case of the direct CP-violating component, since techniques for handling this have been developed over the past few years [34, 35]. Recently there has been a calculation of the rate in which QCD effects are taken into account consistently in the next-to-leading order [36]. Thus, if $B(K_L \to \pi^0 e^+ e^-)_{dir}$ could be isolated, it would indeed be similarly useful to $K_L \to \pi^0\nu\bar{\nu}$. However this proves to be very challenging. Assuming CKM unitarity and the CDF value for m_t:

$$B(K_L \to \pi^0 e^+ e^-)_{dir} \approx 7 \times 10^{-11} A^4 \eta^2 \qquad (11)$$

Comparing Eqs. 10 and 11, one sees $B(K_L \to \pi^0 e^+ e^-)_{dir}$ is several times smaller than $B(K_L \to \pi^0\nu\bar{\nu})$, This makes it difficult to separate from certain competing contributions to $K_L \to \pi^0 e^+ e^-$. These also arise because the final state leptons can couple to photons, as in Fig. 9.

First there is an indirect CP-violating term, $\epsilon A(K_S \to \pi^0 e^+ e^-)$. Unfortunately the approach used to calculate the direct contribution breaks down here because the real parts of the Wilson coefficients get large contributions from regions below m_c, where perturbative QCD can't be trusted. This contribution could be unambiguously determined by a measurement of the CP-conserving decay $K_S \to \pi^0 e^+ e^-$, but the current upper limit on this branching ratio [37], 1.1×10^{-6}, falls at least three orders of magnitude short of the required sensitivity. A rough idea of the ex-

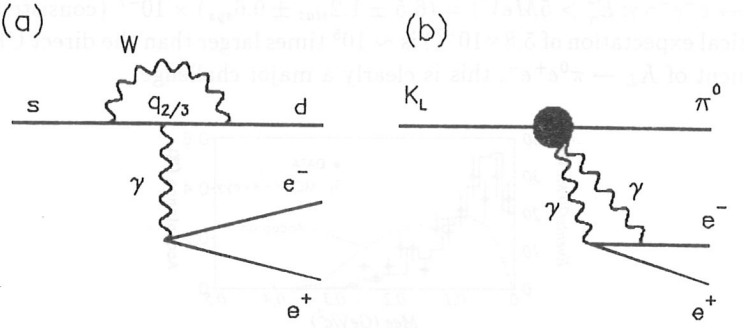

Figure 9: Photon-mediated contributions to $K_L \to \pi^0 e^+ e^-$ (a) CP-violating, (b) CP-conserving.

pected size of this component can be obtained from the well-determined [38] value of $\Gamma(K^+ \to \pi^+ e^+ e^-)$. This yields $B(K_L \to \pi^0 e^+ e^-)_\epsilon \approx 6 \times 10^{-12}$, a number very close to the magnitude of $B(K_L \to \pi^0 e^+ e^-)_{dir}$ implied by Eq. 11. However the precise size of this contribution is currently very uncertain. Attempts [39, 40] to relate $\Gamma(K_S \to \pi^0 e^+ e^-)$ to $\Gamma(K^+ \to \pi^+ e^+ e^-)$ via chiral perturbation theory (χPT) have run into problems [41, 42]. To further complicate the situation, there is also a CP-conserving two photon contribution of roughly the same order as the CP-violating, that arises from the intermediate state $K_L \to \pi^0 \gamma\gamma$ (see Fig. 9 (b)). In principle the size of this contribution can be predicted from data on the latter process. There were a number of contradictory theoretical predictions for $K_L \to \pi^0 \gamma\gamma$ (see Ref. 43 for a summary). The observations by NA31 [44] and FNAL-731 [45] have been a mixed success for χPT. The Dalitz Plot distribution is pretty well predicted by χPT [40], but the observed branching ratio, $\sim 1.7 \times 10^{-6}$, is about three times higher than that originally predicted. Refinements to the theory [46] have reduced this discrepancy, but this born-again agreement is not as convincing as an initially correct prediction would have been. What is more, even the refined theory's implications for $K_L \to \pi^0 e^+ e^-$ are not unambiguous. Ref. 46 predicts $B(K_L \to \pi^0 e^+ e^-)_{CPcons} = 1.8 \times 10^{-12}$, while Ref. 42, which includes dispersive effects, obtains $B(K_L \to \pi^0 e^+ e^-)_{CPcons} = 4.9 \times 10^{-12}$.

In addition to the above, the intrinsic background $K_L \to e^+ e^- \gamma\gamma$ is extremely difficult to overcome. The impact of this background, which was discovered [47] in the course of the first dedicated search for $K_L \to \pi^0 e^+ e^-$, was studied in detail by Greenlee [48]. It is basically a radiative correction to $K_L \to e^+ e^- \gamma$. However, in spite of the give-away tendency of the radiated photon to line up with its parent electron, and the necessity of its pairing with the other photon to make a spurious π^0, this background appears very hard to beat at the 10^{-11} level. Fig 10 shows the $\gamma\gamma$ mass from a recent study of this process [49]. Quite an appreciable fraction of the events have $m_{\gamma\gamma}$ near m_{π^0}. Since the observed branching ratio,

$B(K_L \to e^+e^-\gamma\gamma; E^*_\gamma > 5MeV) = (6.5 \pm 1.2_{stat} \pm 0.6_{sys}) \times 10^{-7}$ (consistent with the theoretical expectation of 5.8×10^{-7}) is $\sim 10^5$ times larger than the direct CP-violating component of $K_L \to \pi^0 e^+ e^-$, this is clearly a major challenge.

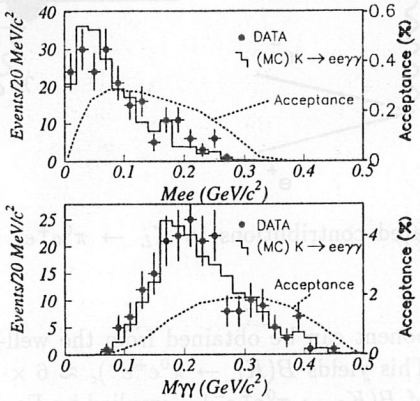

Figure 10: The e^+e^- and $\gamma\gamma$ mass distributions for $K_L \to e^+e^-\gamma\gamma$ (from Nakaya, *et al.*). About 25% of the events are actually $K_L \to e^+e^-\gamma$.

Results on $K_L \to \pi^0\ell^+\ell^-$ have also been reported by FNAL-799 recently. The 2-d plots of Fig. 11 show p_T^2 versus invariant mass of candidates for $K_L \to \pi^0 e^+ e^-$ and $K_L \to \pi^0\mu^+\mu^-$. No events are observed in either signal box, allowing 90% c.l. upper limits of $B(K_L \to \pi^0 e^+ e^-) < 4.3 \times 10^{-9}$ [50] and $B(K_L \to \pi^0\mu^+\mu^-) < 5.1 \times 10^{-9}$ [51] to be obtained. The former limit is only a small advance over previous work, but the latter represents nearly a 250-fold advance in sensitivity. The $K_L \to \pi^0\mu^+\mu^-$ signal region seems quite clean and very significant further progress can be anticipated [52]. The projected single event sensitivity for both processes at KTeV is $10^{-10} - 10^{-11}$. This will not be sufficient for an observation at the S.M. level, but it should clarify the future prospects for these modes in the study of CP-violation.

4.4 $K_L \to \mu^+\mu^-$

The theoretical connection between the short distance contribution to this branching ratio ($B(K_L \to \mu^+\mu^-)_{SD}$) and SM parameters was reviewed by Buras and Harlander [53] and subsequently by Buchalla and Buras [28]. Although the short-distance contribution is dominated by long-distance effects roughly an order of magnitude larger, a measurement of sufficient precision to overcome this difficulty seems possible. In principle, the CKM parameter ρ could be extracted from such a measurement. Both $K_L \to \mu^+\mu^-$ and its close relative $K_L \to e^+e^-$ are also sensitive to new physics beyond the Standard Model.

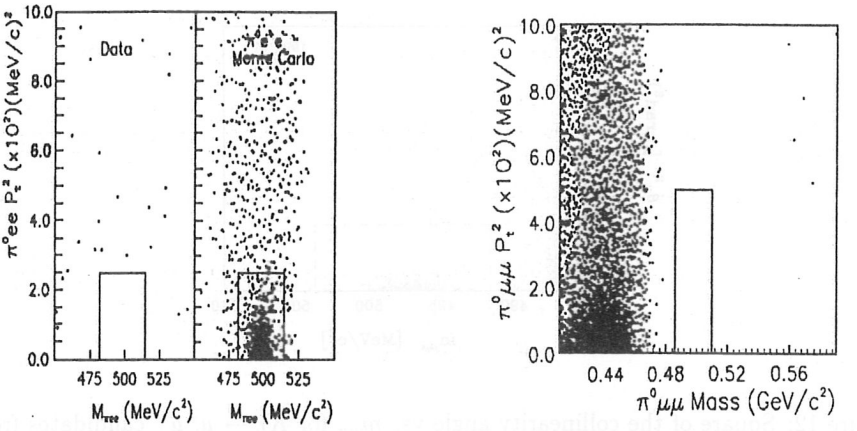

Figure 11: Results of $K_L \to \pi^0 \ell^+ \ell^-$ searches (from FNAL-799).

The short distance contribution to this process comes from the box and electro-weak penguin diagrams of Fig. 6. The hadronic matrix element is given by that occurring in $K^+ \to \mu^+ \nu$. Assuming three-generation unitarity, an approximate expression for the complete result can be written [35]

$$\begin{aligned} B(K_L \to \mu^+\mu^-)_{SD} &= 1.7 \times 10^{-10} x_t^{1.56} A^4 (\rho_0 - \rho)^2 \\ &= 1.9 \times 10^{-9} A^4 (\rho_0 - \rho)^2 \text{ (for } m_t \approx 170) \end{aligned} \tag{12}$$

where $\rho_0 - 1$ measures the charmed quark contribution (including QCD corrections). For typical values of the parameters involved, $\rho_0 \sim 1.27$. Then, for example, if $A = 0.85$ and $\rho = 0.27$, $B(K_L \to \mu^+\mu^-)_{SD} = 10^{-9}$. (For the case of $K_L \to e^+e^-$, this BR is reduced by a factor $\sim (m_e/m_\mu)^2$.) After taking the calculation to the next to leading logarithmic order, Buchalla and Buras [28] estimate the residual theoretical uncertainty in $B(K_L \to \mu^+\mu^-)_{SD}$ to be $\sim 8.5\%$, once the values of the parameters have been fixed. This suggests a target for the precision of possible future measurements.

Unlike most of the processes discussed in this paper, high statistics data are available for $K_L \to \mu^+\mu^-$. Fig. 12 shows the result of a single year's run of AGS-791 [54], in which hundreds of signal events are evident. There are now ~ 1000 events in the world sample of $K_L \to \mu^+\mu^-$, and about ten times this number are expected within a few years from AGS-871. In the absence of long-distance effects, this sensitivity would be more than adequate to satisfy the criterion of Ref 28. Unfortunately, the long-distance contribution dominates this decay, and determines whether $K_L \to \mu^+\mu^-$ can be exploited to determine ρ. By far the largest part of the long distance contribution is given by the two photon intermediate state of Fig. 13. Therefore

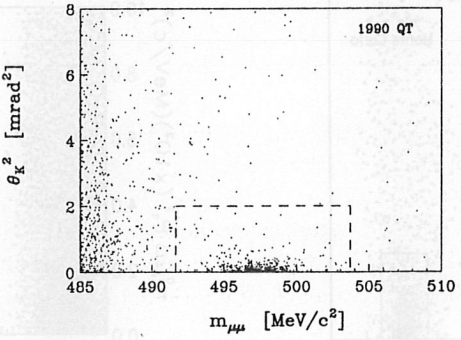

Figure 12: Square of the collinearity angle vs. $m_{\mu\mu}$ for $K_L \to \mu^+\mu^-$ candidates from 1990 data set of AGS-791.

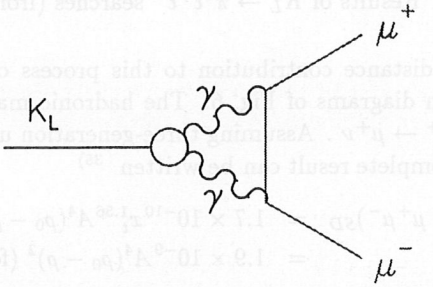

Figure 13: Long distance contribution to $K_L \to \mu^+\mu^-$

the absorptive part of the amplitude is related to the experimental rate for $K_L \to \gamma\gamma$ by [55]:

$$B(K_L \to \ell^+\ell^-)_{abs} = \frac{1}{2}\alpha^2 r_\ell^2 \frac{1}{\beta}\left|\ln\frac{1+\beta}{1-\beta}\right|^2 B(K_L \to \gamma\gamma) \qquad (13)$$

where $\beta \equiv \sqrt{1-4r_\ell^2}$ and $r_\ell^2 \equiv m_\ell^2/m_K^2$.This can be compared to the latest measurements:

$$B(K_L \to \mu^+\mu^-) = \begin{cases} (6.81 \pm 0.32) \times 10^{-9} & \text{absorptive} \\ (7.9 \pm 0.7) \times 10^{-9} & \text{KEK-137 [56]} \\ (6.86 \pm 0.37) \times 10^{-9} & \text{AGS-791 [54]} \end{cases}$$

$$B(K_L \to e^+e^-) = \begin{cases} (3.0 \pm 0.1) \times 10^{-12} & \text{absorptive} \\ < 4.1 \times 10^{-11} & \text{AGS-791 [57]} \end{cases} \qquad (14)$$

where the absorptive contribution is derived by using $B(K_L \to \gamma\gamma) = (5.70 \pm 0.27) \times 10^{-4}$ [26]. Were this the sole long-distance effect, the prospects for a measurement

of ρ via this process would be easy to evaluate. However, there is also a long distance *dispersive* contribution that adds in amplitude with the weak contribution. Unfortunately the relative size and even the relative sign of the two contributions is controversial.

Temporarily ignoring this problem, we can evaluate the potential of a precision measurement of $B(K_L \to \mu^+\mu^-)$ under the most favorable possible assumptions. Table 3 compares the precision on $B(K_L \to \mu^+\mu^-)_{dsp}$ available a decade ago, that available at present (the two latest experiments are averaged), and that which *could* be available after AGS-871, if a very precise measurement of $B(K_L \to \gamma\gamma)$ were also made. In Table 3, the 1997 value of $B(K_L \to \gamma\gamma)$ is assumed to be the same as the present PDG value. Also, $B(K_L \to \mu^+\mu^-)_{dsp}$ is assumed to be 10^{-9}. The precision assumed for the 1997 $B(K_L \to \mu^+\mu^-)$ measurement is slightly worse than that given by the anticipated statistics alone. Finally, the assumption is made that the precision on $B(K_L \to \gamma\gamma)$ can be improved to $< 1\%$ [58]. Applying Eq. 12 to the 1997 value of Table 3 gives a precision on ρ of about $\pm.06$ on the assumption that A is well-known. This precision is a function of the actual value of the dispersive BR, *e.g.* for $B(K_L \to \mu^+\mu^-)_{dsp} = 0.23 \times 10^{-9}$ the precision worsens to ± 0.12, while for $B(K_L \to \mu^+\mu^-)_{dsp} = 2 \times 10^{-9}$ it improves to ± 0.04. A precision on ρ of $\sim \pm 0.06$ would be very welcome in the anticipated time frame. Thus, were the long-distance

Table 3: Precision with which dispersive part of $B(K_L \to \mu^+\mu^-)$ can be extracted

Date	$B(K_L \to \mu\mu)$	$B(K_L \to \gamma\gamma)$	$B(K_L \to \mu\mu)_{abs}$	$B(K_L \to \mu\mu)_{dsp}$
1984	$(9.1 \pm 1.9)10^{-9}$	$(4.9 \pm .4)10^{-4}$	$(5.9 \pm .5)10^{-9}$	$(3.2 \pm 2.0)10^{-9}$
1994	$(7.09 \pm .33)10^{-9}$	$(5.70 \pm .27)10^{-4}$	$(6.85 \pm .32)10^{-9}$	$(.23 \pm .46)10^{-9}$
1997	$(7.85 \pm .10)10^{-9}$	$(5.70 \pm .05)10^{-4}$	$(6.85 \pm .06)10^{-9}$	$(1.00 \pm .12)10^{-9}$

dispersive contribution negligible, for $B(K_L \to \mu^+\mu^-)_{dsp} \sim 10^{-9}$, the ongoing experiments could approach the criterion of Ref. 28.

Unfortunately our knowledge of the long-distance dispersive contribution is very poor. The difficulties in calculating it are outlined in Ref. 41. There have been a number of model calculations [59, 60, 61], and these disagree with one another. However the same models also make predictions about other decays, such as $K_L \to \ell^+\ell^-\gamma$, $K_L \to 4$ leptons, $K^+ \to \pi^+\ell^+\ell^-$, etc. These decays are being studied experimentally and can possibly serve to distinguish among the models. In any case one can hope that further experimental and theoretical work will refine the prediction of the long-distance dispersive contribution. To estimate the experimental progress that might be necessary, let us focus on the model calculation of Ref. 60. In this model, a parameter α_K characterizes the relative strength of K^*-mediated diagrams. This parameter [62] was measured to be $-0.28 \pm 0.083^{+0.054}_{-0.034}$ [63] and -0.28 ± 0.13 [64] in two studies of $K_L \to e^+e^-\gamma$. At the recent DPF meeting, FNAL-799 reported a new measurement [65] of $K_L \to \mu^+\mu^-\gamma$, based on 200 events (see Fig. 14). Their

result, $B(K_L \to \mu^+\mu^-\gamma) = (3.55 \pm 0.25_{stat} \pm 0.23_{sys}) \times 10^{-7}$, implies $\alpha_K = -0.15^{+0.14}_{-0.12}$, consistent with the $K_L \to ee\gamma$ results.

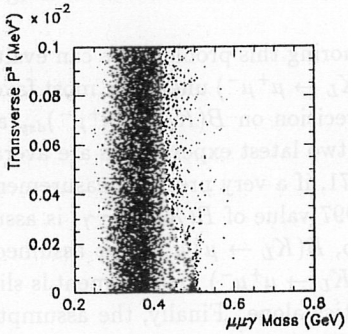

Figure 14: $K_L \to \mu^+\mu^-\gamma$ candidates from FNAL-799. Signal events can be seen near $m_{\mu\mu\gamma} = m_K$ and small p_T^2.

The model of Ref. 60 gives a tiny long distance contribution to the real part, but this is essentially a numerical accident due to the precise value $\alpha_K = -0.28$ ($B(K_L \to \mu\mu)^{l.d.}_{dsp} = 0.76 \times 10^{-9}(1 + \alpha_K/0.27)^2$). If one attributes an error of ± 0.09 to α_K, the corresponding error in the dispersive amplitude is $\pm 1.0 \times 10^{-5}$ (about 1/3 the size of the short distance amplitude if $B(K_L \to \mu\mu)_{sd} = 10^{-9}$). It corresponds to about ± 0.32 in ρ. To reduce it to ± 0.06, α_K would need to be determined to ± 0.017. Scaling from AGS-845 [63], this would require about 30,000 $K_L \to e^+e^-\gamma$ events, which is possible for the upcoming round of CP-violation experiments. Much larger samples of $K_L \to \mu^+\mu^-\gamma$ should also be available.

There has also been significant progress on the related decays mentioned above. FNAL-799 recently published results [66] on $K_L \to e^+e^-e^+e^-$. Based on 28 events, they measured $B(K_L \to e^+e^-e^+e^-) = (3.96 \pm 0.78_{stat} \pm 0.32_{sys}) \times 10^{-8}$ (*cf.* a theoretical expectation of $(3.55 \pm 0.17) \times 10^{-8}$). This sample was sufficient to verify that the final state is mainly $CP = -1$, but it is too small to distinguish among theoretical approaches to off-mass shell behavior of the photons in $K_L \to \gamma\gamma$. However much larger samples will be available in the near future. If a well-motivated theoretical approach can give a good account of high statistics samples of this process as well as $K_L \to \ell^+\ell^-\gamma$, $K_L \to e^+e^-\mu^+\mu^-$, $K_L \to \ell^+\ell^-\gamma\gamma$, etc., a basis will exist for extracting very valuable information on ρ from $K_L \to \mu^+\mu^-$.

4.5 $K^+ \to \pi^+\ell^+\ell^-$

It was originally believed that $K^+ \to \pi^+\ell^+\ell^-$ would be short-distance dominated [67]. However it is now understood to be very difficult to distinguish one-loop effects in

this decay, because of long distance photon exchange contributions that are known to be large but which are very difficult to calculate precisely [68]. AGS-777/851 collected more than 1000 $K^+ \to \pi^+e^+e^-$ events; results based on ~ 500 have been published [38]. These results are consistent with the predictions of χPT [39], but are not sufficiently precise to constitute a real challenge. A successor experiment, AGS-865, now running, anticipates collecting tens of thousands of both $K^+ \to \pi^+e^+e^-$ and $K^+ \to \pi^+\mu^+\mu^-$. The latter decay is particularly interesting because measurements of the parity-violating polarization asymmetry of the μ^+ are sensitive to the short-distance contribution [69]. In particular, such measurements are potentially sensitive to ρ, thus affording an alternative to $K_L \to \mu^+\mu^-$ for determining ρ with kaon decays. Recently Buchalla and Buras [70] have extended the previous analyses beyond the leading logarithmic approximation. For $-0.25 \leq \rho \leq 0.25$, $V_{cb} = 0.040 \pm 0.004$, and $m_t = (170 \pm 20)$ GeV, they found $3.0 \times 10^{-3} \leq |\Delta_{LR}| \leq 9.6 \times 10^{-3}$ ($\Delta_{LR} \equiv \frac{\Gamma_R - \Gamma_R}{\Gamma_R + \Gamma_L}$, where Γ_R and Γ_L are the rates to produce right and left-handed μ^+). To attain this precision with $B(K^+ \to \pi^+\mu^+\mu^-) \sim$ a few $\times 10^{-8}$ is very challenging indeed. If one could measure the polarization of the μ^- as well as that of the μ^+, it is also possible in principle to measure η in this process [71]. However a measurement sufficient to do this is far beyond current experimental capabilities. In any case the first step in exploiting $K^+ \to \pi^+\mu^+\mu^-$ is to observe it. This step has recently been taken by AGS-787. Fig. 15 shows a plot of p_T^2 vs three-body effective mass for $K^+ \to \pi^+\mu^+\mu^-$ candidates. A clear accumulation of events is visible in the signal region near $p_T^2 = 0$ and $m_{\pi\mu\mu} = m_K$.

4.6 One-loop decays and the Standard Model parameters

It's evident from the above discussion that one-loop K decays can be very useful in constraining the unitarity triangle. With the addition of a single measurement from the B system (*e.g.* of $|V_{cb}|$ or of $|V_{ub}/V_{cb}|$), they can actually over-determine the triangle. This is graphically illustrated in Fig. 16. For a given value of m_t, the various dimensions indicated are proportional to the square root of the K branching ratio divided by A^2. Clearly any two of them can determine the apex of the triangle.

The information from K decays can be used in a number of different ways; several have been suggested in the literature. For example, Buchalla and Buras [72] estimate that $sin(2\beta)$ could be determined to ± 0.11, given 10% accuracy on $B(K^+ \to \pi^+\nu\bar{\nu})$ and $B(K_L \to \pi^0\nu\bar{\nu})$. The most advantageous strategy will depend on when results of various levels of precision become available.

5 – B's and K's

At the recent DPF meeting two bounds on $|\frac{V_{td}}{V_{ts}}|$ from B-decays were presented. The first is a limit of $B(B \to \rho(\omega)\gamma)/B(B \to K^*\gamma) < 0.34$ from CLEO [73]. If these

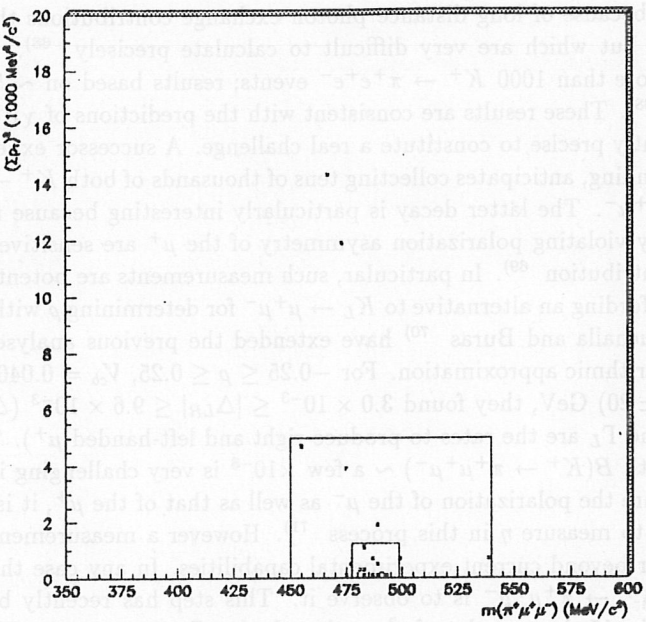

Figure 15: $K^+ \to \pi^+\mu^+\mu^-$ candidates from AGS-787. Smaller box is signal region. Region between smaller and larger boxes is used to estimate background.

decays are mediated purely by short-distance penguin diagrams like that of Fig. 17, one can extract a limit $|\frac{V_{td}}{V_{ts}}| < \frac{0.58}{\sqrt{\xi}}$, where ξ is an SU(3)-breaking parameter between 0.58 and 0.81. Using $\xi = 0.58$ gives $|\frac{V_{td}}{V_{ts}}| < 0.76$. However Atwood, *et al.* [74], point out that the interpretation of this measurement may be afflicted by possible long distance effects in $B \to V\gamma$. This is a problem at present, but it is believed that the long distance contributions, although not negligible, are smaller than the short distance contributions, and that further experimental and theoretical work will eventually make this a viable method of determining $|\frac{V_{td}}{V_{ts}}|$.

The second bound comes from recent work on $B_s - \bar{B}_s$ mixing at LEP [75]. $B_d - \bar{B}_d$ mixing is proportional to $|V_{td}|^2$, but the presence of an *a priori* unknown hadronic matrix element makes extracting $|V_{td}|$ problematical (this is to be contrasted to the case of $K^+ \to \pi^+\nu\bar{\nu}$ where the hadronic matrix element is accurately known from $Ke3$ decay). A measurement of $B_s - \bar{B}_s$ mixing can reduce the theoretical problem to that of determining the ratio of B_d and B_s matrix elements. This ratio is claimed to be known to about 10%, and one has [76] $\frac{\Delta m_d}{\Delta m_s} = \frac{1}{(1.19\pm0.10)} \times |\frac{V_{td}}{V_{ts}}|^2$. The numerator here has been known pretty well for a while via time-averaged measurements, and more recently there have been LEP results exploiting the time de-

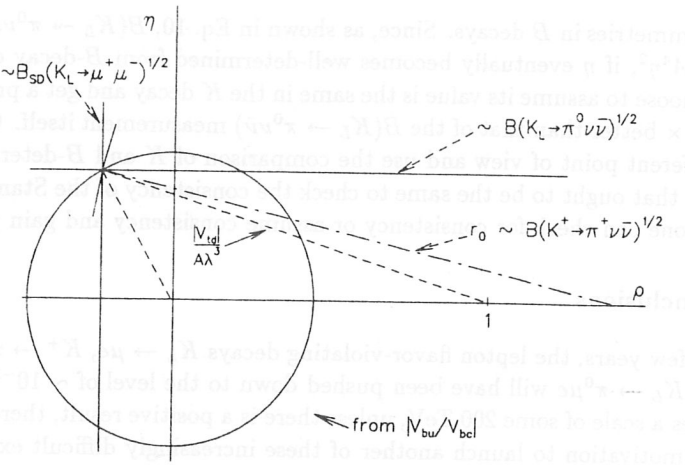

Figure 16: Rare K decays and the unitarity triangle.

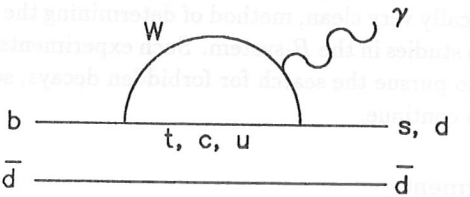

Figure 17: Penguin diagram for $B \to V\gamma$.

pendence. These have now developed to the point where meaningful limits on Δm_s can be extracted. The ALEPH result discussed by Sharma at the DPF Meeting is $\Delta m_s > 6ps^{-1}$. For $\tau_{B_S} = (1.56 \pm 0.14)ps$, they obtain $|\frac{V_{td}}{V_{ts}}| < 0.33$. More conservatively: $|\frac{V_{td}}{V_{ts}}| < 0.36\frac{f_{B_s}\sqrt{B_{B_s}}}{f_{B_d}\sqrt{B_{B_d}}}$. Progress beyond this at LEP is expected to be slow.

By making perhaps invidious assumptions about $|V_{ts}|$, one can beat the $K^+ \to \pi^+\nu\bar{\nu}$ result discussed above into a comparable form: $|\frac{V_{td}}{V_{ts}}| < 1.38$. This is not yet good as the B measurements, but it is very clean theoretically and is limited only by the experiment. Rapid progress is expected if AGS running time is adequate, and the K sensitivity should be comparable to that of the B's within a couple of years.

It's also important to keep in mind that the B and K experiments are not quite measuring the same thing, and that it's possible that non-SM effects will show up as discrepancies between the two.

Buras and his collaborators [72, 77, 78] have explored how complementary information from B's and K's can be combined. One perhaps surprising example is the proposal to extract a precise value for $|V_{cb}|$ from $B(K_L \to \pi^0\nu\bar{\nu})$ plus measurements

of CP-asymmetries in B decays. Since, as shown in Eq. 10, $B(K_L \to \pi^0\nu\bar{\nu})$ is proportional to $A^4\eta^2$, if η eventually becomes well-determined from B-decay experiments, one can choose to assume its value is the same in the K decay and get a precision on A that's $\sim 4\times$ better than that of the $B(K_L \to \pi^0\nu\bar{\nu})$ measurement itself. One can also take a different point of view and use the comparison of K and B-determinations of quantities that ought to be the same to check the consistency of the Standard Model. Basically one can check for consistency or assume consistency and gain precision.

6 – Conclusions

Within a few years, the lepton flavor-violating decays $K_L \to \mu e$, $K^+ \to \pi^+\mu^+e^-$, and probably $K_L \to \pi^0\mu e$ will have been pushed down to the level of $\sim 10^{-12}$. Although this probes a scale of some 200 TeV, unless there is a positive result, there may not be sufficient motivation to launch another of these increasingly difficult experiments in the near future. This is because of the lack of a currently compelling theoretical target, and the fact that according to Eq. 1, one progresses only as $\propto (BR)^{-\frac{1}{4}}$. However the motivation to pursue one-loop K decays is very strong even in the era of B-factories, and should be pushed vigorously. They present the irresistible opportunity of an alternative, theoretically very clean, method of determining the unitarity triangle that is complementary to studies in the B-system. Such experiments almost inevitably also offer opportunities to pursue the search for forbidden decays, so that progress in that area is also likely to continue.

7 – Acknowledgment

This work was supported by the U.S. Department of Energy under Contract No. DE-AC02-76CH00016.

References

1. J. Ritchie and S. Wojcicki, *Rev. of Mod. Phys.* **65** 1149 (1993).

2. W. Buchmüller and D. Wyler, *Nucl. Phys.* **B268** 621 (1986); R. Cahn and H. Harari, *Nucl. Phys.* **B176** 135 (1980); J. Pati and H. Stemnitzer, *Phys. Lett.* **172B** 441 (1986): O. Shanker, *Nucl. Phys.* **B206** 253 (1982); A. Acker and S. Pakvasa, *Mod. Phys. Lett.* **A7** 1219 (1992); W. Marciano and A. Sanda, *Phys. Rev. Lett.* **38** 1512 (1977); W. Marciano, *Phys. Rev.* **D45** R721 (1992); A. Barroso, G. Branco and M. Bento, *Phys. Lett.* **134B** 123 (1984); P. Langacker, S. Uma Sankar and K. Schilcher, *Phys. Rev.* **D38** 2841 (1988)

3. K. Arisaka *et. al.*, *Phys. Rev. Lett.* **70** 1049 (1993).

4. W.J. Marciano, *Vancouver Rare Decay*, 1 (1988).

5. R. Balest *et al.*, **CLEO CONF 94-4** Submitted to the 1994 Glasgow ICHEP.

6. A. M Lee *et al.*, *Phys. Rev. Lett.* **64** 165 (1990).

7. P. Gu, Albuquerque DPF Workshop, 1994.

8. P. Krolak *et al.*, *Phys. Lett.* **B320** 407 (1994).

9. R. Ammar *et al.*, *Phys. Rev.* **D49** 5701 (1994).

10. R. Bolton *et al.*, *Phys. Rev.* **D38** 2121 (1988).

11. U. Bellgardt *et al.*, *Nucl. Phys.* **B299** 1 (1988).

12. C. Dohmen *et al.*, *Phys. Lett.* **B317**, 631 (1993).

13. R. Abela *et al.*, PSI preprint (1994).

14. S. Shotkin, Albuquerque DPF Workshop, 1994.

15. A. Bean *et al.*, *Phys. Rev. Lett.* **70** 138 (1993).

16. J. Bartelt *et al.*, *Phys. Rev. Lett.* **73** 1890 (1994).

17. L. Wolfenstein *et al.*, *Phys. Rev. Lett.* **13** 562 (1964).

18. L. Hall and S. Weinberg, *Phys. Rev.* **D48**, 979 (1993); L. Lavoura, CMU-HEP92-17 (1992); S.M. Barr and E.M. Friere, *Phys. Rev.* **D41**, 2129 (1990); S.M. Barr *Phys. Rev.* **D34**, 1567 (1986); S.M. Barr and D. Seckel, *Nucl. Phys.* **B233**, 116 (1984).

19. M. Kobayashi and T. Maskawa, *Prog. Theor. Phys.* **49**, 652 (1973).

20. A.G. Cohen, D.B. Kaplan, and A.E. Nelson, *Ann. Rev. Nucl. Part. Phys.* **43**, 27 (1993).

21. J. Kambor *et al.*, *Phys. Lett.* **B261**, 496 (1991), S. Fajfer and J.-M. Gerard, *Z. Phys.* **C42**, 425 (1989); H.-Y. Cheng, *Phys. Lett.* B238, 399 (1990).

22. G.B. Thomson *et al.*, *Phys. Lett.* **B337**, 411 (1994).

23. K. Jon-And, *Recent Results of CP, T, and CPT Tests with the CPLEAR Experiment*, Albuquerque DPF Workshop, 1994; T. Ruf, *Measurements of CP and T-violation Parameters in the Neutral Kaon System at CPLEAR*, Glasgow Conference (1994).

24. L.-F. Li and L. Wolfenstein, *Phys. Rev.* **D21**, 178 (1980); J.F. Donoghue *et al.*, *Phys. Rev.* **D36**, 798 (1987); A.A. Belkov *et al.*, *Nucl. Phys.* **B359**, 322 (1991); H.-Y. Cheng *et al.*, *Mod. Phys. Lett.* **A4**, 869 (1989); H.-Y. Cheng, *Phys. Rev.* **D43**, 1579 (1991); H.-Y. Cheng, *Phys. Lett.* **B238**, 399 (1990); Erratum **B248**, 474 (1990);S. Faijfer and J.M. Gérard, *Z. Phys.* **C42**, 425 (1989).

25. Y. Zou, *et. al*, *Phys. Lett.* **B329**, 519 (1994).

26. Particle Data Group 1994, *Phys. Rev.* **D50**, 117 (1994).

27. J. Hagelin and L. Littenberg, *Prog. Part. Nucl. Phys.* **23** 1 (1989);D. Rein and L.M. Sehgal, Phys. Rev. **D39** 3325 (1989); M. Lu and M. B. Wise, Phys. Lett. **B324** 461 (1994).

28. G. Buchalla and A.J. Buras, *Nucl. Phys.* **B412** 106 (1994).

29. M. S. Atiya et al., *N.I.M* **A321**, 129 (1992)

30. M. S. Atiya, *et. al.*, *Phys. Rev.* **D48** 48 (1993).

31. L. Littenberg, *Phys. Rev.* **D39** 3322 (1989).

32. M.B. Weaver, *et. al*, *Phys. Rev. Lett.* **72**, 3758 (1994).

33. T. Inagaki, *et. al*, KEK Proposal 324, 1994.

34. F. Gilman and M. Wise, *Phys. Rev.* **D21** 3150 (1980); C. Dib, I. Dunietz, and F.J. Gilman, *Phys. Rev.* **D39** 2639 (1989); C. Dib, I. Dunietz, and F.J. Gilman *Phys. Lett.* **218B** 487 (1989); J.M. Flynn, *Nucl. Phys.* **B13** 474 (1990); J.M. Flynn and L. Randall, *Nucl. Phys.* **B326** 31 (1989), E.-*ibid.* **B334** 580 (1990).

35. G. Buchalla, A. Buras and M. Harlander, *Nucl. Phys.* **B349** 1 (1991).

36. A. Buras, *et. al*, *Nucl. Phys.* **B423** 349 (1994).

37. G.D. Barr, *et. al*, *Phys. Lett.* **B304** 381 (1993).

38. C. Alliegro *et. al*, *Phys. Rev. Lett.* **68** 278 (1992).

39. G. Ecker, A. Pich and E. de Rafael, *Nucl. Phys.* **B291** 692 (1987).

40. G. Ecker, A. Pich and E. de Rafael, *Nucl. Phys.* **B303** 665 (1988).

41. L.Littenberg and G. Valencia, *Ann. Rev. Nucl. Part. Sci.* **43** 729 (1993).

42. J.F. Donoghue and F. Gabbiani, *Phys. Rev.* **D51** 2187 (1995).

43. B. Winstein and L. Wolfenstein, *Rev. of Mod. Phys.* **65** 1113 (1993).

44. G. D. Barr *et al.*, *Phys. Lett.* **242B** 523 (1990);G. D. Barr, *et, al.*, *Phys. Lett.* **284B** 440 (1992).

45. V. Papadimitriou *et. al.*, *Phys. Rev.* **D44** R573 (1991).

46. A.G. Cohen, G. Ecker, and A. Pich, *Phys. Lett.* **304B**, 347 (1993).

47. W.M. Morse *et al.*, *Phys. Rev.* **D65**, 36 (1992).

48. H.B. Greenlee, *Phys. Rev.* **D42** 3724 (1992).

49. T. Nakaya, *et al.*, *Phys. Rev. Lett.* **73**, 2169 (1994).

50. D.A. Harris *et. al.*, *Phys. Rev. Lett.* **71** 3914 (1993).

51. D.A. Harris *et. al.*, *Phys. Rev. Lett.* **71** 3918 (1993).

52. One expects $B(K_L \to \pi^0\mu^+\mu^-)_{CP-viol} \approx 0.2B(K_L \to \pi^0 e^+e^-)_{CP-viol}$. Also, relative to $B(K_L \to \pi^0\mu^+\mu^-)_{CP-viol}$, the CP-conserving $2\,\gamma$ component is expected to be quite a bit larger and the $K_L \to \ell^+\ell^-\gamma\gamma$ background about a factor two smaller than in the electron case.

53. A. Buras and M. Harlander, *Review Volume on Heavy Flavors*, ed. A. Buras and M. Lindner, World Scientific, Singapore (1992).

54. A. P. Heinson *et al.*, *Phys. Rev.* **D51** 985 (1995).

55. L.M Sehgal, *Phys. Rev.* **183** 1511 (1969).

56. T. Akagi, *et al.*, *Phys. Rev.* **D51** 2061 (1995).

57. K. Arisaka *et. al.*, *Phys. Rev. Lett.* **71** 3910 (1993).

58. Note that one can actually do somewhat better than is indicated in the table, because the normalization uncertainties on $B(K_L \to \mu^+\mu^-)$ and $B(K_L \to \gamma\gamma)$ are correlated (see Ref. 54).

59. C. Quigg and J. D. Jackson, UCRL-18487 unpublished (1968).

60. L. Bergström, E. Massó, P. Singer, *Phys. Lett.* **131B** 229 (1983); L. Bergström *et al.*, *Phys. Lett.* **134B** 373 (1984).

61. P. Ko, *Phys. Rev.* **D45** 174 (1992).

62. Note that an absolute avlue of $.2 - .3$ was predicted for α_K several years in advance of the measurements.

63. K.E. Ohl *et al.*, *Phys. Rev. Lett.* **65**, 1407 (1990).

64. G. D. Barr *et al.*, *Phys. Lett.* **240B** 283 (1990)

65. M. B. Spencer, *A measurement of the branching ratio* $K_L \to \mu^+\mu^-\gamma$, Albuquerque DPF Workshop, 1994.

66. P. Gu, *et al.*, *Phys. Rev. Lett.* **72**, 3000 (1994).

67. M.K. Gaillard and B.W. Lee, *Phys. Rev.* **D10**, 897 (1974).

68. A.I. Vainshtein, *et al.*, *Yad. Phys.* **24**, 820 (1976) [*Sov. J. Nucl. Phys.* **24**, 427 (1976)].

69. M. Savage and M. Wise, *Phys. Lett.* **250B** 151 (1990): M. Lu, M. Wise and M. Savage, *Phys. Rev.* **D46** 5026 (1992);G. Bélanger, C. Q. Geng and P. Turcotte, *Nucl. Phys.* **B390**, 253 (1993).

70. G. Buchalla and A.J. Buras, *Phys. Lett.* **B336**, 263 (1994).

71. P. Agrawal *et. al.*, *Phys. Rev. Lett.* **65** 537 (1991); *Phys. Rev.* **D45** 2383 (1992).

72. G. Buchalla and A.J. Buras, *Phys. Lett.* **B333**, 221 (1994).

73. M. Athanas, *et. al.*, CLEO CONF 94-2.

74. D. Atwood, B.Block, and A. Soni, SLAC-PUB-6635, BNL-60709, TECHNION-PH-94-11.

75. V. Sharma, Albuquerque DPF Workshop, 1994.

76. A. Ali, *Proc. of XXVI int. Conf. on High Energy Physics, Dallas (1992)* **Vol. I**, 484.

77. A.J. Buras, M.E. Lautenbacher, and G. Ostermaier, *Phys. Rev.* **D50** 3433 (1994).

78. A.J. Buras, *Phys. Lett.* **B333**, 476 (1994).

Frascati Physics Series, Vol. III (1994)
HEAVY QUARKS AT FIXED TARGET
University of Virginia, October 7–10, 1994
(pp. 327–342)

RESULTS/PROSPECTS IN E777/851/865

D.M. Lazarus
Brookhaven National Laboratory, Upton, N.Y. 11786, USA

Abstract

E777 has set 90% C.L. branching ratio upper limits of 2.1×10^{-10} for the decays $K^+ \to \pi^+\mu^+e^-$ and 4.5×10^{-7} for $K^+ \to \pi^+A^0$, where A^0 is any particle of mass less than 100 MeV/c^2 decaying into e^+e^- with lifetime less than 10^{-13} sec. E851 measured the BR$(K^+ \to \pi^+e^+e^-) = (2.97^{+0.19}_{-0.22}) \times 10^{-7}$ and BR$(\pi^0 \to e^+e^-) = (8.0 \pm 2.6 \pm 0.6) \times 10^{-8}$. E865 is preparing to take data in 1995 which should greatly improve these results.

1 -Introduction

Over the past two decades, a number of extensions to *The Standard Model* have been proposed which attempt to ameliorate if not cure some of its well known ills. Most of these attempts such as technicolor [1] extended technicolor [2] which connect quark and lepton sectors via horizontal gauge boson exchange, supersymmetry [3], leptoquarks [4] and additional Higgs scalars [4] allow lepton flavor violation as shown in Fig.1.

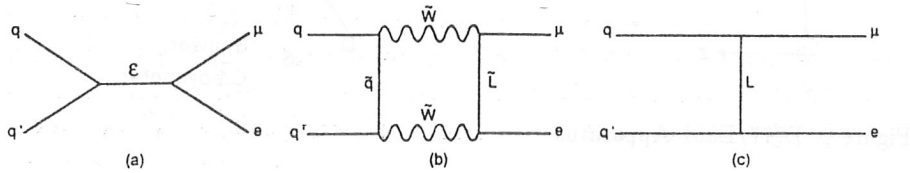

Figure 1. Diagrams for lepton flavor violation. (a) horizontal gauge bosons, (b) supersymmetry, (c) leptoquarks.

Muon decay studies have provided the most sensitive tests for lepton flavor violation with measured branching ratios BR$(\mu^- \to e^-\gamma) < 4.9 \times 10^{-11}$ [5], BR$(\mu^- \to$

$e^-e^+e^-) < 1.0 \times 10^{-12}$ [7] and $BR(\mu^- \rightarrow e^-2\gamma) < 7.2 \times 10^{-11}$ [6] all at the 90% confidence limit. In contrast, the only credible search for lepton flavor violation in kaon decays prior to the present AGS program yielded a branching ratio $K^+ \rightarrow \pi^+\mu^+e^- < 4.8 \times 10^{-9}$ [8] . In the event that generation number conservation [9], i.e., G= +1 for the first generation of fermions, u, d, e^- and ν_e, G=+2 for s, c, μ^- and ν_μ, etc. and -1, -2, etc. for their antiparticles, is a more restrictive constraint than lepton flavor, then $K+ \rightarrow \pi^+\mu^+e^-$ in which $\Delta G = 0$ may prove more sensitive to lepton flavor violation than the muon decay modes in which $\Delta G = 1$.

The search for $K^+ \rightarrow \pi^+\mu^+e^-$, ($K_{\pi\mu e}$), is also complimentary to $K_L^0 \rightarrow \mu^\pm e^\mp$. Although the latter can conserve generation number, it can only proceed via an interaction that transforms as an axial vector or pseudoscalar whereas $K^+ \rightarrow \pi^+\mu^+e^-$ proceeds via scalar or vector currents.

2 -E777/E851 Apparatus

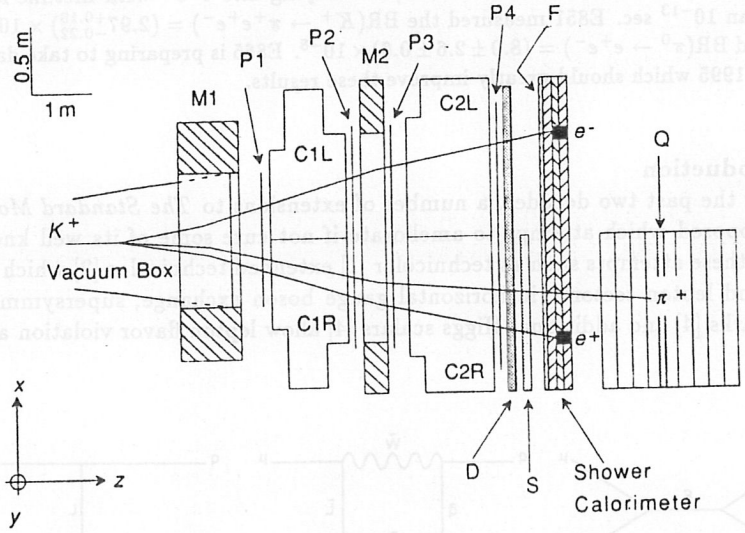

Figure 2. E777/E851 Apparatus

Figure 2 shows the basic experimental apparatus used in E777 and E851. A 6 GeV/c unseparated beam containing approximately 10^7 positive kaons per AGS pulse traversed a 5 meter vacuum decay region immediately upstream of the detectors in which some 10% of the beam kaons decayed. These were accompanied by about 2×10^8 positive pions and protons per cycle. The decay region ended inside a 48D48 (M1 in the figure) spectrometer magnet with a gap of 40 inches which deflected

decay products away from the beam region with positive particles to beam right and negatives to the left. This enabled us to specialize the two sides of the particle identification system to trigger on an electron on the left with a pion and a muon on the right . Four multiwire proportional chambers, P1-P4, each with three views and two mm wire spacing, and a second spectrometer magnet M2, a 72D18, with a 30 inch gap and magnetic field integral producing a deflection of 164 MeV/c which was equal and opposite to that of M1 provided particle tracking and momentum measurement. The measured resolution was $\sigma_P = 0.01P^2$ GeV/c, where P, the momentum of the decay products ranged from 0.6 to 4.0 GeV/c. Particle identification was obtained from three systems, two atmospheric pressure gas Čerenkov counters for pion(muon)-electron identification, a lead-scintillator calorimeter, 11.4 radiation lengths thick, and finally a muon identifier consisting of eight two- view proportional tube packages, interspersed with 9 cm thick steel plates. The Čerenkov counters contained hydrogen gas on the left (Č1L and Č2L)

The identification of an electron on the left side of the detector is of crucial importance to the $K_{\pi\mu e}$ trigger since the most prolific K^+ decay mode to yield an electron is $K^+ \rightarrow \pi^+\pi^0$ followed by the Dalitz decay $\pi^0 \rightarrow e^+e^-\gamma$ which has a combined branching ratio of 2.5×10^{-3} [10]. On the right side, Č1R and Č2R were filled with CO_2 yielding an average of six photoelectrons for an electron with the muon threshold at 3.7 GeV/c, corresponding to the upper limit of the decay muon spectrum. The efficiency for rejecting triggers with a positron signal in either Č1R or Č2R was 99.9%.

The lead-scintillator shower calorimeter was located behind the last proportional chamber, P4, and was segmented into 24 horizontal sections and 2 vertical ones. Requiring the energy deposited to be consistent with an electron increased the pion rejection efficiency of the left side of the detector by a factor of six averaged over all momenta with a loss of 5% in electron detection efficiency. By rejecting particles on the right side with energy deposition greater than 75% of their measured momentum, the overall positron rejection factor was raised to 99.97% with an insignificant loss for detecting pions. The wire chambers were deadened to prevent gas multiplication in the region traversed by the beam. Opaque baffles contained the beam region in the Čerenkov counters so that light produced by the beam did not reach the photomultplier tubes. The shower calorimeter was configured with a hole through which the beam could pass without interacting.

D, F, S and Q in Figure 2 indicate scintillation counter hodoscopes that were used to trigger the data acquisition system. A single F counter firing on the left in coincidence with 2 appropriately correlated (F · S) coincidences on the right was required for all triggers. The $K_{\pi\mu e}$ trigger then had the additional requirement of a (Č1L·Č2L) coincidence with a threshold of 0.4 photoelectron in each counter, no veto from Č1R or Č2R and a potential muon track. A τ trigger resulted from the F and S coincidences with no Čerenkov counters firing and no candidate muon track. Since the τ trigger occurred at a rate of 10^5 per spill, it was prescaled by 8192. Finally, a

$K_{\pi ee}$ trigger was formed by requiring (Č1L·Č2L)·(Č1R·Č2R). The high sensitivity of this trigger to Dalitz decays resulted in it being prescaled by a factor of 8.

3 -$A^0 \rightarrow e^+e^-$

The first results from E777 were prompted by reports of correlated electron-positron pairs produced in heavy ion collisions which suggested the possible existence of a short lived, 1.8 MeV/c^2 particle that decays to e^+e^- [11]. At the time axions and light Higgs bosons were very much in fashion and a search for such a particle, A^0, resulting from the decay $K^+ \rightarrow \pi^+A^0$, $A^0 \rightarrow e^+e^-$ was undertaken [12].

A scatter plot of M_{ee} vs. $M_{\pi ee}$ with the requirements that S, the rms distance of closest approach of the three tracks to a common vertex, was less than 1.4 cm and the reconstructed K^+ momentum vector can be projected back through the beam to the production target is given in Figure 3(a).

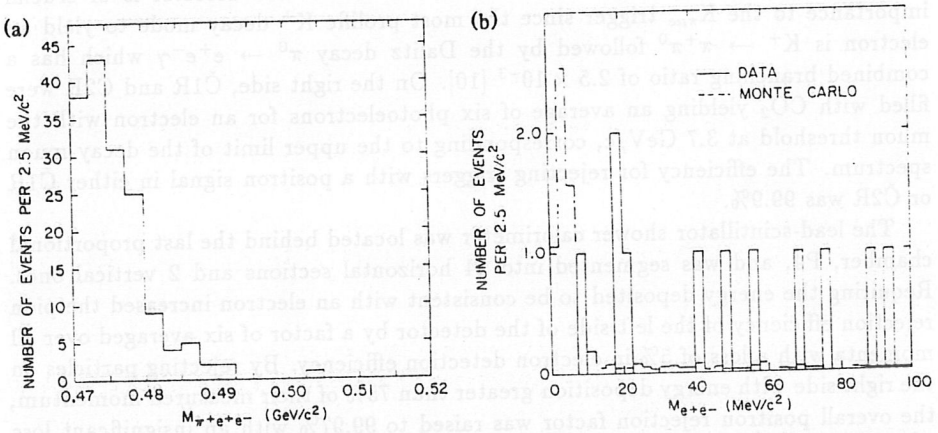

Figure 3. (a) Invariant mass distribution of $M_{\pi ee}$ for $M_{ee} \leq 15 MeV/c^2$. (b) $M_{\pi ee}$ distribution for 492.5 MeV/$c^2 \leq M_{\pi ee} \leq$ 520 MeV/c^2. The dashed line indicates the signal expected from the decay of a 1.8 MeV/c^2 A^0 with a branching ratio BR($A^0 \rightarrow e^+e^-$)= 10^{-6}. The high mass tail on this distribution results from electron bremsstrahlung and multiple Coulomb scattering.

The background from Dalitz decays for $M_{ee} \leq$ 15 MeV/c^2 is apparent from Figure 3(a). Dalitz decays are prominent below the kaon mass and a single event appears on the high mass side. Figure 3(b) gives the low mass M_{ee} distribution for $M_{\pi ee}$ in region of the kaon mass. A 1.8 MeV/c^2 signal would be spread to 10 MeV/c^2 by our resolution. The events observed show no significant structure and are consistent with the Monte Carlo simulation of Dalitz decays. From the known branching ratio

we estimate less than one background event from this decay in this region.

Since the particle detection identification efficiencies for this decay are the same as those for Dalitz decays, the normalization is derived from the known branching ratio for Dalitz decay, the observed number of Dalitz decays and the Monte Carlo calculation of the acceptances for the two decays. The resulting upper limit branching ratios for $M_{A^0} = 1.8$ MeV/c^2 and 100 MeV/c^2 are plotted vs. A^0 lifetime in Figure 4 along with previous results [13], [14]. For lifetimes longer than 10^{-10} second, the probability of the A^0 passing through the apparatus before decaying reduces the sensitivity. For lifetimes shorter than 10^{-13}, a 90% confidence limit of 4.5×10^{-7} for the branching ratio for $K^+ \to A^0$ was obtained.

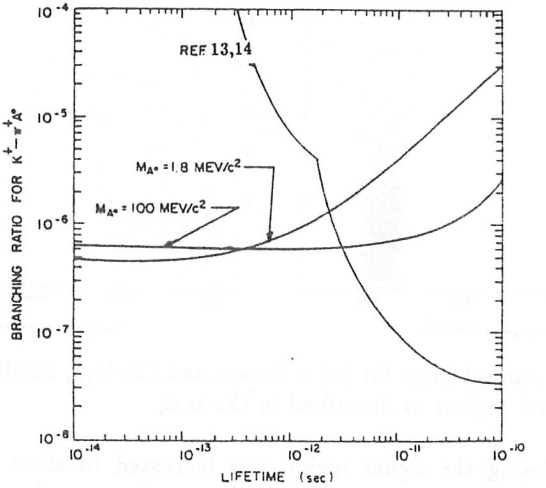

Figure 4. BR($A^0 \to e^+e^-$) for A^0 mass equal to 1.8 MeV/c^2 and 100 MeV/c^2 (this experiment) and 1.8 MeV/c^2 for the data of Refs 13 and 14.

4 -$K^+ \to \pi^+\mu^+e^-$ ($M_{\pi\mu e}$)

The primary backgrounds to the search for $K_{\pi\mu e}$ arise from τ and $K_{\pi 2}$ followed by Dalitz decays. In the former, $K^+ \to \pi^+\pi^+\pi^-$ where a π^+ decays to $\mu^+\nu$ with the ν emitted backwards and the π^- misidentified as an e^-. Kinematics reduces this background to the 10^{-5} level implying the necessity of maintaining the π^-/e^- misidentification probability below 10^{-7}. In the second case, the combined branching ratio for $K^+ \to \pi^+\pi^0$ followed by $\pi^0 \to e^+e^-\gamma$ is 2.5×10^{-3}. If the π^+ decays to $\mu^+\nu$ with the ν going backwards and the e^+ is misidentified as a π^+ kinematic rejection is good but insufficient to reduce this background to a tolerable level. An e^+/π^+ misidentification probability of less than 10^{-4} is necessary. Initial results on

$K_{\pi\mu e}$ were published by Campagnari *et al.* [15]. Figure 5(a) is a scatter plot of S vs. $K_{\pi\mu e}$ invariant mass for events with three charged pions in the final state. A clear τ signal is present at the K^+ mass for small values of S. The box around the signal region represents the boundaries of three standard deviations in invariant mass and 95% of events in S. The distributions are consistent with Monte Carlo simulations with the anticipated mass resolution. Events with the kaon invariant mass but large values of S are mainly due to events in which one of the pions decayed to $\mu\nu$ in while traversing the apparatus. The final results of the search for $K_{\pi\mu e}$ are displayed in Figure 5(b).

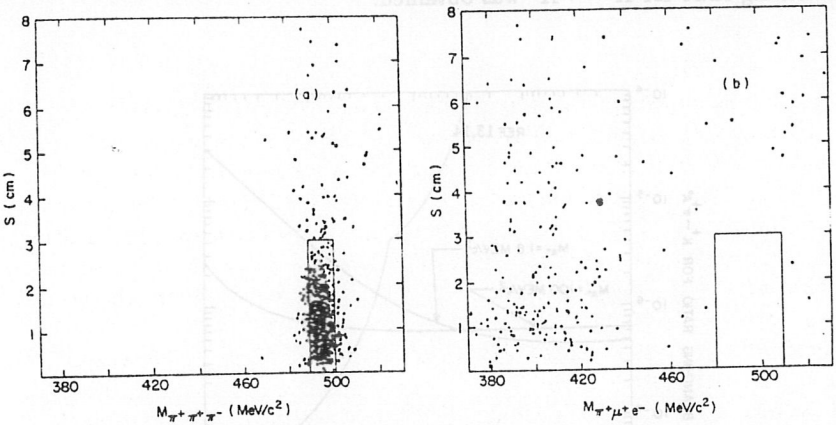

Figure 5. S vs. invariant mass for (a) τ decays and (b) $K_{\pi\mu e}$ candidates. The boxes represent the signal regions as described in the text.

The box enclosing the signal region was increased to allow for the increased kinetic energy released in $\pi\mu e$ decay relative to τ decay as determined by Monte Carlo simulation. The two events nearest the signal region with acceptable S have invariant masses of 474.9 and 512.2 MeV/c^2, 3.8 and 3.7 standard deviations from the kaon mass, respectively. Events below 450 MeV/c^2 result from τ decays in which the π^- was misidentified as an electron and a π^+ as a muon. The events in the high mass region are likely due to Dalitz decays in which the e^+ was taken for a π^+. The distribution of backgrounds is a minimum in the signal region as expected from Monte Carlo calculation which predicts $\sim$0.1 event in the region.

Since (Č1L)·(Č2L) triggers were used for both $K_{\pi\mu e}$ and Dalitz modes, the latter events with invariant mass greater than 350 MeV/c^2 were again used for normalization with appropriate corrections for relative acceptance as determined by Monte Carlo calculation. Other corrections included differences in efficiencies for various cuts in the two modes and differences in particle identification efficiency between positrons and muons whose ratio we estimate as $C = 1.26 \pm 0.10$. An uncertainty of

7% was assigned to the calculated ratio of acceptances. The final upper limit on the branching ratio for $K^+ \to \pi^+\mu^+e-$ is 2.1×10^{-10} at the 90% confidence level [16]. Generic models [17] incorporating horizontal gauge bosons to mediate lepton flavor violating transitions can be used to predict a mass scale for such a boson from the ratio of the limit for $K_{\pi\mu e}$ to the branching ratio for $K^+ \to \pi^0\mu^+\nu$. For a purely vector coupling of strength equal to that of the weak interaction, our result implies a mass, M_{HGB}, greater than 39 TeV/c^2.

Calculating the acceptance for the decay sequence, $K^+ \to \pi^+\pi^0$ followed by $\pi^0 \to \mu^+e^-$, it was also possible to set a limit for $BR(\pi^0 \to \mu^+e^-) < 1.6 \times 10^{-8}$ (90% C.L.).

5 -$K \to \pi^+e^+e^-$ ($K_{\pi ee}$)

$K_{\pi ee}$, is a strangeness changing neutral current decay and is highly suppressed in the *Standard Model* by the GIM mechanism [18]. The branching ratio and e^+e^- invariant mass spectrum have been calculated by a number of authors [19] but until the advent of E777 , the world sample of $K_{\pi ee}$ has been 41 events yielding a branching ratio of $(2.7 \times 10^{-7}$ [20]. Such highly suppressed processes are always attractive in that they might have enhanced sensitivity to new physics. With some model dependent assumptions a measurement of $K_{\pi ee}$ parameters can be related to those for $K_S^0 \to \pi^0e^+e^-$ [21].

Data for $K_{\pi ee}$, were obtained in two runs. In E777, Č1R and Č2R were filled with CO_2 and $K_{\pi ee}$ triggers were prescaled to reduce dead time due to Dalitz decays that would detract from the search for $K_{\pi\mu e}$. E851 was a dedicated to study $K_{\pi ee}$ and to search for $\pi^0 \to e^+e^-$ (π_{ee}). The prescale was eliminated and both sides of the Čerenkov counters were filled with hydrogen gas at atmospheric pressure in order to purify the trigger and data sample at the cost of a reduction in efficiency. A high e^+e^- mass trigger based on vertical separation of the e^+e^- tracks was implemented to enhance trigger sensitivity to $K_{\pi ee}$ and π_{ee} relative to Dalitz decays.

A scatter plot of the e^+e^- invariant mass vs. the $\pi^+e^+e^-$ invariant mass is displayed in Figure 6(a). A band of $K^+_{\pi ee}$ events with little background is prominent at the kaon mass for M_{ee} greater than 150 MeV/c^2. Below $M_{ee} = 150$ MeV/c^2 a band of Dalitz decays dominates the region below the kaon mass. The excellent fit of Monte Carlo simulations using the detector acceptance and the known properties of Dalitz decays to the data lends confidence to the validity of the conclusions for the analysis of $K_{\pi ee}$ and for the measurement of the branching ratio for $\pi \to e^+e^-$ which will be discussed in the next section. Figures 6(b) and 6(c) are the background subtracted M_{ee} and $M_{\pi ee}$ distributions, respectively, for events with M_{ee} greater than 150 MeV/c^2 and in the latter for high mass events with $470 < M_{\pi ee} < 512$MeV/c^2. The solid histograms are based on the known properties of the detector system. In addition the M_ee distribution in Figure 6(b) was fitted with the spectrum $d\Gamma/dM_{ee} = CM_{ee}p_\pi^3(1.0 + \lambda M_{ee}^2/M_\pi^2)$ anticipated from a vector interaction. In this expression, p_π is the pion momentum in the kaon rest frame, C is

an overall normalization constant which depends on the branching ratio, the normalization to Dalitz decays and acceptance and efficiency corrections and λ is a constant which determines the form factor for the decay. Figure 7(a) gives the results of this fit for the branching ratio and λ in contours of constant χ^2+n from E851. The results for the branching ratio and λ obtained in E777, $BR(K_{\pi ee}) = (2.75\pm0.23\pm0.13)\times10^{-7}$ and $\lambda = 0.105 \pm 0.035 \pm 0.015$ have been published [22] and are compared with the E851 results: $BR(K_{\pi ee}) = (2.87 \pm 0.32 \pm 0.13) \times 10^{-7}$ and $\lambda = 0.187 \pm 0.36 \pm 0.124$.

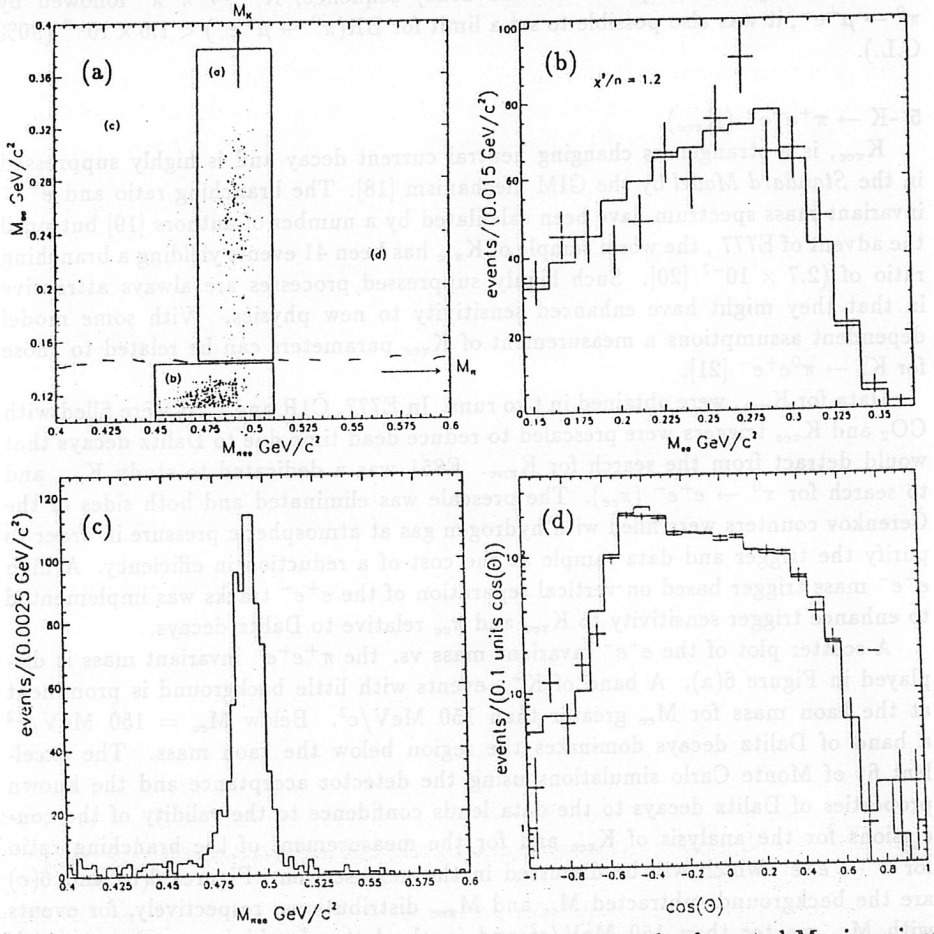

Figure 6. (a) Scatter plot of M_{ee} vs. $M_{\pi ee}$, (b) Background subtracted M_{ee} invariant mass distribution with a fit to the spectrum calculated from a vector interaction indicated by the histogram, (c) Background subtracted $M_{\pi ee}$ invariant mass spectrum, (d) angular correlation between the π^+ and the positron with the correlation calculated from a vector interaction(histogram).

Ecker, Pich and de Raphael have parameterized kaon decays using an effective chiral Lagrangian [23] which relates the decay rates and invariant mass spectra of different decay modes. In their formulation, the invariant mass spectrum M_{ee} can be written as $d\Gamma/dM_{ee} = 16 M_{ee} \bar{\Gamma} p_\pi^3 \mid \hat{\phi}_+(q^2) \mid^2 / M_K^5$ where $\bar{\Gamma}$ is an overall normalization factor and $\hat{\phi}_+ = -(\phi_K(q^2) + \phi_\pi(q^2) + w_+)$. The kinematic dependence of the kaon form factor, ϕ_K, is given by

$$\phi_K(q^2) = -\frac{4M_K^2}{3q^2} + \frac{5}{18} + \frac{1}{3}\left[\frac{4M_K^2}{q^2} - 1\right]^{3/2} \arctan\left[\frac{4M_K^2}{q^2} - 1\right]^{-1/2}$$

The pion form factor is the same with M_K replaced by M_π. The constant w_+ is related to a theoretically undetermined coupling constant which contributes to other rare kaon decays, most notably $K_{\pi\mu\mu}$, $K_L^0 \to \pi^0 e^+ e^-$ and $K_S^0 \to \pi^0 e^+ e^-$.

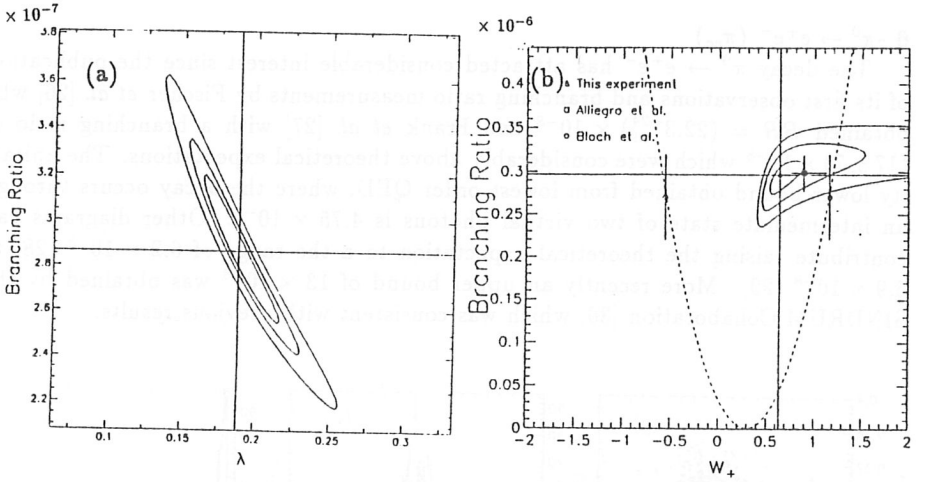

Figure 7. (a)$K_{\pi ee}$ branching ratio vs. λ for constant values of $\chi^2_{\min} + n$. (b) $K_{\pi ee}$ branching ratio vs. w_+ for contours of constant $\chi^2_{min} + n$.

The results of the fits to the spectra are given in Figure 7(b) where the quadratic dependence of the branching ratio on w_+ in chiral perturbation theory is indicated by the dashed curve. The two solutions obtained from the data of Bloch *et al.* [20] whose 41 events yielded only a branching ratio are indicated along with the E777 result of Alliegro *et al.* [22] and the E851 determination which is presented with constant contours of $\chi^2_{min} + n$. The results of the fits to the E777 and the E851 data in this parameterization are $BR(K_{piee}) = (2.99 \pm 0.22) \times 10^{-7}$, $w_+ = 0.89^{+0.24}_{-0.14}$ and $BR(K_{\pi ee}) = (2.97^{+0.19}_{-0.22}) \times 10^{-7}$, $w_+ = 0.64^{+0.25}_{-0.10}$, respectively. Since the theory specifies the kinematic dependence of the form factor up to the constant w for all $K_{\pi ll}$ decays, these results enable us to predict $BR(K_{\pi\mu\mu}) = (5.25^{+0.48}_{-0.24}) \times 10^{-8}$ and

$(4.86^{+0.39}_{-0.29}) \times 10^{-8}$ for the two values of w_+. AGS E787 recently reported 200 $K_{\pi\mu\mu}$ events which will lead to the first branching ratio determination for this decay [24].

The determination of w_+ also leads to a prediction for $BR(K^0_S \to \pi^0 e^+ e^-)$, with the relation $\hat{\phi}_S(q^2) = 2\phi_K(q^2) + w_S$ where $w_S = w_+ + \frac{1}{6} log \frac{m_\pi^2}{m_K^2}$. The resulting branching ratios, $BR(K^0_S \to \pi^0 e^+ e^-) = 4.5 \times 10^{-10}$ and $BR(K^0_S \to \pi^0 e^+ e^-) = 2.7 \times 10^{-10}$ are extremely sensitive to the error in w_+, where one standard deviation in w^+ leads to an order of magnitude increase in the upper limit in branching ratio. The one standard deviation upper bounds are close to the most recent experimental attempt to detect this decay which obtained a 90% C.L. upper limit of 4.3×10^{-9} [25].

These results imply one standard deviation upper limits for the branching ratio $BR(K^0_L \to \pi^0 e^+ e^-) < 1.2 \times 10^{-11}$ and $BR(K^0_L \to \pi^0 e^+ e^-) < 5.5 \times 10^{-12}$ if this decay were to proceed only through the CP violating part of the $K^0 - \bar{K}^0$ mass matrix.

6 -$\pi^0 \to e^+e^-$ (π_{ee})

The decay $\pi^0 \to e^+e^-$ has attracted considerable interest since the publication of its first observations and branching ratio measurements by Fischer *et al.* [26] who obtained $BR = (22.3^{+24}_{-11}) \times 10^{-8}$ and Frank *et al.* [27] with a branching ratio of $(17 \pm 7) \times 10^{-8}$ which were considerably above theoretical expectations. The unitarity lower bound obtained from lowest order QED, where the decay occurs through an intermediate state of two virtual photons is 4.75×10^{-8}. Other diagrams can contribute raising the theoretical expectation to a the range of 6.2×10^{-8} [28] to 6.9×10^{-8} [29]. More recently an upper bound of 13×10^{-8} was obtained by the SINDRUM Collaboration [30] which was consistent with previous results.

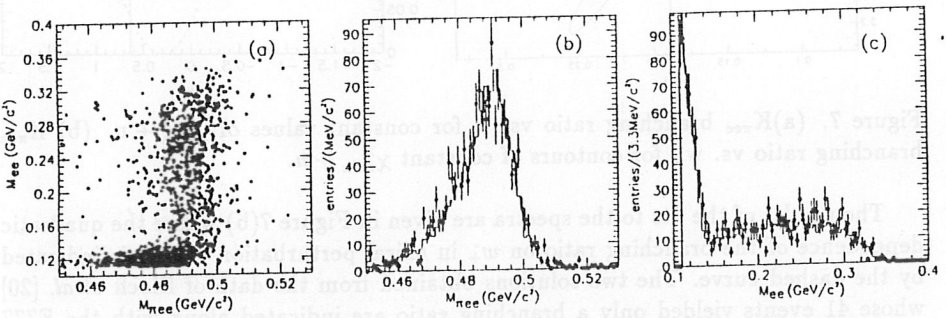

Figure 8. (a) Scatter plot of M_{ee} vs. $M_{\pi ee}$. (b)$M_{\pi ee}$ and (c) M_{ee} distributions with Monte Carlo simulations (histograms).

E851 carried out a search for this decay simultaneously with the measurement of $K_{\pi ee}$ with both the left and right sides of the Čerenkov counters filled with hydrogen. The analysis and normalization procedures were similar to those for the direct

$K_{\pi ee}$ decay but the backgrounds in the low M_{ee} region were somewhat different with contributions from $K_{\pi ee}$ itself, double Dalitz decay, i.e. $\pi^0 \to e^+e^-e^+e^-\gamma$ as well as Dalitz decays which were also used for normalization.

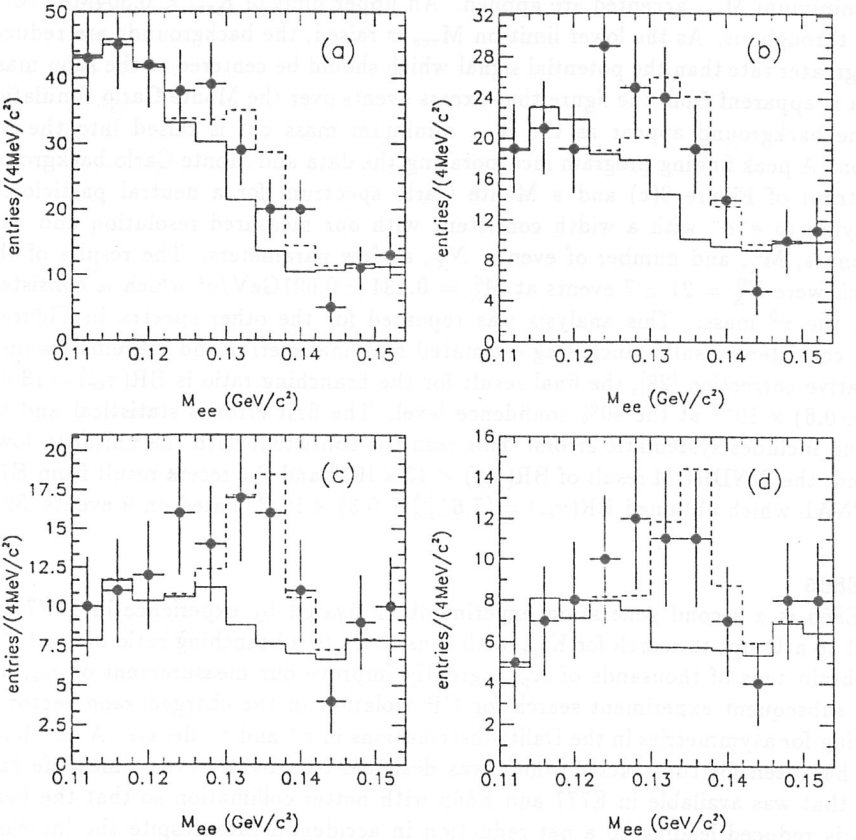

Figure 9. M_{ee} distributions in the vicinity of the π^0 for $M_{\pi ee} < 0.504\ GeV/c^2$ and (a) $M_{\pi ee} > 0.483\ GeV/c^2$, (b) $M_{\pi ee} > 0.487\ GeV/c^2$, (c) $M_{\pi ee} > 0.490\ GeV/c^2$ and (d) $M_{\pi ee} > 0.492\ GeV/c^2$. The solid histogram is the Monte Carlo simulation with no $\pi \to e^+e^-$. The dashed histogram indicates the fit of the peak finding program.

Figure 8(a) is a scatter plot of the M_{ee}vs.$M_{\pi ee}$ distribution for events in which the origin of the reconstructed kaon momentum vector is consistent with the position of the production target. Figures 8(a) and 8(b) give the projections of this distribution on the $M_{\pi ee}$ and M_{ee} axes, respectively. The histograms are the Monte Carlo simulations of our detector response to these background decays. The region below $M_{ee} = .15 MeV/c^2$ is dominated by Dalitz and double Dalitz decays. These events have $M_{\pi ee}$ less than the kaon mass because of the energy carried by the undetected

γ or e^+e^- pair. As the momentum of these particles approaches zero the measured invariant mass, $K_{\pi ee} \rightarrow M_K$ where they are the primary background in the search for $\pi^0 \rightarrow e^+e^-$. Figure 9 represents the M_{ee} spectrum as a successively higher cuts on the minimum $M_{\pi ee}$ accepted are applied. An upper limit of $K_{\pi ee} < 0.504 MeV/c^2$ is used throughout. As the lower limit on $M_{\pi ee}$ is raised, the backgrounds are reduced at a greater rate than the potential signal which should be centered at the kaon mass.

It is apparent from the figure that excess events over the Monte Carlo simulation of the background appear as the $K_{\pi ee}$ minimum mass cut is raised into the M_K region. A peak finding program incorporating the data and Monte Carlo background spectrum of Figure 9(c) and a Monte Carlo spectrum for a neutral particle X^0 decaying to e^+e^- with a width consistent with our measured resolution and with the mass, M_X^0, and number of events, N_X^0, as free parameters. The results of this search were $N_X^0 = 21 \pm 7$ events at $M_X^0 = 0.134 \pm 0.001 GeV/c^2$ which is consistent with the π^0 mass. This analysis was repeated for the other spectra in Figure 9 with consistent results. Including estimated systematic error and a bremsstrahlung radiative correction [28], the final result for the branching ratio is $BR(\pi_{ee}) = (8.0 \pm 2.6 \pm 0.6) \times 10^{-8}$ at the 90% confidence level. The first error is statistical and the second includes systematic errors. This result is consistent with the unitarity lower bound, the SINDRUM result of $BR(\pi_{ee}) < 13 \times 10^{-8}$ and the recent result from E731 at FNAL which obtained $BR(\pi_{ee}) = (7.6^{+3.5}_{-2.8} \pm 0.5) \times 10^{-8}$ based on 9 events [32].

7 -E865

E865 is a second generation experiment motivated by experience in E777 and E851 to attempt to search for $K_{\pi\mu e}$ with sensitivity to a branching ratio of 3×10^{-12}, to obtain tens of thousands of K_{piee}, greatly improve our measurement of π_{ee}, and in a subsequent experiment search for CP violation in the charged kaon sector by looking for asymmetries in the Dalitz distributions in τ^+ and τ^- decays. A new beam line has been for constructed which was designed to provide seven times the kaon flux that was available in E777 and E865 with better collimation so that the beam halo is reduced leading to a net reduction in accidental rate despite the increased beam intensity. The E865 apparatus is shown schematically in Figure 10. Major improvements include a factor of three larger acceptance using a 120D36 spectrometer magnet which also provides a p_t kick of 240 MeV/c compared to 165 MeV/c in the earlier experiments which will significantly improve our resolution. The major limitation experienced in searching for $K_{\pi\mu e}$ was the rate of accidental coincidences due primarily to beam halo. Our ability to reconstruct events with more than three hits in each chamber will be enhanced by the introduction of a fourth view in each multiwire proportional chamber package. A 600 element shower calorimeter has been constructed by the INR (Moscow) group which gives greatly improved pion-electron separation and by virtue of its high degree of segmentation, it provides a powerful tool when used with special modules for triggering the apparatus on topologies that are of physics interest and have desired properties such as crude momentum balance.

The E865 muon identifier covers both sides of the apparatus increasing the acceptance and has finer longitudinal segmentation. Dead time is reduced by means of more sophisticated triggering, tighter coincidence gates and a new data acquisition system that has an order of magnitude greater rate capability than the previous one.

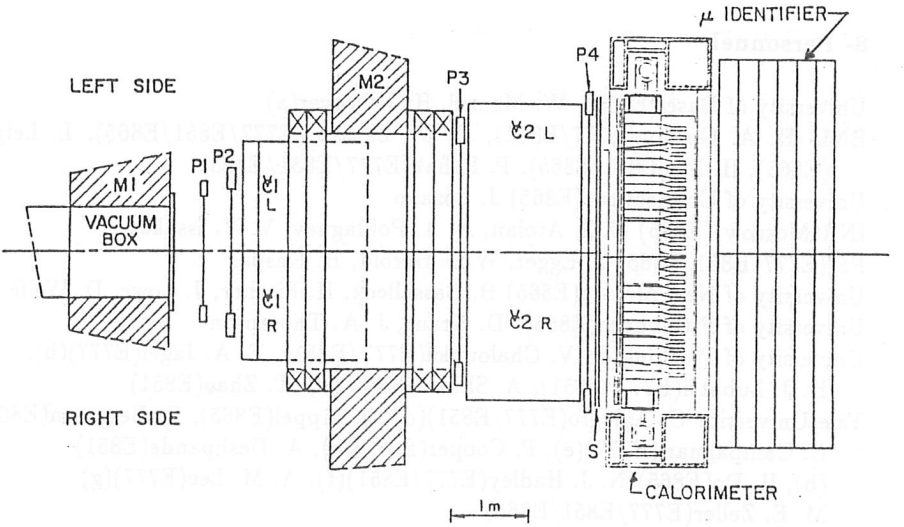

Figure 10. The E865 Apparatus.

An engineering run last year enabled us to determine that the beam performs as designed and to measure trigger rates and study the performance of various detectors some of which are being improved. We expect to begin taking data during the run that will take place next winter and spring.

The E865 apparatus is well suited for searching for CP violation in charged kaon decays by attempting to observe differences in the $\tau^{\pm}(K^{\pm} \rightarrow \pi^{\pm}\pi^{\pm}\pi^{\mp})$ decays. *Standard Model* predictions [33] for differences in rates, $\Delta(\Gamma) \equiv (\Gamma_{\tau^+} - \Gamma_{\tau^-})/(\Gamma_{\tau^+} + \Gamma_{\tau^-}) \simeq 0.094 \mid \epsilon' \mid$. However, in limited regions of the Dalitz plot these can be as large as $0.74 \mid \epsilon' \mid$. Therefore, by comparing the normalized populations of τ^+ and τ^- in each bin of the Dalitz plot and computing an asymmetry $A = (N_{\tau^+} - N_{\tau^-})/(N_{\tau^+} + N_{\tau^-})$ for that bin, a search for a systematic asymmetry across the Dalitz plot allows a sensitive test for CP violation. The previous experiment [34] found no regions of the Dalitz plot where A differed significantly from zero at the level of $\simeq 10^{-3}$ and the overall measurement gave $\Delta(\Gamma) = (5 \pm 7) \times 10^{-4}$, a result that was limited by statistics. In addition, they determined the asymmetry in the slope parameters $\Delta(a) \equiv (a^+ - a^-)/(a^+ + a^-) = (-5 \pm 7) \times 10^{-3}$ where $\mid M^{\pm} \mid^2 \propto 1 + a^{\pm}[(3T - Q)/Q]$ in the linear approximation, T3 is the kinetic energy of the odd charged pion and Q

is the total kinetic energy of the pions in the center of mass.

Predictions for $\Delta(a)$ based on chiral perturbation calculations have been as large as 1.4×10^{-3} [35] and as small as $\leq 4.5 \times 10^{-5}$ [36]. We anticipate the possibility of determining $\Delta(a)$ with a statistical accuracy of 2×10^{-5}. Systematic errors would likely be in the vicinity of 10^{-4}.

8- Personnel

University of Basel(E865)- W. Menzel, H. J. Weyer(a)
BNL- H. A. Gordon(E777/E851), D. M. Lazarus(E777/E851/E865), L. Leipuner (E865), H. Ma(E851/E865), P. Rehak(E777/E851/E865)
University of Connecticut(E865) J. Lozano
INR(Moscow)(E865) G. S. Atoian, A. A. Poblaguev, V. V. Issakov
PSI(E777/E851/E865) J. Egger, W.D. Herold, H. Kaspar
University of New Mexico(E865) B. Bassalleck, H. Fischer, J. Lowe, D. Wolfe
University of Pittsburgh(E865)- D. Kraus, J. A. Thompson
University of Washington V. Chaloupka(E777/E851), E. A. Jagel(E777)(b), H. J. Lubatti(E777/E851), A. Shukla(E865)(c), T. Zhao(E851)
Yale University C. Alliegro(E777/E851)(d), R. Appel(E865), D. Bergman(E865) C. Campagnari(E777)(e), P. Cooper(E777)(e), A. Deshpande(E851) (b), H. Do(E865) N. J. Hadley(E777/E851)(f), A. M. Lee(E777)(g), M. E. Zeller(E777/E851/E865)
University of Zurich(E865) S. Pislak, P. Truoel

Present address: (a) PSI, (b)CERN, (c)Utah State University, (d) Bell Telephone Laboratories, (e) FNAL, (f) University of Maryland, (g) Duke University

References

[1] For a review of technicolor models see E. Fahri and L. Susskind, Phys. Rep. **74**, 277 (1981)

[2] S. Dimopoulos and J. Ellis, Nucl. Phys. **B182**, 505 (1982).

[3] For a review of supersymmetric models see: P.Fayet and S. Ferrara , Phys. Rep. **32**, 249 (1977).

[4] O. Shanker, Nucl. Phys. **B206**, 253 (1982).

[5] R. D. Bolton *et al.*, Phys. Rev. D **38**, 2077 (1988).

[6] R. D. Bolton *et al.*, Op. Cit. [6].

[7] U. Bellgardt *et al.*, Nucl. Phys. **B299**, 1 (1988).

[8] A. M. Diamant-Berger *et al.* Phys. Lett. **62B**, 485 (1974).

[9] R. N. Cahn and H. Harari, Nucl. Phys. **B176**, 135 (1980).

[10] Particle Data Group, Phys. Rev. D **50** 1196, 1200 (1994). (1987).

[11] T.Cowan *et al.*, Phys. Rev. Lett. **56**, 444 (1986).

[12] N. J. Baker *et al.*, Phys. Rev. Lett. **59**, 2832 (1987) .

[13] Y. Asano *et al.*, Phys. Lett. **107B**, 159 (1981).

[14] Y. Asano *et al.*, Phys. lett. **113B**, 195 (1982).

[15] C. Campagnari *et al.*, Phys. Rev. Lett. **61**, 2062 (1988).

[16] A.M. Lee *et al.*, Phys. Rev. Lett. **64**, 165 (1990).

[17] R. N. Cahn and H. Harrari, Op. Cit.[10].

[18] S. L. Glashow, J. Iliopoulos, and L. Maiani, Phys. Rev. D **2**, 1285 (1970).

[19] M. K. Gaillard and B. W. Lee, Phys. Rev. D **10**, 897, (1974); D. V. Nanopoulos and G. G. Ross, Phys. Lett.**56B**, 279 (1975); A. I. Vainshtein, V. I. Zakharov, L. B. Okun, and M. A. Shifman, Yad. Fiz. **24**, 820 (1976)[Sov. J. Nucl. Phys. **24**, 427 (19760]; E. Witten, Nucl. Phys. **B120**, 387 (1977); J. O. Eeg and F. Ravndahl, Lett. Nuovo Cimento **22**, 397 (1978); F. J. Gilman and M. B. Wise, Phys. Rev. D **21**, 3150 (1980); J. O. Eeg, Lett. Nuovo Cimento **29**, 197 (1980); L. E. Ibáñez, C. López, and F. J. Ynduráin, Phys. Rev. D **21**, 1428 (1980); J.O. Eeg, Phys. Rev. D **23**, 2596 (1981); L. Bergström and P. Singer, Phys. Rev. Lett. **55**, 2633 (1985); C. O. dib, I Dunietz, and F. J. Gilman, Phys. Rev. D **39**, 2639 (1989).

[20] P. Bloch *et al.*, Phys. Lett. 56B, 201 (1975).

[21] G. Ecker, A. Pich, and E. de Raphael, Nucl. Phys. **B291**, 692 (1987).

[22] C. Alliegro *et al.*, Phys Rev. Lett. **68**, 278 (1992).

[23] G. Ecker, A. Pich, and E, de Raphael, op. cit.[23]

[24] M. Ito, These proceedings.

[25] D.A. Harris *et al.*, Phys. Rev. Lett. **71**, 3918 (1993).

[26] J. Fischer *et al.*, Phys. Lett. **73B**, 364 (1978).

[27] J. Frank *et al.*, Phys. Rev. D **28**, 423 (1983).

[28] L. Bergström, Z. Phys. C **14**, 129 (1982).

[29] A. N. Kamal and Lo Chong-Huah, Phys. Rev. D **32**, 1744 (1985).

[30] Carsten Niebuhr *et al.*, Phys. Rev. D **40**, 2796 (1989).

[31] A. Deshpande *et al.*, Phys. Rev. Lett. **71**, 27 (1993).

[32] K. McFarland *et al.*, Phys. Rev. Lett. **71**, 31 (1993).

[33] C. Avilez, Phys. Rev. D **23**, 1124 (1981).

[34] W. T. Ford *et al.*, Phys. Rev. Lett. **25**, 1370 (1970).

[35] A. A. Bel'kov, *et al.*, Phys. Lett. **232B**, 118 (1989).

[36] G. D'Ambrosio, G. Isidori, and N. Paver, Phys. Lett. **273B**, 497 (1991)

Frascati Physics Series, Vol. III (1994)
HEAVY QUARKS AT FIXED TARGET
University of Virginia, October 7–10, 1994
(pp. 343–357)

LEPTONIC DECAYS OF NEUTRAL KAONS – RECENT RESULTS AND EXPECTED EXPERIMENTAL PROGRESS

W. Molzon
Department of Physics and Astronomy,
University of California, Irvine, CA 92717

ABSTRACT

There has been recent significant progress in the study of decays of K_L^0 mesons to lepton pairs. A series of new experiments is searching for the possibility of muon- and electron-number violation in the decay $K_L^0 \to \mu e$ and studying the Standard Model physics of the top quark mass and mixing by measuring the rate for the decay $K_L^0 \to \mu\mu$. I summarize the motivation for these studies, present results of Brookhaven E791 on these and related decay modes, and report the status of BNL E871, which will improve the experimental sensitivity by a factor of twenty with respect to E791.

1 – Introduction and motivation

The study of leptonic decays of neutral kaons has resumed in the last few years, after a hiatus in these studies following a series of early experiments [?]. The renewed interest is due to significant advances in accelerators which allows higher flux kaon beams, to advances in detector technology which allow us to utilize the higher fluxes, and to renewed and expanded interest in the physics. This paper discusses two BNL experiments, one completed and one just beginning to take data. The goal of the experiments is to study the three leptonic decays: $K_L^0 \to \mu e$, $K_L^0 \to \mu\mu$, and $K_L^0 \to ee$.

The search for the decay $K_L^0 \to \mu e$ is one of a class of experiments designed to discover evidence for the violation of an additive quantum number associated with each of the three families of leptons: electrons, muons, and tau leptons. To the extent that we have looked, there appears to be a conserved additive quantum number

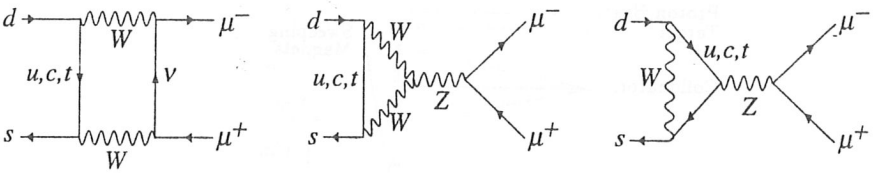

Figure 2: Short distance diagrams contributing to $K_L^0 \to \mu\mu$ decays.

The decay $K_L^0 \to ee$ is related to the decay $K_L^0 \to \mu\mu$; due to the lighter mass of the lepton it is more heavily suppressed by helicity considerations. As in the case of $K_L^0 \to \mu\mu$, the decay can proceed through real intermediate states (the dominant one being two photons) or through virtual intermediate states containing heavy quarks and vector bosons. The decay rate for the latter is suppressed with respect to $K_L^0 \to \mu\mu$ by a factor of m_e^2/m_μ^2. The suppression for the former is not as great; an additional factor of (≈ 17) appears in the ratio for modes involving real intermediate states. Hence this mode is not a fruitful way to study short distance Standard Model physics. However, it is a good way to look for non Standard Model processes, since the expected branching fraction from Standard Model modes is $\approx 3 \times 10^{-12}$. A measured branching fraction larger than this would be evidence for new physical processes.

2 – Results from Brookhaven E791

2.1 Description of the experiment

Brookhaven experiment 791 was conducted at the AGS in the B5 beamline, a neutral beam of 65 μsr produced at 2.75° from an incident proton beam of energy 24 GeV. The beam consisted of K_L^0 and neutrons in the approximate ration of 1:16. The mean K_L^0 energy was approximately 4 GeV, and the useful energy interval extended from 3 to 12 GeV. The neutral beam defining elements (collimators and sweeping magnets) extended for 10m downstream of the copper production target, and was followed by an evacuated decay region of length 8m. The beam and apparatus are discussed in detail elswhere [5] and in reference contained therein.

The apparatus, shown in fig. 3, consisted of a two arm spectrometer with two sequential magnets, each operated with a momentum kick of $\approx$ 300 MeV/c, and of opposite sign. The neutral beam was transported through the center of the apparatus, primarily in He, to a dump at the end of the apparatus. The spectrometer elements were drift chambers with high resolution ($\approx 120\mu$m) and efficiency (> 99%). The magnetic spectrometer was followed by planes of segmented scintillation counters for triggering, a threshhold gas Cerenkov counter and an array of lead

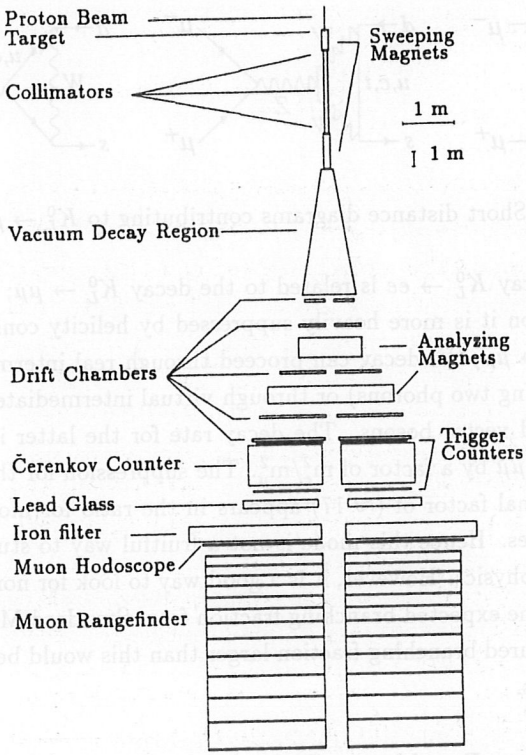

Figure 3: The E791 beamline and detector.

glass shower counters for electron identification, and a steel absorber followed by scintillation counters and a marble/drift tube range stack for muon identification.

The online event selection was done in two stages. The first consisted of fast electronics and was used to require hits in scintillation counters indicating the presence of a charged particle traversing each side of the spectrometer. A highly prescaled sample of such events (the minimum bias sample) was recorded, as were all events which in addition had a signal in either the Cerenkov counter or the muon scintillator hodoscope on each side of the spectrometer (the dilepton sample). For events satisfying these requirements signals in all detectors were transferred into buffer memories of a system of computers in which the events were analysed and further selected. The selection algorithm consisted of pattern recognition in the spectrometer and kinematic analysis of the events. Events consistent with originating from a two-body decay of a neutral kaon were accepted and transferred to a data-logging computer and written to tape.

Data were collected in three running periods, in 1988-90. The proton beam

intensity was up to 5×10^{12} per spill each 3.4 seconds; the spill time varied from 1.0-1.5s in different periods of data taking.

2.2 Analysis

The data were analysed in three stages. The first consisted of pattern recognition and a rough kinematic analysis to further restrict the sample of data consistent with two-body decays. The second consisted of a fitting procedure, by which the kinematic properties of charged particles which best fit the measured positions in the drift chambers were determined. This used a full three dimensional map of the magnetic field in the spectrometer, in which particle trajectories were numerically integrated. The third consisted of associating particle trajectories with signals in the particle identification counters to selected electrons and muons. Criteria by which events were identified as dilepton decays with well measured kinematic properties were derived without studying events in a kinematic region in which signal events were expected (e.g. in the mass interval around the kaon mass and in a region of apparant kaon transverse momentum near zero). We call this a blind analysis, and the purpose is to avoid biases in the selection process based on observations of possible signal events.

2.3 Experimental sensitivity, the $K_L^0 \to \pi\pi$ signal

All branching ratios were normalized to the $K_L^0 \to \pi\pi$ decay mode, with branching fraction $(2.03 \pm .04) \times 10^{-3}$. The normalization sample was chosen from the highly prescaled minimum bias events. The analysis was identical to that for di-lepton events, with the exception that there was no particle identification. The number of observed events was determined from the number of events in a 10 MeV/c^2 mass window around the kaon mass, with a background level subtracted. The shape of the latter was taken from a Monte Carlo simulation of semileptonic decays; the level was normalised to the observed level outside the kaon peak and interpolated under the peak. The $K_L^0 \to \pi\pi$ mass peak, with the background fit superimposed, is shown in fig. 4.

The relative acceptance and efficiency for this normalization mode and the dilepton modes was determined using a combination of measurements from the data and Monte Carlo simulations. For example, efficiencies of the lepton identification counters and of the lepton identification selection criteria were determined using well identified semi-leptonic decays. The relative efficiencies for geometrical acceptances were determined from Monte Carlo simulations of the detector. Trigger efficiencies were determined from the data, by measuring the probability that events from the

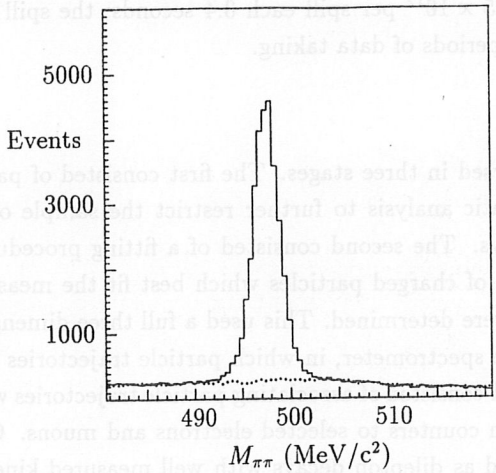

Figure 4: Distribution in $M_{\pi\pi}$ for a subset of the data with a fit to the semileptonic background superimposed.

minimum bias sample which satisfied offline selection criteria had the appropriate trigger bits set.

2.4 Results for $K_L^0 \to \mu e$

The crux of the $K_L^0 \to \mu e$ analysis is eliminating potential backgrounds while retaining high sensitivity and avoiding any bias for or against a possible signal. The analysis of the data proceeded by studying the background events in a region within $5 MeV/c^2$ of the K_L^0 mass and with $144 < p_T^2 < 800 (MeV/c^2)$. Here p_T is the transverse momentum of the charged pair with respect to the kaon direction, determined from the target and vertex position. Events in the signal region were not analysed until the final event selection criteria were chosen.

The distribution in p_T^2 vs. $M_{\mu e}$ for events which satisfiy a set of selection criteria on tracking and particle identification quality is shown in fig. 5. The predetermined area in which $K_L^0 \to \mu e$ signal events are expected is delineated by the box centered on the kaon mass. No events are contained in the signal region.

From these data, an upper limit on the branching fraction for $K_L^0 \to \mu e$ was determined. The limit is normalized to the known branching fraction for the 2π decay mode, correcting for relative acceptances and efficiencies (all numbers of order unity). The resulting 90% confidence limit [3] on the branching fraction is $B(K_L^0 \to \mu e) < 3.3 \times 10^{-11}$. These data have been previously reported [3]. When combined with results from a KEK experiment [4], the limit is $B(K_L^0 \to \mu e) < 2.4 \times 10^{-11}$.

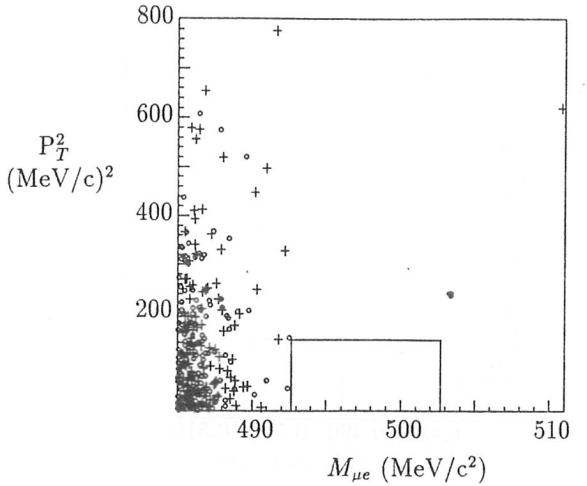

Figure 5: Scatter plot of P_T^2 vs. $M_{\mu e}$ for the final sample of $K_L^0 \to \mu e$ candidate events. Plus signs (circles) are 1989 (1990) data.

2.5 Results for $K_L^0 \to ee$

An analysis similar to that for $K_L^0 \to \mu e$ was applied to the $K_L^0 \to ee$ data set. Again, events in a region surrounding and excluding the signal region were studied to devise background rejection criteria. In addition to a series of selection criteria on tracking quality and particle identification, cuts were applied to remove background from the double Dalitz decay $K_L^0 \to eeee$, or external conversions of photons from $K_L^0 \to ee\gamma$ and $K_L^0 \to \gamma\gamma$ decay modes. Events were rejected if an extra track was detected in both views of the first two drift chamber planes which projected to within one centimeter of the vertex.

Fig. 6 is a scatter plot of θ_K^2 vs. M_{ee} for events passing all selection criteria. Here θ_K is the angle of the charged pair momentum vector with respect to the kaon direction determined from target and vertex positions. The signal region is delineated by the box in the figure, and no events are seen. Due to radiative energy loss from inner bremsstrahlung, the lower mass cut excludes approximately 17% of $K_L^0 \to ee$ events [6]. This cut is crucial in eliminating background processes to this decay. It does not exclude backgrounds from the Dalitz decay $K_L^0 \to ee\gamma$ with a soft photon, a process which is inherently indistinguishable from the inner bremsstrahlung corrected $K_L^0 \to ee$ process.

Again, since no events were observed, an upper limit was calculated [7]. The resulting 90% confidence limit on the branching ratio is $B(K_L^0 \to ee) < 4.1 \times 10^{-11}$ from the total data set. This is consistent with the predictions of the Standard Model. A KEK experiment [8] has also set an upper limit on this branching ratio; they

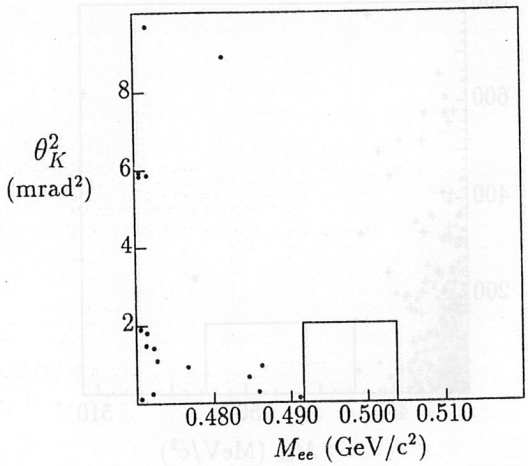

Figure 6: Scatter plot of θ_K^2 vs. M_{ee} for events from the combined 1989 and 1990 data sets which satisfy all selection criteria except those on θ_K^2 and M_{ee}.

saw one event, consistent with background, and quote $B(K_L^0 \to ee) < 16. \times 10^{-11}$

2.6 Results for $K_L^0 \to \mu\mu$

As discussed in the introduction, the short distance contributions to this process, which are of the greatest theoretical interest, probably account for only a small fraction of the decay rate. Hence, a precise measurement of the branching fraction (approaching 1% precision) is required to see the effect of these processes. Unlike the other decay modes, rejecting background is not so critical, since the signal is substantial and backgrounds can be subtracted statisticly if they are well understood. However, a careful analysis of the relative efficiencies and acceptances for detecting muon and pion pairs is required to reduce systematic uncertainties.

The analysis proceeded in much the same way as the searches described above. In this case, choices in the background rejection schemes were made on the basis of minimizing the uncertainty in the relative acceptance and efficiency for the 2π and 2μ decay modes.

Figure 7 shows a scatter plot of θ_K^2 versus $M_{\mu\mu}$ (for the 1990 data) and the distribution in $M_{\mu\mu}$ for events with $\theta_K^2 < 2\ mrad^2$ (for the 1989 and 1990 data). A signal is clearly seen near $\theta_K^2 = 0$ and $M_{\mu\mu} = M_K$. Also visible is a background extending to large $M_{\mu\mu}$ mass. This background is dominated by $K_L^0 \to \pi e\nu$ decays in which the pion decayed in-flight and the electron was misidentified as a muon; the misidentification produces a two-body invariant mass equal to or exceeding m_K. The background also contains a small number of mismeasured $K_L^0 \to \pi\mu\nu$ decays, which,

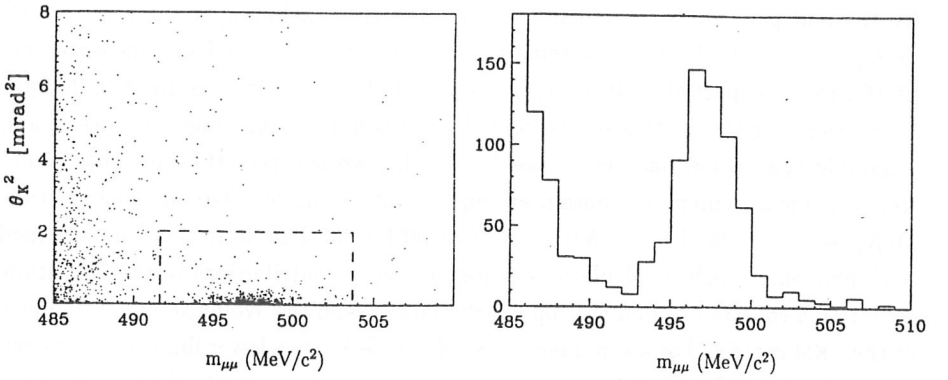

Figure 7: Scatter plot of θ_K^2 vs. $M_{\mu\mu}$ for events from the 1990 data, and the projection to the mass axis for the combined 1989 and 1990 data sets.

for perfect momentum measurement, have a kinematic endpoint at 489 MeV/c^2.

To subtract these backgrounds, the distributions of the dominant background sources were derived from the data by relaxing particle identification cuts. The shapes of these distributions were then normalized to the background outside the signal region, and the background in the signal region deduced. A total of 707 events over a background of 42 events is observed.

A careful study of the systematic uncertainties in the relative acceptance and efficiency for the signal and normalization channels was made. Included were uncertainties in the effects of pion decays and interactions(.5%), background subtractions(.8%), possible level 1(.4%) and level 3(.3%) trigger biases, uncertainties in the relative 2π and 2μ acceptances(2.0%), the absolute efficiencies of the muon identification(.3%), and the uncertainty in the $K_L^0 \to \pi\pi$ branching fraction(2.0%), where the numbers in parenthesis are the contributions to the uncertainty in the $K_L^0 \to \mu\mu$ branching fraction.

The results from the three years of data taking were combined [5], yielding a final result of $B(K_L^0 \to \mu\mu) = (6.86 \pm 0.25(stat.) \pm 0.27(syst.)) \times 10^{-9}$. The earliest of these measurements [10] was below the unitarity limit, although consistent with it within the experimental uncertainties. An experiment at KEK [9] has detected about 170 events and reported a branching fraction $B(K_L^0 \to \mu\mu) = (7.9 \pm 0.6(stat.) \pm 0.2(syst.)) \times 10^{-9}$.

Our result is consistent with the unitarity limit of 6.83×10^{-9} and implies either a small short distance contribution, or a cancellation of the short distribution

by the real part of the long distance contribution. Excluding the uncertainty on $B(K_L^0 \to \pi^+\pi^-)$, the total systematic uncertainty is 3.4% and our measurement of the ratio of partial widths $\Gamma(K_L^0 \to \mu\mu)/\Gamma(K_L^0 \to \pi^+\pi^-)$ is $(3.38 \pm 0.17) \times 10^{-6}$. Deriving the short distance contribution is not an unambigious process, and a sample calculation has been done [5]. Briefly, we subtract the unitarity bound from our measurement and obtain an upper limit on the real part of the amplitude $\mathcal{A}(K_L^0 \to \mu\mu)$: $|Re\mathcal{A}|^2 < 5.6 \times 10^{-10}$ at 90% C.L. This limit can be combined with phenomenological calculations of long-distance contributions to the amplitude to obtain a constraint upon the top quark mass m_t and the Wolfenstein parameter ρ of the CKM matrix. For a top quark mass of 180 GeV/c^2, a lower limit on ρ between -1.0 and -0.5 is derived, depending on the model used to calculate the long distance amplitude [5].

3 – Prospects for Improvement: E871

Experiment 791 at BNL was limited in sensitivity by a number of factors. First, the available proton intensity was limited to about 5×10^{12} protons per pulse by the AGS intensity and demands from other parts of the HEP program. Second, the available computing time in the level 3 trigger processors limited the level 1 trigger rate. Third, accidental triggers were a significant component of the level 1 trigger rate at the highest intensities, exacerbating the problem of limited online computing power. Fourth, the background rejection capabilities of the apparatus were close to being limiting; the predicted background for $K_L^0 \to \mu e$ was about 0.1 events, based on extrapolating measured background rates outside the signal region. These backgrounds seemed to result from a combination of tracking and measurement errors, and particle identification errors, often due to accidental signals in particle identification counters.

With the commisioning of the booster in the AGS complex, the AGS can now deliver greater than 50×10^{12} protons per pulse to experiments. E871 has been designed to use up to 20×10^{12}. This has necessitated a more sophisticated target consisting of a Pt target attached to a Be stem and water cooled heatsink. The sweeping magnet downstream of the target has been replaced with one containing radiation hard coils. To reduce the ratio of neutrons to kaons in the beam, it is produced at 3.75° with respect to the incident beam. This also results in a softer kaon spectrum, for which the detector has been optimized.

To obtain a significant gain in sensitivity over that of E791 a new apparatus was designed and built, using some of the E791 detectors but also using many new detectors and significantly reconfiguring the apparatus. A schematic drawing of the E871 detector is shown in fig. 8. The principle objectives of the new design are as

follows: to increase the acceptance, to use higher beam flux, to improve tracking and kinematic analysis, and to improve the particle identification. The experiment is again a two arm spectrometer with two magnets, these having p_T kicks of about

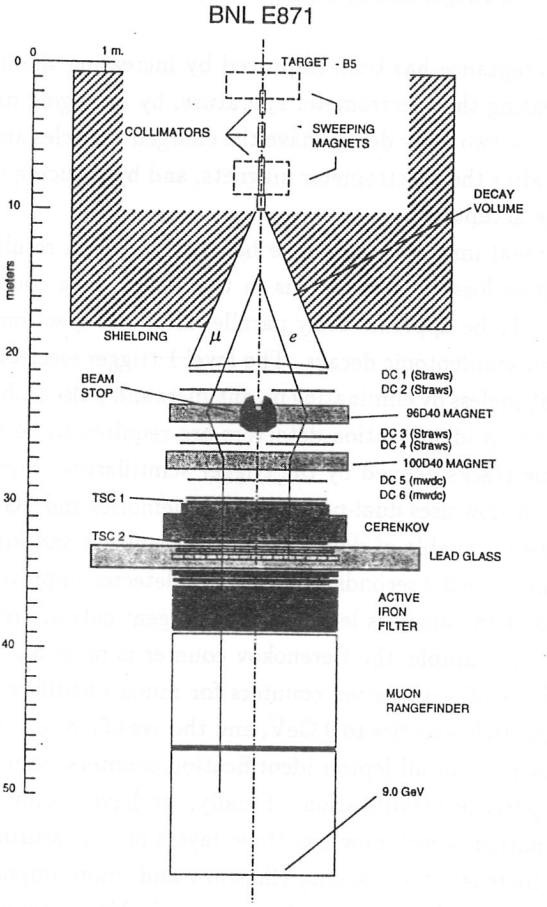

Figure 8: The E871 apparatus.

+440 and -220 MeV/c. An important feature of the design is a beam stop located in the gap of the first analysing magnet, in which the neutral beam is absorbed. This results in significantly reduced rates in detectors after the magnets, and allows detectors to be continuous across the projected beam line to improve the acceptance. All tracking chambers have three layers of detectors per module in the bending (x) view. The chambers before and between the magnets consist of 5mm diameter straw tubes, operated with a CF_4-ethane mixture with 100 μm/s drift velocity. The chambers after the magnets are conventional drift chambers similar in design to

those of E791. Electrons are identified using a H_2 filled Cerenkov counter, more highly segmented than in E791, and a lead glass array reused from E791. Muons are identified using multiple layers of scintillation counters located at positions ranging from 0.6-6.0 GeV of range, and by a range stack with 5% range resolution extending to 9 GeV range.

The acceptance has been improved by increasing the length of the decay region, by increasing the spectrometer aperature, by arranging magnetic fields such that about half the two body decays have the charged particles approximately parallel to the beam after the spectrometer magnets, and by reducing the low momentum limit on particle acceptance.

Additional improvements have been made which result in reduced deadtimes and analysis losses. Correlations in the scintillation counter signals require that particle tracks be approximately parallel after the spectrometer, reducing the trigger rate from semileptonic decays. The level 1 trigger electronics has been made essentially deadtimeless by eliminating meantimers and pulse reshaping circuits. The signals in the lepton identification detectors are required to be spatially correlated with the particle tracks defined by the trigger scintillators. The level 3 trigger has been upgraded; it now uses dual-ported buffer memories and SGI V35 processors in VME crates and is capable of doing pattern recognition and kinematic analysis of over 12000 events each 3.2 seconds. Many of the detector improvements are designed to reduce losses at the analysis level, where stringent cuts are required to eliminate backgrounds. For example, the Cerenokov counter is more finely segmented, there are multiple layers of scintillation counters for muon identification, the rangestack now measures particle energies to 9 GeV, and the use of a beam stop in the analysing magnet reduces rates in all lepton identification counters, resulting in cleaner and more efficient particle identification. Finally, we have significantly increased the tracking information, which now has three layers of x-measuring detectors in each module. This increases the tracking efficiency and, more importantly, reduces the chance of errors in tracking and the large errors in kinematic measurements which result.

The increase in sensitivity of E871 with respect to E791 has been calculated in two ways, by an *ab initio* calculation of the sensitivity, and by scaling the E791 sensitivity by factors for improved intensity, acceptance, and efficiencis. These improvements are summarized in tables 1 and 2.

E871 has now had a short first run, in June 1994, with essentially all detectors in place. Data were collected which have been used for calibrating detectors and developing online and offline analysis code. The first major physics run started January 1 1995. As an example of the performance of the apparatus, fig. 9 shows

	E791 1989 Data	E871 as proposed	Increase
$K_L^0 \to \mu e$ acceptance	0.0113	0.0242	2.14
$K_L^0 \to ee$ acceptance	0.00873	0.0224	2.57
$K_L^0 \to \mu\mu$ acceptance	0.0149	0.0283	1.90
Protons on target	3.8×10^{12}	15×10^{12}	3.95
L1 trigger efficiency	0.72	0.95	1.32
L3 trigger efficiency	0.64	0.95	1.48
Cerenkov electron efficiency	0.89	0.96	1.08
PBG electron efficiency	0.95	0.97	1.02
Running efficiency	0.875	0.92	1.05
Running time	17 weeks	38 weeks (2 years)	2.24

Table 1: Improvement factors of E871 with respect to the 1989 E791 run.

K_L in beam/spill	2×10^8
Fraction of K_L's decaying with $1.7 < p_K < 20$ GeV/c and $11.5\ m < z_{DK} < 26$ m	0.11
K_L decays in normalization region/spill	2.2×10^7
Spills/hour	1200
Beam hours/week	100
K_L's in 38 weeks of running	1×10^{14}
$K_L^0 \to \mu e$ acceptance	0.0242
Particle id efficiency (μe)	0.9
Trigger efficiency (combined)	0.85
Pattern recognition eff. (analysis cuts)	0.7
Running efficiency	0.92
Net efficiency (incl. acceptance)	0.012
Single event sensitivity	8.3×10^{-13}
90% confidence level sensitivity	2×10^{-12}

Table 2: *Ab initio* calculation of the E871 sensitivity.

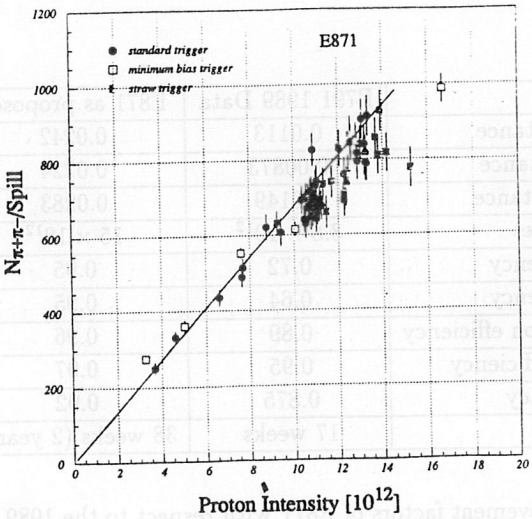

Figure 9: The number of $K_L^0 \to \pi\pi$ events as a function of proton intensity on target.

the number of reconstructed $K_L^0 \to \pi\pi$ events per unit time as a function of the proton beam intensity. The data are consistent with a linear increase in sensitivity with increasing beam intensity, indicating small deadtime and analysis losses even at intensities up to 15×10^{12} protons per pulse on target. The 1995 run is expected to continue through mid June and achieve a sensitivity of approximately 1 event at a branching fractio of 3×10^{-12} (assuming an efficiency and acceptance equal to that for $K_L^0 \to \pi\pi$). A data taking period of 25 weeks next year will allow the experiment to reach a sensitivity approaching 1 event at a branching fraction of 10^{-12}.

4 – Summary

Our knowledge of leptonic decays of neutral kaons has improved substantially in the last few years. From a situation where a total of 27 $K_L^0 \to \mu\mu$ events had been detected by a total of 4 experiments, we have progressed to a total of nearly 1000 events detected in two experiments. The branching fraction for $K_L^0 \to \mu\mu$ is now know to a precision of a few percent, close to the point where Standard Model parameters of top quark weak interactions can begin to be studied. Stringent limits on muon and electron number violation in the decay $K_L^0 \to \mu e$ have been set, approaching 10^{-11} in branching fraction. A similar limit has been set on $B(K_L^0 \to ee)$, and the prospects for detecting this decay at the Standard Model level are in sight. There is an experiment, E871 at Brookhaven National Lab, currently taking data which should improve these measurements by approximately a factor of 20.

Acknowledgements

I acknowledge my collaborators on BNL experiments E791 and E871, whose work I am reporting.

References

1. A.R. Clark *et al.*, Phys. Rev. Lett. **26**, 1667 (1971); W.C. Carithers *et al.*, Phys. Rev. Lett. **30**, 1336 (1973); *ibid.* **31**, 1025 (1971); Y. Fukushima *et al.*, Phys. Rev. Lett. **36**, 348 (1976); M.J. Shochet *et al.*, Phys. Rev. **D19**, 1965 (1979).

2. P. Langacker, S. Uma Sankar and K. Schilcher, Phys. Rev. **D38**, 2841 (1988); S. Dimopoulos and J. Ellis, Nucl. Phys. **B182**, 505 (1981); R. N. Cahn and H. Harari, Nucl. Phys. **B176**, 135 (1980); J. C. Pati and H. Stremnitzer, Phys. Lett. **B172**, 441 (1986); N.G. Deshpande and R. J. Johnson, Phys. Rev. **D27**, 1193 (1983); B. Mukhopadhyaya and A. Raychaudhuri, Phys. Rev. **D42**, 3215 (1990).

3. K. Arisaka *et al.*, Phys. Rev. Lett. **70**, 1049 (1993).

4. T. Akagi *et al.*, Phys. Rev. Lett. **67**, 2614 (1991).

5. A. Heinson, *et al.*, Phys. Rev. **D51**, 985 (1995).

6. L. Bergström, Z. Phys. **C20**, 135 (1983).

7. K. Arisaka *et al.*, Phys. Rev. Lett. **71**, 3910 (1993).

8. T. Inagaki, *et al.*, Phys. Rev. Lett. **67**, 2614 (1991).

9. T. Akagi *et al.*, Phys. Rev. Lett. **67**, 2618 (1991);

10. C. Mathiazhagan *et al.*, Phys. Rev. Lett. **63**, 2185 (1989).

Frascati Physics Series, Vol. III (1994)
HEAVY QUARKS AT FIXED TARGET
University of Virginia, October 7–10, 1994
(pp. 359–364)

RESULTS FROM BNL E787, A SEARCH FOR $K^+ \to \pi^+ \nu \bar{\nu}$

Mark M. Ito
Joseph Henry Laboratories, Princeton University, Princeton, New Jersey 08544

Flavor-changing-neutral-current decays of kaons provide an important tool for testing many features of the Standard Model. The GIM mechanism suppresses the rate of these decays by eliminating simple tree level weak processes, and so for some classes of decays, an observation tests the theory at higher order. The suppression can also be viewed as reducing the "Standard Model background" and allowing new physics to emerge.

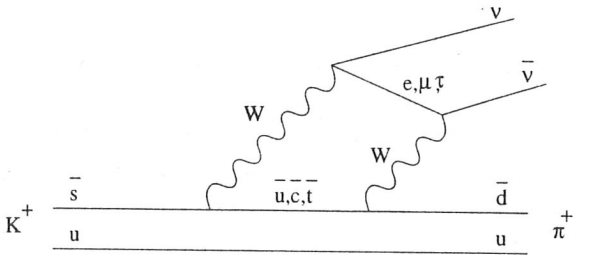

Figure 1: Diagram for $K^+ \to \pi^+ \nu\bar{\nu}$

Fig. 1 shows one of the diagrams that contributes to the decay $K^+ \to \pi^+ \nu\bar{\nu}$. Even at the one-loop level, the rate would vanish if not for the differences in the quark masses which upset the cancellation of the diagrams. Many authors have estimated the rate of $K^+ \to \pi^+ \nu\bar{\nu}$ in the context of the Standard Model.[1–5] The branching ratio is most sensitive to the values of the CKM matrix elements and the top quark mass. Uncertainties in the hadronic matrix element have been largely eliminated by relating this rate to that of $K^+ \to \pi^0 e^+ \nu_e$ and long distance effects have been shown to be negligible[6] for $K^+ \to \pi^+ \nu\bar{\nu}$. The present expectation is that the branching ratio is in the range $(0.5 - 3) \times 10^{-10}$. Most of the uncertainty comes from the CKM matrix element V_{td}. This process is therefore one of the best ways to get at this element. The best previous experimental upper limit on this process[7] is 1.4×10^{-7} at the 90% confidence level.

This leaves a large window in which to search for new physics. An experiment sensitive to $K^+ \to \pi^+\nu\bar{\nu}$ will detect the charged pion coming from the K^+ decay recoiling against a weakly interacting system of particles. Hence it will be sensitive to certain types of new particles which include the familon,[8] and supersymmetric particles.[2,9–10] In addition, the standard model rate may can also be altered with the addition of new virtual particles. For example in models with non-minimal Higgs sectors a virtual charged Higgs can change the flavor of the s quark. Diagrams like these can add to or subtract from the rate for $K^+ \to \pi^+\nu\bar{\nu}$.[11]

The main backgrounds to a measurement of $K^+ \to \pi^+\nu\bar{\nu}$ come from the decays $K^+ \to \mu^+\nu$ ($K_{\mu 2}$) with a branching ratio of 64% and $K^+ \to \pi^+\pi^0$ ($K_{\pi 2}$) with a branching ratio of 21%. These are both topologically similar to the decay of interest, with one charged track in the final state. In order to deal with the background there are three broad areas of attack. First, one must be able to distinguish pions from muons. One way to do this is to observe the unique decay sequence $\pi^+ \to \mu^+\nu$, $\mu^+ \to e^+\nu\bar{\nu}$. Second, the detector must efficiently veto the photons from π^0 decay. This requires a 4π photon detector. And third, one must exploit the differences between the kinematics of the decay and those of the background.

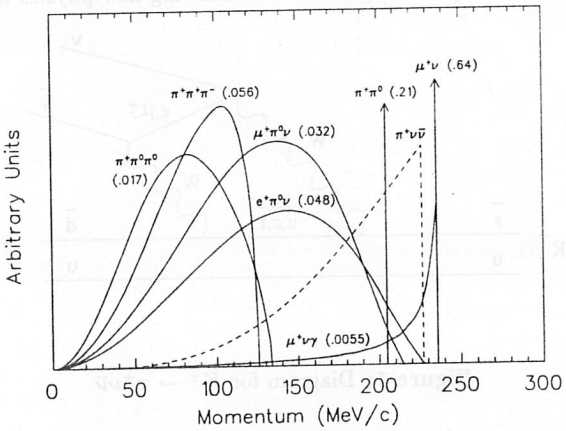

Figure 2: Momentum spectrum for charged particles from K^+ decay. Branching ratios are given in parentheses.

Fig. 2 shows the momentum spectrum of the daughter charged particles from K^+ decay measured in the kaon rest frame. The two-body modes have a unique range. The three-body decay $K^+ \to \pi^+\nu\bar{\nu}$ peaks at its end point and has a significant fraction of its phase space between the $K_{\pi 2}$ and $K_{\mu 2}$ peaks. The data analysis focuses on the area of phase space above the $K_{\pi 2}$ peak. As discussed below, the detector provides three independent measurements of the decay kinematics: momentum, range, and energy. This redundancy

guards against mismeasurement of a single quantity and provides a means of particle identification.

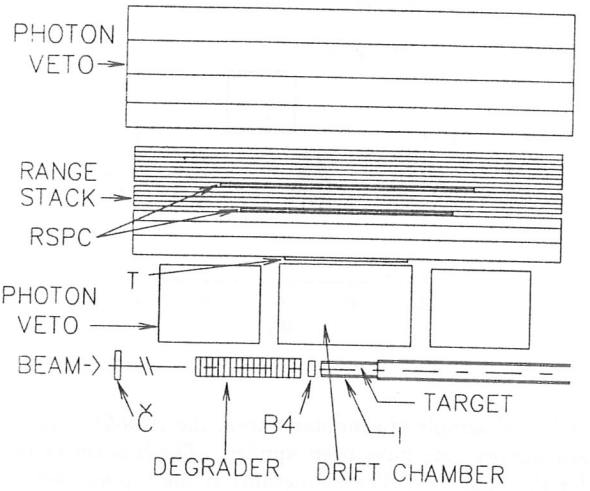

Figure 3: Side view of the E787 detector. Only the top half of the detector is shown. The detector has cylindrical symmetry.

The detector[12] is shown in Fig. 3. It is located at the end of a 775 MeV/c separated beamline at the Brookhaven AGS. The beam was instrumented with a Čerenkov counter, several scintillator hodoscopes, and a small MWPC. The beam passed through a beryllium oxide degrader and kaons were ranged out in a scintillating fiber target. Surrounding the target was a cylindrical drift chamber which provided a momentum measurement of the decay particle. The decay particle entered and was brought to rest in a plastic scintillator range stack. In addition to the range measurement, the kinetic energy was measured by summing the pulse height in struck range stack counters. Outside of the range stack was a lead-scintillator barrel photon veto. Completing the solid angle coverage of the photon veto were lead-scintillator endcaps. Surrounding the entire detector was a conventional copper-coil magnet which provided a 1 T field. The tagging of the $\pi \to \mu \to e$ decay sequence is accomplished by instrumenting the range stack with 180 channels of 500 MHz, 8-bit transient digitizers.

The most recent result from E787 on $K^+ \to \pi^+ \nu\bar{\nu}$ is from data collected in 1989, 1990 and 1991. A preliminary analysis of the data from these years uses a total exposure of 3.47×10^{11} stopped K^+'s. Fig. 4 shows the candidate events before the final cuts on range and kinetic energy have been applied. The events below the accepted region are consistent with $K_{\pi 2}$ decays where both photons from the π^0 have been missed. There are several events above the accepted box consistent with $K_{\mu 2}$ events. No events are seen in the signal region. The acceptance for $K^+ \to \pi^+ \nu\bar{\nu}$ is 0.18%. The acceptance for a two-body decay

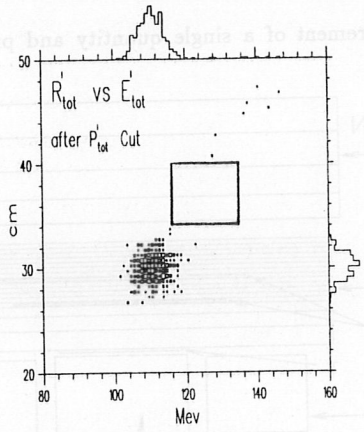

Figure 4: Final sample of candidates from the 1989-91 data before range and kinetic energy cuts have been applied. The box shows the accepted regions for the final cuts. The histograms at the top and left margins are projections of the data.

$K^+ \to \pi^+ X^0$ is 1.1%, assuming that $m_{X^0} = 0$. Preliminary branching ratio limits are:

$$\mathrm{BR}(K^+ \to \pi^+ \nu\bar{\nu}) < 3.7 \times 10^{-9}$$

$$\mathrm{BR}(K^+ \to \pi^+ X^0) < 6.1 \times 10^{-10}$$

at the 90% confidence level.

E787 has also observed a signal for the rare decay $K^+ \to \pi^+\mu^+\mu^-$. This decay has not been seen before and the best existing limit is at a branching ratio of less than 2.3×10^{-7} the 90% confidence level.[13] Theoretical predictions[14–15] are in the range $(3-7) \times 10^{-8}$. Chiral perturbation theory makes a prediction for the shape of the $m_{\mu\mu}$ spectrum that is coupled to the absolute total rate. This decay can be compared to a recent measurement of $K^+ \to \pi^+ e^+ e^-$.[16] The decay has been seen in two independent analyses, one which emphasizes a clean experimental signature by detecting all three charged particles in the central drift chamber and the other which emphasizes high efficiency by summing the observed kinetic energy of the K^+ decay products. In the latter analysis only two of the particles need to be seen in the drift chamber. Fig. 5 shows the final kinetic energy spectrum in the high efficiency search. The lower, small peak is due to decays $K^+ \to \pi^+\pi^+\pi^-$. Other K^+ decays that have subsequent Dalitz decays of π^0's contribute background events across the entire region examined. There is a clear signal of about 200 events at the kinetic energy expected for $K^+ \to \pi^+\mu^+\mu^-$. Both of these analyses are still in progress.

The experiment took data during the summer of 1994 with several improvements. The most important of these was a new separated beam line which increases the K^+ flux by

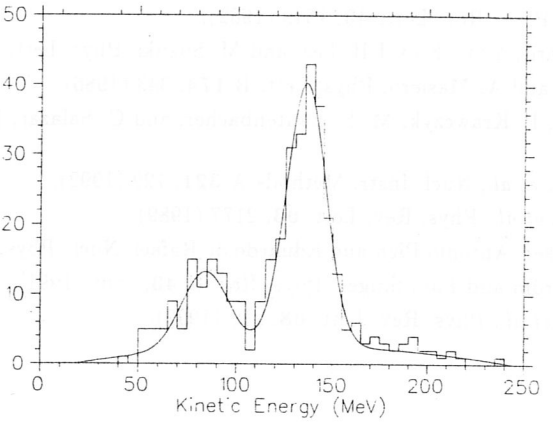

Figure 5: Kinetic energy of final candidate events in $K^+ \to \pi^+\mu^+\mu^-$ analysis.

a factor of about 2.5 per incident proton, and which dramatically improves the purity of the beam, giving a $K{:}\pi$ ratio of 4:1. The ratio was formerly 1:2. Also installed were a new scintillating fiber target, a completely rebuilt trigger system, a new data acquisition computer with associated control software, a new central tracking chamber, new z-tracking chambers in the range stack, cesium iodide crystal endcap detectors, and finer segmentation of the inner layers of the range stack.

The AGS booster will started to increase the intensity of the proton beam in 1995. Eventually, the increase will be a factor of about four over the intensity performance of the recent past. Major detector improvements are being contemplated, including an upgrade of the barrel photon detector and further segmentation of the range stack to deal with potential backgrounds from accidentals in the new high rate environment. The ultimate goal of E787 is to see several events if they occur at the Standard Model rate.

References

1. T. Inami and C. S. Lim, Prog. Theor. Phys. **65**, 297 (1981).
2. J. Ellis and J. S. Hagelin, Nucl. Phys. B **217**, 189 (1983).
3. J. Ellis, J. S. Hagelin, and S. Rudaz, Phys. Lett. B **192**, 201 (1987).
4. C. O. Dib, I. Dunietz, and F. J. Gilman, Mod. Phys. Lett. **6**, 3573 (1991).
5. C. Q. Geng and J. N. Ng, Phys. Rev. D **41**, 2351 (1990).
6. D. Rein and L. M. Sehgal, Phys. Rev. D **39**, 3325 (1989).
7. Y. Asano *et al.*, Phys. Lett. **107B**, 159 (1981).

8. F. Wilczek, Phys. Rev. Lett. **49**, 1549 (1982).
9. M. K. Gaillard, Y.-C. Kao, I-H. Lee, and M. Suzuki, Phys. Lett. **123B**, 241 (1983).
10. S. Bertolini and A. Masiero, Phys. Lett. B **174**, 343 (1986).
11. A. J. Buras, P. Krawczyk, M. E. Lautenbacher, and C. Salazar, Nucl. Phys. B **337**, 284 (1990).
12. M. S. Atiya, *et al.*, Nucl. Instr. Methods A **321**, 129 (1992).
13. M. S. Atiya *et al.*, Phys. Rev. Lett. **63**, 2177 (1989).
14. Gerhard Ecker, Antonio Pich and Eduardo de Rafael, Nucl. Phys. **B291**, 692 (1987).
15. Lars Bergström and Paul Singer, Phys. Rev. D **43**, 1568 (1991).
16. C. Alliegro *et al.*, Phys. Rev. Lett. **68**, 278 (1992).

Frascati Physics Series, Vol. III (1994)
HEAVY QUARKS AT FIXED TARGET
University of Virginia, October 7–10, 1994
(pp. 365–376)

THE FERMILAB RARE KAON DECAY PROGRAM

Robert S. Tschirhart
Fermi National Accelerator Laboratory
Representing the E799–I and KTeV Collaborations

Abstract

Recent results from the new rare kaon decay program at Fermilab are presented. The status and prospects of the new KTeV initiative are discussed with emphasis on recent electron beam test results of a full CsI calorimeter prototype test array.

1 – Introduction.

The principal goal of the Fermilab rare kaon decay program is to search for rare kaon decays that are likely[1] to have a large CP violating component in the decay amplitude. This so called "direct" CP violation is parameterized by ϵ' in the $K \to \pi\pi$ system, whereas CP violation occuring through $K^0 - \bar{K}^0$ mixing is parameterized by ϵ. In contrast to $K_L \to \pi\pi$ decays where $|\epsilon'/\epsilon|$ is very small $(10^{-4} - 10^{-3})$, decays such as $K_L \to \pi^0 e^+ e^-$ are expected[1] to have $|\epsilon'/\epsilon| \sim 1$. Unlike $K_L \to \pi\pi$ decays, the experimental challenge is to *find* examples of these decays, where the expected branching fraction is at the $10^{-12} - 10^{-11}$ level.

The Fermilab rare kaon decay program was initiated with phase-I of E799 which was an eight week test run during the 1991 fixed target running cycle. The total integrated flux collected corresponded to approximately 40

billion kaon decays in the fiducial volume. In addition to triggers tuned for $K_L \to \pi^0 l\bar{l}$ decays, several other triggers were implemented in parallel that were sensitive to rare or forbidden neutral kaon and lambda decays. One of these parallel triggers resulted in the first clear observation of $K_L \to \mu^+\mu^-\gamma$ in a signal of 200 events, where previously[12] only one candidate event had been observed. Experiment E799 will continue in KTeV, which is a new kaon physics initiative at Fermilab that will measure $|\epsilon'/\epsilon|$ with a sensitivity of 10^{-4} and probe rare kaon decays at the 10^{-11} level. This large step in sensitivity is achieved through pure CsI calorimetry, an improved spectrometer, a high speed data acquistion system, transition radiation detectors (TRDs) to provide e/π rejection, and a very hermetic photon veto system. The current status and future prospects $K_L \to \pi^0 l\bar{l}$ searches and $K_L \to \mu^+\mu-\gamma$ are now described.

2 $- K_L \to \pi^0 e^+ e^-$:

Both the direct (ϵ' : $K_2 \to \pi^0 e^+ e^-$) and indirect (ϵ : $K_1 \to \pi^0 e^+ e^-$) CP violating amplitudes of this decay are expected[2] to contribute to the branching fraction at the $(1-10)\times 10^{-12}$ level. The CP conserving amplitude of the branching fraction, $K_L \to \pi^0\gamma^*\gamma^*$, is strongly helicity supressed, and is expected[2] to be less than 1×10^{-11}. Hence extracting the direct CP violating component of $K_L \to \pi^0 e^+ e^-$ may very well be complicated by the presence of other amplitudes. Far more serious than the complication of other amplitudes is a significant background[3] from radiative Dalitz decay, $K_L \to e^+e^-\gamma\gamma$. This process has been observed[4, 6] with a branching fraction of $(6.5 \pm 1.3) \times 10^{-7}$ for events with a minimum energy photon of 5 MeV in the center of mass. The only experimental handle available to reject this background is the reconstructed $m_{\gamma\gamma}$ mass. High performance calorimetry such as the KTeV pure CsI calorimeter can efficiently allow a $m_{\gamma\gamma}$ mass cut of $\pm 5\ MeV$ ($\pm 3\sigma$), which reduces[3] this background to the $(1-3) \times 10^{-11}$ level. The pure CsI KTeV calorimeter is radiation hard to tens of kRads, fast

($25nsec$), and has been proven to provide an energy resolution of less than 1% for rare kaon decay photon energies. Despite this large step in calorimetry instrumentation, it is likely that the direct CP violating component of $K_L \rightarrow \pi^0 e^+ e^-$ will have to be observed above a significant background from $K_L \rightarrow e^+ e^- \gamma\gamma$.

Two recent experiments BNL/E845 and Fermilab/E799-I searched for $K_L \rightarrow \pi^0 e^+ e^-$, and have set comparable limits[4, 5] of less than 5.5×10^{-9} and 4.2×10^{-9} respectively at the 90% confidence level. Both these experiments are background limited at this level of sensitivity. The principal background at this level is $K_L \rightarrow \pi^{\pm} e^{\mp} \nu + \gamma_{(rad\ or\ accidental)} + \gamma_{accidental}$ where the pion is misidentified as an electron. Phase-II of E799 (KTeV) will strongly reject this background process through a better beam design to reduce accidental energy deposits, and dramatically better e/π rejection realized through pure CsI calorimetry and a TRD system. The rare kaon decay experiment KEK/E162 in Japan has now had an engineering run, and is expected to probe $K_L \rightarrow \pi^0 e^+ e^-$ with a single event sensitivity of 1×10^{-10}. Experiment KEK/162 is the first neutral kaon experiment to employ pure CsI calorimetry. KTeV will probe $K_L \rightarrow \pi^0 e^+ e^-$ with a single event sensitivity[2] of 6×10^{-11}. This large step in rare decay reach is realized through the following detector detector improvements and increased flux:

a) $\times 3.5$ increase in proton intensity on target.

b) $\times 3.0$ increase in running time.

c) $\times 1.4$ increase in live time, 50% $\rightarrow$ 70%.

d) $\times 2.0$ increase in acceptance through the use of CsI calorimetry and few accidental losses due to better secondary beam design.

e) An increase in e/π rejection from $\times 70$ (Phase-I) to to $\times 40,000$ (Phase-II) through a combination of CsI calorimetry and a TRD system.

3 – $K_L \to \pi^0 \mu^+ \mu^-$:

Both the direct and indirect CP violating components to this decay are supressed by the reduced phase space to 20% of the $K_L \to \pi^0 e^+ e^-$ branching fraction. The CP conserving amplitude is not as strongly supressed as $K_L \to \pi^0 e^+ e^-$, and hence it is likely that this process will be dominated by the CP conserving component. The Fermilab experiment E799-I has set a background free limit[7] of 5.1×10^{-9}, which is an improvement of $\times 300$ over the previous measurement[12]. The Fermilab/KTeV experiment[2] will probe this mode with a single event sensitivity of 1×10^{-11}.

4 – $K_L \to \pi^0 \nu \bar{\nu}$:

This process is quite intriguing in that the direct CP violating component can be calculated[2, 8] with a high degree of confidence in the context of the Standard Model, and is expected to dominate the branching fraction. In addition, the direct CP violating amplitude is expected to be significantly larger, ($\sim 6 \times 10^{-11}$) than the amplitude in $K_L \to \pi^0 e^+ e^-$, primarily due to three neutrino flavors increasing the number of final states. Unfortunately observing this final state is extremely challenging. In beam experiments where adequate flux may exist but kaon decay verticies and energies vary from event to event, the decay process is poorly constrained. Kinematic constraints in beam experiments can be acquired by requiring Dalitz decay ($\pi^0 \to e^+ e^- \gamma$) of the π^0, but this reduces the effective flux by $\times 70$. The Frascati Φ factory does have adequate kinematic constraints to cleanly observe this process, but the expected sensitivity is limited to well above the 10^{-10} level. An interesting suggestion[11] has been made recently by A. Konaka (TRIUMF) that one can produce a tagged beam of K_L through associated production near threshold, $\pi^- p^+ \to \Lambda^0 K^0$, where the Lambda decay tags the momenta of the K_L.

The first search for this process in a beam experiment was from Fermi-

lab/E731 where a Dalitz decay ($\pi^0 \to e^+e^-\gamma$) was required, and a limit of 2.2×10^{-4} was set on the $K_L \to \pi^0\nu\bar{\nu}$ process and the 90% confidence level[9].

Phase-I of Fermilab/E799 has continued this search using the same method, and sets a limit of 5.8×10^{-5} at the 90% confidence level[10]. The KTeV experiment expects to push the single event sensitivity to this process into the 10^{-8} range while still requiring the Dalitz decay requirement. At this level of sensitivity background from $K_L \to \pi^{\pm}e^{\mp}\nu + \gamma_{accidental}$ where the pion is misidentified as an electron is quite serious, and requires a very high level of π/e rejection from the KTeV CsI calorimeter and TRD system to defeat. Background from $\Lambda^0 \to n(\pi^0 \to e^+e^-\gamma)$ is significant as well, and requires tagging of the neutron with a hadron calorimeter to defeat.

In order to relax the Dalitz decay requirement and gain back a factor of $\times 70$ in sensitivity, a very hermetic veto system is required to veto kaon decay backgrounds with missing photons, the most serious of which is $K_L \to \pi^0\pi^0$. There is great deal of interest in extending this search with a rare kaon decay experiment that would exploit the very high proton flux of the Fermilab Main Injector. A "Kaons at the Main Injector" (KAMI) design report has been prepared[14], where an experiment is discussed that could ultimately probe $K_L \to \pi^0 e^+e^-$ at the 10^{-14} level, and $K_L \to \pi^0\nu\bar{\nu}$ at the 10^{-13} level.

5 – Observation of $K_L \to \mu^+\mu^-\gamma$

The decay $K_L \to \mu^+\mu^-\gamma$ is expected to be dominated by the so-called long distance contributions occuring via the $K\gamma\gamma^*$ vertex[15]. Knowledge of long distance contributions can help to determine the origin of the $\Delta I = \frac{1}{2}$ enhancement in non-leptonic weak interactions. Other rare kaon decays such as $K_L \to \mu^+\mu^-$ depend on similar long distance contributions which must be measured in order to extract Standard Model parameters.[16, 17, 18] The reconstructed $\mu^+\mu^-\gamma$ mass is shown in figure 1, showing a clear signal of aprroximately 200 events over a background of 10 events. The $\mu^+\mu^-$ invariant mass is shown in figure 2, together with the Monte Carlo expectation

based on a Dalitz decay form factor. Clearly the process is dominated by the Dalitz decay amplitude. A combined fit of the branching fraction and the $m_{\mu\mu}$ mass distritubion sensitively probes the $K\gamma\gamma^*$ vertex for contributions beyond the Dalitz form factor. The measured branching fraction[21] of $(3.23 \pm 0.23(stat) \pm 0.19(sys)) \times 10^{-7}$ is in fact 2.9σ greater than the expectation of a pure Dalitz form factor, which is the first evidence of a contribution to the form factor beyond the Dalitz component. KTeV should observe nearly 10,000 of these decays, which will enable precision studies of the non-trivial structure of the $K\gamma\gamma^*$ vertex.

6 – Status of KTeV Preparations.

The most demanding instrumentation requirements of the KTeV detector are with the CsI calorimeter which must provide an energy resolution of better than 1% for photons and electrons between 2 GeV/c^2 and 80 GeV/c^2, and an e/π rejection of better than $\times 500$ over the same range. These high performance goals were tested and met in an electron test beam run at CERN in August of 1994. The 5×5 test-array was a full prototype of KTeV crystals and readout electronics. The readout electronics is a high-speed pipelined ADC system[19] orginally designed for the SDC detector at the SSC. The measured energy resolution of the test-array is shown in figure 3 with and without the resoltion function of the electron beam removed. From figure 3 it is clear that the calorimeter resolution is less than 1% over the required dynamic range. The measured e/π rejection of 30 GeV pions in shown in figure 4 where the momentum width of the beam was increased from 0.3% to 3% in order to acquire a larger sample of data. For an electron acceptance of 95% the measured e/π rejection is $\times 400$. The e/π rejection scales to nearly $\times 900$ for an energy resolution of 1%, which is more than adequate for KTeV. The details of the test beam run and results are documented elsewhere[20]. Installation of the calorimeter will commence with completion of the new experimental hall in July of 1995.

7 – Summary.

Standard model expectations[13] suggest that in the near future the new Fermilab/KTeV and CERN/NA48 initiatives will likely observe direct CP violation through the avenue of $|\epsilon'/\epsilon|$ measurements. Such an observation would invalidate the Superweak hypothesis of CP violation. Theoretical uncertainties[13] in Standard Model predictions for the magnitude of $|\epsilon'/\epsilon|$, will limit tests of Standard Model predictions only to a qualitative level. Precision tests of Standard Model expectations for direct CP violation in the neutral kaon system must wait for observations of the very rare neutral kaon decays, $K_L \to \pi^0 l\bar{l}$. The prospect of quantitatively challenging the Standard Model has generated a great deal of interest in meeting the enormous technical challenge of observing $K_L \to \pi^0 l\bar{l}$ decays at a statistically significant level. The KAMI facility at that Fermilab Main Injector may be able to meet these challenges, and a detailed study of KAMI prospects is now underway.

References

[1] B. Winstein, L. Wolfenstein, Reviews of Modern Physics. (10/93) Modern Physics.

[2] See Fermilab report FN-580 for a conceptual design of the KTeV experiment.

[3] H. B. Greenlee, Phys. Rev. D. **42**, 3724 (1990).

[4] K.E. Ohl et al., Phys. Rev. Lett. **64**, 2755 (1990).

[5] D. H. Harris et, al., Phys. Rev. Lett. **71**, 3918 (1993).

[6] T. Nakaya, et al., Phys. Rev. Lett. **73**, 2169 (1994).

[7] D. H. Harris et, al., Phys. Rev. Lett. **71**, 3914 (1993).

[8] G. Buchalla, A. Buras and M. Harlander, Nucl. Phys. **B349** 1 (1991).

[9] G. E. Graham et, al., Phys. Lett. **B295**, 169 (1992).

[10] M. Weaver, et al., Phys. Rev. Lett. **72**, (1994).

[11] A. Konaka. Proceedings of "Future Directions in Particle and Nuclear Physics" **BNL-52389** 456 (1993).

[12] Carrol et, al., Phys. Rev. Lett. **44**, 525 (1980).

[13] M. Ciuchini et al., CERN-TH.7514/94, Rome prep. 94/1024.

[14] See Fermilab report FN-568 for a conceptual design of the KAMI experiment.

[15] L. Bergstrom, E. Masso, P. Singer, Phys. Lett. **131B**, 229 (1983).

[16] P. Singer,. Nuc. Phys. **A527**, 713c (1991).

[17] G. Belanger, C.Q. Queng, Phys. Rev. **D43**, 140 (1991).

[18] P. Ko, Phys. Rev. **D44** 139 (1991).

[19] R. Yarema et, al., Fermilab-TM-1895, June 1994.

[20] R. Kessler et, al., Submitted for publication in NIM.

[21] M. Spencer et, al., Accepted for publication in Phys. Rev. Lett.

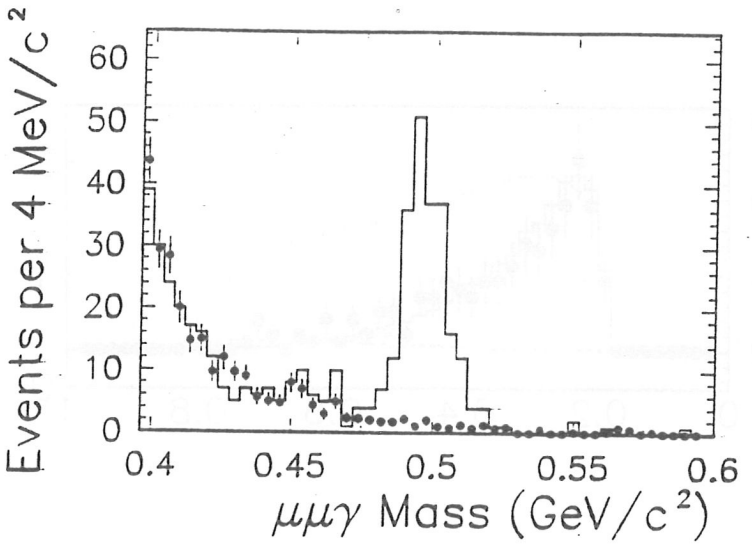

Figure 1: $\mu^+\mu^-\gamma$ mass distribution after cuts. Histogram is data for events with P_t^2 less than 200 MeV^2/c^2 and points are for events with P_t^2 greater than 200 MeV^2/c^2 and less than 1000 MeV^2/c^2 normalized to the low P_t^2 data.

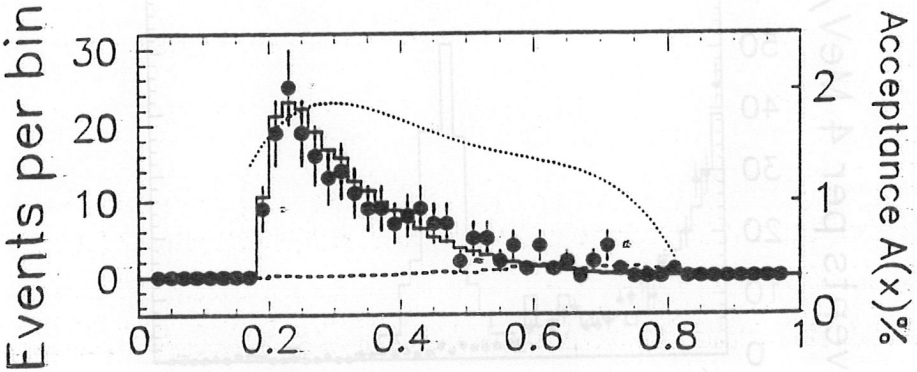

Figure 2: Dimuon mass distribution, points are data, histogram is a Monte Carlo simulation with a Dalitz form factor as a funciton of x where $x = m^2_{\mu\mu}/m^2_K$. The dashed line is the estimated background and the dotted line is the acceptance.

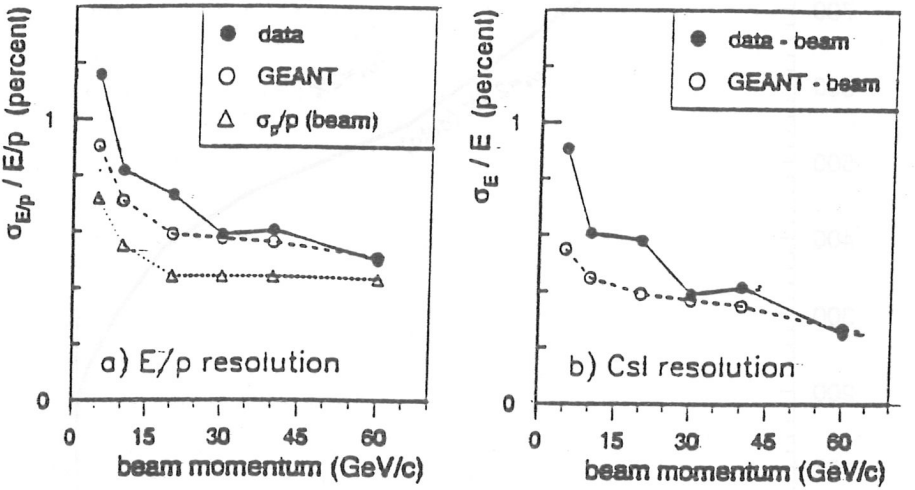

Figure 3: a) *PRELIMINARY* E/p resoultion .vs. beam momentum, and b) the intrinsic CsI resolution with the beam contribution subtracted.

Frascati Physics Series, Vol. III (1994)
HEAVY QUARKS AT FIXED TARGET
University of Virginia, October 7–10, 1994
(pp. 377–398)

RESULTS ON RARE DECAYS OF NEUTRAL KAONS FROM THE NA31 EXPERIMENT AT CERN

Konrad Kleinknecht

Institut für Physik, Johannes Gutenberg-Universität Mainz
55099 Mainz, Germany

ABSTRACT

Experimental data from the neutral Kaon decay experiment NA31 at CERN have been analyzed. Results include the first observation of the mode $K_L \to \pi^o\gamma\gamma$ with a branching ratio of $(1.7\pm0.3)\ 10^{-6}$ and an invariant $\gamma\gamma$ mass spectrum favouring chiral perturbation theory, a measurement of 2021 events of the Dalitz decay $K_L \to \gamma e^+e^-$ yielding a branching ratio of $(9.1\pm0.3^{+0.5}_{-0.6})10^{-6}$ and of 8 events of the double Dalitz decay, $K_L \to e^+e^-e^+e^-$, with a branching ratio of $(10.4\pm3.7\pm1.1)10^{-8}$. Searches are also reported for the decay $K_S \to \pi^o e^+e^-$ ($BR<1.1\times10^{-6}$ at 90% C.L.), $K_L \to \pi^o\pi^o\gamma$ ($BR<5.6\times10^{-6}$ at 90% C.L.) and $K_L \to 3\gamma$ ($BR<2.8\times10^{-7}$ at 90% C.L.).

1. Introduction

The experiment NA31 was originally designed for measuring the CP violating decays $K_L \to \pi^0\pi^0$ and $K_L \to \pi^+\pi^-$. The experiment resulted in the first evidence for direct CP violation with the experimental result for the parameter $\varepsilon'/\varepsilon = (2.30\pm0.65)\ x10^{-3}$ [1]. Concurrently with the 2π decay modes, other rare decays were registered in this detector. This report describes the experimental results on some of these decay modes.

2. The NA31 neutral Kaon detector

This detector is able to measure the neutral and charged two-pion and other decay modes of neutral K mesons. While $\pi^0\pi^0$ decays are detected through four electromagnetic showers and $\pi^+\pi^-$ decays through two charged tracks, for the final states discussed here it is necessary to detect electromagnetic showers ($\pi^0\gamma\gamma$, $\pi^0\pi^0\gamma$, 3γ) or charged particles ($e^+e^-e^+e^-$) or both photons and charged particles (γe^+e^-, $\pi^0e^+e^-$).

The beam and detector for the experiment have been described in detail in ref. [2]. Long-lived kaons are produced with an average momentum of 100 GeV/c by 450 GeV/c protons striking a beryllium target located 244m upstram of the electromagnetic calorimeter. Charged particles are removed by a sweeping magnet, and a neutral beam is selected by collimation to ±0.2 mrad. The final collimator, with diameter 6 cm, is located 124 m upstream of the electromagnetic calorimeter. It is followed by a 95 m long evacuated region. The neutral beam is further transported in an evacuated tube of diameter 20 cm through a central hole in the detectors. Decays occurring downstream of the final collimator over a region of 50 m in length are detected in a setup of wire chambers and calorimeters with outer diameters of 2.5 m typically. The relevant parts of the detector - ordered in downstream direction - are:

- four ring-shaped anti-counters surrounding the decay region, and placed between 60 and 120 m from the final collimator, to veto events with photons missing the calorimeter;
- two wire chambers, spaced 23 m apart, each consisting of four planes, with a resolution of ±0.5 mm in each projection;

- a transition radiation detector (TRD) for electron /pion discrimination composed of four modules, each with a plastic foil radiator and a wire chamber filled with a Xenon (30%)- Helium (55%)-Methane (15%) mixture [3l;
- scintillator hodoscopes triggering on charged and neutral decay modes;
- an electromagnetic lead/liquid argon calorimeter (LAC) with 1.25 cm wide strips measuring the energies of photons and electrons with a resolution of $7.5\%/\sqrt{E(GeV)}$and their impact points with a transverse spatial resolution of ±0.5 mm in each projection;
- an iron/scintillator sandwich calorimeter which measures the energy of charged pions;
- two planes of scintillators behind an absorber of a thickness equivalent to 3 m of iron, which detect penetrating muons.

The wire chambers are used to measure the directions of charged particles and to reconstruct the position of the decay vertex, while the liquid argon calorimeter measures energies and impact positions of electrons and photons. The hadron calorimeter and the transition radiation detector are used to reject events containing charged pions.

3. Event reduction and reconstruction

The trigger requires a minimum total energy of 35 GeV and at least two energy clusters in each projection in the liquid argon calorimeter. For decay modes with charged tracks, in addition more than six hits in the four planes of the first wire chamber are required. In the off-line preselection of candidates, the following criteria are used: more than 45 GeV energy deposited in the liquid argon calorimeter, less than 6 GeV energy seen in the hadron calorimeter, and - for decay modes with charged tracks - at least one spacepoint in each wire chamber. These events were kinematically reconstructed.

A complete reconstruction of the tracks - if any - in the chambers is performed. Independently, narrow energy clusters indicating electromagnetic it any showers are found from the pulse heights in the calorimeter. Electron tracks are reconstructed by linking space points from the two wire chambers with electromagnetic showers.

For events which have only photons in the final state, the longitudinal position Z_K of the decay vertex is calculated from the energy and transverse position of the electromagnetic showers in the LAC under the assumption that the invariant mass is the nominal kaon mass ("neutral vertex"). For events with two or four electron tracks, this longitudinal

position can also be calculated from the tracks ("charged vertex"). For two tracks, this is calculated from the minimum distance of approach of the two tracks, or in events with four tracks this is obtained by requiring the sum of the squared transverse distances d^2 from the four tracks to the transverse vertex position to be a minimum:

$$d^2 = \sum_{i=1}^{4} \frac{(x_{ti} - x_v)^2 + (y_{ti} - y_v)^2}{\sigma_{ti}^2}$$

where x_{ti} and y_{ti} are the coordinates of track i at the longitudinal vertex position z_v, and σ_{ti} ist the resolution in the transverse distance from track i to the vertex.

For each decay mode, different fiducial cuts are made on these vertex positions, depending on the presence of background. Common kinematical fiducial cuts require: i) the total energy deposited in the LAC to be between 50 and 190 GeV (60 to 170 GeV for $\pi^o\gamma\gamma$), ii) the individual electromagnetic shower energy to be between 3 and 100 GeV (for γe^+e^-, $e^+e^-e^+e^-$, and $\pi^o e^+e^-$ decays modes) or between 5 and 100 GeV (for $\pi^o\gamma\gamma$, $\pi^o\pi^o\gamma$, and 3γ), iii) the energy barycentre in the electromagnetic calorimeter to be within 5 cm from the beam axis (7 cm for Dalitz decays γe^+e^- and $e^+e^-e^+e^-$, and 9 cm for $K_S \to \pi^o e^+e^-$). The last requirement rejects events with large missing transverse energy.

4. Decay $K_L \to \pi^0\gamma\gamma$

The decay $K_L \to \pi^o\gamma\gamma$ is of considerable theoretical interest. Firstly, it may be used to estimate the CP conserving contribution to the decay $K_L \to \pi^o e^+e^-$ [4-6] via two-photon intermediate states. The decay $K_L \to \pi^o e^+e^-$ is a candidate for detecting direct CP violation. If the amplitudes for $K_L \to \pi^o\gamma\gamma$ are small enough, then the decay $K_L \to \pi^o e^+e^-$ is dominated by CP violating contributions. This experiment provides a measurement of the dominant J=0, and a limit on the J=2 two-photon contribution to the $K_L \to \pi^o\gamma\gamma$ decay.

Secondly, the decay $K_L \to \pi^o\gamma\gamma$ may be used to test the chiral perturbation theory, and some semi-empirical models describing kaon decays. Lowest order chiral expansion [7] and models involving $\pi^+\pi^-$ intermediate states in addition to the π^o [8] predict a branching ratio around 7×10^{-7} and J=0 for the photon pair. The $\gamma\gamma$ invariant mass spectrum extends from about $2m_\pi$ to the kinematical limit. Higher order chiral expansion and other calculations including vector (or scalar) meson intermediate states [9] predict a

branching ratio between 0.7×10^{-6} and 3×10^{-6} depending on the contribution at low $m_{\gamma\gamma}$, for which the photon pair should have J=2.

This decay was originally observed by NA31 [10]; the present analysis supports this result with more than twice the K_L flux. Events with four electromagnetic showers are required for this experiment. The main problem is then the rejection of unwanted background from $\pi^0\pi^0$ and $3\pi^0$ decays. The four showers are grouped into two pairs. One pair is required to have a mass near the π^0 mass (between 125 and 145 MeV), assuming the "neutral vertex" z_K reconstructed from all four showers and the kaon mass. The other pair should not have the π^0 mass. The rejection of $\pi^0\pi^0$ states is done by requiring the quantity

$$\mu = \left(\frac{m_{ij} - m_{kl}}{12\ \text{MeV}}\right)^2 + \left(\frac{m_{ij} + m_{kl} - 2m_\pi}{8\ \text{MeV}}\right)^2$$

to be above 5 for all possible pairings (ij) and (kl) of the four showers. If, in addition, events with similar energies in the same quadrant of the LAC are removed, 99.94% of the selected $\pi^0\pi^0$ events are removed.

The remaining sample of 5881 candidate events consists mainly of background from $K_L \rightarrow 3\pi^0$ with two photons undetected or with one photon undetected and two photon showers overlapping in the LAC. Here the fine granularity of the LAC helps reducing this background. On the basis of a sample of 9×10^8 simulated $K_L \rightarrow 3\pi^0$ decays, it appears that for both background sources, the reconstructed neutral vertex is shifted by at least 7.5 m downstream relative to the true vertex. Using this property and the fact that in most of the background events there is at least one π^0 reconstructible from the electromagnetic showers in the LAC, it is possible to eliminate 99.6 % of the $3\pi^0$ background and still keep 46% of the $\pi^0\gamma\gamma$ signal. 94 candidates remain after all cuts. Fig. 1 shows a significant peak in the distribution of the invariant two-photon mass m_{12} at the π^0 mass. We define the signal region as the mass interval from 132.5 to 137.5 MeV, corresponding to a $\pm$ 1.4 σ interval. 63 events lie inside this signal region.

The simulations of the remaining backgrounds indicate that the background under the peak may be estimated by linear interpolation. This leads to a background of 6.0±1.7 events and a signal of 57±8.1 $K_L \rightarrow \gamma\gamma$ decays.

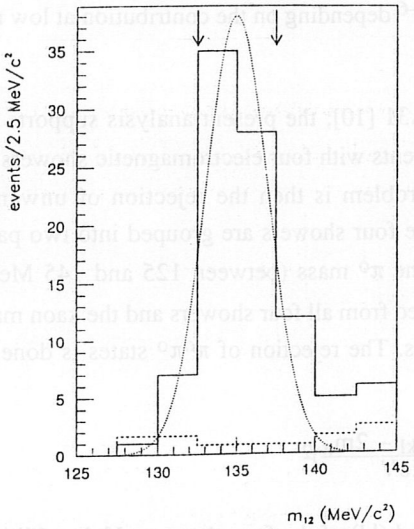

Fig. 1: Invariant mass m_{12} for $K_L \to \pi^0\gamma\gamma$ candidates (solid) and for expected background (dotted). Gaussian represents resolution.

Normalizing this number to the K_L flux using the $K_L \to \pi^0\pi^0$ sample, we obtain the branching ratio $\Gamma(K_L \to \pi^0\gamma\gamma) / \Gamma(K_L \to \text{all}) = (1.7\pm0.3) \times 10^{-6}$ where the error includes the systematic error. This branching ratio is slightly higher than the value from chiral perturbation theory in lowest order p^4 [7]. More involved models including vector meson contributions, presumably substituting the p^6 contributions [9], agree better with this experimental value.

More detailed information about the validity of these theoretical models is obtained from the invariant mass distribution of the two incorrelated photons, m_{34}. The data are shown in Fig. 2. There is a clear concentration of events above a mass of 240 MeV, just as predicted by chiral perturbation theory where the leading effective process corresponds to a charged pion loop radiating two photons. This process yields photon pairs mainly above $2m_\pi = 270$ MeV. The distribution predicted by chiral perturbation theory is shown in the figure as dotted histogram.

There is no evidence for a signal below $m_{34} = 240$ MeV. From this fact, we extract the parameter a_V characterizing the vector meson contribution in the notation of ref. [7], as

$$a_V = -0.05^{+0.14}_{-0.17}.$$

From this, we deduce a limit on the J = 2 two-photon contribution and on the total CP-conserving contribution to the decay $K_L \to \pi^0 e^+ e^-$. We conclude that this contribution is less than 4.5×10^{-13} at 90% C.L., small compared to the expected CP violating contributions.

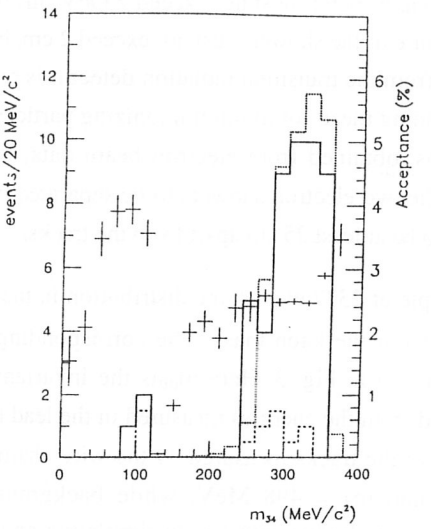

Fig. 2: Invariant mass m_{34} for unambiguous $K_L \to \pi^0\gamma\gamma$ candidates with m_{12} in the signal region (solid), for background (dashed) and for prediction of chiral perturbation theory (dotted). Crosses show acceptance (right-hand scale).

5. Dalitz decay $K_L \to e^+e^-\gamma$

The Dalitz decay of the long-lived neutral K meson, $K_L \to ee\gamma$, is intimately related to its decay into two photons. The Dalitz decay sheds light into the structure of the $K_L \to \gamma\gamma^*$ vertex, through the measurement of the lepton pair produced by the virtual photon [12]. Phenomenological models of this structure include vector meson dominance of the photon propagator [13] and QCD models involving penguin diagrams and pole diagrams [14]. The branching ratio is calculated to be $(9.1\pm0.4)10^{-6}$ without a form factor and $(9.5\pm0.4)10^{-6}$ with a vector meson dominance form factor, using the measured value for the $K_L \to \gamma\gamma$ branching ratio from an experiment using the same detector [15].

The NA31 data have been partially published [16], the full data set is contained in [17]. Apart from the cuts mentioned in section 3, the two tracks measured in the drift chambers are identified to be electrons by the following requirements:

i) the energy deposited by a shower in the first half of the liquid argon calorimeter (12 radiation lengths) must be more than 65% of the total energy deposited by this shower in the liquid argon and the hadron calorimeters; ii) the energy measured in the

first half of the hadron calorimeter must not exceed 2 GeV; iii) the distance between the track impact and the centre of the shower must not exceed 2 cm, iv) the truncated mean of the four pulse-heights from the transition radiation detector is required to be larger than 1.5 times the corresponding mean for minimum ionizing particles. The loss due to these cuts for good electrons, obtained from electron beam data, is 5.3%. In addition we require the centers of the two electron showers to be separated by at least 6 cm, and the photon shower centre to be at least 25 cm apart from the tracks.

For the remaining sample of 2337 events, the distribution in the invariant $(e^+e^-\gamma)$ mass, m_3 shows a clear signal at the kaon mass. The corresponding scatter plot of m_3 vs. $x = m^2_{ee}/m^2_K$ is displayed in Fig. 3. Here $m_{ee}$is the invariant mass of the electron-positron pair, calculated from the energies measured in the lead liquid argon calorimeter and the opening angle of the tracks measured by the wire chambers. The signal events appear as a band around m_3 = 498 MeV, while background events due to e.g., $K \rightarrow \pi\, e\, \nu$ and $K \rightarrow \pi\, e\, \nu\, \gamma$ decays with a pion simulating an electron, are distributed in the lower part of the plot. The resolution of the detector in the $(e^+e\gamma)$ invariant mass was calculated as a function of m_{ee} using a Monte Carlo simulation. The contours corresponding to a four standard deviation (4σ) limit are shown in Fig. 3. Inside these limits, 2021 events remain. The background in the signal region is estimated from an event sample with one identified charged pion to be 4.0±0.4 events.

The acceptance for Dalitz decays is calculated with Monte Carlo simulated events generated according to the QED distribution falling steeply with $q^{-2} = (m_{ee})^{-2}$ [12]. It is (16.9±0.1)%.

The branching ratio is normalized using decays of the mode $K_L \rightarrow \pi^o\pi^o{}_D$ with subsequent pion Dalitz decay $\pi^o{}_D \rightarrow e^+e^-\gamma$. In this way, the geometrical acceptances and identification efficiencies for an electron pair and for photons enter similarly in both decay modes, and the uncertainty in electron identification largely cancels in the ratio of detection efficiencies for the decays $K_L \rightarrow e^+e^-\gamma$ and $K_L \rightarrow e^+e^-\gamma\pi^o$. With selection criteria analogous to those for $K_L \rightarrow ee\gamma$, 1350 events of the type $K_L \rightarrow \pi^o\pi^o{}_D$ are found. The background to this sample comes predominantly from $K_L \rightarrow 3\pi^o$ decays with Dalitz decay of one π^o, and amounts to 29±2 events.Using the acceptance of 4.3% for the decay including electron identification losses, the number of K_L decays in the fiducial volume is (1.41±0.04) 10^9. From this flux, we obtain the branching ratio

$$\Gamma(K_L \rightarrow ee\gamma)/\Gamma(K_L \rightarrow \text{all}) = (9.1\pm0.3\pm0.5)10^{-6}$$

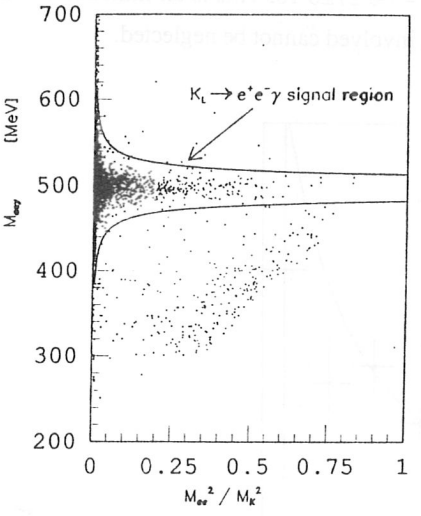

Fig. 3: Scatter plot of $e^+e^-\gamma$ mass vs. the variable $x = m^2_{ee}/m^2_K$. The dashed lines are 4σ resolution contours.

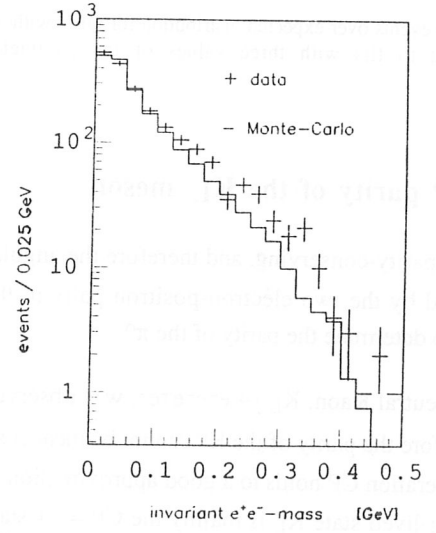

Fig. 4: Invariant e^+e^- mass spectrum. Data (histogram) are compared to the predicted distribution for QED without vector mesons (curve).

The form factor $F(q^2)$ is obtained by comparing the observed distribution in the invariant mass $q^2=m^2_{ee}$ with the distribution calculated from models without form factor, as shown in Fig. 4. There is a clear enhancement at high q^2, consistent with vector meson dominance in the photon propagator. If we divide the experimental distribution by the result of the Monte-Carlo calculation with $F(q^2) = 1$, we obtain the q^2 variation of $F(q^2)$. Radiative corrections to this q^2 variation have been calculated. They are small in this experiment because NA31 has no magnetic field, and photons radiated from an electron hit the shower detector very close to the electron impact point. The photon energy deposited in the shower counter is summed up with the electron shower.

The experimentally measured form factor (Fig. 5) is then compared to the quark model of Bergström et al. [13]. In this QCD-inspired quark model, aiming at explaining the $\Delta I = \frac{1}{2}$ enhancement in non-leptonic weak decays, contributions through $K^*\gamma$ coupling followed by $K^* \to \rho, \omega, \phi$ transitions are considered in addition to conventional quark diagrams. In fact, the amplitude is calculated to be proportional to the function:

$$A(q^2) = A_{\gamma\gamma}/(1 - q^2/m^2_\rho) + \alpha\, A_K^*(q^2)$$

where $A_{\gamma\gamma}$ is the experimental amplitude for $K_L \to \gamma\gamma$ decay and $A_K^*(q^2)$ is the sum of three pole terms with poles at the ρ, ω and ϕ meson mass. The ratio of the

coupling constants belonging to the two different types of contributions is determined from the fit to the data shown in Fig. 5 to be $\alpha = -0.27 \pm 0.10$. This is an indication that the internal weak transitions of the vector meson involved cannot be neglected.

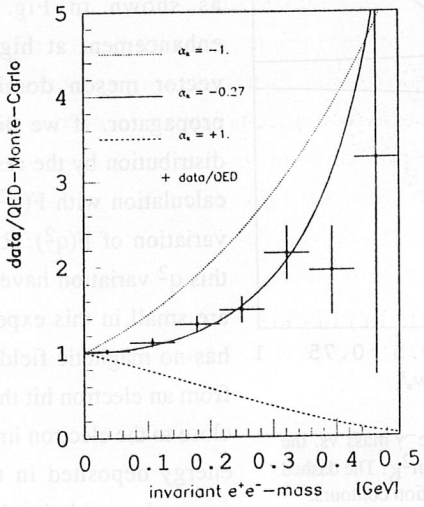

Fig. 5: Ratio of m_{ee} distribution of $K_L \to e^+e^-\gamma$ events over expected distribution for QED without vector mesons. The lines correspond to fits with three values of the parameter α (−1, −0.27, +1).

6. $K_L \to e^+e^-e^+e^-$ and the CP parity of the K_L meson

The two-photon decay of the neutral pion is parity-conserving, and therefore the angular distribution between the two planes defined by the two electron-positron pairs in the decay $\pi^0 \to \gamma^*\gamma^* \to e^+e^-e^+e^-$ can be used to determine the parity of the π^0.

The corresponding decay of the longlived neutral Kaon, $K_L \to e^+e^-e^+e^-$, was observed recently [18]. It is parity violating, and therefore the parity of the K^0 cannot be measured. However, invariance under the combined operation CP holds to a good approximation in weak decays of neutral K mesons. The long-lived state K_L is mainly the CP = −1 state K_2, with a very small admixture of the CP = +1 state K_1: that is $K_L = (K_2 + \varepsilon K_1)/\sqrt{1+|\varepsilon|^2}$ with $|\varepsilon| = 2.3 \times 10^{-3}$. Due to the small value of ε, the decay of the K_1 component can be neglected here. Direct CP violation would lead to a decay of K_2 to a CP = +1 state, and

can also be ignored. The main decay is therefore expected to be the decay of the K_2 state to an $(e^+e^-e^+e^-)$-state with CP = –1. The angular distribution of the angle ϕ between the planes defined by the two e^+e^--pairs is then determined by the CP of the long-lived neutral kaon.

We have investigated a larger sample of $K_L \to e^+e^-e^+e^-$ decays than in our earlier publication [18] in order to study this angular distribution and to obtain a more precise measurement of the branching ratio. Four tracks are reconstructed by linking space-points from the two wire chambers. The space-points are required to be separated by at least 3 cm. Each track is required to match with a separate electromagnetic shower in the LAC to within 2 cm, and all four tracks are required to converge upstream of the detector. The decay vertex is reconstructed by requiring the quantity d^2 (Section 3) to be a minimum. Events with pion tracks are removed by requiring that (a) at least 65% of the total shower energy in the LAC has to be deposited in the first 12 radiation lengths, and (b) the energy in the HAC directly behind the shower does not exceed 2 GeV. 22 events remain.

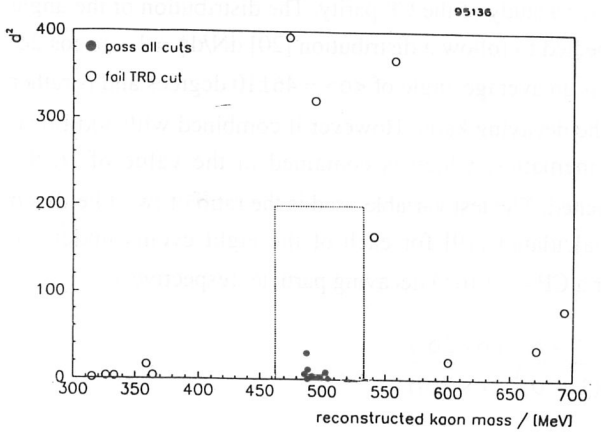

Fig. 6: Reconstructed invariant kaon mass of $K_L \to e^+e^-e^+e^-$ candidates vs. the quantity d^2 from the vertex fit. Solid (open) circles are events which pass (fail) the TRD electron identification cut.

The signal region in the two dimensional plane of the kaon mass and the quantity d^2 is defined to contain 96.5% of the events on the basis of a Monte Carlo simulation: the value for d^2 must not exceed 200 and the reconstructed kaon mass must be within the range from 462 to 532 MeV. Finally each of the four tracks must have a TRD signal consistent with that expected from an electron, that is the pulseheight must be at least 1.5 times that of a minimum ionizing particle. After all cuts eight events remain. Fig. 6 shows the signal events as solid circles and the events that fail the TRD-cut as open circles.

Eight events of the type $K_L \to e^+e^-e^+e^-$ have been observed, including the data of the previous publication [18], with negligible background. The normalization to the K_L flux

has been measured from the number of $K_L \to \pi^0\pi^0_D$ decays in the same sample. Using the acceptance calculated by Monte Carlo simulation, a total flux of 1.3×10^9 K_L decays is obtained. The acceptance for $K_L \to e^+e^-e^+e^-$ decays is calculated by Monte Carlo to be 7.4%. The matrix element for the simulation of the decay was taken from ref. [19] neglecting the interference between the two virtual photons. Including the electron identification cuts and the cuts on the kaon mass and the d^2-value the acceptance is reduced to 5.9%. Radiative corrections are negligible [17] because the experiment does not employ a magnetic spectrometer and therefore radiated photons are not spatially separated from their associated electrons.

From the numbers given above, a branching ratio of $(10.4 \pm 3.7 \pm 1.1) \times 10^{-8}$ for the decay $K_L \to e^+e^-e^+e^-$ is obtained with the statistical and systematical uncertainties given separately. The systematic error given includes uncertainties in the acceptance calculation, the normalization and in the branching ratio for the normalization events.

The events have also been used for a study of the CP parity. The distribution of the angle ϕ between the two planes is expected to follow a distribution [20] $dN/d\phi = 1 - \alpha \cos 2\phi$. The experimental distribution has an average angle of $\langle\phi\rangle = 46 \pm 10$ degrees and is rather insensitive to the CP parity of the decaying kaon. However if combined with additional information from the decay kinematics, which is contained in the value of α, the statistical power can be strengthened. The test variable used is the ratio of two likelihood functions L^- and L^+ with α calculated [19] for each of the eight events under the assumption of a CP = –1 (α^-) or a CP = +1 (α^+) decaying particle, respectively:

$$\frac{L^-}{L^+} = \prod_{i=1}^{8} \frac{(1 - \alpha_i^- \cos 2\phi_i)}{(1 - \alpha_i^+ \cos 2\phi_i)}$$

The data give a value of 22 for this ratio and can be compared to a Monte Carlo simulation including all detector effects with the events generated for the two assumptions of a CP = –1 or a CP = +1 decaying kaon (see Fig. 7). The probability of obtaining a value larger than measured is 25% for the CP = –1 case and 0.6% for the CP = +1 case of the decaying particle. This result favours clearly the CP = –1 assignment for the long-lived neutral kaon.

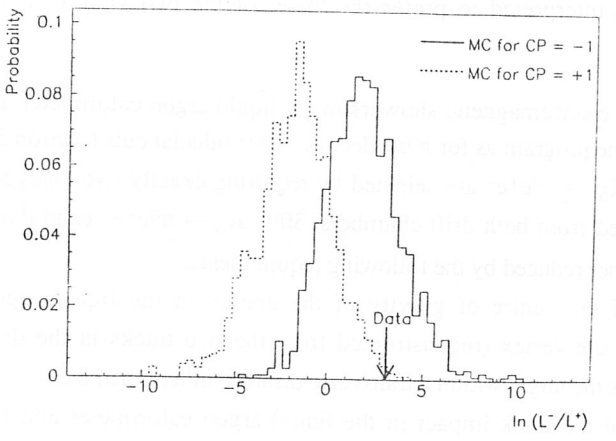

Fig. 7: Logarithm of likelihood ratio L^-/L^+ for the two assumptions of CP partiy −1 (solid) or +1 (dashed) for the K_L state. The data yield ln $(L^-/L^+) = 3.1$.

This measurement of the branching ratio is consistent with our previous published result [18] and with recent measurements at BNL [21], KEK [22] and at FNAL [23]. An analysis of the angular distribution of the decaying particles published recently [23] also agrees with this measurement. This result is also consistent with a calculation [19], based on the assumption that only the decay chain $K_L \rightarrow (\pi^0, \eta, \eta') \rightarrow \gamma\gamma$ contributes, which predicts a branching ratio of $(3.4\pm0.2) \times 10^{-8}$.

7. Search for $K_S \rightarrow \pi^0 e^+ e^-$

A measurement of the decay $K_S \rightarrow \pi^0 e^+ e^-$ is of interest for the interpretation of the $K_L \rightarrow \pi^0 e^+ e^-$ branching ratio. The decay $K_L \rightarrow \pi^0 e^+ e^-$ is a promising candidate for observing direct CP violation in the kaon system [4] apart from the measurement of the ε'/ε parameter in $K_L \rightarrow 2\pi$ decays [24]. There are three possible contributions to the amplitude of the K_L decay, (a) direct CP violating, (b) CP violating from the state mixing of the K_1 and K_2 CP eigenstates and (c) CP conserving. The CP-conserving amplitude can be estimated from recent measurements of the decay $K_L \rightarrow \pi^0\gamma\gamma$ [11]. A measurement of the decay rate of $K_S \rightarrow \pi^0 e^+ e^-$ allows the state mixing contribution to $K_L \rightarrow \pi^0 e^+ e^-$ to be determined. The direct ly CP-violating component of the K_L decay can then be extracted from an experimental measurement of the decay.

An estimate of the $K_S \rightarrow \pi^0 e^+ e^-$ branching ratio may be made by comparing it to the measured decay $K^+ \rightarrow \pi^+ e^+ e^-$ using a model based on chiral perturbation theory and other assumptions [4]. A two fold ambiguity remains, leading to estimated branching ratios, of 5×10^{-9} or 5×10^{-10}. Under the assumptions of the model [25], the

measurement [26] can be interpreted to prefer the lower of the two values of the branching ratio.

Position and energy of the electromagnetic showers in the liquid argon calorimeter are reconstructed using the same program as for $\pi^0\pi^0$ decays. After fiducial cuts (section 3), candidates for the decay $K_S \to \pi^0 e^+ e^-$ are selected by requiring exactly two charged-particle tracks reconstructed from both drift chambers. 3095 $K_S \to \pi^0 e^+ e^-$ candidates remain. This sample is further reduced by the following requirements:

(I) the extrapolation of the centre of gravity of the energy in the liquid argon calorimeter through the vertex (reconstructed from the two tracks in the drift chambers) has to pass the target within a transverse distance of less than 8 cm,

(II) the distance between the track impact in the liquid argon calorimeter and the associated shower must not exceed 2 cm,

(III) electrons are required to have a pulse-height in the TRD, larger than 1.5 times that of a minimum ionizing particle, and to have a shower with more than 65% of the shower energy deposited in the first 12 radiation lengths.

After these cuts, 622 events remain. For these events, the invariant mass m_{ee} of the (e^+, e^-) pair is calculated from the opening angle of the two tracks and the electromagnetic shower energies associated with these tracks. The distribution of these invariant masses shows that there are two sources of background from $K_S \to \pi^0\pi^0$ decays.

The first source comes from $K_S \to \pi^0\pi^0$ decays in which one of the pions undergoes a Dalitz decay ($\pi^0 \to e^+e^-\gamma$) and one photon is lost. The invariant e^+e^- masses of these background events are all below 140 MeV. Background of this type is rejected by requiring the invariant e^+e^- mass to be above 140 MeV. After this cut 39 events remain.

The second source of background comes from $K_S \to \pi^0\pi^0$ decays in which two of four photons convert into an e^+e^- pair in the kevlar window in front of the first drift chamber ("double conversion"). The produced e^+e^- pairs do not in general open up and pairs may be identified as a single "electron" track. Events where the two converted photons come from one pion show a peak at the π^0 mass and are already rejected by the cut against Dalitz decays. In order to reject events where the two converted photons come from different pions, the two combinations of invariant masses of one photon and one "electron" are calculated. The event is rejected if at least one combination is consistent with a $\pi^0\pi^0$ hypothesis. Fig. 8 shows a scatter plot of the two invariant photon electron

masses for the two possible combinations, for 39 events remaining after the cut against Dalitz decays. Events inside the small ellipse indicated satisfy the $\pi^0\pi^0$ hypothesis and are rejected. We find 28 events of this type inside the ellipse compared to 31 events expected from a Monte Carlo simulation for this double conversion background.

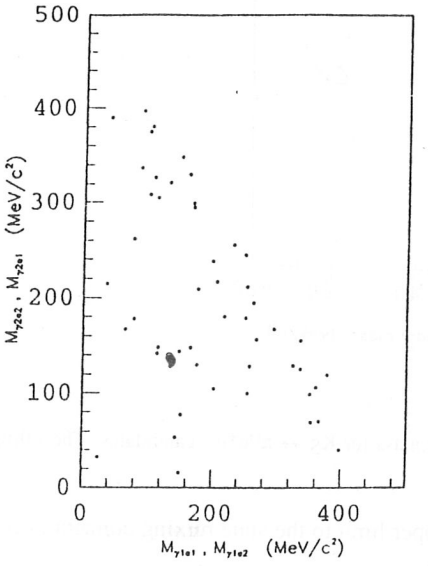

Fig. 8: Scatter plot of the two possible combinations of invariant photon-electron masses for $K_S \to \pi^0e^+e^-$ candidate events (two entries/event). Entries inside the ellipse are due to $\pi^0\pi^0$ events with double conversion.

After these cuts, 11 events remain. For these events, Fig. 9 shows the invariant $\gamma\gamma$ mass versus the total invariant mass of the $K_S \to \pi^0e^+e^-$ candidates. A final cut, shown by the ellipse in fig. 9, restricts these invariant masses by imposing a $3\sigma x3\sigma$ elliptical signal region with resolutions of 2.2 and 30 MeV as calculated by the Monte Carlo simulation. We find no event inside the signal region. An upper limit on the branching ratio is then calculated from a signal level of less than 2.3 events with a 90% confidence level.

The $K_S \to \pi^0\pi^0$ decay is used for normalization. We find 31815 $K_S \to \pi^0\pi^0$ candidates free of background, which corresponds to a flux of $(2.2x0.1)x10^7$ K_S decays. The acceptance for this decay in the detector is calculated to be $(22.8\pm0.6)\%$.

For the decay $K_S \to \pi^0e^+e^-$ the acceptance is calculated from a Monte Carlo simulation using a matrix element with one-photon exchange [25] for the three-body decay. The acceptance is $(9.8\pm0.5)\%$. We find with this normalization and acceptance, an upper limit to the branching ratio for this decay of $\Gamma(K_S \to \pi^0e^+e^-)/\Gamma(K_S \to \text{all}) < 1.1x10^{-6}$ at 90% C.L..

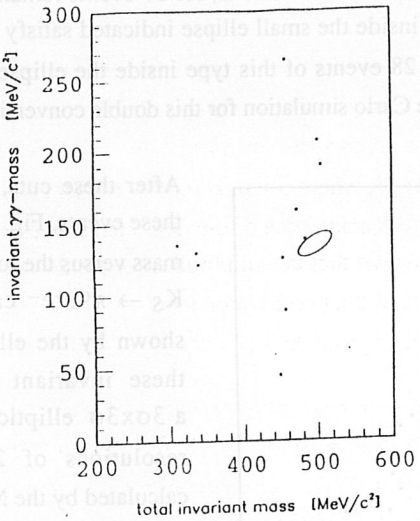

Fig. 9: Invariant $(\gamma\gamma e^+e^-)$-mass vs. invariant $\gamma\gamma$ mass for $K_S \to \pi^0 e^+e^-$ candidates. The ellipse indicates a $3\sigma \times 3\sigma$ signal region.

From this measurement, we can deduce an upper limit to the state mixing contribution to the branching ratio of the decay $K_L \to \pi^0 e^+e^-$:

$$BR(K_L \to \pi^0 e^+e^-, \text{mixing}) = |\varepsilon|^2 \frac{\Gamma_S}{\Gamma_L} BR(K_S \to \pi^0 e^+e^-)$$

This upper limit comes out to be [27]:

$$BR(K_L \to \pi^0 e^+e^-, \text{mixing}) = < 3.2 \times 10^{-9} \text{ at } 90\% \text{ C.L.}$$

8. Search for the decay $K_L \to \pi^o\pi^o\gamma$

In a way similar to the decay $K_L \to \pi^o\gamma\gamma$ (Section 4), this decay mode may be used as a test of chiral perturbation theory. The experimental data on the rate of $K_L \to \pi^o\gamma\gamma$ and the shape of the $\gamma\gamma$ invariant mass spectrum were reproduced well by the chiral perturbation calculations [7] to order p^4, where p stands for the momenta of the decay products in the kaon CMS system, but the magnitude of the $O(p^6)$ terms is still an open question. Funck and Kambor [3] have shown that the amplitudes for the decays $K_{L,S} \to \pi^o\pi^o\gamma$ vanish to $O(p^4)$ for real photons in chiral perturbation theory. Thus a measurement of $K_L \to \pi^o\pi^o\gamma$ should give direct information on the size of $O(p^6)$ contributions.

As pointed out by Heiliger and Sehgal [29] and Ecker, Neufeld and Pich [30], the amplitudes $K_L \to \pi^o\pi^o\gamma$ and $K_S \to \pi^o\pi^o\gamma$ are purely electric and magnetic, respectively, in the limit where CP is conserved. Heiliger and Sehgal estimate $BR(K_L \to \pi^o\pi^o\gamma) = 1\times10^{-8}$. On the other hand, Ecker, Neufeld and Pich use a naive chiral dimensional analysis to estimate the sixth order electric amplitude. They estimate a value for the branching ratio $BR(K_L \to \pi^o\pi^o\gamma) = 7\times10^{-11}$.

The first search for this decay was done by the NA31 collaboration [31]. $K_L \to \pi^o\pi^o\gamma$ candidates must have five reconstructed electromagnetic showers and fulfil the fiducial criteria mentioned in Section 3. Further cuts are applied to reduce the overwhelming background from $K_L \to 3\pi^o$ decays with one photon escaping detection. The first cut uses the two vertices of neutral pions reconstructed from two pairs of photons out of the five. The two "best" pairings of photons are chosen, and the distance of their two π^o vertices is required to be less than 5 m. This cut removes 60% of the $3\pi^o$ background and 10% of the $\pi^o\pi^o\gamma$ signal, and leaves 1.4×10^5 events.

After a few cuts against overlapping showers in the same quadrant of the calorimeter, a very effective cut against $3\pi^o$ events with one escaping photon was designed by studying such events simulated by a Monte Carlo calculation. These five photon events were reconstructed in the normal way, but the identity of each generated photon (1-6) was retained and matched to its reconstructed energy. Because a six photon event was analyzed and reconstructed as a five photon event, its reconstructed vertex position was shifted toward the electromagnetic calorimeter. As a result, when the right pairings of photons were used to determine the invariant masses of the two π^os from which the

photons came, the masses were incorrect. This is illustrated in Fig. 10, which shows the two-dimensional distribution of these reconstructed π^0 masses. The candidate $\pi^0\pi^0\gamma$ events are treated in a similar manner. All combinations of two photon invariant masses are formed for each event and if one or more combinations of the two reconstructed π^0 masses fall within the solid curve shown in Fig. 10, the event is rejected. Only 35% of the Monte Carlo generated $K_L \to \pi^0\pi^0\gamma$ events pass this cut because if any of the 15 independent combinations of two pairs of two photons from the set of five photons falls within the solid curve, the event is rejected. This cut reduces the real data sample to 16 events.

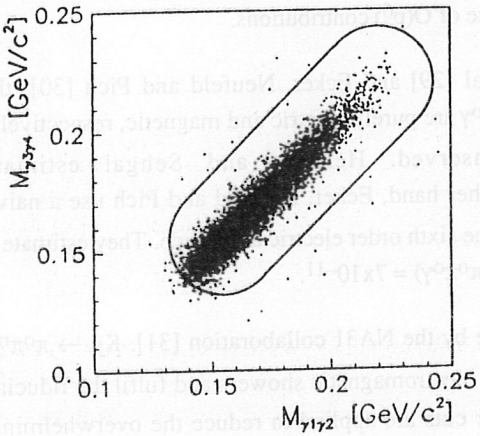

Fig. 10: Distribution of the two invariant $\gamma\gamma$ masses from $K_L \to 3\pi^0$ Monte Carlo events with one lost photon, reconstructed as $\pi^0\pi^0\gamma$ event.

Using the best pairings of photons, these 16 events are plotted in Fig. 11. The signal region is shown in the figure. This region corresponds to 2.9 standard deviations of the two-dimensional mass distribution. Three candidate events lie within the signal region.

The normalization of the number of $K_L \to \pi^0\pi^0\gamma$ events comes from an analysis of the topologically similar $K_L \to \pi^0\pi^0$ events. These normalization events were recorded through the same trigger chain as were the signal events. Thus the trigger efficiency cancels in the branching ratio. 8127 $K_L \to \pi^0\pi^0$ candidates were found with a background of 167 events from $3\pi^0$ with two missing photons. Using the calculated acceptance of 10.4% for $K_L \to \pi^0\pi^0$, we obtain a number of 8.4×10^7 K_L decays in the fiducial volume.

The background to $\pi^0\pi^0\gamma$ is estimated to be 1.2 ± 0.5 events from $3\pi^0$ with one missing photon, 0.6 events from $3\pi^0$ with two missing photons and an accidental photon, and 0.4 events from $2\pi^0$ with an accidental photon. Together these backgrounds add up to 2.2 ± 0.9 events. The upper limit to the $K_L \to \pi^0\pi^0\gamma$ signal is then 4.6 events, and the 90% C.L. upper limit to the branching ratio, using the $\pi^0\pi^0\gamma$ acceptance of 1%, is

$$\Gamma(K_L \to \pi^0\pi^0\gamma)/\Gamma(K_L \to \text{all}) < 5.6 \times 10^{-6}$$

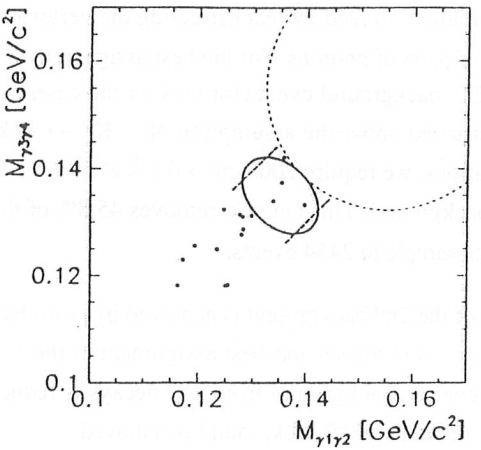

Fig. 11: Two-photon masses for the 16 $K_L \to \pi^0\pi^0\gamma$ candidate events that pass all cuts. The signal region for $\pi^0\pi^0\gamma$ events is shown as solid ellipse. The curve from fig. 10 encircling the background events from $3\pi^0$ is the light-dashed curve. Three events lie within the signal region.

9. Search for $K_L \to 3\gamma$

While the electromagnetic decay $\pi^0 \to 3\gamma$ is forbidden by C invariance, the weak-electromagnetic decay $K_L \to 3\gamma$ is suppressed by a combination of gauge invariance and Bose statistics [32]. The decay is supposed to proceed through the intermediate state $\pi^0\pi^0\gamma$ with two photons coupling to the π^0 loop. The estimated branching ratio is 3×10^{-19} assuming a branching ratio of 10^{-8} for the mode $\pi^0\pi^0\gamma$.

The decay was searched for by requiring three electromagnetic showers in the LAC with a total energy between 50 and 190 GeV and individual shower energies between 5 and 100 GeV. The shower centres are required to be separated by at least 3 cm in both transverse projections. Charged tracks are rejected by admitting at most one space-point in the second and none in the first drift chamber. Fiducial cuts include the longitudinal vertex position between –10 m and 40 m relative to the defining collimator. Events with missing energy are reduced by requiring the transverse gravicentre of energy to be within 5 cm of the beam axis, and events with more than 3 GeV of energy in the hadron calorimeter are rejected. 18981 events survive these cuts.

The main backgrounds for this decay channel are the mode $K_L \to 3\pi^0$ with undetected or overlapping photons, and the mode $K_L \to 2\,\pi^0$ with one photon undetected. The latter

background is essentially removed by reconstructing the vertex of a possible π^0 from all three combinations of pairs of photons. For the best assignment of the pair this is the true vertex $z1(\pi^0)$ of a $2\pi^0$ background event (for 90% of the cases), and is upstream of the vertex $z(3\gamma)$ reconstructed under the assumption of $K_L \to 3\gamma$ kinematics. Guided by Monte Carlo simulations, we require $2000\ \text{cm} + 0.1 \times z1(\pi^0) < z(3\gamma) < z1(\pi^0)$ to remove 97.7% of this $2\pi^0$ background. This cut also removes 45.8% of the $3\pi^0$ background and reduces the candidate sample to 2454 events.

A further reduction of the $2\pi^0$ background is achieved by considering and simulating the relation between $z1(\pi^0)$ and the second-best assignment of the pair, $z2(\pi^0)$. The sample is reduced to 1524 events. Background from $2\pi^0$ decays is reduced by a factor of 137, and also 28% of the remaining $3\pi^0$ background is removed.

The remaining background is reduced by using precise timing information from zero-crossing TDC's processing the pulse-height information of the LAC channels. Pulses in a time interval of 144 ns are accepted. This reduces the background from events with accidental coincidences between two showers and an accidental energy cluster deposited in the LAC. The distribution of the vertex $z_v(3\gamma)$ of the remaining events with and without this timing cut is shown in Fig. 12. The candidate distribution is matched very well by the distribution of the $3\pi^0$ background events with its characteristic increase towards larger z_v, due to the fact that missing energy in the decay shifts downwards the reconstucted vertex of incomplete events.

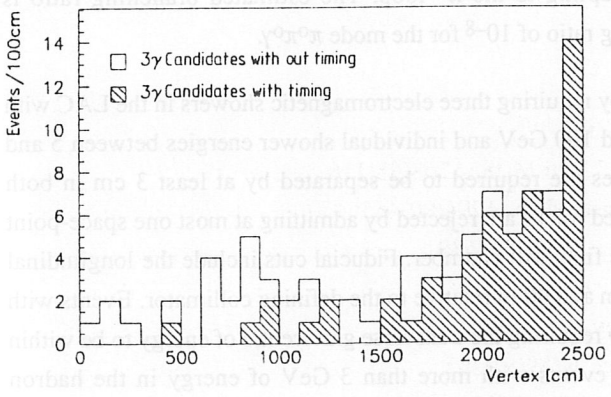

Fig. 12: Vertex distribution for $K_L \to 3\gamma$ candidate events with (shaded) or without (light) tight timing cuts.

For the search for $K_L \to 3\gamma$, the region from 0 to 15 meters in z_v offers the best balance between acceptance for 3γ and suppression of background. 7 events remain in this region. The background is estimated to be 1.2 ± 0.2 events from $3\pi^0$, 0.12 ± 0.04 events from $2\pi^0$, and 3.1 ± 0.6 events from accidental

coincidences, all together 4.4±0.7 events. From these numbers we deduce an upper limit of 7.7 events for $K_L \to 3\gamma$.

The calculated acceptance for the decay $K_L \to 3\gamma$ is 12±2% , and the number of K_L decays in the fiducial volume is obtained from $K_L \to 2\pi^0$ decays to be $(2.43\pm0.02)10^8$.

We conclude that the upper limit for the decay mode is

$$\Gamma(K_L \to 3\gamma)/\Gamma(K_L \to \text{all}) < 2.8\text{x}10^{-7}$$

at 90% C.L..

10. Outlook

The new experiments on CP violation in the K^0 system at CERN and at Fermilab aim at a kaon flux increased by a factor of ten compared to the experiments NA31 and E731. They will also trigger on rare kaon decays of the types discussed above. The sensitivities to the detection of these decays will also be increased by this factor. Single event sensitivities of 10^{-9} for K_L decays and of 10^{-7} for K_S decays are within reach in these experiments which start taking data in 1996.

REFERENCES

1. G.D. Barr et al., Phys.Lett B317(93)233
2. H. Burkhardt et al., Nucl.Instr.Meth. A268(88)116
3. G.D. Barr et al., Nucl.Instr.Meth. A294(90)465
4. C.O. Dib et al., Phys.Rev. D39(89)2639
5. A. Barker et al., Phys.Rev. D61(90)3546
6. K.E. Ohl et al., Phys.Rev.Lett. 64(90)2755
7. G. Ecker et al., Phys.Lett. B189(87)363
8. L.M. Sehgal, Phys.Rev. D6(72)367;
   P. Ko and J.L. Rosner, Phys.Rev. D40(89)3775
9. G. Ecker et al., Phys.Lett. B237(90)481;
   J. Bijnens et al., Phys.Rev. D44(91)3555

10. G.D. Barr et al., Phys.Lett. B242(90)523
11. G.D. Barr et al., Phys.Lett. B284(92)440
12. L.M. Sehgal, Phys.Rev. D7(73)3303; T. Miyazaki, Lett. Nuovo Cim. 3(72)294
13. J.J. Sakurai, Phys.Rev. 156(67)1508;
M. Moshe and P. Singer, Phys.Rev. D6(72)1379
14. M.A. Shifman et al., Nucl.Phys. B120(77)316;
L. Bergström et al., Phys.Lett. B131(83)229
15. H. Burkhardt et al., Phys.Lett. B199(87)139
16. G.D. Barr et al., Phys.Lett. B240(90)283
17. H. Rohrer, Ph.D. thesis, Mainz University 1992
18. G.D. Barr et al., Phys.Lett. B259(91)389
19. N.M. Kroll and W. Wada, Phys. Rev. 98(55)1355;
T. Miyazaki and E. Takasugi, Phys. Rev. D8(73)2051
20. C.N. Yang, Phys. Rev. 77(50)242
21. M.R. Vagins et al., Phys.Rev.Lett. 71(93)35
22. T. Akagi et al., Phys.Rev. D47(93)R2644
23. P. Gu et al., Phys.Rev.Lett. 72(94)3000
24. L.K. Gibbons et al., Phys.Rev.Lett. 70(93)1203;
G.D. Barr et al., Phys.Lett. B317(93)233
25. G. Ecker et al., Nucl.Phys. B291(87)692
26. C. Alliergo et al., Phys.Rev.Lett. 68(92)278
27. G.D. Barr et al., Phys.Lett. B304(93)381
28. R. Funck and J. Kambor, Nucl.Phys. B396(93)53
29. P. Heiliger and L.M. Sehgal, Phys.Lett. B307(93)182
30. G. Ecker, H. Neufeld, A. Pich, CERN-TH 6920/93
31. G.D. Barr et al., Phys.Lett. B328(94)528
32. P. Heiliger et al., Phys.Lett. B327(94)145

SESSION XI

- D. Kaplan
  Panel Discussion: Future Options for Charm Experiments in Fixed Target

- M. Procario
  Charm Baryons at CHARM2000

- P. Karchin
  Comments on Future Charm Measurements

- M. Sokoloff
  Physics of an Ultrahigh-Statistics Charm Experiment

- D. Christian
  CHARM2000 at FNAL Using Crystal Extraction

- R. Cester
  Experiments to Study ($Q\ \bar{Q}$) States. Is There a Future?

Frascati Physics Series, Vol. III (1994)
HEAVY QUARKS AT FIXED TARGET
University of Virginia, October 7–10, 1994
(pp. 401–403)

PANEL DISCUSSION: FUTURE OPTIONS FOR CHARM EXPERIMENTS IN FIXED TARGET

Daniel M. Kaplan
Illinois Institute of Technology

ABSTRACT

The charm future-options panel discussion is briefly summarized. A goal of 10^8 reconstructed charm decays is considered for the Year $\approx$ 2000; at this statistical level, charm becomes a significant probe of physics beyond the Standard Model. An apparatus capable of the required performance is sketched.

1 – Introduction

Charm is now something of a mature subject twenty years since its discovery. But as in the case of the strange quark, the availability of ever-higher statistics has given access to new questions. With 10^5 reconstructed charm decays in E687 and E791 and 10^6 expected from E831 and E781, one is naturally led to ask whether this is the end of the line or whether substantial further advances are feasible and desirable. This was the focus of the recent CHARM2000 Workshop at Fermilab [1], which concluded that $\sim 10^8$ reconstructed decays (with signal-to-background at least as good as in E687 and E791) is a reasonable goal for an experiment to run at the turn of the century. With this sensitivity Standard-Model physics such as the parameters of the CKM matrix, QCD and the Heavy-Quark Effective Theory, the role of final-state interactions, and decay form factors begins to be rivaled in interest by searches for physics beyond the Standard Model: $D^0 - \overline{D}^0$ mixing, *CP* violation, and such rare-decay processes as flavor-changing neutral currents, all of which are expected to be extremely small in the Standard Model.

The main physics topics of interest in such an experiment were discussed by Karchin and Sokoloff. Reasonable goals for physics beyond the Standard Model appear to be sensitivities of order 10^{-5}, 10^{-3}, and 10^{-7} for mixing, *CP* violation, and rare decays (respectively); detailed simulations will be required to establish whether systematic effects can be controlled to these levels. Christian emphasized the variety

of available operating modes for such an experiment: "conventional" fixed-target, collider, or "parasitic" fixed-target running using a crystal-extracted beam during collider runs.

In addition to growth in statistics, another significant trend in charm physics has been the successful application of new techniques, including threshold charmonium studies via $p\bar{p}$-annihilation (Fermilab E760 and E835, discussed by Cester) and optimization for charm-baryon production and detection (CERN WA62 and WA89 and Fermilab E781, discussed by Procario). Kekelidze covered the surprising charm-baryon results from Serpukhov, where the EXCHARM experiment has signals for Λ_c and Ξ_c without even a vertex detector.

2 – CHARM2000 "Strawman" Apparatus

To provide context for the discussion, I briefly described the "existence-proof" experiment discussed at the CHARM2000 Workshop [2] (see Fig. 1). This is a compact fixed-target spectrometer, intended to be of moderate cost (under \$10M), featuring large acceptance and high-rate tracking and particle identification. The use of silicon-strip and scintillating-fiber tracking detectors allows coverage down to 4 mr laboratory polar angle with interaction rate exceeding 5 MHz, two orders of magnitude beyond that achieved in existing open-geometry charm spectrometers. To permit a sufficiently intense beam without unacceptable radiation damage, a "pencil" primary proton beam is focussed on a "point" target, and the detectors are configured around a central beam hole (see Fig. 2). A fast ring-imaging Cherenkov counter provides hadron identification, and calorimeters (possibly augmented by a TRD) identify electrons and allow first-level triggering on transverse energy. A first-level "optical" decay-vertex trigger [3, 4] may also be possible. A second-level trackfinding decay-vertex trigger reduces the event rate sufficiently for recording on tape while remaining relatively bias-free for charm events [5]. Preliminary simulations indicate mass resolution and acceptance for charm decays better than, and vertex resolution comparable to, those of E791.

References

1. D. M. Kaplan and S. Kwan, *eds.*, **The Future of High-Sensitivity Charm Experiments**, Proceedings of the CHARM2000 Workshop, Fermilab, June 7–9, 1994, FERMILAB-Conf-94/190.

2. D. M. Kaplan, "A High-Rate Fixed-Target Charm Experiment," in **The Future of High-Sensitivity Charm Experiments**, *op cit.*, p. 229.

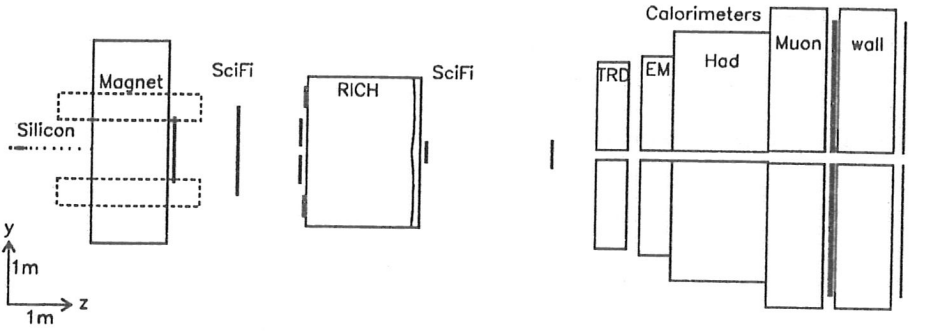

Figure 1: Layout of "existence-proof" spectrometer (bend view).

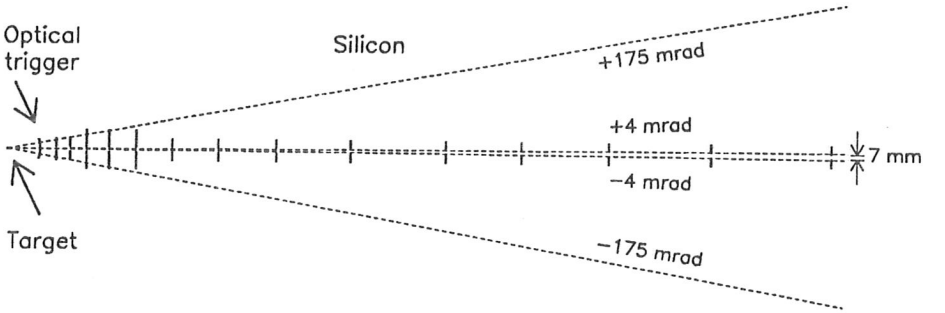

Figure 2: Detail of vertex region (showing optional optical impact-parameter trigger).

3. G. Charpak, Y. Giomataris, and L. M. Lederman, Nucl. Instr. & Meth. **A306**, 439 (1991); D. M. Kaplan *et al.*, *ibid.* **A330**, 33 (1993); G. Charpak *et al.*, *ibid.* **A332**, 91 (1993).

4. A. M. Halling and S. Kwan, Nucl. Instr. & Meth. **A333**, 324 (1993).

5. Further discussion of triggers (secondary-vertex and otherwise) for heavy-quark experiments may be found in D. Christian, "Triggers for a High-Sensitivity Charm Experiment," in **The Future of High-Sensitivity Charm Experiments**, *op cit.*, p. 221, and D. Barberis, "A Secondary Vertex Trigger for Beauty Search: Results from the BEATRICE/WA92 Experiment," *ibid.* p. 213.

Frascati Physics Series, Vol. III (1994)
HEAVY QUARKS AT FIXED TARGET
University of Virginia, October 7–10, 1994
(pp. 405–406)

CHARM BARYONS AT CHARM2000

Michael Procario
Carnegie Mellon University

Some of the questions currently needing experimental input for the study of charm baryon physics are precise ($\sim 5\%$) lifetime measurements; detailed studies of semileptonic decays; an understanding of whether hadronic decays are dominated by resonances, or are multibody; the absolute branching ratio scales; study of production mechanisms such as diquarks; and spectroscopy of the charm baryon system.

The currently planned experiments at Fermilab, E781 and E831, as well as CLEO II/III, will address many of these issues, while some like the absolute branching ratio scale may be better done with BES. These experiments may solve all the open problems, fall short, or discover important new problems, but we will not know this until the experiments run. I know of no important rare phenomena such as mixing, *CP* violation, non-standard model rare decays, that are done better in charm baryons than charm mesons. Given the statistical advantage that charm meson production has over charm baryon production, it appears that charm meson physics will drive the building of CHARM2000.

It is the general understanding of the E781 collaboration that charm baryons are best studied with detectors optimized for their production and detection. E781 expects to observe $\sim 100,000$ $\Lambda_c^+ \to pK^-\pi^+$ decays, $\sim 150,000$ Ξ_c^0 or Ξ_c^+ decays into a variety of modes, and perhaps 5000 Ω_c decays, while if we scale up from E831, a charm meson experiment, to the nominal CHARM2000 experiment, we might expect one million $\Lambda_c^+ \to pK^-\pi^+$ and about 10,000 charm-strange baryons [1].

To the degree that CHARM2000 tries to accommodate charm baryons by including excellent particle identification, the ability to trigger on short lifetimes, and good acceptance and resolution for long-lived hyperons, it could make a significant impact on charm baryon physics. Unfortunately, it is not yet possible to set interesting charm baryon goals that require such an experiment.

References

1. Harry W. K. Cheung and P. Cooper, "Charm Baryon Working Group Report," in **The Future of High-Sensitivity Charm Experiments** Proceedings of the CHARM2000 Workshop, Fermilab, June 7–9, 1994, D. M. Kaplan and S. Kwan, *eds.*, FERMILAB-Conf-94/190, p. 427.

Frascati Physics Series, Vol. III (1994)
HEAVY QUARKS AT FIXED TARGET
University of Virginia, October 7–10, 1994
(pp. 407–410)

COMMENTS ON FUTURE CHARM MEASUREMENTS

Paul E. Karchin
Yale University

1 – Introduction

Fixed target experiments have now provided much of our knowledge of charm decay physics. These experiments have been both competitive and complementary to those at e^+e^- colliders operating either at charm or beauty threshold. My purpose here is to highlight some of the most interesting topics for future experiments and to comment on how future fixed target experiments might contribute.

2 – $D - \overline{D}$ Mixing

$D - \overline{D}$ mixing is characterized by the ratio r_{mix} of "wrong sign" to "right sign" decay rates,

$$r_{mix} = \frac{\Gamma(D^0 \to \overline{f}) + \Gamma(\overline{D}^0 \to f)}{\Gamma(D^0 \to f) + \Gamma(\overline{D}^0 \to \overline{f})},$$

where f represents some particular final state and $\overline{f}$ is the charge conjugate state. An example is $f = K^-\pi^+$. In the standard model, there are both short distance and long distance contributions to $D - \overline{D}$ mixing. The short distance contributions [1] result in $r_{mix} < 10^{-8}$. The long distance contributions are uncertain, although there are some theoretical arguments that these contributions are no more than comparable to that from the short distance effect. Bigi emphasized during the session that the long distance contributions are uncertain. The present experimental limit from Fermilab E691 [2] is $r_{mix} < 3.7 \times 10^{-3}$, a limit far above the value expected from the short distance contribution. If the standard model long distance contributions can be shown theoretically to be small, then an accurate measurement of r_{mix} would be sensitive to new physics [3].

When the final state f is purely hadronic, doubly Cabibbo suppressed decays are a background to mixing. This problem is not present for the semileptonic

decays such as $D^0 \to K^- l^+ \nu$. Morrison [4] "guestimates" that an experiment that can reconstruct 10^8 charm could measure $r_{mix} < 10^{-5}$.

3 – *CP* Violation

It may be possible to observe indirect *CP* violation in D^0 decays to *CP* eigenstates if $D - \overline{D}$ mixing is large enough. The decay rate asymmetry is defined as

$$A = \frac{\Gamma - \overline{\Gamma}}{\Gamma + \overline{\Gamma}},$$

where Γ is the decay rate for D^0 to a *CP* eigenstate and $\overline{\Gamma}$ is the rate for $\overline{D}^0$ to the same *CP* eigenstate. The maximum value for the time-integrated asymmetry is $\sim \sqrt{r_{mix}}$. Using the current upper limit for r_{mix}, $A <\sim 0.06$ is not ruled out. However, in the case that r_{mix} is dominated by short distance physics, $r_{mix} < \mathcal{O}(10^{-8})$ and A cannot be larger than $\mathcal{O}(10^{-4})$, which is not experimentally accessible.

Perhaps the most promising prospect for observing *CP* violation in charm decays is from direct *CP* violation in the decays of singly Cabibbo suppressed final states, for which the theoretical expectation [1] is that $A \sim O(10^{-3})$. The experimental signature is

$$A = \frac{N - \overline{N}}{N + \overline{N}},$$

where N is the number of decays observed for charm state $X_c \to$ final state f, and $\overline{N}$ is the number of decays for $\overline{X}_c \to \overline{f}$. Examples of such decays are $D^+ \to K^+K^-\pi^+$ and $D^0 \to K^+K^-$. One must take caution in that the above formula also describes the production asymmetry! Presumably, the production asymmetry can be measured from Cabibbo allowed decays and used to correct the observed asymmetry for the Cabibbo suppressed decays. Using this technique, the current experimental limits on direct *CP* violation, from Fermilab E687 [5], give $A <\sim 0.1$. The number of reconstructed decays $N + \overline{N}$ necessary to observe an asymmetry A with significance S is given by

$$N + \overline{N} = \left(\frac{S}{A}\right)^2.$$

To observe an asymmetry with significance of 3, an experiment that can reconstruct 10^8 Cabibbo suppressed decays would have (3σ) sensitivity for $A \sim 10^{-3}$.

4 – Charm Decay Form Factors

The form factors for charm and beauty decay are related through heavy quark effective theory. For example, the form factors for $D \to \rho l\nu$ and $D \to \pi l\nu$ are

related to those for B decays to the same final states. Of particular interest are the charm decays $D^+ \to \pi^0 l^+ \nu$, $D^+ \to \rho^0 l^+ \nu$, and $D^0 \to \pi^- l^+ \nu$. Of these decays, only the one with π^0 has been detected, by CLEO. Future measurements of the form factors in these decays can be used as input to the analysis of the corresponding beauty decays to determine $|V_{ub}|$.

5 Flavor Changing Neutral Currents and Lepton Family Number Violation

In the standard model, FCNC processes are highly suppressed – for example, $BR(D^0 \to \mu^+\mu^-) < \mathcal{O}(10^{-15})$ – and lepton family number violation is forbidden. Hence such processes are sensitive to new physics. Current limits on branching fractions, such as those for $D^0 \to l^+l^-$ and $D^+ \to \pi^+ l^+ l^-$, are of order 10^{-5}.

6 – Experimental Prospects

The number of reconstructed charm decays can be roughly estimated from the formula

$$N_c(x_F > 0) = (interaction\ rate) \times \frac{\sigma_{c\bar{c}}}{\sigma_{inel}} \times time \times efficiency\,.$$

These factors are tabulated below for the two new Fermilab fixed target experiments and the proposed one at DESY.

beam	int./sec.	$\frac{\sigma_{c\bar{c}}}{\sigma_{inel}}$	#sec.	eff.	N_c
γ (E831)	10^4	10^{-2}	10^6	10^{-2}	10^6
Σ^- (E781)	10^5	10^{-3}	10^6	10^{-2}	10^6
p (HERA-B)	10^7	10^{-3}	10^7	10^{-2}	10^9

I have been cavalier in assigning the same efficiency for all charm decays for all three experiments! For example, E781 has particularly good acceptance for final states with high momentum $\Lambda's$, E687 has good acceptance for lower momentum charm parents, and HERA-B has a large acceptance for the pions from D^* decay. Nonetheless, the table illustrates the comparative potential of these experiments. What is striking is the potential yield from HERA-B due to the high interaction rate and long running time.

Whether this potential can be fulfilled depends on whether a selective enough trigger can be implemented. One possible trigger scheme is to exploit charm final states with leptons. Three of the four charm topics mentioned above have at least one lepton in the final state. A dilepton level 1 trigger may be possible where either both leptons are from the final state of interest or one lepton is from the "tagging" charm and the other from the final state of interest. The level 2

trigger could exploit the secondary vertex topology. A trigger for hadronic charm final states would require a single lepton from the tagging charm combined with a requirement from the vertex topology. At the least, the HERA-*B* experiment could serve as a proving ground for high-rate fixed target charm experiments.

References

1. Gustavo Burdman, "Charm Mixing and *CP* Violation in the Standard Model," in **The Future of High-Sensitivity Charm Experiments**, Proceedings of the CHARM2000 Workshop, Fermilab, June 7–9, 1994, D. M. Kaplan and S. Kwan, *eds.*, FERMILAB-Conf-94/190, p. 75.

2. J. C. Anjos *et al.* (E691 Collaboration), Phys. Rev. Lett. **60**, 1239 (1988).

3. Sandip Pakvasa, "Charm as Probe of New Physics," in **The Future of High-Sensitivity Charm Experiments**, *op cit.*, p. 85.

4. R. J. Morrison, "Charm2000 Workshop Summary," in **The Future of High-Sensitivity Charm Experiments**, *op cit.*, p. 313.

5. P. L. Frabetti *et al.* (E687 Collaboration), Phys. Rev. D **50**, R2953 (1994).

Frascati Physics Series, Vol. III (1994)
HEAVY QUARKS AT FIXED TARGET
University of Virginia, October 7–10, 1994
(pp. 411–419)

PHYSICS OF AN ULTRAHIGH-STATISTICS CHARM EXPERIMENT

Michael D. Sokoloff
University of Cincinnati
Daniel M. Kaplan
Illinois Institute of Technology

ABSTRACT

We review the physics goals of an ultrahigh-statistics charm experiment and place them in the broader context of the community's efforts to study the Standard Model and to search for physics beyond the Standard Model, and we point out some of the experimental difficulties which must be overcome if these goals are to be met.

The CHARM2000 workshop [1] suggested that the goal for a future experiment be a factor $\sim 10^2$ increase in statistics over the coming round of fixed-target charm experiments at Fermilab (E781 and E831). We consider the physics goals of such an ultrahigh-statistics charm experiment ($\sim$ 100 million reconstuctable D's). Some measurements will test the Standard Model, some will measure its parameters, and some will elucidate heavy-quark phenomenology. We can outline the major goals as follows:

1. Measurements which search for new physics [2]
   - $D^0 - \overline{D}^0$ mixing
   - explicit flavor-changing neutral currents
   - direct CP violation.
2. Measurements which test the heavy-quark symmetry of QCD in the charm sector
   - form factors of semileptonic decays of charmed mesons
   - masses and widths of orbitally-excited charmed mesons.

   These measurements are key to extracting fundamental parameters from future beauty experiments.

3. Measurements which probe aspects of perturbative and nonperturbative QCD (including higher-twist effects)
   - nonleptonic singly and doubly Cabibbo-suppressed decay rates
   - dynamics of charm hadroproduction.

We next discuss these topics in more detail.

1 – Searches for New Physics

1.1 $D^0 - \overline{D}^0$ mixing

$D^0 - \overline{D}^0$ mixing is one of the most interesting places to look for physics beyond the Standard Model. While Wolfenstein [3] once suggested large long-distance or dispersive contributions to Δm_D within the Standard Model, more detailed calculations by Donoghue *et al.* [4] give $|\Delta m_D| \approx 10^{-6}$ eV. Recent analyses [5,6] based on heavy-quark effective theory (HQET) suggest that cancellations lead to $|\Delta m_D| < 3.5 \times 10^{-8}$ eV. Values of $|\Delta m_D|$ as large as 10^{-4} eV are possible in many models beyond the Standard Model [7] – [13]. Thus there is a large window for observing new physics via $D^0 - \overline{D}^0$ mixing.

A particularly intriguing example is discussed in a recent paper by Hall and Weinberg [13], which emphasizes that electroweak theories with several scalar doublets are consistent with all known physics (especially with the approximate *CP* symmetry in the neutral-kaon sector), provide an alternative mechanism for *CP* violation, and have various interesting phenomenological features. In such models, tree-level scalar-exchange contributions to neutral K- and B-meson mass mixing are at about the level observed by experiments if Higgs bosons have masses in the 700 GeV range. Hall and Weinberg say that "although this means that little can be learned about the CKM matrix from Δm_K and Δm_B, the case of $D - \overline{D}$ [mixing] presents different opportunities. ... If we take the typical Higgs boson mass as near 1 TeV to account for the observed values of $|\Delta m_K|$ and $|\Delta m_B|$, then the predicted value of $|\Delta m_D|$ is close to the current experimental limit, $|\Delta m_D| < 1.3 \times 10^{-4}$ eV."

CLEO II has reported a $D^0 \to K^+\pi^-$ signal with a branching ratio about $2 \times \tan^4\theta_C \times B(D^0 \to K^-\pi^+)$ [14]. This "wrong-sign" kaon is a signature either of mixing or of doubly Cabibbo-suppressed decay (DCSD). The two are most easily separated in a fixed-target experiment, in which the lifetime of the D can be directly measured: a DCSD signal decays exponentially, while a mixing signal has an additional t^2 dependence, so that it peaks at $2\tau_D$. If the CLEO II signal is primarily a DCSD signal, then it presents an inescapable background for mixing studies using hadronic final states. Assuming this is the case, an experiment such

as we consider should be sensitive to a mixing signal on top of a DCSD signal with $|\Delta m_D| \approx 2 \times 10^{-5}$ eV. Morrison [15] has pointed out that similar sensitivity might be achievable also in semileptonic decays, which are free of the confounding effects of DCSD. Liu's thorough treatment [16] includes the intriguing suggestion that for mixing arising from the decay-rate difference between the *CP* eigenstates D_1 and D_2, sensitivity an order of magnitude better might be achievable in singly Cabibbo-suppressed modes, by using the interference between mixing and DCSD to enhance the mixing signal.

1.2 Charm-changing neutral currents

Some of the models cited above [11, 12] also allow the possibility of explicit flavor-changing neutral currents (FCNC) in D decays. E791 has reported [17] the best 90%-confidence-level upper limit for the branching ratio of $D^+ \to \pi^+\mu^+\mu^-$ of 1.3×10^{-5}. An ultrahigh-statistics experiment with good lepton identification would have a sensitivity to this and other FCNC decays (and also to lepton-number-violating decays) one to two orders of magnitude lower.

1.3 *CP* violation

The Standard Model predicts that direct *CP* violation (observed as the fractional difference between decay rates of particle and antiparticle to charge-conjugate final states) will be of order 10^{-3} or less in singly Cabibbo-suppressed D decays [18]. (In the Standard Model, *CP* should be an exact symmetry for Cabibbo-allowed and DCSD decays.) Physics beyond the Standard Model might contribute *CP*-violating amplitudes to decay rates, and there is a large window for observing new physics. At the level of statistics we consider here, sensitivity to *CP* asymmetries at the fraction-of-a-percent level in singly Cabibbo-suppressed decays and at the few-percent level in doubly Cabibbo-suppressed decays may be possible. Holding systematic uncertainties to the percent level will be challenging, and experimenters planning to make such measurements must consider carefully how systematic errors will be minimized and how they will be measured.

2 – HQET and Semileptonic Decays

2.1 Testing HQET via orbitally-excited charmed mesons

Within the Standard Model, it is generally agreed that heavy-quark symmetry can be used to predict many nonperturbative properties of hadrons containing a single heavy quark, and the most important of these predictions are for exclusive

semileptonic B-meson decays [19]. These nonperturbative effects will be important in extracting V_{ub} and V_{cb} from measured decay rates. Heavy-quark symmetry also relates the masses and widths of the orbitally-excited D^{**} mesons (including the D_s^{**} mesons), as has been discussed recently in papers by Isgur and Wise [20], Ming-Lu, Isgur, and Wise [21], and Eichten, Hill, and Quigg [22]. While some authors argue that the charm-quark mass is sufficiently large for the limit $m_c \to \infty$ to be a good approximation [22], others [23] have argued that even for B mesons the $m_Q \to \infty$ limit has not been reached. The experiment we consider will measure the masses and widths of the orbitally-excited D^{**} mesons with sufficient precision to confront theoretical models quantitatively. Where E691 [24], ARGUS [25], CLEO II [26], and E687 [27] have measured the D_2^{*0}, D_2^{*+}, and D_1^0 widths with 50% fractional errors, such an experiment should be able to achieve few-percent fractional errors. To untangle the states and reflections which lie on top of each other, it will also be necessary to measure π^0's and (perhaps) single photons well. However, the benefit of making these measurements is that they will establish how well heavy-quark symmetry works for charm and give theorists the numbers they need to develop a more complete phenomenology of B physics.

2.2 Semileptonic form factors

High-statistics charm experiments will also contribute to our understanding of the form factors and helicity amplitudes of the vector mesons which can appear as decay products in both D and B decays. Extracting CP-violation parameters from measurements of branching ratios for decays such as $B_d \to \rho^0\psi$ and $B_d \to K^*\psi$, which Dunietz [28] advocates as the best place to measure the unitarity-triangle angle γ, requires the best possible measurement of the ρ^0 and K^* helicity amplitudes and form factors in the D semileptonic decays $D^+ \to \rho^0 l\nu$ and $D^+ \to K^{*0} l\nu$, as they should be the same in D as in B decay. Assuming single-pole forms for the form factors, the mass of the pole should be measurable with better than 1% precision. In $D^+ \to K^{*0} l\nu$, it should be possible to measure the polarization of the K^*,

$$\Gamma_L/\Gamma_T = \frac{\int P_V^* t |H_0(t)|^2 dt}{\int P_V^* t \left[|H_+(t)|^2 + |H_-(t)|^2\right] dt} \qquad (1)$$

(the ratio of longitudinal to transverse form-factors), with percent statistical and systematic uncertainties. It should be possible to measure the polarization of the ρ^0 in the Cabibbo-suppressed decay with few-percent statistical accuracy. $D_S \to \phi l\nu$ should be measured with similar precision, which will provide another test of the applicability of heavy-quark symmetry to the study of semileptonic decays.

2.3 Studying the CKM matrix with semileptonic decays

Studying semileptonic decays also contributes directly to our knowledge of the CKM matrix. High-statistics charm experiments are able to measure the magnitudes of V_{cs} and V_{cd} from the semileptonic decays of the D mesons. The absolute decay rates depend on various well-measured constants (such as the D masses and lifetimes), the CKM matrix elements, and the form factors of the hadrons produced along with the leptons. Currently, $|V_{cd}|$ and $|V_{cs}|$ are known with $\pm 8\%$ and $\pm 20\%$ precision [29, 30]. From the branching ratios for the semileptonic decays $D^0 \to \pi^- l^+ \nu_l$ and $D^0 \to K^- l^+ \nu_l$, the ratio $|V_{cd}|/|V_{cs}|$ should be determined with a statistical accuracy of $\sim 10^{-3}$. In addition to testing the unitarity of the CKM matrix in the charm sector, this ratio is explicitly required to extract the unitarity angle γ from the ratio $B(B_d \to \rho^0\psi)/B(B_d \to K^*\psi)$ discussed earlier.

3 – Testing QCD with Charm Hadroproduction

At the parton level, $c\bar{c}$ production is supposed to be described by perturbative QCD [31]. At the hadron level, the situation becomes more complicated. Several experiments have reported large leading-particle effects at high x_F [32]. Leading-twist factorization in perturbative QCD predicts that the charm quark's fragmentation is independent of the structure of the projectile, while the data indicate that the produced charm quark coalesces or recombines with the projectile spectator. To test models of higher-twist effects [33], one wants to look at the observed production asymmetries as functions of p_T and x_F jointly. Measuring these asymmetries for different target nuclei (*i.e.* measuring the A-dependence of these asymmetries) will provide an extra handle on how quarks evolve into hadrons.

4 – Experimental Issues

Building an ultrahigh-statistics charm experiment will be a challenge. The next-generation fixed-target experiments at Fermilab each project reconstructed charm samples of order 10^6 events. A Tau-Charm Factory operating at a luminosity of $10^{33}\,\mathrm{cm}^{-2}\,\mathrm{sec}^{-1}$, such as that proposed for SLAC [34], would reconstruct about 5×10^6 charm per year. The B factories planned for KEK and SLAC will produce of order 10^8 $b\bar{b}$ events per year at design luminosity. However, the number of reconstructed charm will be similar to that projected for the Tau-Charm Factory. HERA-B [35] will produce a sufficient number of D's in pp collisions to imagine an ultrahigh-statistics experiment, but the triggering requirements for charm physics differ substantially from those for B physics, and the data acquisition system is currently designed to operate at 10 Hz. In addition, the current design for the HERA-B vertex detector

entails much more multiple scattering and much poorer vertex resolution than are desirable for a charm experiment. There is no clear route to higher luminosities for e^+e^- machines or photon beams, so we are left with the problem of working with a relatively small cross-section in a hadronic environment. Whether it is a fixed-target experiment or a collider experiment that we consider, triggering selectively and efficiently will be the first major problem.

Building a detector which minimizes backgrounds will be another problem. If we are looking for physics beyond the Standard Model, or looking for relatively rare decays expected within the Standard Model, reducing backgrounds will be at least as important as maintaining high efficiency for the interesting signals. Two examples should suffice:

1) The FCNC decay $D^+ \to \pi^+\mu^+\mu^-$ is expected to have a branching ratio less than 10^{-8} in the Standard Model [36] (except for the decay $D^+ \to \phi\pi^+$ followed by $\phi \to \mu^+\mu^-$, which populates a limited region of the Dalitz plot). E791 [17] finds that its sensitivity is greatest when the expected number of background events is between 5 and 10 in the signal region. If one were to scale up from this experiment simply, sensitivity would increase only as the square root of the number of reconstructed charm, since the background would grow linearly with the signal. To increase sensitivity here, it will be important to reduce backgrounds without substantially reducing efficiency for detecting muons. This can be achieved by adding redundancy, *e.g.* a second view in the muon detector or a redundant muon-momentum measurement, so that the double muon-misidentification probability becomes approximately the square of the single muon-misidentification probability.

2) To measure the ratio of CKM matrix elements by comparing the decay rates for $D^+ \to K^*\ell\nu$ and $D^+ \to \rho^0\ell\nu$, it will be critical to separate pions from kaons with a very high degree of confidence; the reflections of these signals feed into each other directly. A fast RICH technology may suffice, but this is another area where redundancy seems necessary to reduce the confusions which lead to systematic errors.

Finally, it seems obvious that silicon pixel devices will be necessary to provide both the spatial resolution and the segmentation that are required for unambiguous vertexing in the high-rate small-angle region.

5 – Summary

Charm physics provides a window into the Standard Model, and possibly beyond, that complements those provided by other types of experiments. In searches for

$D-\overline{D}$ mixing, FCNC, lepton-number-violating decays, or *CP*-violating amplitudes, we are probing physics at the TeV level which may not be accessible to other experiments: down-sector and up-sector quarks can couple differently to new physics, and the charm quark is the only up-sector quark for which such studies are possible. Within the Standard Model, charm is probably the best place to test heavy-quark symmetry quantitatively, and it is the best place to measure some of the CKM matrix elements. While ultrahigh-statistics experiments will be extremely difficult, we can reasonably imagine that the technology will exist in the next decade to reconstruct 100 million charm. Getting from here to there will require a substantial R&D effort, and developing the expertise to design and build such an experiment will require commitment from the individuals who will contribute directly, from the laboratory at which it will be done, and from the community as a whole.

We thank the organizers of this Workshop for offering us this opportunity to discuss heavy-quark physics in such attractive surroundings. We also thank our colleagues from Fermilab proposal P829 [37] for their contributions. This work was supported by NSF grant PHY 92-04239 and DOE grant DE-FG02-94ER40840.

References

1. D. M. Kaplan and S. Kwan, *eds.*, **The Future of High-Sensitivity Charm Experiments**, Proceedings of the CHARM2000 Workshop, Fermilab, June 7–9, 1994, FERMILAB-Conf-94/190 (1994).

2. These topics have also been discussed recently by S. Pakvasa, "Charm as Probe of New Physics," in **The Future of High-Sensitivity Charm Experiments**, *op cit.*, p. 85.

3. L. Wolfenstein, Phys. Lett. B **164**, 170 (1985).

4. J. F. Donoghue, E. Golowich, B. R. Holstein and J. Trampetic, Phys. Rev. D **33**, 179 (1986).

5. Howard Georgi, Phys. Lett. B **297**, 353 (1993).

6. T. Ohl, G. Ricciardi, and E. H. Simmons, Nucl. Phys. **B403**, 605 (1993).

7. E. Eichten, I. Hinchliffe, K. D. Lane, and C. Quigg, Phys. Rev. D **34**, 1547 (1986).

8. I. I. Bigi and A. F. Sanda, Phys. Lett. B **171**, 320 (1985).

9. A. Datta, Phys. Lett. **154B**, 287 (1985).

10. A. Hadeed and B. Holdom, Phys. Lett. **159B**, 379 (1985).

11. W. Buchmuller and D. Wyler, Phys. Lett. B **177**, 377 (1986);
Miriam Leurer, Phys. Rev. Lett. **71**, 1324 (1993).

12. A. S. Joshipura, Phys. Rev. D **39**, 878 (1989).

13. Lawrence Hall and Steven Weinberg, Phys. Rev. D **48**, R979 (1993).

14. D. Cinabro *et al.* (CLEO collaboration), Phys. Rev. Lett. **72**, 1406 (1994).

15. R. Morrison, "Charm2000 Workshop Summary," in **The Future of High-Sensitivity Charm Experiments**, *op cit.*, p. 313.

16. T. Liu, "The $D^0\overline{D}^0$ Mixing Search — Current Status and Future Prospects," in **The Future of High-Sensitivity Charm Experiments**, *op cit.*, p. 375.

17. A. Nguyen *et al.* (E791 Collaboration), "Search for $D^{\pm} \to \pi^+\mu^+\mu^-$," FERMILAB-Conf-94/187-E, contributed to the 27th International Conference on High Energy Physics (ICHEP), Glasgow, Scotland, 1994.

18. F. Bucella *et al.*, Phys. Lett. B **302**, 319 (1993).

19. N. Isgur and M. B. Wise, Phys. Lett. B **232**, 113 (1989) and Nucl. Phys. **B348**, 276 (1991).
Howard Georgi, Nucl. Phys. **B348**, 293 (1991).

20. N. Isgur and M. B. Wise, Phys. Rev. Lett. **66**, 1130 (1991).

21. Ming-Lu, M. B. Wise, and N. Isgur, Phys. Rev. D **45**, 1553 (1992).

22. E. Eichten, C. T. Hill and C. Quigg, Phys. Rev. Lett. **71**, 4116 (1993); "Spectra of Heavy-Light Mesons," in **The Future of High-Sensitivity Charm Experiments**, *op cit.*, p. 345, and "Orbitally Excited Heavy-Light Mesons Revisited," *ibid.*, p. 355.

23. S. Godfrey and R. Kokoski, Phys. Rev. D **43**, 1679 (1991).

24. J. C. Anjos *et al.* (E691 Collaboration), Phys. Rev. Lett. **62**, 1717 (1989).

25. H. Albrecht *et al.* (ARGUS Collaboration), Phys. Lett. B **221**, 422 (1989); *ibid.* **231**, 208 (1989); and *ibid.* **232**, 398 (1989).

26. P. Avery *et al.* (CLEO Collaboration), Phys. Rev. D **41**, 774 (1990).

27. P. L. Frabetti *et al.* (E687 Collaboration), Phys. Rev. Lett. **72**, 324 (1994).

28. Isard Dunietz, "*CP* Violation with Additional *B* Decays," in "*B* **Decays**," Sheldon Stone, *ed.*, World Scientific, Singapore (1992), p. 393, and "Extracting CKM Parameters from *B* Decays," FERMILAB-Conf-93/90-TH, in **Proceedings of the Workshop on B Physics at Hadron Accelerators**, Snowmass, CO, June 21 – July 2, 1993, P. McBride and C. S. Mishra, *eds.*, FERMILAB-Conf-93/267 (1993), p. 83.

29. Particle Data Group, L. Montanet *et al.*, Phys. Rev. D **50**, Part 1 (1994).

30. J. L. Rosner, "The Cabibbo-Kobayashi-Maskawa Matrix," in "*B* **Decays**," Sheldon Stone, *ed.*, World Scientific, Singapore (1992), p. 312.

31. P. Nason, S. Dawson and R. K. Ellis, Nucl. Phys. **B327**, 49 (1989) and ERRATUM, *ibid.*, **B335**, 260 (1990).

32. G. A. Alves *et al.* (E769 Collaboration), Phys. Rev. Lett. **72**, 812 (1994);
T. Carter *et al.* (E791 Collaboration), "Production Asymmetries in x_F and p_T^2 for $D^{\pm}$ Mesons," FERMILAB-Conf-94-185-E," contributed to the 27th International Conference on High Energy Physics (ICHEP), Glasgow, Scotland, 1994.

33. S. J. Brodsky, J. F. Gunion, and D. E. Soper, Phys. Rev. D **36**, 2710 (1987);
S. J. Brodsky, P. Hoyer, A. H. Mueller, and W.-K. Tang, Nucl. Phys. **B369**, 519 (1992);
W.-K. Tang, "Anomalous Charm Production at Large x_F," in **The Future of High-Sensitivity Charm Experiments**, *op cit.*, p. 251.

34. **Proceedings of the Tau-Charm Factory Workshop**, L. V. Beers, *ed.*, SLAC-343, May 1989.

35. W. Hofmann and W. Schmidt-Parzefall, spokespersons, "HERA-*B*: An Experiment to Study CP Violation in the *B* System Using an Internal Target at the HERA Proton Ring," DESY-PRC 94/02 (1994); also H. Albrecht, these Proceedings.

36. A. Schwartz, Mod. Phys. Lett. **A8**, 967 (1993).

37. B. T. Meadows *et al.*, "P829: Continued Study of Heavy Flavors at TPL," a proposal to the Fermi National Accelerator Laboratory, November 1993, and addendum, February 1994.

Frascati Physics Series, Vol. III (1994)
HEAVY QUARKS AT FIXED TARGET
University of Virginia, October 7–10, 1994
(pp. 421–422)

CHARM2000 AT FNAL USING CRYSTAL EXTRACTION

David Christian
Fermilab

ABSTRACT

Discussions of a "10^8 charm" experiment have so far focussed on a traditional fixed target experiment using a resonant-extracted 800 GeV/c proton beam. The purpose of this note is to point out that it would also be possible to achieve the CHARM2000 goals in a fixed target experiment which uses a low intensity 900-1000 GeV/c proton beam extracted from the halo of the circulating TeVatron beam by a bent crystal during collider operation.

At least three options exist for achieving the goals of CHARM2000 at Fermilab. These are a fixed target experiment running as part of a dedicated fixed target run, a collider experiment optimized for charm, and a fixed target experiment running during collider operation using a proton beam extracted from the TeVatron halo by a bent silicon crystal. This third option has not yet been explored, but it appears viable and should not be forgotten.

The first experiment [1] designed to demonstrate the feasibility of crystal extraction from the TeVatron (E853) will begin taking data soon. The goal of this experiment is to remove 4×10^6 protons/second from the TeVatron with a channeling efficiency of 25% (i.e. 1 MHz extracted). This rate was chosen so as to contribute 24 hours to the luminosity lifetime of the TeVatron collider under the current intensity conditions of 10^{12} protons circulating. It should be noted that schemes [2] exist for achieving much higher channeling efficiency.

During the first Main Injector run (TeV Run II), 36 bunches of approximately 1.2×10^{13} protons total will be collided with 36 bunches of approximately 1.3×10^{12} antiprotons [3]. With these conditions, a bent crystal could be used to remove approximately 5×10^7 protons/second from the circulating beam, leading to a 12 MHz extracted beam, assuming 25% efficiency. Furthermore, tests already conducted for E853 [4] indicate that it will be possible to remove (a few) $\times 10^7$ protons/second without significant impact on backgrounds at CDF or D0. Improve-

ments both in extraction efficiency and in the collimation of protons interacting with the crystal are being studied [5].

I have estimated the charm yield for a hypothetical experiment using a 12 MHz crystal extracted beam and a 5% interaction length target to produce a 600 kHz interaction rate. This I have done by scaling from P829 [6], for which conservative yield estimates were made using data and charm signals from E791. P829 assumed a 100 kHz interaction rate during slow spill (with a duty factor of approximately $\frac{1}{3}$). It called for a 500 GeV/c π^- beam, for which the fraction of events containing charm is estimated to be 50% higher than would be the case with a 900 GeV/c proton beam. Together these factors indicate that the experiment using a crystal extracted beam would reconstruct $6 \times 3 \times \frac{2}{3} = 12$ times as much charm as expected by P829 in an equal amount of calender time. In one year of running, approximately 0.5×10^8 reconstructable charm decays would be recorded on tape.

During the second Main Injector run (TeV Run III), the number of proton and antiproton bunches will be increased to as many as 99, or as few as 77. Even if one ignores the possibility of gains due to improvements in crystal extraction techniques, an increase in the number of bunches by a factor of 2-3 can be expected to result in a similar increase in charm yield. At this point, the experiment would be logging to tape more than 10^8 completely reconstructable charm decays per calender year.

References

1. R. A. Carrigan *et al.*, "E853: A Test of Low Intensity Extraction from the TeVatron using Channeling in a Bent Crystal," C. T. Murphy, spokesperson, May 1991.

2. E. Tsyganov and A. Taratin, "Beam Halo Crystal Extraction from the TeVatron during Collider Runs," SSCL-Preprint-569 (1994).

3. K. Stanfield, "Dear Colleagues" letter dated February 14, 1994.

4. G. Jackson, "Results from Beam Diffusion and Collimation Measurements in Preparation for Fermilab Tevatron Crystal Extraction," Proc. 1993 Part. Acc. Conf., Washington, DC (1993).

5. C. T. Murphy, private communication.

6. B. Meadows *et al.*, "P829: Continued Study of Heavy Flavors at TPL," D. Christian and M. Sokoloff, spokespeople, October, 1993.

Frascati Physics Series, Vol. III (1994)
HEAVY QUARKS AT FIXED TARGET
University of Virginia, October 7–10, 1994
(pp. 423–426)

EXPERIMENTS TO STUDY $(Q\overline{Q})$ STATES. IS THERE A FUTURE?

Rosanna Cester
Univ. degli Studi di Torino

The study of $(Q\overline{Q})$ states has been performed in three types of experiments:

- The production mechanism has been studied in high energy hadronic interactions.
- The spectral characteristics and decay mechanisms have been studied at e^+e^- colliders by direct formation through one photon exchange (for states with $J^{PC} = 1^{--}$) and in the radiative decays of ${}^3S_1$ states or, at higher energies, in two photon fusion (for states with positive C-parity).
- Precise measurements of the level structure can also be obtained from direct formation of $Q\overline{Q}$ states in $\bar{p}p$ annihilation. In this kind of experiment there are no constraints on the possible values of J^{PC}, however, due to the high background in hadronic final states, only decays to electromagnetic final states have been observed.

Direct formation experiments at e^+e^- colliders (BEPC, CESR and future B factories) could in principle continue but are at present given low priority. The study of two photon processes will continue at high energy e^+e^- colliders. Similarly the study of production mechanisms (and possibly new discoveries) will come as a by-product of high energy hadron-collider experiments.

The only dedicated experiments to study quarkonium spectroscopy in the near future are those studying direct formation of $(c\bar{c})$ in $\bar{p}p$ annihilation. The history of these experiments (from past to near future) is given in Table 1.

The three experiments have common features: they are fixed target experiments and use stochastically cooled antiprotons circulating in a storage ring as a beam; an internal hydrogen-jet target; and a non-magnetic spectrometer optimized for the detection of electromagnetic final states. Examples of reactions that have been studied are: $\bar{p} + p \to J/\psi \to e^+ + e^-$, $\bar{p} + p \to \chi \to J/\psi + \gamma \to e^+ + e^- + \gamma$,

Table 1:

Experiment	$\mathcal{L}_{max}$ (10^{31} cm^{-2}s^{-1})	$\int \mathcal{L}\, dt$ (pb^{-1})	$\frac{\sigma_P}{P}$	Facility	Period
R704	0.3	3	4×10^{-4}	CERN-ISR	1983-1984
E760	1.0	30	$\sim 10^{-4}$	FNAL-$\bar{p}$ Source	1990-1991
E835	7.0	200	$\sim 10^{-4}$	FNAL-$\bar{p}$ Source	1996-1997

$\bar{p} + p \rightarrow \eta_c \rightarrow \gamma + \gamma$. The advantages of such fixed target experiments are the possibilities of using existing facilities and reaching high luminosities and a superb resolution for the energy of the initial state (see Table 1).

In the charmonium sector three out of four of the $n = 1$ D states (two of which are expected to be narrow) have not yet been detected and two states, the $n = 2\ ^1S_0$ (η_c') and the $n = 1\ ^1P_1$ (h_c) need confirmation. A measurement of mass and width for all these narrow levels would complete the study of the charmonium spectrum, improving our knowledge of spin effects in quark-antiquark interactions and shedding light on the annihilation mechanism. Furthermore there is speculation that the energy region close to the $D\overline{D}$ threshold ($3.7\,\text{GeV} < \sqrt{s} \leq 4.3\,\text{GeV}$) could be populated by exotics, which would preferentially decay by cascading down to lower charmonium levels. One possible example is $D\overline{D}$ molecules, which should show up just below the $D\overline{D}$ threshold.

E835 plans to address these problems, but will probably not integrate enough luminosity to complete the program.

The question we ask is: can this kind of experiment continue in the Main Injector era and how can it be substantially improved?

The strategy of the experiments of Table 1 has been that of selecting final states with a strong signature, namely the two body decay into either e^+e^- or $\gamma\gamma$, or the cascade decay to either a J/ψ or an η_c then decaying to the same two body final states. Since the identification of a $J/\psi \rightarrow e^+ + e^-$ in the final state has proven to be an extremely powerful tool to suppress background, one could retain the same strategy with a new detector of higher performance and larger acceptance. This would probably require also a new target of different geometry to improve on the hermeticity of the detector. The maximum instantaneous luminosity will scale linearly with the stacking rate in the accumulator [1], which is expected to increase by a factor ~ 4. The density of the jet could also be further increased but would reduce the lifetime of the circulating $\bar{p}$ and result in a limited gain in luminosity. At best one could hope to obtain a factor ten improvement on the E835 event rate.

A completely different and new approach would be that of searching for

hadronic decays. As already mentioned the background from light quark hadron production is discouragingly high (with the possible exception of the OZI forbidden $\phi\phi$ channel). It has been suggested [2] that interference effects between non-resonant and resonant amplitudes could provide a signature for the formation of charmonium states decaying to light-quark hadrons. E760 has searched for such effects in neutral final states but, so far, has seen no evidence.

In conclusion, I believe that there is still room for an interesting experiment; how interesting and how worthwhile we will only know after E835. So far I have discussed the feasibility of an experiment to be performed in the Main Injector era at the antiproton source at Fermilab. One should however keep in mind that such experiment has only run parasitically to the Tevatron fixed target data taking. It is conceivable that a better data-taking duty cycle could be obtained by constructing an external $\bar{p}$ beam with low π^- contamination. Proposals to study charmonium spectroscopy with external beams have been presented in the past at CERN [3] and BNL and could be adequate to detect and measure the wider ($\Gamma \geq$ few MeV) resonances.

The next question which is usually asked is: could one perform a similar experiment looking for $(\bar{b}b)$ states formed in $\bar{p}p$ annihilation? Clearly this experiment would be of great interest for two reasons: a) the $\bar{b}b$ system is the best testing ground for potential models since relativistic corrections are small, and b) the $\bar{b}b$ spectrum is poorly known, with only 9 out of the expected 26 narrow states so far detected.

It is a difficult experiment since the cross sections for direct formation of $(\bar{b}b)$ states are predicted to be of order 10^{-4} times smaller than those for charmonium, at best 100 pb integrating over all decay channels. Clearly one can not afford to select a low-branching-ratio decay mode for a signature! It has been suggested that $(\bar{b}b)$ events could be selected with high efficiency by requiring high transverse momenta and a two (three) jet topology [4].

For a fixed target experiment a $\bar{p}$ beam in the range of energy 46 to 58 GeV is needed, which at present is nowhere available.

References

1. S. Y. Hsueh, "The Fermilab $\bar{p}$ accumulator ring for the charmonium experiment," in **Physics at SuperLEAR**, C. Amsler and D. Urner, *eds.*, The Institute of Physics, Bristol, 1991, p. 105.

2. J. Rosen, private communication.

3. P. J. Litchfield *et al.*, ISR proposal, CERN/SPSC/80-62; SPSC/I 132, Aug. 5,1980.

4. P. Dalpiaz, "Bottomonium, a further option of SuperLEAR," in **Physics at SuperLEAR**, *op cit.*, p. 125.

SESSION XII

- T. Nakada
  Prospects for Studying CP Violation in B-Meson Decays at LHC
- T. Matsuda
  CP Reach: The Case of the KEK B-factory
- J. Butler
  B Physics at the Fermilab Collider After the First Main Injector Run

Frascati Physics Series, Vol. III (1994)
HEAVY QUARKS AT FIXED TARGET
University of Virginia, October 7–10, 1994
(pp. 429–434)

PROSPECTS FOR STUDYING CP VIOLATION IN B-MESON DECAYS AT LHC

Tatsuya Nakada
Paul Scherrer Institute, CH-5232 Villigen-PSI, Switzerland

ABSTRACT

Efforts to observe CP violation in the B-meson decays are already made at the existing accelerators and those under construction. Although a positive signal may appear there first, LHC will be the ultimate source of the B-mesons. With the large number of B-mesons expected at LHC, a real precision test will become possible. A short summary of the prospect for CP violation experiments at LHC is presented.

1 – Introduction

The aim of the CP violation study at LHC is the "precision" test. The b-quark cross sections are estimated to be $\sim$ 1 μb in fixed target mode and $\sim$ 500 μb in collider mode. In addition to B^0, $\overline{B}^0$ and $B^{\pm}$, B_s-mesons and Λ_b's are produced. The fraction of the b-quark production in the total p-p interactions is $\sim$ 0.002% in fixed target mode and $\sim$ 0.5% in collider mode. It must be noted that the current fixed target charm experiments operate with $\sigma_{c\bar{c}}/\sigma_{\rm total} \approx 0.5\%$. The large number of B-mesons expected at LHC should allow measuring the angles of the so called "unitarity triangle" [1], α and β (and γ) with a precision of $\sim$ 0.01 ($\sim$ 0.5) or better. This will be the ultimate test of the standard model for CP violation.

On the other hand, an experiment at LHC is a formidable challenge. The detector has to cope with an event rate of 40 MHz and an even higher interaction rate. The trigger, in particular the first-level trigger, must be fast and very selective. One can no longer record all events with B-mesons and particular B-meson decay modes of interest must be selected. This requires the online reconstruction of events in the third-level trigger with all the detector information.

The ultimate limitation of the experiment may come from the radiation damage. It is conceivable that LHC will produce more B-mesons than the experiment can handle due to the radiation damage of the detector.

2 – General Purpose Detectors

ATLAS and CMS [2] are two general purpose collider detectors designed to perform high P_T physics such as studying the top quark and searching the Higgs and super-symmetric particles in p-p interactions at LHC in the central region. The b-quark provides an important means for high P_T physics.

Due to the increasing interest in b-physics itself, both collaborations started to investigate the capabilities of their detectors to study b-physics such as CP violation in the B-meson decays. Those studies are influencing the design of the detectors, in particular the vertex detectors.

It is expected to take several years for LHC to reach its designed luminosity of $\sim 10^{34}$ cm^{-2}s^{-1} which is required to fully exploit LHC for high P_T physics. Thus, b-physics will be an important physics programme for ATLAS and CMS during the first few years of the LHC operation. Once LHC achieves the design luminosity, b-physics will become exceedingly difficult due to the pile-up.

Both ATLAS and CMS have an excellent muon detection capability and the muon is used in the first-level trigger. ATLAS requires a single muon with $P_T \geq 6$ GeV. For the B$\rightarrow$ J/ψ K$_S$ decay mode, the trigger muon can be generated by muons either from the J/ψ decay or from the semileptonic decay of the partner b-quark which is used as the tag.

The CMS first-level trigger demands a single muon with $P_T \geq 10$ GeV or two muons with $P_T \geq 3 \sim 5$ GeV. The double muon trigger is very effective for the B-meson decay final states with J/ψ. The single muon trigger is mainly sensitive to the semileptonic decay of the partner b-quark used for the tag.

The excellent detection capability for the electron allows ATLAS to reconstruct J/$\psi \rightarrow e^+e^-$. Due to the strong magnetic field of the detector (4 T), CMS has a difficulty to use the electron channel.

Both experiments have improved their vertex detectors by placing their first plane much closer to the beam than the original designs shown in the letters of intent. The new designs provide a much better impact parameter resolution which reduces the background in the reconstructed B-mesons and improves the eigentime resolution of the B-meson. However, the radiation damage with the nominal LHC luminosity is a serious concern.

Table 1 summarises the expected performance for measuring sin 2α and sin 2β by ATLAS and CMS using the CP asymmetries obtained form the decay time integrated rates. It is assumed that LHC will run with an average luminosity of 10^{33} for 10^7 s, i.e. roughly one year. The quoted errors are only statistical. The table shows that sin 2β can be measured well. For the measurement of sin 2α, the large amount of the remaining background is a worry. The background comes mainly from other two-body decay modes of b-hadrons such as B $\rightarrow$ Kπ, B$_s$ $\rightarrow$ KK etc.. The momentum resolution is not sufficient to distinguish them from the B$\rightarrow \pi^+\pi^-$ decay.

One way to separate the background in ATLAS and CMS which have no special kaon and pion identification capability, is to study the decay time distribution. The background events are expected to decay (almost) exponentially. In

Table 1: Expected performances of the general purpose detectors at LHC for $\sin 2\alpha$ and $\sin 2\beta$ using the time integrated method.

No.($b\bar{b}$)/10^7 sec	5×10^{12}			
Measurement	sin 2α from $\pi^+\pi^-$		sin 2β from $J/\psi K_S$	
Experiment	ATLAS	CMS	ATLAS	CMS
No.(reconstructed "final state"+tag)				
• μ-tag	3070	3400	$J/\psi \to \mu^+\mu^-$	
			3847	9200
			$J/\psi \to e^+e^-$	
			6041	-
• e-tag	-	-	$J/\psi \to \mu^+\mu^-$	
			4322	-
total	3070	3400	14210	9200
background/signal	1.67	0.84	~ 0.1	~ 0.1
stat. information	0.71	0.47	0.62	0.47
$\sigma_{\text{statistical}}$	0.08	0.09	0.028	0.047

the absence of the penguin diagram, the decay time distribution for $\pi^+\pi^-$ events is given by

$$\propto e^{-\Gamma t}(1 \pm \sin 2\alpha \times \sin \Delta m t)$$

where Δm and Γ are the mass difference between the two weak eigenstates and the decay width of the neutral B-mesons, respectively. Another advantage of studying the decay time distribution is that the errors on $\sin 2\alpha$, and also on $\sin 2\beta$, can be reduced by up to $\sim 20\%$ due to the increased statistical sensitivity of the method.

3 – Dedicated Detectors

3.1 Past

Three different ways to study B-physics in a dedicated manner, COBEX, GAJET and LHB [2], have been initiated. COBEX proposed to work in collider mode, GAJET and LHB in fixed target mode. An internal gas-jet target was considered for GAJET, while LHB proposed to extract parasitically the halo of the LHC beam using a bent crystal. All three experiments were designed to run for many years in different luminosity conditions of LHC.

All three detectors are forward spectrometers equipped with a Si vertex detector very close to (or in) the beam, a large aperture magnet(s), a tracking system, a particle identification system capable of the π/K/p separation over all the necessary kinematic range, an electromagnetic (and a hadronic for GAJET and LHB) calorimeter(s) and a muon system.

COBEX benefits from the larger b-quark production cross section in collider mode. GAJET emphasises its simple and effective trigger strategy based on the point-like target geometry. LHB deploys a vertex detector system in the beam where most of the B-mesons decay within the system.

General advantages of a dedicated detector compared to a general purpose detector are the followings:

- The forward spectrometer geometry allows a more efficient muon P_T trigger with a lower threshold value.
- The vertex detector system close to the beam provides a better vertex resolution.
- The particle identification system reduces the background in the $B \rightarrow \pi^+\pi^-$ decay mode generated by other two-body decay modes of b-hadrons to a negligible amount. It also reduces the combinatorial background and many-body decay modes of B- and B_s-mesons can be reconstructed. This allows to measure the third angle of the unitarity triangle, γ, CP asymmetries which are expected to be very small in the standard model and CP asymmetries in the charge B-meson decays.

Table 2 summarises the performances of the three dedicated experiments. They do indeed better in the difficult decay mode $B \rightarrow \pi^+\pi^-$ than the general purpose detectors, not only statistically but also in the reduction of the background.

3.2 Current Status and Future

Although the LHC committee (LHCC) has repeatedly confirmed the necessity of a dedicated B-physics experiment as one of the baseline LHC experiments along with ATLAS, CMS and ALICE, non of the above described three experiments was recommended for submitting a technical proposal. Instead, LHCC requested the submission of a new letter of intent by a joint collaboration based on collider mode with a newly designed forward spectrometer. A collaboration consisting of most of the members of the original three groups and many other institutes were formed to do this task. The collaboration is currently of optimising the detector and the trigger strategy and intends to submit the letter of intent by the end of February 1995. The performance is expected to be even better and more solid than that given by the originally proposed dedicated experiments.

4 – Conclusions

Active efforts are being made to plan measuring CP violation in the B-meson decays at LHC. The two general purpose experiments, ATLAS and CMS will study CP violation during the initial period of the LHC running with less luminosities than the nominal one. They can measure sin 2β well using the $B \rightarrow J/\psi K_S$ decay

Table 2: Expected performances for proposed dedicated experiments at LHC.

Experiment	COBEX	GAJET	LHB
No.($b\bar{b}$)/10^7 sec	4×10^{12}	2×10^{10}	7.7×10^9
First-level trigger			
High P_T	μ	μ, e, hadron	μ, e
+ Large impact parameter	-	yes	-
Tagging method	μ ($K^{\pm}$)	μ, e, $K^{\pm}$	μ, e, $K^{\pm}$, $B^{\pm}$
sin 2α from $\pi^+\pi^-$			
No.(reconstructed $\pi^+\pi^-$+tag)	30000	4500	3200
background/signal	< 0.23	0.32	< 0.1
$\sigma_{\sin 2\alpha}$ statistical	0.015	0.047	0.069
sin 2β from $J/\psi\, K_S$			
No.(reconstructed $J/\psi\, K_S$+tag)	270000	10000	13000
$\sigma_{\sin 2\beta}$ statistical	0.007	0.028	0.024
final states useful to measure γ			
$B_s \to D_s K$/branching ratio + tag	1.8×10^8	8.3×10^7	2.8×10^7
$B^+ \to \bar{D}^0 K^+$/branching ratio	-	-	1.2×10^8
$B^0 \to \bar{D}^0 K^{*0}$/branching ratio	-	1.9×10^8	–

mode and contribute to the sin 2α measurement. Their limitation is in the particle identification.

A dedicated B-physics detector at LHC will tackle the problem of CP violation in the B-meson decays for many years and try to measure the angles of the unitarity triangle with a precision of ≤ 0.01. It will have a more efficient trigger for the b-quark events than the general purpose detectors. The capability of identifying pion, kaon and proton will ensure the clean reconstruction of many different B-meson decay modes which is important to make the ultimate test of the standard model for CP violation.

Acknowledgements

The author thanks the organizers of the conference for their hospitality.

References

1. See for example contribution from I. I. Bigi in this proceedings.

2. All the activities on b-physics at LHC are nicely summarised by the various articles found in
Proceedings of the Second International Workshop on B-Physics at Hadron Ma-

chines (ed. P. E. Schlein, Le Mont-Saint-Michel, April 1994), Nucl. Inst. and Meth. **A351**, 1 (1994).

Frascati Physics Series, Vol. III (1994)
HEAVY QUARKS AT FIXED TARGET
University of Virginia, October 7–10, 1994
(pp. 435–440)

CP Reach: The Case of the KEK B-factory

T. Matsuda
National Laboratory for High Energy Physics
Tsukuba, Ibaraki, 305 Japan

ABSTRACT

KEK is building an asymmetric B-factory. The goal of the peak luminosity is $1 \times 10^{34}\text{cm}^{-2}\text{sec}^{-1}$. The BELLE collaboration builds a detector to study of CP violation in B meson decays. Our Monte Carlo studies based on the BELLE detector design show that it will become possible to carry out a definitive test of CP violation in the standard model by measuring the three angles and the three sides of the CKM triangles provided with extended theoretical studies.

1 Introduction

Since the first observation of CP violation in the K^0 system in 1964, an enormous amount of theoretical work has been done to try to understand the phenomenon. In addition to the Cabibbo-Kobayashi-Maskawa (CKM) scheme, which explains CP violation within the framework of the Standard Model, many extensions of the Standard Model have been proposed that incorporate CP violation. All of these theoretical proposals are, however, consistent with presently available experimental data.

Observations of CP violation at a B-factory could provide definitive information to settle the theoretical situation. As is well known, all of the KM matrix elements can, in principle, be measured at a B-factory. In addition to clarifying the situation for CP violation, these measurements may provide a first look at phenomena beyond the Standard Model.

2 KEK B-factory

The KEK B-factory [1] is an asymmetric e^+e^- collider operated at $\Upsilon(4S)$. We install the two rings of the KEK B- factory in the existing 3 km TRISTAN tunnel. The

design parameters of the accelerator (as of September 1994) are listed in Table1.

We choose the energy asymmetry of 3.5 x 8 GeV after an intensive comparison of different energy asymmetries. To achieve the 8 GeV injection of electrons and to obtain a necessary intensity of 3.5 GeV positron beam, the energy upgrade of the injection liniac to 8 GeV has been started. The final goal of the peak luminosity of the KEK B-factory is $1 \times 10^{34}\mathrm{cm}^{-2}\mathrm{sec}^{-1}$. Adopting a large angle (± 10 mrad) beam crossing at the interaction point after an intensive study on the beam-beam instability, the effort of increasing the luminosity from an initial achievement to its final goal will be continuos whereas in our previous design with the head-on collision the design luminosity was limited to be 2 $times 10^{33} cm{-}2sec^{-1}$ and a large modification of the interaction region was necessary to go beyond the limit. To achieve this final goal, we choose an accelerator design with the large beam currents, the large beam-beam tune shift and the small beta function at the interaction point. When we compare the design parameters of the KEK B-factory to those for the SLAC B-factory, it is interesting to realize that the design approaches of these two B-factories are much different.

Table 1: Design parameters of the KEK $B-$ factory (as of September 1994).

Energy (GeV)	E	3.5	8.0
Circumference (m)	C	3016	3016
Emittance (nmrad)	ϵ_x/ϵ_y	18/0.36	18/0.36
Beta function at IR (m)	β_x^*/β_y^*	0.33/0.01	0.33/0.01
Tune shift .	ξ_x/ξ_y	0.05/0.05	0.05/0.05
Crossing angle (mrad)		± 10.0	
Momentum compaction	α	1.648×10^{-4}	2.5×10^{-4}
RF frequency (MHz)	f_{RF}	508.887	508.887
RF voltage (MV)	V_c	9.5	≈ 2.5
Bunch length (cm)	σ_z	0.4	0.4
Number of bunches	k_B	5120	5120
Bunch spacing (m)	S_B	0.6	0.6
Damping time (ms)	τ_E/τ_x	40.2/80.5	17.6/35.3
Beam current (A)	I	2.6	1.1
Synch. rad. loss (MeV/turn)	U_o	0.87	4.6
Luminosity ($\mathrm{cm}^{-2}\mathrm{sec}^{-1}$)	L	1×10^{34}	

The KEK B-factory project was approved by Japanese government in April 1994 with the 5 years' construction budget. The LOI for "the study of CP violation in B meson decay at the KEK B-factory" by the BELLE collaboration [2] was accepted in March 1994. The TDR is due at the end of 1994 for a full approval. We plan to complete our BELLE detector by the summer 1998. The commission of the accelerator should take place immediately after the roll-in of the detector. The BELLE detector will be installed at the Tsukuba experimental hall where the TOPAZ detector currently occupies.

3 BELLE Detector

The proposed BELLE detector (as of October 1994) is shown in Figure 1. The tracking detector consists of three devices, Silicon micro-strip Vertex Detector (SVD), Precision Drift Chamber (PDC), Central Drift Chamber (CDC). Three layers of double-side, double-metal silicon strip detectors provide the vertex measurement of B- meson decays. The resolution of the measurement of the distance δ_z between two B meson decay vertices is typically 90 μm, about a half of the decay length of B mesons at the KEK B-factory. CDC has Al anode wires and is filled with a Helium-based gas to minimize the multiple Coulomb scattering. The electromagnetic calorimeter consists of CsI crystal's readout by photo diodes. To identify kons from pions we plan to use a Cerenkov detector in addition to TOF counter and the dE/dx measurement in CDC. The decision on the type of the Cerenkov detector, either the low index silica aerogel counter, the fast-RICH or the DIRC, will be made by the end of March 1995. For the detection of K_L as well as muons, the yoke of the 1.0 Tesla superconducting solenoid is segmented to install a hadron calorimeter of two interaction length. In the fall 1994 we decided to build a new 1.5 Tesla superconducting solenoid instead of using the existing VENUS magnet.

4 CP Reach by the BELLE detector

The physics performance of the BELLE detector was studied by a fast Mont Carlo simulation. In the fast simulation only the effects of the beam pipe and the expected performance of SVD were fully simulated, whereas the performance of other detectors were represented by smeared kinematic variables according to their resolutions and acceptances. The reconstruction efficiency for charged particles and the efficiency of the clustering in the calorimeter were not included. A fast-RICH detector with CsI photocathode was assumed providing a K/π separation of more than 2σ in all the kinematical region.

The experimental sensitivity of the CP asymmetry is expressed as

$$\delta \sin 2\phi = \frac{1}{d}\frac{1}{1-2\omega_t}\sqrt{\frac{1+N_{BG}/N_{obs}}{N_{obs}}}, \qquad (1)$$

here d is a dilution factor due to decaying time evolution, $1-\omega_t$ is a dilution factor due to wrong tagging probability, N_{obs} and N_{BG} are the numbers of observed candidate events and background events respectively. The tagging efficiency ϵ_{tag} of the BELLE detector is estimated to be 43.5 combined lepton-Koan tagging method with the wrong tagging probability ω_t of 9.8

Tables 3 and 4 summerize the experimental sensitivities (100 fb^{-1}) of the measurements of the three angles, β, α and γ of the CKM unitarity triangles.

As can be seen in the table, the most promising channel for the $\sin 2\beta$ measurement is the "gold plated mode" $J/\psi K_S(J/\psi \to \ell^+\ell^-, K_S \to \pi^+\pi^-)$; the next promising channel is $J/\psi K_L(J/\psi \to \ell^+\ell^-, K_L \to$ *nuclear interaction*). The decay channel of $J/\psi K^*$ is also promising mode, especially if it is dominated by

the CP-even final state, as indicated by ARGUS and CLEO measurements. By combining the data from all of the listed channels, the error in $\sin 2\beta$ can be reduced from 0.08, which corresponds to the gold plated mode alone, to 0.06.

Similarly, the error in $\sin 2\alpha$ is reduced from 0.17 for the $\pi^+\pi^-$ mode to $0.09 \sim 0.13$ when the $\rho\pi$ mode is included. The $\sin 2\alpha$ error from the $\rho\pi$ mode depends on the unknown value of $\rho = |A(\overline{B} \to f)/A(\overline{B} \to \overline{f})|$ for $f = \rho^+\pi^-$. Here, for simplicity, we ignore penguin contributions in both decay modes, even though they are thought to be non-negligible. Actual errors after subtracting penguin contributions will likely be larger and the estimated errors given here can be considered as lower limits.

The third angle γ can be measured using neutral and charged B decay into $D_{1,2}K$. The γ error is sensitive to the values of γ, δ and r, where δ is the final-state-interaction phase and $r = |A(B \to \bar{D}K)/A(B \to DK)|$. The γ error from B^0 decays is estimated to be less than 25° (for $\gamma < 90°$), if $|\delta_D - \delta_{\bar{D}}|$ is between 50° and 150° and r is larger than 0.25. The error from $B^\pm$ decays is estimated to be less than 15° (for any γ), if $|\delta_D - \delta_{\bar{D}}|$ is larger than 50° and r is larger than 0.1. Combining the B^0 and $B^\pm$ modes results in a γ error that is less than 13°.

Table 2: Presently available information about the two CKM parameters, ρ and η.

Quantity	Value	comments
$\|Vcb\|$	$.041 \pm .002 \pm .004$	S.Stone, "B Decays",Singapore,1991
$\|Vub/Vcb\|$	0.085 ± 0.035	Includes recent CLEO result
M_t	$132 \pm 31 \pm 19$ GeV	LEP Collab.,Phys. Lett.**B276**,247(1992)
B_K	0.8 ± 0.2	Harris and Rosner,Phys.Rev.**D45**,946(1992)
$\mid \epsilon_K \mid$	$(2.268 \pm 0.023) \times 10^{-3}$	PDG
$Re(\epsilon'/\epsilon)$	$(14.5 \pm 5) \times 10^{-4}$	average of E731 and NA31
x_d	0.677 ± 0.104	CLEO, 1993 Report to the PAC, Jan. 1993
$f_B\sqrt{B_B}$	unconstrained	
τ_B	1.40 ± 0.04 psec	E.Locci, UNK B-Factory Workshop,Jan.1993

The projected β and α measurements for an integrated luminosity of 50 fb^{-1} cover the entire 90% C.L. allowed region. Even for 10 fb^{-1}, the chance for measuring β with a 3 standard deviation significance is as high as 50%. On the other hand the γ measurement may need more than 100 fb^{-1} luminosity and will require quality high-momentum charged K/π separation.

We have also performed Monte Carlo simulation studies for measuring the sides of the KM unitarity triangle, namely, $|V_{cb}|$, $|V_{ub}|$ and $|V_{td}|$. The expected sensitivities of these measurements are summarized in Table 5. The expected statistical errors of $|V_{cb}|$, $|V_{ub}/V_{cb}|$ and $|V_{td}/V_{ts}|$ are estimated for the integrated luminosities of 10 fb^{-1} and 100 fb^{-1}. As shown in the table, the expected statistical errors of the first two parameters are much smaller than the present values even for an integrated luminosity of 10 fb^{-1}. Measurement of the third parameter has not been done so far. The systematic error in $|V_{cb}|$ is expected to improve since the extrapolation

Table 3: Expected sensitivity for $\sin 2\phi_i$ measurements with an integrated luminosity of 100 fb^{-1}. For all modes, a tagging efficiency $\epsilon_{tag} = 0.44$, a wrong-tag fraction $w = 0.10$, and a dilution factor $d = 0.54$ are used. The additional dilution due to final state CP mixing, $d_\pm$, ranges from 1 to ~ 2.7. Here $d_\rho = 2\rho/(1+\rho^2)$, where $\rho = |A(\bar{B} \to \rho^+\pi^-)/A(\bar{B} \to \rho^-\pi^+)|$. For $\rho = 0.24 \sim 4$, $d_\rho = 1 \sim 0.45$.

ϕ_i	decay mode	final states	BR(B)	BR(f) $\times$ ϵ_{rec}	N_{obs}	N_{BG}	$\delta \sin 2\phi$
β	$J/\psi K_S$	$\ell^+\ell^-\pi^+\pi^-$	5.0×10^{-4}	0.084×0.38	802	0	0.083
	$J/\psi K_S$	$\ell^+\ell^-\pi^0\pi^0$	5.0×10^{-4}	0.038×0.14	133	40	0.23
	$J/\psi K_L$	$\ell^+\ell^- K_L$	5.0×10^{-4}	0.122×0.15	444	164	0.13
	$J/\psi K^{*0}$	$\ell^+\ell^-\pi^+\pi^-\pi^0$	1.6×10^{-3}	0.014×0.19	215	53	$0.17 \times d_\pm$
α	$\pi^+\pi^-$	$\pi^+\pi^-$	1.3×10^{-5}	1.00×0.42	274	164	0.17^a
	$\rho^\pm\pi^\mp$	$\pi^0\pi^+\pi^-$	6.0×10^{-5}	1.00×0.25	754	672	$0.11/d_\rho^a$

(a) penguin backgrounds are ignored.

Table 4: Expected sensitivity for γ measurements with an integrated luminosity of 100 fb^{-1}. (a) with assumptions of $50° < \delta_D - \delta_{\bar{D}} < 150°$, $|A(B^\circ \to \bar{D}^\circ K_S)/A(B^\circ \to D^\circ K_S)| > 0.25$, and $|A(B^- \to \bar{D}^\circ K^-)/A(B^- \to D^\circ K^-)| > 0.1$.

decay mode	BR(B)	final states	BR(f) $\times$ ϵ_{rec}	ϵ_{tag}	N_{obs}	N_{BG}	$\delta\gamma^{(a)}$
$B^\circ \to D^\circ K_S$	5.0×10^{-5}	$D^\circ \to K^\pm\pi^\mp$	0.037×0.75	0.40	67	18	
		$D^\circ \to K^\pm\pi^\mp\pi^\circ$	0.119×0.56	0.40	160	185	
		$D_2 \to K_S\pi^\circ$	0.014×0.43	0.40	14	20	$\leq 25°$
		$D_2 \to K_S\omega$	0.019×0.44	0.40	20	9	
		$D_1 \to K^+K^-$	0.005×0.78	0.40	9	10	
		$D_2 \to K_S\phi$	0.004×0.56	0.40	5	2	
$B^\pm \to D^\circ K^\pm$	3.5×10^{-4}	$D^\circ \to K^\pm\pi^\mp$	0.037×0.83	self	1291	17	
		$D^\circ \to K^\pm\pi^\mp\pi^\circ$	0.119×0.55	tag	2730	159	
		$D_2 \to K_S\pi^\circ$	0.014×0.43	self	256	66	$\leq 15°$
		$D_2 \to K_S\omega$	0.019×0.49	tag	396	23	
		$D_1 \to K^+K^-$	0.005×0.86	tag	182	41	
		$D_2 \to K_S\phi$	0.004×0.78	tag	130	4	

Table 5: The expected sensitivities for triangle-side measurements with integrated luminosities of 10 and 100 fb^{-1}. The expected statistical errors of $|V_{cb}|, |V_{ub}/V_{cb}|$ and $|V_{td}/V_{ts}|$ are compared with the presently achieved statistical and systematic errors. The branching ratios of BR($B \to \pi\ell\nu$) $= 1.0 \times 10^{-4}$ and BR($B \to \rho\gamma$) $= 5 \times 10^{-6} - 1 \times 10^{-6}$ are assumed.

side	decay mode		statistical error			systematic error
	B-factory	present	100 fb^{-1}	10 fb^{-1}	present	present
$\|V_{cb}\|$	$B \to D^*\ell\nu$	$B \to D^*\ell\nu$	1%	3%	10 %	15 %
$\|V_{ub}/V_{cb}\|$	inclusive lepton	$B \to \pi\ell\nu$	1.5%	5%	14 %	40 %
$\|V_{td}/V_{ts}\|$	$B \to \rho\gamma/B \to K^*\gamma$	-	12-25%	34-67%	- %	- %

error of the decay rate to the zero recoil point y=1 will be reduced both due to the higher statistics as well as better resolution in y. The systematic error in $|V_{ub}|$ is also expected to improve because of the direct measurement of $b \to u$ decays via the exclusive $B \to \pi l\nu$ channel.

5 Conclusion

The KEK B-factory will start operation in 1998. The design peak luminosity is 1×10^{34}. The construction of the B-factory with the large beam crossing angle is a challenge. The projected β and α measurements by the BELLE experiemnt for an integrated luminosity of 50 fb^{-1} cover the current 90% C.L. allowed region if the penguin effect can be untangled. The γ measurement may need more than 100 fb^{-1} luminosity and will require high- momentum charged K/π separation. The experimental condition at the B-factory is expecetd to be the cleanest and the sensitivity of experiment may much depends on the integrated luminosity to be accumulated.

References

1. A technical design report of the KEK B-factory will soon appear as KEK Report.

2. KEK Report 94-2, April 1994.

Frascati Physics Series, Vol. III (1994)
HEAVY QUARKS AT FIXED TARGET
University of Virginia, October 7–10, 1994
(pp. 441–448)

B PHYSICS AT THE FERMILAB COLLIDER AFTER THE FIRST MAIN INJECTOR RUN

J.N. Butler
Fermi National Accelerator Laboratory
Batavia, Illinois

ABSTRACT

The prospects for a Dedicated B Collider Experiment at the Fermilab Tevatron after the year 2000 are discussed.

1 B Physics at the Fermilab Tevatron

B-physics at the Fermilab Tevatron is currently being done in the two collider detectors, CDF and D0. These detectors are not optimized for B physics and, even after their upgrades [1) 2)], will not have all the characteristics necessary to exploit the full potential of the Tevatron. The design of a 'Dedicated B Collider Detector' for the Tevatron after the first Main Injector run represents a unique opportunity and a difficult technical challenge.

While the main focus of the discussion on B physics has concentrated on a small number of very specific measurements related to indirect CP violation, there is reason to believe that this topic will be of interest for many years for the following reasons:

- B physics is a multifaceted topic which is more than just CP violation. It includes study of B_s mixing, heavy quark symmetries, hadrons containing more the one heavy quark, e.g. $b\bar{c}$, and the search for rare and (SM) forbidden decays.
- CP violation is a 'complex' phenomenon which will not be easily explored by a few measurments both because of experimental difficulties and theoretical ambiguities. It will require a comprehensive attack from many directions.
- It is hoped that even if the SM explanation of CP violation is borne out, very detailed studies may turn up deviations which would indicate physics beyond the Standard Model and would launch new studies.

The Fermilab Tevatron is an attractive site for a comprehensive program of B-physics studies because:

1. The Tevatron Collider, running at a luminosity of 10^{32} produces $\sim 5 \times 10^{10}$ b-pairs/'Snowmass year'. This is to be compared with $\sim 3 \times 10^{7}$ at an e^+e^- B symmetric or asymmetric B factory running on the $\Upsilon(4S)$ at a (design) luminosity of 3×10^{33}.

2. The Tevatron Collider constitutes a **'Broadband, High Luminosity B Factory'**, which simultaneously provides access to B physics for B_d and B_u, B_s, B-baryon, and B_c states. This permits the kind of comprehensive attack on B-physics issues that is needed.

3. While I have my doubts about whether it is possible to really work at luminosities greater than 10^{32} for this physics (I expect the trigger to break first), if it proves possible, then one can take advantage of proposed Tevatron luminosity upgrades to 10^{33}.

The price of the high rate and 'inclusivity' provided by a hadron collider is the very challenging environment in which one must perform a high precision, intrinsically low P_t experiment because:

- The b events are accompanied by a very high rate of background events.
- Even in the b events of interest, there is a complicated underlying event and one does not have available the stringent constraints that one has by running on the $\Upsilon(4S)$ at an e^+e^- collider.

These lead to questions about the overall triggering, tagging, and reconstruction, and particle identification efficiency and background rejection which can be obtained in a hadron collider. These questions must be answered to convince people that B physics at the sensitivity required for CP violation studies can be done at the Tevatron.

It should be noted that the big edge in luminosity at the Tevatron means that the experiments do not have to be as efficient as e^+e^- experiments to be competitive. If they were only 1% as efficient, they would still have a big advantage in statistics.

For many years, most high energy physicists believed that it would be difficult, if not impossible, to meet these technical challenges and successfully design a detector that could do B-physics at a hadron collider. CDF's success in reconstructing B^0, B^+, and B_s and measuring liftimes with its silicon vertex detector is the critical breakthrough 'happening' that convinces people, even e^+e^- proponents, that this physics can possibly be done at a hadron collider. The observation of the B_s, and possibly other higher mass states, eloquently makes the point about the broadband nature of the physics reach. For all their years of work in B physics,

ARGUS and CLEO never observed a B_s, nor could they have since they always ran below threshold for its production. Such choices will always face e^+e^- B-factories and will always lead to compromises.

Given the high rate of B production, one might even ask why these measurements are still viewed as being so difficult. First, one is always looking at decay modes with low branching fractions; second, many of the important studies require flavor tagging; and third the decay products of the states of interest are spread out over a large range of rapdity and occur at relatively low P_t leading to low efficiencies unless one has a highly optimized geometry. Also, there can be large backgrounds from 'typical' events, charm events, or B events which do not contain the decay of interest. These backgrounds dilute the statistical significance of the measured signal events. Table 1 shows the signal surviving the various physics processes and analysis phases for a typical forward geometry for measurements of the asymmetry in the decay

$$B^o \rightarrow J/\psi\ K_s. \tag{1}$$

(This calculation assumes only muon tags. It is expected that electron, charged kaon, and (possibly) topological tags will achieve an increase in the 'effective' number of events by a factor of 3 so the final sensitivity should be a factor of square root of three better than that shown in the table.)

This decay is seen as one of the best candidates for the detection of a CP asymmetry. The size of $\sin 2\beta$, constrained by other CKM measurements, is expected to be in the range 0.2-0.8 so $\delta \sin 2\beta \sim 0.07$ would be a three σ effect, at the low end of the range. Experiments now under construction hope to see evidence of this asymmetry after a few years of running.

The asymmetry in the decay

$$B^o \rightarrow \pi^+\pi^- \tag{2}$$

is more typical of the challenges facing an experiment that starts taking data only after the first Main Injector run. An evaluation similar to the one undertaken for $\psi\ K_s$ indicates that a sensitivity of $\delta\ sin(2\alpha)$ of 0.07 in one year of running (including all tagging techniques) could be achieved. The signal to background ratio for this state is very poor and clean detection of the signal places very difficult demands on the tracking, vertexing, and particle identification.

It is the **realistic** calculation of these efficiencies, whose product turns out to be rather low in the end, along with accurate estimates of the backgrounds, that is the real issue. The other way of saying this is that, despite the large number of B's produced, this measurement is statistically marginal and every attempt should be made to understand how to improve the efficiency and reduce the background. If each of the efficiencies turned out to be optimistic by 20% or the backgrounds turned out to much worse than expected, the CP capability of the experiment would begin to slip away.

Some people at Fermilab have assembled in a group to study possible approaches to performing a comprehensive study of CP violation in the Tevatron

Table 1: Sensitivity Calculation for Observing a CP Asymmetry in $B \rightarrow \psi K_s$ using only a Muon Tag in One Year of running at 10^{32}

CM energy	2 TeV
Cross section	50 μb
Luminosity	10^{32}
N_{B_d}/'Snowmass' year	3.75×10^{10}
Br($B_d \rightarrow \psi K^0$)	5.5×10^{-4}
Br($B_d \rightarrow \psi(\mu^+\mu^-)K_s(\pi^+\pi^-)$)	2.2×10^{-5}
$N(B_d \rightarrow \mu\mu\pi\pi)$/year	8.2×10^5
semi-leptonic decay of away side tag	0.10
Tagged $N(B_d \rightarrow \mu\mu\pi\pi)$/year	8.2×10^4
triggering efficiency	0.8
acceptance for muon tag	0.25
acceptance for $\mu\mu\pi\pi$ tracks	0.2
Vertexing, cleanup	0.7
Detected events	2400
Dilution factors:	
$\frac{x_d}{1.0+x_d^2}$	0.47
muon misid(away side mix)	0.7
muon misid (cascade,π,k decay)	0.8
Background	0.95
Total sensitivity(μ tag):	0.07

Collider. This resulted in an Expression of Interest submitted to Fermilab, which is now called EOI 2 [3]. There are about 10 people active in this effort at the moment and the number is growing (slowly).

The goal of the group is to achieve a good understanding of the tradeoffs among:

- Geometries/Architectures (This includes η coverage, magnetic field configuration, etc);
- Tracking configuration – vertex detector technology(strips, pixels), vertex detector configuration (disks, barrels, roman pots,..), central tracking, resolution, multiple scattering, etc;
- Trigger scheme – leptons, invariant mass, impact parameter – at each level;
- Particle identification – this is important for a complete attack on CP including direct CP, baryons, and is also important for measuring $\sin 2\alpha$ using $B^0 \rightarrow \pi^+\pi^-$;
- Tagging - the semi-muonic branching fraction times muon detection efficiency (due to P_t cuts, geometric acceptance, etc) is a big loss. Other schemes, including K-tagging, B^{**} tagging, electron tagging, and tagging via kinematical correlations of various sorts can have higher efficiency but also may introduce unacceptable backgrounds and need to be studied.

The first project of this group is to develop a fast, hit-level Monte Carlo to quickly run through several geometries and chose the most promising ones for additional studies.

Candidates are:

1. Forward geometry with Roman Pot type silicon vertex detectors with quadrupoles or dipoles (COBEX type geometries).
2. Central dipole or dipoles (BCD type geometries).
3. Central solenoid with forward dipoles or quadrupoles. At least one set of these geometries involves placing dipoles around the CDF solenoid or D0 solenoid.
4. A solenoid (perhaps very long).
5. ANY OTHER GEOMETRIES WHICH LOOK PROMISING.

We are also beginning to develop a full hit level simulation package based on GEANT. After the initial shakeout of geometries and vertex detectors using the fast simulation, GEANT will be used to develop a complete hit level model of the trigger and reconstruction efficiency. THIS WOULD BE USED TO GENERATE AN LOI WHICH IS DUE ABOUT A YEAR AND A HALF FROM NOW.

Meanwhile, there are a large number of physics studies which must be done.

- Generator Level
  1. Do we have a reliable measurement or model of the 'typical hadronic (background) events'? This is a critical question for trigger and background studies.
  2. Do we have a reliable measurement or model of charm production, which could be a major contributor of background?
  3. Do we have a reliable model of the B-pair production dynamics including correlations? Is there anything there we can exploit? Data about the existence/rate/decay modes of B^{**} production would be helpful.

- Trigger and efficiency studies
  1. Selection of key benchmark states
     (a) 'tagged' decays with ψ's, such as ψK_s^o
     (b) 'tagged' $\pi^+\pi^-$
     (c) Decays with photons or π^0 - $K^*\gamma$, $B_s \to \rho\gamma$
     (d) Decays with two D mesons, such as D^+D^-
     (e) Decays with D's and K's
     (f) B_s states for Mixing study
     (g) ...
  2. Geometric Acceptance, tracking efficiency
  3. Mass, momentum resolution
  4. Vertex finding efficiency, proper time resolution, false vertex probability
  5. Lepton (electrons, Muons) Geometric, Reconstruction efficiencies and fake rate, esp. fake tags
  6. Particle identification efficiency and fake rate
  7. Photon reconstruction

- Background studies
  1. Combinatoric background – efficacy of vertex detector in achieving required rejections
     (a) From 'typical events'
     (b) From charm
     (c) From combination of correctly measured and mismeasured B events
  2. Background from kinematic reflections (esp. in states like $B^0 \to \pi\pi, K\pi, \rho\gamma, K^*\gamma$) (mass resolution and particle id are big issues here)
  3. false tags

- Luminosity, pile up studies

1. How serious are multiple interactions to the trigger rejection and efficiency, the reconstruction efficiency, and resolution?
2. Effect of machime backgrounds

- Final analysis cuts, sensitivity to CP type asymmetries

Parallel to this effort must be an effort in understanding and even developing detector technologies, triggering and DA techniques, etc.

I take it as a given that the trigger will be a very sophisiticated pipelined trigger with significant tracking, mass sensitivity, and perhaps even impact parameter selection at level I (or 1.5).

2 Status of the EOI and Relation of a Tevatron B Experiment to Other Efforts

The Fermilab PAC, at its June meeting, endorsed the idea of a dedicated B detector to replace one of the two existing collider detectors for RUN III. The lab is moving towards providing official encouragement and some level of support for the development of LOI's.

The PAC recommendation points to a fully operational B detector in RUN III which one imagines will occur around 2003-2004. At the start of the experiment, the e^+e^- B factories and HERA-B will hopefully have had several years of running at design luminosities. Some of the easiest CP studies may well have been carried out. Any of the proposed hadron collider experiments, except for the ongoing efforts at CDF and D0 at FNAL, will come on late and must be designed as 'second generation' experiments whose goals must be to address the harder measurements, which are likely to be either not done or not very precise.

The arguments I have advanced for a program of B physics at the Tevatron Collider are even stronger for the LHC where the higher energy results in a higher cross section and the luminosity will also be higher. Although all schedules are uncertain, even an optimistic view of the Fermilab schedule and a pessimistic view of the LHC schedule would give the Fermilab experiment a head start of at most 2-3 years. One may then correctly question the competitiveness of the proposed experiment.

I have a several comments. One is that, of course, we would like to find a way to advance the schedule at Fermilab. The second is that Fermilab is now considering upgrades to the machine luminosity (and possibly the energy). These upgrades will surely improve the competitiveness of the Tevatron if they are implemented. We believe that the sensitivity of these experiments will level off at some luminosity around a few 10^{32} due to triggering and reconstruction efficiency problems and therefore there may be no significant luminosity advantage at LHC (this remains to be seen, of course). LHC still would have an advantage due to the higher cross section which may amount to a factor of 5. However, the basic efficiency is low so there is plenty of 'headroom' for differences in experimental approach to further

narrow the gap. At any rate, those of us participating in this effort are acutely aware of the competition, both from e^+e^- and from LHC, and know that these issues will have to be addressed after designs have solidified and more is known about schedules. The challenge now for our group remains to design an optimized dedicated B detector for the Tevatron.

References

1. Expression of Interest in a Future Collider Detector at B0 - CDF Collaboration
2. Expression of Interest Based on the D0 Detector for Run 3 at the Fermilab Tevatron – D0 Collaboration
3. Expression of Interest for a Dedicated Hadron Collider B Experiment at the Fermilab Tevatron – R. Edelstein et al.

PARTICIPANTS

ALBRECHT, HARTWIG
DESY
F15ALB@DSYIBM.DESY.DE
DESY - F15, 22603 HAMBURG, GERMANY
49-4089993188

ARENTON, MIKE
UNIVERSITY OF VIRGINIA
UVAHEP::ARENTON
DEPARTMENT OF PHYSICS, CHARLOTTESVILLE, VA 22901
(804) 982-5374

BELLINI, GIANPAOLO
UNIV. DI MILANO
FNALO::BELLINI
DIPT. DI FISICA, VIA CELORIA 16, I-20133, MILANO, ITALY
39-2-2392370

BERGER, EDMOND L.
ARGONNE NATIONAL LAB.
ELB@HEP.ANL.GOV
HEP 362, ARGONNE, IL 60439
(708) 252-6211

BIANCO, STEFANO
INFN - FRASCATI
FNALV::BIANCO
LAB. NAZIONALI DI FRASCATI, VIA ENRICO FERMI 40, I-00044, FRASCATI (RM) ITALY
39-6-9403409

BIGI, IKAROS I.
UNIVERSITY OF NOTRE DAME
BIGI@UNDHEP.HEP.ND.EDU
DEPT. OF PHYSICS, NOTRE DAME, IN 46556
(219) 631-7108

BONOMI, GERMANO
INFN - PAVIA
BONOMI@PV.INFN.IT
DIPT. DI FISICA NUCLEARE E TEORICA E INFN, VIA BASSI 6, PAVIA ITALY
39-382-507267

BUCHHOLZ, PETER
CERN
BUCHHOLZ@CERNVM.CERN.CH
PPE/48E, CH-1211, GENEVA 23, SWITZERLAND
41-227677178

BUTLER, JOEL N.
FERMILAB
FNALV::BUTLER
MS-120, P.O. BOX 500, BATAVIA, IL 60510
(708) 840-3148

CARBONI, GIOVANNI
INFN - SEZ. DI PISA
CARBONI@HP1LHB.PI.INFN.IT
LAB. DI SAN PIERO, VIA LIVORNESE, 582/A, I-56010, S. PIERO A GRADO (PI) ITALY
39-50-880239

CESTER-REGGE, ROSANNA
UNIV. DEGLI STUDI DI TORINO
CESTER@VAXTO.TO.INFN.IT
DIPT. DI FISICA TEORICA, VIA PIETRO GIURIA 1, I-10125, TORINO, ITALY
39-11-6707310

CHRISTIAN, DAVID C.
FERMILAB
FNALV::DCC
MS-220, P.O. BOX 500, BATAVIA, IL 60510
(708) 840-4001

CHUDAKOV, EUGENE
UNIV. OF MAINZ C/O CERN
GEN@VSNHD7.CERN.CH
PPE CERN, GENEVA 23, CH-1211, SWITZERLAND
41-22-767-8193

CONETTI, SERGIO
UNIVERSITY OF VIRGINIA
UVAHEP::SERGIO
PHYSICS DEPARTMENT, CHARLOTTESVILLE, VA 22901
(804) 982-5371

CORTI, GLORIA
UNIVERSITY OF VIRGINIA
UVAHEP::CORTI
PHYSICS DEPARTMENT, CHARLOTTESVILLE, VA 22901
(804) 982-5386

COX, BRADLEY B.
UNIVERSITY OF VIRGINIA
UVAHEP::COX
PHYSICS DEPARTMENT, CHARLOTTESVILLE, VA 22901
(804) 982-5377
DAMERI, MAURO
INFN - GENOVA
DAMERI@VAXGEA.GE.INFN.IT
DIPT. DI FISICA, VIA DODECANESO 33, I-16146 GENOVA, ITALY
39-10-35-36320

DROPMANN, FRANK
MAX-PLANCK-INSTITUT FUER KERNPHYSIK
FDR@DXNHD1.MPI-HD.MPG.DE
POSTFACH 10 38 80, D-69029 HEIDELBERG, GERMANY

DUKES, CRAIG
UNIVERSITY OF VIRGINIA
UVAHEP::DUKES
DEPARTMENT OF PHYSICS, CHARLOTTESVILLE, VA 22901
(804) 982-6384

EICHTEN, ESTIA J.
FERMILAB - THEORY GROUP
FNALV::EICHTEN
MS-106, P.O. BOX 500, BATAVIA, IL 60510
(708) 840-3751

FABBRI, F.L.
INFN - FRASCATI
FRANCO@VAXLNF.LNF.INFN.IT
LAB. NAZIONALI DI FRASCATI, VIA ENRICO FERMI 40, I-00044, FRASCATI (RO) ITALY
39-6-9403423

FISHBANE, PAUL
UNIVERSITY OF VIRGINIA
PMF2R@VIRGINIA.EDU
DEPARTMENT OF PHYSICS, CHARLOTTESVILLE, VA 22901
(804) 924-6578

GRANCAGNOLO, FRANCO
INFN - SEZ. DI LECCE
FNALV::FRANCO
UNIVERSITA DEGLI STUDI, STRADA PER ARNESANO, I-73100, LECCE, ITALY
39-832-320492

GRECO, MARIO
INFN - FRASCATI
GRECO@LNF.INFN.IT
LAB. NAZIONALI DI FRASCATI, VIA ENRICO FERMI 40, I-00044, FRASCATI (RO) ITALY
39-6-9403383

HAGAN-INGRAM, KARLA
UNIVERSITY OF VIRGINIA
UVAHEP::HAGAN
DEPARTMENT OF PHYSICS, CHARLOTTESVILLE, VA 22901
(804) 982-5372

HANDLER, TOM
UNIVERSITY OF TENNESSEE
TH@UTKHEP.PHYS.UTK.EDU
DEPARTMENT OF PHYSICS, KNOXVILLE, TN 37996-1200
(615) 974-7820

HANLET, PIERRICK
UNIVERSITY OF VIRGINIA
UVAHEP::HANLET
DEPARTMENT OF PHYSICS, CHARLOTTESVILLE, VA 22901
(804) 982-5372

ISGUR, NATHAN
CEBAF - THEORY GROUP
CEBAF::ISGUR
MS-12H2, 12000 JEFFERSON AVENUE, NEWPORT NEWS, VA 23606
(804) 249-7451

ITO, MARK
PRINCETON UNIVERSITY
ITO@PUPHEP.PRINCETON.EDU
DEPARTMENT OF PHYSICS, JADWIN HALL, PRINCETON, NJ 08544
(609) 258-5592

JENSEN, DOUGLAS
FERMILAB
FNALV::DJENSEN
MS-231, P.O. BOX 500, BATAVIA, IL 60510
(708) 840-8194

JESIK, RICHARD L.
UNIVERSITY OF ILLINOIS AT CHICAGO
FNALV::JESIK
DEPARTMENT OF PHYSICS (M/C 273), 845 W. TAYLOR, CHICAGO, IL 60607
(312) 996-5909

KAPLAN, DANIEL M.
ILLINOIS INSTITUTE OF TECHNOLOGY
FNALV::KAPLAN
CHICAGO, IL 60616
(312) 567-3389

KARCHIN, PAUL E.
YALE UNIVERSITY
KARCHIN@YALPH1.PHYSICS.YALE.EDU
DEPARTMENT OF PHYSICS, 509 GIBBS LAB., PO BOX 208121, NEW HAVEN, CT 06520-8121
(203) 432-3362

KEKELIDZE, VLADIMIR
JOINT INSTITUTE FOR NUCLEAR RESEARCH
KEKELIDZE@LSHE6.JINR.DUBNA.SU
LAB. FOR SUPER HIGH ENERGIES, DUBNA, MOSCOW REGION, 141980, RUSSIA
7-09621-62861

KINOSHITA, KAY
VIRGINIA TECH
KINOSHITA@AMY.PHYS.VT.EDU
DEPARTMENT OF PHYSICS, BLACKSBURG, VA 24061
(703) 231-8735

KLIENKNECHT, KONRAD
JOHANNES-GUTENBERG-UNIV.
KLEINKNECHT@VIPMZW.PHYSIK.UNI-MAINZ.DE,
INSTITUT FUER PHYSIK, STAUDINGERWEG 7, D-55099, MAINZ, GERMANY
49-6131-392893

LAU, KWONG H.
UNIVERSITY OF HOUSTON
LAU%UHIBPD@UHIBPD.PHYS.UH.EDU
IBPD, ROOM 632, S&R 1, HOUSTON, TX 77204-5506
(713) 743-3600

LAZARUS, DON
BROOKHAVEN NATIONAL LABORATORY
BNLDAG::LAZARUS
BUILDING 911B, UPTON, NY 11973
(516) 282-3959

LAZZERONI, CRISTINA
INFN - PISA
LAZZERONI@VXCERN.CERN.CH
LAB. DI SAN PIERO, VIA LIVORNESE, 582/A, I-56010, S. PIERO A GRADO (PI) ITALY
39-50-880237

LEDOVSKOY, ALEXANDER
UNIVERSITY OF VIRGINIA
UVAHEP::LEDOVSKOY
DEPARTMENT OF PHYSICS, CHARLOTTESVILLE, VA 22901
(804) 982-5372

LIGUORI, GIUSEPPE
UNIVERSITY OF PAVIA
LIGUORI@VAXPV.PV.INFN.IT
VIA BASSI 6, I-27100, PAVIA, ITALY
39-382-507-419

LITTENBERG, LARRY
BROOKHAVEN NATIONAL LABORATORY
LITTENBE@BNL.GOV
PHYSICS 510A, UPTON, NY 11973

LUK, KAM B.
UNIVERSITY OF CALIFORNIA - BERKELEY
LBL::LUK
DEPARTMENT OF PHYSICS, BERKELEY, CA 94720
(510) 486-7054

MARLOW, DANIEL R.
PRINCETON UNIVERSITY
MARLOW@PUPHEP.PRINCETON.EDU
PHYSICS DEPARTMENT, P.O. BOX 708,
PRINCETON, NJ 08540
(609) 258-4383

MATSUDA, TAKESHI
KEK NATIONAL LABORATORY
MATSUDA@KEKVAX.KEK.JP
FOR HIGH ENERGY PHYSICS, 1-1 OHO,
TSUKUBA-SHI, IBARIKI-KEN 305, JAPAN
1-298-64-5366

MCMANUS, ARTHUR P.
UNIVERSITY OF VIRGINIA
UVAHEP::MCMANUS
PHYSICS DEPARTMENT, CHARLOTTESVILLE, VA 22901
(804) 982-5383

MENARY, SCOTT
UNIVERSITY OF CALIFORNIA SANTA BARBARA
FNALV::LNS62::MENARY
WILSON LAB, UCSB GROUP, CORNELL
UNIVERSITY, ITHACA, NY 14853
(607) 255-8785

MOLZON, WILLIAM R.
UNIVERSITY OF CALIFORNIA - IRVINE
WMOLZON@UCI.EDU
DEPARTMENT OF PHYSICS, IRVINE, CA 92717
714-856-5987

NAKADA, TATSUYA
INSTITUTE FOR INTERMEDIATE ENERGY
PHYSICS OF ETH ZURICH
VILLIGEN PSI CH-5232 SWITZERLAND
NAKADA@PSICLU.CERN.CH
41-56-992111

NELSON, KENNETH S.
UNIVERSITY OF VIRGINIA
UVAHEP::KENNELSON
PHYSICS DEPARTMENT, CHARLOTTESVILLE, VA 22901
(804) 982-5378

PROCARIO, MIKE
CARNEGIE MELLON UNIVERSITY
PROCARIO@FEYNMAN.PHYS.CMU.EDU
DEPARTMENT OF PHYSICS, 5000 FORBES AVENUE, PITTSBURGH, PA 15213
(412) 268-3887

PUROHIT, MILIND V.
UNIVERSITY OF SOUTH CAROLINA
PUROHIT@SCUCH8.PSC.SCAROLINA.EDU
DEPARTMENT OF PHYSICS AND ASTRONOMY, COLUMBIA, SC 29212
(803) 777-6996

RAMACHANDRAN, SATYADEV
UNIVERSITY OF CALIFORNIA LOS ANGELES
FNALV::SATYADEV
FERMILAB MS-221, P.O. BOX 500, BATAVIA, IL 60510
(708) 840-4250

RHOADES, JEAN
UNIVERSITY OF CALIFORNIA LOS ANGELES
FNALV::JRHOADES
FERMILAB MS-330, P.O. BOX 500, BATAVIA, IL 60510
(708) 840-3001

ROBERTS, WINSTON
OLD DOMINION UNIVERSITY
CEBAF::ROBERTS
CEBAF, MS-12H2, 12000 JEFFERSON AVENUE, NEWPORT NEWS, VA 23606
(804) 249-7380

SALA, SILVANO
MILANO UNIVERSITY
FNALV::SALA
DIPT. DI FISICA, VIA CELORIA, 16, 20133, MILANO, ITALY
39-2-2392-312

SANNINO, MARIO
INFN - GENOVA
SANNINO@VAXGEA.GE.INFN.IT
DIPT. DI FISICA, VIA DODECANESO, 33, 16146, GENOVA, ITALY
39-10-353-6334

SELOVE, WALTER
UNIVERSITY OF PENNSYLVANIA
WS@UPENN5.HEP.UPENN.EDU
PHYSICS DEPARTMENT, PHILADELPHIA, PA 19104
(215) 898-8159

SHUKLA, SHEKHAR
FERMILAB
FNAL::SHEKHAR
MS-341, P.O. BOX 500, BATAVIA, IL 60510
(708) 840-4828

SIMONE, JIM
FERMILAB - THEORY GROUP
FNALV::SIMONE
MS-106, P.O. BOX 500, BATAVIA, IL 60510
(708) 840-3748

SMITH, GERALD A.
PENNSYLVANIA STATE UNIVERSITY
SMITH@PHYS.PSU.EDU
303 OSMOND LAB, UNIVERSITY PARK, PA 16802
(814) 863-3076

SOKOLOFF, MICHAEL D.
UNIVERSITY OF CINCINNATI
FNALV::SOKOLOFF
PHYSICS DEPARTMENT, CINCINNATI, OH 45221
(513) 556-0533

SPIEGEL, LENNY
FERMILAB
FNALV::LENNY
MS-220, P.O. BOX 500, BATAVIA, IL 60510
(708) 840-2809

THACKER, HANK
UNIVERSITY OF VIRGINIA
HBT8R@VIRGINIA.EDU
DEPARTMENT OF PHYSICS, CHARLOTTESVILLE, VA 22901
(804) 924-3204

TSCHIRHART, ROBERT
FERMILAB
FNALV::TSCH
MS-122, P.O. BOX 500, BATAVIA, IL 60510
(708) 840-4100

TZAMOURANIS, IOANNIS
UNIVERSITY OF VIRGINIA
UVAHEP::YANNIS
PHYSICS DEPARTMENT, CHARLOTTESVILLE, VA 22901
(804) 982-5385

VALENCIA, GERMAN
IOWA STATE UNIVERSITY
FNALV::VALENCIA
DEPARTMENT OF PHYSICS, AMES, IO 50011
515) 294-4110

VIOLA, LAURA
UNIV. DI PAVIA
VIOLA@VAXPV.PV.INFN.IT
DIPT. DI FISICA NUCLEARE E TEORICA E INFN,
VIA BASSI 6, PAVIA ITALY
39-382-507-268

VITULO, PAOLO
UNIV. DI PAVIA
VITULO@VAXPV.PV.INFN.IT
DIPT. DI FISICA NUCLEARE E TEORICA E INFN,
VIA BASSI 6, PAVIA ITALY
39-382-507268

VOTANO, LUCIA
LAB. NAZ. DI FRASCATI
VOTANO@LNF.INFN.IT
VIA ENRICO FERMI, 40, 00044 FRASCATI (ROMA) ITALY
39-6-9403432

WHITE, SEBASTIAN
BROOKHAVEN NATIONAL LABORATORY
SWHITE%BNLCL7@FNAL.FNAL.GOV
MS-510C, UPTON, NY 11973
(516) 282-5488

WISE, MARK
CALIFORNIA INSTITUTE OF TECHNOLOGY
WISE@THEORY3.CALTECH.EDU
452-48 PHYSICS, PASADENA, CA 91125

WISS, JAMES
UNIVERSITY OF ILLINOIS - URBANA
FNALA::JEW
413 LOOMIS LAB, 1110 W. GREEN ST., URBANA, IL 61801
(218) 333-4873

ZIOULAS, GEORGE
FERMILAB
FNALV::GIORGOS
MS-122, P.O. BOX 500, BATAVIA, IL 60510
(708) 840-2439